

NASA CP-2376
V 6

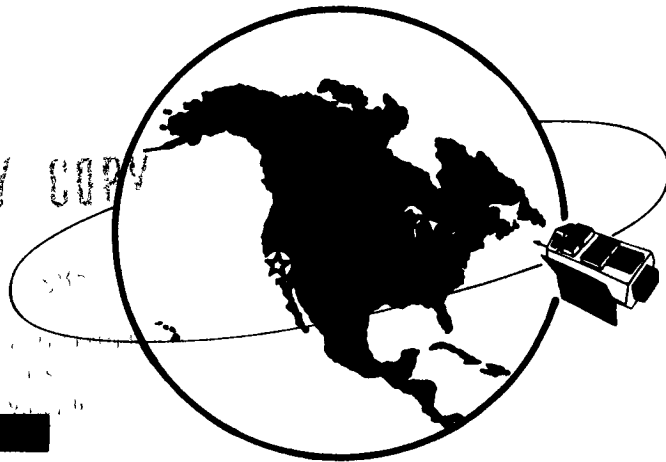
19TH INTERNATIONAL COSMIC RAY CONFERENCE

LA JOLLA, USA AUGUST 11-23, 1985

CONFERENCE PAPERS

NASA-CP-2376-VOL-6
19850027535

LIBRARY COPY



HE
SESSIONS
VOL. 6

THE UNIVERSITY OF TEXAS AT AUSTIN

19TH INTERNATIONAL COSMIC RAY CONFERENCE

LA JOLLA, USA AUGUST 11-23, 1985

CONFERENCE PAPERS



HE

SESSIONS
VOL. 6

PUBLICATION COMMITTEE

F.C. Jones, Chm.

J. Adams

G.M. Mason

NASA Conference Publication 2376

Published by
Scientific and Technical Information Branch
National Aeronautics and Space Administration
Washington, D.C. 20546

August 1985

For sale by the National Technical Information Service, Springfield, VA 22151

PREFACE

The 19th International Cosmic Ray Conference, under the auspices of the Cosmic Ray Commission of the International Union of Pure and Applied Physics, is being held on the campus of the University of California, San Diego, on 11 through 23 August 1985. In keeping with the tradition begun in 1971 by the Australian organizers of the 12th ICRC, the Proceedings of this conference are appearing in two sets of volumes. The first set, consisting of volumes 1 through 8, is being distributed to all participants at the beginning of the conference. This set contains the contributed papers. The second set, distributed after the conference, contains invited, rapporteur, and highlight papers. The papers are reproduced here exactly as they were received from the authors, without refereeing.

For the 19th ICRC, the scientific program was organized according to three major divisions— OG (cosmic rays and gamma rays of Galactic Origin), SH (Solar and Heliosphere), and HE (High Energy). Technical papers are included in each of the three divisions.

This conference depended on funds from several agencies of the United States government, including major financial support from the National Aeronautics and Space Administration and support from the National Science Foundation, the Department of Energy, and the Air Force Geophysics Laboratory. Important financial support also came from the Center for Astrophysics and Space Sciences of the University of California, San Diego, from the California Space Institute of the University of California, from the Department of Physics and Astronomy of the University of Maryland, College park, from the International Union for Pure and Applied Physics, and from several corporate sponsors who will be acknowledged by name in the post-conference volumes.

We appreciate the confidence placed in the conference organizers by the Cosmic Ray Commission, and acknowledge with thanks the role of the Commission members in setting up the rules for the conference and in advising the organizers during its planning.

We are grateful to all of the members of the various organizing committees listed at the front of this volume. The three Program Committees went to great effort to organize a coherent scientific program and to schedule four parallel sessions with a minimum of conflicts. The Local Organizing Committee has worked long and hard to ensure efficient and hospitable accommodations for all the participants, both in the scientific sessions and outside them. The Publications Committee not only took great pains to assemble these volumes but also maintained an orderly data base of papers and authors which was extremely helpful to the program committees. The General Organizing Committee made important contributions of ideas and efforts to make the conference possible; this committee included international representation from all of North America, thus the departure from the traditional name of National Organizing Committee. And the entire effort was coordinated by the dedicated members of the Steering Committee.

Martin H. Israel, Chairman
General Organizing Committee

August, 1985

LETTER FROM THE EDITORS

This conference marks a departure from previous conferences in this series in that the publication of the Conference Papers was carried out an entire continent away from the activities of Local Organizing Committee. This posed some problems but, to the considerable surprise of the Publications Committee members, the one that was expected to be the most trouble turned out not to be significant. The overwhelming majority of those submitting papers and abstracts sent them to the correct address, not to La Jolla as was feared. We wish to thank our many authors for their alertness and commend them for handling a complicated situation so well.

There are eight volumes to be distributed to the conference participants in addition to the Conference Program and Author Index: three volumes for OG, two for SH and three for HE. the detailed makeup of these volumes is described in the prefaces written by the Scientific Program chairmen for their respective volumes. Out of some 1100 abstracts that were accepted by the Scientific Program Committees for inclusion in the conference some 929 papers were finally received in time for inclusion in the Conference Papers. This represents a response of approximately 84 percent, a modest improvement. Even if one excludes the 42 one page papers that should be considered as "confirming abstracts", even though there was no such formal category, the response was somewhat higher than that of recent years. We attribute this to the carrot of a later deadline than before coupled with the stick of there being no printing of post deadline contributed papers. We believe that this decision of the General Organizing Committee was a wise one. Of course invited, rapporteur, and highlight talks will be printed in volumes to be distributed to the participants after the conference as usual.

The Publications Committee had much generous help in performing its duties: from Goddard Space Flight Center we had the help of B. Glasser, L. Harris, E. Schronce, N. Smith, J. Esposito and T. Smith. From the Naval Research Laboratory we were helped by T. Mazzotta, and at the University of Maryland M. L. Snidow and J. Mucha gave much needed assistance. Special thanks are due to Caryl Short, the lone staff member of the Publications Committee. She maintained the computer data base, organized the abstracts as they arrived, and kept track of the papers themselves to see that the finally arrived in the right place at the right time. Without her help the job would have been far more difficult than it was.

PUBLICATIONS COMMITTEE

August, 1985

Frank C. Jones, Chm.
Jim Adams
Glen M. Mason

THE SESSIONS
VOLUME VI

19th INTERNATIONAL COSMIC RAY CONFERENCE
LA JOLLA, USA
AUGUST 11-23, 1985

INTERNATIONAL UNION OF PURE AND APPLIED PHYSICS
MEMBERS OF THE COMMISSION ON COSMIC RAYS OF IUPAP

A.E. Chudakov, Chm.	P.H. Fowler	T.O. Montmerle	B.V. Sreekantan
F.B. McDonald	D. Hovestadt	H. Moraal	K. Suga
G.C. Castagnoli	J. Kota	J.R. Prescott	J. Wdowczyk

STEERING COMMITTEE

F. McDonald, Chm.	T. Gaisser	F. Jones	R. Mewaldt
G. Burbage	M. Israel	R. Lingenfelter	L. Peterson
M. Forman			

GENERAL ORGANIZING COMMITTEE

M. Israel, Chm.	V. Jones	B. Price	J. Simpson
M. Bercovitch	S. Krimigis	R. Ramaty	E. Stone
P. Freier	J. Kurfess	F. Reines	D. Venkatesan
R. Gall	J. Lockwood	M. Shapiro	J. Waddington
R. Jokipii	P. Meyer	M. Shea	S. White
L. Jones			

PROGRAM COMMITTEES

OG SESSIONS	SH SESSIONS	HE SESSIONS	PUBLICATIONS
R. Mewaldt, Chm.	M. Forman, Chm.	T. Gaisser, Chm.	F. Jones, Chm.
G. Cassiday	H. Hudson	K. Lande	J. Adams
C. Fichtel	G. Mason	J. Linsley	G. Mason
A. Harding	B. McKibben	E. Loh	
J. Matteson	M. Pomerantz	G. Yodh	
D. Muller			
W. Webber			

LOCAL ORGANIZING COMMITTEE

L. Peterson, Chm.	A. Buffington	J. Linsley	O. Piccioni
G. Burbidge	M. Burbidge	K. Marti	M. Thiemens
R. Lingenfelter	W. Fillius	G. Masek	W. Thompson
R. Rothschild	R. Gall	J. Matteson	H. Ticho
J. Arnold	R. Gould	C. McIlwain	R. White
W. Baity	H. Hudson	R. Mewaldt	

Sponsored by

National Aeronautics and Space Administration
National Science Foundation
Department of Energy

Center for Astrophysics and Space Science, University of California, San Diego
California Space Institute, University of California
Department of Physics and Astronomy, University of Maryland, College Park

Preface to HE Volumes

Papers contributed to the XIX International Cosmic Ray Conference were arranged into three major divisions: Origin and Galactic phenomena (OG), Solar and Heliospheric (SH), and High Energy (HE). The HE sessions at this conference comprise all the subjects formerly included in the muon and neutrino sessions (MN) and the extensive air shower sections (EA) as well as those on high energy interactions, new particle searches and emulsion chamber results, which were previously classified in HE. In addition, technical papers have not been classified separately, but have been inserted in appropriate subject sections. All the papers now classified as HE are contained in volumes 6, 7 and 8.

Volume 6 includes sessions HE1 (cross sections and interactions of particles and nuclei at high energy) and HE3 (emulsion chamber results). Extensive air shower papers (HE4) are in volume 7. Papers on muons and neutrinos (HE5), searches for new particles and processes (HE6) and some on new techniques (HE7) are in volume 8.

Altogether some 380 abstracts were received for the HE sections. These were divided into the 25 groups listed in the tables of contents of the HE volumes. (These groups correspond only approximately to the 26 contributed paper sessions at the conference.)

Four rapporteurs were selected to cover the subjects of the HE sessions:

L.W. Jones	High Energy Interactions and New Particle Searches (HE1 & HE6);
M. Shibata	Emulsion Chamber Observations and Interpretation (HE3);
R.W. Clay	Extensive Air Showers (HE4);
K. Sivaprasad	Muons and Neutrinos (HE5).

The written versions of the rapporteur talks are contained in the post-conference volume together with highlight and invited papers.

The work of arranging the HE program was shared by a committee consisting of

T.K. Gaisser (Bartol), Chairman
K. Lande (Pennsylvania)
E.C. Loh (Utah)
J. Linsley (New Mexico)
G.B. Yodh (Maryland)

This conference is the 19th in a series. Previous conferences in this series were held at:

Cracow, Poland	-	1947
Como, Italy	-	1949
Bagnères-de-Bigorre, France	-	1953
Guanajuato, Mexico	-	1955
Varenna, Italy	-	1957
Moscow, USSR	-	1959
Kyoto, Japan	-	1961
Jaipur, India	-	1963
London, UK	-	1965
Calgary, Canada	-	1967
Budapest, Hungary	-	1969
Hobart, Australia	-	1971
Denver, USA	-	1973
München, FRG	-	1975
Plovdiv, Bulgaria	-	1977
Kyoto, Japan	-	1979
Paris, France	-	1981
Bangalore, India	-	1983

HE 1.1
CROSS SECTIONS

PAPER CODE		PAGE
HE 1.1-1	PROTON-AIR AND PROTON-PROTON CROSS SECTIONS FROM AIR SHOWER DATA J LINSLEY	1
HE 1.1-2	PROTON-AIR INELASTIC CROSS SECTION AT $S^{*1/2} = 30$ TEV RM BALTRUSAITIS, GL CASSIDAY, R COOPER JW ELBERT, PR GERHARDY, VD KOSLOV, EC LOH Y MIZUMOTO, P SOKOLSKY, D STECK	5
HE 1.1-3	HADRON CROSS SECTIONS AT ULTRA HIGH ENERGIES AND UNITARITY BOUNDS ON DIFFRACTION DISSOCIATION GB YODH, TK GAISSER, UP SUKHATME	9
HE 1.1-4	ON TOTAL CROSS SECTIONS AND SLOPES AT SUPERHIGH ENERGIES SHS YEREMIAN, VM ZHAMKOCHIAN	13
HE 1.1-5	DETERMINATION OF THE CROSS SECTION OF THE PROTON, PION AND NEUTRON INELASTIC INTERACTION WITH LEAD AND CARBON NUCLEI AT 0.5 - 5.0 TEV ENERGIES VV AVAKIAN, GV KARAGJOZIAN EA MAMIDJANIAN, MI KEROPIAN, RM MARTIROSOV GG OVSEPIAN, SO SOKHOYAN	17
HE 1.1-6	P(P)P ELASTIC SCATTERING AND COSMIC RAY DATA FE ALEEM, M SALEEM	21
HE 1.1-7	MEASUREMENT OF INTERACTION CROSS SECTION OF COSMIC RAY FE ($E > 4$ GEV/N) WITH AL TARGET GX REN, YZ ZHOU, RQ HUANG, MY CHEN	25

x
VOLUME 6

- | | | |
|-----------|--|----|
| HE 1.1-8 | HADRON THERMODYNAMICS IN RELATIVISTIC
NUCLEAR COLLISIONS | 28 |
| | P AMMIRAJU | |
| HE 1.1-9 | ESTIMATION OF THE TOTAL INELASTICITY
COEFFICIENT IN INTERACTION OF > 20 TEV
HADRONS WITH LEAD | 31 |
| | BL KANEVSKY, IA MIKHAILOVA
IV RAKOBOLSKAYA, LG SVESHNIKOVA | |
| HE 1.1-11 | THE METHOD FOR THE STUDY OF THE
INELASTIC CROSS - SECTION FOR HIGH
ENERGY PROTONS BY MEANS OF SHOWER ARRAYS
WITH THE LARGE CALORIMETER AREA | 35 |
| | TV DANILOVA, AD ERLYKIN | |
| HE 1.1-12 | INELASTICITY PARTIAL COEFFICIENT K SUB
GAMMA DETERMINATION IN PI C AND PI PB
INTERACTIONS AT 10**14 EV | 39 |
| | FAMIR COLLABORATION | |

HE 1.2
PARTICLE PRODUCTION - MODELS AND
EXPERIMENTS

PAPER CODE		PAGE
HE 1.2-1	SINGLE PARTICLE MOMENTUM AND ANGULAR DISTRIBUTIONS IN HADRON-HADRON COLLISIONS AT ULTRAHIGH ENERGIES TT CHOU,CN YANG	43
HE 1.2-2	QCD-MOTIVATED DESCRIPTION OF VERY HIGH ENERGY PARTICLE INTERACTIONS TK GAISSER,F HALZEN	47
HE 1.2-4	EMPIRICAL DESCRIPTION OF THE HADRON-HADRON AND HADRON-NUCLEUS INTERACTION AT THE ACCELERATOR ENERGY RANGE G KUBIAK, SZABELSKI,J WADOWCZYK,J KEMPA A PIOTROWSKA	51
HE 1.2-5	MULTIPLICITY DISTRIBUTIONS IN INTERACTION MODELS USED FOR CASCADE SIMULATIONS RW ELLSWORTH,RK GAISSER,T STANEV	55
HE 1.2-6	SOME REMARKS ABOUT SIMULATION OF COSMIC RAY PHENOMENA WITH USE OF NUCLEAR INTERACTION MODELS BASED ON THE CURRENT SPS PROTON-ANTIPROTON DATA JA WROTONIAK,GB YODH	56
HE 1.2-7	LOW P**T HADRON-NUCLEUS INTERACTIONS R HOLYNSKI,K WOZNIAK	60
HE 1.2-8	ANGULAR DISTRIBUTION AND MULTIPLICITY OF BACKWARD HADRONS IN HFE INTERACTION AT 0.5-5.0 TEV ENERGIES (PION EXPERIMENT) VV AVAKIAN,MO AZARIAN,KSH EGIYAN EA MAMIDJANIAN,GZH OHANIAN SV TER-ANTONIAN	64

- HE 1.2-9 A TEST OF THE FEYNMAN SCALING IN THE FRAGMENTATION REGION AT THE SQUARE ROOT OF $S = 630$ GEV 68
T DOKE, V INNOCENTE, K KASAHARA, J KIKUCHI
T KASHIWAGI, S LANZANO, K MASUDA
H MURAKAMI, Y MURAKI, T NAKADA, A NAKAMOTO
T YUDA, M HAGUENAUER
- HE 1.2-10 ANGULAR DISTRIBUTION OF SHOWER PARTICLES PRODUCED IN THE COLLISIONS OF 20-GEV/C AND 300-GEV NEGATIVE PIONS WITH EMULSION NUCLEI 72
CO KIM, SN KIM, IG PARK, CS YOON
- HE 1.2-11 NUCLEON-NUCLEUS INTERACTIONS FROM JACEE 76
TH BURNETT, S DAKE, M FUKI, JC GREGORY
T HAYASHI, R HOLYNSKI, J IWAI, WV JONES
A JURAK, JJ LORD, O MIYAMURA, T OGATA
A OLSEZWSKI, TA PARNELL, T SAITO, S STRAUZ
M SZARSKA, T TABUKI, Y TAKAHASHI
Y TOMINAGA, B WILCZYNSKA, JF WEFEL
RJ WILKES, W WOLTER, B WOSIEK
- HE 1.2-13 AN UNIFICATION OF THE INTERACTIONS AND THE DIFFRACTIVE PROCESSES 80
IA KUCHIN
- HE 1.2-14 IS THE INELASTIC CHARGE-EXCHANGE CONTRIBUTION CONSTANT AT THE LARGE X AND SUPERHIGH ENERGIES? 84
IA KUCHIN
- HE 1.2-15 GENERAL CONSEQUENCES OF THE VIOLATED FEYNMAN SCALING 88
G KAMBEROV, L POPOVA
- HE 1.2-16 PROPAGATION OF COSMIC RAYS THROUGH THE ATMOSPHERE IN THE QUARK-GLUON STRINGS MODEL 92
AD ERLYKIN, NP KRUTIKOVA, YM SHABELSKI

HE 1.2-17 SCALING VIOLATION IN THE FRAGMENTATION
REGION OF INCLUSIVE NUCLEON SPECTRUM

96

SK MACHAVARIANI, SI NIKOLSKY, AP CHUBENKO

HE 1.3
NUCLEI AND NUCLEAR MATTER

PAPER CODE		PAGE
HE 1.3-1	DETERMINATION OF PRIMARY ENERGY IN NUCLEUS -NUCLEUS COLLISIONS AND THE HIGH P SUB T TAIL OF GAMMA-PARTICLES PS FREIER, TW ATWATER	100
HE 1.3-4	STOPPING RELATIVISTIC XE, HO, AU AND U NUCLEI IN NUCLEAR EMULSIONS CJ WADDINGTON, DJ FIXSEN, PS FREIER	104
HE 1.3-5	PHYSICAL MEANING OF THE MULTIPLICITIES OF EMITTED NUCLEONS IN HADRON-NUCLEUS COLLISIONS Z STRUGALSKI	108
HE 1.3-6	HOW ARE PARTICLE PRODUCTION, NUCLEON EMISSION, AND TARGET FRAGMENT EVAPORATION PROCESSES INTERRELATED IN HADRON-NUCLEUS COLLISIONS? Z STRUGALSKI	112
HE 1.3-7	EXPERIMENTAL STUDY OF THE SPACE-TIME DEVELOPMENT OF THE PARTICLE PRODUCTION PROCESS IN HADRON-NUCLEON COLLISIONS, USING MASSIVE TARGET NUCLEUS AS A DETECTOR Z STRUGALSKI	115
HE 1.3-8	EXPERIMENTAL EVIDENCE OF THE DECREASE OF KINETIC ENERGY OF HADRONS IN PASSING THROUGH ATOMIC NUCLEI Z STRUGALSKI	118
HE 1.3-9	ENERGY-RANGE RELATIONS FOR HADRONS IN NUCLEAR MATTER Z STRUGALSKI	122

HE 1.3-10	SCATTERING AND STOPPING OF HADRONS IN NUCLEAR MATTER	125
	Z STRUGALSKI	
HE 1.3-11	MEASUREMENT OF HADRON MEAN FREE PATH FOR THE PARTICLE-PRODUCING COLLISIONS IN NUCLEAR MATTER	129
	Z STRUGALSKI	
HE 1.3-13	THE PHI-MESON AND "CHIRAL-MASS-MESON" PRODUCTION IN HEAVY-ION COLLISIONS AS A PROBE OF THE QUARK-GLUON-PLASMA AND THE CHIRAL SYMMETRY TRANSITIONS	133
	Y TAKAHASHI, PB EBY	
HE 1.3-15	SU(2) X U(1) VACUUM AND THE CENTAURO EVENTS	137
	D KAZANAS, VK BALASUBRAHMANYAN RE STREITMATTER	
HE 1.3-16	HEAVY FLAVOURS PRODUCTION IN QUARK-GLUON PLASMA FORMED IN HIGH ENERGY NUCLEAR REACTIONS	141
	J KLOSINSKI	
HE 1.3-17	RINGLIKE INELASTIC EVENTS IN COSMIC RAYS AND ACCELERATORS	145
	IM DREMIN, AM ORLOV, MI TRETYAKOVA	
HE 1.3-18	PHASE SPACE FACTORS IN MULTIPARTICLE PROCESSES	149
	RJ GOULD	

HE 1.4
NUCLEUS-NUCLEUS COLLISIONS

PAPER CODE		PAGE
HE 1.4-1	THE RESPONSE OF A SCINTILLATION COUNTER BELOW AN EMULSION CHAMBER TO HEAVY NUCLEUS INTERACTIONS IN THE CHAMBER TH BURNETT, S DAKE, JH DERRICKSON, M FUKI JC GREGORY, R HAYASHI, T HAYASHI R HOLYNSKI, J IWAI, WV JONEW, A JURAK JJ LORD, CA MEEFAN, O MIYAMURA, H ODA T OGATA, TA PARNELL, E ROBERTS, T SAITO M SZARSKA, T TABUKI, Y TAKAHASHI, B WOSIEK JS WATTS, B WILCZYNSKA, RJ WILKES, W WOLTER	152
HE 1.4-2	HEAVY NUCLEUS COLLISIONS BETWEEN 20 AND 60 GEV/NUCLEON TH BURNETT, S DAKE, M FUKI, JC GREGORY T HAYASHI, R HOLYNSKI, J IWAI, WV JONES A JURAK, JJ LORD, O MIYAMURA, T OGATA TA PARNELL, T SAITO, T TABUKI, Y TAKAHASHI T TOMINAGA, B WILCZYNSKA, RJ WILKES W WOLTER, B WOSIEK	156
HE 1.4-3	CHARACTERISTICS OF CENTRAL COLLISION EVENTS IN FE-NUCLEUS INTERACTIONS FROM 20 TO 60 GEV/N TH BURNETT, S DAKE, JH DERRICKSON W FOUNTAINS, M FUKI, JC GREGORY, T HAYASHI TO HAYASHI, R HOLYNSKI, J IWAI, WV JONES A JURAK, JJ LORD, CA MEEGAN, O MIYAMURA H ODA, T OGATA, TA PARNELL, E ROBERTS T SAITO, S STRAUZ, T TABUKI, Y TAKAHASHI T TOMINAGA, B WILCZYNSKA, RJ WILKES W WOLTER, B WOSIEK	160
HE 1.4-4	NUCLEUS-NUCLEUS INTERACTIONS ABOVE SEVERAL HUNDRED GEV/N TH BURNETT, S DAKE, M FUKI, JC GREGORY T HAYASHI, R HOLYNSKI, J IWAI, WV JONES A JURAK, JJ LORD, O MIYAMURA, H ODA, T OGATA TA PARNELL, T SAITO, S STRAUZ, M SZARSKA T TABUKI, Y TAKAHASHI, T TOMINAGA, JW WATTS JP WEFEL, B WILCZYNSKA, RJ WILKES, W WOLTER B WOSIEK	164

- HE 1.4-5 OBSERVATION OF DIRECT HADRONIC PAIRS IN NUCLEUS-NUCLEUS COLLISIONS IN JACEE EMULSION CHAMBERS 168
- TH BURNETT,S DAKE,M FUKI,JC GREGORY
T HAYASHI,R HOLYNSKI,J IWAI,WV JONES
A JURAK,JJ LORD,O MIYAMURA,H ODA,T OGATA
TA PARNELL,T SAITO,T TABUKI,Y TAKAHASHI
T TOMINAGA,B WILCZYNSKA,RJ WILKES
W WOLTER,B WOSIEK
- HE 1.4-6 EXCESSIVE PRODUCTION OF ELECTRON PAIRS BY SOFT PHOTONS IN LOW MULTIPLICITY ION INTERACTIONS 172
- TH BURNETT,S DAKE,M FUKI,JC GREGORY
T HAYASHI,R HOLYNSKI,J IWAI,WV JONES
A JURAK,JJ LORD,O MIYAMURA,T OGATA
TA PARNELL,T SAITO,S STRAUZ,T TABUKI
Y TAKAHASHI,T TOMINAGA,J WATTS
B WILCZYNSKA,RJ WILKES,W WOLTER,B WOSIEK
- HE 1.4-7 FORWARD PARTICLE PRODUCTION IN INELASTIC **22NE INTERACTIONS IN EMULSION AT 4.1 A GEV/C 176
- B WOSIEK
- HE 1.4-8 ON THE MECHANISM OF ANOMALOUS NUCLEUS-NUCLEUS INTERACTIONS AT ENERGIES ABOVE 1 TEV/NUCLEON 180
- SSH AMEEV,VL SHMONIN
- HE 1.4-10 MESON MULTIPLICITY IN NUCLEUS-NUCLEUS COLLISIONS ABOVE 4 GEV/AMU 184
- TW ATWATER,PS FREIER,MP KERTZMAN
- HE 1.4-11 INCLUSIVE ANGULAR DISTRIBUTION OF SIGMA AND LI FRAGMENTS PRODUCED IN THE FE-C AND FE-PB COLLISIONS AT 1.88 GEV/U 188
- CO KIM,SN KIM,IK CHAE,DH KIM
- HE 1.4-12 EXPERIMENT "PAMIR"-III. COPLANAR EMISSION OF HIGH ENERGY GAMMA-QUANTA AT INTERACTION OF HADRONS WITH NUCLEI OF AIR ATOMS AT ENERGIES ABOVE 10**17 GEV 192

PAMIR COLLABORATION

HE 1.4-13 THE EFFECT OF THE RELATIVE NUCLEAR SIZE
ON THE NUCLEUS-NUCLEUS INTERACTIONS

196

IN EROFEEVA, VS MURZIN, SYU SIVOKLOKOV
LN SMIRNOVA

HE 3.1
GAMMA-RAY AND HADRON SPECTRA

PAPER CODE		PAGE
HE 3.1-1	JAPAN-USSR JOINT EMULSION CHAMBER EXPERIMENT AT PAMIR AS BORISOV, KV CHERDYNTSEVA, ZM GUSEVA VG DENISOVA, AM DUNAEVSKY, EA KANEVSKAYA VM MAXIMENKO, RA NAM, SV PASHKOV VS PUCHKOV, SA SLAVATINSKY, MD SMIRNOVA YA SMORODIN, NG ZELEVINSKAYA, MV ZIMIN GB ZHDANOV, RA MUKHAMEDSHIN, OE NEDEL'KO LP NIKOLAEV, GT ZATSEPIN, TP AMINEVA LT BARADZEI, IF IVANENKO, NP ILIJINA TV LAZAREVA, AK MANAGADZE, IA MIKHAILOVA EA MURZINA, EI POMELOVA, EG POPOVA	200
HE 3.1-2	INTENSITIES OF HIGH-ENERGY COSMIC RAYS AT MT. KANBALA CHINA-JAPAN COLLABORATION, K MIZUTANI	204
HE 3.1-3	HIGH ENERGY GAMMA-RAYS AND HADRONS AT MT. FUJI M AMENOMORI, H NANJO, E KONISHI, N HOTTA K MIZUTANI, K KASAHARA, T KOBAYASHI E MIKUMO, K SATO, T YUDA, I MITO, M SHIBATA T SHIRAI, T TAIRA, N TATEYAMA, S TORII H SUGIMOTO, K TAIRA	208
HE 3.1-6	ON THE CHARACTERISTICS OF EMULSION CHAMBER FAMILY EVENTS PRODUCED IN LOW HEIGHTS G JING, C JING, Q ZHU, L DING	212
HE 3.1-7	HADRON INTENSITY SPECTRUM AT 4380 M ABOVE LEVEL SD CANANOV, EKH CHADRANYAN LA KHIZANISHVILI, DM KOTLYAREVSKI NN ROINISHVILI	216
HE 3.1-8	SOME CHARACTERISTIC COSMIC RAY EVENTS AND AN ATTEMPT AT THEIR EXPLANATION S BHATTACHARYYA	220

XX
VOLUME 6

- HE 3.1-9 THE NUCLEON INTENSITY IN THE ATMOSPHERE AND THE P**T DISTRIBUTION 224
A LILAND
- HE 3.1-10 ENERGY SPECTRA OF PROTON AND NUCLEI OF PRIMARY COSMIC RAYS IN ENERGY REGION > 10 TEV/PARTICLE 228
KV MANDRITSKAYA, GP SAZHINA
NV SOKOLSKAYA, AYA VARKOVITSKAYA
EA ZAMCHALOVA, VI ZATSEPIN
- HE 3.1-11 SCALING VIOLATION IN FRAGMENTATION REGION AT ENERGIES ABOVE 10^{*15} BASED ON THE DATA ON COSMIC RAY HADRON COMPONENT 232
PAMIR COLLABORATION
- HE 3.1-12 CONNECTION BETWEEN VARIATIONS OF THE ATMOSPHERE TEMPERATURE PROFILE AND VARIATIONS OF THE MESON COMPONENT INTENSITY 236
YAL BLOKH, YL BLOCH
- HE 3.1-13 HIGH SENSITIVE X-RAY FILMS TO DETECT ELECTRON SHOWERS IN 100 GEV REGION 239
T TAIRA, T SHIRAI, N TATEYAMA, S TORII
J NISHIMURA, M FUJII, A YOSHIDA, H AIZU
Y NOMURA, M KAZUNO, T KOBAYSHI, A NISHIO

HE 3.2
C-JETS

PAPER CODE		PAGE
HE 3.2-1	JETS IN AIR-JET FAMILY AC FAUTH,K SAWAYANAGI	243
HE 3.2-5	SEARCH FOR ANOMALOUS C-JETS IN CHACALTAYA EMULSION CHAMBER EXPERIMENT H KUMANO	246
HE 3.2-6	EXOTIC INTERACTIONS AMONG C-JETS AND PB-JETS BRAZIL-JAPAN	250
HE 3.2-7	X-RAY FILM CHAMBER WITH CARBON TARGET OF TIEN-SHAN COMPLEX ARRAY KV CHERDYNTSEVA,AP CHUBENKO,AG DUBOVY NP KRUTIKOVA,NM NESTEROVA,SI NIKOLSKY NM NIKOLSKAJA,EI TUKISH,NG VILDANOV TI YAKOVLEVA	254
HE 3.2-8	SCALING VIOLATION IN HADRON-NUCLEUS INTERACTION YG VERBETSKI,YG VERBETTSKI LP GARSEVANISHVILI,DM KOTLYAREVSKI MV MELKU,NG TATALASHVILI,NI SHERER YUM SHABEL'SKI,GZ STEMANETYAN	258
HE 3.2-9	FEW-PARTICLES GENERATION CHANNELS IN INELASTIC HADRON-NUCLEAR INTERACTIONS AT ENERGY ~ 400 GEV NG TATALASHVILI	262
HE 3.2-10	THE MODEL OF INDEPENDENT PARTICLES EMISSION IN THE MULTIPARTICLE PRODUCTION THEORY VV UCHAIKIN,VA LITVINOV	266

HE 3.2-11 THE MULTIPLICITY AND THE SPECTRA OF
SECONDARIES CORRELATED WITH THE LEADING
PARTICLE ENERGY

270

NA KRUGLOV, AS PROSKURYAKOV, LI SARYCHEVA
LN SMIRNOVA

xxiii
VOLUME 6

HE 3.3
A-JETS

PAPER CODE		PAGE
HE 3.3-1	CHARACTERISTICS OF ANOMALOUSLY HIGH MULTIPLICITY COSMIC RAY INTERACTIONS IYA CHASNIKOV, YUA EREMENKO DT MADIGOZHIN, TKH SADYKOV, VG VOINOV	274
HE 3.3-2	TRANSVERSE MOMENTUM DISTRIBUTION OF PI DEGREES IN THE FRAGMENTATION REGION OF SUPER HIGH ENERGY INTERACTIONS JR REN, HH KUANG, AX HUO, SL LU, S SU YX WANG, CR WANG, M HE, NJ ZHANG, PY CAO JY LI, SZ WANG, GZ BAI, ZH LIU, GJ LI QX GENG, WD ZHOU, RD HE	278
HE 3.3-4	STUDY OF HADRON BUNDLES OBSERVED IN CHACALTAYA TWO-STORY EMULSION CHAMBER H AOKI	280
HE 3.3-5	PENETRATIVE NATURE OF HIGH ENERGY SHOWERS OBSERVED IN CHACALTAYA EMULSION CHAMBER Y FUNAYAMA, M TAMADA	284
HE 3.3-6	ANOMALOUS CORRELATION BETWEEN HADRON AND ELECTROMAGNETIC PARTICLES IN HADRON AND GAMMA RAY FAMILIES M TAMADA	288
HE 3.3-7	ATMOSPHERIC INTERACTIONS DETECTED IN BOTH THE UPPER AND THE LOWER CHAMBERS AT CHACALTAYA NM AMATO, N ARATA, RHC MALDONADO	292
HE 3.3-8	LATERAL DISTRIBUTION OF HIGH ENERGY HADRONS AND GAMMA RAYS IN AIR SHOWER CORES OBSERVED WITH EMULSION CHAMBERS T MATANO, M MACHIDA, N KAWASUMI I TSUSHIMA, K HONDA, K HASHIMOTO, CE NAVIA NJ MARTINIC, C AGUIRRE	296

- HE 3.3-9 SIZE DISTRIBUTIONS OF AIR SHOWERS 300
ACCOMPANIED WITH HIGH ENERGY GAMMA-RAY
BUNDLES OBSERVED AT MT. CHACALTAYA
- T MATANO, M MACHIDA, I TSUSHIMA
N KAWASUMI, K HONDA, K HASHIMOTO
NJ MARTINIC, J ZAPATA, CE NAVIA, C AGUIRRE
L SILES, R MAGNANI
- HE 3.3-10 EAS ACCOMPANIED BY GAMMA-FAMILIES AT MT. 301
NORIKURA AND COMPARISON WITH MONTE CARLO
SIMULATIONS
- M SHIMA, T SAITO, M SAKATA, Y YAMAMOTO
K KASAHARA, T YUDA, S TORII, N HOTTA
- HE 3.3-11 COMPARISON OF ABSOLUTE INTENSITY BETWEEN 305
EAS WITH GAMMA-FAMILIES AND GENERAL EAS
AT MT. NORIKURA
- T MITSUMUNE, T NAKATSUKA, K NISHIKAWA
T SAITO, M SAKATA, M SHIMA, Y YAMAMOTO
S DAKE, M KAWAMOTO, M KUSUNOSE, N OHMORI
H SASAKI, N HOTTA

xxv
VOLUME 6

HE 3.4
SUPER FAMILIES I

PAPER CODE		PAGE
HE 3.4-1	A COSMIC RAY SUPER HIGH ENERGY MULTICORE FAMILY EVENT EXPERIMENT AND GENERAL FEATURES	309
	CHINA-JAPAN COLLABORATION	
HE 3.4-2	A COSMIC RAY SUPER HIGH MULTICORE FAMILY EVENT (II) PRODUCTION AND FRAGMENTATION CHARACTERISTICS OF THE JETS	313
	CHINA-JAPAN COLLABORATION	
HE 3.4-3	OBSERVATION OF SUPER HIGH ENERGY BIG FAMILY WITH LARGE SCALE EMULSION CHAMBERS	317
	CHINA-JAPAN COLLABORATION	
HE 3.4-5	A HALO EVENT CREATED AT 200 M ABOVE THE CHACALTAYA EMULSION CHAMBER	320
	NM AMATO, N ARATA, RHC MALDONADO	
HE 3.4-6	A BINOCULAR TYPE ATMOSPHERIC INTERACTION GENERATING SEQUENTIAL EXOTIC FEATURES	324
	NM AMATO, N ARATA, RHC MALDONADO	
HE 3.4-7	GAMMA-HADRON FAMILIES AND SCALING VIOLATION	328
	TK GAISSER, T STANEV, JA WROTONIAK	
HE 3.4-8	SUPER-FAMILY P2 C-96-125 OBSERVED BY JAPAN-USSR JOINT EMULSION CHAMBER EXPERIMENT	332
	EH SHIBUYA	

- HE 3.4-9 ON THE HALO EVENTS OBSERVED BY MT. FUJI 336
AND MT. KANBALA EMULSION CHAMBER
EXPERIMENTS

JR REN, HH KUANG, AX HUO, SL LU, S SU
YX WANG, YG XUE, CR WANG, M HE, NJ ZHANG
PY CAO, JY LI, SZ WANG, GZ BAI, ZH LIU, GJ LI
QX GENG, WD ZHOU, RD HE, M AMENOMORI
H NANJO, N HOTTA, I OHTA, K MIZUTANI
K KASAHARA, T YUDA, I MITO, M SHIBATA
T SHIRAI, N TATEYAMA

- HE 3.4-10 EXPERIMENT "PAMIR"-II: "FIANIT"-A 340
GIGANTIC SUPER-FAMILY WITH HALO (E SUB
O[~]10**17 EV)

PAMIR COLLABORATION

- HE 3.4-11 EXPERIMENT "PAMIR"-IV. ANALYSIS OF 344
ELECTROMAGNETIC HALO SUPERFAMILY
DETECTED IN DEEP XEC

PAMIR COLLABORATION

HE 3.5
SUPER FAMILIES II

PAPER CODE		PAGE
HE 3.5-1	PARTICLE INTERACTIONS AT ENERGIES OVER 1000 TEV INFERRED FROM GAMMA-FAMILIES OBSERVED AT MT FUJI M AMENOMORI, H NANJO, E KONISHI, N HOTTA K MIZUTANI, K KASAHARA, T KOBAYASHI E MIKUMO, K SATO, T YUDA, I MITO, M SHIBATA T SHIRAI, T TAIRA, N TATEYAMA, S TORII H SUGIMOTO, K TAIRA	348
HE 3.5-2	A SEARCH FOR MINI-CLUSTERS IN JAPAN-USSR JOINT CHAMBER AT PAMIR JAPAN-USSR	352
HE 3.5-3	MINI-CLUSTERS JA CHINELLATO, C DOBRIGKEIT, J BELLANDI CMG LATTES, MJ MENON, CE NAVIA, DA PAMILAJU K SAWAYANAGI, EH SHIBUYA, A TURTELLI NM AMATO, N ARATA, FM OLIVERIRA CASTRO RHC MALDONADO, H AOKI, Y FUJIMOTO Y FUNAYAMA, S HASEGAWA, H KUMANO, H SEMBA M TAMADA, S YAMASHITA, T SHIBATA, K YOKOI A OHSAWA	356
HE 3.5-4	GIANT MINI-CLUSTERS AS A POSSIBLE ORIGIN OF "HALO" PHENOMENA OBSERVED IN SUPER FAMILIES BRASIL-JAPAN	360
HE 3.5-7	STRUCTURE OF SUPER-FAMILIES S YAMASHITA, A OHSAWA, JA CHINELLATO	364
HE 3.5-8	EXTREMELY HIGH ENERGY HADRON AND GAMMA RAY FAMILIES (III) S YAMASHITA, A OHSAWA, JA CHINELLATO EH SHIBUYA	368

HE 3.5-9	NUMERICAL ANALYSIS OF ELECTROMAGNETIC CASCADES IN EMULSION CHAMBERS	372
	AV FLYASHESHNIKOV, KV VOROBYEV	
HE 3.5-10	AN EXPERIMENTAL STUDY OF CORRELATIONS IN THE DEVELOPMENT OF THE ELECTRON-PHOTON CASCADES	376
	YUP KRATENKO, SA CHARISHNIKOV	
HE 3.5-11	THE ELECTROMAGNETIC COMPONENT OF ALBEDO FROM SUPERHIGH ENERGY CASCADES IN DENSE MEDIA	380
	RM GOLYNSKAYA, LA HEIN, AV PLYASHESHNIKOV KV VOROBYEV	
HE 3.5-12	INTEGRAL FUNCTIONS OF ELECTRON LATERAL DISTRIBUTION AND THEIR FLUCUATIONS IN ELECTRON-PHOTON CASCADES	384
	IP IVANENKO, BL KANEVSKY, AA KIRILLOV IA LINDE, YG LYUTOV	
HE 3.5-13	ANALYTICO-NUMERICAL METHODS OF CALCULATIONS OF ENERGY AND THREE-DIMENSIONAL PARTICLE DISTRIBUTIONS IN ELECTROMAGNETIC CASCADES	388
	IP IVANENKO, BL KANEVSKY, TM ROGANOVA VV SIZOV, SV TRIPHONOVA	

HE 3.6
EMULSION CHAMBER SIMULATIONS

PAPER CODE		PAGE
HE 3.6-2	MULTIDIMENSIONAL ANALYSIS OF DATA OBTAINED IN EXPERIMENTS WITH X-RAY CHAMBERS AND EXTENSIVE AIR SHOWERS AA CHILINGARYAN,SK GALFAYAN,MZ ZAZYAN AM DUNAEVSKII	392
HE 3.6-3	A NEW METHOD OF DIFFERENTIAL STRUCTURAL ANALYSIS OF GAMMA-FAMILY BASIC PARAMETERS LG MELKUMIAN,SV TER-ANTONIAN YUA SMORODIN	396
HE 3.6-4	LPM EFFECT AND PRIMARY ENERGY ESTIMATIONS MF BOURDEAU,JN CAPDEVIELLE	400
HE 3.6-6	EXPERIMENTAL BASIS FOR THE MODELS OF CASCADE PROPAGATION IN ATMOSPHERE Z STRUGALSKI	404
HE 3.6-7	RELATION BETWEEN GAMMA-RAY FAMILY AND EAS CORE - MONTE-CARLO SIMULATION OF EAS CORE - T YANAGITA	407
HE 3.6-8	COMPARISION OF BIG EVENT WITH CALCULATIONS OF THE AIR SHOWER DEVELOPMENT M NIWA,A MISAKI,T MATANO,K HONDA I TSUSHIMA,N KAWASUMI,K HASHIMOTO	411
HE 3.6-10	THE LATERAL DISTRIBUTION OF CHARGED PARTICLES OF ENERGY GREATER THEN 0.3 E CRIT IN ELECTRON-PROTON CASCADES IN LEAD AND AIR A WASILEWSKI,E KRYS	412

HE 3.6-11 RESULTS OF MONTE-CARLO SIMULATIONS OF 416
ELECTRON-PHOTON CASCADES IN LEAD AND
LAYERS OF LEAD-SCINTILLATOR

A WASILEWSKI, E KRYS

HE 3.6-12 ON THE 'MINI-CLUSTER' OBSERVED BY THE 420
CHACALTAYA EMULSION CHAMBER EXPERIMENT

T TATI

HE 3.7
EMULSION CHAMBER RESULTS

PAPER CODE		PAGE
HE 3.7-1	A COMPARATIVE ANALYSIS OF GAMMA AND HADRON FAMILIES AT THE SUPERHIGH ENERGIES RECORDED IN EXPERIMENT "PAMIR" SA AZIMOV,EJ MULLADJANOV,AN NOSOV H NURITDINOV,DA TALIPOV,DA HALILOV TS YULDASHBAEV	424
HE 3.7-2	STUDY OF GAMMA-FAMILIES GENERATED IN NUCLON-NUCLEUS (NA) AND PION-NUCLEUS (PI A) INTERACTIONS SA AZIMOV,EJ MULLAJANOV,H NURITDINOV TS YULDASHBAEV	428
HE 3.7-3	HADRONS REGISTRATION IN EMULSION CHAMBER WITH CARBON BLOCK A TOMASZEWSKI,Z WLODARCZYK	431
HE 3.7-4	NEW ANALYSIS OF NUCLEAR INTERACTION OBSERVED BY MT. KANBARA EMULSION CHAMBER EXPERIMENT H NANJO	435
HE 3.7-5	ON THE MEAN CHARACTERISTICS OF FAMILY EVENTS OBSERVED AT MT. KANBALA CHINA-JAPAN COLLABORATION	439
HE 3.7-7	STRUCTURED EVENTS IN "PAMIR" CARBON X-RAY CHAMBERS GG LEPTUKH	443
HE 3.7-9	ULTRA HIGH ENERGY EVENTS IN ECHOS SERIES AND PRIMARY ENERGY SPECTRUM JN CAPDEVIELLE,J IWAI,T OGATA	447

HE 3.7-10 PECULIARITIES OF GAMMA-RAY DISTRIBUTION
AT 20 TEV ENERGY

451

PM ERMAKOV, AA LOKTIONOV, YUT LUKIN
TKH SADYKOV

PROTON-AIR AND PROTON-PROTON CROSS SECTIONS FROM AIR SHOWER DATA

John Linsley
 Department of Physics and Astronomy
 University of New Mexico, Albuquerque, NM 87131
 USA

ABSTRACT

Data on the fluctuations in depth of maximum development of cosmic ray air showers, corrected for the effects of mixed primary composition and shower development fluctuations, yield values of the inelastic proton-air cross section for laboratory energies in the range 10^8 - 10^{10} GeV. From these values of σ_{pa} , corresponding values of the proton-proton total cross section are derived by means of Glauber theory and geometrical scaling. The resulting values of σ_{pp} are inconsistent with a well known \ln^2 's extrapolation of ISR data which is consistent with SPS data; they indicate a less rapid rate of increase in the interval $540 < \sqrt{s} < 10^5$ GeV.

1. Introduction. The total inelastic proton-air cross section σ_{pa} , which is interesting in relation to the theory of hadron-hadron and hadron-nucleus interactions, can be derived from data on cosmic ray air showers. Cosmic ray evidence of an increase with increasing energy in σ_{pp} , the total proton-proton cross section, has been confirmed, first at ISR energies and more recently with the CERN SPS collider.¹⁻⁴ In the interval $10 < \sqrt{s} < 540$ GeV the increase, amounting to some 75%, agrees well with a \ln^2 's dependence but is compatible with a slower rate.³ A recent cosmic ray result for $2 \cdot 10^3 < \sqrt{s} < 2 \cdot 10^4$ GeV favors \ln^2 's,⁵ while another result of this kind, for $\sqrt{s} = 3 \cdot 10^4$ GeV, favors a slower increase.⁶ In case of the cosmic ray results, σ_{pp} is derived from σ_{pa} using Glauber theory.

My purpose here is to draw attention to another body of air shower evidence extending to even higher energies ($10^4 < \sqrt{s} < 1.6 \cdot 10^5$ GeV) which also bears on this question.¹⁹ The evidence consists in part of data on the fluctuation of shower elongation x_m , and in part of data on the primary composition. These are combined using an expression for $\{x_m\}$ as a function of $\langle \ln A \rangle$, $\{\ln A\}$ and $\{x_{m,p}\}$, where A is the primary mass number, $\langle \ln A \rangle$, $\{\ln A\}$ are the mean value and dispersion about the mean of $\ln A$ for fixed primary energy, $\{x_{m,p}\}$ is the dispersion of x_m for proton-initiated showers of a fixed energy (allowing for fluctuations in shower origin and development), and $\{x_m\}$ is the observed dispersion of x_m , corrected for reception fluctuations (instrumental dispersion).⁷ Using experimental evidence on $\langle \ln A \rangle$ and $\{\ln A\}$ from other air shower observations, the correction for contamination of the primary beam with heavy nuclei is shown to be small: $\{x_{m,p}\} \cong \{x_m\}$. Cascade simulations have shown that $\{x_{m,p}\}$ is proportional to λ_{pa} , the proton-air mean free path, with a proportionality constant equal to 1.4. From λ_{pa} one obtains σ_{pa} ; σ_{pp} follows by application of Glauber theory.

2. Primary Composition Effect. I have shown elsewhere that if y is an observable such as x_m , whose mean value for proton showers can be graphed vs $\ln E$ as a straight line (over reasonably wide intervals, say 2 decades or more), and if the line width (fluctuation of y) for showers initiated

by various nuclei is approximated by $\{y(A)\} = \{y(1)\}(1 - k \ln A)$, where k is constant, then

$$\{y\}^2 = \{y(1)\}^2 [1 - 2k \langle \ln A \rangle + k^2 (\langle \ln A \rangle^2 + \{\ln A\}^2)] + b^2 \{\ln A\}^2, \quad (1)$$

where b is the slope of the straight-line graph.⁷ This follows from elementary statistical theory and the superposition principle of Peters. For $y = x_m$, b is just $D_{e,p}$, the proton shower elongation rate. With these substitutions I solve (1) for $\{x_{m,p}\}$, obtaining

$$\{x_{m,p}\} = \{x_m\} \left(\frac{1 - (D_{e,p} \{\ln A\} / \{x_m\})^2}{1 - 2k \langle \ln A \rangle + k^2 (\langle \ln A \rangle^2 + \{\ln A\}^2)} \right)^{\frac{1}{2}}. \quad (2)$$

The right hand side of (2) contains, besides the observed quantity requiring correction, 2 parameters which describe phenomenologically the relevant features of air showers ($D_{e,p}$ and k), and 2 parameters which describe the composition of the incoming cosmic ray beam ($\langle \ln A \rangle$ and $\{\ln A\}$).

The fluctuation of x_m has been studied experimentally for more than 10 years using the giant air shower array at Haverah Park,^{8,9} and almost as long using a similar size array at Yakutsk.¹⁰ It has been measured independently at Dugway using an array of atmospheric Cerenkov light detectors,¹¹ and at Akeno using data on the electron lateral distribution.¹² Results are given in Table 1.

I have shown elsewhere that under a wide range of assumptions about hadron-nucleus interactions $D_{e,p}$ cannot be appreciably greater than t_0 , the radiation length. This insures that the numerator in (2) is approximately 1, so the exact value of $D_{e,p}$ is unimportant. For energy independent composition, $D_{e,p} = D_e$ (observed elongation rate). I adopt $D_{e,p} = 28 \text{ g/cm}^2$, practically the experimental value of D_e at these energies.¹⁴ As for the parameter k , Monte Carlo cascade simulations show that its value lies in the range $0.15 \pm .05$, depending on the choice of model.^{11,15} The exact value is unimportant if $\langle \ln A \rangle$ is less than 1.

Data on $\langle \ln A \rangle$ and $\{\ln A\}$ at very high energies are summarized in Ref. 7 (see also conference paper OG5.4-4). They can be combined, as in Fig. 1, by plotting $\{\ln A\}$ vs $\langle \ln A \rangle$ in rectangular coordinates. Note that for any pure composition $\{\ln A\} = 0$. It is assumed that the possibilities range from $\langle \ln A \rangle = 0$ (pure protons) to $\langle \ln A \rangle = 4$ (pure Fe). The maximum dispersion for a given mean occurs for a mixture of protons and Fe nuclei. When the scales are chosen as I have done the locus of binary proton-Fe mixtures is a semicircle. The lower boundary of the diagram consists of smaller semicircles corresponding to other binary mixtures. The region inside the boundary represents all possible compositions. The observed equal-energy composition in the low energy region (10^2 - 10^5 GeV) is indicated by the heavy dashed line. The compositions experimentally allowed at very high energies ($E > 10^8$ GeV) are those within the shaded region. The heavy dotted line

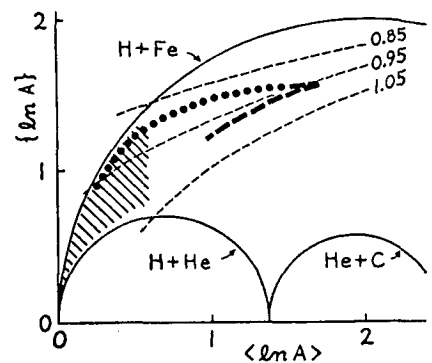


Fig. 1. Cosmic ray composition diagram: 2nd vs 1st moment of the $\ln A$ distribution, explained in the accompanying text.

Table 1. Summary of $\{x_m\}$ data

$\log E_{\text{lab}}$ (GeV)	$\{x_m\}$ g/cm ²	No. of events	Ref.
7.58	89 ± 15	?	12
7.82	90 ± 18	?	12
8.06	86 ± 19	?	12
8.24	80 ± 11	147	11
8.30	70 ± 13	?	12
8.30	69 ± 14	426	8
8.56	62 ± 9	1014	8
8.68	71 ± 6	519	9
8.78	73 ± 10	a	10
8.83	51 ± 7	652	8
8.88	79 ± 4	300	10
9.11	68 ± 10	334	8
9.15	69 ± 6	a	10
9.43	65 ± 11	a	10
9.45	74 ± 11	178	8
9.60	63 ± 5	201	10
10.00	54 ± 11	87	8
10.15	55 ± 13	a	10

^a total of 464 events

where K is a constant. On the basis of Monte Carlo cascade simulations by Walker and Watson⁸ I adopt the value 1.40 for this constant. The resulting values for σ_{pa} are given in Figure 2.

There is of course some uncertainty in the value of K , due mainly to uncertainty about the elasticity of very high energy hadron-air collisions, denoted here by η . The result $K = 1.4$ rests on a conventional assumption that η is distributed uniformly between 0 and 1 with a mean value of 0.5. It has been pointed out by L.W. Jones that according to accelerator data the value of $\langle \eta \rangle$ for proton collisions with light nuclei is appreciably less, about 0.3.¹⁶ The dependence of K on $\langle \eta \rangle$ can be estimated by assuming 1) that x_{av} of the partial electronic cascade originating from each collision of the leading nucleus is perfectly correlated with the depth of that collision, and 2) that $\{x_{m,p}\} = \{x_{av,p}\}$ (neglecting fluctuations in η). It is then easily shown that

$$K \cong \left[\sum_{j=1}^{\infty} j(1-\eta)\eta^{j-1} \right]^{\frac{1}{2}} = (1-\eta)^{-\frac{1}{2}}. \quad (3)$$

For $\eta = 0.5$ one obtains $K \cong 1.41$; for $\eta = 0.3$ the result is $K \cong 1.20$. Thus the effect of assuming a smaller value of $\langle \eta \rangle$ is to reduce the apparent cross sections σ_{pa} and σ_{pp} at air shower energies.

represents a detailed model given in Ref. 7, which describes in a plausible manner the high energy region and the transition from lower energies. The correction factors $\{x_{m,p}\}/\{x_m\}$ for this model to be used with Table 1 according to (2) range in value from 0.91 to 0.95; thus they differ only slightly from 1 (no correction). These corrections have been applied in obtaining the present results, shown in Figures 2 and 3.

Also shown in Fig. 1 are contour lines corresponding to a typical value of $\{x_m\}$ ($= 66 \text{ g/cm}^2$) and the indicated values of the correction factor. By examining these contours one sees that correction factors for any other allowed model will differ only slightly from those used here.

3. Development Fluctuations. The next step is to convert from $\{x_{m,p}\}$ to σ_{pa} allowing for shower development fluctuations. These arise primarily because of the leading particle effect. Thus one expects them to scale as λ_{pa} , so there will be a proportionality: $\{x_{m,p}\} = K\lambda_{pa}$

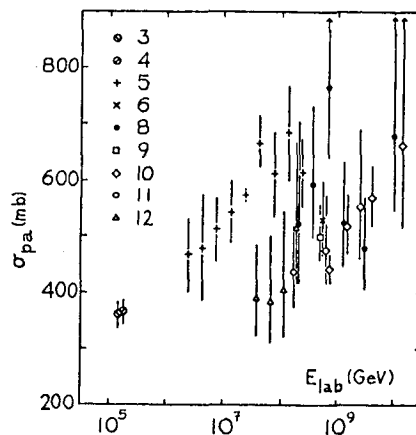


Fig. 2. Results on σ_{pa} . The numbers listed with the symbols are the corresponding references.

4. Results. Examining Fig. 2 one notes good agreement between the present results and one published recently by the Fly's Eye group.⁶ The Fly's Eye result is derived from the decrement of the x_m distribution, rather than the dispersion, using a proportionality between Λ_{xm} and λ_{pa} . The value of the constant is taken as $1.6 \pm 10\%$ from simulations¹⁵ similar to those of Walker and Watson. The present results disagree with those of Ref. 5, based on the zenith angle distribution of generally smaller air showers for fixed N_e and N_μ . Here also the relation between a measured attenuation length and λ_{pa} is found by means of simulations. There is an approximate proportionality, the value of the constant being 1.45-1.55. The value of $\langle \eta \rangle$ for the Akeno model is 0.44. A smaller value would result in a smaller value of the proportionality constant and a smaller apparent rise in cross sections. However it would not remove the discrepancy since a change in $\langle \eta \rangle$ will have a similar effect on results from Λ_{xm} and $\{x_m\}$.

Fig. 3 shows the result of converting the new σ_{pa} values to σ_{pp} . This has been done the same way as in Ref. 6, using Glauber theory with an assumption that the nuclear slope parameter has the same energy dependence as σ_{pp} (geometrical scaling). In parametric form, the relation assumed is $\sigma_{pa} = 24.0 \sigma_{pp}^{0.648}$ (cross sections in mb). Shown for comparison are the SPS results,^{3,4} and well known extrapolations by Block and Cahn, based on ISR data, which successfully predicted those results.¹⁷ Also shown is a recent prediction by Bourrely *et al.*, for the so-called impact picture.¹⁸ The lower Block-Cahn curve is the best fit with $a \neq 0$, where parameter a takes on small positive values to allow for deviations from Froissart bound form. The upper curve is for $a = 0$.

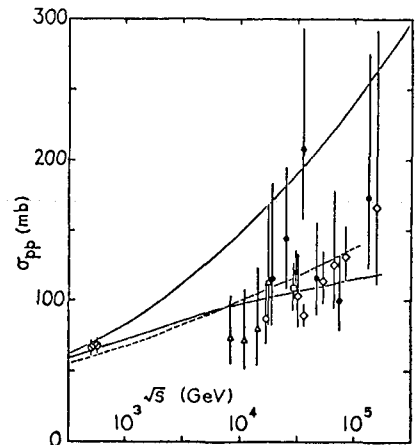


Fig. 3. Results on σ_{pp} (same symbols as Fig. 2). The lower solid curve, from Ref. 17, is a best fit to ISR data allowing deviation from the Froissart bound. The upper solid curve (same Ref.) is a best fit with Froissart bound form. The dashed curve is for the 'impact picture'.¹⁸

References. ¹YODH *et al.* 1972, Phys. Rev. Lett. 28, 1005; ²AMALDI *et al.* 1977, Phys. Lett. 66B, 390; ³BATTISTON *et al.* 1982, Phys. Lett. 117B, 126; ⁴ARNISON *et al.* 1983, Phys. Lett. 128B, 336; ⁵HARA *et al.* 1983, Phys. Rev. Lett. 50, 2058 and Proc. 18th ICRC 11, 354; ⁶BALTRUSAITIS *et al.* 1984, Phys. Rev. Lett. 52, 1380; ⁷LINSLEY 1983, Proc. 18th ICRC 12, 135; ⁸WALKER and WATSON 1982, J. Phys. G: Nucl. Phys. 8, 1131 (also 1983, Proc. 18th ICRC 6, 114); ⁹COY *et al.* 1981, Proc. 17th ICRC 6, 43; ¹⁰DYAKONOV *et al.* 1981, Proc. 17th ICRC 6, 110 and Proc. 18th ICRC 6, 111; ¹¹CHANTLER *et al.* 1982, J. Phys. G: Nucl. Phys. 8, L51; ¹²HARA *et al.* 1983, Proc. 18th ICRC 11, 272; ¹³LINSLEY and WATSON 1981, Phys. Rev. Lett. 46, 459 and references therein; ¹⁴WALKER and WATSON 1981, J. Phys. G: Nucl. Phys. 7, 1297 (see also Ref. 13); ¹⁵ELLSWORTH *et al.* 1982, Phys. Rev. D 26, 336; ¹⁶JONES 1983, Proc. 18th ICRC 5, 17; ¹⁷BLOCK and CAHN 1983, Phys. Lett. 120B, 224 and in Proc. 18th Rencontre de Moriond, Vol. 3; ¹⁸BOURRELY *et al.* 1985, Phys. Rev. Lett. 54, 757; ¹⁹see also LINSLEY 1985, Lett. Nuovo Cimento 42, 403.

PROTON-AIR INELASTIC CROSS SECTION AT $S^{1/2} = 30$ TeV

Baltrusaitis, R.M., Cassidy, G.L., Cooper, R., Elbert, J.W., Gerhardy, P.R., Ko, S., Loh, E.C., Mizumoto, Y., Sokolsky, P. & Steck, D.

Department of Physics, University of Utah, Salt Lake City, UT 84112

ABSTRACT

We have measured the distribution of the maxima of high energy cosmic ray induced extensive air showers in the atmosphere as a function of atmospheric depth. From the exponential tail of this distribution, we determined the p-air inelastic cross section at 30 TeV center-of-mass energy to be 540 ± 40 mb.

1. Introduction. The technique of extracting the p-air cross section from the data obtained by the "Fly's Eye" detector has been described in detail in an earlier paper.(1) We report the results of a recent analysis from data accumulated through the month of April 1985.

2. Discussion. The "Fly's Eye" detector consists of 67 F/1 mirrors, each with 12 or 14 photomultiplier tubes mounted at the focus.(2) These mirrors are arranged so that they cover all but a small portion of the solid angle near the horizon. The detector records the passage of distant extensive air showers by means of the light produced by the shower particles which, depending on the relative geometry between the track and the detector, is usually an admixture of Cerenkov and fluorescent light. The shower direction is reconstructed from the timing information obtained by the photomultiplier tubes. Knowing the reconstructed geometry and the fluorescence efficiency and taking into account the Cerenkov intensity, we calculate the number of particles of each shower as it progresses through the atmosphere. Figure 1 shows the number of particles in a shower as a function of atmospheric depth.

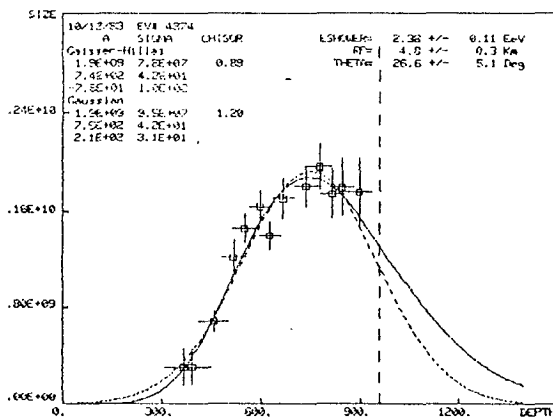


Figure 1. An Extensive Air Shower That Survives All Data Cuts. The solid curve is a GH. shower curve. The dotted curve is a Gaussian distribution.

The shower maximum is obtained by fitting a distribution to the shower profile. We ascertained that the shape of the shower profile can be fitted with either a Gaisser-Hillas (G-H)(3) distribution or a Gaussian distribution. Both distributions yield equally good fits, with the G-H fit consistently giving a slightly lower value (30 g cm^{-2}) to the depth of maxima. Such consistent difference does not affect the over-all shapes of the final data distributions obtained from the two fits.

The error in shower maximum, for showers whose

closest distance of approach of exceed one and one half kilometers, arises almost entirely from the uncertainty in the reconstructed polar angle. Showers with zenith angle larger than sixty degrees are excluded in this analysis to avoid bias toward large depths of maxima due to the exponential behavior of the atmospheric density.

Possible track reconstruction bias has been examined by using light beams generated by a roving light pulser, and a fixed position nitrogen pulse laser. Tracks reconstructed from such light pulses show that, regardless of the angle of the light beams, we can measure the polar angle to the order of one degree with a sigma of about 1.7 degrees. Figure 2 shows the result of one of the runs obtained

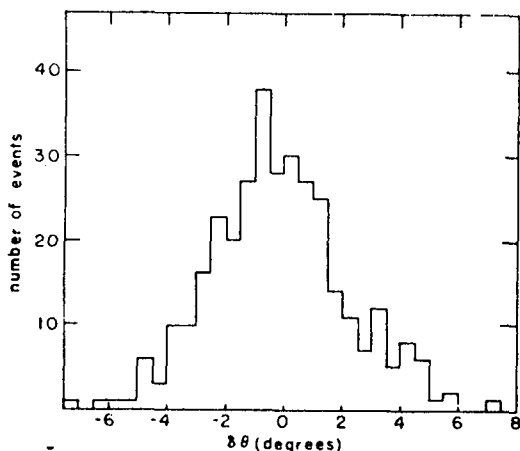


Figure 2. Distribution of differences between known and fitted zenith angles for "upward-going" showers of known geometry generated by a high intensity light flasher. The width of the distribution is $\sigma=1.7^\circ$.

with the roving flasher. Further checks are made with events that are visible from a partially built second detector located about 3.5 kilometers from the "Fly's Eye". In this case, the polar angle is determined from the intersection of the two planes which contain the track. Again, the zenith angles obtained with the coincidence events are in agreement within experimental uncertainties with the angles calculated with the timing information from one eye alone. Figure 3 shows the agreement between the two methods of calculating the zenith angle.

Bias toward large depths of maxima could result from distant showers of very high

energy. Such bias is removed by accepting showers of a narrow band of energy between 10^{17} eV and 2×10^{18} eV. Finally, events with shower maximum uncertainty less than 100 g cm^{-2} are accepted for analysis with the average uncertainty of the order of 70 g cm^{-2} .

3. Results and Conclusions. The resulting distribution of the shower maxima as a function of the atmospheric depth is shown in Figure 4. The effect of the finite resolution of $\delta=70 \text{ g cm}^{-2}$ does not effect the shape of the exponent behavior of the tail of the distribution beyond a distance of δ^2/λ where λ is the slope of the tail of the distribution.

A fit of the data based on events beyond a depth of $\sim 760 \text{ g cm}^{-2}$ is found to be $=70 \pm 6 \text{ g cm}^{-2}$.

From a paper by Sokolsky et al(4) submitted to this conference, it seems likely that the primary particles consist of a considerable amount of light particles, i.e., protons. According to

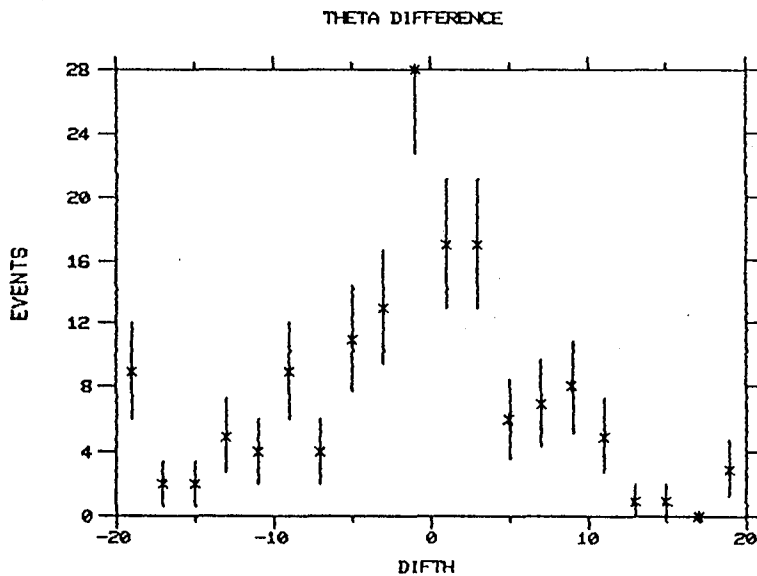


Figure 3. Difference in Zenith Angle for Events Observed by Both Detectors and With One Detector Alone. The average angular length for the track is about 40° .

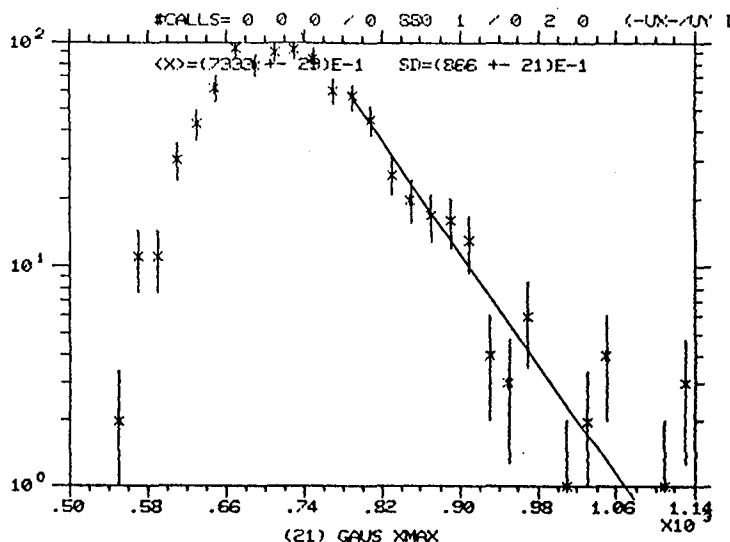


Figure 4. Distribution of Depth of Shower Maxima for Data Whose Fitting Errors Are Less Than $8,100 \text{ g cm}^{-2}$. The slope of the exponential tail is $\lambda = 70 \pm 6 \text{ g cm}^{-2}$.

the paper by Ellsworth et al(5), those protons dominate the tail of the distribution. In this case, the proton-air inelastic cross-section is found to be $540 \pm 50 \text{ g cm}^{-2}$. This result is in agreement with the results published by Hara et al(6).

The extrapolation of proton-proton inelastic cross-section from p-air cross-section is model dependent. With the same assumptions made in our previous paper(1), the p-p inelastic cross-section is found to be $122 \pm 11 \text{ mb}$ at $s^{1/2}$ of 30 TeV (Figure 5).

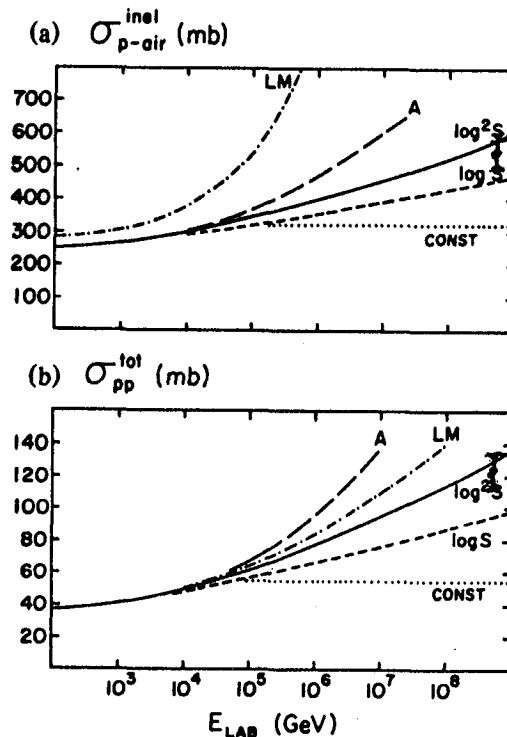


Figure 5.

(a) Pair Inelastic and (b) p-p Total Cross Section With Our Data.

4. Acknowledgements. We gratefully acknowledge the United States National Science Foundation for its generous support of this work under grant PHY8201089.

References.

1. Baltrusaitis, R.M., et al, Phys. Rev. Lett. 52, 1380 (1984).
2. Baltrusaitis, R.M., et al, Nuclear Instruments Methods (to be published).
3. Cassiday, et al, Proceeding of the Workshop on Very High Energy Interactions, Philadelphia, 1982, pp. 72-82.
4. Baltrusaitis, R.M., et al, paper OG 5.1-7
5. Ellsworth, R.W., Gaisser, T.K., Stanev, T., and Yodh, G.B., Phys. Rev. D26, 336 (1982).
6. Hara, T., Hayashida, N., Honda, M., Kamata, K., Kawaguchi, S., Kifune, T., Mizumoto, Y., & Nagano, M. Proceedings of International Symposium on Cosmic Rays and Particle Physics, March 19-23, 1984, Tokyo.

HADRON CROSS SECTIONS AT ULTRA HIGH ENERGIES AND
UNITARITY BOUNDS ON DIFFRACTION DISSOCIATION

G. B. Yodh

Dept. of Physics and Astronomy, Univ. of Maryland
College Park, MD 20742

T. K. Gaisser

Bartol Research Foundation, Univ. of Delaware
Newark, Delaware 19711

U. P. Sukhatme

Dept. of Physics, Univ. of Illinois, Circle Campus
Chicago, Illinois 60680

1. Introduction: The behavior of total cross sections at ultra high energies, above $\sqrt{s} \sim 1$ TeV has been derived from analysis of air shower observation.¹ The proton-air inelastic cross section must be related to the basic proton-proton interaction to determine which of the different models for the asymptotic behavior of the scattering amplitude are consistent with cosmic ray data which may be ruled out. The adjective inelastic for proton-air cross section ($\sigma_{p\text{-air}}^{\text{inel}}$) describes the fact that cosmic ray experiments do not measure all of the absorptive cross section because cascade development is not sensitive to processes that lead to quasi-elastic excitation of the air nucleus (σ_{qe}) or to diffractive excitation of one of the nucleons of the air nucleus (σ_{DD}). The method generally used to calculate p-air inelastic cross section from proton-proton parameters is the Glauber multiple scattering technique.² Application of this method leads to the relation

$$\sigma_{p\text{-air}}^{\text{inel}} = \sigma_{p\text{-air}}^{\text{tot}} - \sigma_{p\text{-air}}^{\text{el}} - \sigma_{qe} - \sigma_D - \Delta\sigma(\text{inelastic screening}) \quad (1)$$

The term $\Delta\sigma(\text{inelastic screening})$ accounts for screening due to multiple scattering with excited nucleon intermediate states. To calculate terms on the right hand side of this relation it is necessary to know the values of σ_{pp}^{tot} , slope parameter $B^{pp}(t=0)$, single and double diffractive cross sections σ_{SD}^{pp} , σ_{DD}^{pp} the shape of $d^2\sigma/dt dM^2$ at t_{min} for the diffractive process $P+P \rightarrow P+X$ and the nuclear density profile.³

2. Discussion of Models of Elementary Interaction: Many different models for the high energy behavior of scattering amplitudes have been proposed, all of which agree with PP and $\bar{P}P$ data up to SPS- $\bar{P}P$ collider energies but give different extrapolations at higher energies. They may be classified into three types: (1) Geometric scaling models,⁴ (2) Diffraction dominance models,³ (3) Chou-Yang type models.⁵

The "Geometrical Scaling" models are those in which the interaction radius increases logarithmically with energy. The ratio $\sigma_{el}/\sigma_{\text{tot}}$ is assumed to be energy independent. The rise in the total cross section comes from all three components, diffractive and inelastic processes.

The diffractive dominance models ascribe all the rise in total cross sections to σ_{el} , σ_{SD} and σ_{DD} , the "inelastic" cross section remaining constant. The ratio $\sigma_{\text{inel}}/\sigma_{\text{tot}}$ decreases with energy, $\sigma_{el}/\sigma_{\text{tot}}$ becomes energy independent, $\sigma_{SD}/\sigma_{\text{tot}}$ slowly decreases with energy while $\sigma_{DD}/\sigma_{\text{tot}}$ will be asymptotically constant.

In Chou-Yang type models the restriction of geometrical scaling that $\sigma_{el}/\sigma_t = \text{constant}$ is released. However the detailed behavior of σ_{SD} or σ_{DD} is not generally prescribed.

This it may seem at first glance that with so much freedom it would be possible to fit the cosmic ray data with a large range of models. This is not so, however, because the range of variation of the diffractive component cross sections are limited by unitarity bounds. There is only one proviso for this statement which is that Glauber techniques are valid at these energies.

3. Unitarity Bounds and Limits on Diffraction: The unitarity bound on elastic and diffractive cross section can be stated as⁶

$$\sigma_{el} + \sigma_{Diff} \leq \frac{1}{2} \sigma_{tot} \quad (2)$$

One can write σ_{tot} in terms of its parts

$$\sigma_{tot} = \sigma_{el} + \sigma_{Diff} + \sigma_{ND} \quad (3)$$

where σ_{ND} is the non-diffractive cross section. It follows from these relations that

$$\sigma_{ND} \geq \frac{1}{2} \sigma_{tot} \quad (4)$$

which means that if $\sigma_{tot}(E)$ increases with energy then σ_{ND} cannot be energy independent.

Assuming the general validity of the bounds we apply it to the specific model of diffractive dominance proposed by Goulianos. The energy variation of σ_{el} , $2\sigma_{SD}$, σ_{DD} and σ_{tot} for this model is shown in figure 1. The value of $\frac{1}{2} \sigma_{total}$ is also graphed. The unitarity bound given by equation (2) is violated by this model at $\sqrt{s} \sim 200$ GeV so is the inequality $\sigma_{ND} \geq \frac{1}{2} \sigma_{tot}$.

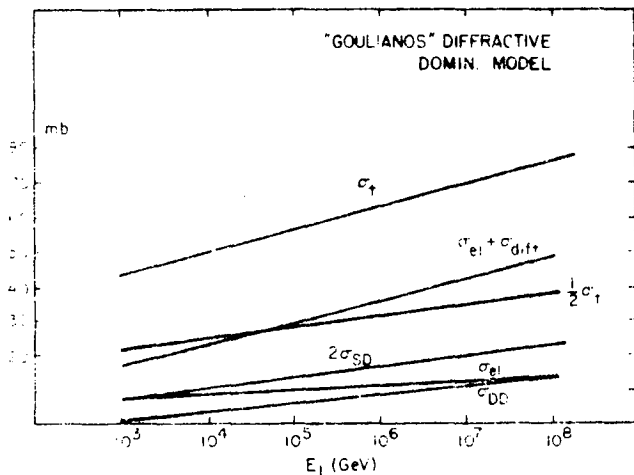


Figure 1: Predictions from a diffractive dominance model (Goulianos 1983) and its relation to unitarity bounds which require $(\sigma_{el} + \sigma_d)/\sigma_t$ to be less than or equal to 0.5

In fact any model which ascribes the increase in cross section entirely to diffractive processes will violate conventional unitarity requirements.

As representative of other models let us consider the model proposed by Block and Cahn. The model gives explicit fits for total and elastic cross sections as well as the slope parameter, (B) , as a function of energy. To obtain σ_{p-air} (inelastic) using equation (1) we must calculate the five terms on the right hand side using Glauber methods. The total, elastic and quasi-

elastic proton-air cross sections can be calculated in straight forward manner using the model parameters: σ_{pp}^{tot} , σ_{pp}^{el} , B and ρ . To estimate σ_D and $\Delta\sigma$ (inel-screening) a knowledge of the single diffractive cross section is needed, which is not given by the model. Of these two terms, $\Delta\sigma$ (inel-screening) depends only on the value of $(d\sigma/dtdM^2)_{tmin}$ which varies as $1/M^2$.² Most of the contribution to this term comes from small values of M^2 and numerical evaluation gives a value for this correction which varies from about 8 mb at ISR energies to saturation at ~ 14 mb at ultra high energies.

The correction for diffractive dissociation of the target nucleon is given by

$$\sigma_D = (\sigma_{SD}^{pp} / \sigma_{inel}^{pp}) \sigma_{p-air}^1 \quad (5)$$

Here σ_{p-air}^1 is the cross section for an absorptive -p-nucleus interaction involving exactly one elementary inelastic scattering encounter. It is easy to show that $\sigma_{p-air}^1 \equiv 2/3 \pi \langle r^2 \rangle$ which corresponds to 142 mb for a root mean square radius of 2.6 fermis. The correction depends on the energy dependence of $\sigma_{SD}^{pp} / \sigma_{inel}^{pp}$ where $\sigma_{inel}^{pp} \equiv \sigma_{tot}^{pp} - \sigma_{el}^{pp} = \sigma_{ND} + 2\sigma_{SD} + \sigma_{DD}$.

What does the unitarity bound tell us about the size of this ratio? From the unitarity bound in equation (2) gives

$$2\sigma_{SD} + \sigma_{DD} \leq \frac{1}{2} \sigma_{tot} - \sigma_{el} \quad (6)$$

The maximum value of σ_{SD} then is obtained by putting $\sigma_{DD} = 0$. The ratio $\sigma_{SD} / \sigma_{inel}$ is bounded by

$$\frac{\sigma_{SD}}{\sigma_{inel}} \leq \frac{1}{4} \left[1 - \frac{\sigma_{el} / \sigma_{tot}}{1 - \sigma_{el} / \sigma_{tot}} \right] \leq 0.25 \quad (7)$$

The maximum value of σ_D is 36 mb if $\sigma_{el} = 0$! In the Block-Cahn model corresponding to a $\ln^2 s$ energy dependence⁵ the ratio of σ_{el} to σ_{tot} varies from 0.175 to 0.37 as energy is varied from $\sqrt{s} \sim 20$ GeV to $\sqrt{s} \sim 10$ TeV, corresponding upper limits to σ_D are 28 mb and 15 mb respectively. At ISR, however, there are direct measurements of σ_{SD} and σ_{inel} which give a 14 mb cross section for σ_D . A reasonable measure of the allowed range of σ_D can be obtained by assuming that the lower bound to $\sigma_{SD} / \sigma_{inel}$ is the ISR value and the upper bound is given by equation (8) with $\sigma_{el} / \sigma_{tot}$ being taken from Block and Cahn's model. The result is shown in figure (2). Also shown in the figure is the sum of the last three terms in equation (1), i.e. $\sigma_{qe} + \sigma_D + \Delta\sigma$ (inel. screening). The

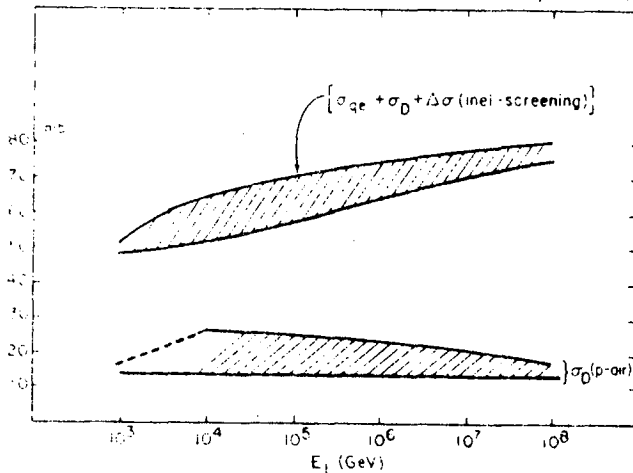


Figure 2: The allowed ranges for the correction for diffractive dissociation of the target nucleon. Also shown is the total correction as a function of energy.

fractional uncertainty in the value of $\sigma_{p\text{-air}}(\text{inelastic})$ is less than three percent.

In figure (3) we compare the predictions of the $\ln s$ and $\ln^2 s$ models of Block and Cahn with air shower cosmic ray cross sections.^{7,8,9} It is seen that the data clearly favor the faster energy dependence.

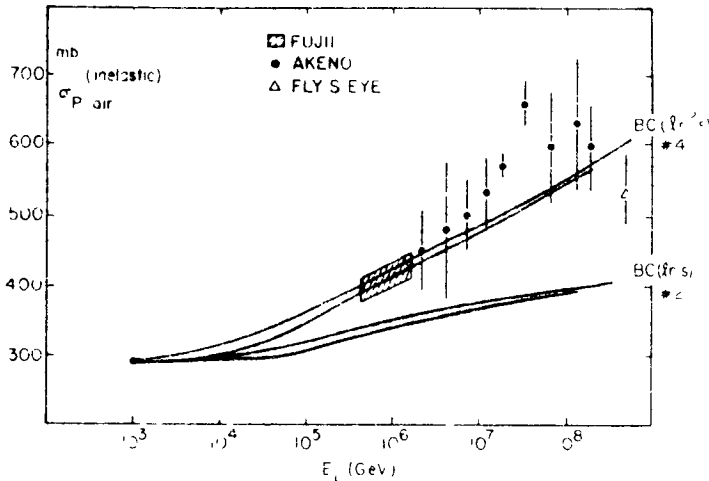


Figure 3: Comparison of predictions for $\sigma_{p\text{-air}}(\text{inelastic})$ from two different models of Block and Cahn: No. 4 for which $\sigma_{pp}^{\text{total}}$ increases as $\ln^2 s$ and No. 2 which has a $\ln s$ dependence

4. Conclusion: We have shown that if unitarity bounds on diffractive cross sections are valid at ultra high energies then (a) diffractive dominance models which ascribe the increase in total hadron-hadron cross sections to diffractive processes only are ruled out and (2) that cosmic ray cross sections derived from air shower experiments at ultra high energies clearly rule out models for hadron-hadron cross sections with $\ln s$ energy dependence and favor those with $\ln^2 s$ variation.

This work was supported in part by the National Science Foundation and the Department of Energy.

5. References:

1. G. B. Yodh, to be published in the Proceedings of the Aspen Winter Conference Series, Jan. 1985, Univ. of MD Physics Preprint PP No. 85-130.
2. V. Barger et al., Phys. Rev. Letters 33, 1051, (1974) and G. B. Yodh et al., Phys. Rev. D27, 1183 (1983).
3. A summary of data prior to 1983 is given in K. Goulianos, Phys. Reports 101, 170 (1983).
4. U. Amaldi, M. Jacob et al., Ann. Rev. of Nucl. Science, 26, 385 (1976).
5. M. M. Block and R. N. Cahn, Rev. Mod. Physics, 57, 563 (1985); T. T. Chou and C. N. Yang, Phys. Rev., 170, 1591 (1968).
6. U. P. Sukatme and F. S. Heyney, Nucl. Phys. B108, 317 (1976) and J. Pampulin, Phys. Rev. D8, 2899 (1973).
7. M. Akashi et al., Phys. Rev. D24, 2353 (1981). This contains the data from Mt. Fujii.
8. T. Hara et al., Proceedings of Int. Symposium on Cosmic Rays and Particles, Tokyo, Japan (1984), p. 756; T. Hara et al., Phys. Rev. Letters 50, 2058 (1983). The 1984 paper gives the revised data points for the Akeno experiment.
9. R. M. Baltrusaitus et al., Phys. Rev. Letters 52, 1380 (1984). This paper contains results from the Fly's Eye experiment.

ON TOTAL CROSS SECTIONS AND SLOPES
AT SUPERHIGH ENERGIES

SH.S.YEREMIAN, V.M.ZHAMKOCHIAN

Yerevan Physics Institute, Markarian st.2
375036, Yerevan, Armenia, USSR

ABSTRACT

Hadron-hadron and hadron-nucleus interactions are investigated in the framework of the Reggeon field theory with critical and supercritical pomerons and multiple scattering theory. A good agreement is obtained with experimental data on cross sections of proton-proton and proton-nucleus interactions at high energies.

The theory with the renormgroup critical pomeron (RCP) ($\alpha_p(0) \equiv 1$) is compared with the supercritical one ($\alpha_p = 1 + \Delta$) - froissarton. The theory with RCP is considered in detail in /1/, and with froissarton - in /2/, therefore, we will present here the basic results only.

In fig.1 total cross sections of pp-interaction at energies E_{LAB} from 10 to 10^{12} GeV are presented. Both models describe well the region of mean and high energies and practically coincide up to $\xi \leq 15$. The cross section given by RCP is presented in the figure by a coarse line. At mean values of energies it grows like ξ^2 , at $\xi > 15$ the rate of growth gradually slows down and turns into asymptotic $\sim \xi^{0.277}$.

The cross section given by the froissarton is presented by thin lines.

The upper line corresponds to $\Delta = 0.12$, and the lower one to $\Delta = 0.07$. The cross section with $\Delta = 0.12$ rapidly

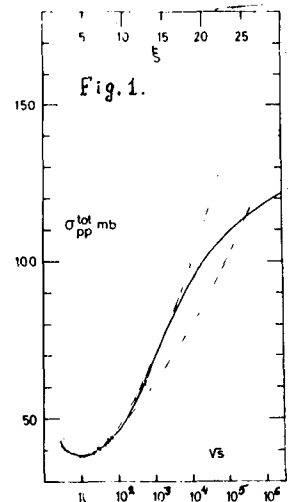


Fig.1. Total cross section of pp-interaction σ_{p-p}^{tot}

grows from the very beginning and at $\xi \geq 15$ begins to exceed the RCP and passes to its asymptotic regime $\sim \xi^2$. It is seen that σ_{pp}^{tot} cannot serve as a test for separating a correct model.

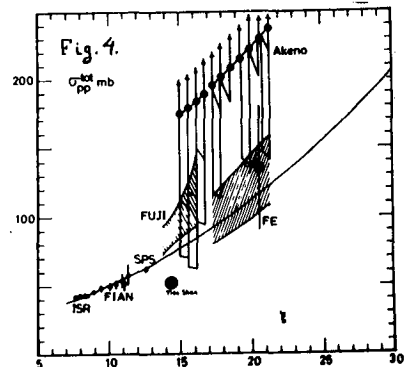
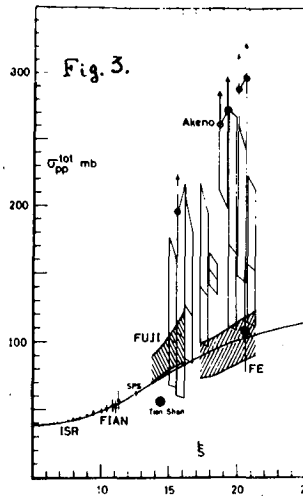
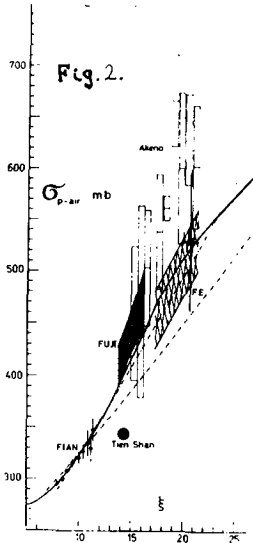


Fig. 2. Production cross section on the nuclei of air atoms $\sigma_{p-air}^{\text{prod}}$ in theories with critical and supercritical pomerons (— RCP, — — — froissarton).

Fig. 3. Total cross section of pp-scattering in the theory with a critical pomeron.

Fig. 4. Total cross section of pp-scattering in the theory with a supercritical pomeron.

In fig. 2 theoretical curves are presented that describe the production cross section on nuclei of air atoms in the two theories considered (the calculation technique of the hadron-nucleus interaction characteristics is presented in /1/). The coarse curve corresponds to RCP, and the dot-and-dash curves to the supercritical pomeron with $\Delta = 0.07$ and 0.12 . The curve corresponding to the froissarton lays systematically lower than RCP in the range $15 < \xi < 25$.

In figs. 3 and 4 total cross sections of pp-interactions in both theories as well as results of the pp cross sections extraction from experimental data on proton-nucleus interaction at cosmic energies are presented. The rings with arrows denote the values of separated points that lay above the unitarity limit for the given theory. It

should be noted that according to /1/ the cross-section values σ_{p-aiz}^{p2od} depend essentially on the slopes of diffraction cone of the pp-interaction predicted by the given theory. It is clear that experiments with cosmic rays require a more rapid growth of slopes than the one which may be given by both theories. The theory with RCP seems preferable.

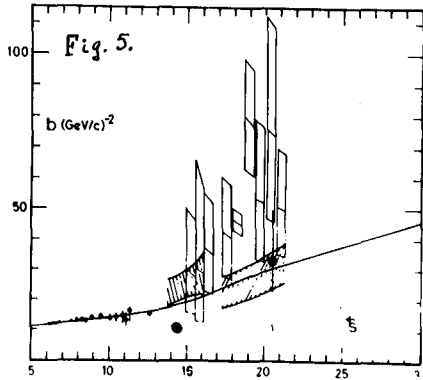


Fig.5. Slope of the diffraction cone of pp-scattering in the theory with a critical pomeron.

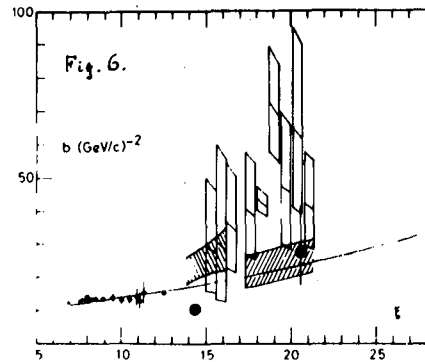


Fig.6. Slope of the diffraction cone of pp-scattering in the theory with a supercritical pomeron.

In figs. 5 and 6 diffraction cone slopes in RCP and froissarton theories are presented. The experimental data presented were extracted proceeding from the fixed cross sections of the elementary act in the given theory and are conventional, nevertheless, they indicate a necessity in a more rapid growth of slopes as compared with the theoretical one.

In fig.7 the ratio σ^{el}/σ^{tot} is presented. This value is crucial for the revelation of the question, which of these two theories is consistent at superhigh energies. In the RCP theory this ratio at $S \rightarrow \infty$ behaves like $\xi^{-0.862}$. In the froissarton theory we have $\sigma^{el}/\sigma^{tot} \rightarrow 1/2$. However, in the region of attainable energies we have an inverse picture: up to $\xi \approx 17$ σ^{el} and σ^{el}/σ^{tot} in RCP grow much more rapidly than in the froissarton, after which the RCP begins to slowly fall, and the froissarton continues to grow.

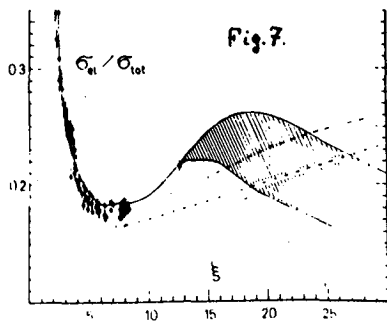


Fig. 7. Ratio σ_{el}/σ_{tot}
 (— RCP,
 - - - - - froissarton).

REFERENCES

- /1/ Yeremian Sh.S., Zhamkochian V.M., Yad.Fiz., 1984, 40, 1016.
 /2/ Kaidalov A.B., Ter-Martirosian K.A., Yad.Fiz., 1984, 39, 1545.

Summing up the abovementioned, one may state that even at ultracomic energies it is apparently impossible to obtain an unambiguous answer to the question: which of these theories is consistent at superhigh energies?

DETERMINATION OF THE CROSS SECTION
OF THE PROTON, PION AND NEUTRON INELASTIC INTERACTION
WITH LEAD AND CARBON NUCLEI AT 0.5 - 5.0 TEV ENERGIES
(PION Experiment)

V.V.AVAKIAN, G.V.KARAGJOZIAN, E.A.MAMIDJANIAN,
M.I.KEROPIAN, R.M.MARTIROSOV, G.G.OVSEPIAN, S.O.SOKHOYAN

Yerevan Physics Institute, Markarian st. 2
375036 Yerevan, Armenia, USSR

ABSTRACT

Experimental results on the cross section of the single pion, proton and neutron inelastic interaction with carbon and lead nuclei in the 0.5-5.0 TeV energy interval obtained on the PION installation (mount.Aragats, Armenia, 3250 m) are presented. For this purpose the N_{π} / N_p and $\sigma_{PFe}^{in} / \sigma_{JFe}^{in}$ ratios measured directly on the installation as well as the calculated $\sigma_{PA}^{in} / \sigma_{JA}^{in}$ dependence on the target nucleus atomic number were used.

The PION installation combining an X-ray transition radiation multimodule detector (XTR detector) and an ionization calorimeter (IC) is shown in fig.1. The detailed description of the installation is given in /1/. 3 rows of multiwire proportional chambers (MWPC) identical to the chambers located in the XTR detector were used as detectors of the hadron interaction with the graphite nuclei. The thickness of the two graphite layers is 12 cm. The interactions in lead were registered by two rows of ionization chambers located under 3 cm (I layer) and 2 cm (II layer) of lead in the upper part of the IC.

To determine σ^{in} with the C and Pb nuclei, events were chosen that satisfied the following selection criteria: the energy release in the IC should be higher than 500 GeV;

the axis of the nuclear-electromagnetic cascades (NEMC) should be within the solid angle of the installation (its geometric factor is $G = 1,28 \text{ m}^2\text{sr}$); the ionization distribution in each row of the ionization chambers should have one maximum at a distance of 20 cm from the IC edge (\sim two chamber diameters); the air accompaniment density should not exceed 1 part./m (the hadron "singleness" condition).

In selecting the events identified as interactions in the graphite target the fulfillment of two additional criteria was required. The energy release in the interaction detector under the graphite target should correspond to the passage of > 2 relativistic particles, and the summary energy release under the first layer should exceed 100 relativistic particles.

The additional condition for selecting the events identified as interactions in lead was the presence of energy release in the second row of ionization chambers in the absence of energy release in the first row.

According to these criteria 548 neutral and 876 charged hadrons having interacted in graphite as well as 1364 neutral and 1090 charged hadrons identified as having interacted in the second layer of lead were selected.

In determining the inelastic interaction cross sections corrections were introduced for "albedo" particles, the difference in the angular distribution of charged and neutral hadrons, the contribution of the cascades generated by muons, the transition effect Pb - ionization chamber wall. The measured cross sections of charged and neutral hadron

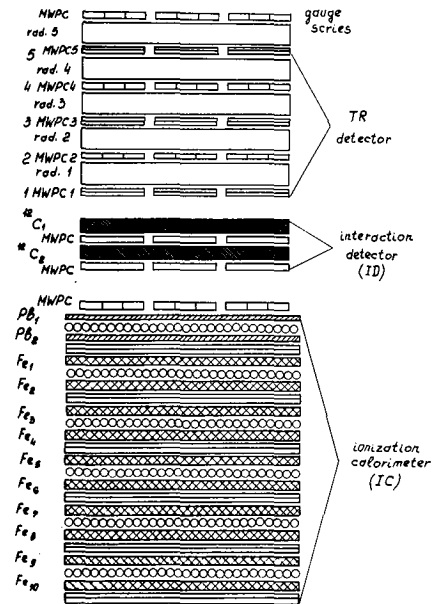


Fig. 1

interactions with the C and Pb nuclei are plotted in Table 1.

Table 1

	500-1000 GeV	1000-2000 GeV	2000 GeV
σ_{nc}^{in}	254 \pm 21	263 \pm 28	261 \pm 34
σ_{chc}^{in}	214 \pm 19	228 \pm 21	247 \pm 36
σ_{pc}^{in}	236 \pm 23	236 \pm 30	255 \pm 39
σ_{jc}^{in}	179 \pm 18	179 \pm 23	193 \pm 30
σ_{npb}^{in}	1980 \pm 60	2100 \pm 81	2215 \pm 104
σ_{chpb}^{in}	1693 \pm 80	1762 \pm 94	1890 \pm 114
σ_{ppb}^{in}	1762 \pm 108	1809 \pm 101	1916 \pm 116
$\sigma_{\pi pb}^{in}$	1587 \pm 89	1630 \pm 83	1726 \pm 97

By means of these data the σ^{in} of pions and protons with the carbon and lead nuclei were determined. For this purpose we have used the calculated curve of the ratio $\sigma_{PA}^{in} / \sigma_{JA}^{in}$ dependence on the nucleus atomic number obtained in /2/ according to which $f(A) = \sigma_{PA}^{in} / \sigma_{JA}^{in}$ is practically independent of energy. The experiment shows a good agreement with the calculated curve, $\sigma_{pp}^{in} / \sigma_{jp}^{in} = 1.61 \pm 0.03$ at $E = 345$ GeV /3/, and $\sigma_{pFe}^{in} / \sigma_{jFe}^{in} = 1.19 \pm 0.05$ for $E = 1000$ GeV /4/. On the PION installation the pion-to-proton ratio N_{π} / N_p for various intervals of hadron energy was directly measured /5/. The calculated values of $\sigma_{PA}^{in} / \sigma_{JA}^{in}$ for the C and Pb nuclei are equal to 1.32 ± 0.4 and 1.11 ± 0.03 , respectively. The final revised data on the proton and pion cross sections are also plotted in Table.1.

Figure 2 presents the experimental results on σ_{pc}^{in} and σ_{ppb}^{in} obtained both on accelerator /5/ and in cosmic rays /6/. The curves denote the recalculation by the multiple scattering theory from the PP to PPb and PC interactions.

The authors are grateful to A.Ts.Amatuni and S.G.Matinyan for their interest in the work as well as to A.P.Garyaka, S.R.Gevorkian and V.M.Zhamkochian for stimulating discussions.

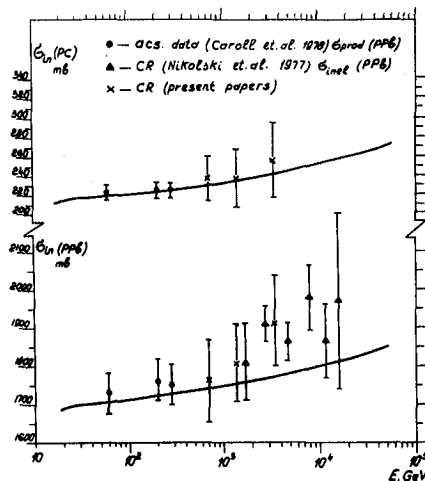


Fig. 2

REFERENCES

- /1/ Avakian V.V. et al., XVI ICRC, Kyoto, 1980, 13, 61.
- /2/ Badalian A.R., Gevorkian S.R., Mamidjanian E.A., XVIII ICRC, Bangalore, 1983, 5, 510.
- /3/ Carroll A.S. et al., Fermilab-Pub., 78/85, 7110, 104, 1978.
- /4/ Avakian V.V. et al., VANT, ser.tekh.fiz.eksp, 1983, 4(16), 56.
- /5/ Avakian V.V. et al., XVIII ICRC, Bangalore, 1983, 5, 263.
- /6/ Nam R.A., Nikol'sky S.I. et al., Preprint FIAN N.85, 1977.

P(\bar{p})P ELASTIC SCATTERING AND COSMIC RAY DATA

Fazal-e-Aleem and Mohammad Saleem
 Centre for High Energy Physics
 University of the Punjab
 Lahore-20, Pakistan.

ABSTRACT

It is shown that the total cross section σ_T for pp elastic scattering at cosmic ray energies, as well as the total cross section $\sigma_{\bar{p}p}$, the slope parameter $b(s,t)$ and the differential cross section $d\sigma/dt$ for small momentum transfer at ISR and collider energies for p(\bar{p})p elastic scattering can be simultaneously fitted by using a simple Regge pole model.

1. Introduction. The total cross sections for proton-proton and proton-antiproton scattering for $20 < \sqrt{s} < 2 \times 10^5$ GeV have been measured at ISR and SPS collider and derived from the cosmic ray data[1,2]. The data show that the total cross section keeps on rising throughout the measured range. The results of these measurements are shown in Figs.1 and 2. The slope parameter $b(s,t)$ for pp \rightarrow pp at $\sqrt{s}=53$ GeV has been measured by various authors[3] and the results are shown in Fig.3. Accurate measurements of $b(s,t)$ at collider energy $\sqrt{s}=546$ GeV were made by using luminosity independent technique[3] and are shown in Fig.4. It may be noted that the value of 15.3 ± 0.3 (GeV/c) $^{-2}$ of slope parameter for $0.03 < -t < 0.1$ (GeV/c) 2 as measured by this group differs significantly from the earlier measurement of the slope parameter at $\sqrt{s}=540$ GeV which gives a value of 17.2 ± 1.0 (GeV/c) $^{-2}$ in the range $0.05 < -t < 0.19$ (GeV/c) 2 [4].

Simultaneous measurements of differential cross sections for $\bar{p}p$ and pp elastic scatterings at $\sqrt{s}=31, 53$ and 62 GeV in the interval $0.05 < -t < 0.85$ (GeV/c) 2 have been made by Breakstone et al[5] at the CERN ISR. At 53 and 62 GeV, for $0.17 < -t < 0.85$ (GeV/c) 2 both $\bar{p}p$ and pp data show simple exponential fall. At $\sqrt{s}=31$ GeV, the data in the interval $0.05 < -t < 0.85$ (GeV/c) 2 are consistent with a change in slope near $-t=0.15$ (GeV/c) 2 . Results of these ISR measurements are plotted in Fig.5. Very recently, UA4 collaboration[6] has measured the differential cross section of proton-antiproton elastic scattering at $\sqrt{s}=546$ GeV. The $d\sigma/dt$ distribution shows a steep exponential decrease, with a change of slope around the same value of $-t$ as at ISR energies. The data for this reaction for $-t < 0.8$ (GeV/c) 2 are shown in Fig.6.

2. Calculations and Discussion. Following Refs.7 8, we find that for both the reactions a very good fit with the total cross section, the slope parameter and the differential cross section for small momentum transfers is obtained by choosing

the residue function as a sum of two exponentials. Thus the scattering amplitude may be written as

$$T(s,t) = \beta(t) \xi(t) s^{\alpha(t)} = (Ae^{Bt} + Ce^{Dt}) \xi(t) s^{\alpha(t)}$$

The differential cross section is then given by

$$d\sigma/dt = \frac{1}{s^2} |T|^2 = (Ae^{Bt} + Ce^{Dt})^2 s^{2\alpha(t)-2}$$

The expression for the slope parameter $b(s,t)$ can be obtained by using the formula

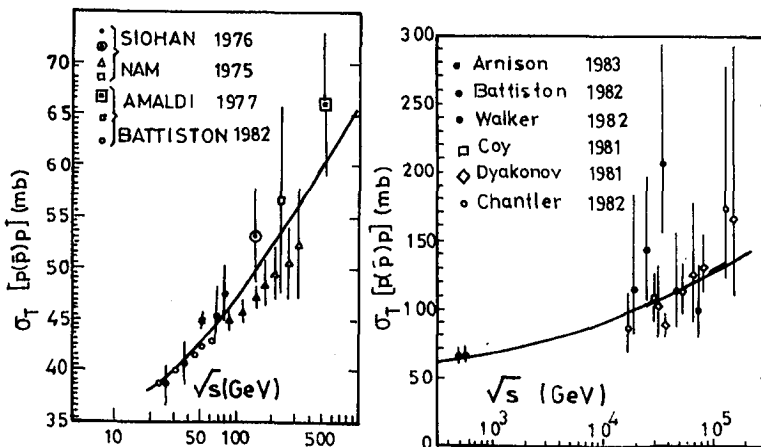
$$b(s,t) = d/dt (\ln d\sigma/dt)$$

It is found that a good fit with the experimental data, including the most recent results, is obtained by the following choice of residue function $\beta(t)$:

$$\beta(t) = 4.35e^{2.72t} + 1.45e^{10.93t}$$

The equation of the Pomeron has been chosen as [9,10]

$$\beta(t) = 1.069 + 0.3t$$

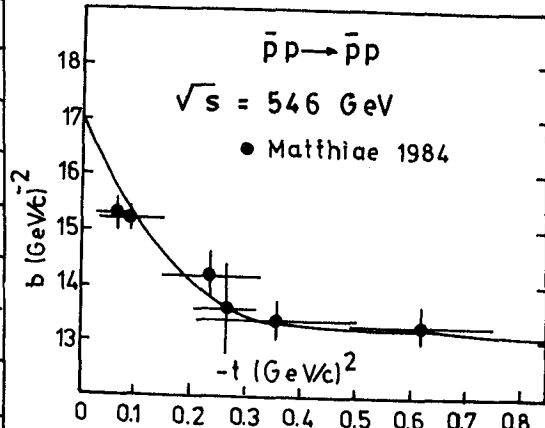
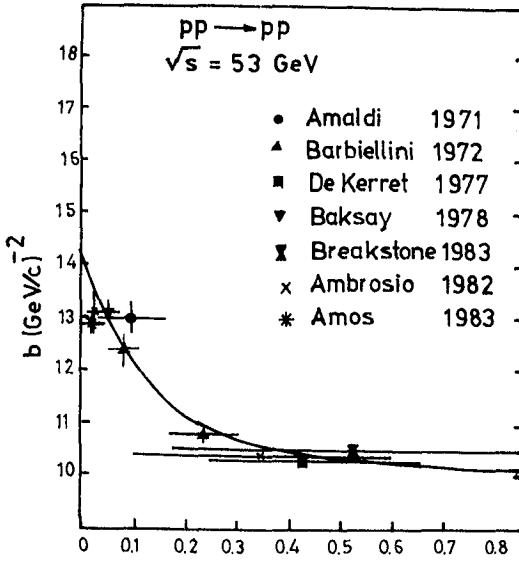


Figs.1 and 2. The total cross sections for $20 < \sqrt{s} < 2 \times 10^5$ GeV. Theoretical curves are the predictions of the model described in the text.

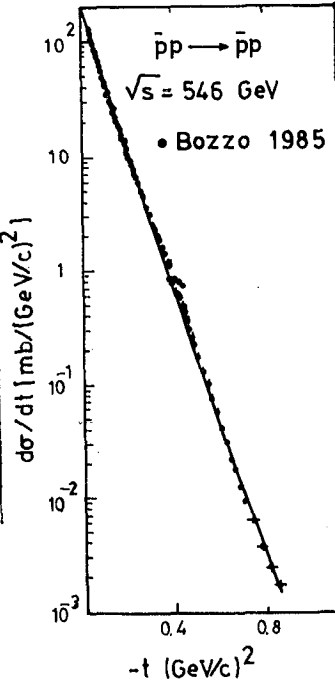
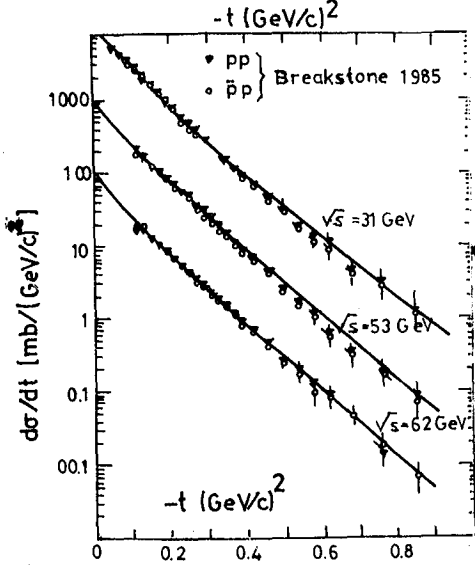
In Figs.5 and 6 the measured differential cross sections for pp and $\bar{p}p$ elastic scatterings at ISR and collider energies have been plotted together with the predictions of the model described in the text.

The CERN SPS proton-antiproton collider, after modifications which have enhanced the peak energy it can achieve, is back in action again. This time the collider is providing 630 GeV collision energy compared to the 546 GeV in previous runs. The results are expected to be available shortly. We predict the slope parameter at $\sqrt{s}=630$ GeV for $-t < 1$ $(\text{GeV}/c)^2$. The curve in Fig.7 shows the predicted values.

Figs.1 and 2 show the total cross sections for $20 < \sqrt{s} < 2 \times 10^5$ GeV. Theoretical curves are the predictions of simple Regge pole model. Figs.3 and 4 show the results of the slope parameter for $p(\bar{p})p$ elastic scattering at $\sqrt{s}=53$ and 540 GeV respectively. The curves represent predictions of the



Figs.3 and 4. The slope parameter at $\sqrt{s}=53$ and 540 GeV. Theoretical curves are the predictions of the model described in the text.



Figs.5 and 6. The differential cross sections at ISR and collider energies. Theoretical curves are the predictions of the model described in the text.

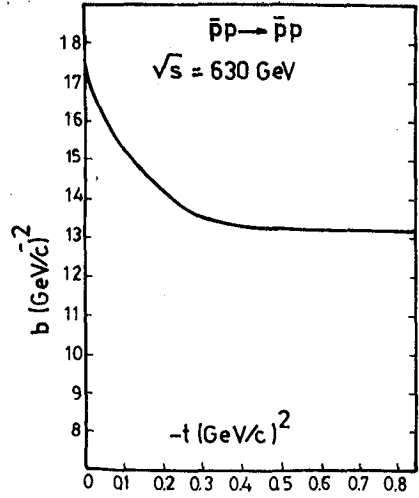


Fig.7. Predictions of the model described in the text for the slope parameter at $\sqrt{s}=630$ GeV.

3. Conclusions. We conclude that at high energies where pomeron is believed to dominate the behaviour of elastic scattering, a simple Regge pole model can be used to explain the total cross section for proton-proton elastic scattering at cosmic ray energies together with the total cross section, the slope parameter and the differential cross section for small momentum transfers at ISR and collider energies for $p(\bar{p})p$ elastic scattering.

4. Acknowledgement. The financial assistance from the Pakistan Science Foundation under contract No.P-PU/Phys(11/2) is gratefully acknowledged.

References.

1. G.B.yodh et al., Phys.Rev.(1983) 27D, 1183 (Also see references quoted therein).
2. J.Linsley, UNML-5/4/84-2 (Also see references quoted therein).
3. G.Matthiae, CERN/EP 84-119, 11 September 1984 (Also see references quoted therein).
4. R.Battiston et al., Phys.Lett.(1982) 115B, 333; Phys.Lett.(1982) 117B, 126.
5. A.Breakstone et al., Nucl.Phys.(1984) 248B, 253.
6. M.Bozzo et al., CERN/EP 85-31, 7 March 1985.
7. M.Saleem and Fazal-e-Aleem, Pramana (1985) 24, 429.
8. Fazal-e-Aleem, Hadronic J. (In press).
9. P.D.B.Collins et al., Phys.Lett.(1973) 43B, 171; Nucl. Phys.(1974) B80, 135.
10. S.Y.Chu et al., Phys.Rev.(1975) 13D, 2985.

MEASUREMENT OF INTERACTION CROSS SECTION
OF COSMIC RAY Fe NUCLEI ($E > 4$ GeV/N) WITH Al TARGET

G.X. Ren, Y.Z. Zhou, R.Q. Huang, M.Y. Chen

Institute of High Energy Physics

Academia Sinica

Beijing China

1. Introduction

Although the study of relativistic heavy ion interaction encumbered by the low intensities of the incident heavy nuclei in cosmic ray experiments, however, one can use a suitable structure of detector to attain a result with a reasonable accuracy.

In this paper we present a cross section value of Fe($E > 4$ GeV/N) with Al. We use CR-39 as detector and Al as target.

The cross section value is estimated using maximum likelihood method.

2. Detector

The detector which consists of a stack of CR-39 sheets sandwiched by Al plates is designed for measuring Fe-Al interaction cross section, the Al serving as target and CR-39 serving as detector. The thicknesses of a CR-39 sheet and an Al plate are 1.6 mm and 1.8 cm, respectively. There are 6 layers altogether.

3. Experiment procedure

The detector was launched by a balloon near Beijing in 1982 to a ceiling height of 37 km and lasted for 10 h. The effective cutoff rigidity is 9.4 GV, the recorded threshold for Fe $E > 4$ GeV/N, a value slightly higher than the one reached by heavy ion accelerator so far.

The CR-39 sheets were etched in 6.8 normal NaOH

solution with temperature of 70°C for 40 h. The reduced etch rate of CR-39, $V_T/V_B - 1$, and dip angle of impinge particle are obtained from the measurement of the major and minor axes of etch pit ellipses.

Among the recorded nuclei with charge $Z \gg 10$, 322 tracks are identified as Fe nuclei with resolution of 0.6 e.

According to the position and dip angle of impinge particle in a sheet of CR-39 and the thickness of target plate, one can calculate the expected position of the particle in the next sheet of CR-39 below target easily. If an etch pit at the expected position possesses a major and minor axes within the error $1.5 \mu\text{m}$ with the impinge particle at former sheet, namely possesses a charge within the error 1 e and a dip angle within 2° with the impinge one, then this particle is thought to pass through the target without interaction, otherwise a nucleus-nucleus interaction is assumed.

Every Fe track is followed downwards until an interaction takes place or it goes out the detector. 205 interactions satisfying this criterion mentioned above are observed and the total track length been followed $\sum_{i=1}^{N_0} L_i = 1854.3 \text{ cm}$ ($N_0 = 322$, the number of incident particles)

A maximum likelihood estimation of Fe-Al collision mean free path gives

$$\lambda = \frac{\sum_1^{N_0} L_i}{N} \quad (1)$$

where N is the number of interactions.

The variance of λ is

$$\text{Var}(\lambda) = \lambda^2 / N \quad (2)$$

4. Result and discussion

According to eqs (1) and (2), the maximum likelihood estimation of Fe-Al collision mean free path is obtained as $\lambda = 9.04 \pm 0.63$ cm which corresponds to the cross section value $\sigma_{\text{Fe-Al}} = 1.83 \pm 0.13$ bar.

In our analysis the interaction point is assumed in the middle of plate when an interaction takes place inside it. The error of λ caused by the uncertainty of interaction points is estimated by

$$\Delta \lambda \cong H \sqrt{N_0} / N \sqrt{12} \quad (3)$$

where H is the thickness of target plate.

In order to increase the measuring accuracy of λ , larger number of interactions is needed. It means H should be increased. However, increase of H is limited by the relation $\Delta \lambda < [\text{Var}(\lambda)]^{1/2}$. In our case, $\Delta \lambda = 0.04$ cm is still much less than the statistical error. Even if the number of incident particles is not so large, we can obtain a comparable result with work performed on accelerator.

References

- Li Tipei, "Treatment in experiments", Science Press, Beijing, 1980.
- F. Fumuro, R. Ihara, 16th ICRC., 6 (1979), 166.

HADRON THERMODYNAMICS IN RELATIVISTIC
NUCLEAR COLLISIONS

P. Ammiraju

Instituto de Física 'Gleb Wataghin'

UNICAMP-CAMPINAS

BRASIL

1. Introduction. The current interest¹ in the study of nuclear collisions at very high energies - especially nucleus-nucleus collisions at several GeV/nucleon - stems from the expectation that one can investigate under laboratory conditions the early beginnings of our present universe. Thereby, one hopes to observe qualitatively new states of matter - such as density isomers, pion condensates, quark-gluon plasma (QGP), etc. The question whether the anticipated phase transition from hadron gas to QGP is a sharp or continuous one can only be answered through experiments devoted to the subsequent decay modes of this phase transition since the various theoretical models suffer in one way or other in their ability to pin point clear cut signals of this phase transition.

The search for QGP is basically a search for collective phenomena in strong interactions. Among them are the Cronin effect, the EMC effect, the production of secondaries with a kinetic energy above the kinematic limit in collisions of nucleons with targets of varying mass number, strange hadrons such as K, Λ , Σ and the leptons. However, from the data obtained, it is difficult to separate the purely QGP signals from the predictions of non-equilibrium QG-dynamics which can equally well explain the observed phenomena.

2. Relativistic Hadron Thermodynamics. The application of thermodynamics formalism to the study of high energy hadron-hadron central collisions has been in vogue for over forty years. What is now new is the use² of transformation laws of temperature and quantity of heat in the special relativistic thermodynamic formalism which preserves all the laws of classical thermodynamics by giving specific prescriptions in the

application of Lorentz transformation to the various thermodynamic quantities.

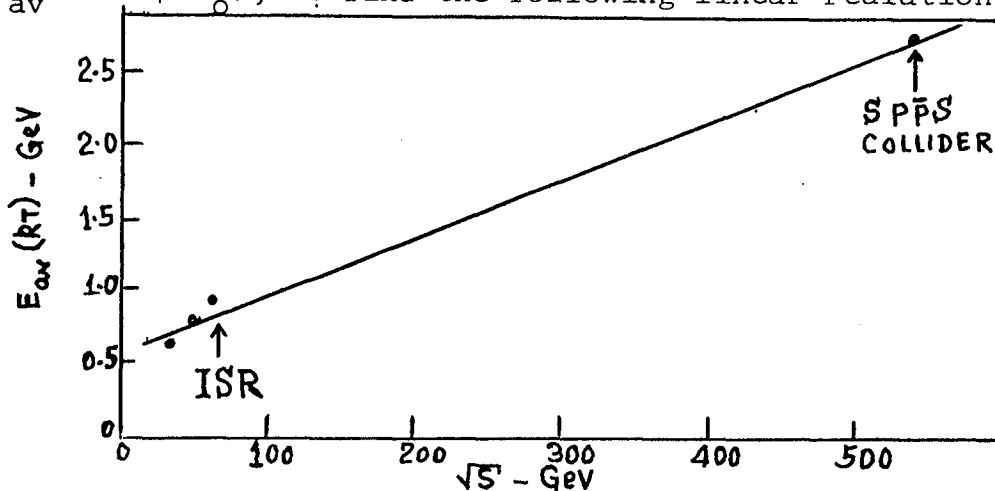
It is generally agreed that the entropy S is a Lorentz invariant and a unique answer is provided by statistical mechanics. In order to ensure the invariance of the entropy $dS = \delta Q/T$, the amount of (reversible) heat δQ and temperature T must transform in the same way. The problem comes in trying to preserve the first law $\delta Q = dU - \delta W$. The internal energy, U , cannot be considered as the fourth component of a four-vector as is done in the case of a mechanical point mass. The interpretation is to be modified for hadrons considered as extended bodies. Statistically, the distinction between heat and work, though both represent some form of energy transfer, rests on the essentially disordered nature of energy which is regarded as heat. Also, the systems considered in thermodynamics are not isolated. Thermodynamic space and ordinary phase space must be treated in a similar Lorentz invariant way to be logically consistent.

3. "Derivation" of law of Lorentz transformation of temperature. In the literature there exist various "derivations" of the law of Lorentz transformation of temperature and other thermodynamic quantities. The transformation formulae for temperature accepted for over fifty years is the following

$$T = T_0 (1 - v^2/c^2)^{1/2}$$

and consequently $\delta Q = \delta Q_0 (1 - v^2/c^2)^{1/2}$. Where the subscript 0 refers to the rest system and quantities in the lab system without subscript and \vec{v} is the velocity of the rest system with respect to the lab system. In the rest system all the energy is of a disordered form but, in the lab system, a fixed amount equal to v^2/c^2 of the net increase goes over into the ordered form, leaving $(1 - v^2/c^2)$ of the net increase as disordered energy. However, the statistical measure of disorder (i.e. entropy) is an invariant and this requires a lower temperature, compatible with a lower quantity of heat observed in the lab system³.

4. Experimental 'evidence' from large P_T phenomena. Chiu et al⁴ and Chew et al⁵ used the "two-temperature" concept for large P_T phenomena and fitted reasonably well the single particle inclusive cross-sections as a functions of P_T in a thermodynamically based statistical distribution. If we identify their values of $\langle kT_1 \rangle$ and $\langle kT_2 \rangle$ with the E_{av} in formula of ref. 2 ($E_{av} \sim \sqrt{s}/\mu T_0$), we find the following linear relationship.



5. Conclusions: Various phenomenological models based on statistical thermodynamical considerations have been used to fit the experimental data at high P_T to a two-temperature distribution. Whether this implies that the two-temperatures belong to two different reaction mechanisms, or consequences of Lorentz-contraction factor, or related in a fundamental way to the intrinsic 'thermodynamics of Space-Time' can only be revealed by further theoretical and experimental investigations of high P_T phenomena in extremely energetic hadron-hadron collisions.

6. References.

1. P.Ammiraju, et al: Il Nuovo Cimento 78A, 172 (1983)
2. P.Ammiraju, Lett. Al Nuovo Cimento 39, 424 (1984)
3. R.K.Pathria, Proc.Ray.Soc.88, 791 (1966)
4. B.K.Chiu et al, Phys.Rev. D.12,2725 (1975)
5. C.K.CheW et al, Phys.Rev. D.29, 2127 (1984)

ESTIMATION OF THE TOTAL INELASTICITY COEFFICIENT
IN INTERACTION OF ≥ 20 TeV HADRONS WITH LEAD

Kanevsky B.L., Mikhailova I.A.,
Rakobolskaya I.V., Sveshnikova L.G.

Institute of Nuclear Physics, Moscow State University,
Moscow 119899, USSR

Experimental data on the interaction mean free path of hadrons with energy $E_0 \geq 20$ TeV in lead obtained with multilayer X-ray emulsion chambers (XEC) are compared with results of simulation of nuclear-electromagnetic cascades in lead chamber. It is shown that, to explain experimental data, the value of the total inelasticity coefficient, $\langle K \rangle \sim 0.8$ should be assumed.

Multilayer XEC allow determination of gamma-ray and electron energy, E_γ , the energy $E_\lambda^{(e)}$ released into the electron-photon cascade (EPC) in hadron-lead nuclear interaction, and the origin depth Δt of an electron-photon cascade induced in a chamber by gamma-rays, electrons, and hadrons. The experimental procedure and chamber design have been described in detail in /1/.

In paper /2/ of the "Pamir" Collaboration, the results have been presented of measurement of the hadron interaction mean free path, λ_{meas} , in lead chambers obtained by analysing the hadron flux (about 700 events) over an area of 140 m^2 . After efficiency of hadron registration in chambers of different thickness has been allowed for more accurately, the authors of /2/ obtained the following results:

$$\begin{aligned} \lambda_{\text{meas}} &= 185 \pm 40 \text{ g/cm}^2 \text{ for energy } E_h = 5-10 \text{ TeV,} \\ \lambda_{\text{meas}} &= 213 \pm 24 \text{ g/cm}^2 \text{ for energy } E_h^{(e)} \geq 10 \text{ TeV,} \\ \lambda_{\text{meas}} &= 197 \pm 29 \text{ g/cm}^2 \text{ for energy } E_h^{(e)} \geq 20 \text{ TeV.} \end{aligned}$$

The measured value of λ_{meas} can be seen to be independent of $E_h^{(e)}$ within errors and $\lambda_{\text{meas}} = 207 \pm 17 \text{ g/cm}^2$.

The measured value of λ_{meas} concerns the summary flux of nucleons and charged pions with energies $E_0 \geq 20$ TeV. The pion fraction in this flux can be estimated based on calculations in terms of quasiscaling models, e.g., from /3/. This magnitude is almost independent of a model and, on average, pions present $\sim 30\%$ and nucleons $\sim 70\%$ in the total hadron flux at the given depth (596 g/cm^2).

The value of λ_{meas} may differ from the proper interaction mean free path for hadrons in lead, λ_{prop} , due to the following causes:

- A. The influence of an admixture of electron-photon component

When determining λ meas, cascades with $\Delta t > 8$ c.u. were taken into account. The number of EPC induced by gamma-rays and electrons at depth 8-10 c.u. from the chamber boundary was less than 2% of the hadron-induced cascades.

B. The influence of the boundary effects.

Using the angular distributions of $\cos \theta^{5.3}$ for hadrons and $\cos \theta^{5.8}$ for gamma-rays and the power law energy spectrum with the differential power index 3, obtained in /4/, the procedure of hadron and gamma-ray registration in a 2mx5m chamber (a standard size of lead chambers in the "Pamir" Collaboration) was Monte-Carlo simulated. The cascades interacting in a chamber and leaving its volume and additional cascades arriving from air, when taken into account, change the value of λ meas by less than 3%.

C. Allowance for secondary interactions.

The impossibility to follow entirely the hadron cascades in a chamber due to a high registration threshold leads to appearing the hadron-induced cascades for which we measure Δt of the second and subsequent interactions instead of the first one. So, there exist cascades in which in first interaction the energy $E_n^{(1)}$ lower than threshold was released while the energy released in one of subsequent interactions exceeds the threshold. There are also the cascades with energy released in the first and second interactions being higher than the threshold and the second interaction occurs at a point of 15-20 c.u. far from the first one. So, the second interaction was mistaken as the first one of another hadron.

The existence of these cascades leads to overestimation of λ meas compared with λ prop, Monte-Carlo simulations were performed to eliminate the distortions of λ meas. The scheme of simulations used is presented in /5/. Energy E_0 of the primary protons inducing in a chamber nuclear-electromagnetic cascades was simulated with respect to the spectrum with the differential power index 3. The point of the first interaction in a chamber was computed with λ prop = 190 g/cm². Random stars imitating nuclear interaction were simulated according to /6/.

In the first version of simulations, the difference in inelastic interaction of incident hadron with protons and nuclei was neglected, leading particles being simulated in the x-presentation with respect to the inclusive spectrum from /7/, and the mean value $\langle K \rangle$ being equal to .5. In the second version of simulations, use was made of the data on the inclusive spectrum of leading particles obtained in terms of an additive quark model regarding the atomic number of the target-nucleus in /8/, the mean value being $\langle K \rangle = .8$. The electromagnetic cascades resulting from the decay of π^0 -meson for particles with energy $E_p > E_{thr}$ ($E_{thr} = .5 \cdot 10^{12}$ eV) were also Monte-Carlo simulated allowing for the processes of pair production, bremsstrahlung radiation, and Rutherford scattering. To obtain the electron number and

the optical density of X-ray film within a circle of given radius ($R=140 \text{ um}$) caused at an observation level by the initial gamma-rays and electrons (with energies $E_{\gamma} < E_{em}$) use was made of the averaged cascade curves calculated to the core approximation. Optical densities in X-ray film produced by simulated cascades at various depths in lead were processed by the same program as experimental ones /1/.

(2) For each version of calculations, ~ 1000 events with $E_{\gamma} \geq 4 \text{ TeV}$ and $8 \text{ c.u.} \leq \Delta t \leq 64 \text{ c.u.}$ were simulated. The λ_{meas} -values obtained for the two versions of calculations are listed in Table 1 together with the corresponding values of λ_{prop} deduced from the experimental values of λ_{meas} and from ratios of λ_{prop} and λ_{meas} obtained in different versions of calculations.

Table 1. Ratios of λ_{prop} and λ_{meas} obtained when analysing simulated cascades

	calculation		experiment	
	$\lambda_{\text{prop}} \text{ g/cm}^2$	$\lambda_{\text{meas}} \text{ g/cm}^2$	$\lambda_{\text{meas}} \text{ g/cm}^2$	$\lambda_{\text{prop}} \text{ g/cm}^2$
$\langle K \rangle = 0.5$	190	340 ± 30	207 ± 17	115 ± 22
$\langle K \rangle = 0.8$		230 ± 20		173 ± 39

The contribution of the pion component allowed for do not practically change the obtained ratios of λ_{meas} and λ_{prop} . In the energy region $\sim 200 \text{ GeV}$ an inelastic cross section σ_{inel} in the π -Pb-interaction is by a factor of 1.1-1.3 less than in the pPb-interaction that may lead to an increase in λ_{prop} for the total hadron flux by less than 5%. σ_{inel} of the pion and nucleon interactions on lead are expected to come closer with increasing energy/9/. $\langle K \rangle$ in the π Pb-interaction is larger than in the pPb-interaction, leading to a less diversity of λ_{meas} from λ_{prop} in the π Pb-interaction.

Experimental data obtained at accelerators and in cosmic rays for the hPb-interaction shows that up to energies of several TeV, an increase in $\sigma_{\text{inel}}^{\text{hPb}}$ within errors is absent and $\sigma_{\text{inel}}^{\text{hPb}} = 1800 \text{ mb}/10/$. For higher interaction energies, in /9/, using the Glauber model, the following values have been obtained: $\sigma_{\text{inel}}^{\text{pPb}} = 1900 \text{ mb}$ that corresponds to $\lambda_{\text{prop}}^{\text{pPb}} = 180 \text{ g/cm}^2$ and $\sigma_{\text{inel}}^{\pi\text{Pb}} = 1734 \text{ mb}$ that corresponds to $\lambda_{\text{prop}}^{\pi\text{Pb}} = 199 \text{ g/cm}^2$ for $E_0 = 20-100 \text{ TeV}$.

Thus, the experimental value $\lambda_{\text{meas}} = 207 \pm 17 \text{ g/cm}^2$ for the summary hadron flux is consistent with the expected value $\lambda_{\text{prop}}^{\text{hPb}} = 180 \text{ g/cm}^2$ for $E_0 \geq 20 \text{ TeV}$ for the total inelasticity coefficient $\langle K \rangle \sim .8$ only.

References

1. Bayburina S.G. et al. Trudy FIAN, 1984, v.154.
2. Borisov A.S. et al. Proc. of Intern. Symp. on Cosmic Rays and Particle Physics, Tokyo, 1984, 426-430.
3. Erlikin A.D., Kuzuna N.P., Preprint N 95 FIAN, 1980.

4. Bayburina S.A. et al. Proc. 18th ICRC, 1983, 7, 420-423.
5. Belyaev A.A. et al. EPC in cosmic rays at superhigh energies, Moscow, "Nauka", 1981.
6. Astafiev V.A. et al. Proc. 14th ICRC, 1975, 7, 2593.
7. Eilten et al., Nucl. Phys., B44, 333, 1972.
8. Anisovich V.V., Braun Yu.M., Shabelsky Yu.M., Yadernaya Fizika, 1984, 39, vyp.4, 934-946.
9. Jofa M.Z., Pukhov A.E., Yadernaya Fizika, 1985, 40, vyp. 7.
10. Garyaka A.P. et al. Izv. AN Arm. SSR, 78, vyp.1, 1983, 66-78.

THE METHOD FOR THE STUDY OF THE INELASTIC CROSS-SECTION FOR HIGH ENERGY PROTONS BY MEANS OF SHOWER ARRAYS WITH THE LARGE CALORIMETRIC AREA.

Danilova T.V., Erlykin A.D.

P.N. Lebedev Physical Institute, Leninski pr. 53,
Moscow, 117924, USSR.

Proton initiated showers could be reliably separated from showers initiated by cosmic ray nuclei by means of arrays with large calorimetric area, using distributions of energy fractions for EAS electromagnetic muon and hadron components. Proton initiated showers penetrate deeper into the atmosphere and have relatively lower energy fraction in muons. Distribution of that energy fraction is sensitive to the value of the proton inelastic cross-section. It is shown that the analysis of this distribution let one distinguish between $\log^2 S$ -rise and $\log S$ -rise of the cross-section at energies above 10^{15} eV.

Methods of the direct study of interactions stop working at energies above 10^{15} eV since intensities of primary particles and particles in the atmosphere are small at such energies. In connection with this future arrays for the study of interactions must be based on arbitrary methods, that is mainly on the study of EAS cores.

The absolute value and the energy dependence of hadron cross-sections determine the distribution of interaction points of hadrons in the atmosphere. This distribution determines the speed of the cascade development, if all other factors are identical. For the analysis of EAS detected at arrays with large calorimeter areas like ANI or AKENO it was proposed to use new classification parameters: the total energy of the shower E_0 or its energy at the observation level E_z /1/. Here $E_0 = E_{e\gamma} + E_h + E_{\mu\nu} + E_Q$ (1) for EAS where one succeeded to measure the Čerenkov light and by this way - the energy E_Q , lost by the shower in the atmosphere and $E_z = E_{e\gamma} + E_h + E_{\mu\nu}$ (2) for EAS without measurements of the Čerenkov light. Calorimeters with large areas let one measure rather accurately the energy carried by electromagnetic $E_{e\gamma}$ and hadron E_h components in every individual shower. The measure of the energy for the muon and neutrino component $E_{\mu\nu}$ is the total number of muons in the shower /1/.

In the paper / 1/ it was suggested to use the multidimensional analysis of tetrahedron and triangle diagrams - distributions of $E_{e\gamma}$, E_h , $E_{\mu\nu}$ and E_Q for the study of

primary mass composition. Such an analysis helps to analyse the cross-section behaviour too, since
 a) providing the good energy resolution it let better determine the energy of primary particles;
 b) among primary particles with the given energy it let reliably separate proton induced showers;
 c) the analysis of the shape of distributions $W(\delta_e, \delta_\mu, \delta_h)$ or $W(\Delta_e, \Delta_\mu, \Delta_h, \Delta_Q)$, where $\delta_i = E_i/E_z$, $\Delta_i = E_i/E_0$ in "proton" part of these diagrams is equivalent to the analysis of distributions for the speed of the cascade development of proton induced showers and finally, let one find the value of the cross-section at chosen energies.

Accuracy estimates for the energy determination of different EAS components at ANI array show that the shower energy at the observation level E_z will be measured with $\sim 11\%$ accuracy. In the fig.1 the distribution of E_0/\bar{E}_0 ratio is shown for showers selected by E_{700} classification parameter from 100 up to 316 TeV at the mountain level 700 g/cm² (full line) compared with similar distributions for showers selected by the total electron number N_e in the interval $(1 - 1,58) \cdot 10^5$ (dotted line) and the muon number $N_\mu (> 5 \text{ GeV})$ in the interval $(1-1.58) \cdot 10^3$ (dashed line). All distributions are obtained by means of the simulation program /2/ for EAS with zenith angles $\theta \leq 30^\circ$. Mass composition of primaries is similar to that at energies $\cdot 10^{11} \text{ eV}$ /2/. It is seen that the total shower energy E_0 may be determined by its energy at the observation level E_{700} with inaccuracy $\sim 19\%$. It is better, than in the case, when the primary energy is determined by N_e or N_μ , where the error is $\sim (37-38)\%$. In the combination with the error of E_{700} determination this distribution gives on the average $\sim 22\%$ error in the determination of E_0 at ANI array when energies of three EAS components are measured. Measurements of the fourth component E_Q let one reduce the error down to 8%.

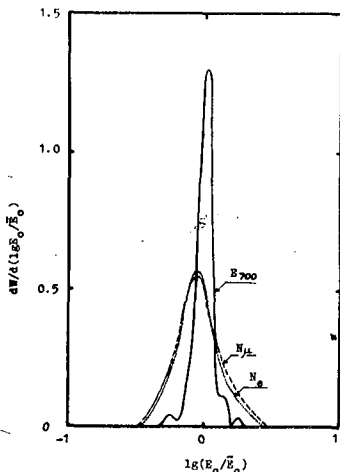


Fig. I.

The triangle diagram in the fig.2 demonstrates positions of gravity centres of $\delta_e, \delta_\mu, \delta_h$ distributions for primary particles of different masses, which induce showers with $E_{700} = 31.6 - 100 \text{ TeV}$ and $100-316 \text{ TeV}$. Here

stars indicate positions of gravity centres for mixed composition. It is seen that all centres are located at one trajectory. Their position is determined by the energy

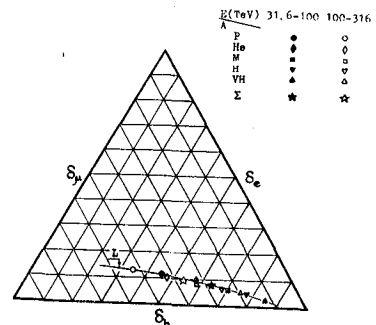


Fig. 2.

and the mass of the primary particle, i.e. depends in fact on the speed of the shower development. From this point of view the trajectory marked by the letter L may be called "the speed line".

Showers which develop faster are usually concentrated around points located at the right side of this line. In the left part on the average proton induced showers are concentrated which on the opposite, penetrate deeper into the atmosphere. The probability of such penetration and hence the $\delta_e, \delta_\mu, \delta_h$ -distribution depends on the magnitude of the cross-section. The value of δ_μ varies most quickly along "the speed line", therefore δ_μ -distribution in the left part of the triangle diagram must be most sensitive to the proton cross-section σ_{PA}^{prod} . The ideology of this method is similar to that suggested by Ellsworth et al. /3/ for σ_{PA}^{prod} determination by the distribution of shower maximum depth in the region of large depths, i.e. again by showers with slowest development.

The analysis of diagrams $W(\delta_e, \delta_\mu, \delta_h)$ for primary particles of different masses demonstrates that proton induced showers may be effectively selected from the mixture corresponding to the normal mixed composition, if to restrict the region by values $\delta_\mu = \bar{\delta}_\mu - (0.1 \div 0.15)$. For example, for $E_{700} = 100-316$ TeV $\bar{\delta}_\mu = 0,514$. The probability for the proton induced shower to hit the region $\delta_\mu < 0,35$ is 0,492, the same probability for helium induced shower is 0,155. For other primary nuclei it is 0. For the region

$\delta_\mu < 0,4$ these probabilities are $W_p = 0,647$; $W_{He} = 0,246$, $W_{M, H, VH} = 0$. Taking into account that protons in the ordinary mixed primary composition are about twice as abundant compared with helium nuclei, one can say that in the region $\delta_\mu < 0,35$ 86% of showers are proton induced and only 14% of them are helium induced. For $\delta_\mu < 0,4$ these values correspond to 83% and 17%.

Shower distributions for different values of σ_{PA}^{prod} and σ_{hA}^{prod} differ most strongly just in the extreme left region of δ_μ . In the fig.3 distributions $W(\delta_e, \delta_\mu, \delta_h)$ are shown for proton induced showers with $E_0 = (1-3,16) \cdot 10^{10}$ eV and for two versions: with logarithmic ($\sigma_{hA}^{prod} \sim \log S$) and maximum rising ($\sigma_{hA}^{prod} \sim \log^2 S$) cross-section. The quantitative analysis of these bilateral diagrams made by means of Kolmogorov criterium shows that in the region $\delta_\mu < 0.4$ these versions may be considered different with the probability to be wrong no more than 4%. At the same time the analysis of similar diagrams, calculated with constant or rising inelasticity does not reveal such a sensitivity.

In the fig.4 folded unilateral distributions $\Delta W / \Delta \delta_\mu$ are shown in the interval $\delta_\mu = 0-0,4$. Essential difference in the shape of these distributions confirms above mentioned expectations and let one hope for the practical realizability of this method.

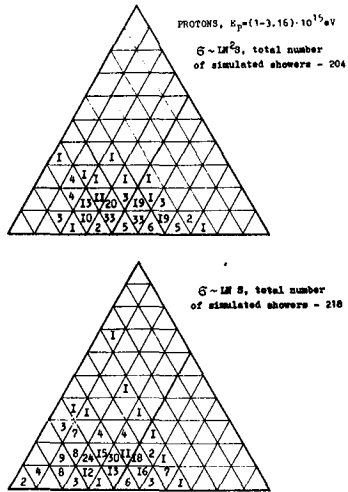


Fig. 3

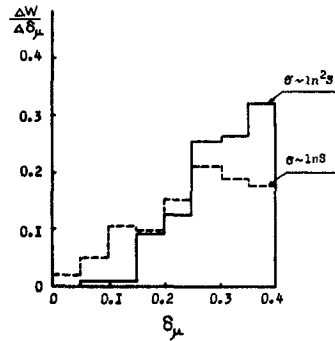


Fig. 4

References.

1. Danilova T.V., Erlykin A.D. 18 ICRC, 1983, Bangalore, 6, 262.
 Preprint FIAN N°155, 1982.
2. Danilova T.V. et al. 17 ICRC, 1981, Paris, 6, 146.
 Preprint FIAN N°14, 15, 1984.
3. Ellsworth R.W. et al. Phys. Rev. 1982, D26, 336

ON A POSSIBILITY OF INELASTICITY PARTIAL COEFFICIENT K_{γ}
 DETERMINATION IN πC AND πPb INTERACTIONS AT 10^{14} EV
 (EXPERIMENT "PAMIR" I)

Pamir Collaboration:

Borisov A.S., Cherdyntseva K.V., Guseva Z.M., Denisova V.G.,
 Dunaevsky A.M., Kanevskaya E.A., Maximenko V.M., Nam R.A.,
 Pashkov S.V., Puchkov V.S., Slavatinsky S.A., Zimin M.V.,
 Smirnova M.D., Smorodin Yu.A., Zelevinskaya N.G. and Zhdanov
 -P.N. Lebedev Physical Institute, Academy of Sciences of
 USSR, Moscow

Mukhammadshin R.A., Nedel'ko O.E., Nikolaeva L.P.,
 -Institute for Nuclear Research, Academy of Sciences of
 USSR, Moscow

Amineva T.P., Baradzei L.T., Ivanenko I.P., Iljina N.P.,
 Lazareva T., Managadze A.K., Mikhailova I.A., Murzina E.A.,
 Pomelova E.I., Popova E.G., Rakobolskaya I.V., Roganova T.M.,
 Ryabova N.G., Sveshnikova L.G.

-Institute of Nuclear Physics, Moscow University, Moscow
 Cananov S.D., Chadranyan E.Kh., Khisanishvili L.A., Ladarina N
 Leptukh G.G., Roinishvili N.N., Svanidze M.S.

-Institute of Physics, Georgian Academy of Sciences,
 Tbilisi

Asimov Z.A., Bobodjanov I.B., Gubar' N.E., Gulov Yu.A.,
 Normuratov F., Shoboronov Kh.

-Institute of Physics and Engineering, Tajik Academy of
 Sciences, Dushanbe

Azimov S.A., Khalilov D.A., Mulladjanov E.G., Nuritdinov Kh.,
 Talipov D.A., Yuldashbaev T.S.

-Institute of physics and Engineering, Uzbek. Academy of
 Sciences, Tashkent

Bakhtigireev S.E., Dobrotin N.A., Emeljanov Yu.A., Zaitseva E
 -Institute of High Energy Physics, Kazakh. Academy of
 Sciences, Alma-Ata

Bielawska H., Linke M., Malinowski J., Novicka A., Podgorzak,
 Tomaszewski A., Wlodarczyk Z., Wrotniak A.

-Institute of Physics, University of Lodz, Poland

and Sharvadze Z.SH.*, Institute of Physics, Georgian Academy
 of Sciences, Tbilisi

The investigation of hadron-nuclear interactions in
 "Pamir" experiment is carried out by means of X-ray emulsion
 chambers of two types: carbon (C) and lead (Pb) ones [1].

While comparing the results from the chambers of both
 types [2] it was found a discrepancy in $\langle n_h \rangle$ and $\langle E_h^{(0)} \rangle$
 values.

* This article only

Here $\langle n_h \rangle$ is an average hadron multiplicity normalized to one γ -h-family fitted the following selection criterion A: $\sum E_\gamma \geq 100$ Tev, $n_h \geq 0$, $E_h^{(v)} \geq 4$ Tev; $\langle E_h^{(v)} R \rangle$ is a space-energetic characteristics of hadrons in families fitted the criterion B: $\sum E_\gamma \geq 100$ Tev, $n_h > 3$, $E_h^{(v)} \geq 4$ Tev; $E_h^{(v)}$ is the energy registered in hadron block. n_h values are corrected on interaction probability in each chamber.

Tables I and II represent our experimental results, where ν and χ parameters defined as

$$\nu = \frac{\langle n_h \rangle_{Pb}}{\langle n_h \rangle_c} \quad (1) \quad ; \quad \chi = \frac{\langle E_h^{(v)} R \rangle_{Pb}}{\langle E_h^{(v)} R \rangle_c} \quad (2)$$

Table I

	N_{fam}	$\langle n_h \rangle$	$\beta - 1$
C	169	3.0 ± 0.2	1.0 ± 0.1
Pb	41	4.2 ± 0.3	1.1 ± 0.1
ν	-	1.4 ± 0.2	

Table II

	N_{fam}	$E_h^{(v)} R_{num}$
C	33	350 ± 30
Pb	22	455 ± 70
χ	-	1.3 ± 0.2

N_{fam} is a number of families in C and Pb chambers fitted the above mentioned criteria, $\beta - 1$ is a slope of integral energy spectrum of hadrons from families selected by A-criterion

In the present paper we connect the observed discrepancy between $\langle n_h \rangle$ and $\langle E_h^{(v)} R \rangle$ in C and Pb chambers with the difference in values of effective coefficients of energy transfer to the soft component K_{eff} for C and Pb chambers. The following considerations can be a ground of this suggestion:

1) It is known that a probability of hadron registration (in case of power like spectrum) is equal to $\langle K_\gamma^{\beta-1} \rangle$. Thus, the ratio of multiplicities

$$\nu = \frac{\langle n_h \rangle_{Pb}}{\langle n_h \rangle_c} = \frac{\langle K_\gamma^{\beta-1} \rangle_{Pb}}{\langle K_\gamma^{\beta-1} \rangle_c}$$

As $\beta - 1 \approx 1$ (see Table I) we have:

$$\nu = \langle K_\gamma \rangle_{Pb} / \langle K_\gamma \rangle_c \quad (3)$$

2) $\langle E_h^{(v)} R \rangle$ value can be written down as $\langle K_\gamma \rangle \langle E_h R \rangle$ (in case of K_γ independent of E_h). Hence: $\chi = \langle K_\gamma \rangle_{Pb} / \langle K_\gamma \rangle_c$ (4).

To test this considerations some simulations on nuclear electromagnetic cascades in the atmosphere were made on the basis of fireball scaling model (S-model) [3]. Hadrons passage through the chamber was imitated in the simulations. For each hadron the value of K_γ coefficient was found by means of $f(K_\gamma)$ distribution function taken in the form of $f(K_\gamma) \sim K_\gamma^\alpha \cdot \exp(-K_\gamma/\beta)$ [4]. The parameters α and β define the momenta of this distribution. Two series of simulation with various $\langle K_\gamma \rangle$ values were carried out. One of them with $\langle K_\gamma \rangle = 0.17$ imitated the situation in C-chamber, the other with $\langle K_\gamma \rangle = 0.30$ in Pb-chamber. The latter value is greater than

the real one in Pb-chamber, was chosen especially to emphasize the effects connected with K_γ variations. The ratio of simulation values of $\langle K_\gamma \rangle$ is equal to

$$\langle K_\gamma \rangle_{\text{Pb}} / \langle K_\gamma \rangle_{\text{C}} = 1.76 \quad (5)$$

A hadron was considered registered one in case of $E_h^\gamma = K_\gamma E_h \geq 4$ Tev.

For $\langle E_h^\gamma R \rangle$ determination we selected the families with number of registered hadrons $n_h > 3$. Table III represents the obtained results.

Table III

	N_{fam}	$E_h K$ Tev mm
C	126	285 ± 20
Pb	275	510 ± 15
χ		1,80 ± 0.1

Table IV

	N_{fam}	$\langle n \rangle$	$\beta - 1$
C	505	2.3 ± 0.1	0.9 ± 0.05
Pb	505	3.9 ± 0.1	1.0 ± 0.05
γ		1.7 ± 0.1	

As it is seen from Table III

$$\chi = \langle E_h^{(\gamma)} R \rangle_{\text{Pb}} / \langle E_h^{(\gamma)} R \rangle_{\text{C}} = 1.80 \pm 0.10 \quad (6)$$

and that is in good agreement with value (5).

The incoming to the installation hadron families with $n_h > 3$ and $\sum E_h \geq 250$ Tev were selected to calculate γ parametre. The last condition provides registration of the same events in both sets of simulation (in "both chambers").

Table IV represents the obtained values of mean multiplicities and energy spectra slope. γ value which is equal to 1.70 ± 0.10 is also in agreement with the given ratio of $\langle K_\gamma \rangle$ (5). Thus, the experimental estimation of χ and γ values in the two types of chambers gives an opportunity to get a ratio of $\langle K_\gamma \rangle$ coefficients for lead and carbon nuclei.

Returning to preliminary experimental evaluations of χ and γ parametres (Table 1) one can see that the coefficients ratio turned to be roughly equal to 1.2 ± 1.5 . This ratio corresponds to K_γ coefficients for pion-nuclear interactions as the majority of hadrons in families are π -mesons.

Experiments carried out in the low energy range yield that K_{π^0} partial inelastic coefficient dependence on atomic number of target nucleus is described as $K_{\pi^0} \sim A^\alpha$. Using this dependence and $\langle K_\gamma \rangle_{\text{Pb}} / \langle K_\gamma \rangle_{\text{C}}$ value we can estimate α -index at energy $\sim 10^4$ ev. Here we should bear in mind, that $K_\gamma^{\text{Pb}} \approx K_{\pi^0}^{\text{Pb}}$, while K_γ^{C} can considerably differ from $K_{\pi^0}^{\text{C}}$. However, it was shown in simulations [5] K_γ value in carbon chamber in $E_h^{(\gamma)}$ energy range from 3 up to 30 Tev is similar to K_{π^0} value in pion-nucleon interactions. In such case

$$\frac{\langle K_\gamma \rangle_{\text{Pb}}}{\langle K_\gamma \rangle_{\text{C}}} \approx A^{\alpha} \text{Pb} \quad \text{and} \quad \alpha \approx 0.06 \pm 0.02. \quad \text{This value is}$$

not in contradiction to α -measureings at lower energies

and confirms a possibility of the suggested method.

To determine α -value with 20% accuracy it is necessary to have approximately 100 families with $\sum E_{\gamma} \geq 100$ Tev in each chamber as well as to make precise simulations of connection between partial K_{π^0} and effective K_{γ} inelasticity coefficients in chambers of both types.

References

1. Trudy FIAN, v.154, 1984, (in Russian)
2. Pamir Collaboration. Proc. of International Symposium of Cosmic Rays and Particle Physics, Tokyo, P292, 1984
3. Wrotniak I.A. Zess.Nauk.Univers.Lodz, vol.60, p.73, 1977
4. Malinowski A. et.al. Pamir Coll. Workshop, p.49, UL, Lodz, 1980
5. Wlodarczyk Z. et.al. Proc. of International Symp. of Cosmic Rays and Particle Physics, Tokyo, p 451, 1984

SINGLE PARTICLE MOMENTUM AND ANGULAR DISTRIBUTIONS
IN HADRON-HADRON COLLISIONS AT ULTRAHIGH ENERGIES

T. T. Chou
Department of Physics
University of Georgia
Athens, GA 30602, USA

Chen Ning Yang
Institute for Theoretical Physics
State University of New York
Stony Brook, NY 11794, USA

1. Introduction. The forward-backward charged multiplicity distribution $P(n_F, n_B)$ of events in the 540 GeV $\bar{p}p$ collider has been extensively studied by the UA5 Collaboration. It was pointed out that the distribution with respect to $n = n_F + n_B$ satisfies approximate KNO scaling and that with respect to $Z = n_F - n_B$ is binomial [1]. The geometrical model of hadron-hadron collision interprets [2] the large multiplicity fluctuation as due to the widely different nature of collisions at different impact parameters b . For a single impact parameter b , the collision in the geometrical model should exhibit stochastic behavior. This separation of the stochastic and non-stochastic (KNO) aspects of multiparticle production processes gives conceptually a lucid and attractive picture of such collisions [3], leading to the concept of partition temperature T_P and the single particle momentum spectrum to be discussed in detail below.

2. Description of Model. Assuming the separation of stochastic from non-stochastic aspects of collision to remain valid as $n \rightarrow \infty$, we expect [1] that the distribution in the two-dimensional $(n_F/\bar{n}) - (n_B/\bar{n})$ plane would become more and more concentrated in a narrow region. For 540 GeV $\bar{p}p$ collisions this region is in the form of an ellipse as shown in Fig. 1(a). When \bar{n} becomes large, it becomes thinner and eventually collapses into a line segment (Fig. 1(b)). This line segment is a collection of points, at each of which $n_F \approx n_B$ and both n_F and n_B fluctuate only to the extent of $\sqrt{n_F}$ (i.e., like a stochastic distribution). For example; if $n = 2 \times 10^6$, then n_F could easily be as small as 0.5×10^6 or as large as 2×10^6 . But in either case, one can predict that $n_B \approx n_F$ with fractional

errors of the order $(\bar{n})^{-1/2} \sim 10^{-3}$.

Accepting this picture for very high energies, we see that for fixed n_F , the distribution of n_B is stochastic. How then is the energy partitioned in the backward hemisphere? We shall assume that the energy partition for each hemisphere for a fixed $z = (n_F + n_B)/\bar{n}$ is also stochastic but subject to a number of conditions: (a) that the total energy of all outgoing particles on each side is $E_0 h$, (b) Bloch-Nordsieck factor $d^3 p/E$ for each particle, and (c) transverse momentum (p_T) cutoff factor $g(p_T)$. In other words, the probability distribution for central particles on each side will be taken as

$$\delta(\sum_i E_i - E_0 h) \prod_i (d^3 p_i / E_i) g(p_{Ti}) \quad (1)$$

where $E_0 = \sqrt{s}/2$, $E_0(1-h)$ = total energy of all leading particles, and $i = 1, 2, \dots$ ranges over all the particles (positive, negative, and neutral) on one side minus the leading particles. h is a parameter that describes the fraction of E_0 that fragments into all particles in the central region.

Now the mathematical problem (1) is well-known in statistical mechanics as describing a microcanonical ensemble. By the well-known Darwin-Fowler method the single particle distribution of such an ensemble is given by the canonical ensemble:

$$dn = K (d^3 p/E) g(p_T) \exp(-E/T_p) \quad (2)$$

where T_p will be called the partition temperature and K is a normalization constant. Notice that all particles, positive, negative, and neutral, kaons, nucleons as well as pions, share the same T_p .

3. Comparison with Experimental Angular Distribution at 540 GeV. As Fig. 1(a) shows, at the 540 $\bar{p}p$ collider, the distribution is still an ellipse. We shall nevertheless test the validity of (2) at 540 GeV by evaluating the single particle angular distribution from it. We write

$$dn/d\eta = 2\pi K \sin^2 \theta \int_0^{E_0 h} p^2 (dp/E) g(p \sin \theta) \exp(-E/T_p) \quad (3)$$

where η = pseudo-rapidity, $\cosh \eta = \csc \theta$, and

$$g(p \sin \theta) = \exp(-\alpha p \sin \theta). \quad (4)$$

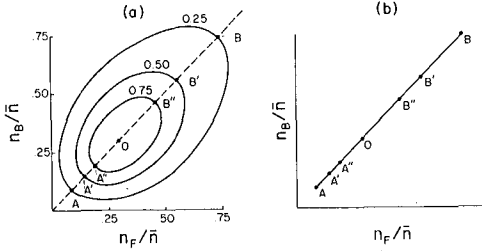


Fig. 1 Schematic diagram for forward-backward multiplicity distribution at very high energies. (a) The contour lines represent $P(n_F, n_B)$ at constant fractions of its maximum value at $\sqrt{s} = 540$ GeV where $\bar{n} \approx 29$. (b) The same contour lines degenerate to straight lines for extremely large \bar{n} .

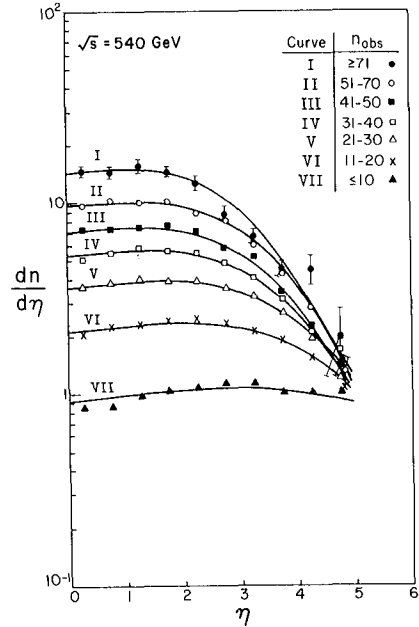


Fig. 2 Calculated and experimental $dn/d\eta$ vs. η at $\sqrt{s} = 540$ GeV.

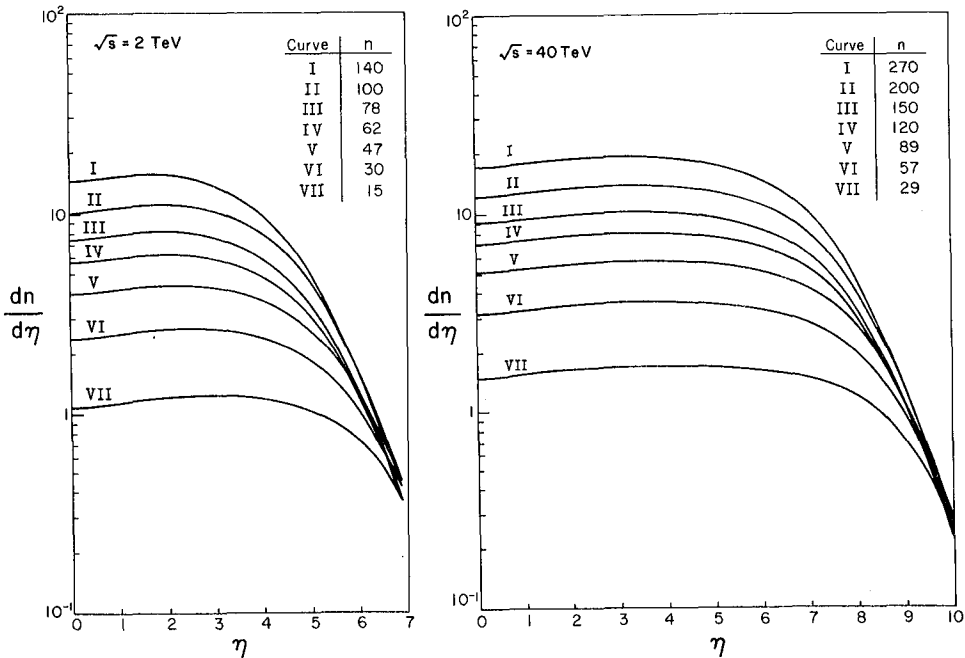


Fig. 3 Calculated $dn/d\eta$ versus η at $\sqrt{s} = 2$ TeV and 40 TeV.

We take α to be equal to $5.25(\text{GeV}/c)^{-1}$. Only pions are included in this calculation. The angular distribution is evaluated from (3) and compared with the results [4] of UA5 in Fig. 2. It is found that the UA5 curve for each multiplicity n is well fitted by (3) for one value of T_p . We emphasize that there are no adjustable parameters in this computation, the cutoff α having been taken from experiments [5] concerning p_T distributions. The parameter h and normalization constant K are both determined from the curves themselves.

We conclude that the angular distribution (3) that results from (2) is in excellent agreement with experiment. Furthermore, we believe (2) would give a complete description of the single particle momentum distribution for central particles.

4. Extrapolation to Higher Energies. We made extrapolations of the angular distribution to $\sqrt{s} = 2$ TeV (Tevatron) and 40 TeV (SSC). The assumptions made in these computations are as follows: (i) The values of α for these energies are taken to be 5.0 and 4.4 $(\text{GeV}/c)^{-1}$, respectively [5]. (ii) The parameter h is taken to be a function of the KNO variable $z = n/\bar{n}$ only. (iii) The values of \bar{n}_{ch} for these energies are taken to be 41 and 78, respectively, by extrapolation. The results are presented in Fig. 3.

5. Acknowledgments. This work is supported in part by the U.S. DOE Grant No. DE-FG09-84ER40160, and by the U.S. NSF Grant No. PHY 81-09110 A01.

References

1. T. T. Chou and C. N. Yang, Phys. Lett. 135B, 175 (1984).
2. T. T. Chou and C. N. Yang, Phys. Lett. 116B, 301 (1982).
3. T. T. Chou, C. N. Yang, and E. Yen, Phys. Rev. Lett. 54, 510 (1985).
4. J. G. Rushbrooke, in Proc. XIV Int. Symp. Multiparticle Dynamics, Lake Tahoe, 1983, edited by J. F. Gunion and P. M. Yager (World Scientific, 1984).
5. J. G. Rushbrooke, in Proc. DPF Workshop on $\bar{p}p$ Options for the Supercollider, Chicago, 1984.

QCD-MOTIVATED DESCRIPTION OF VERY HIGH ENERGY*
PARTICLE INTERACTIONS

T. K. Gaisser
Bartol Research Foundation
University of Delaware
Newark, DE 19716

F. Halzen
Physics Department
University of Wisconsin
Madison, WI 53706

ABSTRACT

Cross sections for the production of secondaries with large transverse momentum can become comparable to the total cross section in the TeV energy range. We argue that the onset of this effect is observed at sub-TeV energies via (i) an increase of the rapidity distribution near $y = 0$, (ii) an increase of $\langle p_T \rangle$ with energy and, most directly, via (iii) a correlation between $\langle p_T \rangle$ and multiplicity. If indeed scaling violations are associated with the hard scattering of partons, then scaling violations are largely confined to the central region and have little effect on cosmic ray data which are sensitive to the forward fragmentation region.

Recent $p\bar{p}$ -collider experiments confirmed the observation by the Brazil-Japan emulsion group that the average transverse momentum of secondaries is larger in events with high multiplicity,¹ see Fig. 1. QCD allows for a straightforward interpretation¹ of this observation: large p_T results from hard scattering of partons, and hard scattering is accompanied by abundant gluon radiation resulting in an increased multiplicity. This effect is most dramatically observed in hard quark + antiquark \rightarrow weak boson events where the hadronic activity accompanying W,Z is larger² than that in average minimum bias events despite the fact that roughly 1/5 of the c.m. energy $\sqrt{s} = 0.54$ TeV is taken away by the W or Z mass. This interpretation of the $\langle p_T \rangle$ -multiplicity correlation received further confirmation by the recent observation³ that high multiplicity events indeed show jet-like final state structure. A large fraction of them contained at least one identified jet with $p_T \geq 5$ GeV. Although the QCD origin of large p_T jets has been quantitatively verified we are here discussing events where the "large" p_T is not much larger than $\langle p_T \rangle$ and perturbative calculations are difficult. We discuss this next.

Perturbative calculations of jet cross sections are made possible by the fact that hadrons interact over a distance scale $O(1/p_T)$ which is small. The hadrons interact via a single quark or gluon in each hadron. When p_T becomes small many relative soft constituents are stacked in the interacting hadrons and therefore multiple parton-parton interactions become likely in a single hadron-hadron collision. Perturbation theory breaks down; e.g. for the SSC energy $\sqrt{s} = 40$ TeV we estimate following Ref. 4 that the cross section for double parton-parton interactions is $100 \sim 200$ mb for $p_T \geq 6$ GeV. This is roughly

equal to the conventional single hard scattering cross section for $p_T \geq 6$ GeV as we will see further on. Conversely one might actually hope that naive perturbation theory yields reliable results for p_T -values as low as 5 - 10 GeV which corresponds to $x (= p_T/\sqrt{s}) \approx 10^{-3}$ at $\sqrt{s} = 40$ TeV!

Using perturbative QCD jet calculations down to $x \approx 10^{-3}$ we have made a toy model of hadronic interactions at all energies and all p_T . The basic idea is to integrate the perturbative QCD expressions for hard scattering of constituents down to an energy-dependent $p_{T \text{ min}}$ defined by

$$\sigma_{\text{tot}} = \sigma_0 + \sigma_{\text{jet}}(p_{T \text{ min}}), \quad (1)$$

where

$$\sigma_{\text{jet}}(p_{T \text{ min}}) = \iiint_{p_{T \text{ min}}} F(x_1)F(x_2)\sigma(\theta). \quad (2)$$

$F(x_i)$ are the probabilities for finding constituents with fractional momenta x_i in the incident hadrons and $\sigma(\theta)$ is the elementary cross section for scattering of constituents to angle θ defined in the parton-parton c.m. system. Unlike the calculation of Ding, et al.⁵ we have no cutoff in θ except that required by $p_T > p_{T \text{ min}}$. The factorization displayed in Eq. (2) is an approximate result suitable for practical calculations. σ_0 represents the soft hadronic cross section and further results will depend on assumptions regarding its magnitude and energy dependence. For illustration we assume $\sigma_0 = 38$ mb at all energies. Table I shows values of σ_{jet} , $p_{T \text{ min}}$ and mean values of Feynman x and rapidity of the scattered jet obtained from Eqs. (1, 2). For details of the calculation see Ref. 1. The values of $p_{T \text{ min}}$ have been adjusted so that Eq. (1) reproduces the total cross section data shown in Fig. 2. Our calculation also reproduces the p_T -distribution measured at the $p\bar{p}$ collider, see Fig. 3.

Because of the large cross sections involved, such semihard processes can be expected to produce dramatic effects at high energy. Figure 4 illustrates the expected energy dependence of the rapidity distribution at various energies of interest. We have assumed that beam fragments in hard collisions produce rapidity distributions of secondary pions as in soft collisions, with two charged particles per unit of rapidity. The scattered jets are assumed to produce rapidity distributions of the same shape as beam fragments at the kinematic limits, and also with an asymptotic density of two charged particles per unit of rapidity. In the absence of significant scaling violation effects in the fragmentation functions, we would predict an asymptotic rapidity density of four charged particles.

By energy conservation one expects a violation of scaling in the fragmentation region as the central component grows with energy. The magnitude of this effect can be estimated from the values of $\langle x_{\text{jet}} \rangle$ tabulated above. At high energies, where semihard scattering events represent a significant fraction of the cross section, $\langle x_{\text{jet}} \rangle \approx 0.05$ so we expect fragmentation region scaling violation only at the level of 5%. This is a smaller effect than suggested in Ref. 5.

We therefore conclude that if the association between hard scattering and increasing cross section described here is qualitatively correct, then scaling violations should have little effect on the behavior of the electromagnetic component of cosmic ray cascades because these depend primarily on the fragmentation region. In particular, use of scaling-type models to interpret the Fly's Eye experiment should be essentially correct. A non-trivial result of the calculation that increases our confidence in the correctness of the association between growing cross section and hard scattering is represented by the last column of Table I. The jet rapidities that come out of the QCD calculation are such that the excess rapidity density from the scattered jets joins smoothly onto the underlying rapidity plateau from beam fragments. The Gaussian-type rapidity distribution observed at $\sqrt{s} = 540$ GeV is thus naturally reproduced.

REFERENCES

1. For a detailed discussion and further references see T. K. Gaisser and F. Halzen, *Phys. Rev. Lett.* 54, 1754 (1985) and Proceedings of the Aspen Winter Physics Conference (1985).
2. F. Halzen in Multiparticle Dynamics 1984, World Scientific, G. Gustafson and C. Peterson (editors).
3. G. Ciapetti, Proceedings of the pp Collider Workshop, Aosta, Italy (1985).
4. B. Humpert and R. Odorico, *Phys. Lett.* 154B, 211 (1985).
5. L. K. Ding, et al., ICR Report 107-83-1, Tokyo (1983).

ACKNOWLEDGEMENTS

We thank A. Mueller for discussions.

TABLE I. Properties of jet cross sections with $p_T > p_{T \text{ min}}$ at different energies.

E (TeV)	\sqrt{s} (GeV)	$p_{T \text{ min}}$ (GeV)	σ_{jet} (mb)	$\langle x \rangle_{\text{jet}}$	$\langle y \rangle_{\text{jet}}$
1	43.	1.25	4	0.17	1.8
150	540.	2	26	0.07	2.9
10^4	4330.	3.2	63	0.05	4.2
10^6	43300.	6	127	0.05	5.9

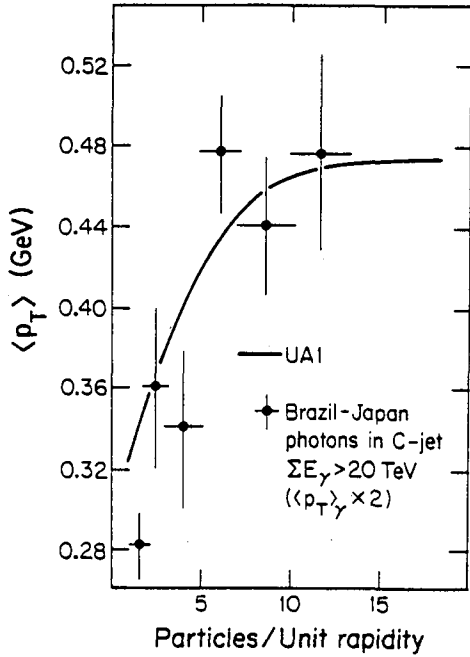


FIGURE 1. Increase of $\langle p_T \rangle$ associated with increasing multiplicity.

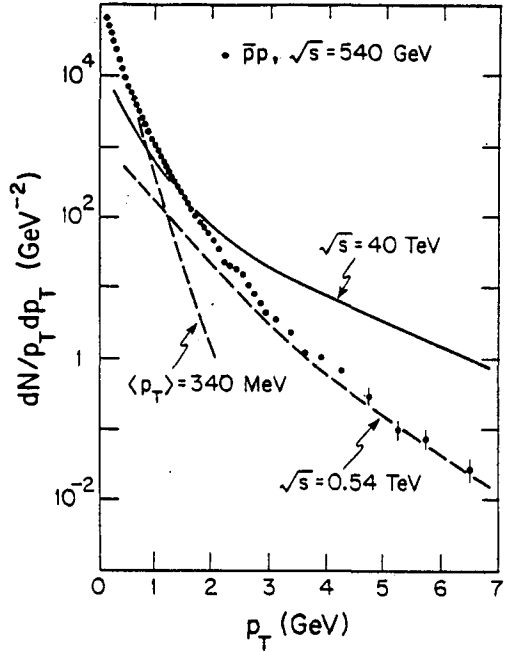


FIGURE 3. Two-component description of the charged particle transverse momentum distribution. The low- p_T component is described by an exponential fall-off with $\langle p_T \rangle = 340 \text{ MeV}$. The "high"- p_T component corresponds to hadrons which are the fragments of parton jets with $p_T > p_{T \text{ min}}$ chosen as in Table I. Data from the UA1 experiment.

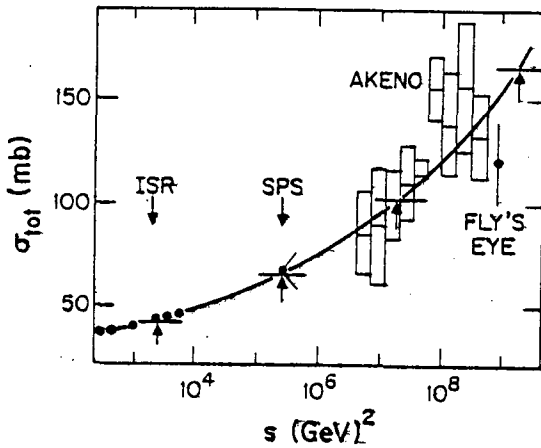


FIGURE 2. The increasing cross section associated with jets of moderate transverse momentum.

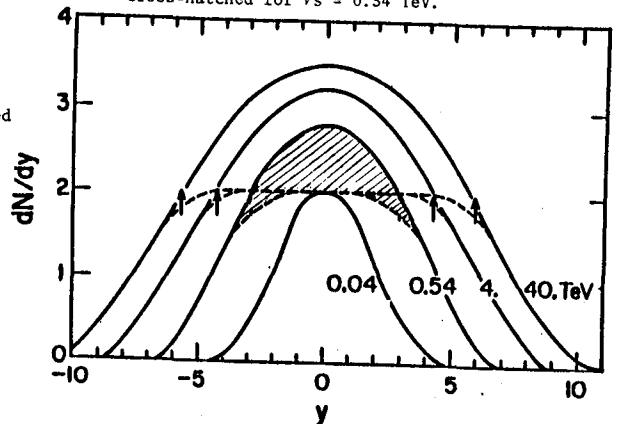


FIGURE 4. Sketch of the two-component rapidity distribution corresponding to the two-component total cross section shown in Fig. 2. At each energy the rapidity distribution consists of a plateau on which is superimposed the excess of hadrons near $y = 0$ due to fragmentation of the scattered jets. Rapidities of the scattered jets are indicated by arrows. The excess is cross-hatched for $\sqrt{s} = 0.54 \text{ TeV}$.

EMPIRICAL DESCRIPTION OF THE HADRON - HADRON AND HADRON -
NUCLEUS INTERACTION AT THE ACCELERATOR ENERGY RANGE

G. Kubiak, J. Szabelski, J. Wdowczyk

Institute of Nuclear Science and Technology,
90-950 Lodz, ul Uniwersytecka 5, Box 447, Poland

J. Kempa and A. Piotrowska

Department of Physics, University of Lodz,
90-236 Lodz, ul Nowotki 149-153, Poland

1. INTRODUCTION

It has been demonstrated by Wdowczyk and Wolfendale (1984) that the energy spectrum of the secondary pions produced in p - p interactions with energies up to a few times 10^{14} eV can be described well by a scaling violation formula of the form

$$P(E_{\pi}) = (E_0/205)^{\alpha} q((E_{\pi}/E_0) (E_0/205)^{\alpha}) \frac{k(E_0, 205)}{E_{\pi}}, \quad (1)$$

where the parameter α , which is a measure of the scaling violation, is gradually increasing with energy. The coefficient $k(E_0, 205) = K_{\pi}(E_0)/K(205)$ describes the variation of inelasticity coefficient for charged pion production.

The energy spectra of the others secondary particles can be obtained by similar transformations.

For purpose of numerical calculations the function $q(x)$ is usually taken from Fermilab data at 205 GeV and approximated by the following formula (for $\pi^+ + \pi^-$)

$$q(x) = .692(1-x)^{7.4} \exp(2.185x) + .807(1-x)^{6.2} \exp(2.968x), \quad (2)$$

which is obtained by integration over p_t of the more general expression fitting simultaneously the x_t and p_t variation for the same Fermilab data at 205 GeV (Kafka et al 1977). The expression has the form

$$q(x, p_t) = 9.524(1-x)^{6.2} \exp(-5.963 p_t^2 \exp(-2.968x)) + 8.744(1-x)^{7.4} \exp(-6.318 p_t^2 \exp(-2.185x)) \quad (3)$$

As a reasonable choice for α and k_{π} variation it is taken $\alpha = .815((E_0/205)^{0.135} - 1) \ln(E_0/205)$, for $E_0 \leq 7.7 \cdot 10^4$ GeV
 $\alpha = .072 + .0163 \ln(E_0/205)$, for $E_0 > 7.7 \cdot 10^4$ GeV. (4)

$$k_{\pi\text{tot}}(E_0, 205) = (E_0/205)^{-0.042}, \quad k_{\pi^\pm}(E_0, 205) = (E_0/205)^{-0.061} \quad (5)$$

It is also assumed that formula (1) and (2) can be used for describing the energy spectra of kaons and baryons (antibaryons). All those are taken together but relative role of baryons and antibaryons increases with primary energy according to the expression

$$F = 1 - .77(E_0/205)^{-0.043} \quad (6)$$

It is assumed that the average energy of kaons and baryons (antibaryons) increases with energy faster than that of pions and the relative inelasticity coefficient for production of those also increases with energy. The expression giving the ratio of the particles average energy and their inelasticity coefficient to those of pions are respectively

$$b = .45 + .253 \ln \sqrt{E_0}, \quad R = 1.81 - 1.5(E_0/205)^{-0.042} \quad (7)$$

The interactions of mesons with protons are also assumed to be described by the same expressions except that the total inelasticity coefficient is taken to be 0.6 instead of 0.5 with total multiplicity the same and average energy increased by factor of 1.2 .

Taking into account all these assumptions formula (1) is transformed into the following expressions for kaon and baryon plus antibaryon production in proton interaction and for pion production in pion interactions

$$P(E) = (E_0/205)^\alpha q((E/b/E_0)(E_0/205)^\alpha) \frac{R}{E} \quad (8)$$

$$P(E) = (E_0/205)^\alpha q((r/1.2/E_0)(E_0/205)^\alpha) \frac{k(E_0, 205)}{E} \quad (9)$$

Combining both formulae we can obtain expression for the spectrum of kaons and baryons plus antibaryons produced in the meson interactions.

2. APPROXIMATE FORMULAE FOR INTERACTIONS WITH AIR NUCLEI

For analysis of the cosmic ray propagation in the atmosphere in actual fact, instead of the formulae for interactions of protons and mesons with protons, we have to use formulae appropriate for interactions with air nuclei. Using the method outlined among others by Elias et al (1980) we have introduced simple corrections to the above given expressions to account for the fact that target is an air nucleus.

Similarly as Elias et al (1980) we have assumed that an interaction of hadron with nucleus is an superposition of subsequent interactions of leading nucleon. The nucleon interacting with nucleus is assumed to undergo with certain probabilities one, two or more interactions with nucleons in the nucl-

eus. The probabilities for the number of interactions used by us are given in the table I. The energy spectrum of the secondaries and the inelasticity coefficient distribution the case of one interaction are the same as for interactions with protons. When the number of interactions is higher those distributions are obtained by summing the contribution from subsequent interactions.

$$P_n(E, E_0) = P_{pp}(E, E_0) + \sum_1^n P_{pp}(E, E_0(1-K_1)(1-K_2)\cdots(1-K_i)), \quad (10)$$

where K_i is the inelasticity coefficient in the i - th subsequent interaction.

In similar way the inelasticity coefficient for p-nucleus interaction can be obtained. Overall spectra of secondary particles can be easily obtained adding the contributions from various number of interactions with probabilities given in table I. The distribution of the inelasticity coefficient for pA collision can be obtained by Monte Carlo allowing the subsequent inelasticities in p-nucleon interactions to fluctuate according to the assumed fluctuations of the inelasticity coefficient in pp interactions.

Table I

Probability of an incident proton having n collision within a carbon nucleus

n	1	2	3	4	5
P_n	.511	.301	.131	.044	.013

Detailed calculations showed that the obtained energy spectra of the secondaries can be well represented by very simple modification of the expression (1) and also the expressions (8) and (9). The modified formula (1) becomes

$$P(E_\pi) = (FC)^{1.5} (E_0/205) q((E_\pi/E_0)(E_0/205) FC^{.5}) \frac{k(E_0, 205)}{E_\pi}. \quad (11)$$

$FC = 1.32$

The inelasticity coefficient distribution calculated by the outlined above method is consistent with an expression which we have developed (Kempa and Wdowczyk 1985) on the basis of experimental data compiled by Jones (1983).

The expression is

$$P(K) = 1.9 \exp(-2(1-K)), \text{ for } K \gg .1 \text{ and } P(K) = \sqrt{K}, \text{ for } K < .1 .$$

Kempa and Wdowczyk (1985) gives also additional expression for the quasielastic interactions but those practically can be neglected here. In spite of the fact that they give almost 20% of the total cross - section their contribution to the flux of secondaries is negligible. Their role practically amounts to an increase of the effective mean free path by a factor of 1.2

Predictions based on the formula (11) are compared with data of Elias et al (1980) in figure 1 where the distributions of pseudorapidities are given for various assumptions about relation of between p_{tpA} and p_{tpp} . It seems that the best value is obtained if we take

$$\langle p_{tpA} \rangle = 1.15 \langle p_{tpp} \rangle .$$

The above described picture of hadron-hadron interaction have been used in our calculations of cosmic ray propagation in the atmosphere presented elsewhere in this proceedings.

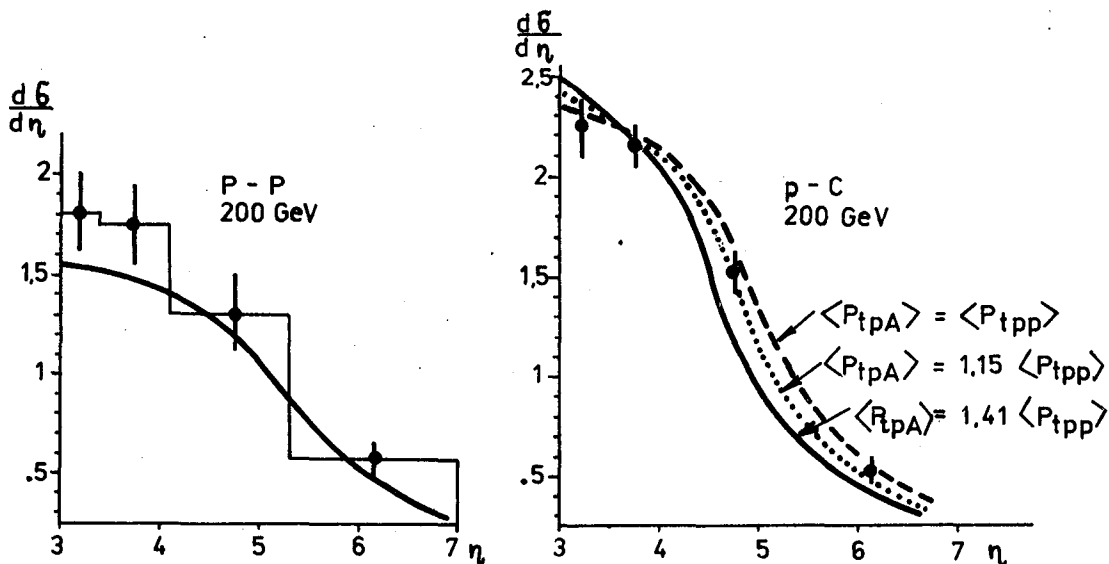


Figure 1

REFERENCES

- Elias J E et al 1980 Phys.Rev.D, p.13
 Jones L W 1983 18th ICRC, Bangalore, 5, p.17
 Kafka T et al 1977 Phys.Rev.D, 16, p.1261
 Kempa J and Wdowczyk J 1985 Presented to the 1st Symposium on
 Underground Physics, Italy, Saint-Vincent, 25 - 28 April
 Wdowczyk J and Wolfendale AW 1984 J.Phys.G:Nucl.Phys.10, p.257

MULTIPLICITY DISTRIBUTIONS IN INTERACTION MODELS
USED FOR CASCADE SIMULATIONS

by

R. W. Ellsworth
Department of Physics
George Mason University
Fairfax, VA 22030T. K. Gaisser and Todor Stanev
Bartol Research Foundation of the Franklin Institute
University of Delaware
Newark DE 19716A b s t r a c t

In cascade simulations, conservation of energy is of paramount importance. We point out that it is possible to construct algorithms in which energies of secondaries are chosen from physically correct distributions in such a way as to conserve energy, and give physically correct multiplicity distributions without further adjustment. The resulting non-Poissonian nature of the distribution and the approximate KNO^k scaling are related to the large fluctuations in the energy available for pion production and to the detailed shape of the inclusive momentum distribution.

We describe two multiparticle production algorithms which have these features. One is the algorithm used in the simulation of C-jets²; the other is for a hadron-nucleus interaction model used in the calculation of muon and neutrino fluxes^{3,4}.

References

1. Z.Koba, H.B.Nielsen and P.Olesen, Nucl Phys B40, 317 (1972)
2. R.W.Ellsworth, T.K.Gaisser and G.B.Yodh, Phys Rev D23, 764 (1981)
3. T.K.Gaisser and Todor Stanev, NIM A235, 183 (1985).
4. T.K.Gaisser et al., Phys Rev Lett 51, 223 (1983).

SOME REMARKS ABOUT SIMULATION OF COSMIC RAY PHENOMENA
WITH USE OF NUCLEAR INTERACTION MODELS BASED ON THE
CURRENT SPS PROTON-ANTIPROTON DATA

J.A.Wrotniak(*) and G.B.Yodh

Department of Physics and Astronomy
University of Maryland
College Park, MD 20742, U.S.A.

We demonstrate, that claims about "models based on SPS collider particle distributions" do not unambiguously predict properties of EAS generated by Monte Carlo simulation.

One of the main difficulties in interpreting extensive air shower data to derive the properties of particle production in the elementary act is that the data available at the highest accelerator energies (SPS proton-antiproton collider) do not include the features of interaction most essential in air shower propagation (e.g. x -distributions).

Therefore, one could think of different models of particle production, each of them adequately fitting the measured pseudo-rapidity distributions at SPS $p\bar{p}$ energies, but possessing different properties in other variable, for example the \bar{d} distributions in x .

In addition to this x - y ambiguity, there are some other degrees of freedom in utilizing the collider data in a phenomenological model of nuclear interaction:

- * distribution in inelasticity,
- * the fact that nucleon-air and (especially) meson-air interactions may differ from nucleon-nucleon interaction,
- * the extrapolation of scaling violation at interaction energies above 155 TeV.

(*) On leave from Łódź University, Poland.

(**) Work supported in part by the U.S.National Science Foundation under Grant No. PHY 82-07425 .

However, in this study we will limit ourselves just to the x-y controversy, introducing models with as many features (except for x- and y-distributions) in common, as possible; to avoid the extrapolation problem, we consider only primary energies of 500 TeV (2*485 GeV in the CMS).

To prove our point, we have performed Monte Carlo simulations of EAS generated by 500 TeV vertical primary protons; four different nuclear interaction models were used. Two of them are described elsewhere in this volume [1] (also, a detailed writeup of models and the general simulation scheme in which they were immersed is available [3]); here we will only name them:

- @ Model M-Y00 - with inclusive x- and y-distributions behaving in a "scaling" way (except for the rise in the total inelastic cross-sections, see below),
- @ Model M-F00 - at and below ISR energies (1 TeV in Lab) exactly equivalent to the above, then gradually changing to provide the distributions in rapidity at 155 TeV as given by SPS p \bar{p} [4]. This was achieved by gradual decrease in the "scale unit" in x-distributions of produced secondaries (see [1]), as interaction energy increases.

In addition to this pair, we modified the M-Y00 model by removing secondaries at x around and above 0.1 (this energy was used for production of low-x particles, to keep the inelasticity distribution unchanged). The probability of this removal was changed logarithmically between 0 at 1 TeV and 1 at 100 TeV. The resulting rapidity distribution at 150 TeV is much closer to that for M-F00 than for M-Y00. Thus, one could say that - at least as far as the rapidity distributions are considered - the modification resulted in

- @ Model M-T00 (T standing for "truncated"), together with M-F00 reasonably well describing the rapidity distributions at ISR and SPS p \bar{p} energies.

To check the effect of charge exchange (about which we know nothing from the collider data, either), a modification of M-T00 was introduced:

- @ Model M-T01 - similar to M-T00, but 1/3 of interacting charged pions may emerge from the collision as pi-zeros.

Except for the differences mentioned above, all remaining simulation assumptions (including mean free paths and inelasticity) were the same for four models [1,3].

The x- and y-distributions for our four models at 1.5 TeV (ISR) and at 150 TeV (SPS p \bar{p}) are shown in Figs.1 and 2. At 1 TeV the distributions for all of them are exactly the same.

(Rapidity for M-Y00 at 150 TeV, not shown, behaves just like it should).

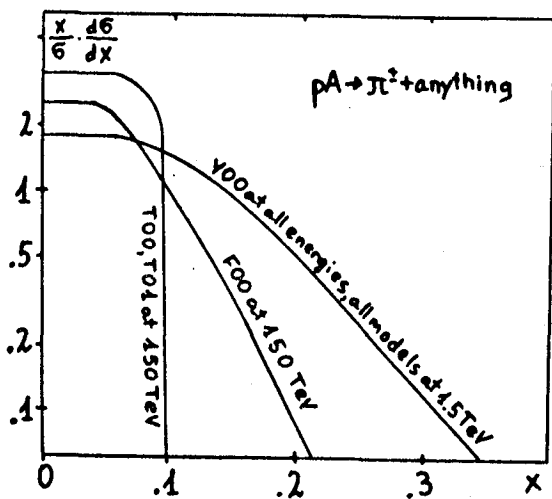


Fig.1 The distributions in x (in high energy approximation: $E/E[\text{inter}]$) for four models used in our study.

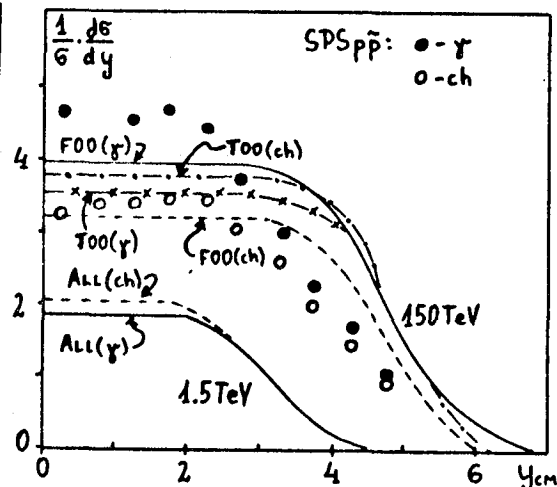


Fig.2 The distributions in rapidity for our models compared with the SPS $p\bar{p}$ data [4] on pseudorapidity.

We are limiting the scope of this paper only to demonstration of the validity of the statement made in the abstract above; more detailed and systematic study of extensive air showers for a variety of models (including two of these) is presented by us in another contribution to this Conference [1,2].

The Table below presents a brief sample of Monte Carlo results for extensive air showers predicted by our four models (numbers in brackets denote mean square statistical errors in last decimal digit units).

Model :		M-Y00	M-T00	M-T01	M-F00
N_e at maximum		$288(3) \cdot 10^3$	$284(3) \cdot 10^3$	$316(4) \cdot 10^3$	$310(3) \cdot 10^3$
at 1000 g/cm ²	N_e	$80(3) \cdot 10^3$	$61(3) \cdot 10^3$	$75(4) \cdot 10^3$	$64(3) \cdot 10^3$
	$N_\mu (> 2 \text{ GeV})$	$6.5(1) \cdot 10^3$	$7.1(1) \cdot 10^3$	$5.0(1) \cdot 10^3$	$6.1(1) \cdot 10^3$
	$N_\mu (> .2 \text{ TeV})$	30(1)	36(1)	31(1)	32(1)
	$N_h (> 2 \text{ GeV})$	237(11)	194(9)	109(9)	168(8)
	$N_h (> .2 \text{ TeV})$	12.3(4)	9.7(4)	6.4(3)	7.9(4)

One can notice, that the average shower size at maximum for M-T00 is basically the same as for M-Y00 (and not for M-F00, in spite of the similarity in rapidity distributions), the transfer of energy into the electromagnetic component had to be speeded up by charge exchange (M-T01) for maximum to reach the M-F00 level. The situation at 1000 g/cm^2 is just reversed. The increase in number of low-energy muons for M-T00 may be understood easily, though for high-energy ones it is not so obvious. For hadrons M-T00 gives results half way between M-Y00 and M-F00. Hadrons are affected to a greater degree than muons by introduction of charge exchange.

Therefore, statements about "models fitting the SPSpp data" may be often misleading; as the comparison of M-F00 and M-T00 shows, the shape of rapidity distribution (especially with the smallest angles excluded from the collider data) does not determine the interaction features most relevant to EAS development (and lack of information on inelasticity and on meson-nucleus interactions makes situation significantly worse).

Such statements may lead to a false belief, that one knows, what to expect from a nuclear interaction at a few hundred TeV, so (this factor fixed) the extensive air showers supply us with unequivocal information on other subjects: inelastic free path, primary composition. This is clearly not the case; air showers still remain one of basic information sources on the multiple production phenomenology in this energy region.

References

1. J.A.Wrotniak and G.B.Yodh; HE 4.1-7 in this volume
2. J.A.Wrotniak and G.B.Yodh; HE 4.1-2 in this volume
3. J.A.Wrotniak; SHOWERSIM/84, Univ.Md.Rep. PP 85-191 [1985]
4. N.Yamdagni; Workshop on Very High Energy Cosmic Ray Interactions, Univ.of Philadelphia, 36 [1982]

LOW P_T HADRON-NUCLEUS INTERACTIONS

R. Hołyński and K. Woźniak

Institute of Nuclear Physics,
Kawiorzy 26 A, 30-055 Kraków, Poland.

Introduction. We are discussing the possibility of describing hadron-nucleus (hA) interactions in terms of a number of independent collisions of the projectile inside the target nucleus. This multiple rescattering may occur on a particle or quark-parton level. To investigate the characteristics of hA interactions as a function of $\bar{\nu}$ we are taking advantage of the correlation between the average number $\bar{\nu}$ of collisions of the projectile inside the nucleus and the number N_g of fast protons ejected from the struck nucleus. We shall use the relation $\bar{\nu}$ vs N_g obtained in [1] (see Fig. 1). For a given target nucleus this allows us to select interactions occurring at different impact parameters.

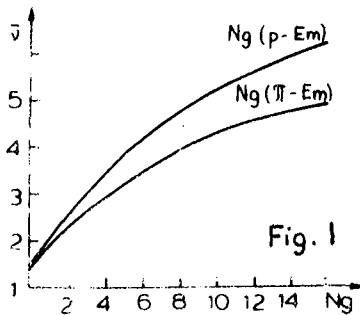


Fig. 1

For a given energy the events were binned in five N_g -groups which correspond to the different $\bar{\nu}$. Details are given in Table 2.

Experimental material. Our data consist of more than eight thousand interactions of negative pions and protons with emulsion nuclei (see Table 1).

Table 1.

π^- -Emulsion		p-Emulsion	
E_0 (GeV)	# of events	E_0 (GeV)	# of events
60	789	67	1183
200	973	200	2595
300	2115	400	853

Table 2.

N_g - interval	0	1	2-3	4-8	9-15
$\overline{N_g}$ (π^- -Em)	0	1	2.40	5.40	10.6
$\bar{\nu}$ (π^- -Em)	1.39	1.82	2.42	3.30	4.40
$\overline{N_g}$ (p-Em)	0	1	2.40	5.52	10.9
$\bar{\nu}$ (p-Em)	1.44	1.97	2.71	3.98	5.40

Thus for fixed target, by choosing events characterized by a given number of fast protons N_g , we have the possibility to investigate the characteristics of hA interactions in significantly greater interval of $\bar{\nu}$ than that, achieved by varying the atomic number of target nucleus. In the latter method by changing targets from hydrogen to uranium we get following $\bar{\nu}$ variation range: $1 \leq \bar{\nu} \leq 4$ and $1 \leq \bar{\nu} \leq 3$ for proton and pion induced reactions respectively.

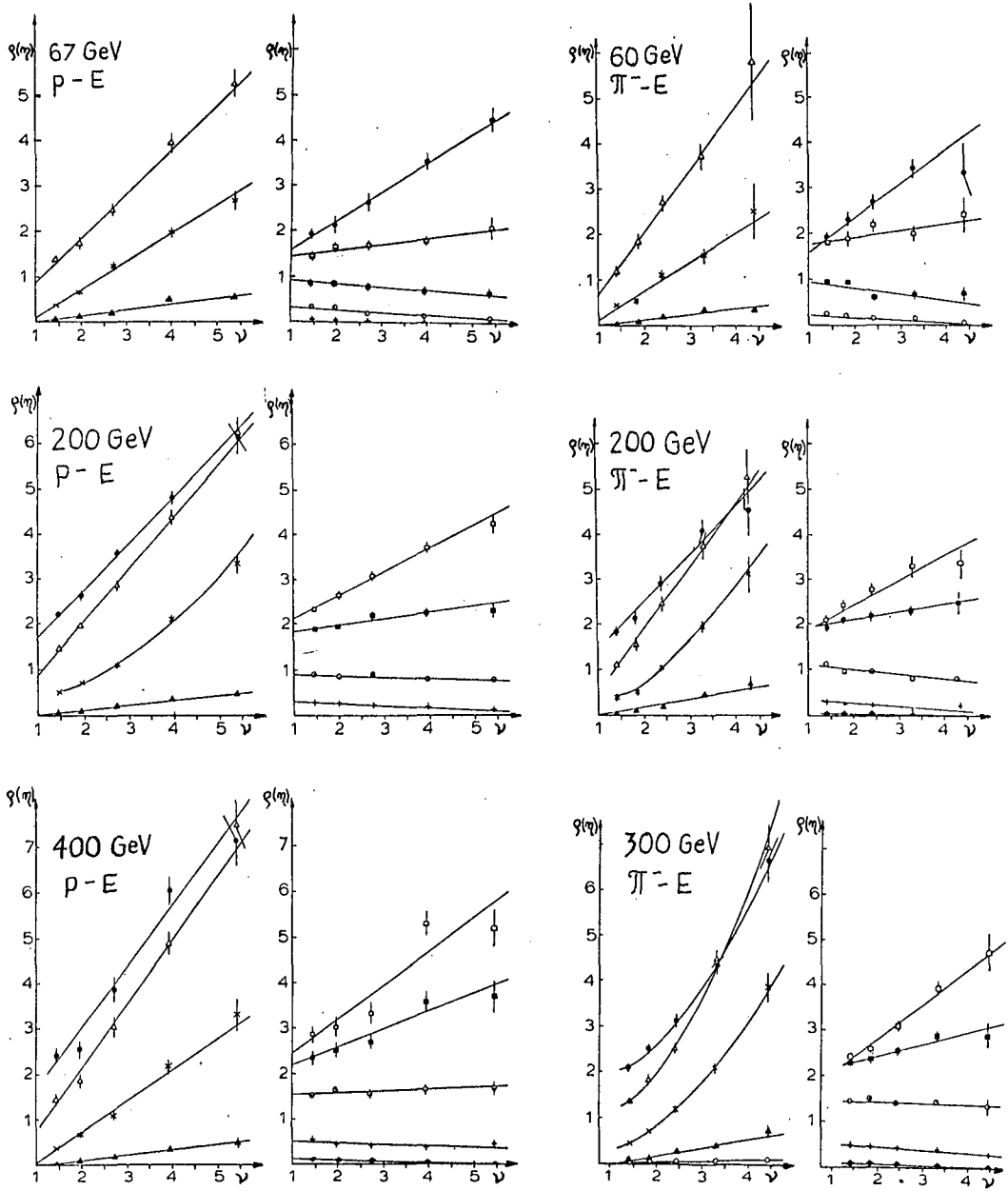
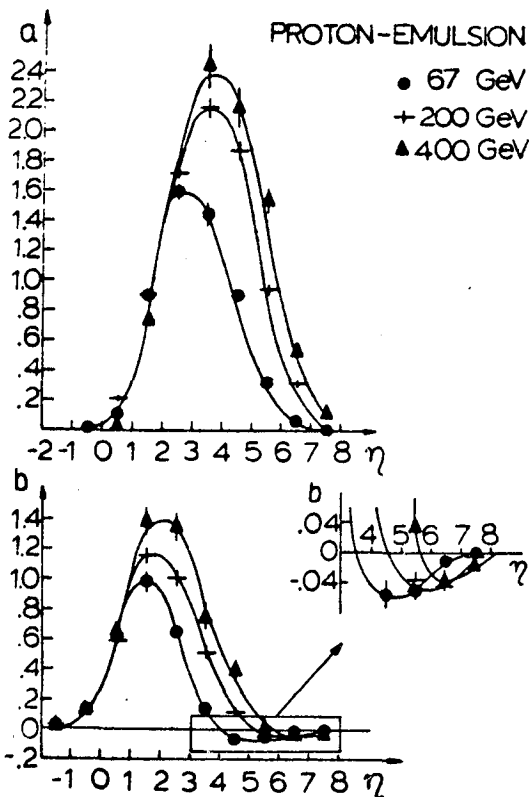


Fig. 2. Particle densities $\rho(\eta)$ vs $N\eta$ for different η - bins: \blacklozenge $8 < \eta \leq 7$, $+$ $7 < \eta \leq 6$, \circ $6 < \eta \leq 5$, \blacksquare $5 < \eta \leq 4$, \square $4 < \eta \leq 3$, \bullet $3 < \eta \leq 2$, Δ $2 < \eta \leq 1$, \times $1 < \eta \leq 0$, \blacktriangle $0 < \eta \leq -1$, \circ $-1 < \eta \leq -2$.

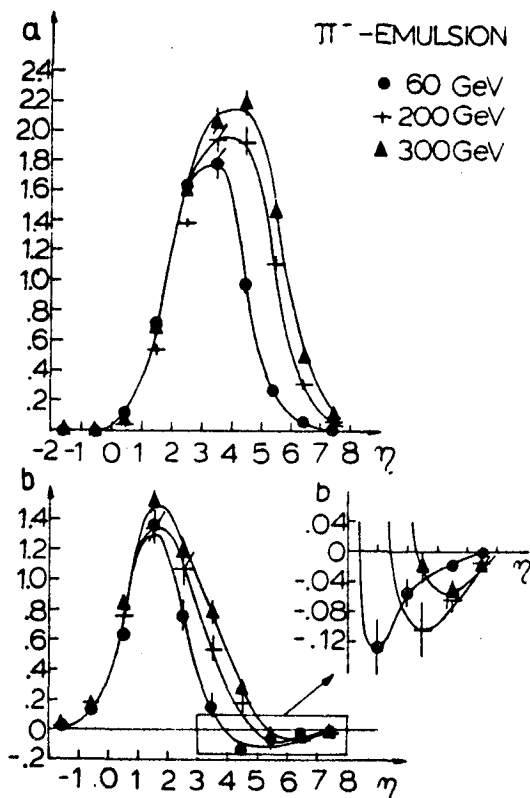
Results. In Fig. 2 the shower particle densities $\varrho(\eta) = 1/N_{\text{ev}} \frac{dn_s}{d\eta}$ in ten pseudorapidity intervals of unit width as a function of $\bar{\nu}$ are presented. The $\varrho(\eta)$ vs. $\bar{\nu}$ dependence can be parametrized by the linear relation:

$$\varrho(\eta) = a(\eta) + b(\eta)(\bar{\nu} - 1) \quad (1)$$

It should be stressed that for data analysed here the linear parametrization gives always satisfactory χ^2 values in projectile fragmentation region and forward central region ($\eta \geq 2.5$). Some intervals in target fragmentation region and backward central region are only approximately described by linear parametrization (see Fig.2). Better parametrization is obtained when the quadratic term equal $c(\eta)(\bar{\nu} - 1)^2$ in eq.(1) is added. The $a(\eta)$ and $b(\eta)$ coefficients for pion and proton interactions in emulsion are depicted in Figs.3a, b and Figs. 4a,b. For sake of clarity the errors are indicated in central and projectile fragmentation region only. The solid curves are to guide the eye. Using the obtained dependences of a and b on η one can construct, according to(1), the inclusive pseudorapidity distribution of shower particles for any value of $\bar{\nu}$.



Figs. 3a,b



Figs. 4a,b

Discussion and Conclusions. The dependence of particle densities $q(\eta)$ as a function of \bar{v} is not universal in the whole pseudorapidity range. For the highest pseudorapidity values the $q(\eta)$ decreases with the increasing number of \bar{v} . In the forward region ($\eta \geq 2.5$) there is no evidence of intranuclear cascade because the ratio $b(\eta)/a(\eta)$ in this region is always less than unity. In backward region ($\eta \leq 2.5$) the increase of multiplicity is much faster than the multiplicity in elementary collision multiplied by \bar{v} . This should be interpreted as an evidence for the existence of cascade effect inside the target nucleus. This cascading is caused by interactions of pions produced in target fragmentation region. From the above, one can argue that in order to discriminate between different superposition models the experimental results in the forward region should be compared with the theoretical predictions. The agreement in the backward region can be obtained by excluding or including cascading of slow pions in the model. Having this in mind the attempt was made in [2] to describe the experimental results obtained in this work for forward region by the additive quark model (AQM). It was tested whether the particle production, in π^- -emulsion interactions can be described by the following relation resulting from AQM:

$$q(\eta, Ng) = F_w(\eta) \bar{w}(Ng) + F_s(\eta)(2 - \bar{w}(Ng)) \quad (2)$$

where F_w and F_s are the fragmentation functions of wounded and spectator quark respectively and $\bar{w}(Ng)$ for a sample of events characterized by a given Ng is an average number of wounded quarks. To obtain $\bar{w}(Ng)$ the relation between \bar{v} and Ng was used [1] and Glauber calculations were performed. It was found at η antylab $\simeq -3.0$, the values of F_w and F_s obtained from experimental data are equal. Thus, as follows from (2), the particle production at this η value should not depend on $\bar{w}(Ng)$ and $q(\eta) = 2F_s$. Our π^- -emulsion data are in good agreement with this prediction for all primary energies considered.

- References: [1] E. Stenlund and I. Otterlund, Nucl. Phys. B198 (1982) 407.
 [2] R. Hołynski, M. Jeżabek and K. Woźniak, to be published.

ANGULAR DISTRIBUTION AND MULTIPLICITY
OF BACKWARD HADRONS
IN hFe INTERACTIONS AT 0.5-5.0 TEV ENERGIES
(PION Experiment)

V.V.AVAKIAN, M.O.AZARIAN, K.SH.EGIYAN,
E.A.MAMIDJANIAN, G.ZH.OHANIAN, S.V.TER-ANTONIAN

Yerevan Physics Institute, Markarian st.2
375036, Yerevan, Armenia, USSR

ABSTRACT

Basing on the analysis of $\sim 5 \cdot 10^3$ events registered on the PION installation, data are obtained on the angular distribution and multiplicity of particles, flying back into the laboratory coordinate system (LCS) that are identified mainly as hadrons produced in the reactions of $hFe \rightarrow h'x$ type. The inclusively produced hadron energy is > 200 MeV. The experimental data are compared to the results of the cumulative particle production in hA processes observed on accelerators at lower energies.

A large number of experimental studies (see e.g./1/) were devoted to the regularities and nature of backward particles. In generating the energetic charged and albedo particles the cumulative processes may also play a significant role /2/.

Basing on the analysis of ~ 5000 events we report here the experimental data on multiplicity and angular distribution of albedo particles generated at $t > 100$ g/cm² depths of the PION installation calorimeter material. The detailed description of the installation is given in /3/. It consists of an ionization calorimeter (IC) and an X-ray transition radiation detector (XTR). The summary quantity of material in the IC is equal to ~ 900 g/cm². A 5-module XTR detector is located above the calorimeter. The efficiency of the charged particle registration by one XTR proportional chamber is 96-98%, the accuracy of measuring the azimuthal angle of the charged hadron track is $\pm 2^\circ$.

The average number of backward particles is determined by the expression

$$\langle W_3 \rangle = \frac{\sum n_3}{N}$$

where $\sum n_3$ is the number of backward charged particles tracks in events considered.

The efficiency of detection of particles, having escaped backward at various angles, versus the interaction depth and the zenith angle was defined by the Monte-Carlo calculations. $\sim 78\%$ of the 5346 events considered are the cases with albedo. The multiplicity of detected backward charged particles averaged over the whole effective depth of the calorimeter per one event equals $\langle W_3 \rangle = 0.55 \pm 0.06$ at the hadron energy $E > 500$ GeV.

The multiplicity of charged backward particles generated by hadrons with the same energy at the calorimeter material depths > 100 g/cm² equals $\langle W_3 \rangle = 0.37 \pm 0.04$.

Figure 1 shows the multiplicity distribution of backward charged particles produced at the depths > 100 g/cm². The data from /1/ are given ibidem. As is seen from the figure, the probability to observe backward particles with the large multiplicity grows with the increase in the primary hadron energy.

The dependence of the backward particle multiplicity on their generation depth in the interval > 100 g/cm² obeys the exponential law $\sim \exp(-t/\lambda)$, where λ equals 181 ± 32 g/cm². Such a large value of λ may testify the presence of hadrons with the energy > 400 MeV in the albedo flux.

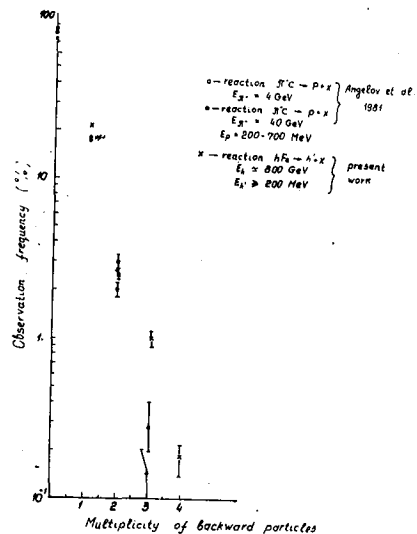


Fig. 1. Probability of observing the cases with various multiplicities of backward charged particles produced at the IC material depths > 100 g/cm².

Figure 2 presents the distributions of amplitudes of signals from backward particles generated by hadrons with the energy > 500 GeV for the calorimeter two depths: small ($Pb_1 + Pb_2$) and middle ($Fe_2 \dots Fe_5$), on the output of the multiwire proportional chambers (MWPC) of the XTR detector first row. The average values of the amplitude are equal to 84.67 ± 3.62 and 58.19 ± 2.10 relative units, respectively, and this result confirms our

assumption that the nature and energy spectrum of backward charged particles detected on the installation

from various depths are not identical. To a similar conclusion leads also the experimental fact that the average amplitude of energy release in the MWPC from charged particles of the average depths ($t > 100$ g/cm²) 1.30 times exceeds the single charged hadron averaged energy release, while the corresponding ratio for the small depth of production ($Pb_1 + Pb_2$) equals ~ 1.9 .

Figure 3 presents the backward angular distribution of 3 particles with the registration efficiency corrections. The 3 particles production cross section in the $120^\circ - 160^\circ$ angle interval does not contradict the results obtained at the primary hadron low energies for cumulatively produced protons and pions /4/. In the $\approx 160^\circ$ interval a peculiarity is observed at $\Theta \approx 170^\circ$ as a minimum. For the first time a similar behaviour of the angular distribution has been observed for cumulative protons and π^- mesons

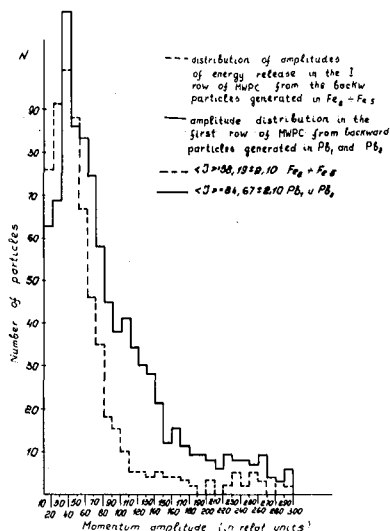


Fig.2. The backward particle energy release amplitude distribution in the first row of MWPC.

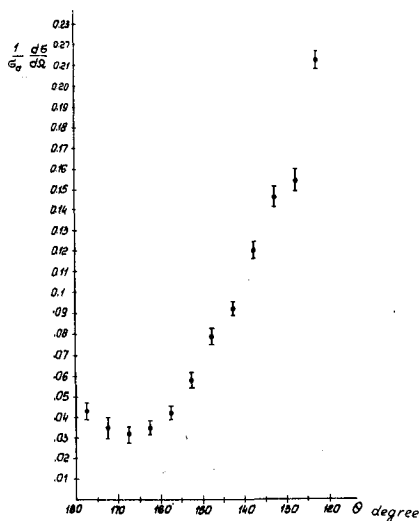


Fig.3. Angular distribution of backward charged particles generated at the calorimeter material depths $> 100 \text{ g/cm}^2$.

produced in dA collisions at the primary energy $\sim 4.5 \text{ GeV/nucleon}$ /4/.

The authors are indebted to A.Ts.Amatuni, S.G.Matinyan, A.G.Oganessian for helpful discussions.

REFERENCES

- /1/ Azarian M.O., Zazian M.Z., Mamidjanian E.A., *Yad.Fiz.*, 1977, 26, N.1.
Avakian V.V. et al., *Izv.AN SSSR, ser.fiz.*, 1981, 45, N.7, 1249-1254.
Ellsworth R.-W., Goodman J.A., Ito A.S. et al., *NIM*, 1982, 203, 167-177.
- Angelov N., Litpulaev S.L., Nikitina V.F., *Yad.Fiz.*, 1981, 33, N.1, 190-193.
- /2/ Baldin A.M., *E.Ch.A.Ya.*, 1977, 8, 429.
- /3/ Avakian V.V. et al., 17th ICRC, Kyoto, 1980, 13, 61.

A Test of the Feynman Scaling in the Fragmentation Region

at $\sqrt{s} = 630$ GeV

T. Doke⁵⁾, V. Innocente^{1) #}, K. Kasahara²⁾, J. Kikuchi⁵⁾,
 T. Kashiwagi⁵⁾, S. Lanzano¹⁾, K. Masuda⁵⁾, H. Murakami³⁾, Y. Muraki²⁾,
 T. Nakada⁴⁾, A. Nakamoto³⁾, T. Yuda²⁾ and M. Haguenaer⁶⁾ #

1) Instituto di Fisica, Univ. of Naples, Naples, Italy

2) ICRR, Univ. of Tokyo, Tanashi, Tokyo, Japan

3) Dep. of Physics, Rikkyo Univ, Toshima, Tokyo, Japan

4) SIN, Villingen, Switzerland

5) Sci. Eng. Lab, Waseda Univ., Shinjuku, Tokyo, Japan

6) CERN UA-4 collaboration

#) Ecole Polytechnique, Palaiseau, Paris, France

(CERN UA-7 collaboration)

abstract

The result of the direct measurement of the fragmentation region will be presented. The result will be obtained at the CERN $p\bar{p}$ collider, being exposed the Silicon calorimeters inside beam pipe. This experiment clarifies a long riddle of cosmic ray physics, " whether the Feynman scaling does violate at the fragmentation region or the Iron component is increasing at 10^{15} eV".

1. Introduction

This experiment aims to measure the inclusive cross-section of neutral pions emitted into the very forward region in $p\bar{p}$ collision at $\sqrt{s} = 630$ GeV. Fig. 1 represents an experimental result¹⁾ which predicts the primary composition of cosmic rays is either proton dominant and Feynman scaling violates or iron dominant and scaling valid.

Until now, no direct measurement inside beam pipe of colliders was made due to a technical difficulty. We have developed a very compact silicon calorimeter with the tungsten target and they will be installed in the Roman pot of UA-4 at CERN

$p\bar{p}$ collider. The direct observation of the energy of the secondary particles with $X_F = 0.05 - 0.5$ gives rise to the final conclusion to a long riddle of cosmic ray physics and also gives a good data for the understanding of the forthcoming cosmic ray phenomena.

2. Geometry

The shower calorimeter consists of 20 layer of silicon wafers with diameter of 10 cm alternating with tungsten converters of thickness 3.5 mm and 7 mm. The total thickness of the calorimeter amounts to 21 radiation lengths.

All electrodes are segmented at the front and rear side of the silicon wafer into x and y electrodes with 5 mm pitch. The first layer of the silicon wafer is used to identify whether the incident particles are charged or photons. At the 8 radiation length from the front, 45° oriented u-chamber is installed to resolve the multi-hit events. Total number of electronics channel is 90 for one detector. The signal is recorded by Le Croy ADC 2281.

One chamber is located at 13 m from the interaction vertex and outside of beam pipe, while the other detector will be installed at 22 m away from the vertex inside the Roman pot (Fig. 2). The tracking chamber is also located to obtain the interaction vertex, which covers $\eta = 4.4 - 5.6$, in front of the silicon detector at 13 m. The properties of the silicon calorimeter has been published elsewhere²⁾.

3. Trigger and Detector resolution

The trigger is made by UA-4 trigger logic³⁾. The identification of the interaction vertex with use of tracking chamber is necessary for the single arm trigger (=single diffractive trigger) selects beam-beam collisions with 75 % probability. Even if the background rate becomes of the same order as the beam-beam collision for the triggered events, we could clearly find the pinote peak as in Fig. 3. For the double arm trigger

(double diffractive trigger) ($3.0 < |\eta| < 5.6$), the beam-gas collision is selected with a rate of 2 %.

Under a typical low- β run with a luminosity of $L = 1 \times 10^{28} \text{ cm}^{-2} \text{ sec}^{-1}$, and the exposure time of 2 minutes, 60,000 minimum bias events will be obtained which is already sufficient to measure the inclusive π^0 and η production spectra but in order to obtain K_S^0 and η' , we need further 20 minutes.

4. Energy calibration and Detection efficiency

The π^0 -mass distribution can be determined with the accuracy of $\Delta M \approx 8 \text{ MeV}$. The double photon mapping technique provides a good energy calibration for the photon detector with an accuracy of $\pm 3 \%$ of its absolute value.

Fig. 4 represents the detectable region of photons by the present detector. Former UA-5 experiments observe the polar angle region greater than 30 m rad. Present experiment covers the polar angle between 0.5 and 17 m rad. Fig. 5 represents the detection efficiency of π^0 by each chamber located at 13 m and 22 m.

5. Schedule

The test exposure will be made on Jul. 10 - 16th with the use of 3" silicon calorimeter. The preliminary results will be presented at this conference. The experiments with the use of two 4" Si-calorimeters will start this September.

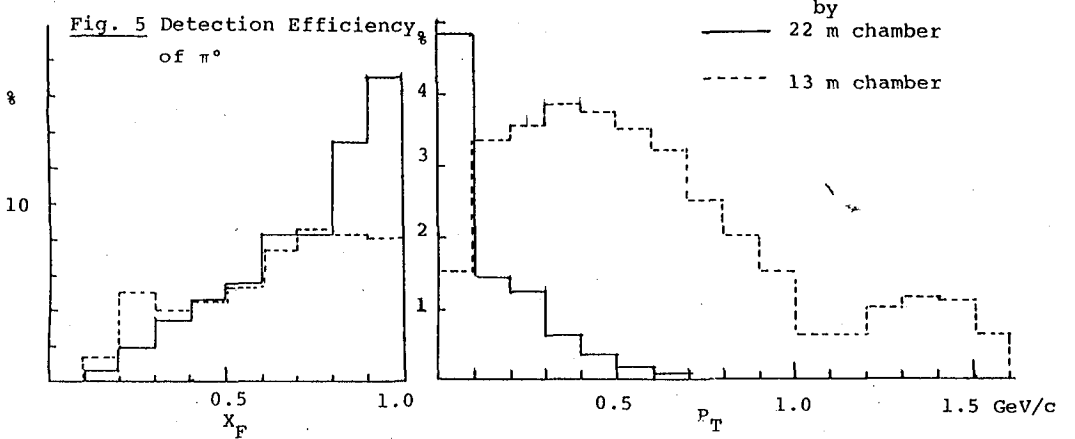
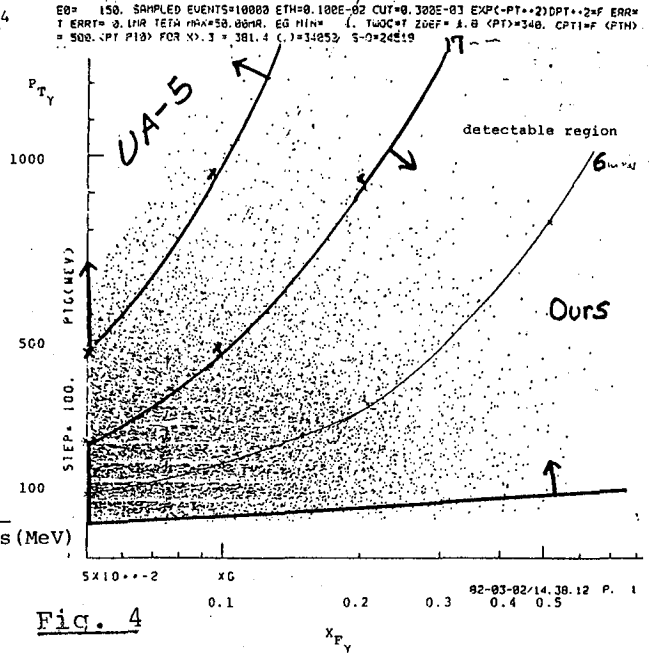
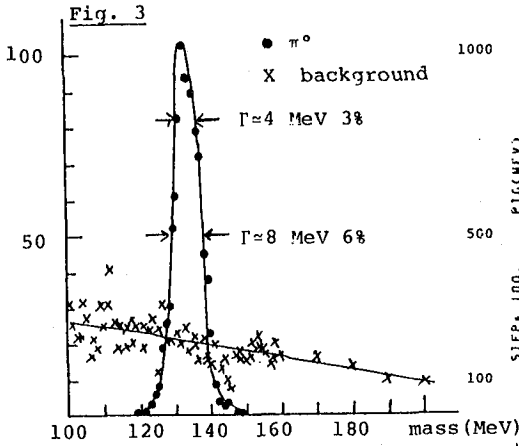
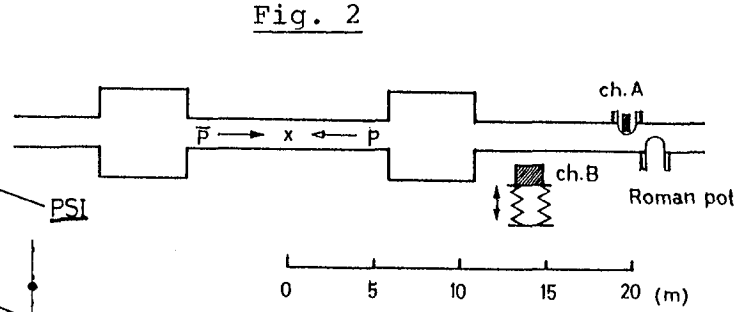
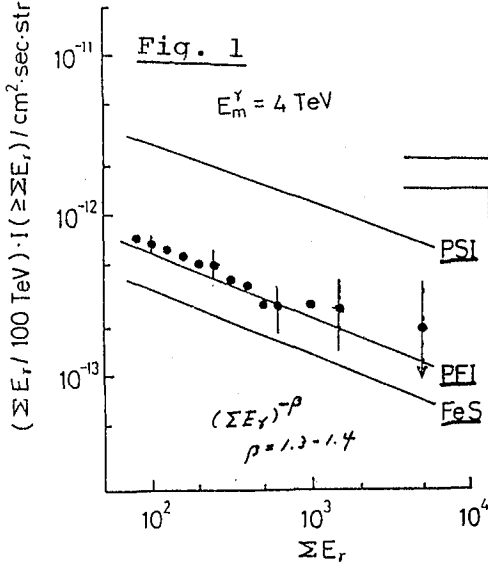
Acknowledgements

The authors would like to express their sincere thanks to Prof. G. Matthiae, spokesman of UA-4 collaboration, for his warm support and valuable suggestions.

We also thank to Prof. A. Staude for valuable discussions.

References

- 1) Mt. Fuji emulsion chamber collaboration: Phys. Rev. D24(81)2353.
- 2) A. Nakamoto et al.: N.I.M. (1985).
- 3) CERN UA-4 collaboration : N.I.M. (1985) and CERN EP 84-156.



ANGULAR DISTRIBUTION OF SHOWER PARTICLES PRODUCED
IN THE COLLISIONS OF 20-GeV/c AND 300-GeV
NEGATIVE PIONS WITH EMULSION NUCLEI*

C. O. Kim, S. N. Kim, I. G. Park, and C. S. Yoon
Department of Physics, Korea University, Seoul 132, KOREA

ABSTRACT

For 435 accelerator-produced π^- jets of 20-GeV/c¹ and 300 GeV^{2,3} in nuclear emulsion, $\langle\eta(\theta)\rangle$'s have been individually calculated for each jet, where $\eta(\theta)$ is a kinematic parameter introduced by one of us in 1967 in order to approximate the LS(laboratory system) rapidity, $\eta = \text{arctanh}(\beta \cos \theta)$.⁴ By taking further averages by dividing the samples into groupings of the LS energy $E_\pi = m_\pi \cosh \eta_\pi$, N_h , the number of heavy prongs with LS velocity $\beta < 0.7$, and n_s , the number of charged shower particles with LS velocity $\beta \geq 0.7$, $\langle\langle\eta(\theta)\rangle\rangle$ have been obtained. By use of the KNO (Koba-Nielsen-Olesen) scaling variable, $\xi = n_s/\langle n_s \rangle$,⁵ we find good fit of our data to the regression function,

$$\langle\langle\eta(\theta)\rangle\rangle - \eta_\pi/2 - \frac{1}{2} \ln(m_\pi/m_p) = A + B/\xi, \quad (1)$$

where m_p is the proton mass.

1. Introduction. With the use of the samples of 3987 accelerator-produced proton jets of 30 - 400 GeV, one of us reported that the regression function,

$$\langle\langle\eta(\theta)\rangle\rangle - \eta_p/2 = A' + B'/\xi, \quad (2)$$

fits the angular data well, where the constants, A' and B' do not have any dependence on $E_p (= m_p \cosh \eta_p)$.⁶ In fact, Eq. (2) as well as Eq. (1) stem from the "scaling" asymmetry parameter R by Tavernier:^{7,8}

$$R \equiv m_t \sinh(\langle\eta\rangle - \eta_t)/m_b \sinh(\eta_b - \langle\eta\rangle), \quad (3)$$

where m_b , m_t , η_b , η_t are masses and "initial" rapidities of beam and target, respectively. By putting, in the LS, $\eta_t = 0$, $m_t = \nu m_p$, $\langle\eta\rangle = \langle\langle\eta(\theta)\rangle\rangle$, the RHS of Eqs. (1) and (2) become equal to $\frac{1}{2} \ln(R/\nu)$, which can be represented by the LHS of Eqs. (1) and (2). Thus, the present paper is the similar analysis to Ref. 6, with the samples of 318 jets¹ of 20 GeV/c π^- and 117 jets^{2,3} of 300 GeV π^- .

2. Experimental Material and Methods. Two stacks of glass-backed plates of Ilford K 5 nuclear emulsion of the size, 7.5 x 8 x 0.06 cm³ (A stack, 21 plates; B stack, 20 plates)

* Research supported partly by the Korea Science and Engineering Foundation (1984 - 87).

were exposed "horizontally" to 300 GeV π^- beam at Fermilab in 1978 with a track density of about 3×10^4 particles/cm². The along-the-track scanning method was employed in order to find 207 inelastic events in tracing 100.374 m of the primary tracks; this gives the mean free path of 300 GeV π^- in Ilford K 5 nuclear emulsion, 48.5 ± 3.4 cm. Among these events, by following the procedure taken by Refs. 2 and 3, 126 interactions, whose origins were located more than 50 μ m away either from the air surface or from the glass surface inside the processed emulsion plates, were subjected the analysis of counting the numbers of tracks to obtain $\langle N_h \rangle = 7.0 \pm 0.4$ and $\langle n_s \rangle = 13.2 \pm 0.6$. Further, we performed angular measurements to the charged shower particles of 117 interactions among the 126 interactions by applying the reference-track method of Ref. 6. The material and experimental procedure concerning the 20-GeV/c pion jets were reported in Ref. 1.

3. Dependence of $\langle\langle \eta(\theta) \rangle\rangle$. The LS emission angles of the charged shower particles were converted to $\eta(\theta)$ (Ref. 4) and for each jet $\langle \eta(\theta) \rangle$'s were calculated. Then, by grouping the 435 jets into subgroups, according to E_π , $N_h = 0, 1, 2-4, 5-8, \geq 9$, $n_s = 1, 2, 3, \dots, 9, 10-14, 15-19, \dots$, $\langle\langle \eta(\theta) \rangle\rangle$ were calculated. As noticed in Refs. 1, 4, and 6, the trends shown in the values of $\langle\langle \eta(\theta) \rangle\rangle$, as a function of n_s and N_h , are:

- (i) For $n_s \gg \langle n_s \rangle$ (i. e., $\xi \gg 1$), $\langle\langle \eta(\theta) \rangle\rangle$ becomes unreasonably larger. (Small $x_T = p_T/m$ effect.)
- (ii) As N_h increases, $\langle\langle \eta(\theta) \rangle\rangle$ becomes smaller. (Nuclear target effect.)

As shown in Figs. 1 (a) - (e) and the values of A, B and χ^2/DF (and also A', B' and χ^2/DF for the 3987 proton jets of 30-400 GeV in parentheses) in Table I, our angular data of 435 π^- jets fit Eq. (1) rather well. The solid-line curves show

TABLE I. The values of A and B obtained by the least-squares fits for the 435 π^- jets (and those for the 3987 proton jets to Eq. (2)).

N_h	A (A')	B (B')	χ^2/DF
0	-0.18 ± 0.11 (-0.22 ± 0.03)	0.35 ± 0.09 (0.22 ± 0.02)	0.04 (1.63)
1	-0.08 ± 0.28 (-0.36 ± 0.05)	0.24 ± 0.20 (0.27 ± 0.04)	8.26 (1.35)
2-4	-0.38 ± 0.08 (-0.48 ± 0.03)	0.41 ± 0.06 (0.27 ± 0.03)	1.39 (1.87)
5-8	-0.53 ± 0.21 (-0.66 ± 0.05)	0.43 ± 0.25 (0.34 ± 0.06)	2.55 (1.46)
≥ 9	-1.12 ± 0.005 (-1.03 ± 0.03)	0.75 ± 0.004 (0.48 ± 0.02)	4.12 (2.38)

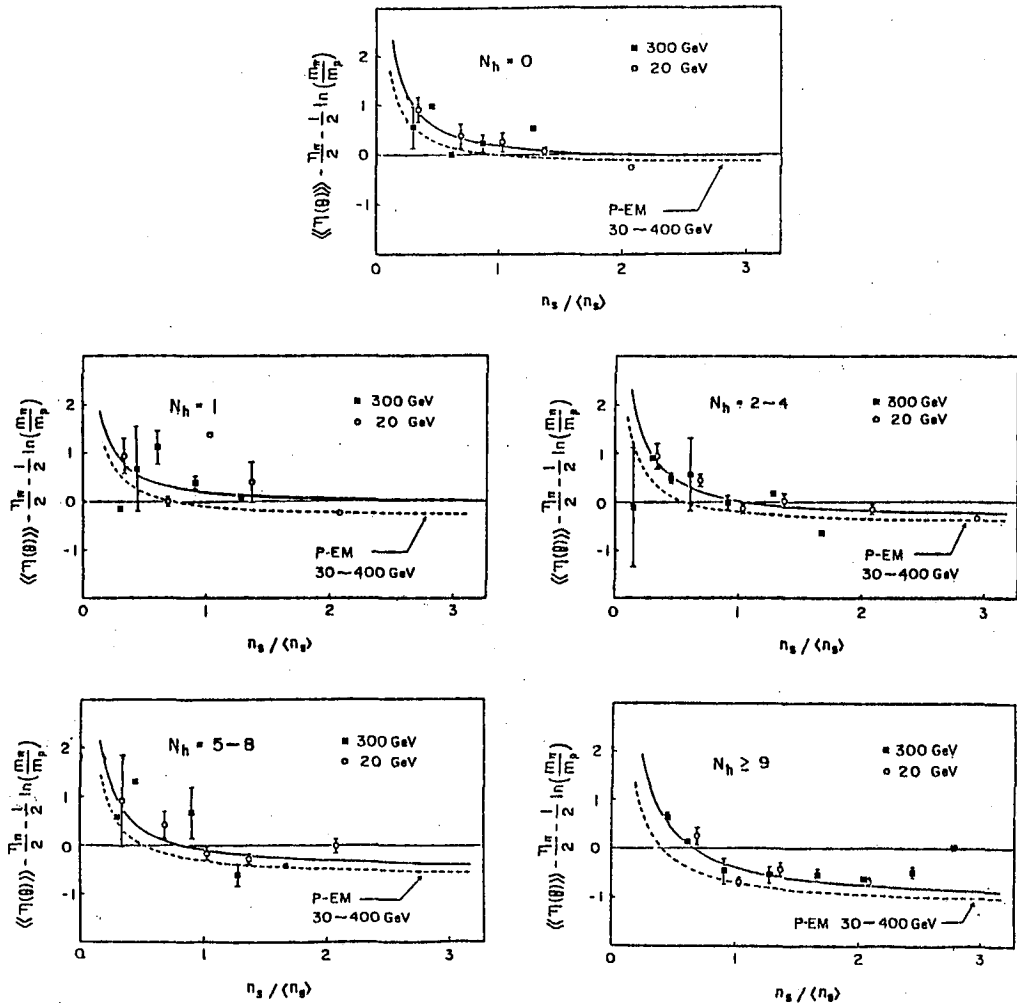


Fig. 1. Dependence of $\langle\langle\eta(\theta)\rangle\rangle$, according to Eq. (1) for the pion jets (solid-line curves) and to Eq. (2) for the proton jets (broken-line curves), for (a) $N_h = 0$, (b) for $N_h = 1$, (c) for $N_h = 2-4$, (d) for $N_h = 5-8$, and for $N_h \geq 9$.

the values of $\langle\langle\eta(\theta)\rangle\rangle - \gamma_\pi/2 - \frac{1}{2} \ln (m_\pi/m_p)$ versus ξ , and the broken-line curves show the values of $\langle\langle\eta(\theta)\rangle\rangle - \gamma_p/2$ versus ξ for proton jets of 30 - 400 GeV.

4. Discussion and Conclusion. As E. Gibbs *et al.*⁹ first noted, the N_h dependence of A , listed in Table I, can be fitted by the regression function,

$$A = \alpha (1 + \gamma N_h) / (1 + \delta N_h), \quad (4)$$

where the results are $\alpha = -0.152 \pm 0.001$, $\gamma = 0.520 \pm 0.004$,

and $\delta = 0.020 \pm 0.005$ with $\chi^2/DF = 0.4/2$.⁶ And as in Ref. 6, N_h -dependence of B , listed in Table I, can be fitted well by the regression function,

$$B = \kappa + \zeta N_h, \quad (5)$$

where the results are $\kappa = 0.33 \pm 0.05$ and $\zeta = 0.025 \pm 0.03$ with $\chi^2/DF = 0.4/3$. Altogether, with the use of the data of angular measurements of 435 accelerator-produced jets of $E_\pi = 20$ and 300 GeV, we have obtained the empirical formula,

$$\langle\langle \eta(\theta) \rangle\rangle - \frac{\eta}{2} - \frac{1}{2} \ln(m_\pi/m_p) =$$

$$(-0.152 \pm 0.001) \frac{[1 + (0.520 \pm 0.004) N_h]}{[1 + (0.020 \pm 0.05) N_h]} +$$

$$[(0.33 + 0.05) + (0.025 \pm 0.03) N_h] / \xi.$$

We find the value of ν in Ref. 6 is almost in accord between the one obtained from the proton jets and the other obtained from the pion jets. But there exists some difference between the values of R of Refs. 7 and 8, which is indeed scaling, for proton and pion jets, reflecting the fact that pion jets do not have two surviving baryons but one.^{4,6}

REFERENCES.

- ¹E. R. Goza, S. Krzywdzinski, C. O. Kim, and J. N. Park, Phys. Rev. 2, 1838 (1970).
- ²M. Jurić, Dj. Krmpotić, O. Adamović, V. Gerc, L. Rak, J. Lory, D. Schune, Tsai-Chü, B. Willot, K. P. Hong, C. O. Kim, S. N. Kim, K. A. Moon, R. Schmidt, I. Otterlund, G. Baumann, M. Lopez Agüera, R. Niembro, A. Ruiz, E. Villa, Z. Phys. C 22, 131 (1984).
- ³Lj. Simić, O. Adamović, M. Jurić, J. Lory, D. Schune, Tsai-Chü, B. Willot, K. P. Hong, C. O. Kim, and K. A. Moon, Nuovo Cimento 82A, 327 (1984).
- ⁴C. O. Kim, Phys. Rev. 158, 1261 (1967).
- ⁵Z. Koba, H. B. Nielsen, and P. Olesen, Nucl. Phys. B40, 317 (1972).
- ⁶C. O. Kim, Phys. Rev. D 31, 513 (1985).
- ⁷S. P. K. Tavernier, Nucl. Phys. B105, 241 (1976).
- ⁸S. P. K. Tavernier and M. Gijsen, Phys. Rev. D 16, 2818 (1977).
- ⁹E. Gibbs et al., Phys. Rev. D 10, 783 (1974).

NUCLEON-NUCLEUS INTERACTIONS FROM JACEE

The JACEE Collaboration:

T. H. Burnett^h, S. Dake^b, M. Fuki^c, J. C. Gregory^g, T. Hayashi^g, R. Holynski^{e,i},
 J. Iwai^h, W. V. Jones^e, A. Jurak^{e,i}, J. J. Lord^h, O. Miyamura^d, T. Ogata^a,
 A. Olszewski^{e,i}, T. A. Parnell^f, T. Saito^a, S. Strausz^h, M. Szarska^{e,i},
 T. Tabuki^a, Y. Takahashi^f, Y. Tominaga^d, B. Wilczynskaⁱ,
 J. P. Wefel^e, R.J.Wilkes^h, W. Wolterⁱ, B. Wosiek^{e,i}

a) Institute for Cosmic Ray Research, Tokyo; b) Kobe University; c) Okayama University of Science; d) Osaka University; e) Louisiana State University; f) NASA Marshall Space Flight Center; g) University of Alabama, Huntsville; h) University of Washington; i) Institute for Nuclear Physics, Krakow.

ABSTRACT

Results on hadron-nucleus interactions from the JACEE experiment are presented. Angular distributions for charged particles, and angular and transverse momentum spectra for photons have been measured for a sample of events with $\Sigma E_\gamma \geq 1$ TeV. Results on central rapidity density and transverse energy flow are discussed.

1. Introduction

JACEE (Japanese-American Cooperative Emulsion Experiment) was organized to study cosmic ray nucleus spectra and interactions at total energies approaching 100 TeV. The use of conventional emulsion chamber techniques permits the observation of secondary charged particles and individual high energy gamma rays. The results presented here were obtained from a series of balloon flights at 3.5-8 g/cm² altitudes¹.

The apparatus used in the experiment has been described in detail elsewhere². All emulsion plates are made from 500~800 μm acrylic bases, coated on both sides with Fuji emulsion. Incident particles are identified in the primary charge detector section using grain, gap and delta-ray counts from thick (150~200 μm) emulsion layers, as well as pit measurements from CR39 etchable plastics. Charge resolution is typically 0.2~2.0 units. The target section contains thin (50-75 μm) emulsion plates interleaved with acrylic or Fe target sheets. Thick emulsions and CR39 sheets are inserted at intervals to permit identification of projectile fragments. Interactions occurring in the upper Pb layers of the calorimeter can also be fully analyzed. The spacer section permits gamma rays to diverge before reaching the calorimeter section, so that individual photon cascades can be observed.

The calorimeter contains ~5 vertical radiation lengths of Pb interleaved with 18-20 layers of emulsion plates and x-ray films. Cascades of energy ≥ 300 GeV make spots visible to the naked eye in the x-ray films, which serve both as threshold detectors and as templates for locating events in the emulsions. In addition, densitometric measurements in x-ray films provide an estimate of the shower energy.

Once an event has been located, a region of diameter 1-2 mm (depending upon vertex height) around the event axis is scanned for lower energy cascades.

Accurate energy determinations are made by performing track counts in the emulsion layers and comparing the results with calibration curves obtained from analytical shower theory calculations³ and monte carlo simulations⁴ which have been checked by accelerator calibration experiments⁵. The error in a single cascade energy measurement is $\sim 20\%$. The directly measured event energy parameter is ΣE_γ , the total energy observed in the electromagnetic calorimeter. The primary energy E_0 can be estimated from ΣE_γ by using the gamma-ray inelasticity factor k_γ derived from measurements on protons at Fermilab⁶, and independently from the charged particle angular distribution using the Castagnoli method.

2. Proton-Nucleus Interactions

Charged track angles are measured relative to the energy-weighted center of the event. Interactions occurring in acrylic base or target plates are assumed to be on carbon targets. Angular distributions are normally presented in terms of the pseudorapidity, $\eta = -\log_e \tan(\theta/2)$. In order to combine events of different energies, one can define a normalized pseudorapidity parameter, $\eta^* = -\log_{10} \tan(\Sigma E_\gamma * \theta)$. The normalized $\log \tan \theta$ distributions for nucleon interactions in C and Pb are shown in Fig. 1. For this sample, $\Sigma E_\gamma > 1$ TeV and $\langle \Sigma E_\gamma \rangle = 4.9$ TeV (carbon) and 3.5 TeV (Pb).

The central pseudorapidity density ρ_c for each event has been estimated by excluding the forward 1.5 rapidity units (projectile fragmentation region) and calculating $dn/d\eta$ over the next 2 rapidity units. In Fig. 2 we plot $\langle \rho_c \rangle$ versus the target mass A . The data are well represented by the relation $\langle \rho_c \rangle = kA^{0.31}$.

For photons observed in the calorimeter, transverse energy flow as a function of rapidity y can be analyzed by defining an integral transverse energy flow parameter,

$$F(y) = \sum_{y_i > y} E_{ti}$$

where $E_{ti} = E_i \sin(\theta_i)$. Plotting $F(y)$ vs η for individual events, and excluding the low- y region where detection bias may be present, one finds that $F(y)$ can be well represented by the form $F(y) \sim e^{-by}$. The fitted values for the slope parameter b have a bimodal distribution shown in Fig. 3, with about 15% of the events displaying a significantly steeper slope than the rest. In Fig. 4a we show several typical events displaying large b ; the low- b events shown for comparison in fig 4b have been chosen to have a similar distribution of target mass and ΣE_γ . The data in Fig. 4 have been displaced vertically for clarity.

3. Acknowledgements

This work supported in part by DOE, NSF and NASA in the US, and JSPS in Japan.

4. References

1. T. Burnett, *et al*, paper HE-1.4-4, this conference.
2. R.W. Huggett, *et al*, 17th Int. Cosmic Ray Conf. (Paris), **8**, 80 (1981).
3. J. Nishimura, *Handbuch der Physik* **46/2**, 1 (1967).
4. S. Dake, private communication.
5. N. Hotta, *et al*, Phys. Rev. **D22**, 1 (1980).
6. S. Dake, *et al*, 15th Int. Cosmic Ray Conf. (Plovdiv), **7**, 322 (1977).

5. Figure Captions

1. Normalized angular distributions for charged tracks observed in p-Pb interactions (solid line) and p-C interactions (dashed line). The normalized pseudorapidity parameter is defined as $\eta^* = -\log_{10}\tan(\Sigma E_\gamma * \theta)$.

2. Central pseudorapidity density ρ_c versus target mass A. Interactions in plastic and emulsion are taken to be on A=12 and 82 respectively. The solid line shows the results of a fit to $\langle \rho_c \rangle \sim A^\delta$, with $\delta=0.31$.

3. Distribution of fits to slope parameter b in the relation $F(y) \sim e^{-by}$. See text for definition of the integral transverse energy flow parameter $F(y)$.

4. Plots of the integral photon transverse energy flow $F(y)$ for individual events a) with slope parameter $b > 1.25$ and b) with $b < 1.25$. The events have been displaced vertically for clarity; the scales shown apply to the lowest data set.

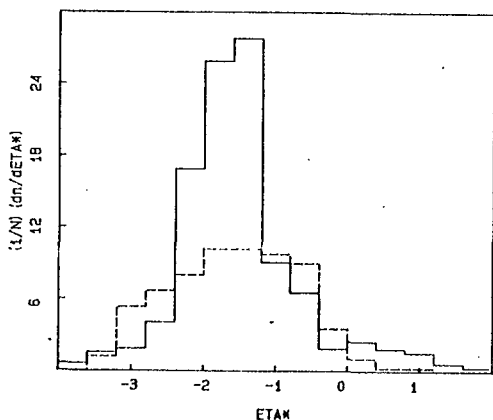


Figure 1

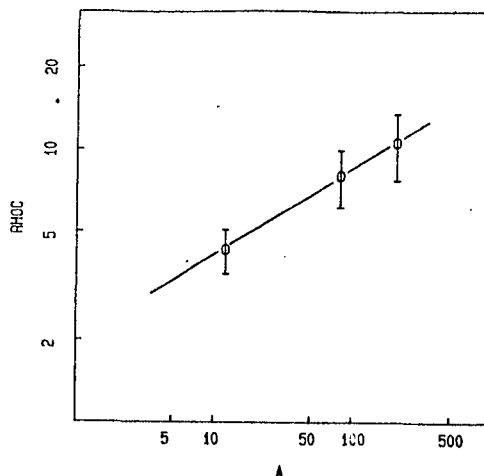


Figure 2

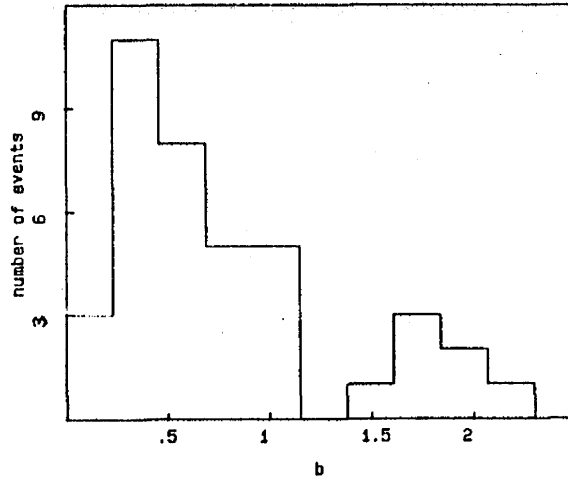


Figure 3

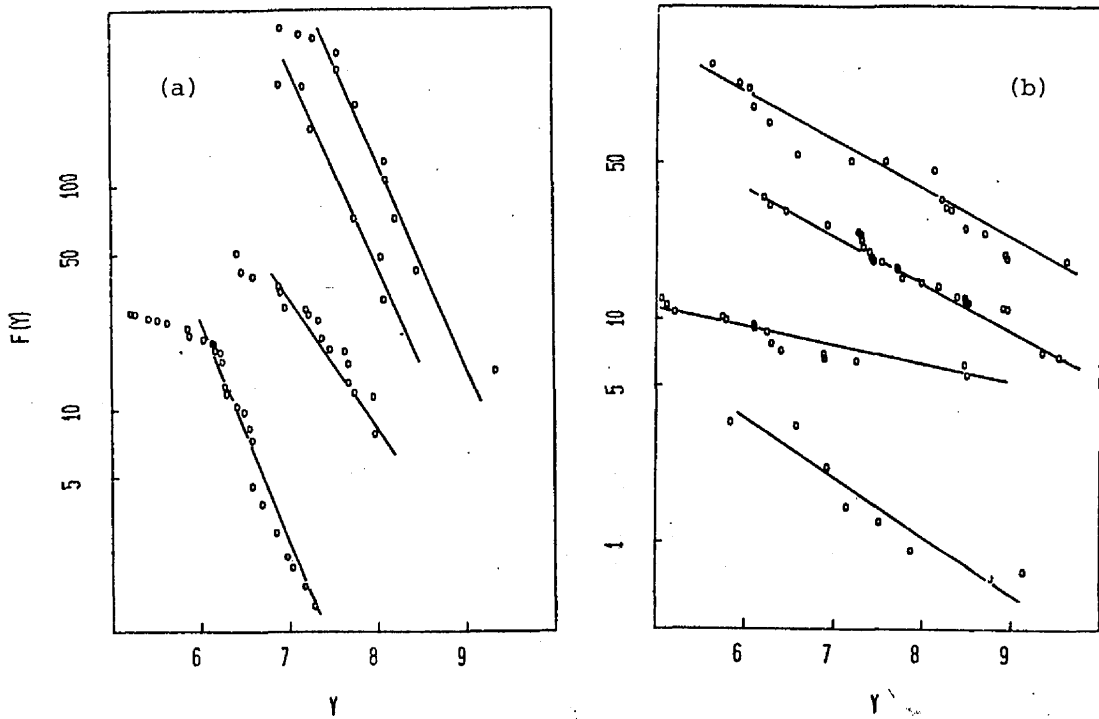


Figure 4

AN UNIFICATION OF THE INTERACTIONS
AND THE DIFFRACTIVE PROCESSES

Kuchin I.A.

High Energy Physics Institute
Academy of Sciences of Kazakh SSR,
480082, Alma-Ata, USSR

Abstract. The transition of a number of hadronic process characteristics to a certain universal regime is interpreted as an indication to the early origination of the unification regime of the interactions.

I. Introduction.

Correspondingly to the rapprochement of the electroweak and strong interaction constants in grand unification (GU) models, one can expect a partial loss of the specific character of the mentioned interactions and the transition of their global characteristics to some general regime [1].

Though one expect GU coming at superhigh energies (10^{16} GeV according to proton decay), nevertheless the various GU models have been approbated and conformed really at $E_0 \leq 10^5$ GeV. On the whole, it is the argumentation on the particle spectroscopy and SU(5)-symmetry confirmation level.

If evidences of such sort really bear a relation to GU, then in the same energy region ($E_0 \leq 10^5$ GeV) it is logical to expect the GU manifestation on the dynamical level too, that is in particle scattering characteristics. Below we shall show a possible GU-manifestation in the attainable now energy interval.

2. Two sources, two forms of the unification of the particle interactions.

As it is known, the local gauge-invariant principle defines the form of all interactions, irrespective of their physical nature, and gives a theory such a form that it permits the purely geometrical interpretation of the scattering process. Namely, one bring the arbitrary gauge field into correspondence with a definite geometry of the fiber space, which may be received from the usual space-time by the replacement of its points with an "internal" spaces, where the gauge group acts [2].

At very short space-time intervals ($\sim 10^{-4} \div 10^{-3}$ fm) the scattering picture reduces to the following: structurless particles (leptons and quarks) exchange by massive vector bosons, and the values of coupling "constants", which depend on the transfer of the 4-momentum, come close (by magnitudes) as the energy increases, so that the strong interactions are weakened while a weak interaction and an electromagnetic one become stronger. If the universality of the interactions means the presence of one general coup-

ling constant, then the unification of the interactions may take place, as it is expected, at the energies of the order of 10^{16} - 10^{18} GeV, when it is necessary to take into account gravitation too.

On the other hand, right now (at FNAL- and ISR-energies) we are witnesses of the transition of a number of hadronic characteristics (the total cross-sections, the parameters of the diffractive cone for different pairs of the colliding particles) to a certain universal regime (Fig.1). This phenomenon is known to be caused by the diffraction predominance [4].

The contribution of the diffractive channel of the scattering does not depend on the nature of the colliding particles. To describe the diffraction the only quantum-mechanical (wave) properties of the scattering, some extent of the dynamical symmetry and the unitarity are essentially necessary. All these are discriminating features of some universal mechanism of the interaction.

Thus we may point out two sources (and two forms) of the unification of the interactions: the first comes from the processes at very short distances (for pointlike, structureless particles), the other- from a processes at comparatively large distances ($\sim 1-2$ fm), in soft interactions of the extensive objects.

3. The principle connection between the diffraction and gauge fields.

There is no satisfactory theory of diffractive high energy scattering of particles at present. In particular, it should be cleared up what "the internal spaces" are responsible for the gauge-invariance principle for the diffractive processes. Nevertheless, a principle connection between the diffraction and the Yang-Mills-type fields exists. It is traced e.g. in that line, which connects non-Abelian gauge theories and the Weyl's geometrical electrodynamics and a string-type solution of nonlinear equations [2]. After all, in the particle physics the string represents the neutral gluonic field - the carrier of the diffractive properties of the interactions on quark-parton level.

4. The predominance of the diffraction in hadronic interactions at high energies.

So one can think, that the more profound general understanding of the particle diffraction will lead to an essential expansion of the area of the diffractive phenomena, though even now their contribution to the total cross-section, by no means, is not small. According to special analysis [4] (the author makes use of the theoretical understanding of the diffraction in gauge theories (in RQT) and of the conception of the pomeron in QCD) in the FNAL - ISR energy interval, the contribution of the diffraction interactions is not less than 95 per cent from 6.2 up. The role

*) It is worth notice a tendency to growth of the total σ_p -interaction cross-section in the region of $E_{\text{cm}} \geq 100-200$ GeV (see ref. on the data in [3]).

of diffraction seems to be so large, that one may speak about true "regeneration" of the strong interactions in the $E_0 \gtrsim 10$ GeV region.

Since the universal properties of the scattering, which act in the diffraction, are important even for GU theory, then all these properties (and, together with them, the diffraction too) work up to complete strengthening of the GU regime. Therefore, there is no reason to expect the decrease of the diffractive contribution when passing to the region of higher energies. On the contrary, it should be expected the increase of its role, because the total unification of the interactions assumes the confluence of its two forms into one.

5. Conclusion. Taking into account that due to a large value of the coupling constant the strong interactions earlier than the others reach a large value of the cross-section and approach GU regime "from above" (whereas the electroweak interactions approach it "from below"), one may conclude, that the observed transition of a number of hadronic process characteristics to certain universal regimes (Fig.1) is the early evidence of the unification regime, in which strong interactions enter.

6. Proposal for cosmic ray investigators.

The interval from the energies of the electroweak unification ($\sim 10^5$ GeV) to the grand synthesis ($\sim 10^{16}$ GeV) is vast. Here one may expect for manifesting of quite new physics. We should remind that up to now any increase of the energy by several orders results in discovery of a new class of the phenomena. The possibility of the phenomenological generalization of the canonical commutation relations for processes at very high energies has been already discussed elsewhere.

For example, it is proved that such modification of the quantum mechanics becomes important at the energies which are typical for GU scheme ($\sim 10^{16}$ GeV) [5]. The other possibilities may appear in the course of more profound understanding both the phenomenon of the diffraction and the mechanism of the unification of the interactions.

A considerable part of the foregoing energy interval of the saturation of the GU regime is available for the cosmic ray particle experiments (up to $E_0 \gtrsim 10^{11}$ GeV) [6]. Due to specific conditions of cosmic ray experiments (limited statistics, high registration thresholds of interaction products) practically only inelastic diffraction of incident hadrons and nuclei is observed in these experiments [7]. This allows to study the process of unification just in the experiments with cosmic ray particles.

References

- [1] Freedman D.Z., van Nieuwenhuizen P. - Scien. Amer., 238, 1978, 126.
- [2] Konopleva N.P., Popov V.N. - Kalibrov. polya, Atomisdat

1980.

- [3] Roos M. et al. - Phys.Lett., B111, 1982, 45.
 [4] White A.R. - Prep. Fermilab-Conf-82/I6-THY, 1982.
 [5] Giffon M., Predazzi E. - Lett. Nuovo Cim., 37, 1983, 430.
 [6] Gusev G.A. et al. - Pisma v ZHETF, 36, 1982, 216.
 [7] Kuchin I.A. - Proc. of the XVIII ICRC, II, 1983, 157.

Figure I.

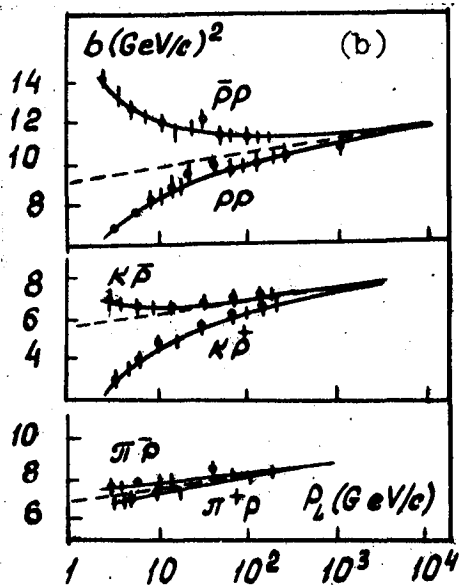
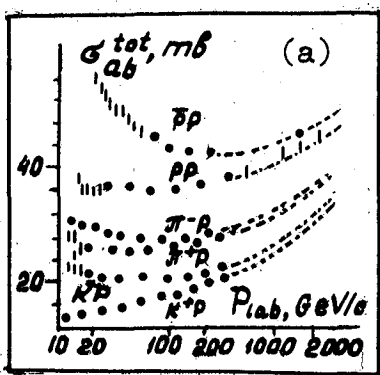


Figure captions.

(a) - The rapprochement of the total cross-section for the interactions of the particle and anti-particle and their transition to some universal regime.

(b) - The same for the slope parameters of the elastic scattering b_{el}^{ab} (s).

IS THE INELASTIC CHARGE-EXCHANGE CONTRIBUTION CONSTANT
AT THE LARGE x AND SUPERHIGH ENERGIES ?

Kuchin I.A.

High Energy Physics Institute
Academy of Sciences of Kazakh SSR,
480082, Alma-Ata, USSR

Abstract. The mechanism explaining the decrease of the inelastic charge-exchange contribution at $x \approx 1$ and $s \rightarrow \infty$ has been proposed.

I. Introduction.

It is customary to think that inelastic charge-exchange (CEX) processes with pions $\pi^+h \rightarrow \pi^0X$ and with nucleons do not decrease with energy growth and along with the processes of the diffraction dissociation (DD), play an important role in production of leading hadrons and \bar{v} -quanta. Sometimes it is motivated by lack of obvious energy-dependence of the RRP-term of the triple Regge expansion of the cross-section for the inclusive reactions [1]. At the same time already from Regge-pole parametrisation of the total cross-section, σ_{ab}^{tot} , one can see that the contribution of the reggeon exchange ($R \neq P$) into σ_{ab}^{tot} as a whole decreases with the growth of total energy \sqrt{s} , as $1/\sqrt{s}$, providing the rapprochement of the total cross-sections of the particle and antiparticle interactions [2].

In this report we shall point out concrete factors, which are responsible for CEX-contribution decrease at $s \rightarrow \infty$ and work near the kinematical limit of the reaction $pp \rightarrow nX^{++}$.

2. Points of departure and formulas.

When discussing the relative contribution of the CEX and DD near the kinematics limit two factors should be taken into account: the limited value of the mass of the particle beam ($M_x^2 \neq \text{const.}$ at $s \rightarrow \infty$) and the dual meaning of the M -dependence in the formula of the triple Regge expansion:

$$s \frac{d^2\sigma}{dt dM_x^2} = \sum_{ijk} G_{ijk}(t) s^{\alpha_i(t) + \alpha_j(t) - 1} (M_x^2)^{\alpha_k(0) - \alpha_i(0) - \alpha_j(0)}$$

the terms with $\alpha_k(0) = 1$ give the background of the resonances in resonance mass region and the terms with $\alpha_k(0) = 1/2$ give the resonances itself as a certain function of M .

Near the kinematical limit one may represent the ijk -term contribution as

$$\frac{d\sigma^{ijk}}{dM_x^2} = \int_{-\infty}^{t_{max}} dt \left(\frac{d^2\sigma}{dt dM_x^2} \right) = \bar{F}_{ijk}(s, M_x^2) \cdot T(s, M_x^2),$$

-where $T(s, M_x^2)$ - is the result of integration of the t -dependence of the process:

$$T(s, M_x^2) = \int_{-\infty}^{t_{max}} dt G_{ijk}(t) \left(\frac{s}{M_x^2} \right)^{(\alpha_i + \alpha_j)t} \cong \frac{\lambda_1}{B_{ij1}} + \frac{\lambda_2}{B_{ij2}}$$

Here the two component form of the $G_{ijk}(t)$

$$G_{ijk}(t) = \sum_p \lambda_p e^{\mu_p t}, \quad B_{ijl} = \mu_l + (\alpha_i' + \alpha_j') \zeta_l \left(\frac{s}{M_x^2} \right)$$

and small value of $t_{max} \approx \frac{m_p^2}{x} (1-x)^2$ in the region of $x \approx 1$ ($1-x = M_x^2/s$) are used. $T(s, M_x^2)$ is a weak (logarithmic) dependence of its arguments, and the behaviour of the triple Regge contributions is determined mainly by the F_{ijk} -function, the explicit form of which is given in the table for different sets of ijk . (Only two trajectories are considered: $\alpha_R(t) = 1/2 + t$ and $\alpha_P(t) = 1 + \epsilon + \delta t$ ($\epsilon = 0.06$, $\delta = 0.3$)).

To elucidate differences in CEX- and DD-behaviour near the kinematical limit we have considered the integral cross-section of the PPR- and RRR-contributions as a function of the upper limit for the integration over the mass.

Numerical estimations of the CEX- and DD- contributions have been carried out using the parametrisation of $G_{ijk}(t)$ from [3].

3. Results of the calculation and discussion.

If only the terms with $k=P$ and $i=j$ are taken into account, then the relative contribution of the CEX does not depend on the energy of the interaction and decreases with the growth of x :

$$R \equiv \sigma_{RRP}^{ex} / \sigma_{PPP}^{DD} \approx (1-x)^{1+2\epsilon}$$

Then, the DD-contribution predominates over the CEX one, beginning with $x \approx 0.85$ (fig.1).

However, it is impossible to extrapolate this dependence into the point $x=1$, without falling into contradiction with the experimental data. Near the kinematical limit of the inclusive reaction $hh \rightarrow hX$ the relation σ^{ex}/σ^{DD} is determined by cross-section of the relevant quasi-two-particle reactions:

$$\frac{\sigma^{ex}}{\sigma^{DD}} \xrightarrow{M_x^2 \rightarrow M_{Res}^2} \frac{\sigma(pp \rightarrow n\Delta^{++})}{\sigma(pp \rightarrow pN^*)} = \text{Const}(M^2) \frac{s^{2[\alpha_R(0)-1]}}{s^{2[\alpha_P(0)-1]}} \approx c \cdot s^{-(1+2\epsilon)}$$

Such behaviour is described by the terms with $k=R$ and $i=j$ or, alternatively, by the two-reggeon-approximation, which effectively takes into account the resonance and background contributions into the reggeon-hadron amplitude.

The ratio of the cross-section σ^{ex} to σ^{DD} , which is expressed via the contributions of the RRR- and PPR-terms, behaves as $\sim 1/s$ with the limited upper value of the mass M

$$\tau \equiv \sigma_{RRR}^{ex}(s, M) / \sigma_{PPR}^{DD}(s, M) \approx \text{Const}(M^2) \cdot s^{-(1+2\epsilon)}$$

However, on energy dependence, the relevant behaviour of the x -distributions (terms with $k=R$) does not join with the regime of the terms, which are dual to background ($k=P$) (fig.1.). To guarantee the smooth transition between them one should take into account the interference terms with $i \neq j$ and different k . The s - and M -dependences of the crossed terms at a given k obey the rule

$$\text{inter} = \sqrt{\text{diff} \cdot \text{nondif}}$$

The accounting of the interference leads to that, the energy-dependent form of the x-distributions (the contribution of the terms with $k=R$) extends from the vicinity $x \approx 1$ to the broader region of $x < 1$ *. At large M_x , when only terms with $k=P$ become essential, the cross-section will depend only on x , and the scaling regime is reconstructed (if $\varepsilon = 0$). The effect of the scaling reconstruction at large M is known [4]. We accent our attention on the factors, which break it down at small M_x .

4. Conclusions.

When prognosing the x-distribution behaviour in super-high energy region ($s \rightarrow \infty$) it is impossible to neglect non-scaling terms with $k=R$, extrapolating the scaling behaviour of the terms with $k=P$ to the point $x=1$.

In the resonance and nearresonance mass region the diffractive and non-diffractive processes, $hh \rightarrow hX$, behave in essentially different way. The energy dependence of resonance diffractive production is approximately the same as for elastic scattering processes (one can expect even a weak growth ($\varepsilon \neq 0$!) of the contribution of the reaction $pp \rightarrow pN_i^*$), whereas the non-diffractive channel decreases as $\sim 1/s$, involving the neighbour regions of the x-spectrum, owing to the action of the interference terms (with $i \neq j$), which decrease only as $\sim 1/\sqrt{s}$ **).

All this taken together should lead to the gradual decrease of the CEX-contribution with energy growth at $s \rightarrow \infty$, which begins close to $x=1$ and extends then to the region of the smaller x .

The study of the CEX processes in the experiments with cosmic ray particles is usually carried out at not too high energies ($E_0 \lesssim 10^{12} - 10^{14}$ eV) and in the limited region of moderately large x ($x \lesssim 0,7 - 0,8$). Apparently, this is not enough to detect the considered effect. It is interesting to observe the CEX-behaviour directly in the region of the utmost large x .

References

- 1 Murzin V.S. et al. - Vzaimod. adr. vys. en., M., 1983, p.20.
- 2 Mukhin S.V. et al. - Yad. Fiz., 30, 1979, 1680.
- 3 Chu S.-Y. et al. - Phys. Rev., D13, 1976, 2967.
- 4 Mukhin S.V. et al. - El. Part. Atomic Nuclei, 8, 1977, 1030.
- 5 Breastone A. et al. - Prep. CERN/EX 84-105.
- 6 Favier J. - In: Proc. XII Rencontre de Morion, 1977, II, 37.
- 7 Webb R. et al. - Phys. Lett., B55, 1975, 331.

*) It is even better to consider together the three - and one-reggeon formulas for one-particle distribution in the incident hadron fragmentation region.

**) By parameterisation of the $G_{ijk}(t)$ the role of the interference terms is not always taken into account, as e. g. in [3].

Table

		$d\sigma_{ijk}/dM^2$	
		$\epsilon = 0$	$\epsilon \neq 0$
diff	PPP	I/M^2	$s^{2\epsilon} M^{-2}(I+\epsilon)$
	FPR	I/M^3	$s^{2\epsilon} M^{-(3+4\epsilon)}$
bond	RRP	I/s	$s^{-I} M^{2\epsilon}$
	RRR	$I/(sM)$	$s^{-I} M^{-I}$
inter	PRP	$I/\sqrt{sM^2}$	$s^\epsilon/\sqrt{sM^2}$
	PRR	$I/(M^2\sqrt{s})$	$s^\epsilon/\sqrt{s} \cdot M^{-2}(I+\epsilon)$

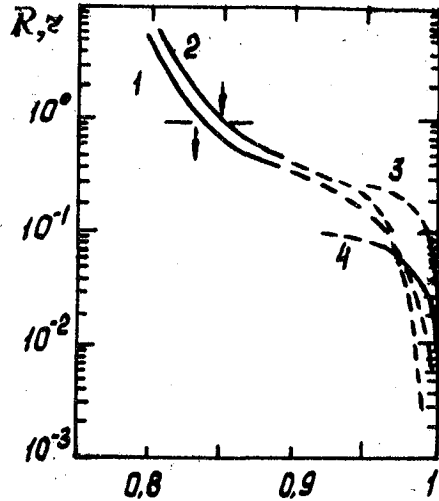


Fig. I.

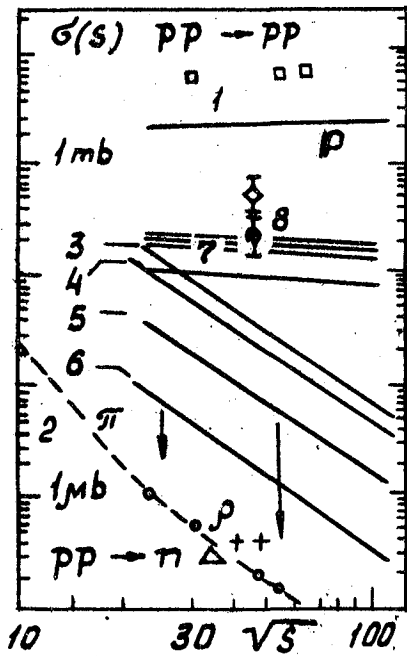


Fig.2.

Figure captions.

Fig. I. The behaviour of the x- distribution. 1- the ratio R for $3I \leq \sqrt{s} \leq 100$ at $\epsilon = 0.06$; 2- the same at $\epsilon = 0$; 3, 4- the ratio r for $\sqrt{s} = 3I$ and 100, respectively.

Fig. 2. The behaviour of the contributions with $k=P$ and $i=j$ near the kinematical limit ($M_x \rightarrow m_\pi$). 1- the elastic scattering cross-section and the contribution of the P-pole (without accounting for the interference with f- and ω - poles); 2- the cross-section of the reaction $pp \rightarrow n\Delta^{++}$ (π - and ρ -regimes) from [6]; 3- 6 - $\sigma^{RRR}(s, M_x^2)$ for $M = 10$; 7.1; 3.2; and 1.4, respectively; 7- $\sigma^{PPR}(s, M)$ for the same values of M; 8 - the contribution of the reaction $pp \rightarrow pN_z^*$ from [7].

GENERAL CONSEQUENCES OF THE VIOLATED FEYNMAN SCALING

G. Kamberov

Department of Mathematics and Mechanics, Sofia State University, Bld. A. Ivanov 5, Sofia, Bulgaria

L. Popova

Institute of Nuclear Research and Nuclear Energy, Bld. Lenin 72, Sofia, Bulgaria

1. Introduction The problem of scaling of the hadronic production cross sections represents an outstanding question in high energy physics especially for interpretation of cosmic ray data. A comprehensive analysis of the accelerator data⁽¹⁾ leads to the conclusion for existence of broken Feynman scaling. It was proposed that the Lorentz invariant inclusive cross sections for secondaries of a given type approach constant in respect to a broken scaling variable x_s . Thus, the differential cross sections measured in accelerator energy \sqrt{s}_0 can be extrapolated to higher cosmic ray energies

$$\frac{E d^3\sigma}{dp_1 dp_2^2} = g(x_s, p_{t1}) = f(x(s/s_0)^{\alpha/2}, p_{t1}) (s/s_0)^{\alpha/2}, \quad (1)$$

where $x = x(s/s_0)^{\alpha}$, $\alpha = 0.26$.

This assumption leads to some important consequences. In this paper we'll discuss the distribution of secondary multiplicity that follows from the violated Feynman scaling, using a similar method of Koba et al⁽²⁾.

2. Derivation of multiplicity distribution in the case of broken Feynman scaling. The distribution of secondary particles in high energy hadron interactions is an object from the first to the recent observations with accelerator facilities. On the other hand, assuming Feynman scaling it was theoretically derived by Koba et al⁽²⁾ that asymptotically $m, n(s)$ is only a function of n/n

$$P_n(s) = G_n(s)/\sigma_{tot}(s) = \frac{1}{\langle n \rangle} \Psi(n/\langle n \rangle), \quad (2)$$

where $G_n(s)$ is the cross section for multiplicity being n at CMS energy \sqrt{s} , $\langle n \rangle$ is the average multiplicity and $\Psi(z)$ is independent function of \sqrt{s} except through the variable $z=n/\langle n \rangle$. The shape of multiplicity distribution has been obtained in a variety of models with rather different theoretical inputs (uncorrelated cluster model⁽³⁾, geometrical models⁽⁴⁾, quark parton model⁽⁵⁾ and dual parton models^(6,7). The theoretical predictions for multiplicity distribution have been found to be approximately true from $\sqrt{s} = 1.5$ Gev up to ISR energy $\sqrt{s} = 63$ Gev⁽⁸⁾, where violation of Feynman scaling was observed. When studying the multiplicity distribution at the collider region at $\sqrt{s} = 540$ Gev the KNO scaling does not necessarily holds for part of the phase space corresponding to higher multiplicities⁽⁹⁾. There is a clear indication of an increa-

sing high multiplicity tail. It causes that many of the original models have been amended to accommodate the observed scaling violation by assuming that between the collider and ISR energies some new physical mechanism (rescattering, three gluon coupling) characterized by higher multiplicity started becoming important. We will examine what follows from breaking of Feynman scaling. Let us assume scaling on x for the distribution functions integrated over the transverse momentum

$$\begin{aligned} \tilde{g}^{(q)}(x_{s1}, \dots, x_{sq}) &= \int g^{(q)}(x_{s1}, p_{t1}, \dots, x_{sq}, p_{tq}) dp_{t1}^2 \dots dp_{tq}^2 = \\ &= \left[\frac{s}{s_0} \right]^\alpha \tilde{g}(x_1 \left[\frac{s}{s_0} \right]^{-\alpha}, \dots, x_q \left[\frac{s}{s_0} \right]^{-\alpha}) \end{aligned} \quad (3)$$

There is needed only that the transverse momentum is limited as \sqrt{s} goes to infinity. In eq.3 are used functions which incorporate q particular semi-inclusive cross sections. We can derive the moments of multiplicity distribution in an analogical way to that of Koba et al. Thus, for secondaries with rest mass m we set

$$\langle n(n-1) \dots (n-q+1) \rangle = \sum_n P_n(s) n(n-1) \dots (n-q+1) =$$

$$\begin{aligned} &= \int g^{(q)}(x_{s1}, p_{t1}, \dots, x_{sq}, p_{tq}) \prod_{i=1}^q \frac{dx_{si} dp_{ti}^2}{x_{si}^2 + \frac{p_{ti}^2 + m^2}{(s/4)^{1-\alpha}}} = \\ &= 2 \int \left\{ \left[g^{(q)}(x_{s1}, p_{t1}, \dots, x_{sq}, p_{tq}) \cdot \ln \left(x_{s1} + \sqrt{x_{s1}^2 + \frac{p_{t1}^2 + m^2}{(s/4)^{1-\alpha}}} \right) \right]_0^{\sqrt{s}} - \right. \\ &\quad \left. - \int dx_{s1} \frac{\partial}{\partial x_{s1}} g^{(q)}(x_{s1}, p_{t1}, \dots, x_{sq}, p_{tq}) \cdot \ln \left(x_{s1} + \sqrt{x_{s1}^2 + \frac{p_{t1}^2 + m^2}{(s/4)^{1-\alpha}}} \right) x \right. \\ &\quad \times \left. \prod_{i=2}^q \frac{dx_{si} dp_{ti}^2}{x_{si}^2 + \frac{p_{ti}^2 + m^2}{(s/4)^{1-\alpha}}} \dots \frac{dx_{sq} dp_{tq}^2}{x_{sq}^2 + \frac{p_{tq}^2 + m^2}{(s/4)^{1-\alpha}}} \right. \\ &= \int \ln \frac{(s/4)^{1-\alpha}}{(p_{t1}^2 + m^2)} \left[g^{(q)}(0, p_{t1}, x_{s2}, p_{t2}, \dots, x_{sq}, p_{tq}) + \frac{W}{\ln \frac{(s/4)^{1-\alpha}}{(p_{t1}^2 + m^2)}} d^2 p_{t1} \right. \\ &\quad \times \left. \frac{dx_{s2} d^2 p_{t2}}{x_{s2}^2 + \frac{p_{t2}^2 + m^2}{(s/4)^{1-\alpha}}} \dots \frac{dx_{sq} d^2 p_{tq}}{x_{sq}^2 + \frac{p_{tq}^2 + m^2}{(s/4)^{1-\alpha}}} \right] \end{aligned} \quad (4)$$

where the integral $W = \int dx_{s1} \frac{\partial}{\partial x_{s1}} g^{(q)}(x_{s1}, p_{t1}, \dots, x_{sq}, p_{tq}) \ln \left(x_{s1} + \sqrt{x_{s1}^2 + \frac{p_{t1}^2 + m^2}{(s/4)^{1-\alpha}}} \right)$ converges. After integration of eq.4 we obtain

$$\langle n(n-1)\dots(n-q+1) \rangle = \int \ln \frac{(s/4)^{1-\alpha}}{p_{t1}^2 + m^2} \dots \ln \frac{(s/4)^{1-\alpha}}{p_{tq}^2 + m^2} \left[g^{(q)}(0, p_{t1}, \dots, 0, p_{tq}) \right. \\ \left. + O\left(\frac{1}{\ln s^{1-\alpha}}\right) \right] dp_{t1}^2 \dots dp_{tq}^2 = \tilde{g}^{(q)}(0, \dots, 0) (\ln s^{1-\alpha})^q + O((\ln s^{1-\alpha})^{q-1}),$$

where $O((\ln s^{1-\alpha})^{q-1})$ means terms that at most go like $(\ln s^{1-\alpha})^{q-1}$. Consequently the same asymptotic behaviour has not only the mean value of any q -order polynomial of n but the mean value of n as well. Taking into account eq.3 we can set

$$\int_0^\infty n^q \cdot p_n(s) \cdot dn = \sqrt{\frac{s}{s_0}}^\alpha \tilde{f}^{(q)}(0, \dots, 0) (\ln s^{1-\alpha})^q + O((\ln s^{1-\alpha})^{q-1}). \quad (5)$$

Dividing eq.5 by $\sqrt{\frac{s}{s_0}}^\alpha (\ln s^{1-\alpha})^q [\tilde{f}^{(1)}(0)]^q$ we obtain

$$\int_0^\infty z \cdot p_z(n)(s) \cdot \tilde{f}^{(1)}(0) \sqrt{\frac{s}{s_0}}^\alpha \ln s^{1-\alpha} \cdot dz = \frac{\tilde{f}^{(q)}(0, \dots, 0)}{[\tilde{f}^{(1)}(0)]^q} + O\left(\frac{1}{\sqrt{s} \ln s^{1-\alpha}}\right), \quad (6)$$

where

$$z = \frac{n}{\tilde{f}^{(1)}(0) \sqrt{\frac{s}{s_0}}^\alpha \ln s^{1-\alpha}} \quad (7)$$

We assume that the function

$$\tilde{f}^{(1)}(0) \sqrt{\frac{s}{s_0}}^\alpha \ln s^{1-\alpha} p_z(n)(s) = \Psi(z) + O\left(\frac{1}{\sqrt{s} \ln s^{1-\alpha}}\right)$$

is determined uniquely by the moments (5). Thus, to the highest order in $\sqrt{s} \ln s^{1-\alpha}$ we have the following broken scaling result

$$p_n(s) = \frac{1}{\langle n \rangle} \Psi(z) + O\left(\frac{1}{\langle n \rangle^2}\right), \quad (8)$$

where the mean multiplicity as function of \sqrt{s} is

$$\langle n \rangle \sim \tilde{f}^{(1)}(0) \sqrt{\frac{s}{s_0}}^\alpha \ln s^{1-\alpha}. \quad (9)$$

3. Comparison of the broken Feynman scaling results for the multiplicity distribution with experimental data in accelerator energy range. In figure 1 we have compared the multiplicity distribution function specified by the semi-inclusive cross sections from FNAL which are published in the paper of Kafka et al/14/ for multipartical production up to above two times larger than the mean value of multiplicity. It is seen that the distribution of relative multiplicity scales at least for the range of not very large multiplicities which are responsible for the typical events in cosmic ray experiments.

As far as the average multiplicity is concerned the assumption for breaking of Feynman scaling gives a good agreement with the acceleration observations in wide energy range up to 10^5 Gev. The energy dependence of mean multiplicity according eq.9 is compared in figure 2 with accelerator data taken from Carlson/15/.

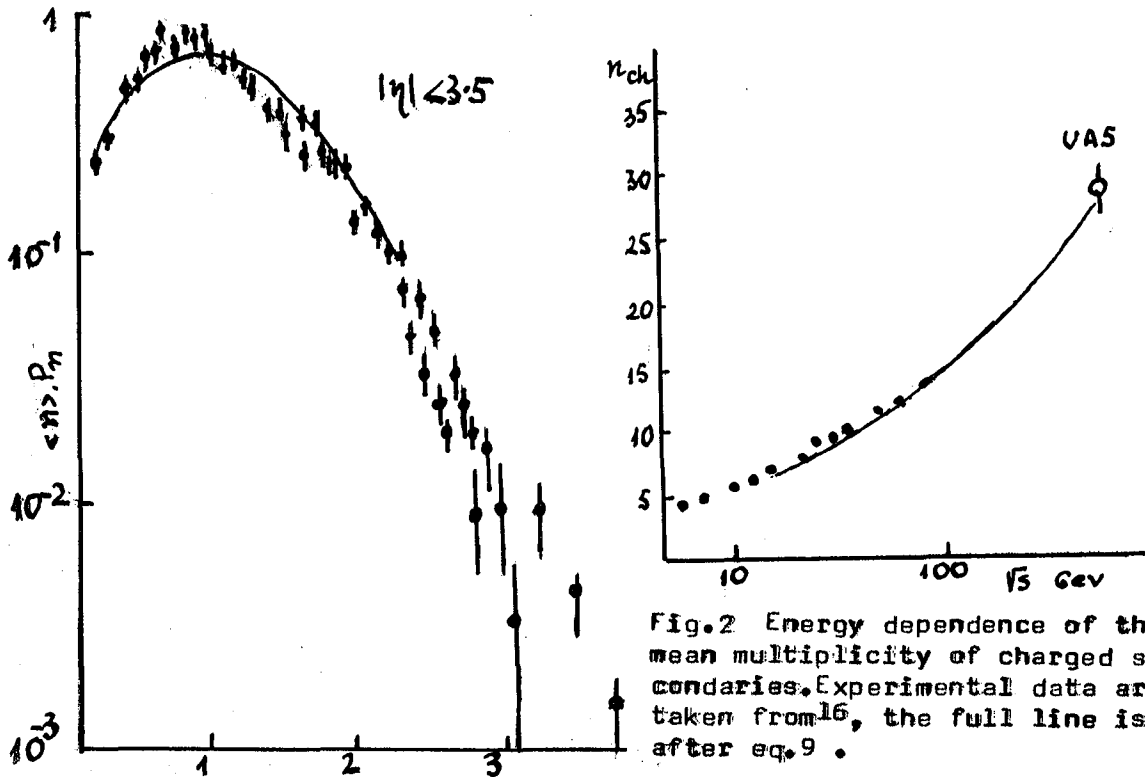


Fig.2 Energy dependence of the mean multiplicity of charged secondaries. Experimental data are taken from¹⁶, the full line is after eq.9 .

Fig.1 Comparison of our parametrisation of the multiplicity distribution (made on the basis of FNAL data) with SPS data for $|\eta| < 3.5$. The latter are representative of the shape of the full distribution.

$$Z = n / \langle n \rangle$$

We can conclude that for the purposes of cosmic ray investigation: scaling of multiplicity distribution derived from broken Feynman scaling can be assumed in order to prescribe the semi-inclusive cross sections at very high energies.

References

1. Wdowczyk J. and Wolfendale A. Nuovo Cimento 54, A, 4, 433, 1979
2. Koba Z., Nielsen H.B. and Olesen P. Nucl. Phys. 840, 317, 1972
3. DeGroot E.H. Phys. Lett. 57B, 159, 1975
4. Chow T.T. and Yang C.N. Phys. Lett. 116B, 301, 1982
5. Takagi F. Zeit. fur Phys. C13, 301, 1982
6. Kafidalov A.B. and Ter-Martirosyan K.A. Phys. Lett. 117B, 247, 1982
7. Capella A. and J. Tran Thanh Van, Phys. Lett. 114B, 450, 1982
8. Thome W. et al. Nucl. Phys. B129, 365, 1977
9. Almer G.J. et al. Phys. Lett. 138B, 305, 1984
10. Pancheri G. Invited Talk XV Symp. Multipart. Dyn. Lund, 1984
11. Capella A. and J. Tran Thanh Van, Orsay reprint LPTHE 83/39, 1983
12. Pancheri G. and Srivastava Y.N. Frascati Preprint 1984
13. Cai Xu and Liu Lian-sou, Lettere al Nuovo Cimento 37, 495, 1983
14. Kafka T. et al Phys. Rev. D16, 5, 1261, 1977
15. Per Carlson XI Intern. Winter Meet. on Fundamental Phys., Toledo, 83

PROPAGATION OF COSMIC RAYS THROUGH THE ATMOSPHERE
IN THE QUARK-GLUON STRINGS MODEL.

Erlykin A.D., Krutikova N.P.

P.N. Lebedev Physical Institute, Leninski pr. 53,
Moscow, 117924, USSR.

Shabelski Yu.M.

Leningrad Nuclear Physics Institute, Gatchina,
Leningrad district, 188350, USSR.

Quark-gluon strings model succeeds in the description of multiple hadron production in the central rapidity region of nucleon-nucleon interactions. This model has been developed for hadron-nucleus interactions and used for calculation of the cosmic ray propagation through the atmosphere. It is shown that at energies $10^{11} - 10^{12}$ eV this model gives a satisfactory description of experimental data. But with the increase of the energy up to $\sim 10^{14}$ eV results of calculations and of experiments begin to differ and this difference rises with the energy. It may indicate that the scaling violation in the fragmentation region of inclusive spectra for hadron-nucleus interactions is stronger than in the quark-gluon strings model.

Quark-gluon strings model (QGSM) describes successfully rather wide set of experimental data on the multiple hadron production in nucleon-nucleon collisions /1,2/. One of us (Yu.M.Sh.) developed this model for hadron-nucleus interactions. The weak scaling violation typical for that model becomes stronger after the transition from hp to hA collisions. In the fig.1 inclusive spectra of charged pions are shown. They were calculated according to QGSM with a magnitude of pomeron intercept $\Delta = 0.14$ for pN^{14} -collisions at energies 10^{11} and 10^{16} eV. It is seen that spectra become considerably softer in this energy range. For instance pion spectra at $x=0.5$ fall down by the factor 2,17. This model was used to calculate the penetration of cosmic rays through the atmosphere. The calculation routine was worked

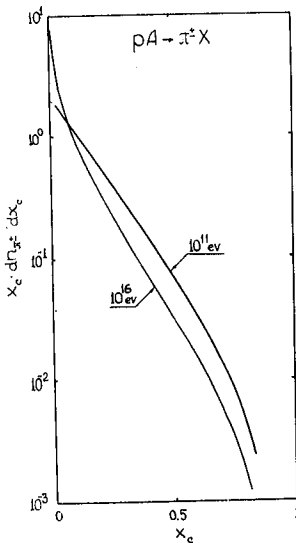


Fig. 1.

$$I(\geq E) = 8.04 \cdot 10^{-4} (E/0.1)^{-1.70} [B_p (1 + 6 \cdot 10^{-4} \cdot E)^{-0.4} + \sum_A B_A (E/0.1)^{\Delta\gamma_A} (1 + 10^{-2} A^{-1} E)^{-0.4}] \text{ cm}^{-2} \text{ sec}^{-1} \text{ ster}^{-1} \quad (1)$$

where E - in TeV, $B_p = 0.41$, $B_4 = 0.22$, $B_{15} = 0.13$, $B_{27} = 0.14$, $B_{56} = 0.10$, $\Delta\gamma_4 = 0$, $\Delta\gamma_{15} = \Delta\gamma_{27} = \Delta\gamma_{56} = 0.04$.

From the comparison of calculated and observed energy spectra of muons and hadrons at mountain level, which were measured by the most precise calorimetric method (fig.2,3), from similar comparison of mass and charge ratios of hadrons (data are not presented here due to the lack of space) one can conclude that QGSM gives a satisfactory agreement with experimental data at energies 10^{11} - 10^{12} eV. Perhaps the only desirable improvement of this model at accelerator

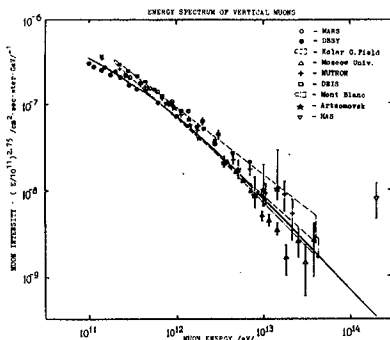


Fig. 2.

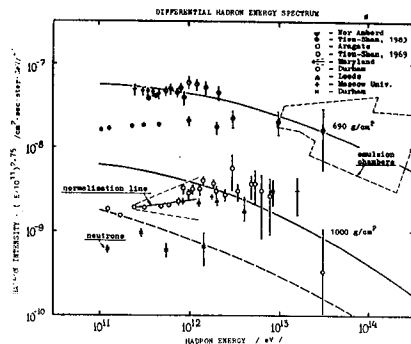


Fig. 3.

out and used in papers /3,4/. Figures 2,3,4 demonstrate results of calculations compared with experimental data on energy spectra of muons at sea level, hadrons and gamma-quanta at different levels in the atmosphere. Energy spectrum and the mass composition of primaries were taken on the base of direct measurements at energies 10^{11} - 10^{13} eV and small EAS data at energies 10^{13} - 10^{15} eV /5/. These spectrum and the mass composition may be presented as

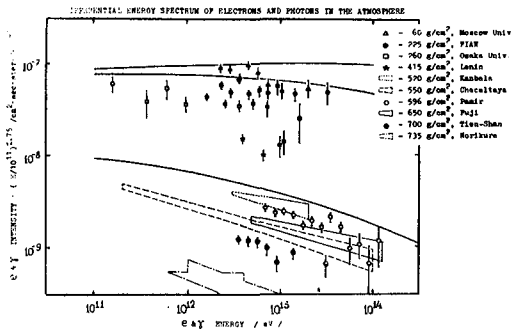


Fig. 4. *)

primary particles with energies above 10^{14} eV are responsible. It is seen in the figure 4 that calculation gives gamma-quanta intensities which exceed as a rule experimental values. This excess at mountain level is about the factor of 1.5. Uncertainties in the primary energy spectrum and mass composition could hardly explain the difference between calculations and experiments, since the spectrum (1) has the intensity at $\sim 10^{15}$ eV, which is at the lower end of the existing uncertainty. For example, spectra proposed by Nikolsky /6/ and by Maryland group /7/ give by ~ 1.4 higher intensities at this energy. It is not possible to vary the mass composition too, not coming to a contradiction with experimental data /8/. It is known that energy spectra of muons and gamma-quanta are most sensitive to the scaling violation in the fragmentation region of pion and kaon inclusive spectra. The observed excess of calculated intensities above experimental ones, the latter being stable in the future, indicates that the scaling violation for hadron-nucleus interactions is evidently stronger than in the present version of QGSM ($\Delta = 0,14$). This conclusion agrees with results of the analysis of lateral and energy characteristics of gamma families, according to which inclusive spectra in the fragmentation region go down not less than by the factor $3 \div 5$ when the collision energy increases from accelerator energies to 10^{16} eV /9/. Such a conclusion indicates possible direc-

energies is some reduction of the neutron flux, which influence on the muon charge ratio too.

Energy spectra of gamma-quanta are most sensitive to the high energy region. For gamma-quanta with energies 10^{13} eV at mountain level

tions of further improvement of this model at high energies.

References.

1. Kaidalov A.B. Phys.Lett 116B,459,1982.
2. Kaidalov A.B., Ter-Martirosyan K.A. Phys.Lett.117B,247, 1982; Yad.Fiz.39,1545,1984;40,211,1984.
3. Erlykin A.D., Kuzina N.P. 17 ICRC, Paris, 1981, 5, 243.
4. Adamov D.S. et al. 18 ICRC, Bangalore, 1983, 5, 275.
5. Danilova T.V. et al. VANT, 3/20/, 20, 1984 (in Russian).
6. Nikolsky S.I. Workshops on cosmic ray interactions and high energy results, La-Paz-Rio de Janeiro, July 1982, 336. JETP, 87, 18, 1984 (in Russian).
7. Cowsik R. et al. 17 ICRC, Paris, 1981, 2, 120.
8. Stamenov J.N. et al. 18 ICRC, Bangalore, 1983, 2, 111.
9. "Pamir" coll. 18 ICRC, Bangalore, 1983, 5, 425.

*) Upper full curve in the Fig.4 corresponds to calculations for the depth 60 g/cm^2 , middle one - for 260 g/cm^2 and the lower one - for 600 g/cm^2 .

SCALING VIOLATION IN THE FRAGMENTATION
REGION OF INCLUSIVE NUCLEON SPECTRUM

S.K. Machavariani, S.I. Nikolsky, A.P. Chubenko

P.N. Lebedev Physical Institute

Moscow, USSR

Spectra of EAS associated with hadrons of various energies from 5 to 80 TeV have been investigated. Results could be interpreted as scaling violation in the fragmentation region of secondary particles generated in inelastic interactions of primary protons at the energy above 30 TeV.

Simultaneous observation of high energy hadron and EAS let us investigate inclusive spectra of hadrons in the fragmentation region.

Significant part of hadron flux in the atmosphere are nucleons. The connection between the nucleon flux at the depth and the spectrum of primary nucleons is

$$F(>E, t) = \sum_{n=0}^{\infty} F(>E_0) e^{-t} (t^n/n!) x^{\gamma-1}$$

where γ - the index of the primary spectrum, $x=E/E_0$, t - the observation depth in units of mean free path for inelastic collisions. It should be noted that events with $n \leq 3$ at the depth of 700g/cm² dominate. Qualitative experimental picture is not changed considerably if one takes into account the energy dependent cross-section of hadron interaction as well as the inclusive spectrum of secondary hadrons.

The table shows the percentage of the primary protons which had only one inelastic collision at 700g/cm². The calculation was made with the accelerator cross-sections and inclusive spectra.

x	0.9	0.82	0.67	0.54	0.44	0.36	0.3
n=1	100	70	60	55	50	40	35

If we add to mention above that at $x \geq 0.3$ all observed hadrons are produced by primary protons then it is clear that analysis of hadron data and EAS accompanying them give us good opportunity to investigate hadron inclusive spectra in the fragmentation part.

In this paper the total EAS spectrum of accompanying hadrons of given energy is considered.

It appears that for scaling model and constant mass composition of primaries the investigated spectrum of EAS for various E_0 must be similar or must have scaling behavior.

The experimental data of Tien-Shan complex installation /1/ on the spectrum of EAS associated with hadrons for energy intervals (5-7.5), (10-20) and (40-80) TeV are present-

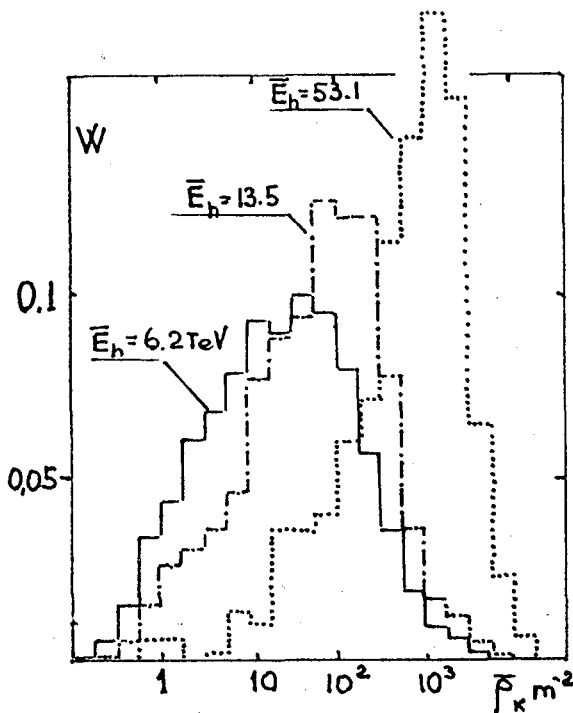


Fig.1 Spectra of EAS associated with hadrons of various energy (exper.) $\bar{\rho}_k$ - average density of particles in the centre $N_e = \bar{\rho}_k \cdot 10^3$, $E_0 = 3 \cdot \bar{\rho}_k \text{ TeV}$.

ted at fig.1. Separation of hadrons and measurement of its energy have been made by means of ionization calorimeter. The space resolution of the calorimeter is about $0.25 \times 0.25 \text{ m}^2$, that is why the hadron jet may consist of several hadrons. Our experimental data are related to the most energetic hadron jets in the calorimeter which occupy less than $0.75 \times 0.75 \text{ m}^2$. We calculate the distribution of EAS for the average density of particles in the array which consists of 64 scintillator detectors and cover the area about 100 m^2 ($\bar{\rho}_k$). The density of particles in the EAS centre has large fluctuations but it does not require knowledge of the lateral distribution of particles for E_0 estimation.

One can see that the experimental $\bar{\rho}_k$ distributions for various \bar{E}_h presented in fig.1 have not the scaling character. The most probable value of $\bar{\rho}_k$ is not proportional to \bar{E}_h ($\bar{\rho}_k \sim \bar{E}_h^{3/2}$) and the $\bar{\rho}_k$ distribution becomes narrower with increasing \bar{E}_h . We can suggest three following reasons for this result:

1. Systematic errors in the experiment.
2. Mass composition of primary cosmic rays is not constant.
3. The scaling violation in the fragmentation region of secondary hadrons.

The methodical effect can be evaluated by the following way. The fig.2 shows the fluxes of recorded hadron jets. In the first case the energy was obtained in the calorimeter over the square at $0.75 \times 0.75 \text{ m}^2$ and in the second - the energy was determined over the square of $0.25 \times 0.25 \text{ m}^2$ and multiplied by 1.5. The coefficient 1.5 was estimated from data on the lateral energy distribution for single hadron. The index of the hadron jet spectrum in the first case is $1 + \gamma = 1.6$ for larger square and $1 + \gamma = 1.75$ in the second case.

The results of our measurements of the total hadron jet flux in the energy range (200-2000) GeV /2/ are also shown in fig.2. The lack of calorimeter resolution doesn't effect intensities at these energies. It seems that our value for intensity is close to calculated one /2/ as well as to data /3/ obtained with spark chamber calorimeter. The power law fit for the data on hadron flux obtained with the help of X-ray film chamber /4/ in the energy range (20-500) TeV has

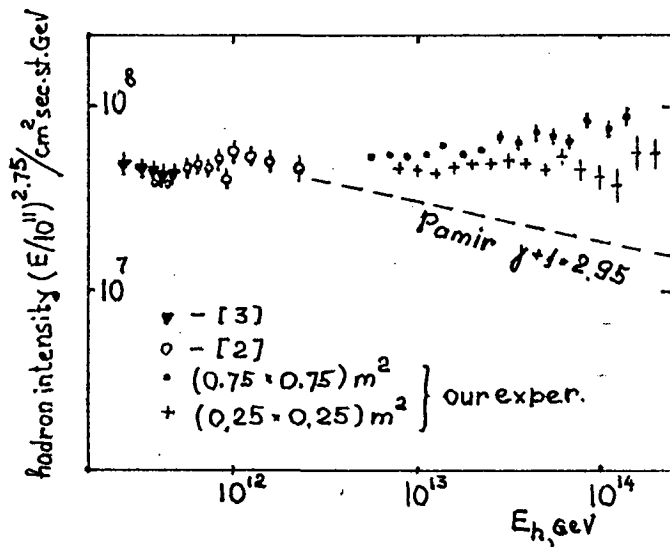


Fig.2 Hadron energy spectrum at mountains ($H=700 \text{ g/cm}^2$)

the exponent $\gamma+1=1.95\pm 0.05$ (and in the X-ray chamber with thick carbon layer $1+\gamma=1.8\pm 0.15$).

The exponent γ is the most reliable value among X-ray film data and as one can see it does not differ much from our value of $1+\gamma=1.75$ obtained for hadron jets in calorimeter region $0.25 \times 0.25 \text{ m}^2$.

We extrapolated the hadron spectrum for $E \leq 1 \text{ TeV}$ with exponent $\gamma+1=1.95$ to the energy range $E > 5 \text{ TeV}$ in order to estimate

the error in determining the energy due to recording of jets. At the energy $E \sim 5 \text{ TeV}$ the value of overestimation is about 1.25 and at $E=100 \text{ TeV} \sim 1.5$. The spectrum of EAS associated with hadron may be distorted due to different overestimation of the hadron energy but the difference is not more than 20% for energy changing from 5 TeV to 100 TeV. Therefore we can neglect this methodical effect.

The distortion of experimental spectrum may be due to primary nuclei. In this case the lateral combination of nucleons into jets increases the number of observed events with the same energy per nucleon because the energy losses of the leading nucleon are compensated by another nucleons of the primary nucleus. This ability will be studied.

We have simulated only two possibilities. We assumed the model of hadron nucleus interaction /5/ based on accelerator data. In the first version of calculation we proposed that the index of primary energy spectrum changes from $\gamma+1=2.6$ to $\gamma+1=3.6$ at the primary proton energy $E_p=10 \cdot E_h$, where E_h is the energy of hadrons (histogram h_2 in fig. 3^h). In the second version we suggested the reduction of the inclusive cross-section for the production of secondary nucleons with $X \geq 0.5$ by the factor 2 at the expense of increasing number of nucleons and pions with $x \leq 0.3$.

As one can see in fig.3 (histogram 3) the second version is in better agreement with the experiment than the first one which assumes the change of primary composition.

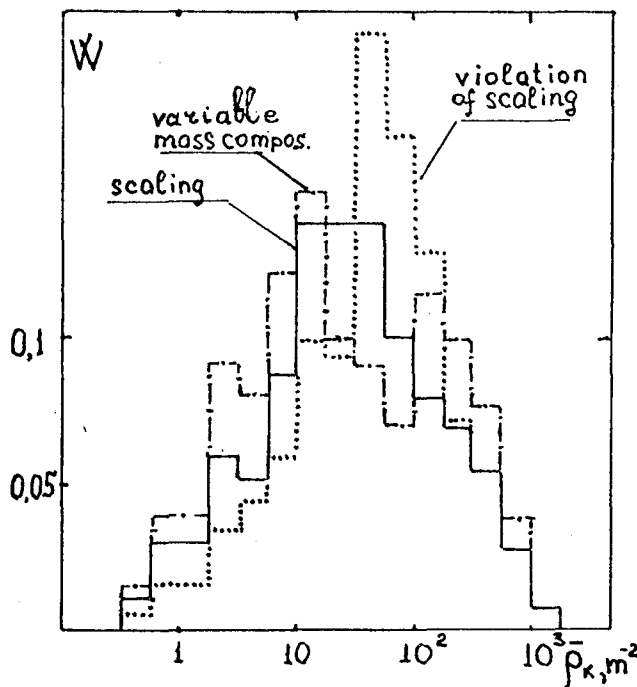


Fig.3 Spectra of EAS associated with hadrons (simulation).

Our conclusion about scaling violation in the fragmentation region of inclusive nucleon spectrum is not quite well-grounded. More detailed analyses of experimental data, especially at $x \geq 0,3$ (pure proton region), and comparison with model simulation are necessary.

References

1. Amineva T.P., (1970), TRUDY FIAN, 46, 157
2. Adamov D.S., et al, (1983), 18 ICRC, Bangalore, 5, 275.
3. Shmeleva A.P. et al (1983), 18 ICRC, Bangalore, 5, 271.
4. "Pamir" coll., (1984), TRUDY FIAN, 154.

**DETERMINATION OF PRIMARY ENERGY IN NUCLEUS-NUCLEUS COLLISIONS
AND THE HIGH p_T TAIL OF α -PARTICLES**

P. S. Freier and T. W. Atwater
School of Physics and Astronomy, University of Minnesota
Minneapolis, Minnesota 55455

Abstract. A determination of primary energy is required in order to study the energy dependence of meson multiplicity in A-A collisions in cosmic rays. Various procedures which estimate the energy of a primary nucleus from its interaction have been investigated. We have used an average of two methods, one using the pions and wounded protons and the other using spectator protons and α -particles. The high p_T tail observed for $Z = 2$ fragments requires a modification of the latter method.

1. Introduction. From accelerator studies of 1.7 and 3.7 GeV/amu of A-emulsion inelastic collisions, the distribution in p_T for projectile fragments has been measured for ^{12}C , ^{14}N , ^{16}O and ^{56}Fe beams.¹⁻⁴ Although the distribution in p_T for $Z = 1$ fragments is consistent with a Gaussian-like distribution

$$\frac{dN}{dp_T} = \frac{p_T}{\sigma^2} \exp(-p_T^2/2\sigma^2) \quad (1)$$

with $\sigma = 100$ MeV/c ($\langle p_T \rangle = 125$ MeV/c),³ for fragments of $Z \geq 2$ there is a marked deviation from this shape due to the presence of a tail of large momentum transfers. This high p_T tail results in $\langle p_T \rangle$ being significantly larger than the $\langle p_T \rangle$ expected from eq. (1). For $Z = 2$ fragments from ^{12}C , $\langle p_T \rangle = 241 \pm 8$ MeV/c,¹ and from ^{56}Fe , $\langle p_T \rangle = 370 \pm 10$ MeV/c.³ $\langle p_T \rangle$ seems to depend only weakly on target A, ($\sim A^{0.05}$) but the dependence on projectile A is more pronounced ($\sim A^{0.25}$).³ This increase in $\langle p_T \rangle$ is mainly due to the enhancement of the high p_T tail with A of the projectile. We shall show that the high p_T tail is also enhanced as the energy of the projectile is increased.

2. Measurements on Beam Projectiles. We have analyzed 105 ^{55}Mn -emulsion interactions at $\langle E \rangle = 1.69 \pm 0.3$ GeV/amu, measuring the emission angles of fragments, α -particles, protons, and mesons. The angular distribution of α -particles is shown in Fig. 1. The transverse momentum, p_T , is calculated from the angle assuming ^4He is emitted at the same momentum per nucleon, p_0 , as the projectile had at the interaction:

$$p_T = 4 p_0 \sin \theta \quad (2)$$

The peak in the angular distribution corresponds to p_T (peak) = 240 MeV/c, while $\langle p_T \rangle = 356 \pm 20$ MeV/c. This $\langle p_T \rangle$ value agrees very well with the value 370 ± 10 MeV/c measured by Chernov et al.³ for α -particles from ^{56}Fe at 1.7 GeV/amu.

The emission angles of α -particles from ^{179}Au -emulsion interactions at 0.5 - 1.0 GeV/amu are also shown in Fig. 1. (The energy at each interaction was calculated by correcting for ionization loss of the

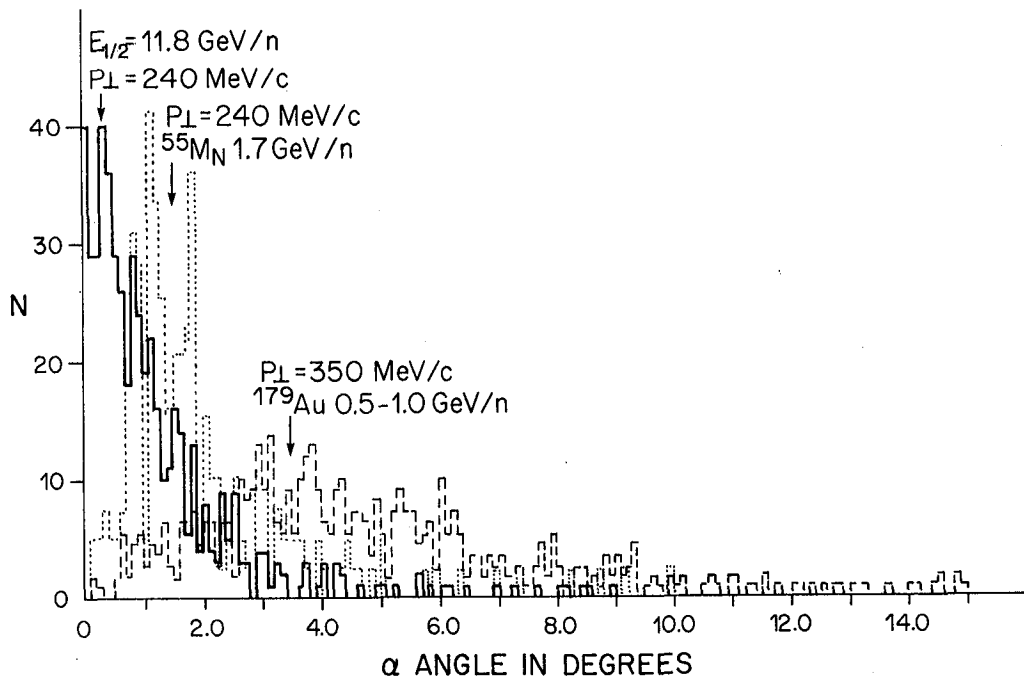


Fig. 1. Angular distributions of α -particles from A-emulsion interactions. Mn at 1.7 GeV/amu; --- Au at 0.5-1.0 GeV/amu; — cosmic rays, $Z = 6-26$ at $E \geq 7.5$, $E_{1/2} = 11.8$ GeV/amu. The arrows show the angles corresponding to the measured $p_T(\text{peak})$ for Mn and Au and to $p_T(\text{peak}) = 240$ MeV/c at the median energy for cosmic rays.

projectile.) There is a marked shift of the angular distribution to larger angles due both to the lower primary energy but also to an increase in $p_T(\text{peak})$ and an enhanced tail of high momentum transfers. The peak corresponds to $p_T = 350$ MeV/c but $\langle p_T \rangle = 520$ MeV/c.

We have used the angles of emitted mesons, protons, and α -particles from ^{55}Mn -emulsion interactions to calculate the energy of the Mn projectile using two different methods: one uses the participant protons (WP) and produced mesons (M), and the second uses the spectator protons (SP) and α -particles. Paper HE 1.4-10 of these proceedings discusses the first method and the separation of spectator and participant protons.⁵ This paper discusses the second method and what adjustments are required in applying it to higher energy cosmic ray projectiles.

Providing p_T is approximately independent of energy, we can estimate the primary energy from

$$P_{\text{primary}} = \frac{p_{T\text{SP}}^{\text{eff}} \sum_i N_{\text{SP}} \frac{1}{\sin \theta_i} + \frac{1}{4} p_{T\alpha}^{\text{eff}} \sum_i N_{\alpha} \frac{1}{\sin \theta_i}}{N_{\text{SP}} + N_{\alpha}} \quad (3)$$

where P_{primary} is the momentum per nucleon and the p_T are effective values of spectator and α -particle transverse momentum given in the

Table. This estimate of energy (eq. 3) will be dominated by spectator protons since $\langle N_{SP} \rangle \sim 4 \langle N_{\alpha} \rangle$. The Table shows the peak values of p_T for α -particles and spectator protons measured in the interactions of the ^{55}Mn beam. The p_T used for wounded protons and mesons (discussed in Paper HE 1.4-10) are also shown in the Table. The "beam" average and median energies are shown in columns 2 and 3 of the Table and can be compared to the calculated energies in columns 8 and 9. The calculated energies are simply averaged from the spectator and participant energy determinations. Figure 2 shows this average energy for the Mn beam. Some 70% of the particles have measured energies within $E \pm E/2$.

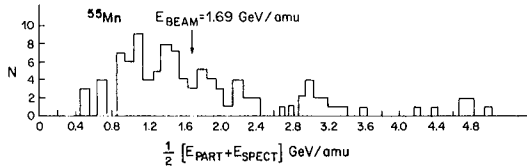


Fig. 2. The distribution in measured energy, $1/2[E(\text{participant}) + E(\text{spectator})]$, for a 1.69 GeV/amu Mn beam.

Table. Effective p_T used in Energy Determination

Beam	p_T^{eff} (MeV/c)						Energy (GeV/amu)		Tail/Peak
	\bar{Z}	$\langle E \rangle$	$E_{1/2}$	SP	α	WP	M	$\langle E \rangle$	
25.0	1.69	1.68	101	232	575	175	2.03	1.51	0.020
13.0	5.50	3.00	106	232	438	179	5.67	2.82	0.084
14.5	19.60	11.80	255	680	691	384	19.90	12.40	0.218

3. Energy Measurements on Cosmic Ray Nuclei. Using the same techniques as used for Mn, we determined the energy of each cosmic ray primary from its interaction. For the 1000 nuclei measured over Texas where $E \geq 1.7$ GeV/amu, the p_T values determined from the Mn beam gave reasonable measurement of energy (see Table). However, for the 500 nuclei measured over India where $E \geq 7.5$ GeV/amu, the energies determined from the spectators using the same values of p_T were far too low. A remeasurement of many of the angles showed they were correct to within $\pm 0.1^\circ$. The observed peak in the α -particle angular distribution is consistent with the beam value $p_T(\text{peak}) = 240$ MeV/c and the median cosmic ray energy, $E_{1/2} = 11.8$ GeV/amu (see Fig. 1). However, the tail to peak ratio, where the cut is defined as six times the peak angle, is much larger in India (see Table). The result is too many low energy events. (For a higher angle cut there were no particles in the Mn tail; the tail to peak ratio for Au is 0.005.)

The effective p_T for the cosmic rays given in the Table were determined by the requirement that the calculated energies fit the cosmic ray energy spectrum as closely as possible. Figure 3 shows the resulting energy spectrum of the 500 particles measured in India compared to a power law in total energy of $E^{-1.7}$. The energy measured from 1000 particles at Texas ($E > 1.7$ GeV/amu) fits equally well.

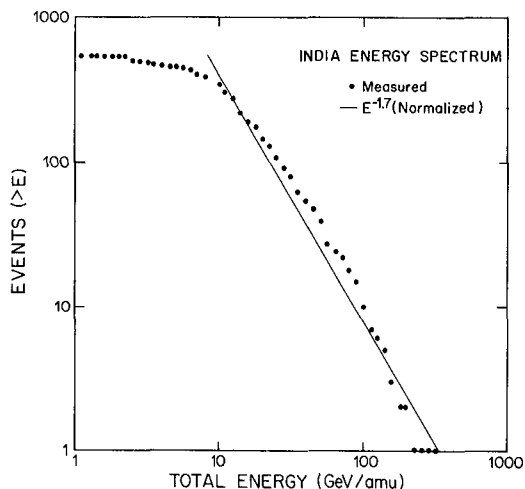


Fig. 3. The integral energy spectrum measured by $1/2 [E_{\text{part}} + E_{\text{spect}}]$ compared to the accepted cosmic ray spectrum, $J > E = kE^{-1.7}$.

4. Conclusions. Calculation of energies of primary cosmic rays using a method assuming constant p_T of fragments fits the known energy spectrum for a low energy data set ($E > 1.7$ GeV/amu). The required effective p_T for cosmic rays > 7.5 GeV/amu are high. The high p_T^{eff} for α -particles can be attributed to the high p_T tail. Since p_T^{eff} for protons must be increased by about the same factor to fit the cosmic ray spectrum, it appears that a high p_T tail must also be present for spectator protons. The high p_T tail increases with energy.

5. Acknowledgements. This work was supported in part by NSF Grant PHY-8405852 and NASA Grant NGR 24-005-050.

References

- ¹Bucharest-Warsaw-Dubna-Kosice-Leningrad-Moscow-Tashkent collaboration (1980), Sov. J. Nucl. Phys. **32(5)**, 716.
- ²Bjarle, C., et al. (1982), Nucl. Phys. A **381**, 544.
- ³Chernov, G. M., et al. (1984), Nucl. Phys. A **412**, 534.
- ⁴Bhalla, K. B., et al. (1981), Nucl. Phys. A **367**, 446.
- ⁵Atwater, T. W., et al. (1985), this conf., Paper HE 1.4-10.

STOPPING RELATIVISTIC Xe, Ho, Au AND U NUCLEI IN NUCLEAR EMULSIONS

C.J. Waddington, D.J. Fixsen and P.S. Freier

School of Physics and Astronomy, University of Minnesota
Minneapolis, MN 55455

Abstract. Nuclei of ^{54}Xe , ^{67}Ho , ^{79}Au and ^{92}U accelerated at the Bevalac to energies between 1200 and 900 MeV/n have been stopped in nuclear emulsions. The observed residual ranges have been compared with those calculated from various models of energy loss and shown to be most consistent with a calculation that includes those higher order correction terms proposed previously to describe the energy loss of highly charged particles, for which the first Born approximation is not valid.

1. Introduction. We have previously reported, Waddington et al. (1983), on the stopping of 200 GeV gold nuclei in nuclear emulsions. Here we describe a new study of the residual ranges of energetic Xe, Ho, Au and U nuclei in nuclear emulsions.

2. Measurements. A single small stack of Ilford G5 nuclear emulsion pellicles, placed so that the pellicles were parallel to the beam, was exposed at the Lawrence Berkeley Laboratory Bevalac to beams of krypton (^{84}Kr), xenon (^{132}Xe), holmium (^{165}Ho), gold (^{197}Au) and uranium (^{238}U) nuclei. These exposures were made over a period of less than a week to nuclei accelerated at maximum rigidity of 5.6 GV and incident on the same edge of the pellicles. Those nuclei which did not interact in the emulsions were, apart from Kr-nuclei, brought to rest in the emulsions by energy loss, thus permitting their residual ranges to be measured. In order to determine the mean ranges of each nuclei species, individual tracks were not followed from the top edge of the emulsions,

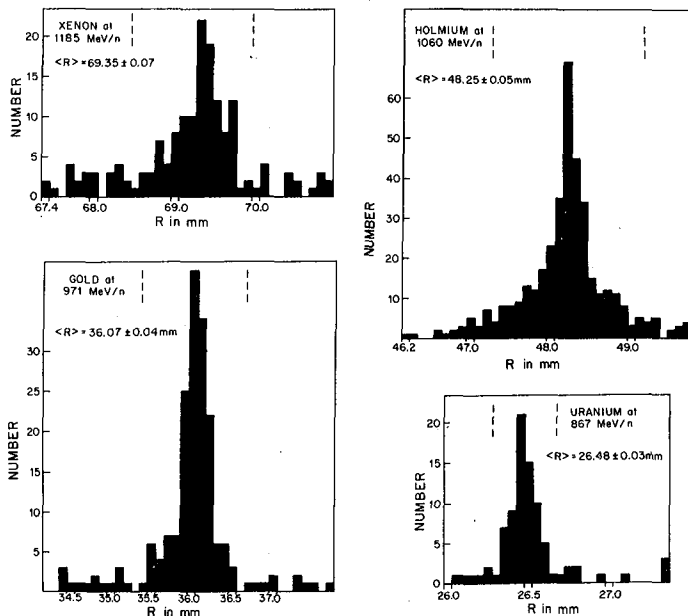


Fig. 1. The residual ranges, R , in mms of nuclear emulsions, measured for each beam. The mean values of range, $\langle R \rangle$, are the arithmetic means taken between the values indicated by the dashed lines and the errors are the formal errors in the mean, not those in the width of the distribution.

but were detected by a line scan made a few mms above the estimated depth of stopping for each species. Each track recorded was then followed for a distance that at most would be a few mms beyond the expected stopping point for that species. Tracks of different primary nuclei than the one being studied could be readily eliminated by visual inspection. Hence each sample consisted of a group of primary nuclei with an admixture of fragments produced from interactions occurring above. The resulting range distributions, Fig. 1, show clearly defined peaks, superimposed on a background of secondary fragments. The peaks observed define the mean residual ranges of each species with adequate accuracy, given the uncertainties in the energies.

3. Discussion. Our previous study of Au-nuclei and that of Ahlen and Tarle (1983) on U-nuclei, both showed that there are large deviations in the residual ranges of highly charged nuclei from those calculated using the standard Bethe-Born formalism of energy loss. In order to fit the observations it is necessary to consider terms which are of higher order in Z than the Z^2 terms that result from assuming the validity of the first Born approximation. Instead, it is necessary to include additional terms that take account of the finite size of the projectile nucleus and the electron binding to the target nucleus. Ahlen (1980, 1982) has modified the energy loss expression by including the terms M , B and B_R as follows:

$$\frac{dE}{dx} = \frac{4\pi NZ_m e^4}{mc^2} \frac{Z_p^2}{\beta^2} \cdot J \left[\ln \frac{2mc^2}{I_m} \cdot \frac{\beta^2}{(1-\beta^2)} - \beta^2 - S - D + M - B + B_R \right]$$

Here the effective charge on the projectile, Z_p , is corrected for the effects of energy dependent electron pickup and D is a density correction that is ≈ 0 at these moderate energies. J is a correction for distant collision polarization effects. Energy losses calculated only using terms up to and including D we consider as the classical Bethe formalism, Fano (1963), denoted as Bethe + and will compare with the earlier calculation of Barkas (1963, 1973). Successive inclusion of the Mott correction for the finite size of the projectile, M ; the Bloch correction for electron binding, B ; and the relativistic Bloch corrections for relativistic terms of the electron binding, B_R , lead to a series of further estimates of dE/dx and hence to calculated residual ranges. Ahlen and Tarle (1983) showed that their observations on the range of U nuclei in a mostly copper medium were consistent with the calculated value using all the terms of the modified dE/dx expression. Our results on Au nuclei in nuclear emulsions were slightly more consistent with an expression that disregarded the relativistic Bloch term, unless the parameters assumed to be valid in that term were modified from those used to fit the U data. Whether there was a significant discrepancy between these two results was not clear, and as a consequence we decided to take advantage of the opportunity to study several different nuclei under as uniform conditions as possible.

The energy of each beam was measured by determining the magnetic field needed to guide the beam in a transport line. Similar measurements have been made many times before and checked by time of flight determinations. Provided that the beam is well focused these measurements should be reliable to ± 3 MeV/n. In this case these

exposures were made during a calibration of the HEAO C3 UH-nuclei satellite detector, Binns et al. (1981), and an image of the beam spot was available in real time as output from a thin multi-wire proportional counter. Except for the U-beam a well-focused spot was obtained in every case and the energies should be reliable. For Uranium there were clearly multiple charge states present in the beam and the energy estimate is based on the assumption that the state with both K-shell electrons attached was dominant in the beam transport line. The Table shows the assigned energies for each beam.

Table of Energies and Ranges

Nuclei	E_{measured}	ΔE	E_{enter}	R_{measured}
	Mev per nucleon			mms
$^{132}_{54}\text{Xe}$	1239 ± 4	54	1185	69.35 ± 0.30
$^{165}_{67}\text{Ho}$	1128 ± 3	68	1060	48.25 ± 0.17
$^{197}_{79}\text{Au}$	999 ± 3	27.5	971.5	36.07 ± 0.17
$^{238}_{92}\text{U}$	899.4 ± 3	32.4	867	26.48 ± 0.08

The emulsions were exposed to particles after they had traversed the vacuum window, an air path and the light tight window in front of the emulsions. The MWPC counter used to examine the footprint of the beam was removed after defocusing to ensure a uniform exposure, but for the Xe and Ho exposures a scintillation counter was also present in the beam. The energy loss in these materials, ΔE , has been calculated from the full expressions for dE/dx , using all terms, for each Z and initial energy.

The charge or energy dependencies of these higher correction terms, M , B , and B_r are not obvious by inspection and indeed are not simple. We have calculated dE/dx and hence residual ranges, R , using the same assumptions as in our previous report. It is found that in every case the Bethe + terms lead to the lowest value of dE/dx , which would imply the largest range, and that the Mott correction alone leads to the highest dE/dx . Application of the Bloch and rel Bloch corrections gives intermediate values of dE/dx but reverse in magnitude as Z increases.

Integration of these dE/dx curves allow us to calculate the residual ranges. In practice these integrations have only been carried down to a residual energy of 10 MeV/n and a very small correction made for the additional range. These calculated ranges have been compared with those predicted from the proton ranges in nuclear emulsions determined by Barkas, scaled by A/Z^2 . The ratios of $R_i/R(\text{Barkas})$ are shown in Fig. 2 for each beam at the appropriate energy, Table. This figure shows that as Z increases the Bethe + expression deviates from the scaled proton range, being some 3% too high at U. All three of the higher order correction terms give ranges less than those predicted from Barkas, and, as suggested by the behavior of dE/dx , the Bloch and relativistic Bloch corrections interchange between Au and U. The experimental observations are in all four cases in good agreement with those predicted by including all terms, including the relativistic Bloch

term. This result is not entirely consistent with our previous Au result, which was more consistent with the predictions that did not include the relativistic Bloch term. The magnitude of the correction

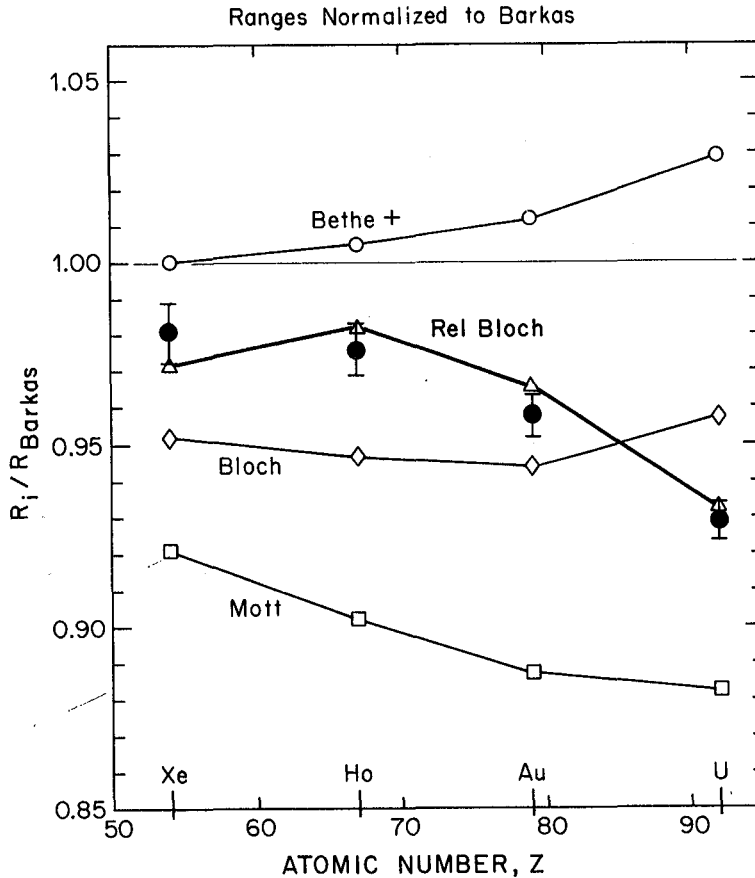


Fig. 2. Ranges normalized to those of Barkas (1973). Values calculated from the dE/dx equation are shown as open symbols, those from the measured ranges as solid with error bars.

that it is necessary to apply to the Barkas ranges steadily increases with increasing Z , reaching some 7% for U. However, it should be remembered that these four measurements are all at different energies and the corrections suggested by Fig. 2 do not truly represent solely the Z dependence of the corrections.

4. Acknowledgements. This work was partially supported by NASA Grants NGR 24-005-050 and NAG8-500 and by NSF Grant PHY-8405852.

References

- Ahlen, S.P., and Tarle, G. (1983), Phys. Rev. Lett., **50**, 1110.
 Ahlen, S.P. (1980), Rev. Mod. Phys., **52**, 121.
 Ahlen, S.P. (1982), Phys. Rev. A, **25**, 1856.
 Barkas, W.H. (1963, 1973), Nuclear Research Emulsions, Vol. I and II, Academic Press, N.Y.
 Binns, W.R., Israel, M.H., Klarmann, J., Scarlett, W.R., Stone, E.C., and Waddington, C.J. (1981), Nucl. Inst. Meth., **185**, 415.
 Fano, U. (1963), Ann. Rev. Nucl. Sci., **13**, 1.
 Waddington, C.J., Freier, P.S., and Fixsen, D.J. (1983), Phys. Rev. A, **28**, 464.

PHYSICAL MEANING OF THE MULTIPLICITIES OF EMITTED NUCLEONS
IN HADRON-NUCLEUS COLLISIONS

Strugalski Z.

Institute of Physics of the Warsaw Technical University
ul. Koszykowa 75
00-662 Warsaw, Poland

and

Joint Institute for Nuclear Research, High Energy Lab.
Dubna, USSR

ABSTRACT

The analysis of experimental data on hadron-nucleus collisions at energies from about 2 up to about 400 GeV was performed in order to discover a physical meaning of the multiplicity of emitted nucleons. Simple relations between the multiplicities and the thickness of the nuclear matter layer involved in collisions were obtained.

1. Introduction

It is commonly known that when atomic nuclei are bombarded by high energy hadrons, with energies higher than the pion production threshold, the emission of nucleons from the target nucleus, the particle production, and the evaporation of nuclear fragments take place. The presence of events in which intensive emission of nucleons and fragment evaporation appear without particle production leads to the conclusion that the nucleon emission process can proceed independently of the particle production, Strugalski Z., Pluta J. (1974), Strugalski Z., Pawlak T., Pluta J. (1982); the emitted nuclei are with kinetic energies from about 20 up to about 400 MeV, in the emulsion technique the nuclei are known as the so called g-track leaving particles.

In considerations about the nucleon emission, the emission process can be treated separately, because the influence on it by the particle production process is negligible, Strugalski Z. (1984 a,b), and the fragment evaporation is due to the target nucleus destruction in the nucleon emission process, Strugalski Z. (1984 c).

But, the emitted nucleons are constituents of the target nucleus, and it is reasonable to expect that characteristics of these nucleons should be connected with the parameters of the target - with its size and nucleon density distribution in it. When the connections will be found, simple physical meaning of the multiplicities of the emitted nucleons, of the protons in particular, may be achieved.

The subject matter in this paper is to present results of our investigations in question.

2. Method

The method of experimental investigations is based on two facts: a) It is possible now to realize experiments, using heavy liquid chambers as 4 π geometry detectors, in which emitted protons and produced pions of any electric charge including zero are registered with the efficiency near to 100 %; additional supplementary information about the target nuclei fragmentation can be obtained from emulsion experiments. Characteristics of the outcomes in hadron-nucleus collisions, such as multiplicities of produced or emitted particles, and momentum and angular spectra can be obtained fully as well. This way, experimental data obtained now are of such a sort as data which one can expect to obtain in a total experiment. b) Now many aspects about the nuclear matter distribution in atomic nuclei are so firmly established that it has been possible to use them in order to investigate other physical quantities, Elton IRB (1961). It is possible, therefore, to estimate the number of nucleons, or protons only, contained within any cylindrical volume centered on the hadron course in an atomic nucleus.

The method of investigation of the physical meaning of the multiplicities of the emitted nucleons, or of the emitted protons in particular, consists in comparison of the data on nucleon multiplicity distribution, obtained in investigations of collisions of definite hadrons with definite target nucleus, with data on distributions of the nucleon numbers contained within some cylindrical volumes centered on various possible hadron courses in the target nucleus; the distributions are determined from the information about the target nucleus size and nucleon density distribution in it.

3. Experiment

In our investigations we have used the 26 and 180 litre xenon bubble chambers, Kanarek T.I. et al. (1959), Kuznetsov E.V. et al. (1970). The first one was exposed to 2.34 GeV/c, 5 GeV/c, 9 GeV/c momentum pions from the synchrotron of the Joint Institute for Nuclear Research at Dubna. The second one was exposed to 3.5 GeV/c negatively charged pions from the accelerator of the Institute of Experimental and Theoretical Physics in Moscow. About 20 000 pion-xenon nucleus collision events were analysed, Strugalski Z. et al. (1982, 1983). Additionally, compilations of corresponding data obtained in emulsion experiments were used, Andersson B. et al. (1978), Babecki J. and Nowak G. (1978), Busza W. (1977), Gurtu A. et al. (1974), Otterlund I. et al. (1978), Tsai-Chü et al. (1977).

4. Results

It was found that the thicknesses of nuclear matter layers involved in hadron-nucleus collisions should be naturally and conveniently expressed in number of nucleons per some area $S = \pi D_0^2 \approx 10 \text{ fm}^2$, where D_0 is the diameter of the nucleon; they can be expressed as well in protons/S, or in neutrons/S. We use these units only later on.

The analysis of the experimental data, in the light of the data on the target nuclei, leads to conclusions that:
1. The number n_p of protons (or of the g-track leaving particles) emitted in a collision is a measure of the thickness λ in protons/S of the nuclear matter layer involved in the collision:

$$n_p = \lambda \cdot S \quad (1)$$

2. The mean number $\langle n_p \rangle$ of protons emitted in a sample of the hadron-nucleus collisions equals the mean thickness $\langle \lambda \rangle$ in protons/S of the nuclear matter layer involved in the collisions:

$$\langle n_p \rangle = \lambda S \quad (2)$$

3. At the incident hadron energy larger than a few GeV, the mean number of protons $\langle n_p \rangle$ emitted in hadron-nucleus collisions is:

$$\langle n_p \rangle = \langle \lambda \rangle S (1 - \exp(- \langle \lambda \rangle / \langle \lambda_t \rangle)) \quad (3)$$

where $\langle \lambda_t \rangle$ in protons/S is the mean free path for interaction of the incident hadron with a nucleon in nuclear matter, $\langle \lambda_t \rangle = 1 / \sigma_{\text{tot}}$, and σ_{tot} is the cross-section for the hadron-nucleus any-type collision.

More information can be found in my previous works , Strugalski Z. (1984 a - c).

5. Remarks

From formula (1) it follows that the nucleon emission proceeds monotonically. But, this formula is accurate when the multiplicity of the emitted protons n_p is not larger than DS , where D is in protons/s the diameter of the target nucleus. In some small number of collision events, in no more than about 10 %, $n_p > DS$. The appearance of such values of $n_p > DS$ is due to the perturbations in nucleon emission process, Strugalski Z. (1984 b)

Formulas (1) - (3) were tested experimentally within the incident hadron energy interval up to about 2000 GeV, where the nucleon emission intensities were under studies. Nevertheless, we hope that the formulas are valid through the total region of the projectile energies above the pion production threshold.

We have investigated mainly the proton emission only, but additional analysis, Strugalski Z. (1984), provided results which incline us to think that formulas (1) - (3) are valid for both the nucleons together, and for the neutrons only, as well.

References

- Andersson B. et al., 1978, Physics Letters, B73, 343.
Babecki J. And Nowak G., 1978, Acta Physica Polonica, B9, 401.
Busza W., 1977, Acta Physica Polonica, B8, 333.
Gurtu A. et al., 1974, Pramana, 3, 311.
Elton L.R.B., 1961, Nuclear Sizes, Oxford University Press, Oxford.
Kanarek T.I. et al., 1959, Proc. Intern. Conf. on High Energy Accelerators and Instrumentation, CERN, p. 508.
Kuznetsov E. V. et al., 1970, Sov. Journ. PTE, vol. 2, p. 56.
Otterlund I. et al., 1978, Nuclear Physics, B142, 445.
Strugalski Z., Pluta J., 1974, Sov. Journ for Nuclear Physics, 27, 504.
Strugalski Z., Pawlak T., Pluta J., 1982, Communications JINR, Dubna: E1-82-718, E1-82-719, E1-82-841.
Strugalski Z., 1984 a, Communications JINR, Dubna E1-84-268.
Strugalski Z., 1984 b, Communications JINR, Dubna E1-84-854.
Strugalski Z., 1984 c, Communications JINR, Dubna E1-84-195.

HOW ARE PARTICLE PRODUCTION, NUCLEON EMISSION, AND
TARGET FRAGMENT EVAPORATION PROCESSES INTERRELATED
IN HADRON-NUCLEUS COLLISIONS ?

Strugalski Z.

Institute of Physics of the Warsaw Technical University
ul. Koszykowa 75
00-662 Warsaw, Poland
and
Joint Institute for Nuclear Research, High Energy Lab.
Dubna, USSR

ABSTRACT

Relations between particle production, nucleon emission, and fragment evaporation processes were searched for in hadron-nucleus collisions. It has been stated that: 1. The nucleon emission and target fragment evaporation proceed independently of the particle production process. 2. Relation between multiplicities of the emitted protons and of the evaporated charged fragments is expressed by simple formula.

1. Introduction

When high energy hadrons - with energies larger than the pion production threshold - collide with atomic nuclei, nucleons are emitted always, target fragment evaporated, and particles may be generated, as it has been stated experimentally.

The emission of nucleons with kinetic energies of about 20 - 400 MeV, or of the so called g-track leaving particles, and the evaporation of the target nucleus fragments may occur without particle production. The question arises therefore: "How are the particle production, nucleon emission, and target fragment evaporation processes interrelated?"

The answer to this question should be found experimentally. In this paper, results obtained in our searches for the relations in question are presented.

2. Method

In investigations we have used the 26 and 180 litre xenon bubble chambers, Kanarek T.I. et al. (1959), Kuznetsov E.V. et al. (1970), exposed to pion beams from the synchrotron of the Joint Institute for Nuclear Research at Dubna and from the accelerator of the Institute of Experimental and Theoretical Physics in Moscow.

General information about pion-xenon nucleus collisions is contained in a set of Communications of the Joint Institute for Nuclear Research at Dubna, Strugalski Z. et al. (1982, 1983); we applied for the analysis in this work the DST used in them. Additional appropriate information at higher energies we have found in various emulsion works : Andersson B. et al. (1978), Babecki J. and Nowak G. (1978), Bannik B. P. et al. (1980), Gurtu A. et al. (1974), Meyer H. et al. (1963), Otterlund I. et al. (1978), Tsai-Chü et al. (1977), Winzelel H. (1965); the accelerator data there are up to 400 GeV of the incident hadron energy in the laboratory system, some data from cosmic rays, Meyer H. et al. (1963) are up to about 3 500 GeV.

The method of investigation is based on the fact that at energies much larger than the pion production threshold hadron-nucleus collision events occur in which intensive emission of nucleons proceeds without particle production, without pion production in particular. It consists in preparation of various characteristics of the emitted nucleons - of the emitted protons in particular - in dependence on the multiplicity $n_{\pi} = 0, 1, 2, 3, \dots$ of produced pions of any electric charge. Clearly : 1. We prepare firstly a set of various dependences of the characteristics of the emitted protons on the multiplicities n_{π} of produced pions, at 2 - 9 GeV/c momentum, and we discover general features of these dependences. It should be mentioned here that in the xenon chambers we register practically all the emitted protons and all the produced pions of any electric charge. 2. Secondly, we compare available characteristics of the proton emission process at higher energies, up to about 3 500 GeV, with corresponding characteristics in pion-xenon nucleus collisions at 2 - 9 GeV. Results of such a comparison allow to conclude about the behaviour of the nucleon emission process with the incident hadron energy increase, in other words - with increase of the multiplicity of produced particles. 3. Thirdly, we investigate the dependences of characteristics of the fragment evaporation process on the multiplicity n_p of the emitted protons at various hadron energy.

This way, the effects of the particle production process on the nucleon emission and fragment evaporation processes, and the relation between the nucleon emission process and fragment evaporation process may be discovered.

3. Results

In result of the analysis of various characteristics in question, Strugalski Z. (1984), it can be concluded that:

- a) The particle production process in hadron-nucleus collisions does not effect on the nucleon emission process in them at any energy of the incident hadron.
- b) The evaporation process of the fragments from the

target nuclei in hadron-nucleus collisions is not influenced by the particle production process at any projectile energy.

The analysis in details of the sequence of the three processes - particle production, nucleon emission, and target fragment evaporation allows to conclude that: Any hadron with energy higher than the pion production threshold causes emission of nucleons with kinetic energies from about 20 up to about 400 MeV from the target nucleus, in passing through it; the nucleon emission may, in many cases, go in advance of the particle-producing collision of the incident hadron inside the target nucleus; the fragment evaporation process appears in result of the target nucleus damage due to the nucleon emission; the multiplicity n_p of protons emitted and the multiplicity $\langle n_p \rangle$ of the charged fragments evaporated are connected by simple formula

$$\langle n_p \rangle = 1.25 \left(n_p + \frac{A-Z}{Z} \right)$$

where A and Z are the mass and charge numbers of the target nucleus, Strugalski Z. (1984).

References

- Andersson B. et al., 1978, Physics Letters, 73B, 343.
 Babecki J., Nowak G., 1978, Acta Physica Polonica, B142, 445.
 Bannik B.P. et al., 1980, Communications JINR, Dubna, R1-13055.
 Gurtu A. et al., 1974, Pramana, 3, 311.
 Kanarek T.I. et al., 1959, Proc. Internat. Conf. on High Energy Accelerators and Instr., CERN, p.508.
 Kuznetsov E.V. et al., 1970, Sov. Journ. PTE, 2, 56.
 Meyer H. et al., 1963, Nuovo Cim., 28, 1399.
 Otterlund I. et al., 1978, Nuclear Physics, B142, 445.
 Strugalski Z., Pawlak T., Pluta J., 1982, Communications JINR, Dubna, E1-82-718, E1-82-719, E1-82-841.
 Strugalski Z. et al., 1983, Communications JINR, Dubna R1-83-68, R1-83-237, R1-83-564, R1-83-568.
 Strugalski Z., 1984, Communications JINR, Dubna: E1-84-268, E1-84-853, E1-84-854, E1-84-195.
 Winzeler H., 1965, Nuclear Physics, 69, 661.

EXPERIMENTAL STUDY OF THE SPACE-TIME DEVELOPMENT OF THE
PARTICLE PRODUCTION PROCESS IN HADRON-NUCLEON COLLISIONS,
USING MASSIVE TARGET NUCLEUS AS A DETECTOR

Strugalski Z.

Institute of Physics of the Warsaw Technical University
ul. Koszykowa 75
00-662 Warsaw, Poland

and

Joint Institute for Nuclear Research, High Energy Lab.
Dubna, USSR

ABSTRACT

Experimental study of the space-time development of the particle production process in hadronic collisions at its initial stage was performed. Massive target nuclei have been used as fine detectors of properties of the particle production process development within time intervals smaller than 10^{-22} s and spatial distances smaller than 10^{-12} cm. In hadron-nucleon collisions, in particular in nucleon-nucleon collisions, the particle production process goes through intermediate objects in $2 \rightarrow 2$ type endoergic reactions. The objects decay into commonly observed resonances and particles.

1. Introduction

In searches for plausible mechanisms to explain the particle production in hadron-nucleon collisions, in nucleon-nucleon collisions in particular, characteristics of the collision reaction products appeared after relatively long time after the collision - not shorter than the life times of resonances - are usually analysed. It cannot be excluded a priori that the known particles and resonances are the decay products of some super-particle or super-particles created firstly as well.

Now experimental information is needed, adequate and of a new quality - relevant to the time intervals τ of the most short-living particles known up to now, and within the spacial distances z much smaller than $\tau c \gamma$, where γ accounts the Lorentz dilatation of the lifetime in the laboratory.

The shortest decay times of the known resonances are $\tau_s \approx 10^{-23}$ s which corresponds to the smallest spacial distances z of some 10^{-13} cm in the laboratory, when $\gamma \approx 1$. So, the qualitatively new and adequate information which has to be used for elucidation of the process in question should be obtained at the times

$\tau \leq 10^{-22}$ s within the spacial distances $z \leq 10^{-12}$ cm. These space distances and time intervals we shall call "short". Experimental information about the particle production process obtained at larger time intervals and spacial distances only may yield false ideas of the collision reaction products and of the particle systematics in a whole as well.

The collision reaction products appeared in the initial stage - within the short time intervals and spacial distances - should interact with a surrounding medium and the interaction must produce observable effects, if one would study these products experimentally. The only tool available now to realize such experiments is to apply massive target nuclei as fine detectors, therefore, Strugalski Z. (1980, 1981, 1982 a);

The subject matter in this paper is to present results of our experimental study of the space-time development of the particle production process in hadronic collisions at its initial stage. In the study, our own experimental data on pion-xenon nucleus collisions obtained at 2 - 9 GeV/c momentum, Miller K. et al. (1976), Pluta J. et al. (1976), Okhrimenko L. et al. (1978), Strugalski Z. et al. (1974, 1981, 1982 a-c, 1983 a-g) and the wealth of experimental data on hadron-nucleus, Bannik B.P. et al. (1980), Busza W. (1975), Faessler M.A. et al. (1979), Gurtu A. et al. (1974 a and b), Otterlund I. et al. (1978), Tsai-Chü et al. (1977) and the data on hadron-nucleon collisions, Famino V. et al. (1979), Goldschmidt-Clermont Y. (1973), collected in the past by other physicists were used.

2. Method

The atomic nucleus used as the target in hadron-nucleus collisions serves as a fine detector. Its size r_A can be roughly up to about 10 fm, Elton L.R.B. (1961). The basic physical process underlying the operation principle of this fine detector is the emission of nucleons, Strugalski Z. (1983, 1984). Information in details about the method can be found in one of my papers, Strugalski Z. (1985).

3. Results

In result of the investigations performed, we can conclude that:

1. In hadron-nucleus collisions, particles are produced via some intermediate objects which decay after having left the parent nucleus into usually observed resonances and particles. We called these objects "generons".

2. It is reasonable to think that the particle production in elementary hadron-nucleon collisions, in nucleon-nucleon collisions in particular, goes through such intermediate objects as well, in endoergic $2 \rightarrow 2$ type reaction; the objects decay into commonly known resonances and particles.

It has been shown that the above presented mechanism of the particle production process allows to derive formulas which in a convincing manner can account for hadron-nucleus data in terms of our knowledge of hadron-nucleon data, Strugalski Z. (1982 b).

4. Remarks

The consequences of the picture of the particle production process, presented above, were proved experimentally, Strugalski Z. (1982 a), Sredniawa B. and Strugalska-Gola E. (1983, 1984), in hadron-nucleus collisions within incident hadron energy values from a few up to a few thousands GeV. Quantitative agreement of the predictions based on the picture presented with corresponding experimental data has been found.

References

- Bannik B.P. et al., 1980, Communications JINR, Dubna, R1-13055.
- Busza W., 1975, Proc. Intern. Conf. on High Energy Phys. and Nucl. Struct., Santa-Fe, p. 211.
- Elton L.R.B., 1961, Nuclear Sizes, Oxford Univ. Press
- Faessler M.A. et al., 1979, Nucl. Phys., B157, 1.
- Famino V. et al., 1979, CERN-HERA, 79-01, 79-02, 79-03.
- Goldschmidt-Clermont Y., 1973, Acta Physica Polonica, B4, 805.
- Gurtu A. et al., 1974, a) Phys. Lett., 50B, 391; b) Pramana, 3, 311.
- Miller K. et al., 1976, Sov. Journ. of Nucl. Phys., 23, 754.
- Otterlund I. et al., 1978, Nucl. Phys., B142, 445.
- Pluta J. et al., 1976, Sov. Journ. Nucl. Phys., 24, 766.
- Sredniawa B. and Strugalska-Gola E., 1983, Communications JINR, Dubna, E1-83-277.
- Sredniawa B. and Strugalska-Gola E., 1984, Communications JINR, Dubna, E1-84-411.
- Strugalski Z. et al., 1974, Sov. Journ. Nucl. Phys., 20, 204.
- Strugalski Z. et al., 1981, Communications JINR, Dubna, E1-81-578.
- Strugalski Z. et al., 1982, Communications JINR, Dubna, E1-82-718, E1-82-719, E1-82-841.
- Strugalski Z. et al., 1983, Communications JINR, Dubna, a) R1-83-68, b) R1-83-155, c) R1-83-234, d) R1-83-237, e) R1-83-344, f) R1-83-564, g) R1-83-568.
- Strugalski Z., 1980, Communications JINR, Dubna, E1-80-548
- Strugalski Z., 1981, Comm. JINR, Dubna, E1-81-576, 81-577
- Strugalski Z., 1982, Comm. JINR, Dubna, E1-82-401, 82-287
- Tsai-Chu et al., 1977, Nuovo Cim. Lett., 20, 257.

EXPERIMENTAL EVIDENCE OF THE DECREASE OF KINETIC ENERGY OF
HADRONS IN PASSING THROUGH ATOMIC NUCLEI

Strugalski Z.

Institute of Physics of the Warsaw Technical University
ul. Koszykowa 75
00-662 Warsaw, Poland

and

Joint Institute for Nuclear Research, High Energy Lab.
Dubna, USSR

ABSTRACT

Hadrons with kinetic energies higher than the pion production threshold lose their kinetic energies monotonically in traversing atomic nuclei, due to the strong interactions in nuclear matter. This phenomenon is a crude analogy to the energy loss of charged particles in their passage through materials. Experimental evidence is presented.

1. Introduction

We have observed, in the 26 and 180 litre xenon bubble chambers that GeV pions can be deflected or absorbed in nuclei without causing particle production, without causing pion production in particular, when are falling on layers of nuclear matter thick enough, Strugalski Z. and Pluta J. (1974), Strugalski Z., Pawlak T., and Pluta J. (1982); the deflection or absorption is always accompanied by intensive emission of nucleons with kinetic energies from about 20 to about 400 MeV.

The energy and angular distributions of the protons in such deflected and stopped events are the same, and they are identical with the distributions of protons in collisions with particle production as well. It is remarkable and leads to the opinion that it is reasonable to think that hadrons lose their kinetic energies, in traversing nuclear matter, by causing nucleon emission.

The subject matter in this paper is to present shortly our results of experimental investigations of degradation of hadron energy through nuclei.

2. Experimental Evidence

We found experimentally that the number n_N of emitted nucleons which accompany the passage of a hadron through a nucleus along a path λ fm equals the number of nuc-

leons contained within the volume $v = \pi D_0^2 \lambda \text{ fm}^3$ centered on λ in the target nucleus:

$$n_N = \pi D_0^2 \langle \rho \rangle \lambda, \quad (1)$$

where $\langle \rho \rangle$ nucleons/ fm^3 is mean density of nucleons in the target nucleus along λ , D_0 is approximately as large as the nucleon diameter, Strugalski Z. (1978,1979), Pluta J. and Strugalski Z. (1985).

Relation (1) may be rewritten in a more convenient form:

$$n_N = \lambda S \quad (2)$$

if the path length λ is expressed in nucleons per the area S , and $S = \pi D_0^2$; the number n_p of the emitted protons is:

$$n_p = \lambda S \frac{Z}{A} = \lambda' S \quad (3)$$

where λ' is in protons per S , Z and A are the charge and mass numbers of the target nucleus.

The simplest observable effects which provide crucial evidence and support for formulas (1) - (3) are: a) At energies high enough, higher than a few GeV, the mean number $\langle n_p \rangle$ of emitted protons in the deflected events is constant and almost equals $\langle \lambda \rangle S$, where $\langle \lambda \rangle$ is the mean thickness of the target nucleus in protons/ S . b) At some projectile energy, definite for a given incident hadron and a given target nucleus, the distribution of multiplicities of protons emitted in the stopped events is symmetrical and its maximum lies at the multiplicity n_p as large as $D S$, where D is the diameter of the target nucleus in protons/ S . c) The probability of an appearance of the stopped events, in collisions of a given hadron with a given nucleus, decreases with the increase of the incident hadron energy; at energies high enough, the stopped events do not appear at all, only the deflected events present themselves in some portion of the collision events, Strugalski Z., Pawlak T., Pluta J. (1984).

An analysis in details of the experimental facts led to the conclusion that: A hadron of kinetic energy E_h larger than the pion production threshold loses its kinetic energy in passing through nuclear matter; the fraction ΔE_h of the energy lost on the path length λ nucleons/ S is:

$$\Delta E_h = \epsilon_h \lambda \quad (4)$$

where ϵ_h MeV/(nucleon/ S) is the measurable coefficient which depends on the hadron identity - for pions $\epsilon_h = \epsilon_\pi \approx 180$ MeV/(nucleon/ S), for protons $\epsilon_h = \epsilon_p \approx 360$ MeV/(nucleon/ S), Strugalski Z. (1983).

In support for this conclusion, some additional experimental facts of the crucial value may be adduced: a) The mean number $\langle n_p \rangle$ of emitted protons in the stopped events is quantitatively predictable by simple relation

$$n_p = (E_h / \epsilon_h) \cdot S \quad (5)$$

which is valid for such values of E_h when $(E_h / \epsilon_h) S \leq DS$ where D in nucleons/S is the target nucleus diameter times Z/A , Strugalski Z. (1983). b) The mean multiplicity $\langle n_p \rangle$ of emitted protons is energy-dependent at the incident hadron energies $E_h \leq D \epsilon_h$, and the energy-dependence is predictable quantitatively if formulas (3) and (4) are used for a given target nucleus and for a given incident hadron, Strugalski Z. (1984). c) Indirectly, the degradation of the incident hadron energy manifests itself in observed degradation of the kinetic energy and of the momenta of produced pions with the increase of the nuclear matter layer thickness $n_p = \lambda S$ the incident hadron of a given kinetic energy interacted with, as it is shown in Fig..

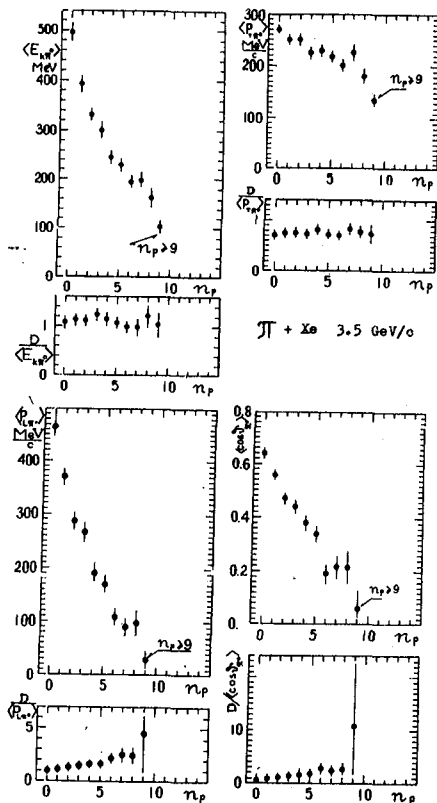


Fig. Mean kinetic energy $\langle E_{k\pi^0} \rangle$, mean longitudinal momentum $\langle P_{L\pi^0} \rangle$, mean transverse momentum $\langle P_{T\pi^0} \rangle$ and mean cosine of the pion emission angle $\langle \cos \theta_{\pi^0} \rangle$ of neutral pions produced in pion-xenon nucleus collisions at 3.5 GeV/c momentum, in dependence on the multiplicity n_p of emitted protons; the multiplicity n_p is connected with the nuclear matter layer thickness λ the incident hadron interacted with as: $n_p = \lambda S$, where $S = \pi D_0^2 \approx 10 \text{ fm}^2$ and D_0 is the diameter of the nucleon. $D/\langle \rangle$ are the normalized dispersions of corresponding quantities.

3. Conclusions

It should be concluded that, in studying hadron-nucleus collisions, we have met a phenomenon which may

be regarded as a crude analogy to the phenomenon consisting in the energy loss of a charged particle in materials; simi

larly, hadrons lose their energies in traversing nuclear matter. But, the newly observed energy loss of hadrons is due to the strong interactions of hadrons with nuclear matter.

In many cases, when particle-producing reactions occur, the nucleon emission and therefore the incident hadron energy loss, due to this emission, is going in advance of the particle-producing reaction; the incident hadron covers firstly some path in the target nucleus without particle-producing reaction and then it causes this reaction in the nucleus; in many cases it may happen on the end of the hadron path in the target nucleus.

The effects caused by the hadron energy loss are observed clearly when the incident hadron energy is not larger than $\epsilon_h D$, where ϵ_h is in GeV/(nucleons/S) and D in nucleons/S is the target nucleus diameter.

References

- Pluta J. and Strugalski Z., 1985, to be published in Communications JINR, Dubna.
- Strugalski Z. and Pluta J., 1974, Sov. Journ. of Nucl. Physics, 20, 504.
- Strugalski Z., Pawlak T., Pluta J., 1982, Communications JINR, Dubna: E1-82-718, E1-82-719, E1-82-841.
- Strugalski Z., Pawlak T., Pluta J., 1984, Communications JINR, Dubna, E1-84-855.
- Strugalski Z., 1978, Communications JINR, Dubna, E1-11976.
- Strugalski Z., 1979, Communications JINR, Dubna, E1-12086.
- Strugalski Z., 1983, Communications JINR, Dubna, E1-83-850.
- Strugalski Z., 1984, Communications JINR, Dubna, E1-84-268.

ENERGY-RANGE RELATIONS FOR HADRONS IN NUCLEAR MATTER

Strugalski Z.

Institute of Physics of the Warsaw Technical University

ul. Koszykowa 75

00-662 Warsaw, Poland

and

Joint Institute for Nuclear Research, High Energy Labor.

at Dubna, USSR

ABSTRACT

Range-energy relations for hadrons in nuclear matter exists, similarly to the range-energy relations for charged particles in materials.

1. Introduction

When hadrons of GeV kinetic energies collide with atomic nuclei massive enough, events occur in which incident hadron is stopped completely inside the target nucleus without causing particle production - without pion production in particular. The "stoppings" are always accompanied by intensive emission of nucleons with kinetic energy from about 20 up to about 400 MeV, Strugalski Z., Pluta J. (1974), Strugalski Z., Pawlak T., Pluta J. (1982). We showed experimentally that the mean number $\langle n_N \rangle$ of the emitted nucleons is a measure of the mean path $\langle \lambda \rangle$ in nuclear matter in nucleons/S on which the incident hadrons are stopped, where $S = \pi D_0^2 \approx 10 \text{ fm}^2$ and D_0 is the nucleon diameter, Strugalski Z. (1978, 1979, 1984):

$$\langle n_N \rangle \approx \langle \lambda \rangle S \quad (1)$$

Similar relation can be written for the mean multiplicity $\langle n_p \rangle$ of emitted protons only, usually observed in experiments:

$$\langle n_p \rangle \approx \langle \lambda \rangle S \frac{Z}{A}, \quad (2)$$

where Z and A are the charge and mass numbers of the target nucleus.

It is known as well, from our experiments, that the mean number $\langle n_p \rangle$ of protons emitted in the "stopped" events decreases with the incident hadron energy E_h decrease.

The question arises: Is the mean path $\langle \lambda \rangle$, in nucleons/S, of the incident hadron in nuclear matter related definitely to its kinetic energy E_h or not? The answer to the question should be found primarily in experiments, and we would like to find it.

2. Experimental Determination of the Range-Energy Relation

The method of determination of the relation between the hadron range R_h and the incident hadron energy E_h is simple - it consists in a determining of the mean multiplicities $\langle n_N \rangle$ or $\langle n \rangle$ in the "stopped" collision events of a definite hadron with a definite massive target nucleus at various energies E_h . Such measurements have been performed at two values of E_h : $E_h = E_\pi = 2.12$ GeV and $E_h = E_\pi = 3.2$ GeV, using pion-xenon nucleus collisions. For both the values of E_h the ratio

$$\epsilon_h = \frac{E_h}{\langle n \rangle} = \frac{E_h}{R_h} \quad (3)$$

is practically the same: $\epsilon_h = \epsilon_\pi = 180$ MeV/(nucleon/S). It enables us to suppose that the relation exists

$$E_h = R_h \epsilon_h, \quad (4)$$

where E_h is in MeV, R_h is in nucleons/S, and ϵ_h is in MeV/(nucleons/S).

Using data on the "stopped" events in proton-AgBr collisions, Sumbera M. and Vokal S. (1982), we determined the quantity $\epsilon_h = \epsilon_p = 360$ MeV/(nucleon/S), for incident protons.

The results obtained are based only on a few experimental points, at two values of E_h for the pion-xenon nucleus collisions and on one value of E_h for the proton-AgBr collisions. It would be not needless to test relation (4) in some other way. We have done it. Namely, we have made an expectation for the probability for the occurrence of the "stopped" events in dependence on the incident hadron energy E_h in pion-xenon nucleus collisions at values of E_h : 2.1, 3.2, 5, 9 GeV. Predictions are based on the relation (4), they are in agreement with corresponding experimental data, fig. ; more details concerning the calculations one can find in one of my works, Strugalski Z. (1983).

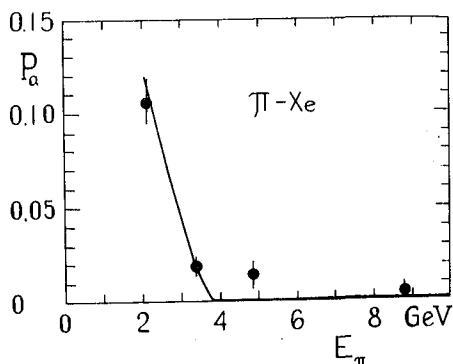


Fig. Probability P of the appearance of the pion-xenon nucleus collision events in which incident pion is stopped inside the target nucleus, in dependence on the incident pion momentum P_π . ● - experimental data, — - calculations, using formula (4) and data on the xenon nucleus, Strugalski (1983).

3. Conclusions

In result of the measurements, we obtained that definite relation exists in nuclear matter between the hadron range R_h and the kinetic energy E_h of this hadron. This relation is an analog to similar range-energy relation in materials, for electrically charged particles.

Relation (4), together with relations (1) and (2), allows to understand the energy-dependences of the mean multiplicity of the emitted nucleons in hadron-nucleus collisions at energies smaller than a few GeV, Strugalski Z. (1984), Abdurakhimov E.O. et al. (1978).

Relation (4) helps to determine the hadron energy loss in nuclear matter, from the energy-dependence of the mean multiplicity $\langle n_p \rangle$ of emitted protons in any-type hadron-nucleus collision reactions, as well, Strugalski Z. (1985).

References

- Abdurakhimov E.O. et al., 1978, Sov. Journ. of Nuclear Physics, 27, 1020.
 Strugalski Z., Pluta J., 1974, Sov. Journ. of Nuclear Physics, 20, 504.
 Strugalski Z., Pawlak T., Pluta J., 1982, Communications JINR, Dubna: E1-82-234, E1-82-718, E1-82-719, E1-82-841.
 Strugalski Z., 1978, Communications JINR, Dubna, E1-11976.
 Strugalski Z., 1979, Communications JINR, Dubna, E1-12086.
 Strugalski Z., 1983, Communications JINR, Dubna, E1-83-850.
 Strugalski Z., 1984, Communications JINR, Dubna: E1-84-268, E1-84-853, E1-84-194.
 Strugalski Z., 1985, Communications JINR, Dubna, E1-85-231.
 Sumbera M., Vokal S., 1982, Acta Physica Slov. 32, 265.

SCATTERING AND STOPPING OF HADRONS IN NUCLEAR MATTER

Strugalski Z.

Institute of Physics of the Warsaw Technical University
ul. Koszykowa 75
00-662 Warsaw, Poland

and

Joint Institute for Nuclear Research, High Energy Lab.
Dubna, USSR

ABSTRACT

We have observed, in the 180 litre xenon bubble chamber, that when hadrons with kinetic energy higher than the pion production threshold fall on a layer of nuclear matter - on an atomic nucleus in other words - in many cases they can pass through it without causing particle production but they are deflected through some deflection angles; if the energy is lower than a few GeV and the nuclear matter layer is thick enough, the hadrons can be stopped in it. The amount of the deflection at a given incident hadron energy varies with the way the hadron strikes the atomic nucleus; the probability of the occurrence of stopping depends on the incident hadron identity and energy, and on the way the hadron passed through the nucleus, as well.

1. Introduction

Almost 75 years ago H. Geiger and E. Marsden, two of E. Rutherford students, directed a beam of alpha particles onto a thin foil of gold. With a screen of fluorescent material they then counted the number of particles scattered at various angles as a result of encounters with the gold atoms, Geiger H. and Marsden E. (1909). It was E. Rutherford who supplied the interpretation of findings obtained in the experiments; in the interpretation he had also introduced a method whose importance is indiminished today, Rutherford E. (1911).

I would like to communicate, in this paper, that now it is possible to perform similar experiments in which instead of the metallic foil the "foil" of nuclear matter of definite thickness will be used, and the projectiles employed will be the strongly interacting particles, pions or protons for example, raised to high energy by an accelerator.

In contrast to the Geiger-Marsden-Rutherford experiments, where the scattered alpha particles have been observed only, in the experiments with nuclear matter foils an

emission of nucleons from the "foil" is observed always and three general kinds of events occur against the background of this emission: a) Events in which the projectile is deflected only, without causing the particle production, Strugalski Z., Pluta J. (1974), Strugalski Z., Pawlak T., Pluta J. (1982). b) Events in which incident hadron is stopped completely without causing the particle production, Strugalski Z., Pluta J. (1974), Strugalski Z., Pawlak T., Pluta J. (1982). c) Events in which particles are produced.

The emitted nucleons are of kinetic energy from about 20 up to about 400 MeV, as it has been seen experimentally, Strugalski Z., Pawlak T., Pluta J. (1982).

2. A Massive Atomic Nucleus as the "Foil" of Nuclear Matter

Any of the atomic nuclei massive enough can be regarded as the lens-shaped "foil" or "slab" of nuclear matter, if the thickness $\lambda(b)$ of the nuclear matter layer at any distance b from the nucleus center is measured in units of number of nucleons per some area $S \text{ fm}^2$, like the Earth atmosphere thickness is expressible usually in grams/cm², Strugalski Z. and Pawlak T. (1981).

Such a "slab" should be characterized generally by the maximum thickness of the nuclear matter layer - λ_{max} , the mean thickness $\langle \lambda \rangle$, and the thickness $\lambda(b)$ at any distance b from the nucleus center; the values of these quantities for many nuclei can be found in one of our works, Strugalski Z. and Pawlak T. (1981).

Results of experimental studies of the nucleon emission process in hadron-nucleus collisions, Strugalski Z., Pawlak T., Pluta J. (1982), prompt to us the procedure by which we can determine the quantity $\lambda(b)$; it has been concluded that relation exists between the multiplicity of the emitted nucleons n_N and $\lambda(b)$ expressed in nucleons per $S \approx 10 \text{ fm}^2$:

$$\lambda(b) \cdot S = n_N \quad (1)$$

When the multiplicity n_p of the emitted protons is measured only, relation (1) should be rewritten:

$$\lambda(b) \cdot S \cdot \frac{Z}{A} = n_p \quad (1')$$

where Z and A are the charge and mass numbers of the target nucleus, and $S = \pi D_0^2 \text{ fm}^2$, and D_0 is the nucleon diameter, Strugalski Z. (1985).

3. Experiment

Experimental information about pion deflection in its passage through nuclear matter was obtained by means of the 26 and 180 litre xenon bubble chambers, Kanarek T.I. et al. (1959), Kusnetsov E.V. et al. (1970). The small chamber was exposed to the pion beam from the synchrophasotron of the Joint Institute for Nuclear Research at Dubna, 2.34 GeV/c;

the larger chamber was exposed to the beam of negatively charged pions of 3.5 GeV/c momentum from the accelerator of the Institute of Theoretical and Experimental Physics in Moscow. The massive nucleus of the xenon 131 atom was used as the nuclear matter slab, Strugalski Z., Pawlak T., Pluta J. (1982).

4. Results

It has been found experimentally that: a) A definite simple relation exists between the incident pion deflection angle θ_π and the average multiplicity n_p of emitted protons; in other words - a definite simple relation exists between the pion deflection angle θ_π and the thickness in protons/S of the nuclear matter layer traversed by this pion. b) The mean value of the cosine of the pion deflection angle, $\langle \cos\theta_\pi \rangle$, depends definitely and simply on the number n_p of emitted protons; in other words, the deflection angle of the incident pion increases in a definite manner with increasing the thickness λ of the nuclear matter layer traversed by the pion.

The analysis of experimental data, Strugalski Z. (1982), leads to the recognition: a) The observed deflection angle distribution is a result of two sorts of hadron deflections in nuclear matter - one is due to a multiple scattering from objects with the rest mass as large approximately as the pion rest mass is, the second one is due to a single scattering from massive objects with the rest mass as large as the rest mass of the nucleon. b) The multiple scattering may be described quantitatively by simple formula with a simple physical meaning, Strugalski Z. (1982):

$$\langle \theta_\pi \rangle^2 = \langle \mathcal{D}_\pi \rangle^2 \cdot \lambda \quad (2)$$

where $\langle \theta_\pi \rangle$ is the mean deflection angle occurred on the thickness λ nucleons/S, $\langle \mathcal{D}_\pi \rangle$ is the mean deflection angle occurred on the thickness $\lambda = 1$ nucleon/S. Formula (2) is similar to the Rutherford's formula, Rutherford E. (1911).

When the incident hadron energy is smaller than a few GeV, events occur in which the hadron is stopped, Strugalski Z., Pluta J. (1974), Strugalski Z., Pawlak T., Pluta J. (1982). In pion-xenon nucleus collisions, the "stopped" events occur when the incident pion energy is smaller than about 4 GeV.

Simple relation exists between the range R_h of the hadron in nuclear matter and its kinetic energy E_h , Strugalski Z. (1983):

$$R_h = \frac{E_h}{\epsilon_h} \quad (3)$$

where R_h is in nucleons/S, E_h in GeV, ϵ_h is experimentally determined coefficient in GeV/(nucleon/S) - for pions

$\epsilon_h = \epsilon_p \approx 0.18 \text{ GeV}/(\text{nucleon}/S)$ and for protons $\epsilon_h = \epsilon_p \approx 0.36 \text{ GeV}/(\text{nucleon}/S)$.

5. Conclusions

Hadron deflections and hadron stoppings were observed experimentally. These phenomena are observed clearly at energies smaller than a few GeV. Many effects occur due to these phenomena - energy dependence of the mean multiplicity $\langle n_p \rangle$ of the emitted nucleons, for example. At energies high enough these phenomena do not influence on the observed outcomes in h-A collisions.

It should be noted that the energy spectra, the longitudinal and transverse momentum distributions of the emitted nucleons do not depend on the hadron deflection angle, at angles not larger than about 60 degrees; they are independent of the hadron range in nuclear matter as well.

References

- Geiger H., Marsden E., 1909, Proc. Roy. Soc., A82, 495.
 Kanarek T. et al., 1959, Proc. Intern Conf. on Accelerators and Instrumentation, CERN, p. 508.
 Kuznetsov E.V. et al., 1970, Sov. Journ. PTE, 2, 56.
 Rutherford E., 1911, Phil. Mag., May, ser. 6, 21, 669.
 Strugalski Z., Pluta J., 1974, Sov. Journ. of Nuclear Phys., 20, 504.
 Strugalski Z., Pawlak T., 1981, Communications JINR, Dubna, E1-81-378.
 Strugalski Z., Pawlak T., Pluta J., 1982, Communications JINR, Dubna, E1-82-718, E1-82-719, E1-82-841.
 Strugalski Z., 1982, Communications JINR, Dubna, E1-82-455.
 Strugalski Z., 1983, Communications JINR, Dubna, E1-83-850.
 Strugalski Z., 1984, Communications JINR, Dubna, E1-84-853.

MEASUREMENT OF HADRON MEAN FREE PATH FOR THE
PARTICLE-PRODUCING COLLISIONS IN NUCLEAR MATTER

Strugalski Z.

Institute of Physics of the Warsaw Technical University
ul. Koszykowa 75
00-662 Warsaw, Poland

and

Joint Institute for Nuclear Research, High Energy Lab.
Dubna, USSR

ABSTRACT

It is not obvious a priori that the cross-section for a process in hadron collisions with free nucleons is the same as that for the process in hadron collisions with nucleons inside a target nucleus. The question arises: "What is the cross-section for a process in a hadron collision with nucleon inside the atomic nucleus?". The answer to it must be found in experiments. The mean free path for particle-producing collisions of pions in nuclear matter is determined experimentally using pion-xenon nucleus collisions at 3.5 GeV/c momentum. Relation between the mean free path in question λ_i in nucleons/fm² and the cross-section σ_i in units of fm²/nucleon for collisions of the hadron with free nucleon is: $\lambda_i = k / \sigma_i$, where $k = 3.00 \pm 0.26$.

1. Introduction

One of the main concepts which is useful in hadron-nucleus collision analysis is that of the mean free path λ ; it always has a subscript denoting a particular process. Usually, the mean free path λ fm for a process is related to the cross-section σ fm²/nucleon for such a process in collisions of the hadron with free nucleon as:

$$\lambda = \frac{1}{\rho \sigma} \quad (1)$$

where ρ in nucleons/fm³ is the mean nucleon density in the target nucleus along λ . Relation (1) can be expressed as

$$\lambda = \frac{1}{\bar{\sigma}} \quad (2)$$

when λ is in nucleons/fm². It is convenient to express λ

in units of nucleons/S where $S = \pi D_0^2 \approx 10 \text{ fm}^2$ and D_0 is the diameter of the nucleon.

The subject matter in this paper is to determine experimentally the mean free path λ , nucleons/S for the particle-producing hadron-nucleon collisions in nuclear matter.

2. Method

Two experimental findings provide the basis for experimental determination of the hadron mean free path for the particle-producing collisions in nuclear matter: a) The discovery of hadron-nucleus collisions in which incident hadron is stopped or deflected only in accompaniment by intensive nucleon emission from the target nucleus without causing the particle production; the emitted nucleons are with kinetic energies from about 20 up to about 400 MeV, Strugalski Z. and Pluta J. (1974), Strugalski Z., Pawlak T., Pluta J. (1982). b) The discovery of definite relation between the intensity of the emitted nucleons and the thickness of the nuclear matter layer involved in any-type collision events - when particles are produced or not, Strugalski Z. (1984 a).

We can consider a sample of hadron-nucleus collisions as a result of interaction of a beam of hadrons with a lens-shaped "slab" of nuclear matter, Strugalski Z. (1984 b). In fact, in any collision event the target nucleus is destroyed, but in any of the collisions a hadron collides with identical nucleus.

Let us consider a hadron flux I_0 incident on a layer of nuclear matter of the thickness dt . The differential intensity loss dI due to interactions is given by the relation $dI = -I_0 \sigma dt$, and so $I = I_0 \exp(-\sigma t) = I_0 \exp(-t/\lambda)$. The mean free path λ in fm can be replaced by λ in nucleons/S, where $S \approx 10 \text{ fm}^2$; the thickness t in fm can be replaced by t in nucleons/S as well, and

$$I = I_0 \exp(-t/\lambda) \quad (3)$$

The thickness of the nuclear matter layer t in nucleons/S, involved in any type collision, is given from the relation between this thickness and the number n_p of the protons emitted in the event, Strugalski Z. (1984^a), as:

$$n_p = t \cdot S \cdot \frac{Z}{A} \quad (4)$$

In measurements of the mean free path λ in nucleons/S the quantity I_0 is simply the number of hadron-nucleus collisions analysed, the quantity I equals the number of events without causing an effect - the particle production, for example; all the quantities I_0 , I , and t are measurable ones. Then, λ can be estimated simply from relation

(3).

For determination of the λ -s, the collision events observed in the 26 and 180 litre xenon bubble chambers, Kanarek T.I. et al. (1959), Kuznetsov E.V. et al. (1970), exposed to beams of pions were used.

3. Experiment

The smaller chamber was exposed to the positively charged pions with 2.34 GeV/c momentum from the synchrotron of the Joint Institute for Nuclear Research at Dubna. The bigger chamber was exposed to negatively charged pions with 3.5 GeV/c momentum from the accelerator of the Institute of Experimental and Theoretical Physics in Moscow.

In photograph scanning, any-type collision events were selected, a total information about the outcome in any of collisions was obtained, as it concerns the emitted nucleons and produced pions of any electric charge, including neutral pions, Strugalski Z., Pawlak T., Pluta J. (1982), Strugalski Z. et al. (1983).

4. Results

We measured the mean free path λ_i in nucleons/S for the particle-producing collisions, and the mean free path λ_d in nucleons/S for collisions without particle production when the incident hadrons were deflected through the deflection angles larger than $\theta_{\pi} \geq 30$ degrees, Strugalski Z. (1983). We obtained for the particle-producing mean free path $\lambda_i = 12.4 \pm 1.7$ nucleons/S and for the mean free path $\lambda_d = 12.8 \pm 1.5$ nucleons/S.

We found that the formula for determination of λ_i from $\bar{\sigma}_i$ taken from elementary hadron-nucleon collisions should be, instead of formula (2):

$$\lambda_i = \frac{k}{\bar{\sigma}_i} \quad (5)$$

where λ_i and $\bar{\sigma}_i$ are in nucleons/S and S/nucleon correspondingly. $k = 3.0 \pm 0.26$.

5. Conclusions

The mean free path λ_i for particle-producing hadron collisions in nuclear matter, determined by means of formula (2), does not correspond to the mean free path determined experimentally.

This path λ_i , for particle-producing collisions, and the path λ_d , for the deflections through angles larger than 30° degrees, are practically the same.

But, the deflections through large angles are from collisions of incident hadron with hard constituents of the nucleons, Strugalski Z. (1982). The observed equality between λ_i and λ_d may mean that particles are produced when collisions occur with the hard constituent of the nucleon.

The inequality of values of the quantity λ_i evaluated from formula (2) and determined experimentally using the method presented above may be regarded as an appearance of a nucleon structure in hadron-nucleus collisions, Strugalski Z. (1984 c).

References

- Kanarek T.I. et al., 1959, Proc. Intern. Conference on Accelerators and Instrumentation, CERN, p.508.
- Kuznetsov E.V. et al., 1970, Sov. Journ. PTE, 2, 56.
- Strugalski Z. and Pluta J., 1974, Sov. Journ. for Nuclear Physics, 20, 504.
- Strugalski Z., Pawlak T., Pluta J., 1982, Communications JINR, Dubna: E1-82-718, E1-82-719, E1-82-841.
- Strugalski Z. et al., Communications JINR, Dubna, 1983 R1-83-68, R1-83-237, R1-83-564, R1-83-568.
- Strugalski Z., 1982, Communications JINR, Dubna, E1-82-455.
- Strugalski Z., 1983, Communications JINR, Dubna, E1-83-563.
- Strugalski Z., 1984, Communications JINR, Dubna: a) E1-84-853, b) E1-84-268, c) E1-84-365.

THE ϕ MESON AND "CHIRAL-MASS-MESON" PRODUCTION IN HEAVY-ION COLLISIONS AS POTENTIAL PROBES OF QUARK-GLUON-PLASMA AND CHIRAL SYMMETRY TRANSITIONS

Y. Takahashi⁺ and P. B. Eby

(NAS-NRC)⁺, ES62 and ES63, Space Science Laboratory
NASA Marshall Space Flight Center, Huntsville, Alabama 35812, USA

ABSTRACT

Possibilities of observing abundances of ϕ mesons and narrow hadronic pairs, as results of QGP and Chiral transitions, are considered for nucleus-nucleus interactions. Kinematical requirements in forming close pairs are satisfied in K^+K^- decays of $S(975)$ and $\delta(980)$ mesons with small P_T , and $\phi(1020)$ mesons with large P_T , and in $\pi\pi$ decays of familiar resonance mesons (ρ , ω , A_1 , ...) only in a partially restored chiral symmetry. Gluon-gluon dominance in QGP can enhance ϕ meson production. High hadronization rates of primordial resonance mesons which form narrow hadronic pairs are not implausible. Past cosmic ray evidences of anomalous ϕ production and narrow pair abundances are considered.

1. Introduction. First (or second) order phase transitions have been demonstrated for Quark-Gluon-Plasma(QGP) and Chiral Symmetry Restoration in various lattice QCD calculations.¹ Phenomenological consequences of new states of matter have been discussed rigorously in the past few years. Some signatures which may discriminate new states from ordinary hadronic processes are considered for on-going and future experimental investigations: (i) direct photons and lepton-pairs;² (ii) large average P_T ;³ (iii) rapidity-azimuth fluctuations;⁴ (iv) strangeness production;⁵ (v) "fade-out" of resonance mass peaks.⁶

The first issue has been most quantitatively studied so far, but the results of calculations are found less prominent than initially expected.⁷ The second item, large P_T , has been attracting some critical attentions, since there are some experimental indications in the JACEE cosmic ray data⁸ and in SppS data,⁹ which can be discussed as influences of hydrodynamical expansion¹⁰ and thermodynamical manifestation¹¹ of plasmas. The third issue has been only naively conjectured,¹² but some expectations are made on the basis of super-cooling and deflagration.¹³ The fourth issue, strangeness, has been emphasized by several people,¹⁴ however, negative arguments against its abundant production are also raised recently (based on large entropy consumption in pions).¹⁵ The last issue, being least studied to date, seems to be of particular interest, because it has been the only predicted diagnosis of Chiral transitions.

We examine other potential probes of new states of matter, considering several anomalous symptoms uniquely shown for nucleus-nucleus interactions in the past cosmic ray experiments. First, the possibility of abundant ϕ meson production in QGP is considered. Then, we shall study the possibility of observing reduced-mass resonance mesons in partial chiral symmetry.

2. ϕ Meson Abundance. Koshiba et al.¹⁶ and Kim¹⁷ observed multiple Kaons in nucleus-nucleus collision events in Brawley Stack emulsion. The former, particularly, have shown that the observed Kaons are mostly due to ϕ mesons which are identified by an invariant-mass study of two Kaons. This is,

however, inconceivable at first glance, because strong suppression of ϕ mesons has been established in elementary particle interactions. This suppression is best understood by (1) its large mass ($1,020 \text{ MeV}/c^2$), (2) small coupling constant of s-quark, and (3) Okubo-Zweig-Iizuka (OZI) rule for disconnected quark diagrams (small mixing of $s\bar{s}$ with $u\bar{u}$ and $d\bar{d}$).

These fundamental suppressions do not seem quite obvious in nucleus-nucleus collisions for the following reasons: (1) large mass suppression in the Boltzman factor may not be valid among different flavors; primordial $s\bar{s}$ can be as many as $u\bar{u}$ and $d\bar{d}$ in QGP, as often stressed by Rafelski.⁵ (2) a small coupling constant is not unique for s-quark at high temperature as QCD reduces strengths of light quark couplings. Even if not, their intrinsic difference is small. (3) The OZI suppression is effective to $q\bar{q} \rightarrow q\bar{q}$ process, but it is absent for stronger (more rapid) $gg \rightarrow q\bar{q}$ process. In a gluon-rich environments(QGP) $s\bar{s}$ production is dominated by the latter.

The ϕ/π ratio should be enhanced in QGP at least to the 1 % level, apart from well-known low values ($< 0.1 \%$). If we follow Rafelski's calculation of $s\bar{s}$ abundance in QGP, and separately apply the Boltzman factor to strange particles, we get ϕ/π ratio upto 23 %. (The P_T distribution of them may be different as well, if hydrodynamical flow of QGP is strong. A universal P_T formula, $dN/dP_T \propto \exp(-m_T/T_0)$; $T_0 = 170 \text{ MeV}$, may not be valid in universal CM system, but only in the rest system of the hydrodynamical front plane.) Such a high ϕ/π ratio, though possible, is not guaranteed only from above considerations. Particularly, an alteration of the universal Boltzman factor for different flavors remains too arbitrary.

On the other hand, the Koshiba data implies ϕ/π ratio $32 \pm 17 \%$ in the target fragmentation region. It is also interesting to note that K/π ratios for nucleus-nucleus and proton-nucleus events in the same data turned out to be 0.41 ± 0.15 and 0.17 ± 0.11 , respectively.²¹ This value is consistent with the latest Rafelski estimate²² and the upper bound given by McLerran.¹⁵ If we accept Kaon data of Koshiba et al., we are inevitably compelled to reconsider the strangeness suppression.

The ϕ meson is an unique particle in the sense that it does not decay ($\tau \approx 20 \text{ fm}/c$) before leaving a "fireball", and its decay particles (K^+K^-) remain closely associated with each other. In this regard, it is interesting to note another cosmic ray data which showed pronounced narrow pairs in nucleus-nucleus collisions.^{18,19} These data, if explained by ϕ mesons, require $P_T(\phi)$ more than $1.5 \text{ GeV}/c$ (for pairs with $\Delta y < 0.2$ and $\Delta\phi < 30^\circ$).²³ S and δ mesons make "too narrow" K^+K^- pairs ($\Delta y, \Delta\phi \approx 0$). The required high $\phi(P_T \geq 1.5 \text{ GeV}/c)/\pi(\text{all } P_T)$ ratio (\sim several %) to account for all the pair abundances is unacceptable by any means, which eliminates the candidacy of high P_T ϕ mesons for the observed pairs. Nevertheless, as discussed later, ϕ mesons and other familiar resonance mesons can make very narrow hadronic pairs without high P_T in partial chiral phase.

3. Mesons in Partial Chiral Symmetry. Chiral Symmetry Restoration is shown by many calculations to take place at almost the identical critical temperature (T_{ch}) as the deconfinement (QGP) transition (T_C). The consequence of the chiral symmetry at high temperature is the reduction of resonance masses. Chiral transition above T_{ch} may not alter the main scenario of dynamical processes of nucleus-nucleus interactions, at least, that of hydrodynamical expansion of QGP. Nonetheless, an influence on the hadronization process must be considered, because the hadronization process is at the same time a process of dynamical symmetry breaking of chirality.

At temperature just below the QGP phase transition ($T \leq T_C$) when early

hadronization starts, chiral symmetry breaking is incomplete. The mass of a resonance meson composed of u or d quarks is significantly light at high temperature, while those of π 's and K's remain almost normal. Chiral counterparts, for example, $\rho((1^-)^-)$ and $A_1((1^+)^+)$, have different masses, 770 and 1,270 MeV/c², respectively in normal nuclear phase. Their mass difference vanishes above T_{ch} . The mass formulae in the quark model gives a degree of symmetry breaking as a function of the temperature:²⁰

$$m(T)/m_0 \Big|_{T \sim T_{ch}} \rightarrow 2.03 \{(T_{ch} - T)/T_{ch}\}^{1/2}, \quad (1)$$

where m_0 represents the constituent quark mass (~ 300 MeV). Using a formula given by Pisarski,²⁰ we get ρ meson mass at different T . When $T_{ch} = 215$ MeV and $T_c = 207$ MeV, for example, m_ρ increases rapidly with decreasing T :

$$m_\rho \approx 290 \text{ MeV } (T = 206 \text{ MeV}), 341 \text{ MeV } (T = 205 \text{ MeV}), \dots \quad (2)$$

The decay P_{max} values for $\rho(T = 206, 205 \text{ MeV}) \rightarrow \pi\pi$ are only 63 MeV and 96 MeV, respectively, which can explain observed narrow pairs ($dN/d(\Delta\phi)$ for $\Delta y \leq 0.2$) satisfactorily without assuming high P_T .²³ Other resonance mesons are similarly lighter than their ordinary values in normal nuclear phase.

The number of primordial $q\bar{q}$ mesons can be evaluated by the combination rate at unit space-time,

$$A \equiv \frac{dN}{dt dx^3} = (1/2) \int_{4m^2}^{\infty} s ds \cdot \delta(s - (k_1 + k_2)^2) \int \frac{d^3 k_1}{(2\pi)^3 |k_1|} \int \frac{d^3 k_2}{(2\pi)^3 |k_2|} \\ \times \{C_g f_g(k_1) f_g(k_2) \bar{\sigma}_{gg \rightarrow q\bar{q}}(s) + C_q f_q(k_1) f_q(k_2) \bar{\sigma}_{q\bar{q} \rightarrow q\bar{q}}(s)\}, \quad (3)$$

where C_g and C_q are determined by the number of degrees of freedom for gluons and quarks, and $\bar{\sigma}(s)$'s are cross sections for gluons and quarks to form a specific $q\bar{q}$ state. The ratio of $(q\bar{q})$ states frozen out in the temperature intervals $T_c - T$ and $T_c - T_f$ can be estimated by

$$R(T) \equiv \int_T^{T_c} dT \cdot A(T) \int_{\Omega} d^4x \delta(T - T(x)) / \int_{T_f}^{T_c} dT \cdot A(T) \int_{\Omega} d^4x \delta(T - T(x)) \\ \approx \{(T_c/T)^6 - 1\} / \{(T_c/T_f)^6 - 1\}, \quad (4)$$

where $T_c > T > T_f$, with T_f being a final temperature ($T_f = T_0 \approx 170$ MeV). When we consider R at $T = 205$ MeV, about 3 % of all final states are shared by primordial mesons in the earliest chiral breaking phase. Though the evaluation is crude (neglecting many dynamical factors), it is interesting to note that "chiral mesons" are not negligible in discussing the final state pair correlation. A question still remains how $\pi\pi$'s from chiral mesons can survive during meson-meson final state interactions. We tentatively neglect this, as the decay width Γ is proportional to $\{(T_c - T)/T_c\}^{3/4}$,²⁰ and the lifetime of "chiral ρ meson" is correspondingly long (several fm/c).

Chiral symmetry does not affect s-quark mesons very much. Nevertheless, a few times 10 MeV mass reduction is not unreasonable for ϕ mesons. This permits primordial ϕ mesons decay into narrow K^+K^- pairs even with small P_T .

The above discussions are highly speculative, as many assumptions are left unjustified. However, the hadronization mechanism from QGP, particularly from chiral symmetry, seems to have potential sources of narrow pairs.

4. Conclusions. The ϕ meson abundance in nucleus-nucleus interactions can be much higher ($\phi/\pi \geq 1$ %) than that in proton-proton collisions ($\phi/\pi < 0.1$ %). The highest possible value in QGP may be 23 %, though this is too optimistic. Some cosmic ray data suggest much higher values ($\phi/\pi \approx 30$ %) in a narrow target fragmentation region. It is too high for a plausible

explanation without assuming some strangeness abundances in cosmic ray heavy-ion events. Though inspiring, the observed data are limited to only several events ($E > 1$ TeV/amu). Follow-up experiments are required to consider new states of matter for them.

The hadronic narrow pairs might involve decay products of "chirally symmetric primordial mesons" (bound state of $q\bar{q}$: cf. Cooper-pair, i.e. phonon). However, the existing pair correlation data might be mostly accounted by some unclarified experimental errors and by more conventional mechanism such as the HBT effect.¹⁹ Further studies may be required for confirming non-trivial pair abundances in the existing data. We do not consider at present any direct relationship of the experimental data to the above described scenario, though tempting, because both studies are still very primitive. Experimentally, measurements of $\langle P_T \rangle$ and invariant mass of a pair (with identity of the particle species) are possible in the backward hemisphere within nuclear emulsion techniques. If these data become available, the study of pairs will be more interesting. However, pair observations have some difficulties to deal with very high multiplicity/high energy density events; too high a particle density obscures any meaningful narrow-pair correlations. (Rapidity densities for the study of pair abundances may be limited to, probably, $dN/dy \sim 100$.) In this sense, light nuclei collisions and/or intermediate impact parameter events at high energy would best suit for observations, but with a risk to fall short of energy densities for the phase change. Theoretical developments for early hadronization processes are important in confirming the suggested scenario of (chiral transition \rightarrow primordial "chiral mesons" \rightarrow narrow hadronic pairs).

No definitive judgements for existing data are possible at this stage, however, we conclude that these kinds of observations can be potential probes of QGP and Chiral Symmetry Restoration when new states of matter are actually realized in high energy nucleus-nucleus collisions with moderate rapidity densities.

5. Acknowledgements. The authors acknowledge discussions with Drs. O. Miyamura, T. A. Parnell, and T. Tabuki.

References. 1. H. Satz, Quark Matter '84, p.278(1984), Springer Verlag. 2. E.L. Feinberg, Nuovo Cimento 34A, 391(1976); G. Domokos and J.I. Goldman, Phys. Rev., D23, 203(1981). 3. E.V. Shuryak, Phys. Reports, 61, 71(1980). 4. M. Gyulassy et al., LBL preprint, 16277(1983). 5. J. Rafelski and B. Muller, Phys. Rev. Lett., 48, 1066(1982). 6. J. Kapusta, Phys. Rev., C15, 1580(1977). 7. L. McLerran, Quark Matter '84, p. 1 (1984), Springer Verlag. 8. O. Miyamura and JACEE, Quark Matter '84, p. 187 (1984), Springer Verlag. 9. K. Kajantie, H.I. Mittenen, Z. Phys., C9, 341(1981); C14, 356(1982). 10. M. Gyulassy, Nucl. Phys., A418, 59c(1984). 11. L. van Hove, Phys. Letters, 118B, 138(1982). 12. T.D. Lee, Columbia University preprint, CU-TP-170(1981). 13. L. van Hove, CERN preprint, TH3592 (1983). 14. J. Rafelski, Nucl. Phys., A418, 215c(1984). 15. L. McLerran and T. Matsui, private communication, 1985. 16. M. Koshiya et al., J. Phys. Soc. Japan, 22, 1321(1967). 17. C.O. Kim, Phys. Rev., 136, 515(1964). 18. P.S. Freier and C.J. Waddington, AIP 49, 87 (1979). 19. The JACEE Collaboration, this conference, HE 1.4-5, (1985). 20. R.D. Pisarski, Phys. Letters, 110B, 155(1982). 21. Y. Takahashi, talk presented at Quark Matter '84, Helsinki, (1984). 22. J. Rafelski, private communication at Quark Matter '84, Helsinki (1984). 23. P.B. Eby, T.A. Parnell and Y. Takahashi, preprint (unpublished) NASA/MSFC, (1985).

SU(2) x U(1) VACUUM AND THE CENTAURO EVENTS

D. Kazanas, V. K. Balasubrahmanyam and R. E. Streitmatter
 NASA/Goddard Space Flight Center
 Greenbelt, MD 20771
 USA

ABSTRACT

We propose that the "fireballs" invoked to explain the Centauro events are bubbles of a metastable superdense state of nuclear matter, created in high energy ($E \sim 10^{15}$ eV) cosmic ray collisions at the top of the atmosphere. If these bubbles are created with a Lorentz factor $\gamma \approx 10$ at their CM frame, the objections against the origin of these events in cosmic ray interactions are overcome. A relationship then between their lifetime, τ , and the threshold energy for bubble formation, E_{th} , is derived. The minimum lifetime consistent with such an interpretation is $\tau \sim 10^{-8}$ sec, while the E_{th} appears to be insensitive to the value of τ and always close to $E_{th} \sim 10^{15}$ eV. Finally it is speculated that these bubbles might be manifestations of the SU(2) x U(1) false vacuum excited in these collisions. The absence of π^0 's in the Centauro events is then explained by the decay modes of these excitations.

1. Introduction. The Centauro, events (Lattes et al. 1973) are high energy $\approx 10^{15 \pm 1}$ cosmic ray events detected in nuclear emulsion chambers at high altitudes (> 4000 m) with characteristics which defy explanation in terms of "standard" high energy cosmic ray collisions and subsequent cascading of the produced particles. The characteristics which set these events apart from the typical events expected at these energies ($\approx 10^{15}$ eV) are the following:

- a. They are observed deep in the atmosphere (≈ 500 g cm $^{-2}$), only a few hundred meters above the emulsion chamber detector.
- b. They have very high multiplicity.
- c. They have very large mean transverse momentum, $\langle P_t \rangle$, 3-5 times larger than that of a typical nuclear fragmentation interaction.
- d. There is a deficiency of neutral pion production.

Direct nuclear collisions fail to account for any of the above features, especially for the observed rate, $R \approx 10^{-2}$ m $^{-2}$ sr $^{-1}$ yr $^{-1}$, since the probability of penetration of strongly interacting particles to such depth is negligible. It was pointed out though, that most of the above features (multiplicity, $\langle P_t \rangle$), could be accounted for in terms of the explosive decay of an unknown state of matter. Bjorken and McLerran (1979) postulate a new metastable form of quark matter, introducing a new component in the cosmic ray spectrum, while Kinnunen and Rubbia (1981) argue that these events cannot be due to high energy cosmic ray interactions, thus in effect agreeing with the previous authors. In the present note we accept the interpretation of the Centauro events as the explosive decays of an unknown yet high energy particle deep in the atmosphere. However, contrary to the previous treatments, we relate the Centauro flux to the flux of high energy cosmic ray particles at the top of the atmosphere, thus avoiding the introduction of a new, unknown component in the primary cosmic ray spectrum. Then, the requirement that Centauros are

due to the explosive decay of a bubble of a metastable superdense nuclear matter, produced in a high energy collision on the top of the atmosphere, leads to a relation between the formation of such a metastable state and to its lifetime. This is done in the next section.

2. The Centauro Event Rate. In relating the Centauro rate to that of high energy cosmic ray interactions, we shall assume that a large fraction of high energy cosmic rays have interacted within 50 g cm^{-2} from the top of the atmosphere, which sets the interaction height to about 21 km. Given that the Mt. Chacaltaya detector is at a depth $\sim 500 \text{ g cm}^{-2}$ or a height of $\sim 6 \text{ km}$, the bubbles of metastable matter will have to traverse a distance of about 15 km before they decay. We further assume that any decay at a distance $d_L > 100 \text{ m}$ from the detector does not classify as a Centauro event, because the ensuing cascade will not have the characteristics of a Centauro (i.e. closeness to the detector, few π^0 's). Then if τ_0 is the lifetime of the bubble and γ_L its Lorentz factor in the laboratory frame, the decay rate of bubbles as a function of time after the interaction will be

$$N(t) = N_T e^{-t/\gamma_L \tau_0} \quad (1)$$

or in terms of the distance d from the high energy interaction point,

$$N(d) = N_T e^{-d/c\gamma_L \tau_0} \quad (2)$$

Where N_T is the rate of bubble production at the top of the atmosphere. Then the differential rate with respect to the pathlength d_l within which decays are identifiable as Centauro events is

$$\frac{dN(d)}{d_l} = \frac{1}{c\gamma_L \tau_0} N(d)$$

and the Centauro event detection rate should be

$$R = \frac{d_l}{c\gamma_L \tau_0} N_T e^{-d/c\gamma_L \tau_0} \quad (3)$$

Solving this relation for the rate of events at the top of the atmosphere, N_T , one obtains

$$N_T = R \frac{\gamma_L^c \tau_0}{d_l} e^{d/c\gamma_L \tau_0} \quad (4)$$

Since we expect the formation of bubbles to have a threshold energy E_i , N_T should be the integrated cosmic ray flux at the top of the atmosphere with $E > E_i$ or

$$N_T = \eta K E_i^{-1.7} = \eta 1.1 \cdot 10^4 E_i^{-1.7} \text{ m}^{-2} \text{ Sr}^{-2} \text{ S}^{-1} \quad (5)$$

with E_i measured in GeV. The factor η denotes the fraction of these events that produce bubbles of metastable nuclear matter, which we will presently assume to be of the order of 1 ($\eta \approx 1$). If M_b is the mass (rest energy) of the bubble and E_b^* its CM energy then its Lorentz factor in the interaction CM frame will be

$$f = E_b^*/m_b$$

Hence the Lorentz factor of the CM will be $\gamma_{CM} = (\frac{E_i}{2m_p})^{1/2}$. Consequently the Lorentz factor of the bubble in the laboratory frame, γ_L , will be

$$\gamma_L = \frac{E_{b,lab}}{M_b} = \gamma_{CM} f + (\gamma_{CM}^2 - 1)^{1/2} \cdot (f^2 - 1)^{1/2} \cos\theta^* \approx f (\frac{E_i}{2m_p})^{1/2} \quad (6)$$

Substituting equations (5) and (6) into equation (4) and solving for E_i we obtain the transcendental equation

$$E_i = [\frac{1}{n\kappa} \frac{R}{dl} \cdot (\frac{E_i}{2})^{1/2} f \tau_0 \exp(d/c (\frac{E_i}{2})^{1/2} f \tau_0)]^{-0.59} \quad (7)$$

where $R = 10^{-2} \text{ m}^{-2} \text{ sr}^{-1} \text{ yr}^{-1}$ is the Centauro event rate, $dl = 10^4 \text{ cm}$, $d = 15 \text{ km} = 1.5 \times 10^6 \text{ cm}$, κ is defined by equation (5), and m_p has been taken as 1 GeV. Substituting the numerical values equation (7) reads

$$E_i = [\frac{1}{n} 5.68 \times 10^8 E_i^{1/2} f \tau_0 \exp(7.07 \cdot 10^5 / E_i^{1/2} f \tau_0)]^{-0.59} \equiv F(E_i, \tau_0)$$

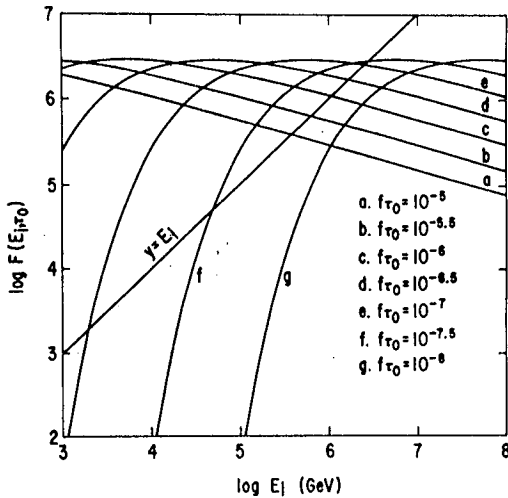


Figure 1

Equation (7a) can be solved graphically by plotting the curves $y = E_i$ and $y = F(E_i, \tau_0)$. The results are shown in figure 1 where the families of curves $F(E_i, \tau_0)$ are shown as a function of E_i with τ_0 as a parameter. One can distinguish two major features: (i) For sufficiently small values of the parameter τ_0 ($< 10^{-8}$) no solution to equation (7a) exists. This means that for sufficiently small bubble lifetimes ($\tau_0 < 10^{-8}$) not enough of them will survive deep enough in the atmosphere to account for the observed Centauro flux, (ii) For $\tau_0 > 10^{-8}$ there are always two solutions to equation (7a) since the curve $y = E_i$ intersects the curve $y = F(E_i, \tau_0)$

at two points. It is interesting to note that of these two solutions the highest ones are always close to an energy $E_i = 10^6 \text{ GeV}$ for a wide range of values of the parameter τ_0 , ($10^{-6} - 10^{-8}$), which corresponds to a CM energy of $\approx 1 \text{ TeV}$.

One can of course assume that the increased penetration is due to the smaller cross section of the "bubble". The difference in heights between 21 km (where presumably the metastable state forms) and 5 km where the fireball occurs and corresponds to $\sim 500 \text{ g cm}^{-2}$ or a cross section > 10 times smaller than that of strong interactions. This corresponds to a linear dimension > 3 times that of a proton and hence a $P_t \sim 3$ times that of strong interactions as indeed observed.

The assumption that the bubbles of the superdense metastable nuclear

state are produced with a certain kinetic energy at the CM of the collision can actually sidestep the arguments of Kinnen and Rubia (1981) against the origin of Centauros in high energy cosmic ray collisions. The latter authors have concluded so by noting that the kinematics of the Cenaturo event demand $\gamma \approx 10^4$ and $M_{\text{fireball}} \approx 200$ GeV. Assuming further (as they did) that all the primary energy goes into making the rest mass energy of the fireball (i.e. $\gamma = \gamma_{\text{CM}}$), they derived from the latter figures a primary energy $E_i \approx \gamma_{\text{CM}}^2 M_{\text{fireball}} \approx 10^{17}$ eV. The flux of cosmic rays at these energies is much too low to account for the observed Centauro rate. Eq. (6) however shows that if the bubble is created in the CM frame with a Lorentz factor $f \approx 10$ then $\gamma_i = 10^4$ implies $\gamma_{\text{CM}} \approx 10^3$ and hence a primary energy $E_i \approx 10^{15}$ which provides sufficient flux to account for the observed rate.

3. Discussion - Conclusions. The next question one is called to answer is the nature of these "fireballs". (See Kazanas et al. 1984). We consider the possibility of the SU(2)xU(1) vacuum as a means for producing these "fireballs". At the restoration of the symmetry there is a contribution to the energy density from the SU(2)xU(1) vacuum. The total energy density, ϵ , is then

$$\epsilon = An^{4/3} + \rho$$

The first term is the energy density due to the quarks participating in the collision (assumed to be cold) and the second term the energy density of the vacuum. The pressure of the mixture can then be calculated using the thermodynamic relation

$$P = n \frac{d\epsilon}{dn} - \epsilon = \frac{1}{3} An^{4/3} - \rho .$$

One can now observe that for $An^{4/3} \approx \rho$ (i.e. close to the phase transition point) the pressure of the mixture goes to zero and the medium becomes unstable to bubble formation. It is assumed that at $T \approx T_c$ the two phases with $\langle \phi \rangle = 0$ and $\langle \phi \rangle \neq 0$ coexist since the height of the barrier between them is smaller than the thermal energy for $T > T_c$ (Sher and Flores 1983). Neglecting surface effects, the bubbles are in pressure equilibrium between the positive particle pressure and the negative vacuum tension. The bubbles should therefore decay primarily into Higgs particles. It has been suggested (Willey 1984) that the particle $\xi(2.2)$ observed in the decay $J/\psi \rightarrow \gamma + \xi(2.2)$ might be the Higgs boson. Such an identification would indeed fit the signatures of the Centauros. A ~ 100 GeV bubble would decay into ~ 50 Higgs and subsequently into ~ 100 KR ($\xi(2.2) \rightarrow RK$ dominantly). These K's would have $P_t \sim 1$ GeV and would explain the absence of π^0 's. Also only explosions close to the detector would classify as Cenaturos since for $dL > 300$ m the K's would have a chance to decay into π^0 's, and then into photons.

4. References

1. Bjorken, J. D. and McLerran, L. D. Phys. Rev. D20 (1979), 2353.
2. Kazanas, D. et al. 1984, Phys. Lett. 142 23.
3. Kinnunen, R. and Rubbia, C. 1981, Proc. 17th ICRC, Paris, 11, 112.
4. Lattes, C. et al. 1973, Proc. 13th ICRC, Denver, 3, 2227; 4, 2671.
5. Sher, M. and Flores, R., Anny. Phys. 148 (1983), 95.
6. Willey, R. S., Phys. Rev. Lett. 52 (1984), 585.

HEAVY FLAVOURS PRODUCTION IN QUARK-GLUON PLASMA
FORMED IN HIGH ENERGY NUCLEAR REACTIONS

J. KLOSINSKI *

RIVERS STATE UNIVERSITY OF SCIENCE AND TECHNOLOGY
Physics Department
P.M.B. 5080
Port Harcourt, Nigeria

A B S T R A C T

Results on compression and temperatures of nuclear fireballs and on relative yield of strange and charmed hadrons are given in this paper. The results show that temperatures above 300 MeV and large compressions (≥ 10) are unlikely achieved in average heavy ion collision. In consequence thermal production of charm is low. Strange particle production is, however, substantial and indicates clear temperature - threshold behaviour.

1. Introduction: Observation of QGP is one of the most desired arguments in favour of correctness of our understanding of strong interactions. Its formation needs a large deposition of energy in large enough volume. The interactions of cosmic ray particles, primarily nuclei, offer the unique opportunity of its detection.

One of the signatures of QGP formation is increased rate of heavy flavours as compared to the hadronic systems at the same temperature without QGP formation (1). The role of charm may be also peculiar; we foresee charmed quarks as a centers of hadronic bubble formation in hot QGP and as a stabilizing factor in cold multicharmed globs (2). Both phenomena may lead to unusual events. Here we present only some of our results. The full paper will be published elsewhere.

2. The model: Several arguments, based on experimental observations (the transparency of nuclei being strongest one) and on results of relativistic of two fluid - hydrodynamics allows us to treat the beam nucleus (for definiteness we will work in the lab frame) as a penetrating, shock-like discontinuity propagating with (almost) velocity of light through the nuclear matter. In equations of hydrodynamics its propagation is represented

as a source term of energy, momentum and colour (but not baryon number) transferred to the nuclear matter. These equations allow us to find (with assumed equation of state for nuclear matter) the heating curve i.e. temperature T and compression factor $f (= n_B/n_0, n_0 = 0.17/\text{fm}^3)$ behind the front. Whenever T and f are in QGP sector of QGP-hadron phase diagram we assume that, within the slice 1-2 fm behind the traversing beam nuclei thermalized QGP is formed.

We tried several models of nuclear matter to get equation of state, but finally our results represented here are based on Walecka mean field model, Statistical bootstrap model of point particles, and Hybrid model of free N, Δ, π - gas with phenomenological repulsion potential fitted at low energies. The qualitatively the results for all models are the same.

QGP is described by standard model of four fermions (u, d, s, c - quarks) and eight bosons (massless gluons). The partition function with several sets of parameters tried, has been calculated up to the lowest order of perturbative expansion. The masses and coupling constant are taken density and temperature dependend with the running momentum $q = ((2T)^2 + (\mu_B/3)^2)^{\frac{1}{2}}$.

The evolution of QGP (its expansion and flow) is governed by hydro-and thermodynamics. One of the strongest constraints is given by baryon number conservation and entropy production condition (1), (3): i.e. surface hadronic deflagration of QGP at thermal and chemical equilibrium is forbidden prior to the reversed phase transition QGP-Hadronic gas. In consequence all hadrons are produced at transition temperature, which (for $f \lesssim 10$) is roughly 160-180 MeV and, as entropy production in deflagration is low, they preserve degrees of freedom of QGP close to the transition.

3. Results: Our model gives a unique possibility to relate T and f when equation of state is given. According to the authors knowledge this result is unique and original (4). In the approximations used the result for $T(f)$ do not depend on size of the neither beam not target nuclei. The result for assumed (ud) , (uds) , $(udsc)$ QGP is presented on Fig. 1.

The second result of our model which we wish to present to the Conference is strangeness and charm relative yield when QGP is formed in nuclear collision. Due to high entropy per baryon and, in principle, unlimited temperature as well as due to peculiar properties of QGP evolution its presence offers more abundant production of heavy flavours than any hadronic process without QGP.

Due to the finite relaxation times the production of heavy flavours at lower temperatures is damped by finite life time of QGP. In consequence the production of strangeness and charm displays a pronounced temperature-threshold enhancements. For nuclear fireball created according to the our scenario the strange particles start to be copiously produced at $T \gtrsim 240$ MeV, (see Fig. 2) whereas charmed particles have threshold at $T \approx 500$ MeV.

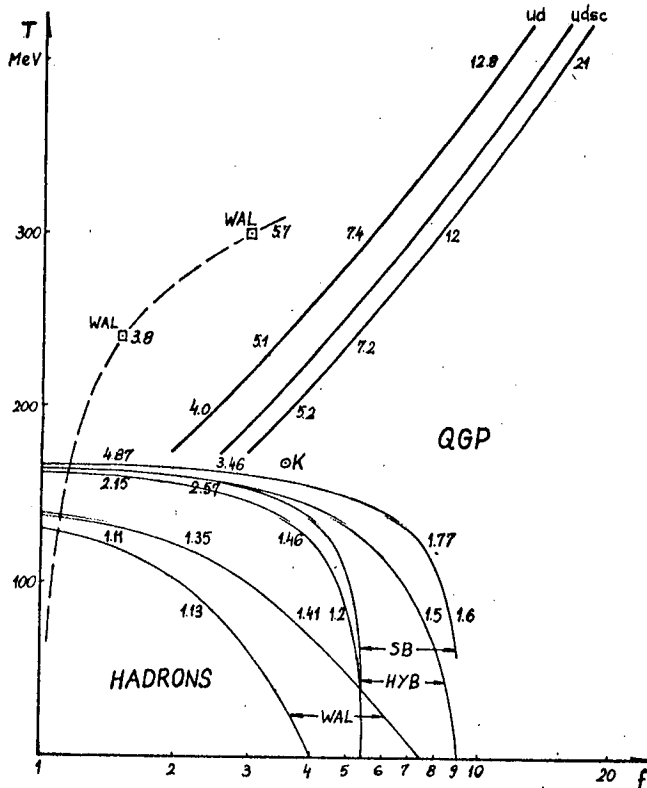


Fig. 1

Temperature T and compression factor (f) of nuclear fireball together with phase diagram for Walecka (WAL), Hybrid (HYB) and stat. Bootstrap (SB) models of hadronic gas.

T - f curve for hadronic fireball has been got for ud , uds and $udsc$ flavours. WAL-curve has been got when compressed matter is assumed to be Walecka nuclear matter. K is "Kajantie point". All numbers refer to energy per baryon.

4. Conclusions: According to our model and within the approximations done our results indicates:

- (i) High temperatures in nuclear fireballs are not likely to be common phenomenon at high energy interactions. It is relatively easy to heat nuclear fireball up to $T = 200 - 240$ MeV.

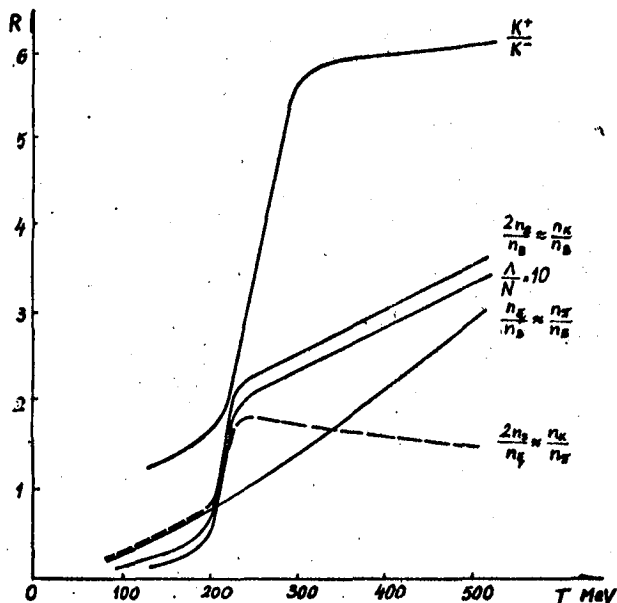


Fig. 2

Ratio R of strange quarks and hadrons yield v.s. initial temperature of nuclear fireball. The threshold behaviour is seen only for strange hadron yield but not for nonstrange component. For charmed particles yield similar threshold is expected for temperatures above 500 MeV.

- (ii) Nuclear fireball decays in a deflagration - like process at $T = 160-180$ MeV when almost all hadrons are produced.
- (iii) Heavy flavours are easily produced provided relaxation time is shorter than life time of QGP droplet. Their production displays threshold - like enhancement which may serve as indicator of QGP-formation.
- (iv) Energy transferred to heavy flavour component is almost steady ($\approx 30\%$) fraction of total energy.
- (v) Charmed quarks and consequently charmed particles are produced in very low amount (at $T = 500$ MeV n_c/n_B is $\approx 10^{-6}$).

* On leave of absence from University of Lodz, Poland.

References:

1. Quark matter Formation, Ed. M. Jacob, H. Satz: Singapore, 1982.
2. J. Klosinski, Proc. of 18th ICRC, Vol.II, p. 166.
3. L. Van Hove, Z, Phys. C, 21, (1983) 93-98.
4. R. Anishetty et al, Phys. Rev. 22 (1980) 2793.

RINGLIKE INELASTIC EVENTS IN COSMIC RAYS AND ACCELERATORS

I.M.Dremin, A.M.Orlov, M.I.Tretyakova
P.N.Lebedev Physical Institute,
Leninsky Prospect 53, Moscow, 117924, USSR

In cosmic rays ¹⁻³ and in accelerators ⁴ there were observed single inelastic processes with densely produced (azimuthally isotropic) groups of particles exhibiting spikes in the pseudorapidity plot of an individual event (i.e. ringlike events).

Theoretically the existence of such processes was predicted ⁵ as a consequence of Cherenkov gluon radiation or, more generally, of deconfinement radiation ⁶.

Nowadays some tens of such events have been accumulated at 400 GeV ⁷ and at 150 TeV ⁸.

Analyzing ringlike events in proton-nucleon interactions at 400 GeV/c we show ⁷ that they exhibit striking irregularity in the positions of pseudorapidity spikes' centers which tend to lie mostly at 55, 90 and 125° in cms. It implies rather small deconfinement lengths of the order of some fermi.

We have chosen high-multiplicity events with $n_{ch} \geq 12$ among all proton-nucleon interactions at 400 GeV in the photoemulsion experiment ⁹. There were 284 events available. To select ringlike events we use some criteria (for more details see ⁷) which single out those events with dense groups in the pseudorapidity plot containing more than 6 charged particles within the unit pseudorapidity interval.

In total 59 among 284 event have been chosen as ringlike events what corresponds to 1 mb of their production cross section.

The very important feature of ringlike events is the position of rings. The center of a ring should be in some way close to the direction of the gluon emission in the above treatment. We have determined the positions of the

centers of rings in all 59 events. They are shown in Fig.1.

In Fig.2 we show the example of one ringlike event (among 59 available).

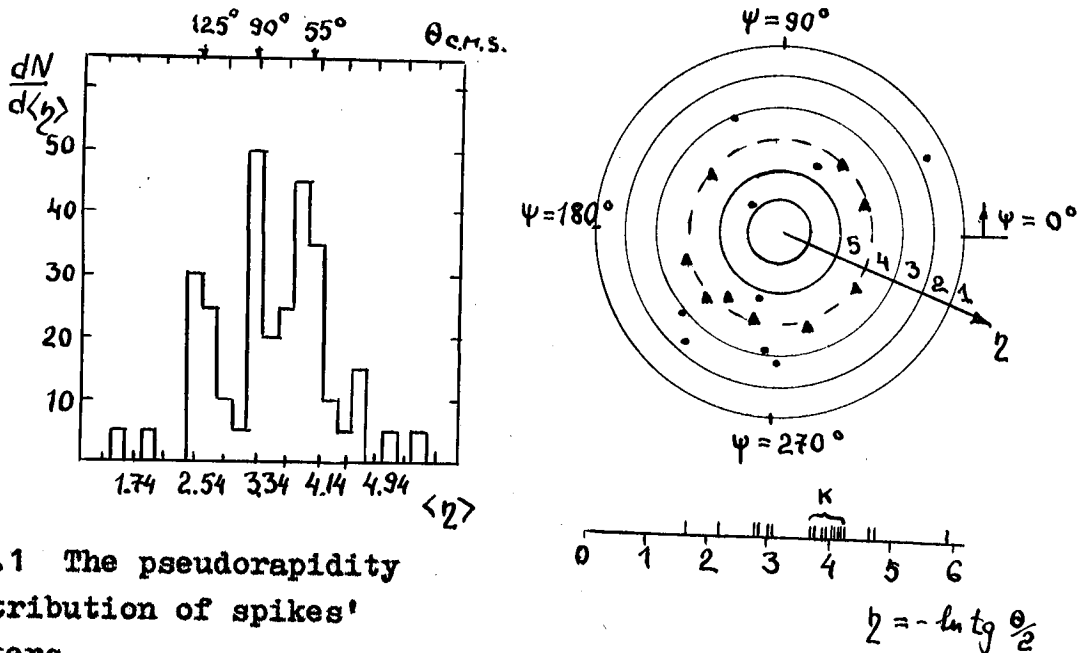


Fig.1 The pseudorapidity distribution of spikes' centers.

Fig.2 The pseudorapidity distribution (a) and the pseudorapidity azimuthal plot (b) of a pN-event ($0+0+18p$) with a ring of 9 charged particles ($\langle \eta \rangle = 4.02$, $\langle \Delta \eta \rangle = 0.066$). Triangles mark the particles, points correspond to other particles.

The most striking feature of Fig.1 is the irregularity in appearance of rings ^{*}) and their tendency to rather large cms angles (upper axis).

The only reliable explanation is that the particles within the rings are produced by some process the formation length of which is rather short. Actually, the large emission angles of Cherenkov gluon radiation were predicted ⁵ in 1979

^{*}) The indirect confirmation to such irregularity can be drawn from ISR-data ¹⁰ about two-particle rapidity correlations (for more details see ⁷).

as a consequence of a thinness of hadronic targets. Later it was shown⁶ that the deconfinement of quarks within hadronic targets can provide stronger effect at the same angles. The maximum of forward (in cms) emission of gluon jets appears at the laboratory angle

$$\theta_{lab} \approx (2\pi/\omega\ell)^{1/2}, \quad (1)$$

where ω is an energy of a gluon jet (i.e. of a group of particles) and ℓ is a formation length which should be close to the deconfinement length. Let us remind that an analogous value for protons usually increases with primary energy E of an emitting particle as $\omega^{-1}\gamma^2 \cong \omega^{-1}(E/m)^2$ i.e. it must be very large at 400 GeV and correspondingly the emission angle is small (of the order of m/E according to (1)).

The average number of emitted within the ring gluons in an individual event is estimated⁶ as about 3 at 400 GeV and about 6 at 150 TeV. Therefore the rings could be totally isotropic at 150 TeV while some azimuthal substructure may be noticeable at 400 GeV. We have not investigated it in detail.

If the maxima at 55 and 125° shown in Fig.1 are interpreted as ones due to gluon emission by deconfined quarks then using (1) together with the obvious inequality

$\omega < E$ one gets

$$\ell \gtrsim 2 fm. \quad (2)$$

The hadron momenta have not been measured⁹ and therefore we can not estimate the value of ω in (1). However reasonable assumptions about transverse momenta show that the gluon radiation length ℓ can not be much larger than, say, 10 fm.

This conclusion is strikingly different from above estimates for photon radiation length. It shows the fundamental difference between the electromagnetic and colour currents, the last one being strongly confined within small space regions. The formula (1) provides unique means to

determine the extension of that region.

In conclusion, the ringlike events (i.e. events with high density of secondary particles within a narrow pseudorapidity interval) provide an unique possibility to define the length of action of deconfined colour currents. The above investigation shows that this length appears to be quite short (of the order of the hadron size). They also could reveal such important facts as the vector nature of gluons and the macroscopic features of the quark-gluon medium (for example, its refractivity). Further experimental work with higher statistics is needed for detailed study of those problems.

References

1. Apanasenko A.V. et al. (1979), JETP Lett., 30, 157.
2. Dremin I.M., Tretyakova M.I., (1981), Proc. XVII ICRC, V5, p.149.
3. Arata N., (1978), Nuovo Cim., 43A, 455.
4. Marutyan N.A. et al., (1979), Sov. J. Nucl. Phys., 29, 1566.
5. Dremin I.M., (1979), JETP Lett., 30, 152; (1981), Sov. J. Nucl. Phys., 33, 1357.
6. Dremin I.M., (1981), JETP Lett., 34, 617; (1983), Sov. J. Nucl. Phys., 37, 649.
7. Dremin I.M., Orlov A.M., Tretyakova M.I., (1984), JETP Lett., 40, 320.
8. Rushbrooke J.G., (1983), Preprint CERN EP 84034.
9. AGMT-collaboration, (1979), Sov. J. Nucl. Phys., 29, 678.
10. Cavalinni V. et al., (1984), Z. Phys. C, 21, 299.

PHASE SPACE FACTORS IN MULTIPARTICLE PROCESSES

Robert J. Gould
 Physics Department B-019
 Univ. of Calif., San Diego
 La Jolla, CA 92093 USA

ABSTRACT

General phase space theorems are discussed for the cases (A) with only energy conservation applied and (B) with energy and momentum conservation applied. It is shown that in the non-relativistic limit for N particles there is a very close relationship between the multiparticle phase space integral in case B and that for case A and $N-1$ particles.

1. Introduction. There are in physics many phenomena that can be described as phase space effects. By this is meant effects that are determined essentially by the number of states available to the system. Examples may be found in equilibrium statistical mechanics and in the evaluation of dynamical processes. In particular, the cross sections and rates associated with processes initiated by binary collisions are determined by the interaction that causes the process and also by the number of final states associated with the various products or channels for the reaction. Applications or examples of this kind of effect occur in electronic and atomic processes, chemical kinetics, nuclear reactions, and elementary particle processes. All of these processes can be represented as a reaction of the type



In the c.m. frame and for given energy (E) available to the outgoing particles, the total momentum-space volume available to these particles is, with momentum and energy conservation imposed,

$$\phi^{(N)} = \int \dots \int \prod_{j=1}^N d^3 p_j \delta^{(3)} \left(\sum_{j=1}^N p_j \right) \delta \left(\sum_{j=1}^N E_j - E \right). \quad (2)$$

This quantity, proportional to the number of available final states, is fundamental and simple expressions for $\phi^{(N)}$ can be derived for small N when the outgoing particles are non-relativistic (NR), extremely-relativistic (ER), or even of general energy. When all are NR or ER (or even a mixture), it is possible to derive expressions for $\phi^{(N)}$ for general N , using various mathematical methods or tricks. One such trick will be illustrated in this paper.

In the limit where one of the outgoing particles (say, particle N) has a large mass, its energy ($p_N^2/2m_N$) is small and can be neglected. Then, the $\delta^{(3)}$ function can be eliminated by integrating over $d^3 p_N$, and

$$\phi^{(N)} \xrightarrow{m_N \gg g} \psi^{(N-1)} = \int \dots \int \prod_{j=1}^{N-1} d^3 p_j \delta \left(\sum_{j=1}^{N-1} E_j - E \right); \quad (3)$$

that is, the heavy particle just plays the role of satisfying the momentum-conservation restriction. The phase space integral (3), with only the energy-conservation restriction applied is the one appearing in statistical mechanics in the so-called microcanonical ensemble. It turns out, however, that, in the NR limit, $\phi^{(N)}$ is very closely related to $\psi^{(N-1)}$ for an arbitrary distribution of masses m_1, m_2, \dots, m_N ; we shall demonstrate this in a simple way.

Before proceeding to consider the very special problem mentioned just above, a few other introductory remarks should be made. In modern particle physics the use of the invariant phase space volume $\phi^{(N)}$ is more common; this quantity is the same as $\phi^{(N)}$ except each factor d^3p_j is divided by $2E_j$, yielding Lorentz-invariant factors; the two δ -functions are also combined to a single invariant $\delta^{(4)}$ factor. The factors ϕ are certainly more convenient than Φ in relativistic calculations, but it is not clear which is actually more fundamental. In a sense Φ is, since it is proportional to the number of states. For examples of the use of the invariant ϕ -factors the book by Perl [1] may be consulted; this work also gives references to earlier papers on the general subject. A general survey is also given in a monograph [2] in preparation by the author.

2. General Expressions: NR Limit. If we make the change of variable

$$p_j = (2Em_j)^{1/2} x_j, \quad (4)$$

thereby introducing dimensionless momentum variables x_j , the integral can be written in more convenient form. It is also convenient to introduce dimensionless masses in terms of the total mass M :

$$m_j = v_j^2 M; \quad \sum_{j=1}^N v_j^2 = 1. \quad (5)$$

Then, in the NR limit,

$$\phi^{(N)} = (2M)^{3(N-1)/2} \left(\prod_{j=1}^N v_j \right)^{3E^{3(N-1)/2-1}} I_N, \quad (5)$$

where

$$I_N = \int \cdots \int \prod_{j=1}^N d^3 x_j \delta^{(3)} \left(\sum_{j=1}^N v_j x_j \right) \delta \left(\sum_{j=1}^N x_j^2 - 1 \right) \quad (7)$$

is a dimensionless integral. In terms of the variables x_j and parameters v_j , the phase space integral ψ [eq. (3)] is

$$\psi^{(N)} = (2M)^{3N/2} \left(\prod_{j=1}^N v_j \right)^{3E^{3N/2-1}} J_N, \quad (8)$$

where

$$J_N = \int \cdots \int \prod_{j=1}^N d^3 x_j \delta \left(\sum_{j=1}^N x_j^2 - 1 \right). \quad (9)$$

In the following section we shall outline the proof that

$$I_N = J_{N-1} \quad (10)$$

This is, at first sight, a remarkable result that means, for example, that I_N is independent of the mass spectrum v_1, v_2, \dots, v_N . The integral (9) for J_N can be evaluated easily by a number of methods (see [2] or almost any book on statistical mechanics):

$$J_N = \pi^{3N/2} \Gamma(3N/2) . \quad (11)$$

3. Theorem [eq. (10)] on Phase Space Integrals. The theorem is easy to prove for $N=2$ and 3, but it is of interest to prove it for general N . This can be done by considering the indices $j=1, 2, \dots, N$ labelling the particles as designating an N -dimensional space. With \hat{e}_j as a unit vector along the j^{th} axis of this space, the axes are taken to be orthogonal: $\hat{e}_j \cdot \hat{e}_k = \delta_{jk}$. In this space $\hat{v} = (v_1, v_2, \dots, v_N)$ is a vector of unit length: $\hat{v} \cdot \hat{v} = 1$, because of (5). Also, in terms of $\hat{x} = (x_1, x_2, \dots, x_N)$, and

$$d^3 \hat{x} = \prod_{j=1}^N d^3 x_j = dx_1 \dots dx_N dy_1 \dots dy_N dz_1 \dots dz_N , \quad (12)$$

the integral (7) can be written

$$I_N = \int d^3 \hat{x} \delta(\hat{x}^2 - 1) \delta^{(3)}(\hat{v} \cdot \hat{x}) \quad (13)$$

But $\hat{v} \cdot \hat{x}$ is invariant to a rotation of the axes in the N -dimensional space, as is \hat{x}^2 . Essentially, such a rotation corresponds to a relabelling of the particles. With this invariance, it is convenient to choose an orientation such that the vector \hat{v} is along one axis such that, say, $\hat{v} = (0, 0, \dots, 1)$ corresponding, physically, to the case $m_N \gg m_{j < N}$. The δ -function $\delta^{(3)}(\hat{v} \cdot \hat{x})$ is then simply $\delta^{(3)}(x_N)$ which can be eliminated by integration over $d^3 x_N$. The resulting integral is then just J_{N-1} and the identity (10) is obtained.

It is interesting how in this problem we make use of the mass spectrum m_1, m_2, \dots, m_N to prove a theorem and simplify a derivation. In the ER limit we have no such device to employ and the evaluation of the corresponding $\Phi^{(N)}$ is more complicated. However, the same trick employed to prove the result (10) can be used to derive results when we have, say, N NR particles and N' ER particles. For more details, see [2].

4. Acknowledgements. This research is supported by NASA through Grant NGR 05 005 004.

References

- [1] M. L. Perl, High Energy Hadron Physics (New York: John Wiley and Sons, 1974).
- [2] R. J. Gould, High Energy Phenomena in Astrophysics (in preparation, Princeton Univ. Press).

THE RESPONSE OF A SCINTILLATION COUNTER BELOW AN EMULSION
CHAMBER TO HEAVY NUCLEUS INTERACTIONS IN THE CHAMBER

THE JACEE⁺ COLLABORATION

T.H. Burnett(h), S. Dake(b), J.H. Derrickson(f), W.F. Fountain(f), M. Fuki(c), J.C. Gregory(g), T. Hayashi(b), T. Hayashi(g,j), R. Holynski(e,i), J. Iwai(h), W.V. Jones(e), A. Jurak(e,i), J.J. Lord(h), C.A. Meegan(f), O. Miyamura(d), H. Oda(b), T. Ogata(a), T.A. Parnell(f), E. Roberts(f), T. Saito(a), T. Tabuki(a), Y. Takahashi(f), T. Tominaga(d), J.W. Watts(f), B. Wilczynska(i), R.J. Wilkes(h), W. Wolter(e.i), and B. Woziek(e,i).

(a) Institute for Cosmic Ray Research, University of Tokyo, Tokyo, Japan; (b) Department of Physics, Kobe University, Kobe, Japan; (c) Department of Physics, Okayama University of Science, Okayama, Japan; (d) Department of Applied Mathematics, Osaka University, Osaka, Japan; (e) Department of Physics and Astronomy, Louisiana State University, USA; (f) Space Science Laboratory, NASA/Marshall Space Flight Center, USA; (g) Department of Chemistry, University of Alabama, Huntsville, USA; (h) Department of Physics, University of Washington, Seattle, USA; (i) Institute for Nuclear Physics, Krakow, Poland; (j) Science and Engineering Research Laboratory, Waseda University, Tokyo, Japan.

ABSTRACT

In 1982 a hybrid electronic counter-emulsion chamber experiment was flown on a balloon to study heavy nucleus interactions in the 20 to ~ 100 GeV/AMU energy range. A gas Cerenkov counter, two solid Cerenkov counters, and a proportional counter hodoscope gave the primary energy, the primary charge and the trajectory of the particles, respectively. Using the trajectory information cosmic ray nuclei of $Z > 10$ were found reliably and efficiently, and interaction characteristics of the Fe group nuclei were measured in the chamber. A plastic scintillator below the emulsion chamber responded to showers resulting from interactions in the chamber and to non-interacting nuclei. Data on the response of the counter have been compared with simulations of hadronic-electromagnetic cascades to derive the average neutral energy fraction released by the heavy interactions, and to predict the performance of this kind of counter at higher energies. For the interacting events of highest produced particle multiplicity comparison between various simulations and the shower counter signal have been made.

1. The Instrument. The hybrid electronic counter-emulsion chamber instrument has been described¹ and some results of the interactions studies are presented at this conference^{2,3}. Information on the measurements of primary charge and energy with the electronic counters is also presented⁴. For the purpose of this paper the counters above the emulsion chamber give a sample of heavy nuclei, carbon and above, energy of 22 GeV/AMU and above with charge known within $Z \pm 1$ and energy differentially to 65 GeV/AMU and integrally above 65 GeV/AMU. The data available in this energy range contain 2,408 total particles. The

relevant emulsion chamber features are: Dimensions 50 cm x 50 cm x 21.5 cm ; 65 gm/cm² thick; 7.0 total radiation lengths; 1.4 interaction lengths thick for oxygen and 2.5 for Fe.

The burst scintillator was a 0.635 cm thick sheet of Ne 102 plastic, 57 cm x 57 cm, enclosed in a diffusion box viewed by two sets of two 7.62 cm photomultiplier tubes. One set of two tubes covered the pulse height range to 200 equivalent minimum ionizing particles (MIP). The other set (using dynode pulses) covered the range to 6000 equivalent MIP. The usable range of overlap included the fraction ($\sim 20\%$) of C to Si nuclei which passed through the emulsion chamber and allowed in-flight calibration. Figure 1 shows the pulse height spectrum caused by oxygen nuclei with the prominent non-interacting peak. The use of only two photomultipliers resulted in nonuniformity ($\pm 15\%$) which was mapped with muons and checked with in-flight calibration for use in corrections. Because of the lateral spread of the showers in this energy range this correction has some residual error.

2. Simulations. A simulation program was developed to predict the shower signal in equivalent minimum ionizing particles [(Z fragments)² + protons + charged pions + (electrons > 1 MeV)]. The simulation program is modular with options allowed for processes such as fragmentation, pion generation, and electromagnetic cascade. Most shower counter simulations used a wounded nucleon model (WNM) with the average number of wounded nucleons equal to 0.3, an average inelasticity of 0.5, number of pions from $\langle N \rangle = 2.3E^{1/4}$, pion energies from the CKP model, and pion angles from a distribution with average $P_T = 300$ MeV/c. The electromagnetic cascade was a linear shower development function at the correct angle based on Rossi-Greisen but adjusted to later experimental results⁵.

3. Results. Figure 2 shows the data from the burst counter for individual events with $Z = 24$ to 28. Also shown are results of simulations at 20 GeV/AMU and 60 GeV/AMU. These simulations were done by choosing, according to interaction length, a random location in the chamber at an incident angle of 30° . The results of repeated event simulations match well in average values the data from $Z = 6$ through 26 over the narrow energy range available to this experiment. Table I shows the results of simulations up to 200 GeV/AMU and data from this experiment. The results agreed with the average value of heavy nucleus energy going into electromagnetic cascades (0.12 for Fe), which has been used for energy estimation in passive emulsion chamber experiments at higher energies.

TABLE I

Pulse height and standard deviation for burst counter and simulations. Burst signal is in range 21 to 25 and > 55 GeV/AMU. Simulations are average of 40 events.

E(GeV/n)	20	60	200
0 Burst	252 \pm 190	604 \pm 468	
0. SIM	231 \pm 132	640 \pm 455	1554 \pm 1200

Fe Burst	951 ± 333	2082 ± 856	
Fe SIM	851 ± 239	2130 ± 934	5861 ± 2716

It is noted from Figure 2 that the events of highest produced particle multiplicity (as determined from the emulsions, see paper HE1.4-3 this conference) do not give exceptional burst counter signatures. Some simulations of these events have been attempted, using as a starting point the first interaction characteristics from the emulsions. One method of simulation started with the primary angle, interaction position, and number of wounded nucleons. The remainder of this simulation was the same as the WNM simulation described above. Another used the produced particle angular distribution list (reduced by a number of leading particles equal to the primary charge); and assumed a pion transverse momentum distribution of average $P_{t\pi^0} = 340$ MeV/c and conservation of isotopic spin. These simulation results for the five highest multiplicity events generally exceeded the burst counter pulse height by one to four standard deviations. An analysis of individual event simulation results to varying parameters in the models is in progress. For peripheral interactions, such simulations are more obscured by subsequent fragment interactions which are not usually measured in the chamber.

4. Discussion. The behavior of the burst counter described above and the results of the simulations using the WNM compare well in average values and variance in the energy range of this experiment. Several effects, including the loss of shower particles from the sides of the scintillator, effect of shower lateral spread on uniformity corrections, and knock-on electrons cascading in the calorimeter have been estimated but not modeled in detail.

References

1. Austin, R.W. et al., Papers of the 18th ICRC, T2-15 (1983).
2. Burnett, T.H. et al., presented by B. Wosiek, this conference.
3. Burnett, T.H. et al., presented by S. Dake, this conference.
4. Paper OG4.1-9, this conference.
5. Müller, D., Phys. Rev., 5:11, 2677-2683, 1972.

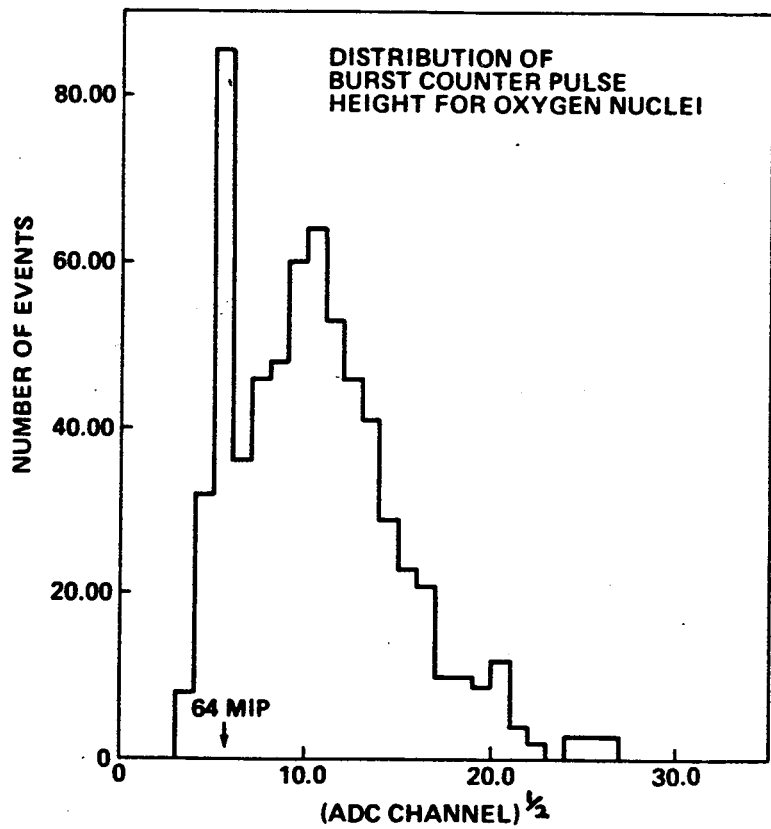


FIGURE 1

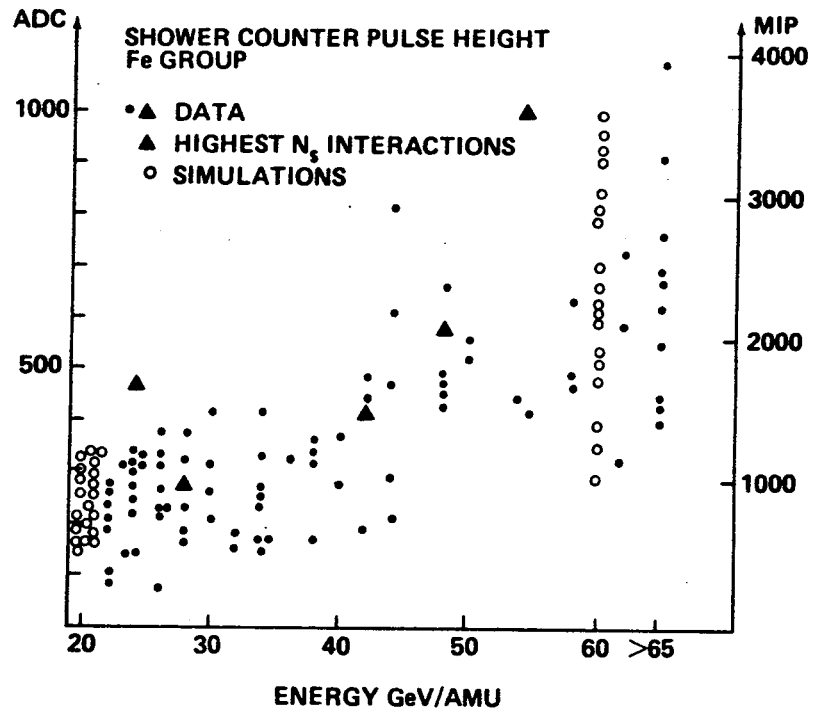


FIGURE 2

HEAVY NUCLEUS COLLISIONS BETWEEN 20 AND 60 GeV/NUCLEON.

The JACEE Collaboration

T.H.Burnett^{h)}, S.Dake^{b)}, M.Fuki^{b)}, J.C.Gregory^{g)},
 T.Hayashi^{d)}, R.Holynskiⁱ⁾, J.Iwai^{h)}, W.V.Jones^{e)},
 A.Jurakⁱ⁾, J.J.Lord^{h)}, O.Miyamura^{c)}, T.Ogata^{a)},
 T.A.Parnell^{f)}, T.Saito^{a)}, T.Tabuki^{a)}, Y.Takahashi^{g)},
 T.Tominaga^{c)}, B.Wilczynskaⁱ⁾, R.J.Wilkes^{h)}, W.Wolterⁱ⁾,
 B.Wosiekⁱ⁾.

- a) ICR, University of Tokyo; b) Kobe University;
 c) Osaka University; d) Waseda University;
 e) Louisiana State University;
 f) Marshall Space Flight Center;
 g) University of Alabama in Huntsville;
 h) University of Washington;
 i) Institute of Nuclear Physics, 30-055 Kraków, Poland.

1. Introduction

Interest in studying relativistic nucleus-nucleus interactions arises from the fact that they offer an opportunity to probe nuclear matter at high density and temperature. It is expected that under such extreme conditions a transition from hadronic matter into quark-gluon plasma occurs and that in the interactions of highly relativistic nuclei such conditions are created [1]. Before energetic nuclei beams will be available at new ion accelerators, cosmic rays remain a unique source of high energy heavy nuclei. JACEE-3 experiment was designed for study the collisions of heavy cosmic ray nuclei with different nuclear targets at energies beyond 20 GeV/nucleon.

2. Experimental method

JACEE-3 experiment was carried out using a combined electronic counters and an emulsion chamber detector, which was exposed to the cosmic rays on a balloon at an altitude of 5 g/cm². The electronic counters were placed on the top of a 50 x 50 cm² emulsion chamber. The counter system measures the energies (between 20 and 60 GeV/nucleon), charges (from Z=6) and determines trajectories of incident nuclei. It registers also the burst energies released in the interactions. The emulsion chamber serves simultaneously as both target and coordinate/ionization recorder. Details of the apparatus are given in [2].

The charges of projectile fragments and emission angles of all charged secondaries were measured in consecutive layers of emulsion and/or CR-39 plates downstream the interaction vertex. Charged particles in the forward cone were detected in the emulsion chamber without ambiguity. For each event the following multiplicities were determined:

N_F - number of multicharged projectile fragments ($Z \geq 2$);

N_p - number of released protons from incident nucleus,

$$N_p = Z_p - \sum_{i=1}^{N_F} Z_{F,i}, \text{ where } Z_p \text{ is the charge of primary nucleus;}$$

N_{sf} - number of relativistic ($\beta \geq 0.7$) singly charged secondaries emitted in the forward hemisphere: $\theta \leq \theta_{1/2}$, where $\theta_{1/2}$ corresponds to $\pi/2$ in the center of mass of proton-proton collision;

$N_{mf} = N_{sf} - N_p$, number of produced charged particles (mesons);

N_{sp} - number of spectator protons (see explanation below);

$N_{part} = N_p - N_{sp}$, number of protons participating in the collision.

Spectator nucleons are not involved in the collision. The number of spectator protons, N_{sp} , can be determined for each event by selecting from singly charged particles those fulfilling a given emission angle criteria [3]. Among participated nucleons (N_{part}) are wounded nucleons which interact inelastically in the target and nucleons which do not contribute to the particle production but still participate in the collision as the secondaries scatter off them. It is not possible to distinguish experimentally between wounded protons and those originating from cascade processes, however it is natural to assume that N_{part} is related to the number of wounded protons.

3. Results

The analysis was performed on an unbiased sample of heavy primary ($Z_p \geq 22$) interactions with three different targets:

light target=CHO, emulsion and lead. The detailed measurements have been completed for 70 interactions with $E_p \leq 60$ GeV/n

out of 120 heavy nuclei recorded. Table 1 summarizes the inclusive data for interactions of "iron" group nuclei on different targets. Multiplicities and dispersions are calculated for the forward cone only. The values of the N_{mf}/D ratio

are close to 1 independently of the target mass being consistent with the predictions of the superposition models for nucleus-nucleus interactions [4]. In Figs. 1a, b, c the inclusive pseudorapidity distributions obtained on different targets are presented. The increased of the particle production on heavier targets in forward region is seen. In Table 2 we compare our results with the data for proton collisions with the same targets [5]. The p-nucleus data are taken in the same angular region and are extrapolated to the same primary energy $\langle E_p \rangle$. The ratio of the average multiplicity in nucleus-

nucleus collisions to the mean multiplicity in p-nucleus interactions can be compared to the average number of wounded nucleons in projectile nucleus N_{wn} , calculated from the simple geometrical formula: $N_{wn} = A_p \sigma_{pA} / \sigma_{AA}$. Within the limits

of statistical errors these two quantities agree with each other. Thus, we observe an extension of p-nucleus data to nucleus-nucleus ones on the base of simple superposition of independent collisions of nucleons from projectile nucleus.

If we select the events with different number of wounded nucleons than, we expect (basing on a superposition picture) that the multiplicity in nucleus-nucleus collisions will depend linearly on the number of wounded nucleons. Experimentally it is only possible to do a selection according to the number of participating nucleons, so the quantitative comparison with model predictions is not possible. Qualitatively we observe the increase of the multiplicity with increasing number of participating nucleons (Fig.2), but this dependence is much weaker than the one expected from superposition of p-nucleus collisions. This discrepancy may be explained by the fact that among N_{part} there are protons which do not contribute efficiently to the particle production. On the other hand we do not expect a dependence of \bar{N}_{mf} on the number of spectator nucleons, unless the latter are not correlated with participating nucleons. Only for events with a total disintegration of primary nucleus into singly charged fragments such correlation exists. In Fig.3 the dependence of \bar{N}_{mf} on the number of spectator nucleons is shown.

From the central rapidity densities we can estimate the energy density created in the collision. Using the formula given by Bjorken [1] and taking $\bar{P}_1 = 0.4$ GeV/c we obtain mean energy densities smaller than 0.5 GeV/fm³. This is below the critical value required for the phase transition [1]. For the highest multiplicity events the energy density approaches 1 GeV/fm³. The characteristics of these events will be presented separately at this conference.

4. Conclusions

The presented results from JACEE-3 experiment (multiplicities, \bar{N}/D ratios, comparison with p-nucleus data) support the hypothesis that nucleus-nucleus interactions can be considered as a simple superposition of independent p-nucleus collisions. The similar conclusion was obtained from an analysis of ²²Ne-emulsion interactions at primary momentum 4.1 A GeV/c and with a high event statistics [6]. No evident signals of phase transition have been observed, suggesting that the detection of exotic phenomena requires a high statistics experiments with a possibility to look for specific signatures.

References

1. See for example: E. Shuryak, Phys. Rep. 61, 71 (1980), J. D. Bjorken Phys. Rev. D 27, 140 (1983), J. Cleymans et al., Z. Phys. C 17, 341 (83).
2. JACEE Collaboration, 18th ICRC Conf. Papers 9, 375, 379 (1983).
3. A. S. Goldhaber, Phys. Lett. B 53, 306 (1974).
4. A. Bialas et al., Nucl. Phys. B 111, 461 (1976), K. Kinoshita et al., Z. Phys. C 8, 205 (1981), A. Capella et al., preprint TH.3700-CERN.
5. W. Busza et al., Phys. Rev. D 22, 13 (1980).

6.B.Wosiek et al., this conference paper HE1.4-7.

Table 1.

A_T TARGET MASS	No. of events	$\langle Z_p \rangle$	$\langle E_p \rangle_{60/h}$	\bar{N}_{mf}	\bar{N}_{mf} / D
CHO	45	25.1	36	21.9 ± 3.0	$1.09 \pm .19$
Emulsion	10	25.0	28	28.9 ± 11.4	$.80 \pm .36$
Pb	15	24.8	34	41.1 ± 10.6	$1.00 \pm .32$

Table 2.

A_T	$\bar{N}_m^{FeAT} (\eta \geq 2)$ ($\eta \geq 2$)	$\bar{N}_m^{PAT} (\eta \geq 2)$ ($\eta \geq 2$)	$\bar{N}_m^{FeAT} / \bar{N}_m^{PAT}$	$\bar{N}_{un}^{Fe} (A_T)^{calc.}$
CHO	22.8 ± 3.3	2.6 ± 0.2	8.8 ± 1.4	6.6
Em	29.8 ± 11.6	3.0 ± 0.3	9.9 ± 4.0	10.3
Pb	45.5 ± 12.3	3.0 ± 0.45	15.2 ± 4.7	18.3

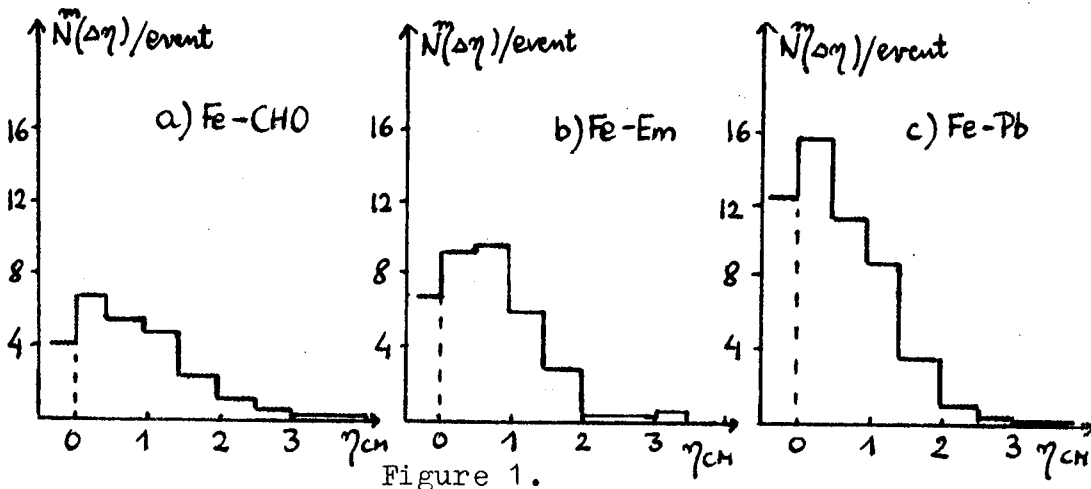


Figure 1.

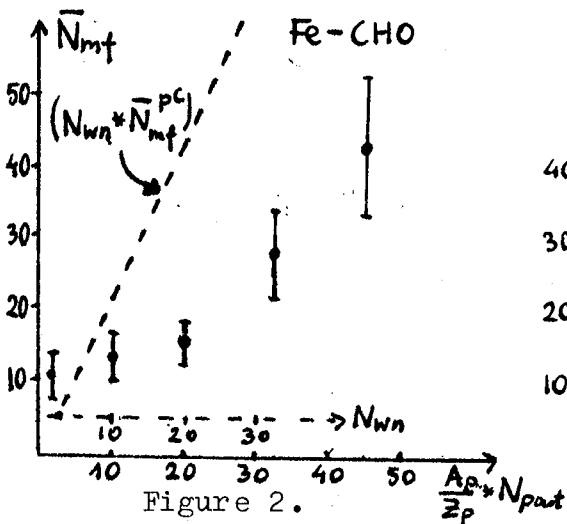


Figure 2.

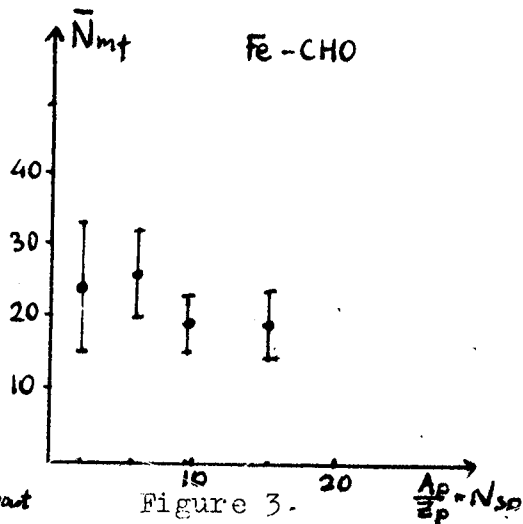


Figure 3.

CHARACTERISTICS OF CENTRAL COLLISION EVENTS
IN FE-NUCLEUS INTERACTIONS FROM 20 TO 60 GEV/NUCLEON

T. H. Burnett (h), S. Daka (a), J. H. Derrickson (f), W. Fountains (f), M. Fuki (c), J. C. Gregory (e), Ta. Hayashi (e), To. Hayashi (a), R. Holynski (i), J. Iwai (h), W. V. Jones (g), A. Jurak (i), J. J. Lord (h), C. A. Meegan (f), O. Miyamura (d), H. Oda (a), T. Ogata (b), T. A. Parnell (f), E. Roberts (e), T. Saito (b), S. Strausz (h), T. Tabuki (b), Y. Takahashi (e), T. Tominaga (d), B. Wilczynska (i), R. J. Wilkes (h), W. Wolter (f) and B. Wosieek (i)

(a) Kobe University, Nada-ku, Kobe 675, JAPAN

(b) ICR, University of Tokyo, Tanashi, Tokyo 188, JAPAN

(c) Okayama University of Science, Ridai-cho, Okayama 700, JAPAN

(d) Osaka University, Toyonaka, Osaka 560, JAPAN

(e) Department of Chemistry, University of Alabama in Huntsville, Huntsville, Alabama, U. S. A.

(f) Space Science Laboratory, Marshall Space Flight Center, National Aeronautics and Space Science Administration, Huntsville, Alabama, U. S. A.

(g) Department of Physics and Astronomy, Louisiana State University, Baton Rouge, Louisiana, U. S. A.

(h) Department of Physics, University of Washington, Seattle, Washington, U. S. A.

(i) Institute for Nuclear Physics, Krakow, Poland

ABSTRACT

Fe nucleus interactions with per-nucleon energies 20 to 60 GeV in JACEE-3 seem to suggest the existence of compression and of collective flow in nuclear matter.

1. Introduction

A counter-emulsion hybrid chamber in JACEE-3¹⁾ was flown on a balloon at the altitude (5.4 g/cm²) in 1982 with objective of probing the heavy nuclear collisions above 20 GeV per nucleon. In the energy region, it is suggested that nucleus-nucleus collisions provide dense collision complex through compression and secondary particle production²⁾. In the lower energy region, an evidence of collective flow has been reported³⁾. And also, at higher energy region, it has been argued that nucleus has rather large stopping power⁴⁾. In this paper, the high multiplicity characteristics of Fe-nucleus central collisions with energies 20 to 60 GeV/nucleon will be presented. This is considered to be relevant to compressibility and collective flow of nuclear matter.

2. Results and Discussions

In the energy region 20 to 60 GeV/nucleon, events induced by nuclei with primary charge around Z=26 have been sampled and analyzed selectively. Inclusive characteristics will be described separately elsewhere⁵⁾. Multiplicity (Nsh) in forward cone is given by number of secondary produced charged tracks in forward hemisphere, $\sum_{i} Z_i - Z_p$, where $\theta_i < \theta_h$

angle defined by $\tan \theta_h = 2m / (m(m+Ec))^{1/2}$.

The scattering plot between multiplicity and incident energy/nucleon is shown in Fig. 1. Average values of multiplicity in Fe-CHO collisions are represented by crosses. These values are consistent with factor 8.8 times of average forward multiplicities in proton-proton collisions as presented by a dotted curve in the figure.

The high multiplicity events of Fe-nucleus collisions are summarized in Table 1.

Table 1
List of High Multiplicity Events

Event	Nsh	Ec	Zp	Mode	Non-sp	dN/dy	aF
< CHO Target >							
#6- 869	101	55.	Fe	128ch+3He	37	40.	0.9
#5- 393	60	45.	Cr	108ch+ He+Be	33	35.	1.3
#1-1214	57	28.	Fe	104ch+ He	41	40.	1.2
#5-1834	55	37.	Cr	87ch+2He	37	35.	1.8
#6-1596	51	51.	Fe	90ch+2He	41	25.	1.0
#7-1357	51	46.	Ti	73ch+2He	37	35.	1.1
#2- 191	46	40.	Fe	84ch+5He	24	30.	1.2
#5-1215	40	22.	Fe	75ch+ He	43	25.	1.2
#7-1689	36	55.	Fe	56ch+ He+N+Li	17	25.	1.3
#6-1114	36	30.	Cr	58ch+ He	30	25.	1.9
#6-1409	35	58.	Fe	59ch+2He+O	15	25.	1.3
#5- 607	34	22.	Fe	57ch+ He+B	26	25.	2.0
#6- 141	34	22.	Fe	62ch+3He	44	25.	1.5
#4- 876	34	35.	Fe	66ch+ Be	37	20.	1.0
#6- 733	35	30.	Cr	62ch+2He+Li	28	20.	
#2- 497	30	38.	Ti	53ch+3He	26	15.	1.0
< Pb Target >							
#7- 642	134	41.	Ti	267ch	48	125.	2.0
#8- 378	105	33.	Fe	160ch	54	100.	2.0
#1-1542	93	51.	Fe	123ch+ He	43	50.	1.3
#6-1927	82	24.	Fe	164ch	56	60.	1.8
#4-2006	52	25.	Cr	90ch+3He+Li	30	50.	2.0
#1- 308	41	34.	Fe	68ch+3He	28	25.	1.3
#4- 400	36	48.	Cr	56ch+5He	15	20.	1.3
< AgBr Target >							
#4- 749	150	26.	Ti	265ch	48	95.	1.8
#8-1063	38	23.	Fe	77ch+ He+Si	38	25.	1.8
#1-1004	39	27.	Fe	70ch+ He+C	24	25.	1.4

Notes : Ec:primary energy (GeV/nucleon), Zp:incident charge
 Non-sp:number of non-spectator nucleons
 dN/dy:max of rapidity density, aF:slope of F-plot;
 $F/(1-F)=(\tan(\theta))^{aF}$

In Fig. 2, pseudo-rapidity distributions of Ti(41 GeV/nucleon)/Pb and Ti(26 GeV/nucleon)/Em are shown. In the figure, curves are calculations of multi-chain model(MCM)⁶⁾. Both events have more tracks in the central region in comparison with the model calculation. The forward multiplicity (Nsh) of these events are 134 and 150,

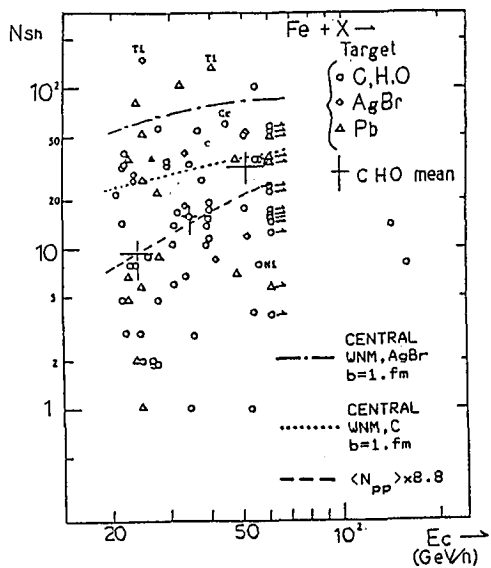


Fig. 1
Scatter Plots between Energy (E_c GeV/n) and Multiplicity (N_{sh})

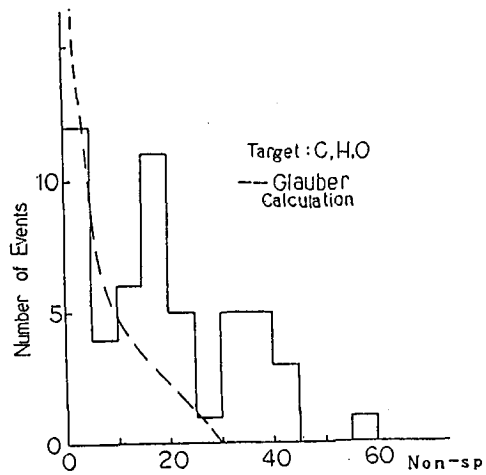


Fig. 3
Number Distribution of Non-spectator Nucleons

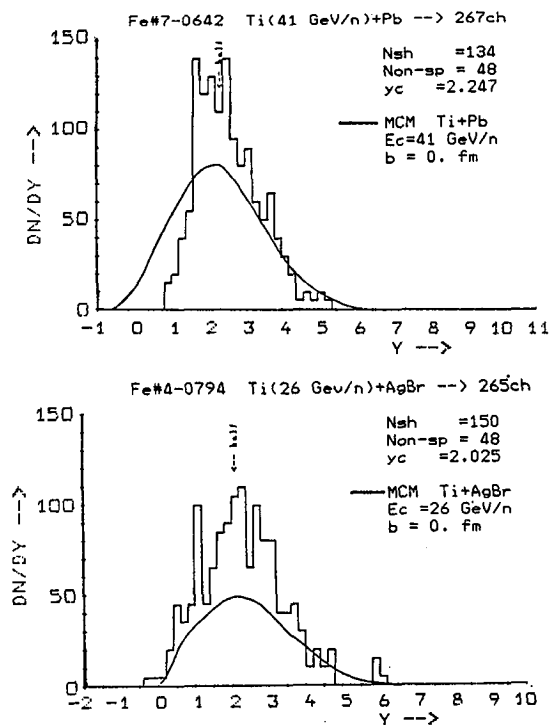


Fig. 2
Pseudo Rapidity Distributions of High Multiplicity Events

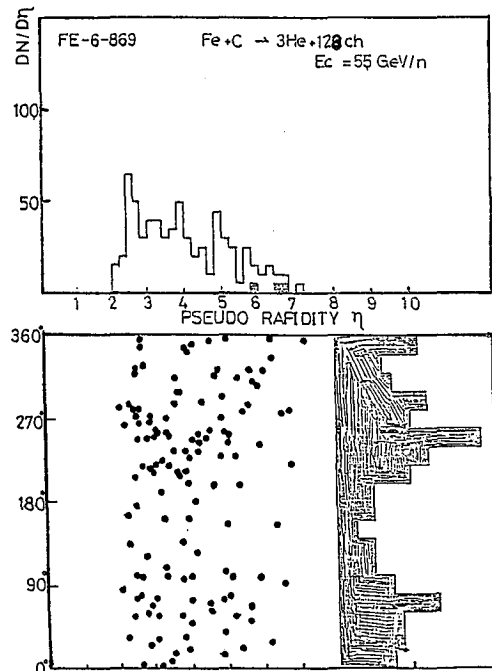


Fig. 4
Azimuth Angle and Pseudo Rapidity

respectively, which are three standard deviation from average value. The maximum heights of pseudo-rapidity densities are 125 and 95, respectively. These values are comparable with the maximum height in high multiplicity events above TeV/nucleon region.

In the iron collisions with CHO-target, number of spectator protons was obtained by consecutively adding all relativistic singly charged tracks starting with the most forward until mean value of $\tan \theta_i$ coincides with that of evaporation formula of Goldhaber⁸⁾ boosted by projectile velocity (evaporation temperature was assumed as 10 MeV). Number of non-spectator projectile protons (which may or may not be 'wounded') are defined by Z_p (projectile charge) - $\sum Z_f$ (fragment) - N_{sp} (number of spectator protons). The number of non-spectator nucleon (Non-sp) is estimated by $(Z_p - \sum Z_f - N_{sp}) \times A_p / Z_p$, where A_p is mass number of projectile. The distribution of the non-spectator nucleon number (Non-sp) is shown in Fig. 3.⁹⁾ The curve in the figure is a calculation of Glauber's model⁹⁾. Thus, we find a lump of events (12 events) in the region $25 < \text{Non-sp} < 56$. We can define such events as central collisions. Six events of them have more tracks at the central region in comparison with multi-chain model assuming head on collision. This feature may be interesting⁴⁾ in connection with the stopping power problem.

One of them, event Fe(55 GeV/nucleon)/CHO has very large multiplicity and dipole type azimuthal distribution as shown in Fig. 4. And also the slope of F-plot in this event is 0.9. The existence of such event is considered to be suggestive for collectiveness of nucleus-nucleus collision in the energy region. However, high multiplicity events Ti(41 GeV/nucleon)/Pb and Ti(26 GeV/nucleon)/Em show isotropical distributions of azimuthal angles and their slopes of F-plot are 2.0 and 1.8, respectively.

References

- 1) S. Dake et al. JACEE collaboration, Proceedings of the 18th International Cosmic Ray Conference, Bangalore (1983).
T. A. Parnell et al. JACEE collaboration, Quark Matter 84.
O. Miyamura et al. JACEE collaboration, Quark Matter 84.
- 2) T. Ludlum and H. Wegner (Ed. s), Proceedings of the Quark Matter 83, Nucl. Phys. A418 1(1984).
- 3) H. A. Gustafsson et al., Phys. Rev. Lett. 52 1950(1984).
- 4) W. Busza and A. S. Goldhaber, Nucl. Phys. A418 635c(1984).
- 5) T. H. Burnett et al. JACEE collaboration, Proceedings of this conference.
- 6) K. Kinoshita, A. Minaka and H. Sumiyoshi, Z. Phys. C8 205 (1981).
- 7) T. H. Burnett et al. JACEE collaboration, Phys. Rev. Letters 50 2062 (1983) and ibid 51 1010 (1983)
- 8) A. S. Goldhaber, Phys. Letters 53B 306(1974)
- 9) A. Bialas, M. Bleszynski and W. Czyz, Nucl. Phys. B111 461 (1976).

Nucleus-Nucleus Interaction above Several Hundred GeV/n

The JACEE Collaboration

T.H.Burnett(h), S.Dake(b), M.Fuki(c), J.C.Gregory(g), T.Hayashi(g),
 R.Holynski(e,i), J.Iwai(h), W.V.Jones(e), A.Jurak(e,i), J.J.Lord(h),
 O.Miyamura(d), H.Oda(b), T.Ogata(a), T.A.Parnell(f), T.Saito(a),
 S.Strausz(h), M.Szarska(e,i), T.Tabuki(a), Y.Takahashi(f),
 T.Tominaga(d), J.W.Watts(f), J.P.Wefel(e), B.Wilczynska(i),
 R.J.Wilkes(h), W.Wolter(e,i), and B.Wosiek(e,i).

- (a) Institute for Cosmic Ray Research, University of Tokyo, Tokyo, Japan
 (b) Department of Physics, Kobe University, Kobe, Japan
 (c) Department of Physics, Okayama University of Science, Okayama, Japan
 (d) Department of Applied Mathematics, Osaka University, Osaka, Japan
 (e) Department of Physics and Astronomy, Louisiana State University,
 Baton Rouge, Louisiana, USA
 (f) Space Science Laboratory, NASA Marshall Space Flight Center,
 Huntsville, Alabama, USA
 (g) Department of Chemistry, University of Alabama in Huntsville,
 Huntsville, Alabama, USA
 (h) Department of Physics, University of Washington, Seattle,
 Washington, USA
 (i) Institute of Nuclear Physics, Krakow, Poland

1. Introduction

At an extreme condition of high pressure, constituents of hadron, quark and gluon, are expected to be deconfined and then transit into a plasma phase(Quark-Gluon-Plasma). Such an extreme condition can be realized through high density hadronic matter and at present, we have no means other than to observe signals from such state through high energy heavy ion collision[7].

The Japanese-American Cooperative Emulsion Experiment(JACEE) have been investigating high energy nuclear interactions of cosmic ray nuclei by mean of balloon-borne emulsion chamber. Current exposure parameters are listed on Table 1. Analysis of last two experiments(JACEE4 and JACEE5) are still in progress. The quasi-inclusive characteristics of nucleus-nucleus collisions above TeV/n region obtained by first three experiments and some anomalous phenomena observed in our experiment had been already reported[1,2]. We present here, a result of semi-inclusive analysis of sample set of central collision events, concerning to multiplicity, rapidity fluctuation for extremely high multiplicity events and correlation between transverse momentum and estimated energy density.

	Flight Altitude (g/cm ²)	Time (hrs)	Area (m ²)
JACEE0	8.0	29.0	0.20
JACEE1	3.7	26.5	0.80
JACEE2	4.0	29.6	0.80
(JACEE3	5.0	39.0	0.25)
JACEE4	4.5	56.0	0.80
JACEE5	5.0	15.0	0.80

Table 1. Exposure Parameter

2. Method

The emulsion chamber have primary, target, space and calorimeter

*) Address for correspondence: Institute for Cosmic Ray Research,
 University of Tokyo, 3-2-1, Midori-cho, Tanashi-shi, Tokyo 188, JAPAN

sections. The primary section contains emulsion layers of high and low sensitivity (Fugi ET7B and ET-6B), coated 0.150-0.200 mm thick on both side of 0.800 mm acrylic base, and CR-39, where primary charge is measured by grain counting, delta ray counting on emulsion and etched pitch rate in CR-39, errors contained in charge measurement being 0.2e, 0.5e and 1e, respectively. The target section contains sandwich of 2.0 mm thick acryl plate and thin (0.050 - 0.075 mm) doubly coated emulsion plates to follow secondary tracks from nuclear collision, thick emulsion plates are also placed in this section for measurement of heavy fragment charge, the spacer of honeycomb is located at the downstream thereof to separate secondary particle. The calorimeter contains 1.0 - 2.5 mm thick lead plates, X-ray films and thin emulsion plates, where gamma ray, most of all from π^0 , makes electron cascade shower which is visible on X-ray films for high energy event. The shower energy is measured by electron counting method for the most of events which shower cores are separated enough for electron counting, error in energy measurement for shower core being 22%. Emission angle of charged particle is measured by track position on emulsion plates. Relative error in angle measurement is less than 0.1 in unit of pseudo-rapidity. Transverse momentum of shower core is obtained from the energy and an angle measured from energy weighted center of shower cores. The average transverse momentum of an event is estimated by fitting of the distribution assuming exponential function. The above procedure with energy measurement overestimates average Pt by 3-7% in average depending on observed gamma ray multiplicity. In addition to this, one should note that, in exclusive analysis, event to event fluctuation may be larger than the above error. As an estimation of Pt of π^0 from observed gamma ray $P_{T\gamma}$, $\langle 2P_{T\gamma} \rangle$ is used for conventionally, which procedure, from kinematic reason, overestimates 43%, 5% and 0.9% for π^0 Pt 100, 300 and 700 MeV/c, respectively, and average Pt of pion in the concerning energy region is known to be over 340 MeV/c [4]. For the case that shower cores overlap with each other in the most forward region depending on vertex location in the calorimeter, the transverse momentum of secondary π^0 is estimated from shower transition in forward restricted angular region, since profile of such superposed shower is determined by both angular and energy/Pt distribution of the secondary. Some events in calorimeter permit measurement with each core separated at large angular region probably due to their very high transverse momenta. In such case, Pt of shower core should be regarded as that of π^0 . For the primary energy estimation, the mean Castagnoli method as well as total radiated cascade energy ΣE_{γ} are used.

3. Results

Tables 2-a and 2-b shows seven high multiplicity events of Ns greater than 400 and of two events of light nucleus with Carbon target events. Three events in Table 2-a were already reported, where observed multiplicity can be interpreted within calculation of Multi-Chain-Model (MCM) [3]. And also, all

Event Type	E_0 (TeV/n)	Nch	$2P_{T\gamma}$ (GeV/c)	$P_{T\pi^0}$ (cone) (GeV/c)	dn/dn nc #
Ca + Pb	1.5	1050 ⁺³⁰⁰ ₋₅₀	0.95±0.31	0.55±0.05	258±12 A88
Si + Ag/Br	4.1	1010±30		0.55±0.05	183±10 G03
Ca + C	100.	760±30	0.525±0.04		81±10 G00
Si + Pb	4.	780	not yet		not yet B02
Ca + Pb	0.5	670±40	not yet		142±8.4 H60
Ca + Pb	1.8	457	2.1±0.1		100±16 D27
Ar + Pb	1.0	416	1.2±0.2		134±8 C27

Table 2-a. High multiplicity events (Nch > 400) in JACEE

observed multiplicity in Table 2-a are still within prediction at impact parameter $b=0$ fm, (maximum predictable multiplicity is not necessary realized at $b=0$ fm for heavy nuclei, $A > 16$, depending on nuclear density distribution), however events in Table 2-b are out of MCM calculation.

The averaged transverse momentum of listed events, which are considered to be central collision, exhibit extremely high Pt values comparing to interpolation value from CERN ISR and SPS collider experiments[4].

We now estimate energy density of event, for which we use that was proposed by Bjorken[5], as in the following.

$$\epsilon \equiv \sqrt{\langle Pt \rangle^2 + m\pi^2} \cdot dn/d\eta|_{\eta_c} \cdot 1.5/V,$$

where $dn/d\eta|_{\eta_c}$ is a pseudo-rapidity density of charged particle at CMS system, V being an interaction volume for which we choose $V=C A_{min}^2/3$, $C=2\pi$. A_{min} is the minimum of A_{proj} and A_{target} . In the case of heavy fragment(s) existing in the secondary, mass number reduction is applied for A_{proj} . Fig. 1 shows scatter diagram between estimated energy density and Pt for which we used $2\langle Pt \rangle$ for the most case, which procedure does not significant influence on the result as previously mentioned, for the events apparently giving π^0 Pt, measured values are used as themselves.

At present, pseudo-rapidity fluctuation analysis had been performed for two high multiplicity events (G0 and G3), wherein multiplicity and its dispersion in windows of width δ on pseudo-rapidity are estimated from Independent Emission Model(IEM) of pure statistical assumption and from MCM, respectively. Results is that both of event are favor for IEM but for MCM, due to the observed fluctuation is not so large comparing to MCM, events G0 and G3 deviating 3σ from MCM and within 1σ and 1.4σ from IEM, respectively.

Azimuthal angle distribution of four events from high multiplicity events(A88, G0, G3 and H66) are also analyzed by Fourier transformation method. Similar analysis had been already proposed by F.Takagi on pseudo-rapidity distribution[6]. According to this analysis, three events (A88, G3 and H60) exhibit dipole structure, which probability is expected to be one event among several ten to several hundred events assuming independent

Event Type	E_0	Nch	2Pty	$dn/d\eta _{\eta_c}$	Nch(MCM)	D
Li + C	15.	217	0.76 ± 0.08	37.5 ± 4.3	154	37
He + C	20.	156	0.62 ± 0.08	26.5 ± 3.6	122	30

Table 2-b. Unit same as Table 2-a. 6 and 7-th column are model calculation by MCM at $b=0$ fm.

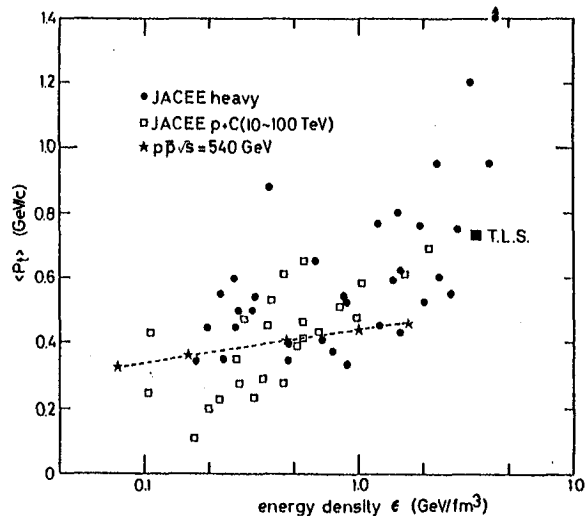


Fig.1 Correlation between energy density and Pt.

emission of secondary, while event G3 is almost isotropic in azimuth.

4. Discussions and summary

As shown in Fig.1, the average transverse momentum seems to grow rapidly over the energy density around 2 GeV/fm. Multiple scattering effect for possible interpretation for this correlation does not describe qualitatively. If the observed correlation is attributed to phase transition of QGP, the observed characteristic energy density is consistent with the predicted critical value for deconfinement of quark and gluon at temperature around 200 MeV[7]. Though there still exists ambiguity in quantitative estimation for energy density such as volume estimation, the observed correlation characteristics might not change substantially.

From the view point of multiplicity, MCM gives fairly good estimation for high multiplicity events, however there still exist the events above maximum prediction of MCM. In the lower energy region of 20-60 GeV/n, there also observed extremely high multiplicity events from minimum bias sample of Fe group primary[8]. Because of a freedom of impact parameter, event to event analysis for multiplicity in nucleus-nucleus collision can not result in fruitful conclusion. However, this kind of analysis not only is a test for assumed conventional picture but also gives a key to reveal a mechanism which determines a final state of nuclear collision.

The present fluctuation analysis requires more statistics to get constructive conclusion. The current result indicates that angular distribution on pseudo-rapidity as well as on azimuth can not be interpreted by simple superposition of nucleus-nucleus collisions for some high multiplicity events.

While the present fluctuation analysis is related to many particles correlation in final state, few particles correlation analysis of charged particle is also possible from our data sample. Detail analysis and discussions on this regard from a short range pair correlation is presented in this conference[9].

Although there exists still theoretical ambiguity in final state estimation from QGP, it seems that we might come close to QGP signal.

Acknowledgements

This work is supported in part in Japan by ICR, JSPS and the Kashima foundation, and in part in the USA by DOE, NASA and NSF.

References

1. Proc. of 18-th ICRC, 5, 214, (1983); Recent review see AIP Conf. Proc., No.123, 723(1984), and Proc. of Quark Matter '84.
2. Proc. of 18-th ICRC, 5, 218, (1983);
T. H. Burnett et al., Phys. Rev. Lett., 50, 2062(1983)
3. K. Kinoshita et al., Zeit. fur Phys., C8, 205(1981)
4. G.Giacomelli et al., Phys. Rep., 55, No. 1(1979);
UA1 Collaboration, Phys. Lett., 118b, 167(1982)
5. J. D. Bjorken, Phys. Rev., D27, 140(1983)
6. F. Takagi, Phys. Rev. Lett., 53, 427(1984)
7. E.V.Shuryak, Phys. Rep., 61C, 71(1980); M.Jacob et al., Phys. Rep., 88C,(1982); Proc. of Quark Matter '83, Nucl. Phys., A418(1984)
8. The JACEE Collab., presented by S. Dake and B.Wosiek in this conference
9. The JACEE Collab., presented by Y. Takahashi in this conference

OBSERVATION OF DIRECT HADRONIC PAIRS IN NUCLEUS-NUCLEUS
COLLISIONS IN JACEE EMULSION CHAMBERS

The JACEE Collaboration[†]

T.H. Burnett(h), S. Dake(b), M. Fuki(c), J.C. Gregory(g), T. Hayashi(g),
T. Hayashi(b), R. Holynski(i), J. Iwai(h), W.V. Jones(e), A. Jurak(i),
J.J. Lord(h), O. Miyamura(d), H. Oda(b), T. Ogata(a), T.A. Parnell(f),
T. Saito(a), T. Tabuki(a), Y. Takahashi(f), T. Tominaga(d),
B. Wilczynska(i), R.J. Wilkes(h), W. Wolter(i), and B. Wosiek(i)

+ Japanese-American-Cooperative-Emulsion-Experiment

- (a) Institute for Cosmic Ray Research, University of Tokyo, Tokyo, Japan
- (b) Department of Physics, Kobe University, Kobe, Japan
- (c) Department of Physics, Okayama University of Science, Okayama, Japan
- (d) Department of Applied Mathematics, Osaka University, Osaka, Japan
- (e) Department of Physics & Astronomy, Louisiana State University, USA
- (f) ES62, Space Science Laboratory, NASA Marshall Space Flight Center,
Huntsville, Alabama 35812, USA
- (g) Department of Chemistry & Res. Inst. Univ. of Alabama, Huntsville, USA
- (h) Department of Physics, University of Washington, Seattle, USA
- (i) Institute of Nuclear Physics, Krakow, Poland

ABSTRACT

In a number of high energy (≥ 1 TeV/amu) nucleus-nucleus collisions observed in JACEE emulsion chambers, non-spatial association of produced charged particles, mostly hadronic pairs, are observed. Similar narrow pairs are observed in about 100 events at much low energy (20 - 60 GeV/amu). Analysis shows that 30 - 50 % of Pair abundances are understood by the Hambury-Brown-Twiss effect, and the remainder seems to require other explanations.

1. Introduction. Frequent association of produced particles in pairs have been noticed in measurements of charged particle angular distributions in nucleus-nucleus collisions. Several high energy events manifested significant abundances in JACEE emulsion chambers. Statistical analyses of larger samples (106 events) at lower energy (20 - 60 GeV/amu) also indicate non-trivial pair abundances.

From the viewpoint of independent superposition models it is not unnatural to expect weaker particle correlations in nucleus-nucleus collisions than those in proton-proton collisions, as long as no space-time structures and no coherent mechanism are considered. Observed pair data does not seem to support an idea of statistical obscuration of correlations.

Recent development in QCD lattice calculations¹ and experimental studies of high multiplicity/high energy density phenomena² encourage searches for signatures of Quark-Gluon-Plasma, a new state of matter. Central or quasi-central collisions are most promising to realize the required high density for QGP transitions, while peripheral collisions are least likely to contain possible QGP signals. Inclusive studies of collisions are generally governed by a large fluctuation of impact parameter which only enhances peripheral phenomena, and are very insensitive to the interaction models.³ Unlike these insensitive parameters ($\langle N \rangle$ and $\langle N \rangle / D$), an exclusive character of pair abundances may not be much obscured even in

an inclusive analysis. We examine in this paper whether there are any non-trivial abundances of narrow hadronic pairs in both individual and inclusive nucleus-nucleus interactions.

2. Methods. The charged tracks emanating from the first collision vertices are measured for individual events. The pseudo-rapidity (η) and azimuth angle (ϕ) of a track are given by spatial coordinates measured at many emulsion layers downstream the vertex. Secondary interaction tracks and early $\gamma \rightarrow e^+e^-$ conversions are removed from the track data as much as possible. (Fine triangulation of tracks allows this elimination of contaminations whose origins are located at more than 50 - 150 μm downstream the first vertex, depending on η and vertex depth.) Obvious nuclear fragments (including spectator protons) are also excluded from the data.

All charged tracks thus defined are used for obtaining the following three different measures of pair correlation.

$$[\text{Measure I}] \quad P(\leq \alpha, \beta) \equiv \frac{\text{No. of pairs } (\Delta\eta \leq \alpha, \Delta\phi \leq \beta)}{\text{No. of all charged tracks } (N_{\text{ch}})} \quad (1)$$

$$[\text{Measure II}] \quad W(\alpha_1 \leq \Delta\eta \leq \alpha_2) \equiv \int_{\alpha_1}^{\alpha_2} \frac{dN}{d(\Delta\eta)d(\Delta\phi)} d(\Delta\eta) \quad (2)$$

$$[\text{Measure III}] \quad S(\text{all}) \equiv \frac{dN}{dR^2}, \text{ with } R^2 \equiv \left\{ \frac{\cosh(\Delta\eta)^2 - \cos(\Delta\phi)^2}{(\Delta\eta)^2 + (\Delta\phi)^2} \right\}, \text{ or} \quad (3)$$

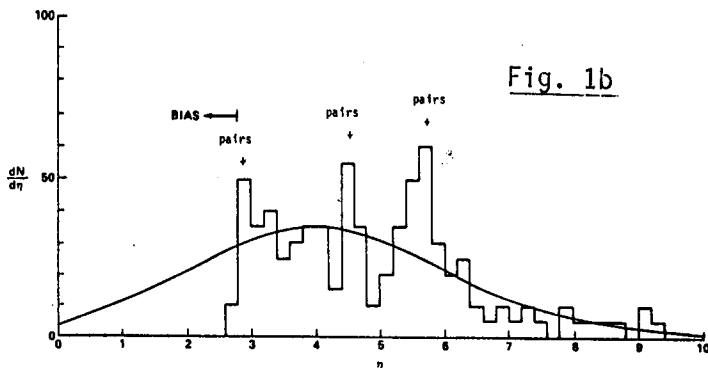
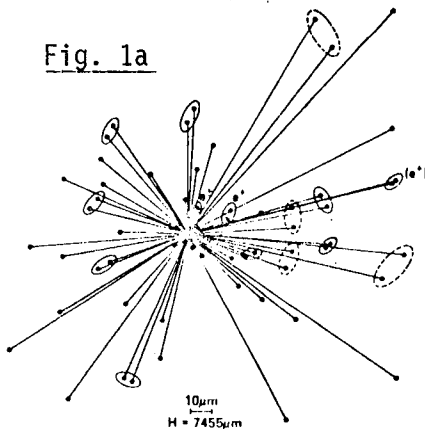
Measure I is useful in the analysis of individual events, and Measure II enhances narrow pairs. Measure III convolves the correlation of the rapidity with that of azimuth angle over the entire available $\eta - \phi$ space.

3. Results. An example, event (G12), shows abundant pairs in its forward rapidity region: Figs. 1a and 1b show its linear target diagram and pseudo-rapidity distribution, respectively.

It is interesting to note that these pairs in this event seem to form a "ring" structure in rapidities as well as a "jet" structure in the azimuth plane. (This event also contains two "direct e^+e^- pairs" [$m_{e^+e^-}$ being ~ 100 and 300 MeV] in the same forward rapidity region.) Measure I is used for individual event analy-

Event Name: Zp(TeV/n) + Zr + Nch + (N _g)	Number of Pairs $\beta < 5^\circ 10^\circ 15^\circ$	Event Name: Zp(TeV/n) + Zr + Nch + (N _g)	Number of Pairs $\beta < 5^\circ 10^\circ 15^\circ$	Event Name: Zp(TeV/n) + Zr + Nch + (N _g)	Number of Pairs $\beta < 5^\circ 10^\circ 15^\circ$
A-5: F _g (3) + C + 86 ch.	DATA 9 14 22 BG.I 5 9 13 BG.II 8 12 16	B-146: F _g (3) + C + 72 ch.	DATA 11 15 20 BG.I 3 5 8 BG.II 5 7 9	G-12: V(1) + C + 150 ch + (8)	DATA 28 47 56 BG.I 24 39 55 BG.II 27 43 38
A-52: F _g (1) + C + 71 ch.	DATA 4 12 16 BG.I 3 6 8 BG.II 5 8 10	C-255: C(3) + C + 76 ch.	DATA 8 12 15 BG.I 4 8 12 BG.II 7 11 15	G-20: S(2) + C + 96 ch.	DATA 17 37 60 BG.I 8 15 22 BG.II 13 20 27
B-4: C(6) + C + 100 ch.	DATA 16 23 28 BG.I 5 10 14 BG.II 8 13 18	D-2: C(10) + C + 159(110)ch	DATA 34 63 89 BG.I 12 28 41 BG.II 25 37 50	G-44: O(2) + C + 76(38) ch.	DATA 7 9 10 BG.I 2 3 5 BG.II 3 4 6
B-20: H _g (9) + C + 95 ch.	DATA 13 22 32 BG.I 6 11 15 BG.II 9 14 19	F-250: C(20) + AgBr + 240 ch.	DATA 60 113 158 BG.I 27 52 78 BG.II 46 72 97	G-54: H _g (20) + C + 80 ch.	DATA 14 19 23 BG.I 5 9 14 BG.II 8 13 17
B-22: H _g (12) + C + 117 ch.	DATA 31 49 65 BG.I 7 13 20 BG.II 12 18 24	G-1: C(40) + C + 101 ch.	DATA 14 27 38 BG.I 8 14 21 BG.II 13 19 26	G-102: H _g (7) + C + 178(100)+(28)	DATA 13 24 32 BG.I 10 19 28 BG.II 13 22 31

TABLE I Number of Pairs in events with high energy ($> \text{TeV/n}$) and medium multiplicity ($70 < N_{\text{ch}} < 250$). Background estimates (BG.I and BG.II) are without and with the HBT effect. (Preliminary) Blackets for Nch refer to the number of tracks used in the analysis.



ses at high energy (≥ 1 TeV/amu). Table. I gives $P(\leq 0.2, 15^\circ) \times N_{ch}$ for 15 events (1532 tracks) with background expected from random coincidence of two particles (BG I) and that includes the HBT effect (BG II). The data show significant excess above background levels for several events. (Four events (B22, D2, F250, G20) show anomalous pair excess, while the other 11 events give $P(\leq 0.2, 15^\circ, -BG II) = 6.9\%$).

For low energy events the statistics (106 events for $N_\pi \geq 2$; 3,695 tracks from 20 - 60 GeV/amu Fe + C, AgBr and Pb reactions) is sufficient that both Measure II and III are taken for all samples. $W(0 \leq \Delta\eta \leq 0.1)$ and $W(0.1 \leq \Delta\eta \leq 0.2)$ distributions as a function of $\Delta\phi$ are given in Figs. 2a and 2b, respectively. Since $W = dN/d(\Delta\phi)$ is constant for a random background (shown in Fig. 2 by dotted lines), a signal of pair correlation is apparent in the region $\Delta\phi < 30^\circ$.

The same signals can be seen in the inclusive Measure III as well, though the S/N ratio is obviously reduced in dN/dR^2 as a result of inclusion of large population at $\Delta\phi > 0.2$. In Figs. 3a and 3b, the purely random (η, ϕ) background is a flat distribution (dotted lines), while a random distribution in ϕ only is evaluated by a Monte Carlo method; using real η and randomly reassigned ϕ values: (dashed-dot lines).

The remainder in Figs. 3a and 3b indicates that there are non-trivial rapidity- and azimuth-correlations.

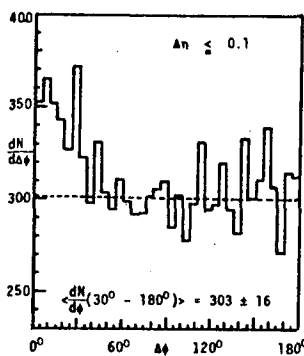


FIG. 2 a.

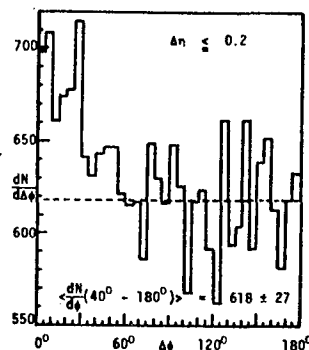
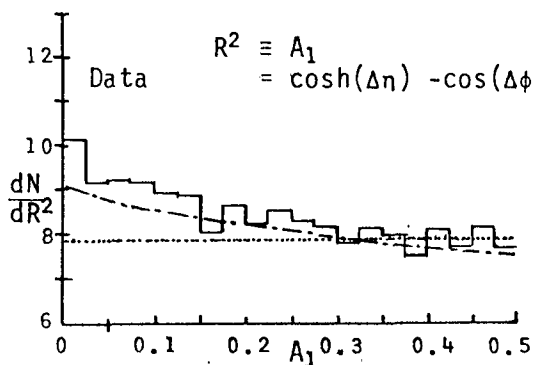
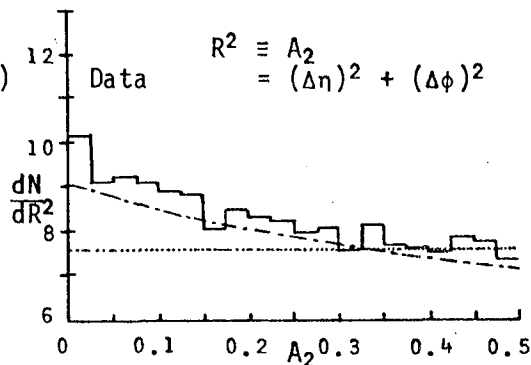


FIG. 2 b.

Fig. 3 a. dN/dR^2 ($R^2 \equiv A_1$)Fig. 3 b. dN/dR^2 ($R^2 \equiv A_2$)

4. Discussions. Results presented above indicate a significant non-trivial correlation of short range nature. To evaluate the magnitude of signals we introduce a trial source of a hypothetical parent meson (X) decaying in two pions (or Kaons) with very small Q-values ($\lesssim 100$ MeV). Non-random signals ($P(\text{Data}) - P(\text{BG I})$) are estimated for eleven high energy events ($\Delta\eta \leq 0.2, \Delta\phi \leq 15^\circ$), and low energy events for ($\Delta\eta \leq 0.1, \Delta\phi \leq 30^\circ$) and ($\Delta\eta \leq 0.2, \Delta\phi \leq 30^\circ$) in terms of $x/\pi \approx 10.2\%$, 8.2% and 13.9% , respectively.

Let's discuss non-random backgrounds. First, Dalitz pairs in $\pi^0 \rightarrow \gamma e^+ e^-$ decay (branching ratio: 1.2%) can be contained in above x/π ratios.

However, this accounts for only $1.2 \times (\pi^0/(\pi^+ + \pi^-)) \approx 0.6\%$. Next, some early conversions of γ -rays can contaminate the data. As mentioned earlier, our track identification is not efficient for eliminating them within $150\mu\text{m}$ from the vertex, we expect this contamination upto $(150/344,000) = 0.04\%$. Even when we fully include proposed internal bremsstrahlung sources⁴ in addition to $\pi^0 \rightarrow \gamma\gamma$ photons, they are not able to contribute more than 0.2%. Thus, electron backgrounds from both internal and external conversions do not account for more than 0.8%. Other experimental errors possibly inherent in measurements are not critically examined at present.

The Hambury-Brown and Twiss effect,⁵ the fourth order quantum interference of Bose-Einstein particles, may possibly explain some of the observation, since this effect is of very short range nature for nucleus-nucleus collisions:

$$C \equiv \sigma_0 \frac{d^2\sigma}{d\vec{p}_1 d\vec{p}_2} / \left(\frac{d\sigma}{d\vec{p}_1} \frac{d\sigma}{d\vec{p}_2} \right) \approx 1 + \exp\left(-\frac{q^2 R^2}{2}\right). \quad (4)$$

The hadron source in nucleus-nucleus collisions is considered to be expanded to the size larger than the colliding nuclear volume, and its known⁶ radius 3 - 4 fm gives the effective momentum difference $|q| < 100$ MeV. This is sufficiently small that $\pi^+\pi^+$ and $\pi^-\pi^-$ form narrow pairs (mostly in $\Delta\eta < 0.1$ region). The HBT estimate by eq.(4) and flat η distributions gives $P(\text{HBT}) \approx 2 \times 0.5 \times n/2C_2 \times \alpha\beta/(2\pi\{\ln s - y_0\})/(n/2) \approx 3 \sim 7\%$ at $\Delta\phi < 30^\circ$. (Note that this approximation depends on the event multiplicity and effective rapidity range.) An enhanced measure $W(0 \leq \Delta\eta \leq .1)$ would contain $0.5 \times \int W_{b.g.} d(\Delta\phi)$ HBT pairs, where the range of the integral must cover $\Delta\phi$ upto $.5 \times \tan^{-1}(100 \text{ MeV}/\langle PT \rangle) \approx 30^\circ$. It is noticed that the observed pair correlation increased for $\Delta\eta \leq 0.2$ (see Fig. 2b), while the HBT particles should not. This, with the analysis in Fig. 3, favors consideration of some hypothetical parent particles (X).

Freier and Waddington⁷ showed similar pair abundances in 2900 tracks obtained from much lower energy (≥ 7.5 GeV/amu) collisions. We estimated $P(0 \leq \Delta\eta \leq .1) = 255/2900 = 8.8\%$. For this result similar to our low energy data (20 - 60 GeV/amu), an HBT estimate explains about 67 pairs, which, with 20 Dalitz pairs, accounts for 35% of all extracted abundances.

In conclusion, about 30 ~ 50% of non-random signals can be attributed to the HBT effect from a large nuclear volume (3 ~ 4 fm). Nevertheless, there seem to remain some "unexplained signals" of narrow hadronic pairs. The net signals for "X" (not attributable to known backgrounds) in the present analysis become $X/\pi \rightarrow \sim 7\%$; 3.5% and 6.3%, for three groups defined previously. A particular group of events at high energies that had the enormous X/π ratio ($\sim 30\%$) are by no means reconciled in the present analysis. All these results might require further examinations of systematic errors and background estimates before seriously considering (X) sources.

Further experimental and theoretical analyses of hadronic pairs seem to be interesting, not only because unexplained abundances still exist, but also because some exclusive characteristics of QGP, and particularly Chiral phase transitions, can be considered in the narrow pair phenomena.⁸

References: 1. J. Polonyi et al., Phys. Rev. Lett. 53, 644(1984). 2. T.H. Burnett et al. (JACEE), Phys. Rev. Lett. 50, 2062(1983). 3. T.H. Burnett et al. (JACEE), AIP 123, 723(1984). 4. J.D. Bjorken and L. McLerran, Phys. Rev. D31, 63(1985). 5. R. Hambury Brown and R.O. Twiss, Nature, 177, 27(1956). 6. W.A. Zajc et al., LBL-12652, 350(1981); D. Beavis et al., Phys. Rev. C27, 910(1983). 7. P.S. Freier and C.J. Waddington, AIP 49, 87(1979). 8. Y. Takahashi and P.B. Eby, this conference HE 1.3-13.

EXCESSIVE PRODUCTION OF ELECTRON PAIRS
BY SOFT PHOTONS IN LOW MULTIPLICITY ION INTERACTIONS*

The JACEE Collaboration†

T. H. Burnett^h, S. Dake^b, M. Fuki^d, J. C. Gregory^g,
T. Hayashi^g, R. Holynskiⁱ, J. Iwai^h, W. V. Jones^e, A. Jurakⁱ,
J. J. Lord^h, O. Miyamura^c, T. Ogata^c, T. A. Parnell^f, T. Saito^a,
S. Strausz^h, T. Tabuki^a, Y. Takahashi^f, T. Tominaga^c, J. Watts^g,
B. Wilczynskaⁱ, R. J. Wilkes^h, W. Wolterⁱ, and B. Wosiekⁱ

^a Institute for Cosmic Ray Research, University of Tokyo;

^b Department of Physics, Kobe University;

^c Department of Applied Mathematics, Osaka University;

^d Okayama University of Science;

^e Department of Physics and Astronomy, Louisiana State University;

^f Space Science Laboratory, NASA Marshall Space Flight Center;

^g Department of Chemistry, University of Alabama, Huntsville;

^h Visual Techniques Laboratory, University of Washington;

ⁱ Institute for Nuclear Physics, Krakow.

Abstract

We report here on three multiply charged primary cosmic ray interactions with carbon nuclei, in which the number of materialized electron pairs within a distance of about 0.3 conversion length is larger than predicted from isospin considerations. These are the most energetic ($\Sigma E_{\nu} > 4$ TeV) of the low multiplicity (< 15 tracks) events observed in the JACEE-2 emulsion chamber.

1. Introduction.

The Japanese-American Cooperative Emulsion Experiment (JACEE) employs balloon-borne emulsion chambers to study the energy spectra, charge composition, and nuclear interactions of ultrahigh energy cosmic rays. Following exposure and processing, the emulsion plates are distributed to the participating laboratories for detailed scanning, tracing, and subsequent measurements using optical microscopes. Preliminary analysis is carried out on the data collected in the individual laboratories before it is combined with data from the other laboratories in the JACEE data bank. Comparisons among the datasets from the various laboratories are used to control the overall quality of the data.

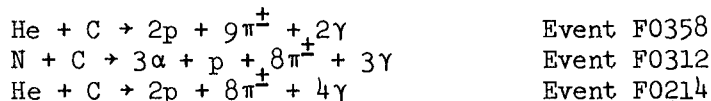
The data presented herein were collected in the plates of the JACEE-2 (second in the JACEE series of annual balloon flights) emulsion chamber. The unusual nature of the events was discovered during a study of the techniques used for determining the transverse momenta of high energy gamma rays emanating from a primary vertex in the target section of the emulsion chamber.

The JACEE-2 chamber consisted of a target section upstream of a thin calorimeter, which was used to measure the energies of cascades initiated by energetic gamma rays. The target was comprised of approximately 50 layers of double-sided emulsion plates (50 micron emulsion films on both sides of an 800 micron acrylic base plate) interleaved with 2 mm thick acrylic sheets. The calorimeter, which was a multilayer sandwich of lead sheets, x-ray films, and emulsion plates, had a vertical thickness of about 7 c.l.

Except for high multiplicity events, individual tracks of hadrons and leptons can be resolved near the vertex and then followed plate-to-plate to the calorimeter section. Consequently, cascades developing in the calorimeter can be correlated with tracks from the vertex.

2. Results.

The cones defined by the tracks of energetic charged particles from low multiplicity (< 15 tracks) interactions were scanned for possible evidence that cascading had begun in the target section of the emulsion chamber, i.e., upstream of the calorimeter. In this report we discuss the observations on the three most energetic ($\Sigma E_Y > 4$ TeV) events in the sample. Using standard nomenclature the three events are of the types:



where C represents the material of the acrylic target plates.

The detailed characteristics of the events are presented in Table 1. A total of 9 electron pairs were found near the interaction vertices. This is more than twice the number expected from photon conversions, assuming that the number of emitted photons in the volume scanned for pairs is equal to the number of charged pions emitted in that volume.

The pseudo-rapidity distributions of the produced hadrons in the forward cone are given in Fig. 1, which also shows the pseudo-rapidities of proton fragments, p, from the interactions and the photons, γ , producing the observed electron pairs. Proton fragments from the

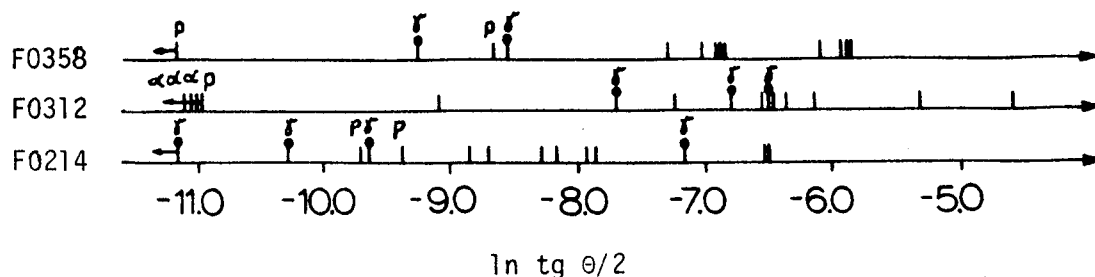


Fig. 1. Pseudo-rapidity distributions of produced particles, proton fragments, and gamma rays.

projectile were assumed to have the smallest emission angles among the charged particle tracks.

Figure 2 shows the dependence of the number of photons converted into electron pairs as a function of distance z from the interaction vertex. The solid line represents the number of materialized gamma rays, N_γ , producing electron pairs inside the scanned volume while the dashed line shows the number of pairs expected in that volume from isospin considerations.

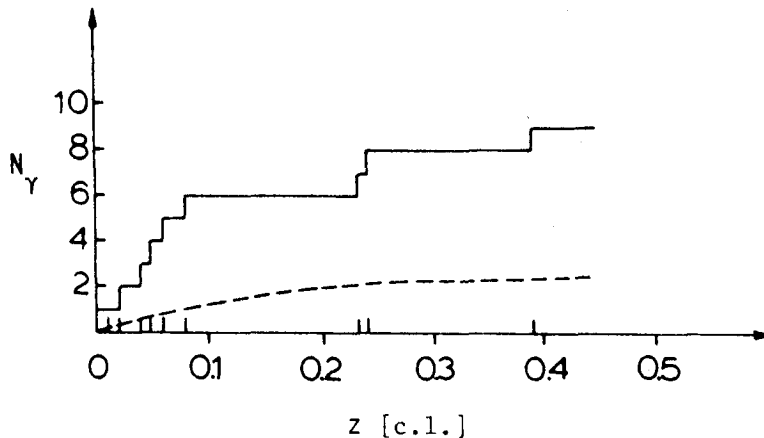


Fig. 2. Number of gamma rays producing electron pairs as a function of distance from the vertex.

3. Discussion.

The largest excess of pairs was observed in the most energetic event ($E \sim 60$ TeV), in which 4 photons materialized within a distance of 0.1 c.l. Three of the pairs were found in a very narrow cone of 0.0001 radians. The pairs evolved to 18 electrons in a distance of 0.4 c.l. and to 30 electrons in 0.5 c.l. A comparison with the results of cascade theory (Table 1, Col. 6) indicates that the materialization of one photon in the vicinity of the vertex is unlikely to produce the fast developing cascade. The observed pairs are most likely first generation and not fluctuations in the cascade development.

A characteristic feature of all the observed pairs is their narrow collimation, which suggests that they were emitted by the fragmenting projectile. Internal bremsstrahlung²⁾ from the deceleration of charged particles (or quarks) may explain the observed excess of pairs, since at projectile energies $E > 10^{12}$ eV the Doppler shift could raise the energy of soft photons above the ~ 0.5 GeV detection threshold. At the present stage, however, fluctuations in production of pairs can not be ruled out, and larger statistics are needed to give a quantitative description of these anomalous pairs.

Table 1. Characteristics of the interactions.

Event	E_0 (TeV)	Pair	z (c.l.)	n_e	n_e^+	n_e^*
F0358	24.0	1	0.04			
		2	0.23	4	2.1	
F0312	24.6	1	0.05			
		2	0.24	4	1.2	
F0214	60.0	1	0.01	2		
		2	0.02	4		
		3	0.06	6		
		4	0.08	8	1.1	
					
			0.36	17		
			0.55	30		6
			0.73	30		9

Table Captions

E_0 - primary energy estimated from the neutral component (ΣE_γ) and inelasticity coefficient $k = 0.5$.

z - distance to point of conversion (in conversion units).

n_e - number of electrons at given z .

n_e^+ - number of electrons predicted from the probability of pair conversion, based on isospin considerations.

n_e^* - number of cascade theory electrons with energies $w > 0.5$ GeV produced by an electron pair of energy $W_0 = 5$ TeV¹⁾. The cascade energy W_0 is estimated from the longitudinal development of the cascade downstream in the calorimeter.

References

* Research supported in part in the USA by DOE, NASA, and NSF and in part in Japan by JSPS and ICR.

† Mailing address for this paper: Institute for Nuclear Physics, ul. Kawioro 26A, 30-055, Krakow, Poland or Department of Physics and Astronomy, Louisiana State University, Baton Rouge, LA 70803, USA.

- 1) Janossy, L. and Messel, H., (1951) Proc. Royal Irish Acad. 54(A), 217.
- 2) Bjorken, J. D. and McLerran, L., (1983) Fermilab-Pub-84/35-T.

FORWARD PARTICLE PRODUCTION IN INELASTIC ^{22}Ne
INTERACTIONS IN EMULSION AT 4.1 A GeV/c.

Alma-Ata, Bucharest, Dubna, Dushanbe, Erevan,
Gatchina, Kosice, Kraków, Leningrad, Moscow,
Tashkent, Tbilisi, Ulan-Bator Collaboration.

Presented by B. Wosiek,

Institute of Nuclear Physics, Kawiory 26 A,
30-055 Kraków, Poland.

1. Introduction

The collisions of high energy nuclei are likely to be the subject of intense experimental investigation in the near future. In this paper we present the results on multiple meson production in forward cone in inelastic interactions of ^{22}Ne nuclei in emulsion at a primary momentum 4.1 GeV/c per nucleon. The detailed characteristics of particle production and the fragmentation processes in collisions of ^{22}Ne nuclei in emulsion will be described in [1].

2. Experimental procedure

Stacks of BR-2 photographic emulsions were exposed to a 4.1 A GeV/c neon beam at the synchrotron of Joint Institute of Nuclear Research in Dubna. The intensity of the exposure was 10^4 particles/cm². In along the track scanning 10,000 neon interactions were found in emulsion. The detailed measurements (emission angles of all charged secondaries as well as charges of projectile fragments) for about 4000 inelastic interactions have been completed. The present paper is devoted to the study of fast ($\beta \geq 0.7$) particle production in the forward hemisphere. We define a forward hemisphere in the center of mass of proton-proton collision at the same primary momentum: $\Theta_{\text{forward}} \leq 90^\circ_{\text{cms,pp}}$. We restrict ourselves to the analysis of forward particle production since in this hemisphere we can define experimentally the number of produced mesons. In a backward hemisphere it is not possible to separate produced mesons (both fast and slow) from a proton fragments of target nucleus. The presented investigation was carried out on a sample of 2031 inelastic interactions. For each event the following multiplicities were determined:

N_F - number of multicharged projectile fragments ($Z \geq 2$);

N_p - number of protons released from ^{22}Ne , can be evaluated from the charge balance between primary charge and sum of charges of heavier fragments: $N_p = 10 - \sum_{i=1}^{N_F} Z_i$

N_{sf} - number of all relativistic ($\beta \geq 0.7$) singly charged tracks emitted in forward hemisphere;

$N_{mf} = N_{sf} - N_p$, number of produced mesons in forward cone;
 N_{sp} - number of spectator protons (see explanation below);
 $N_{part} = N_p - N_{sp}$, number of protons participating in the collision.

Not all nucleons released from incident nucleus ($\frac{A}{Z} \cdot N_p$) participate in the collision. Part of them remains spectators. Spectator protons (N_{sp}) were identified by momentum measurements and from the angular distribution of singly charged secondary particles [2]. Thus, we can obtain the number of protons participating in the collision*.

The data presented in this paper are averaged over all emulsion components and over different impact parameters and are investigated in dependence of the number of participating nucleons from projectile nucleus only.

3. Results

The data on inclusive forward multiplicities are summarized in the Table. The errors quoted in the Table and in Figures include statistical uncertainties only.

In Figure 1 we present the inclusive distribution of produced mesons. Distribution is peaked at small multiplicities due to the low primary energy per nucleon with a very long tail of large multiplicities, which contribute to a large value of the dispersion. The ratio:

$$\bar{N}_{mf}/D = 1.06 \pm .03.$$

Different superpositions models

[3] predict for this ratio a value close to 1 for inclusive nucleus-nucleus data (data averaged over all impact parameters and over all wounded nucleons). The measured value is consistent with these predictions.

It is interesting to study the characteristics of forward particle production in dependence of the number of participating protons from incident nucleus. In Fig.2 we show the distributions of N_{mf} for interactions with different values

Multiplicity	Average
$N_F, Z \gg 3$	$.42 \pm .01$
$N_F, Z = 2$	$.84 \pm .02$
N_p	$5.63 \pm .08$
N_{sp}	$1.89 \pm .03$
N_{part}	$3.74 \pm .08$
N_{mf}	$3.76 \pm .08$

*) Among participating nucleons there are wounded nucleons which interact inelastically in the target and produce secondaries as well as nucleons which undergo the elastic scatterings on wounded nucleons and other secondaries. It is not possible to separate experimentally wounded nucleons from those originated in second generation processes. It is natural to assume that participating nucleons are related to the wounded ones.

of N_{part} . With increasing N_{part} (more central collisions) the distributions shift towards the larger multiplicities and change the shape. The dependence of the moments of these distributions on N_{part} are shown in Figs.3a,b. One can observe that both average multiplicity and dispersion increase with increasing N_{part} . If we assume a simple superposition of independent elementary processes, we expect that the ratio \bar{N}_{mf}/D^2 will be independent of N_{part} . Qualitatively such an independence is observed for $N_{part} \gg 2$ and is illustrated in Figure 4.

We have separated from the released protons of ^{22}Ne projectile the spectator ones. Spectator protons are not affected by the collision and we do not expect the strong dependence of the average number of produced mesons on the number of spectator protons unless the N_{sp} is not correlated with the number of participating protons. A strong correlation between N_{sp} and N_{part} occurs only for events with a total desintegration of primary nucleus into singly charged fragments: $N_{part} = 10 - N_{sp}$. In other cases the spectator part of the incident nucleus may evaporate as protons as well as alpha particles and heavier fragments. The observed very weak dependence of \bar{N}_{mf} on N_{sp} is shown in Figure 5.

4. Conclusions

The presented data on the multiplicities of mesons produced in forward cone and on the dependence of the production process on the number of participating nucleons from primary nucleus can be qualitatively explained by the hypothesis that a simple superposition of elementary collisions describes the interaction between nuclei. However it should be mentioned that some other characteristics of nucleus-nucleus collisions (collective behaviour, cascade processes in the target fragmentation region etc.) can not be described by such a simple model [1,4].

References

1. Alma-Ata, Bucharest, Dubna, Dushanbe, Erevan, Gatchina, Kosice, Kraków, Leningrad, Moscow, Tashkent, Tbilisi, Ulan-Bator Collaboration, papers to be published in Yad.Fiz. (1985).
2. A.S.Goldhaber, Phys.Lett. B53,306(1974).
3. A.Bialas et al., Nucl.Phys. B111,461(1976),
K.Kinoshita et al., Z.Phys. C8,205(1981),
A.Capella et al., preprint TH.3700-CERN.
4. A.M.Baldin et al., Yad.Fiz. 20,1201(1974),
L.S.Schroeder et al., Phys.Rev.Lett. 43,1787(1979).

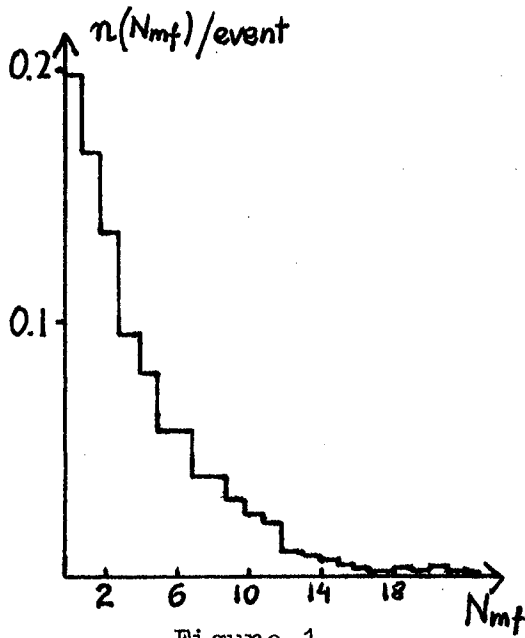


Figure 1.

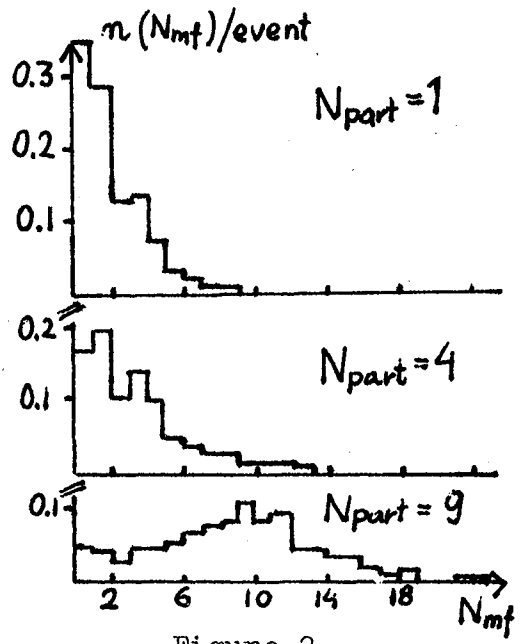


Figure 2.

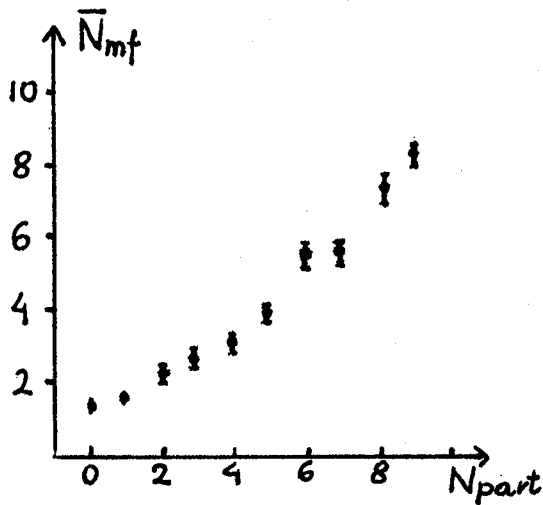


Figure 3a.

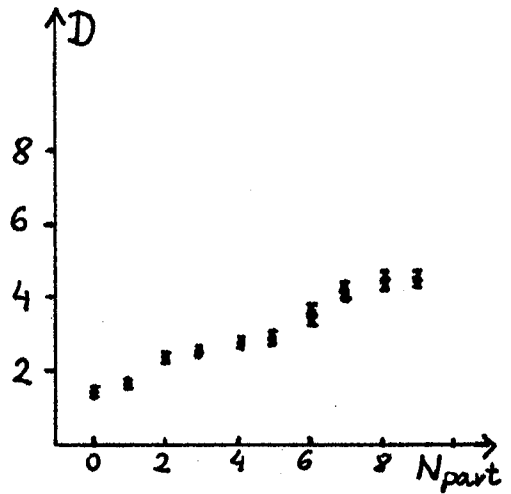


Figure 3b.

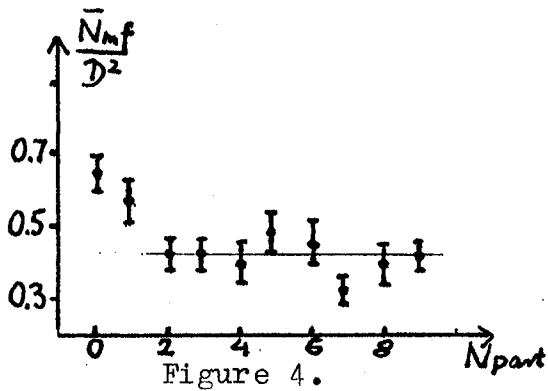


Figure 4.

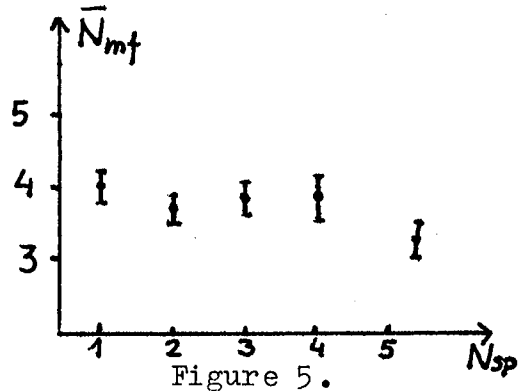


Figure 5.

ON THE MECHANISM OF ANOMALOUS NUCLEUS-NUCLEUS
INTERACTIONS AT ENERGIES ABOVE 1 TEV/NUCLEON

S.Sh.Ameev, V.L.Shmonin

High Energy Physics Institute of the Kazakh SSR
Academy of Sciences, Alma-Ata, 82, USSR

Abstract. Two anomalous interactions of cosmic ray nuclei with photoemulsion nuclei are considered within the framework of the nuclear pionization model. It is shown that the observed regularities of nuclear collisions at the given energy range are satisfactorily reproduced by the model.

The observation and determination of the number of the characteristics of the two heavy ion collisions at energies of 4 TeV/nucleon (Si+Ag) and of 100 TeV/ nucleon (Ca+C) [1] allow to examine roughly the notions of the mechanism of nuclear interactions at the given energy range. The most interesting features of these events are follows. The mean transverse momentum $\langle P_T \rangle_{\pi}$ of π -mesons produced is significantly higher than that for pp-collisions at approximately the same energies of ISR [2] and of SPS [3] (see Table 1) . High multiplicity of secondaries and low number of h-tracks do not agree within the existing classification scheme of events according to which the number of nonrelativistic products of target disintegration in the central collisions should be large.

In this report we analyse the possibility of an interpretation of such events within the framework of the nuclear pionization model [4+6].

According to this model an interaction of relativistic nuclei occurs through the stages of the formation, development and decay of the three intermediate systems : the central pionization cluster and two baryon ones formed by leading components of interacting nucleons. Later a similar sche-

me was used as the base of the model [7]. The numbers of interacting nucleons of the projectile, N_1 , and target, N_2 , are determined for a fixed impact parameter b from the formulae:

$$\begin{aligned} N_1 &= \int dx_1 dy_1 T_1(x_1, y_1, b) [1 - \exp(-\alpha \sigma_{NN}^{in} T_2(x_2, y_2, b))] \\ N_2 &= \int dx_2 dy_2 T_2(x_2, y_2, b) [1 - \exp(-\alpha \sigma_{NN}^{in} T_1(x_1, y_1, b))] \end{aligned} \quad (1)$$

Here $\alpha = 1$, $x_2 = x_1 - b$, $y_2 = y_1$, $T_i = \int \rho(b, x_i, y_i, z) dz$, ($i=1,2$), ρ is the Fermi distribution of the nucleon density in a nucleus. It was pointed out [8] that the existence of the channel of the total compound-system formation in nucleon-nucleon interactions [9,10] leads to the fact that the part of the interacting nucleons in A-A collisions turns out to be captured into the central pionization cluster. The numbers of such nucleons, N_1' and N_2' , are also determined in terms of (1) with $\alpha = 1/3 + 1/4$. The numbers of nucleons entered the baryon clusters can be found from the equations:

$$N_1'' = N_1 - N_1' \quad N_2'' = N_2 - N_2' \quad (2)$$

In the system where the nuclei collide with equal speeds the energies, masses and momenta of the baryon clusters are defined by the expressions:

$$E_i'' = N_i'' [(1 - \langle \delta \rangle)^2 p^2 + m_n^2]^{1/2}, \quad M_i'' = N_i'' (m_n + \mathcal{E}_\kappa), \quad P_i'' = (E_i''^2 - M_i''^2)^{1/2} \quad (i=1,2) \quad (3)$$

In (3) $\langle \delta \rangle = 0.3$ is a part of a baryon cluster nucleon momentum spent on the central cluster production. $\mathcal{E}_\kappa \approx 0.2$ GeV is an average kinetic energy of the nucleon in a baryon cluster rest system.

Taking into account the conservation laws one can determine the energy, momentum and mass of the central cluster $E_c = E_1 + E_2 - E_1'' - E_2''$, $P_c = P_1 + P_2 - P_1'' - P_2''$, $M_c = (E_c^2 - P_c^2)^{1/2}$, (4) where E_1 and E_2 are the energies of the interacting parts of the nuclei before their collision.

The thermodynamical model [4+6,8] is used to describe the decay of the clusters. The pionization cluster decay temperature is determined from the equation of the energetic balance with an account of π -, K -, ρ -, ω -mesons, nucleons and antinucleons among the secondaries. The decay

volume is defined by formula from [11]

$$V = \frac{4}{3}\pi(R_0 + \alpha\tau_h)^2(2R_0/\gamma + \alpha\tau_h)$$

Here R_0 is the initial size of the central cluster Lorentz compressed in longitudinal direction (γ is the Lorentz-factor of the motion of a nucleus in the equal speed system). The parameter R_0 is taken to be equal to the radius of the smaller colliding nucleus for the central collisions.

$\tau_h = 1.2 \text{ GeV}\cdot\text{fm}/c$ [12] is the hadronization time of the quark-gluon plasma forming the cluster matter. The value $\alpha \gg 1$ takes into account the possible increase of τ_h in nuclear collisions in comparison with hadronic ones [13]. According to [14] the contribution of longitudinal collective motion in cluster is taken into account in the energetic balance. The results of the calculation of the multiplicity and average transverse momentum $\langle P_T \rangle_{\pi}$ for π -mesons from the considered events are given in the Table 1.

Table 1.

	E_0 , TeV	Nch		$\langle P_T \rangle_{\pi}$, GeV/c		
		exper.	theor.	exper.	theor.	ISR* SPS**
Si+AgBr	4	1010 ± 30	835	0.550 ± 0.100	0.541	0.340 ± 0.002
Ca+C	100	760 ± 30	597	0.700 ± 0.050	0.708	0.424 ± 0.001

* - data from Ref.[2]

** - data from Ref.[3]

For the second event the energy, transverse momentum and pseudorapidity restrictions for photons have been accounted in the same way as in the experiment[1]. All calculations were carried out for $\alpha = 3$. The relativistic particle pseudorapidity distributions for these two events are shown in the Figs. 1. and 2. (histogram (experiment[1]), curves (this model)).

Taking into account that fact that the considerable fluctuations are possible in these unique events one can conclude that the nuclear pionization model satisfactorily

reproduces the observed regularities of nuclear interactions at the given energy range.

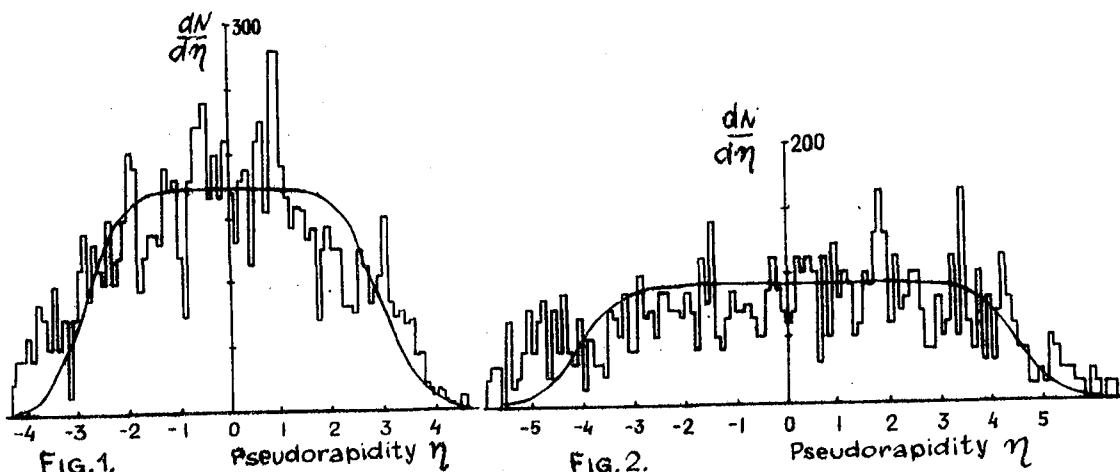


FIG.1. The CMS pseudorapidity distribution of charged particles in the Si+AgBr event.

FIG.2. The CMS pseudorapidity distribution of charged particles in the Ca+C event.

References

1. Burnett T.H. et al., 1983, Phys.Rev.Lett., v50, 26, 2062
2. Alper B. et al., 1975, Nucl.Phys., B100, 237
3. Arnison G. et al., 1982, Phys. Lett., 118B, 167
4. Kalinkin B.N., Koltotechnick S.N., Shmonin V.L., 1978 Preprint HEPI 61-78, Alma-Ata; 1980, Phys.Scr., v21, 792
5. Baranov D.G. et al., 1978, Pis'ma v JETP, v28, 7, 475
Varyukhin V.V. et al., 1979, Proc.16th ICRC, Kyoto, v6, 154-159
6. Ameev S.Sh. et al., 1982, Preprint HEPI 81-16, Alma-Ata
7. Bjorken J.D., 1983, Phys. Rev., D27, 140
8. Ameev S.Sh. et al., 1981, Proc.17th ICRC, Paris, 5, 80
9. Kalinkin B.N., Cherbu A.V., Shmonin V.L., 1980, Fortschr. Phys., 28, 35
10. Kalinkin B.N., Shmonin V.L., 1981, Phys.Scr., v24, 3, 498
11. Ameev S.Sh., Shmonin V.L., 1984, J.Phys.G., v10, 1311-1317
12. Kalinkin B.N., Cherbu A.V., Shmonin V.L., 1979, Acta Phys. Austr. v50, 165; 1980, Phys.Scr., v21, 797-801
13. Kalinkin B.N., Gagarin Yu.F., 1984, FTI im A.F.Ioffe Preprint, 848, Leningrad
14. Varyukhin V.V. et al., 1982, FTI im A.F.Ioffe Preprint, 756, Leningrad.

MESON MULTIPLICITY IN NUCLEUS-NUCLEUS COLLISIONS ABOVE 4 GeV/amu

T.W. Atwater, P.S. Freier and M.P. Kertzman
 School of Physics and Astronomy, University of Minnesota
 Minneapolis, Minnesota 55455

Abstract. Dependence of meson multiplicity on energy for 1486 cosmic ray nucleus-emulsion nucleus interactions is examined. Comparison is made to predictions of the Multi-Chain Model.

1. Introduction. In the near future, relativistic heavy ion accelerators will for the first time probe energies larger than 4 GeV/amu with heavy nuclei. Cosmic rays are currently the only available "beam" at such energies. To date little data has appeared which utilizes the cosmic rays in an unbiased manner to measure the meson multiplicity as a function of energy. This work presents data on the multiplicity per interacting projectile proton up to 100 GeV/amu.

2. Description of Data. Nuclear emulsions were exposed on three balloon flights: two each at cutoff energies $E > 1.7$ GeV/amu (over Texas) and one at $E > 7.5$ GeV/amu (over India). 1486 events have been completely analyzed, including angle measurements of mesons, protons, alphas and heavier projectile fragments. Projectile charge ranged from $Z_p = 6$ to 30, with average $Z_p = 13.5$. The number of charged mesons produced in one interaction is defined by charge conservation:

$$n_{\pi^\pm} = n_s - (Z_p - \sum_i Z_i)$$

where n_s is the number of singly-charged particles with ionization $< 1.4 I_{\min}$, Z_p is projectile charge, and Z_i denotes projectile fragments with $Z_i \geq 2$. Identified lower energy mesons are also included. Error in determining n_{π^\pm} is less than one per event. Angle measurements, used to determine energy of the primary, have an estimated error of 0.1° . The number of wounded (inelastically interacting) projectile protons Q_p is estimated on an event-by-event basis, utilizing the fact that in many of the events projectile and central regions of the pseudorapidity histograms are well separated. Target diagrams, i.e., cross-sections of the secondary beam 1000 μ downstream from the interactions, are also used. While this method of determining Q_p is clearly approximate, it is justified by the fact that rough agreement is obtained with Glauber-type calculations of $\langle Q_p \rangle$.

Data taken from emulsions exposed to the 1.75 GeV/amu ^{55}Mn beam at the Bevalac were also used both to calibrate the energy determination and to supplement the n_{π^\pm} data.

It should be emphasized that all of the data was taken in an unbiased manner so as to detect all inelastic interactions. Defining the latter as those collisions in which the projectile charge is changed, it can be said that essentially all of the inelastic interactions in "along-the-track" scanning were found and measured. Due to time considerations many of the events with zero meson multiplicity were not completely analyzed for angles of nuclear fragments, most of which were in the lower energy (Texas) part of the data. A correction factor based on events that were completely measured has been applied to

correct for this. Thus the measured values should represent the true meson multiplicity for inelastic interactions.

The energy per nucleon of the primary cosmic ray nucleus is measured by utilizing the angular distribution of all charged secondaries. Several methods are employed, all of which depend on the relative constancy of the transverse momentum. One method uses wounded protons and mesons, as suggested by Varyukhin et al.¹ The primary momentum per nucleon is given by

$$P_{\text{prim}}(\text{GeV/amu}) = \frac{\left(\frac{3}{2} f_{\pi} \langle p_{\perp} \rangle_{\pi} + \frac{A}{Z} f_Q \langle p_{\perp} \rangle_Q\right) \sum_i^{n_{\pi} + Q_p} \frac{1}{\sin \theta_i}}{Q_p}$$

where $n_{\pi}^{\pm}(Q_p)$ is the number of charged mesons (wounded projectile protons) in an event, $f_{\pi}(f_Q)$ is the relative number fraction, and the factor $3/2(A/Z)$ accounts for π^0 's (neutrons).² The factor $1/Q_p$ is used because all of the momentum of the wounded protons and mesons after the interaction must arise from the Q_p wounded protons. For the first try at computing P_{prim} , values of $\langle p_{\perp} \rangle$ measured at accelerator energies were used, viz.: $\langle p_{\perp} \rangle_{\pi} = 235$ (320) MeV/c for the Texas (India) data set;³ $\langle p_{\perp} \rangle_Q = 575$ MeV/c⁴ for both data sets. The resultant energy distribution was then compared to the known cosmic ray energy spectrum, $N(>E) \sim E^{-1.7}$ (E = total energy/amu). The values of $\langle p_{\perp} \rangle$ are subsequently modified by a suitable factor so that agreement with the known spectrum is as close as possible. This factor is 0.76 for the Texas data set and 1.20 for the India data set. Primary energy is also measured using the spectator particles, i.e., protons and alphas. This is detailed in a separate paper.⁵ The energies obtained by these two separate methods are simply averaged. The resultant energy distribution is considered to order the events in energy. For a comparison of the result to the cosmic ray energy spectrum, see Ref. 5. The fit to the high energy part of the spectrum is fairly good, but at the low end there are too many ($\sim 25\%$) events below the known cutoffs. A Monte Carlo simulation was performed assuming a Gaussian in energy with $\sigma \sim 0.5 E$, as seen in the Mn beam data. The result implies that many of the events below the cutoff may be due to the inherent spread in the measurement. However, when consolidating the data by binning the particles in energy, this does not matter, as long as the ordering in energy is correct. (For this reason also the precise values of $\langle p_{\perp} \rangle$ used are relatively unimportant.) The average energy of each bin is calculated using the number of events in the bin and the known energy spectrum.

3. Model. Comparison is made to the Multi-Chain Model (MCM) as formulated by Sumiyoshi,⁶ which is essentially an independent particle picture utilizing Glauber theory concepts.⁷ Input to MCM is the inelastic p-p cross-section σ_{inel} and the p-p total charged multiplicity $\langle n_{\text{ch}} \rangle_{\text{pp}}$. Colliding nucleons^{pp} are connected by chains which exchange energy. Equipartition of energy among chains is required. Cascade effects are roughly included by adding 1 to $\langle n_{\text{ch}} \rangle_{\text{pp}}$ for all collisions but the first for each wounded nucleon. Since the model predicts meson plus wounded proton multiplicity, in the model $\langle n_{\text{ch}} \rangle / \langle Q_p \rangle - 1$ should be compared to the data. The model is not claimed to be valid below 10 GeV/amu.⁸

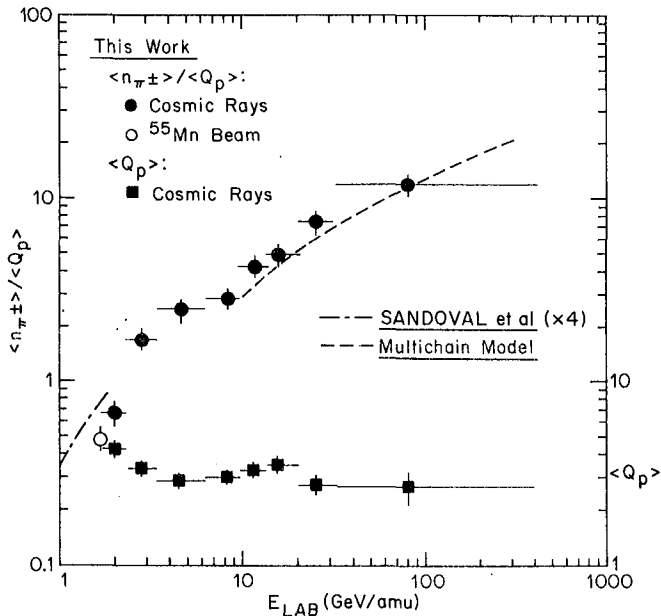
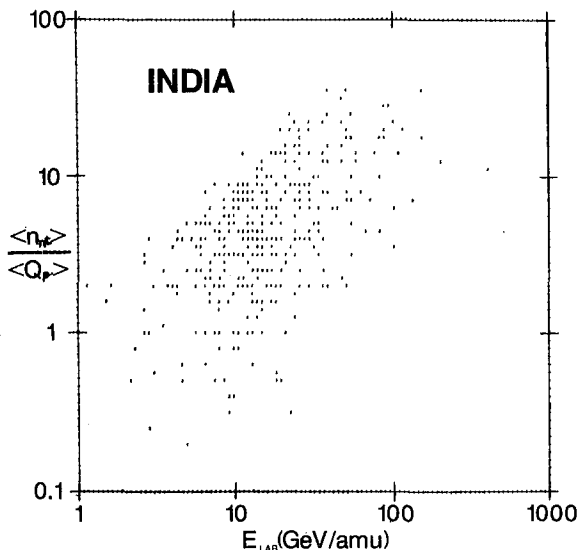


Fig. 1. Meson multiplicity per wounded projectile proton $\langle n_{\pi^{\pm}} \rangle / \langle Q_p \rangle$ vs. energy for cosmic rays in emulsion. Shown also are: ^{55}Mn -emulsion point; streamer chamber data of Sandoval et al.,⁹ multiplied by 4 to account for target protons and π^{\pm} s; Multi Chain Model prediction,⁷ valid for $E > 10$ GeV/amu; and average wounded projectile protons vs. energy. Note large uncertainty in assigning energy value to highest energy point.

4. Results. Meson multiplicity per interacting projectile proton $\langle n_{\pi^{\pm}} \rangle / \langle Q_p \rangle$ as a function of energy is shown in Fig. 1. Also shown is the ^{55}Mn -emulsion value at 1.69 GeV/amu. The experimental number of wounded projectile protons $\langle Q_p \rangle$ is also included on the plot. It is seen that $\langle n_{\pi^{\pm}} \rangle / \langle Q_p \rangle$ varies with energy approximately as $E^{0.7}$ above 4 GeV/amu. The data seem to follow the trend of the MCM prediction. Both the cosmic ray data and the Mn beam point fall below the Ar-KCl data of Sandoval et al.⁹ For the cosmic ray data, this may partly be due to an overestimate of the number of wounded protons $\langle Q_p \rangle$ at this energy (see Fig. 1). However, for the Mn case, this is not true since $\langle Q_p \rangle$ (expt) = 5.2 while $\langle Q_p \rangle$ (Glauber) = 5.0. According to Glauber theory $\langle Q_p \rangle$ is only a weak function of energy, viz. $< 3\%$ variation from 2-100 GeV/amu. $\langle Q_p \rangle$ (Glauber) = 3.1 for the average cosmic ray projectile on emulsion while $\langle Q_p \rangle$ (expt) = 3.3 integrated over energy.



To show the spread in the data, Fig. 2 gives a scatter plot of the 482 events from the India flight ($E > 7.5$, $E = 19.6$, median $E = 11.8$ GeV/amu).

Fig. 2. Scatter plot of meson multiplicity per wounded projectile proton vs. energy for India flight data.

Table 1 shows the projectile charge dependence of the multiplicity per wounded projectile proton integrated over energy. Higher Z_p appears to give lower $\langle n_{\pi^{\pm}} \rangle / \langle Q_p \rangle$. This can only partly be accounted for by the fluctuation in $\langle Q_p \rangle$ as shown in Table 1. As an aside, note that the value of $\langle n_{\pi^{\pm}} \rangle / \langle Q_p \rangle$ for high Z_p (≥ 20 , $\bar{Z} = 23.3$) in the lowest energy cosmic ray bin is very close to the value for the Mn beam ($Z = 25$), both showing internal consistency of the results and lending credibility to the cosmic ray energy determination.

Table 1. $\langle n_{\pi^{\pm}} \rangle / \langle Q_p \rangle$ vs. Projectile Charge^a

Flight	Projectile Z_p	Events	$\langle Q_p \rangle$		$\langle n_{\pi^{\pm}} \rangle / \langle Q_p \rangle$
			Expt	Glauber	
Texas ($E > 1.7$ GeV/amu)	6-9	412	2.2 ± 0.1	2.22	2.9 ± 0.3
	10-19	508	3.7 ± 0.2	3.13	1.9 ± 0.2
	20-26	332	4.4 ± 0.3	4.53	1.5 ± 0.2
India ($E > 7.5$ GeV/amu)	6-9	141	2.4 ± 0.2	2.24	5.5 ± 0.7
	10-19	236	2.8 ± 0.2	3.17	5.7 ± 0.7
	20-26	142	5.5 ± 0.5	4.58	3.8 ± 0.6

^aValues are corrected for unmeasured zero meson events.

5. Conclusion. For the first time a systematic unbiased study has been made of the meson multiplicity in relativistic heavy ion collisions from 2 to 100 GeV/amu. Multiplicity per wounded proton rises roughly as $E^{0.7}$ at $E > 4$ GeV/amu. Heavier projectiles show a somewhat lower multiplicity per wounded projectile proton than lighter ones do. The data roughly follows the Multi-Chain Model prediction.

6. Acknowledgements. We thank Mary Olson and Hilde Rahlenbeck for the careful measurements of interactions. We acknowledge useful conversations with J. Kapusta and L. Csernai. We thank J. Mevissen for computing assistance. This work was supported in part by NSF Grant PHY-8405852, NASA Grant NGR 24-005-050, and the University of Minnesota Computer Science Center.

References

- ¹Varyukhin, V. V., et al. (1984), Phys. Scr. 29, 37.
- ²Note that Ref. 1 uses the same $\langle p_{\perp} \rangle$ for both mesons and wounded protons.
- ³The value 235 MeV/c is taken from an average over nucleus-nucleus data for $\langle p_{\perp} \rangle_{\pi^-}$ at 4.5 GeV/c/amu measured by Anikina et al. (1983), JETP Lett. 36, 331; the value 320 MeV/c was extrapolated from the latter value using the energy dependence of $\langle p_{\perp} \rangle$ from proton-proton data.
- ⁴This value was derived from a distribution in Agakishiev et al. (1983), Sov. J. Nucl. Phys. 38, 90.
- ⁵Paper HE 1.3-1, these proceedings.
- ⁶Sumiyoshi, H. (1983), Phys. Lett. 131B, 241.
- ⁷Glauber, R.J. (1959), Lectures in Theoretical Physics, ed. W.E. Brittin, Vol. 1, Springer, Berlin, p. 315.
- ⁸Kinoshita et al. (1981), Z. Phys. C8, 205.
- ⁹Sandoval et al. (1980), Phys. Rev. Lett. 45, 874.

INCLUSIVE ANGULAR DISTRIBUTION OF α AND Li FRAGMENTS PRODUCED
IN THE Fe-C AND Fe-Pb COLLISIONS AT 1.88 GeV/u*

C. O. Kim and S. N. Kim
Department of Physics, Korea University, Seoul 132, Korea
and

I. K. Chae and D. H. Kim
Department of Physics, Sookmyung Women's University
Seoul 140, Korea

ABSTRACT

The LS (laboratory system) emission angles θ for 2188 α and 298 Li fragments, produced inclusively in relativistic Fe-C and Fe-Pb collisions, have been measured in reference to incident Fe-ion beam tracks nearby in nuclear emulsion. An empirical differential frequency formula,

$$dN(\cot \theta) = \exp(a + b \cot \theta) d(\cot \theta) \quad (1)$$

is obtained with the constant $b \cong -0.026$ at 1.88 GeV/u, which seems to be independent on the kinds of target nucleus as well as on the kinds of projectile fragments. Equation (1) supports the conventional Kaplon's formula,¹ which has been a convenient tool for estimating the unknown primary energy of cosmic-ray primaries;

$$\langle \theta^2 \rangle^{\frac{1}{2}} = \zeta/u \delta_p, \quad (2)$$

with $\zeta = -0.056$, where $u \delta_p$ is the primary energy in GeV/nucleon. Also, the significance of Eq. (1) is discussed.

1. Introduction. When nuclear interactions produced by high-energy singly-charged hadrons in nuclear emulsion ("stars") are observed in the LS, very slow fragments of the constituent nuclei (Ag, Br, C, N, O, H) of nuclear emulsion can be readily distinguished from relativistic shower particles. Nevertheless, it is usually difficult to identify these nonrelativistic fragments, mainly due to their high ionization and short track lengths. Now, owing to recent development in accelerating heavy ions, the "heavy evaporation fragments" in the projectile rest system (ALS; anti-laboratory system) can be observed as 'relativistic particles' in the LS. Particularly, the relativistic α and Li fragments are identified with ease in nuclear emulsion just by simple inspection through an optical microscope, since the former have about four times the grain density of minimum-ionizing tracks, and the latter about nine times. This very technique of identifying α fragments has been used by some recent angular measurements.²

* Research supported partly by Korea Science and Engineering Foundation (KOSEF) (1984-87).

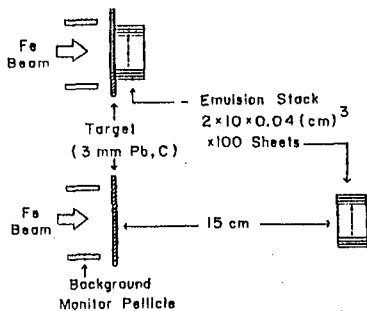


Fig. 1. Experimental Setup.

pellicles were exposed 'horizontally' to the Fe-ion beam with a track density of about 5×10^3 ions/cm².

Because of large distortion present up to $\sim 500 \mu\text{m}$ from the entrance edges of pellicles, α and Li fragments were picked usually at $\sim 500 \mu\text{m}$ from the edges, and angular measurements were typically performed at ~ 1 mm downstream from the entrance edges. Special attention was given not to miss such α and Li fragments as were produced with large θ . In order to avoid the effect due to the distortion inherent in the processed emulsion plate, the LS emission angles θ were measured by use of the reference-track method,³ i. e., always in reference to nearby Fe-ion beam tracks, which had the angular deviation of 2.3 ± 0.3 and 3.7 ± 0.3 mrad., respectively, for the pellicles behind the carbon and lead targets at the site of angular measurements.

3. Experimental Results. As shown in Fig. 2, the differential frequency $dN(\theta)$ versus θ (vacant circles for Fe-C collisions and filled circles for Fe-Pb collisions) resemble closely those of Ref. 2. The two plots in the above for each of S-stacks and L-stacks shown separately and the combined data are shown in the lowest in Fig. 2. There seem to be tendencies of more population of α fragments in the extreme angular regions of $\theta > 10^\circ$ and of $\theta \leq 1^\circ$ for Fe-C collisions than for Fe-Pb collisions. The results of fitting the angular data of $\theta \leq 3^\circ$ with the Gaussian regression function (χ^2/DF , 10 - 30) and those of $\theta \leq 5^\circ$ with the exponential regression function (χ^2/DF , 1 - 2) are also indicated as the curves and equations in the figure.

The root-mean-square angles of fragments (Li fragments) $(\langle \theta^2 \rangle)^{1/2}$, for $\theta < 5^\circ$, as advocated in Ref. 1, are 0.037 ± 0.02 and 0.038 ± 0.01 (0.032 ± 0.02 and 0.035 ± 0.01), respectively, for Fe-C and Fe-Pb collisions, which correspond to $\bar{\lambda} = 0.057$ and 0.067 (0.056 and 0.062) in Eq. (2).

But, we find it most reasonable and revealing to plot the differential frequency $dN(\cot \theta)$ versus, as shown in Fig. 3 (a) for Fe-C collisions and (b) for the Fe-Pb collisions. In the figures the filled circles represent the angular data from 2188 α fragments, and the vacant circles those from 298 Li

2. Experimental Setup and Method. The specific arrangements of the experiment to the Fe-ion beam of 1.88 GeV/u at the Lawrence Berkeley Bevalac are illustrated in Fig. 1. The 3 mm-thick target was made of either carbon or lead. The detector of fragments and incident Fe ions is an emulsion stack (made of 100 Fuji ET7B pellicles of sheet size, $2 \times 10 \times 0.04 \text{ cm}^3$) and is either placed just behind the target plate ("S-stacks") or 15 cm away from the back of the target plate ("L-stacks") in downstream. The shorter edges of

fragments. Since no statistically significant differences between the angular data of S-stacks and those of L-stacks were detected, only the combined data are shown in the figure. For the least-square fit, we used the regression function,

$$\frac{dN(\cot \theta)}{\exp(a + b \cot \theta) d(\cot \theta)} \quad (1)$$

with reasonable fits to most of the angular data, as seen from the best fitted values of a and b and χ^2/DF , separately, for Fe-C and Fe-Pb collisions in Table I. In Figs. 3, the straight lines in the figures and the dotted lines in the inserts show the best-fitted curves. For the interval of $\cot \theta = 0-20$, the amplified version of $dN(\cot \theta)$ versus $d(\cot \theta)$ with one-tenth the interval in the main figures are shown as the inserts, sharp fall-offs of $dN(\cot \theta)$ for $\cot \theta \leq 4$ can be seen. But those portions of α and Li fragments, with extremely small and large θ , which deviates appreciably from the general trends represented by Eq. (1) constitute only several percents.

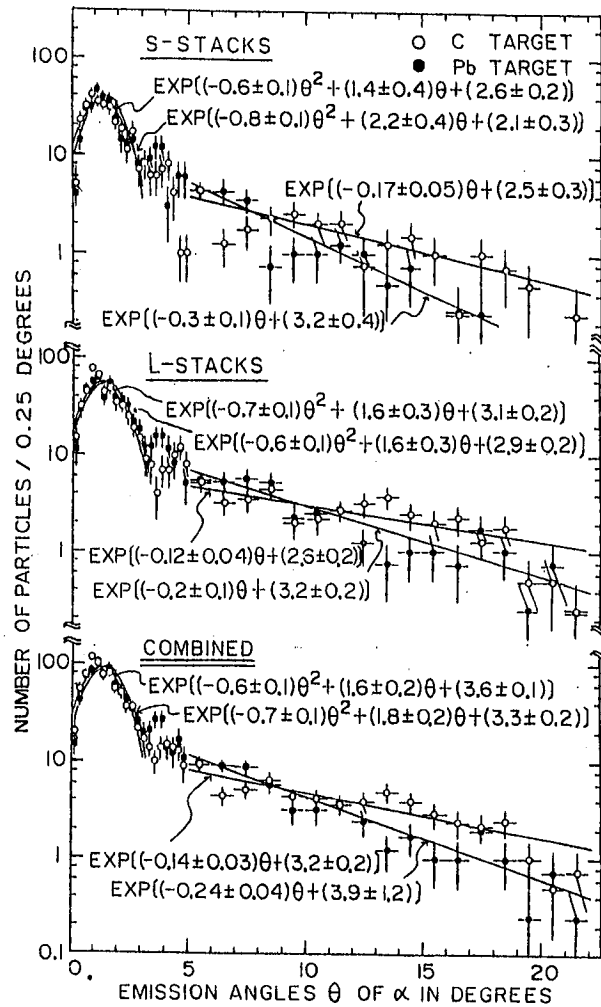


Fig. 2

Table I. The fitted values of a and b of Eq. (1) from the angular data of α fragments (and of Li fragments inside the brackets).

Target	# of α fragments = # from S-stacks + # from L-stacks	a	b	χ^2/DF
Carbon	1103 = 408 + 695 (138 = 35 + 103)	6.3 ± 0.05 (4.4 ± 0.1)	0.0248 ± 0.0009 (0.029 ± 0.003)	21/9 (6/5)
	1085 = 408 + 677 (160 = 62 + 98)	6.3 ± 0.04 (4.4 ± 0.1)	0.0265 ± 0.0009 (0.030 ± 0.003)	27/10 (11/5)

4. Discussion and Conclusion.
From the Lorentz transformation of $\cot \theta$ from the LS to the ALS,

$$\cot \theta = \frac{M_F \bar{\gamma}_p \bar{\beta} (\bar{\beta} \cos \bar{\theta} + \beta_p)}{M_F \bar{\gamma} \bar{\beta} \sin \bar{\theta}} \approx \bar{\gamma}_p \beta_p / (\bar{\beta} \sin \bar{\theta}), \quad (3)$$

where we used the fact that

$$\bar{\beta} \cos \bar{\theta} \ll \beta_p \quad (4)$$

from the observation of D. E. Greiner et al.⁴ as well as our experience with the heavy evaporation prongs produced in high-energy jets in nuclear emulsion. Thus, we obtain the target-independent formula,

$$dN(1/\bar{\beta} \sin \bar{\theta}) \approx (\kappa/b) \times \exp(a + \kappa/\bar{\beta} \sin \bar{\theta}) \times d(1/\bar{\beta} \sin \bar{\theta}), \quad (5)$$

with a Lorentz-invariant constant,

$$\kappa = \bar{\gamma}_p \beta_p b. \quad (6)$$

In fact, Eq. (1) along with Eq. (6) is in accord with the Kaplon's formula, Eq. (2), by finding the median angle through integration of Eq. (1), as

$$\cot \theta_{\frac{1}{2}} = \ln 2/|b| = (\ln 2) (\bar{\gamma}_p \beta_p)/|\kappa|. \quad (7)$$

This method gives the value of $\zeta = 0.06 - 0.07$ in Eq. (2).

REFERENCES

- 1M. F. Kaplon et al., Phys. Rev. 85, 295 (1952).
- 2H. H. Heckman et al., Phys. Rev. C 17, 1735 (1978); K. B. Balla et al., Nucl. Phys. A367, 446 (1981); M. M. Aggarwal et al., Phys. Rev. C 27, 640 (1983); G. M. Chernov et al., Nucl. Phys. A412, 534 (1984).
- 3C. O. Kim, Phys. Rev. D 31, 513 (1985).
- 4D. E. Greiner et al., Phys. Rev. Lett. 35, 152 (1975).

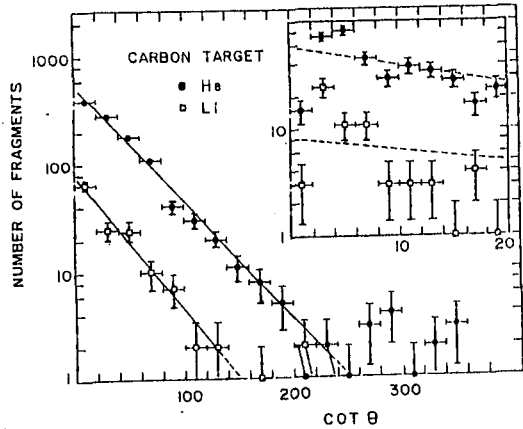


Fig. 3 (a)

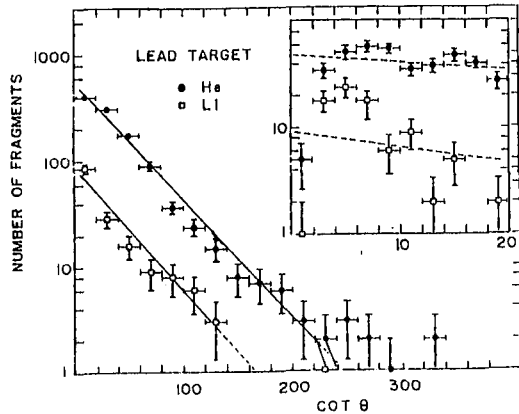


Fig. 3 (b)

EXPERIMENT "PAMIR"-III. COPLANAR EMISSION OF HIGH ENERGY γ -QUANTA AT INTERACTION OF HADRONS WITH NUCLEI OF AIR ATOMS AT ENERGIES ABOVE 10^7 GEV

Collaboration of the Experiment 'Pamir' *

ABSTRACT

At a systematic analysis of large γ -families, detected in X-ray-emulsion chambers, cases of multicore halos have been observed, and among them five events in which the halo is divided into three or four separate cores with their alignment observed in the target diagram (coplanarity of axes of corresponding electron-photon cascades). The halo alignment (tendency to the straight line) leads to the azimuthal asymmetry ("thrust"). The analysis of lateral and momentum distributions of particles in these families shows that they also have "p thrust" that correlates with the direction of the halo core alignment.

1. Introduction

Recently halos - diffuse zones of darkening on X-ray films in the central part of large γ -families - are intensively studied in the framework of experiment "Pamir" /1,6/. While scanning on microdensitometers, five standard levels of electron number density (excess over the background) in the range $\Delta n = 0.015-0.16 \mu\text{m}^{-2}$ are used. The area S_i bounded by the corresponding isodense, and the total number of electrons N_i confined at this area, have been determined for each level /2,3/. For quantitative evaluations a family with halo is defined as the family in which (1) the number of electrons N_3 on the third level of observation ($\Delta n = 0.04 \mu\text{m}^{-2}$) satisfies the condition $N_3 \geq 2 N_3^{(g)}$, where $N_3^{(g)}$ is the calculated number of electrons for the same level of observation in electron-photon cascades (EPC) from above-threshold γ -e particles of the family; (2) the area $S_3 \geq 1 \text{ mm}^2$; (3) the number of above-threshold particles providing the first two conditions are fulfilled is > 1 .

Analysis of the halo on the third level of observation has shown that its basic characteristics (spatial distribution of energy density, axial symmetry, values N_3 , S_3 and their dependence on the depth in the chamber) allow to interpret most of them as a certain stage of the EPC development from the γ -e particle that has been formed with a large value of the Feynman variable ($X \geq 0.1$) /2/.

Thus, the presence of halo indicates the production of high energy γ -e particles in atmospheric cascades.

* Full list of authors see in HE 1.2-12. The authors of this paper are also T.L.Asatiani, L.E.Genina (Yerevan Physical Institute) and G.T.Zatsepin (Institute for Nuclear Researches, Moscow).

By the densitometric scanning of ~ 80 γ -families with $\sum E_\gamma \geq 250$ TeV 36 events with halo have been detected, and in 15 of them several halos (2-4) are observed (multicore or multiple halos). Each component or core was considered as a separate halo, if the above conditions were satisfied, the number of electrons in it was not less than 5% of N_3 , and the distance between the cores exceeded that between the neighboring density level isodensities. In three- and four-core events a quasilinear alignment of halo cores is observed, i.e. coplanarity of axes of corresponding EPC /2,5/.

In the present report we continue investigating the nature of halo, structure of multicore halo, their alignment as well as correlations of the γ -family particles alignment with that of halo.

2. Structure of halo on upper density levels

The study of the halo structure on higher ($\Delta h = 0.08$ and 0.16 mm^2) shows that the ratios N_5/N_3 and N_4/N_3 fluctuate not much which should be the case with EPC, and that large (1.5 order) fluctuations of the size of halo at the given energy of families $\sum E_\gamma$ occur at all levels.

In Fig.1 the correlation field of points (N_i/S_i ; S_i) for separate halo axes is shown. Crosses denote the results for high energy EPC according to calculations /4/.

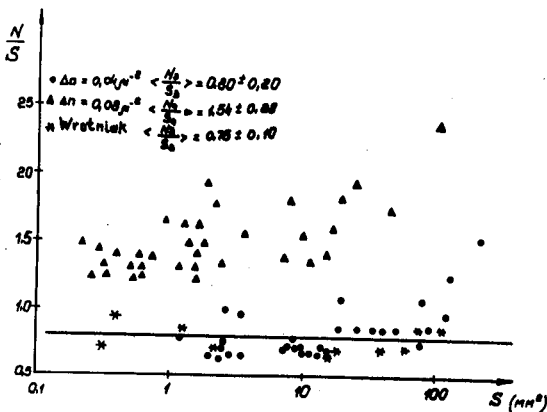


Fig.1

Small fluctuations ratios and proximity of the experimental mean value to the calculated one support the interpretation of halo as a definite stage of EPC development induced by a high energy quantum.

In the upper part of Fig.1 there are events with large halos which apparently begin to differ essentially from "electromagnetic" ones at the large depths of the chamber.

3. "Thrust" of halos and γ -quanta

Densitograms of events with multicore halos and their characteristics are presented in Fig.2a and Table 1, respectively. Each core of such halos may be considered as an event of generation of γ -e particle at a high altitude. Thus nuclear-electromagnetic cascades (NEC) are detected when several such particles are produced. Densitograms show an obvious tendency of halo components to be arranged

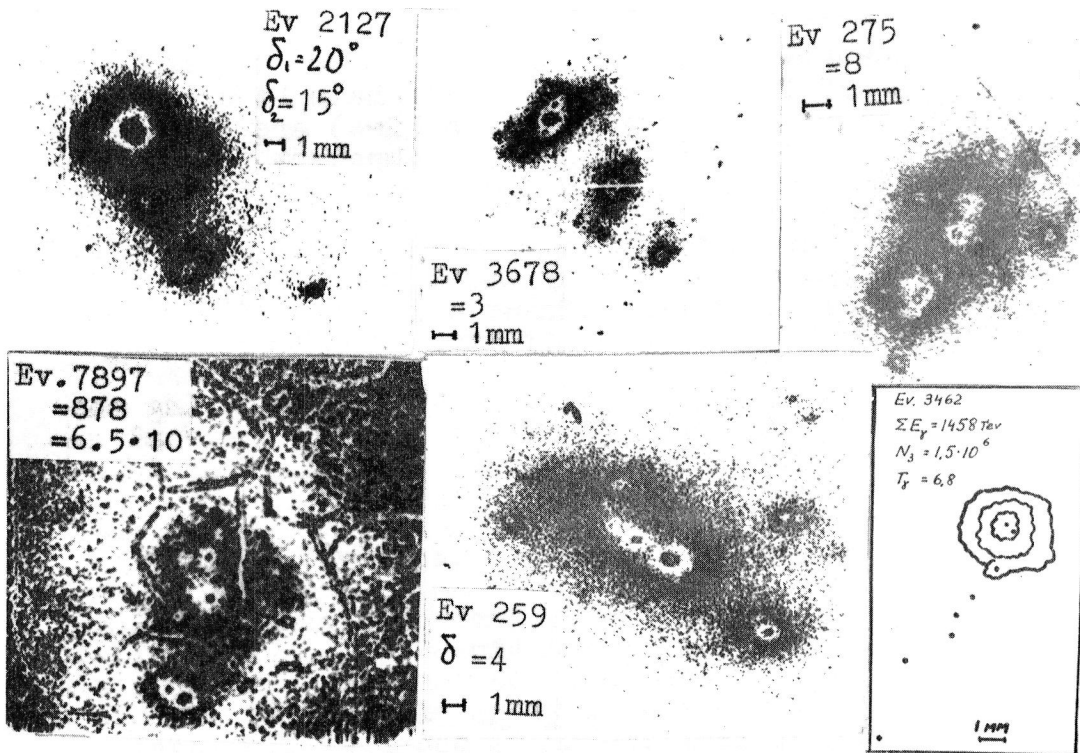


Fig.2a

Fig.2b

on the target diagram along one line, i.e. coplanarity of axes of corresponding EPC (alignment). As a quantitative measure of the alignment may serve the angle formed by lines that connect the second in number $N_3^{(2)}$ halo core with the first one and all the others. The estimate, based on experimental values of these angles, shows that the probability of a random imitation of the observed coplanarity in all five events makes $\sim 10^{-4}$.

The alignment of multicore halos leads to asymmetry in the distribution of transverse momenta - "thrust". As a quantitative dimension of "thrust" of halos or particles in families serves the value $T' = \frac{\sum_{i \neq k} |Z_{ik} \cos \theta_{ik}|}{\sum_{i \neq k} |Z_{ik} \sin \theta_{ik}|}$ where $Z_{ik} = R_{ik} E_i E_k / (E_i + E_k)$; E_i, E_k are the energies of i-th and k-th core of the halo or particle, respectively; θ_{ik}, R_{ik} is the difference of azimuthal angles and distances in the plane of target diagram between appropriate objects. (The value T' by its physical meaning is close to thrust used in analysis of collisions at high energies). Values of T' are plotted in table 2 for halo cores and above-threshold γ -e particles of the family with $f' = E_{\gamma} / \sum E_{\gamma} \geq 0.04$. It is seen from table that the "thrust" of γ -quanta in families correlates with that of halos in events with multiple halos.

As far as most low energy γ -quanta come from low altitudes, this cor-

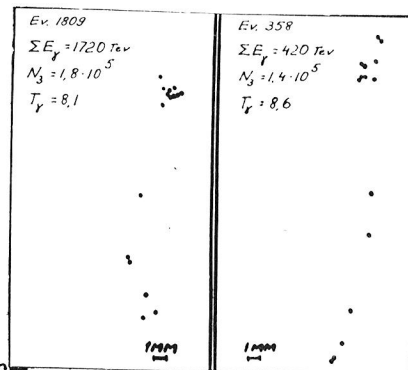


Fig.2b

Table 1. Data on multicore halos

N event	$\sum E_{\gamma, \text{TeV}}$	$\frac{N_3}{S_3} / 10^5$ S_3, mm	$x = N_3^{(i)} / N_3, \%$	$\sum E_{\gamma, \text{TeV}}$ in core	T'
275	2350	10.3 14.7	46, 25, 20	525, 678, 230	2.6
259	506	7.5 11.4	76, 12, 6	92, 80, 98	5.6
3678	1638	11.7 16.7	67, 17, 6	564, 248, 120	5.3
2127	1720	7.2 10.4	80, 6, 5, 8	375, 21, 121, 141	4.2

Table 2. Mean "thrust" of γ -quanta and halo axes

Number of axes	0	1	2	3	4
Number of events	38	10	10	4	1
Mean "thrust" of halo axes				4.4 \pm 1.2	4.2
Mean "thrust" in γ -e partic- les with $f' \geq 0.04$	1.4 \pm 0.24*)	1.15 \pm 0.2*)	6.1 \pm 2	2.8 \pm 0.6	5.2
	2.8 \pm 0.4	3.0 \pm 0.4	6.4 \pm 1.9	3.1 \pm 0.6	5.2

*) for the arbitrarily chosen direction

relation shows that along with the generation of γ -e particles whose "thrust" is established by halo, at high altitudes other particles (hadrons?) are also generated with "thrust" that provide the conservation of the direction of "thrust" in the further development of NEC in atmosphere.

The "thrust" of quanta occurs not only in events with multicore halos but is observed also ($T' \geq 5$) in some families without or with one halo. Examples of target diagrams of such events are presented in Fig. 2b for γ -e particles with $f' \geq 0.04$.

REFERENCES

- /1/ Pamir Collaboration Proc. 18th ICRC, HE 5-28, Bangalore.
- /2/ Baradzei L.T. et al. Proc. Int. Symp., Tokyo, 1983, p. 136.
- /3/ Genina L.E. et al. Prepr. FIAN, N 54, 1981, Moscow.
- /4/ Wrotniak I.A. 17th ICRC, Paris 11(1981)191.
- /5/ Pamir Collab. Kratk. soobsh. fiz. FIAN, N 12, 1984, 39, Moscow.
- /6/ Gulov Yu.A. et al. Preprint FIAN, N 143, 1983, Moscow.

THE EFFECT OF THE RELATIVE NUCLEAR SIZE ON THE NUCLEUS-NUCLEUS INTERACTIONS

I.N.Erofeeva, V.S.Murzin, S.Yu.Sivoklokov and L.N.Smirnova
 Institute of Nuclear Physics, Moscow State University,
 Moscow II9899, USSR

Abstract. The experimental data on the interactions of light nuclei (d , He^4 , C^{12}) at the momentum $4.2 \text{ GeV}/c \cdot A$ with the carbon nuclei were taken in the 2-m propane bubble chamber. The distributions in the number of interacting nucleons, the spectra of protons, the mean energies of secondary pions and protons, the mean fractions of energy transferred to the pion and nucleon components are presented. The results of investigation of the mechanism of nucleus-nucleus interactions can be used to calculate the nuclear cascades in the atmosphere.

Experimental Data

We analyze 2400 dC , 1160 He^4C^{12} and 1800 $C^{12}C^{12}$ events detected in the 2-m propane chamber at the momentum of projectile nuclei $P_0 = 4.2 \text{ GeV}/c \cdot A$. The momenta of all protons and nuclear fragments with $P > 150 \text{ MeV}/c$ and charged π^\pm mesons with $P_\pi > 70 \text{ MeV}/c$ have been measured. All negatively charged particles were regarded as π^- -mesons (the admixture of other species $< 1\%$). The event was identified as an interaction on carbon if one of the following conditions was satisfied /1/: a) $n_+ - n_- > (Z_A + 1)$; b) $n_p > 1$; c) $n_p^- > 0$; d) $n_+ > 2$; e) n_+ is odd for the dC events. Z_A is the incident nucleus charge, n_p is the number of slow (with $P < 750 \text{ MeV}/c$) protons, n_p^- is the number of backward emitted protons in the lab-system, n_+ is the number of charged particles in the event. Using these criteria we selected 70 to 80% of inelastic interactions on the carbon nucleus. The remainder events were statistically separated taking into account the known cross sections on a proton and carbon /2/ and the detection efficiency.

The spectra of protons are obtained by the subtraction of the π^- -meson spectrum from the spectrum of all positive particles. The spectra of π^+ and π^- -mesons were assumed to be identical because of the isotopic symmetry of colliding nuclei.

The Number of Interacting Nucleons

The distribution $P(\nu)$ in the number of interacting nucleons of the projectile nucleus in dC and He^4C^{12} -interactions was obtained on the basis of the data on the number of stripping particles and on the multiplicity of π^- -mesons in the events with a different total charge of the stripping particles. The stripping particles are those ones with momentum $P > 3 \text{ GeV}/c$ and emission angle $\theta < 4^\circ$. The production in the interaction of a nucleon of the projectile nucleus is assumed to be independent of the other nucle-

on's interactions. The use of additional data on the multiplicity of π^- -mesons in pC and dC-interactions /3/ enabled us to obtain six equations with unknown $P(\nu)$ ($\nu = 1...4$) for $\text{He}^{4\text{C}}$ interactions /4/. The obtained probabilities $P(\nu)$ of the interaction of ν nucleons of the projectile nucleus for dC and $\text{He}^{4\text{C}}$ interactions are given in Table I together with the predictions of the multiscattering model (MSM) /5/. $P(1)$ and $P(4)$ in $\text{He}^{4\text{C}}$ -interactions are in disagreement with the MSM results.

Table I
The interaction probabilities $P(\nu)$ of ν nucleons of the projectile nucleus A_i

$A_i A_t$	$P(\nu)$	$P(1)$	$P(2)$	$P(3)$	$P(4)$
dC		0.68 ± 0.04	0.32 ± 0.04	-	-
$\text{He}^{4\text{C}}$		0.24 ± 0.06	0.33 ± 0.15	0.20 ± 0.13	0.23 ± 0.05
$\text{He}^{4\text{C}}$ /5/		0.44	0.25	0.19	0.12
					1.32 ± 0.08 2.42 ± 0.08 2.00

Table 2
The mean characteristics of dC, $\text{He}^{4\text{C}}$ and CC-interactions

	d C	$\text{He}^{4\text{C}}$	CC
$\langle n_- \rangle$	0.61 ± 0.03	1.00 ± 0.04	1.51 ± 0.05
$\langle E_- \rangle$ GeV	0.62 ± 0.02	0.64 ± 0.02	0.64 ± 0.02
$\langle n_p \rangle$	2.7 ± 0.1	3.9 ± 0.1	5.2 ± 0.2
$\langle T_p \rangle$ GeV	0.67 ± 0.06	0.80 ± 0.06	1.11 ± 0.06
ϵ_{π^-} GeV	0.38 ± 0.02	0.64 ± 0.03	0.97 ± 0.04
ϵ_p GeV	1.6 ± 0.2	3.1 ± 0.2	5.7 ± 0.3
$\sum \epsilon_i$	4.3 ± 0.2	8.1 ± 0.5	14.5 ± 0.5
T_0 GeV	4.4 ± 0.2	8.1 ± 0.2	12.9
α_{π}	0.26 ± 0.02	0.24 ± 0.02	0.23 ± 0.02
α_N	0.74 ± 0.07	0.76 ± 0.07	0.91 ± 0.09

The Partial Coefficients of Inelasticity of Pions and Nucleons

Table 2 lists the mean multiplicities and energies $\langle E_- \rangle$ of π^- -mesons, the multiplicities and kinetic energies $\langle T_p \rangle$ of protons and also the mean energy of all π^- -mesons ϵ_{π^-} and protons ϵ_p in an event.

Assuming that the mean multiplicities and energies of all species of π^- -mesons and nucleons are equal ($\langle n_{\pi^-} \rangle = \langle n_{\pi^0} \rangle = \langle n_{\pi^+} \rangle$, $\langle E_{\pi^-} \rangle = \langle E_{\pi^0} \rangle = \langle E_{\pi^+} \rangle$, $\langle n_p \rangle = \langle n_n \rangle$, $\langle T_p \rangle = \langle T_n \rangle$) we can determine the total energy of all secondaries: $\sum \epsilon_i = 2 \epsilon_p + 3 \epsilon_{\pi^-}$. This value must coincide with the initial kinetic energy of interacting nucleons $T_0 = 3.37 \langle \nu \rangle_{AC}$ (GeV) to within the energy of particles below the detection threshold. For CC-interactions the magnitude $\langle \nu \rangle_{CC} = 3.83$ was taken from ref./3/. Table 2 presents also the partial coefficients of inelasticity for pions $\alpha_{\pi} = 3 \epsilon_{\pi^-} / T_0$ and protons $\alpha_N = 2 \epsilon_p / T_0$. The fraction of energy transferred to π^- -mesons is considered to be the same for all reactions in question. It is

much lower than the value of σ/π for the nucleonic interactions at the energies > 20 GeV /6/.

The Momentum Spectra of Protons

The momentum spectra of protons in dC, He⁴C and CC-interactions in the lab-system are presented in fig.1. The spectra are normalized to the mean number of protons in an event. Approximation of the spectra by the function $\exp(-\beta P)$ at $P = 1-3$ GeV/c gives the following values of the parameter β : 0.62 ± 0.04 for dC, 0.49 ± 0.05 for He⁴C and 0.29 ± 0.03 for CC-interactions. At the momenta > 3 GeV/c the spectra tend to steepen slightly, which is well seen in the case of CC interactions, yet, they are everywhere well outside the value $P_0 = 4.2$ GeV/c. If in dC-collisions the part of the plot $P > P_0$ is due to the errors in measuring of the particles momenta and to the cumulative particles contribution the increased yield of fragments with $Z=1$ in this part in He⁴C and CC-interactions requires an additional mechanism. The interacting many-nucleon fragments of the projectile nuclei with $P > P_0$ can contribute to the high-momentum part of the spectrum in these interactions.

The mean momenta of protons in dC, He⁴C and CC-interactions are plotted in fig.2 versus the ratio of atomic weights of the colliding nuclei A_i/A_t . The mean value of $\langle P_p \rangle$ increases by a factor of 1.5 in the transition of A_i from d to C, approaching the estimated value of the mean momentum of a proton in pp-collisions at 4.2 GeV/c. This implies that the cascade becomes less important inside the carbon nucleus for secondary nucleons in He⁴C and CC-interactions. This effect is seemingly present in any collisions of the nuclei with comparable sizes.

Conclusions

The chief results are the following: 1) the distribution in the number of interacting nucleons of the He⁴ nucleus in the carbon nucleus is nearly uniform which is in contradiction to the MSM results /5/; 2) the partial coefficients of inelasticity for pions and nucleons are actually the same for dC, He⁴C and CC-interactions; 3) the momentum spectra of protons and the mean values of their momenta are different for each type of interactions. The experimental results permit us to infer the presence of many-nucleon fragments in the spectrum of interacting particles and the minor role of cascade in the interactions of nuclei with identical atomic weights.

References

1. Agakishiev H.N. et al. JINR, I-83-662, Dubna, 1983.
2. Angelov N. et al. JINR, PI-80-473, Dubna, 1980; Yad.Fiz. 1981, 33, 1046.
3. Agakishiev H.N. et al. JINR, EI-84-32I, Dubna, 1984; Proc. XXII Int.Conf. on High Energy Physics, Leipzig, 1981.

4. Gasparyan A.P. et al. Proc. 16th ICRC, Kyoto, 1979, 6, HE 3-6, 176.
5. Gasparyan A.P. et al. JINR, I-80-853, Dubna, 1980; Yad.Fiz., 1981, 34, 1328.
6. Vlasov E.V. et al. Z.Phys.C, 1982, 13, 95.

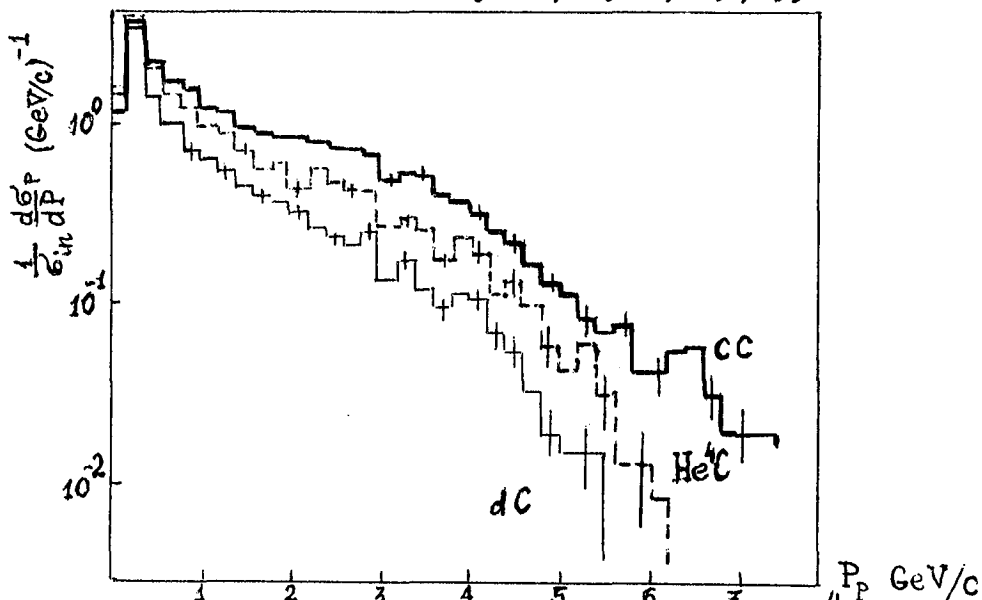


Fig. 1. Momentum spectra of protons in dC , He^4C and CC -interactions

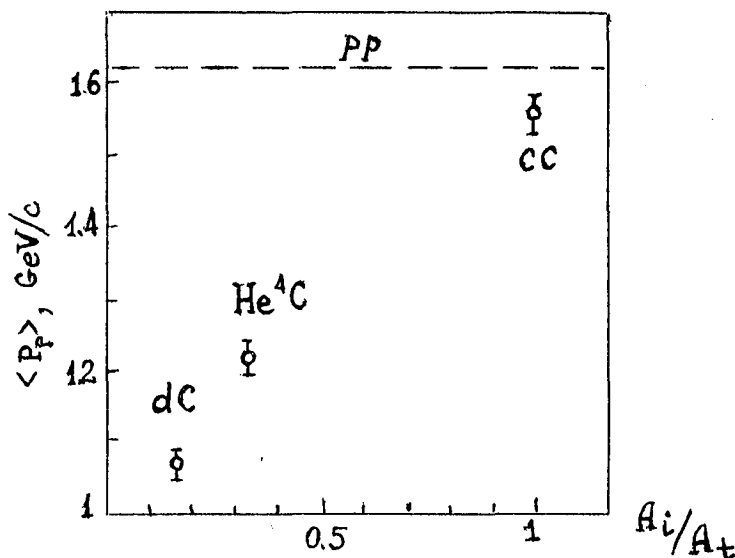


Fig. 2. Mean momentum of protons versus the ratio of atomic weights of colliding nuclei.

JAPAN-USSR JOINT EMULSION CHAMBER EXPERIMENT AT PAMIR

JAPAN-USSR JOINT EXPERIMENT (I)

USSR : A.S.Borisov, K.V.Cherdyntseva, Z.M.Guseva, V.G.Denisova,
 A.M.Dunaevsky, E.A.Kanevskaya, V.M.Maximenko, R.A.Nam, S.V.Pashkov,
 V.S.Puchkov, S.A.Slavatinsky, M.D.Smirnova, Yu.A.Smorodin,
 N.G.Zelevinskaya, M.V.Zimin, G.B.Zhdanov, R.A.Mukhamedshin,
 O.E.Nedel'ko, L.P.Nikolaev, G.T.Zatsepin, T.P.Amineva, L.T.Baradzei,
 I.P.Ivanenko, N.P.Ilijina, T.V.Lazareva, A.K.Managadze, I.A.Mikhailova,
 E.A.Murzina, E.I.Pomelova, E.G.Popova, I.V.Rakobolskaya, T.M.Roganova,
 N.G.Ryabova, L.G.Sveshnikova, S.G.Cananov, L.Kh.Chadranyan,
 L.A.Khisanishivili, G.G.Leptukh, N.N.Roinishivili, M.S.Svanidze,
 Z.A.Azimov, I.B.Bobodjanov, N.E.Gubar, Yu.,A.Gulov, F.Normuradov,
 Kh.Shoboronov, S.A.Azimov, D.A.Khalilov, E.G.Mullajanov, Kh.Nuritdinov,
 D.A.Talipov, T.S.Yuldashbayev, S.E.Bakhtigireev, N.A.Dobrotin,
 Yu.A.Emelyanov and E.G.Zaitseva

POLAND : H.Bielawska, B.Juskiewicz, J.Malinowski, A.Maciaszzyk,
 K.Milczarek and A.Tomaszewski

JAPAN : H.Aoki, Y.Fujimoto, Y.Funayama, S.Hasegawa, H.Kumano, H.Semba,
 M.Tamada, S.Yamashita, K.Yokoi, A.Ohsawa and E.H.Shibuya*

Abstract

The results are presented for the systematic measurement of showers in the first carbon chamber of Japan-USSR joint experiment at Pamir. The intensity and the energy distribution of electromagnetic particles, of hadrons and of families are in good agreement with the results of other mountain experiment if we take into consideration the relative error in energy estimation.

1. Introduction.

Japan-USSR joint emulsion chamber experiment at Pamir plateau (4370m) has been continuing since 1981. The purpose of the experiment is a test for the future large scale emulsion chamber experiment to observe nuclear interaction at the energy region of $10^{16} \sim 10^{17}$ eV and is also to work as a interface among different emulsion chamber experiment of mountain altitude. In Table 1 we show the exposure list of joint chambers. The chamber 'Pamir-1' is for the energy calibration and it is found that upto the shower energy ~ 20 TeV there are no appreciable difference of energy determination between in Soviet group and in Japanese group[1]. The present paper gives the results of systematic measurement of the first joint carbon chamber 'Pamir-2'.

2. Carbon chamber 'Pamir-2'.

The carbon chamber designed to observe hadron and gamma families consists of three parts, that is, Γ -block of 6 cmPb, H-block of 5 cmPb and carbon layer of 60 cm thick between the two. The effective thickness of the chamber is about $1.5 \lambda_{geo.}$. Fig.1 shows the basic structure of the carbon chamber. Two types of Japanese (SAKURA N-type and FUJI #100-type) and Soviet (PTGM-type and PTCW-type) X-ray films are used as sensitive materials. About half, ~ 33 m², of the chamber 'Pamir-2' has been systematically analysed[2].

*) On leave from UNICAMP,IFGW, Sao Paulo, Brasil

Table 1. Exposure list of joint chamber at Pamir (4370m)

chamber	area(m ²)	period (days)	type	sensitive layers	remarks
Pamir-1 81/82	11.2	253 Oct.'81 ~ June'82	flat 7 cmPb (calibration)	3, 3*	[1]
Pamir-2 82/83	72.0	415 June'82 ~ Aug.'83	carbon chamber	2, 3* in Γ-block 2, 3* in H-block	present paper
	6.0	343 Aug.'82 ~ July'83	flat 6 cmPb (calibration)	2, 3*	
Pamir-3 83/84	90.0	350 July'83 ~ July'84	carbon chamber	2, 2* in Γ-block 2, 2* in H-block	under analysis
	4.0		flat 7 cmPb (calibration)	5, 5*	
Pamir-3' 83/85	~ 100	Oct.'83 ~	carbon chamber	2 in Γ-block 2 in H-block	under exposure
Pamir-4 84/85	~ 17	Aug.'84 ~	thick lead 50 cmPb		under exposure

*) number of sensitive layers of Soviet films.

3. Energy estimation.

Here we describe the procedure of Japanese group[2]. The detail procedure of Soviet group is described in Ref.[1,4]. The darkness of shower spot on X-ray films are measured by microphotometer with square slit of $200 \times 200 \mu\text{m}^2$. In this joint chamber, we have only two layers of Japanese X-ray films in each part of the chamber, Γ-block and H-block. Then we must estimate shower energy by using spot darkness on two layers of X-ray films except for the case that showers penetrate both Γ-block and H-block. The two different methods are applied. One (Method-I) is to use the following semi-empirical formula[2],

$$D_m^0 = D_{\max} (D_{10}^\Gamma / D_8^\Gamma)^{-\beta}, \quad \beta = 0.812 - 0.70 \tan^2 \theta$$

$$E = 10 \cdot (D_m^0 \sqrt{1 + \tan^2 \theta} / 0.54) 1.234$$

where D_8^Γ and D_{10}^Γ are darkness of a shower spot at 4 cmPb and 5 cmPb in Γ-block and D_{\max} is larger one between the two. θ is zenith angle of shower direction. For the showers (hadrons) observed in H-block, D_8^Γ and D_{10}^Γ are replaced with D_6^H and D_8^H , where D_6^H and D_8^H are darkness of a shower at 3 cmPb and 4 cmPb in H-block. The other (Method-II, [3]) is to estimate the shower maximum by fitting experimental points, only two points except for penetrating showers, with calculated shower transition curve. Above two methods were applied to the individual simulated cascade showers of gamma-ray primaries[5] and it is found that the average value has expected one though the relative error, $\Delta E/E$, is rather large (20 ~ 30%). When the shower energy increases, $\gtrsim 50$ TeV, Method-I gives underestimation (by ~ 20%) of the energy. The common shower spots are measured by Japanese group and by Soviet group. Fig.2 shows a correlation diagram on the energy of showers estimated by Soviet group and by Japanese group. As is seen in the figure there are no appreciable difference of energy estimation between the two.

4. Energy spectrum of (e,γ), of hadrons and of families.

Energy spectrum of (e,γ) Fig.4 shows integral energy spectrum of showers found in Γ-block. The spectra are expressed by the power function above energy 5 TeV. The Method-I gives steeper energy spectrum because of the underestimation of shower energy in high energy region. The straight line in the figure is a power function with index 2.0. Showers in Γ-block are mixture of electromagnetic showers and those from nuclear interaction of hadrons in Γ-block. About 20% of showers in Γ-block are considered as hadronic origin.

Energy spectrum of hadrons

The visible energy spectrum of hadrons

constructed by showers observed in H-block is shown in Fig.3 by cross mark. The spectrum is also expressed by the power function with index 2.0 above energy 5TeV. The detection probability of hadrons in H-block is $\sim 33\%$. The spot darkness in H-block of hadronic showers becomes smaller because showers spread over during passage through the carbon layer, and then the visible energy is underestimated (by $\sim 20\%$). The flux of hadrons arriving at the chamber, indicated by broken line in the figure, is obtained by applying above two corrections. The relative ratio of intensity, $I_h/I_{e,\gamma}$, at the visible energy greater than 10 TeV, between hadrons and electromagnetic particles is about 2.

Energy spectrum of gamma-families Fig.5 shows integral energy spectrum of gamma-ray families. The spectrum is again well expressed by the power function with index 1.3, above total observed energy ~ 20 TeV.

5. Comparison with the other experiment.

The relative error, $\Delta E/E$, in energy estimation affects the power index and the flux value of the energy spectrum. Suppose that the relative error in energy estimation has Gaussian type distribution with energy dependent dispersion $\sigma = \sigma_0 (E/\text{TeV})^\delta$ and spectrum is power type, then the ratio between the observed intensity, I , and the true one, I_0 , is given by $I(>E)/I_0(>E) \approx 1 + \varepsilon E^{2\delta}$. In the present experiment we have $\sigma_0 \sim 0.12$ and $\delta \sim 0.19$. Then we get $\varepsilon \sim 0.15$ under the assumption that power index of spectrum is 2.0. At the energy $E=10\text{TeV}$, observed intensity is considered $\sim 30\%$ higher than the true one according to the above formula. The true intensity of (e,γ) is obtained by applying corrections for contamination of hadrons (20%) and for the effect of relative error in energy estimation (30%) to the observed intensity shown in Fig.3. Fig.6 shows the altitude dependence of the vertical flux of (e,γ) with energy greater than 10 TeV. As is seen in the figure, all experimental points are distributed around the expected exponential attenuation with $\Lambda_{\text{att}} \sim 120 \text{ gr/cm}^2$. Thus we can conclude that there are no appreciable systematic difference of energy estimation between in the present experiment and in the other mountain experiments.

6. Discussions.

The relative error in energy estimation, by using two layers of X-ray films in the carbon chamber, is rather large, especially in high energy region. However, the vertical flux and the power index of spectra of electromagnetic particles, of hadrons and of families obtained in present measurement are not inconsistent with those of the other mountain experiment.

Acknowledgement. The collaboration experiment is financially supported in part by Grant-in-Aid from the Ministry of Education and Waseda University, in Japan.

References.

- [1] H.Kumano, A.Ohsawa and V.Puchkov ; ICR-Report-115-84-4 (1984)
- [2] M.Koike, T.Hibi, H.Tanaka, M.Tsuchiya and K.Teramura ; to be published
- [3] A.Okamoto, A.Kashimura and K.Takewaka ; to be published
- [4] Pamir Collaboration ; Trudi FIAN Vol.154(1984)
- [5] M.Okamoto and T.Shibata ; Proc. 17th ICRC, Paris, 5(1981)p.214, 218
- [6] Mt.Fuji Collaboration ; Proc. 18th ICRC, Bangalore, 11(1983) 57
- [7] China-Japan Collaboration ; Proc. 18th ICRC, Bangalore, 5(1983) 285

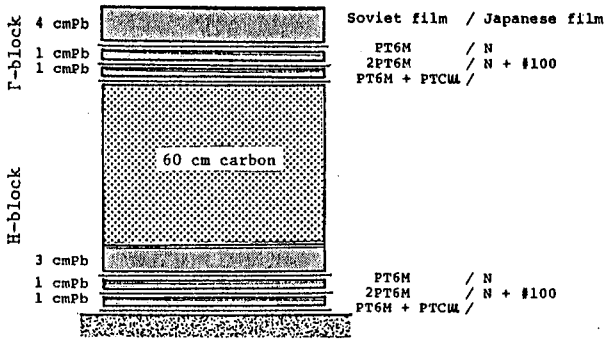


Fig.1 Basic structure of carbon chamber.

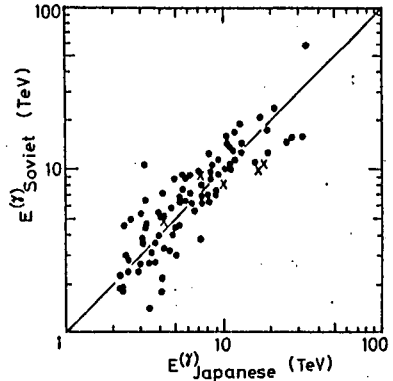


Fig.2 Correlation diagram on the shower energy estimated by Japanese group and by Soviet group. ● : (e, γ), x : hadrons

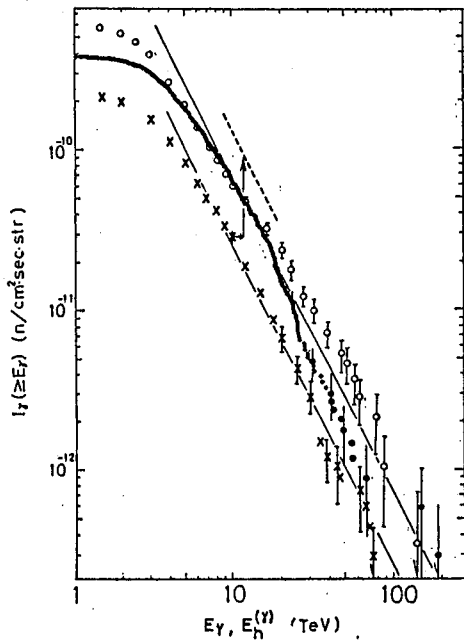


Fig.3 Integral energy spectra of (e, γ) and hadrons.

● : (e, γ) by Method-I
 ○ : (e, γ) by Method-II
 x : hadrons by Method-I
 Lines are power function with index 2.0. Broken line is corrected spectrum of hadrons.

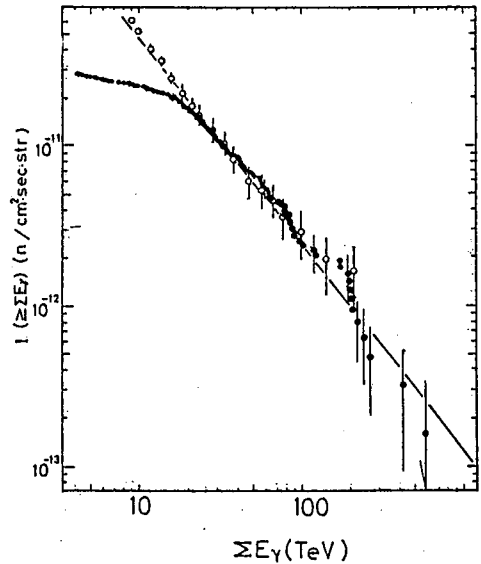
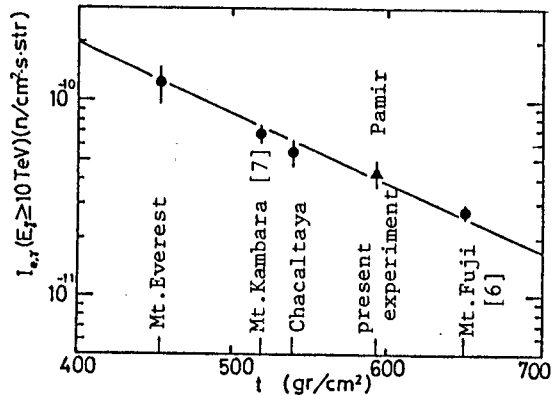


Fig.4 Integral energy spectrum of gamma-ray families.

● : by Method-I
 ○ : by Method-II

Fig.5 Vertical intensity of (e, γ) with energy greater than 10 TeV.



INTENSITIES OF HIGH-ENERGY COSMIC RAYS AT MT. KANBALA

China-Japan Emulsion Chamber Collaboration

Ren, J.R., Kuang, H.H., Huo, A.X., Lu, S.L., Su, S., Wang, Y.X. and Xue, Y.G. (Inst. of High Energy Physics, Academia Sinica, Beijing, China), Wang, C.R., He, M., Zhang, N.J., Cao, P.Y. and Li, J.Y. (Shandong Univ., Jinan, China), Wang, S.Z. (Zhengzhou Univ., Zhengzhou, China), Bai, G.Z., Liu, Z.H., Li, G.J. and Gang, G.X. (Chongqing Inst. of Architecture and Engineering, Chongqing, China), Zhou, W.D. and He, R.D. (Yunnan Univ., Kunming, China), Amenomori, M. and Nanjo, H. (Hirosaki Univ., Hirosaki, Japan), Hotta, N., Ohta, I. and Sakai, M. (Utsunomiya Univ., Utsunomiya, Japan), Mizutani, K. (Saitama Univ., Urawa, Japan), Kasahara, K. and Yuda, T. (Inst. for Cosmic Ray Research, Univ. of Tokyo, Tokyo, Japan), Shibata, M. (Yokohama National Univ., Yokohama, Japan), Shirai, T., Tateyama, N. and Torii, S. (Kanagawa Univ., Yokohama, Japan), Sugimoto, H. and Taira, K. (Sagami Inst. of Technology, Fujisawa, Japan).

Abstract

The energy spectra of atmospheric cosmic rays at Mt. Kanbala (520 g/cm^2) are measured with emulsion chambers. The power indices of the spectra are values of about 2.0 for both gamma-rays and hadrons. Those fluxes are consistent with the ones expected from the model of primary cosmic rays, with heavy nuclei of high content in the energy around 10^{15} eV.

1. Introduction

The China-Japan Cooperative Emulsion Chamber Experiment is continued with a large-area exposure at Mt. Kanbala, Tibet in China (5500 m above sea level, atmospheric depth 520 g/cm^2), in order to observe big families with energy over 1000 TeV . Details of characteristics of those families are discussed in another paper (1), by concerning with primary cosmic rays in the energy around 10^{16} eV or more. Also, uncorrelated particles of atmospheric cosmic rays, such as gamma-rays (hereafter, these mean high energy photons and electrons) and hadrons, are observed in a lower energy region with the same emulsion chambers. The intensities of those particles as well as the members of families are presented in this paper.

2. Experimental procedure

The emulsion chamber used in the Mt. Kanbala experiment consists of photosensitive materials and metal plates, piled up alternately. Several sorts of X-ray film with different sensitivity are generally used as the photosensitive materials, such as type-N (Sakura), type-III (Tianjin), type-100 (Fuji), Gongyuan (Shantou) and type-5F (Shanghai).

Two kinds of metal are used at Mt. Kanbala, as listed in Table 1. One is the lead emulsion chamber (Pb-EC), as generally

used in mountain experiments. Another is the iron one (Fe-EC) which is exposed to observe efficiently hadron components. In this paper, the results are presented given from the Fe-ECs as well as the Pb-ECs whose preliminary data are shown in the previous paper(2).

Table 1. Exposure list at Mt. Kanbala.

Series	Date	Exposure ($m^2 y$)	Material	Thickness (c.u.)
K0	Sep.1980-Sep.1981	3.7	Pb	14
		11.0	Pb	30
K1	Sep.1981-Sep.1982	1.0	Pb	14
		49.0	Pb	28
K2	Oct.1982-May 1984	143.0	Pb	14
		39.1	Fe	29
K3	May 1983-May 1984	6.3	Pb	14
		31.1	Fe	29
K4	May 1984-May 1985	85.0	Pb	14
		58.0	Fe	29

The showers produced by high energy particles are observed as the series of shower spots on X-ray films over several layers and the energy of each shower is estimated by measuring optical density of those spots. Details of the method for the Pb-EC are found in the previous paper(2). For the analysis of the Fe-EC, the similar manner is applied. For the purpose of energy determination of showers in the Fe-EC, massive simulations have been made on the cascade showers developing in iron.

3. Results

In order to get the intensities of atmospheric cosmic rays, a part of the emulsion chambers of thick type (28 - 30 c.u. thick) has been analysed with careful scanning for the exposure of $7.0 m^2 y$ in the Pb-EC and $6.0 m^2 y$ in the Fe-EC.

The starting point of the observed showers is displayed in Fig. 1. The distribution of a deep region gives us the attenuation length of hadrons indicating 42.0 c.u. in lead and 13.5 c.u. in iron. Those values

correspond to the collision length of 28.0 c.u. in lead and 9.0 c.u. in iron, both of which are consistent with the values expected from the respective interaction cross section. By taking the attenuation into account, the detection probabilities of hadrons are determined to be 39 % in the Pb-EC and 78 % in the Fe-EC. A statistical separation of gamma-rays and hadrons has been performed by using those detection probabilities(2),(3).

The resulting vertical energy spectra at Mt. Kanbala are shown

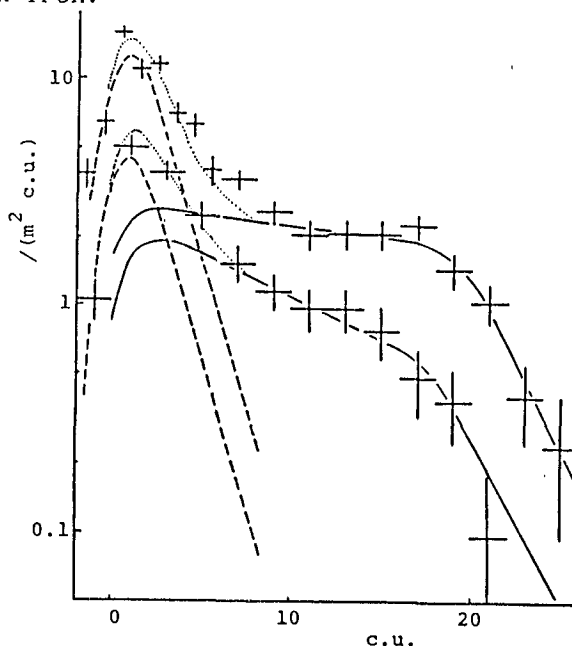


Fig. 1. Starting point distribution of showers in the emulsion chamber of thick type. The upper and lower crosses represent the number of detected showers with energy above 3 TeV for the Pb-EC and above 5 TeV for the Fe-EC, respectively. The dashed and solid curves are expected from gamma-rays and hadrons, respectively.

in Fig. 2 and Fig. 3 for the showers initiated by gamma-rays and hadrons, respectively. Both results given from the Pb-ECs and the Fe-ECs are consistent with each other. Those power indices and fluxes are listed in Table 2.

Table 2. Spectra of atmospheric cosmic rays at Mt. Kanbala.

	Spectral index	Intensity at 5 TeV ($\text{m}^2 \text{ s sr}$)
gamma-rays	2.00 ± 0.08	$(2.8 \pm 0.2) \times 10^{-6}$
showers induced by hadrons	2.03 ± 0.08	$(6.0 \pm 0.6) \times 10^{-6}$

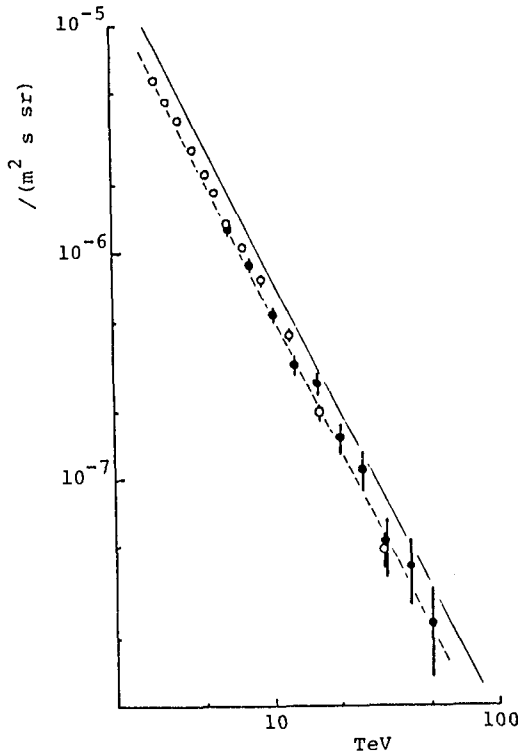


Fig. 2. Integral energy spectrum of vertical gamma-rays at Mt. Kanbala. The open and solid circles represent the results given from the Pb-EC and the Fe-EC, respectively. The dashed line is the best fit. The solid curve is expected by the assumptions mentioned in the text.

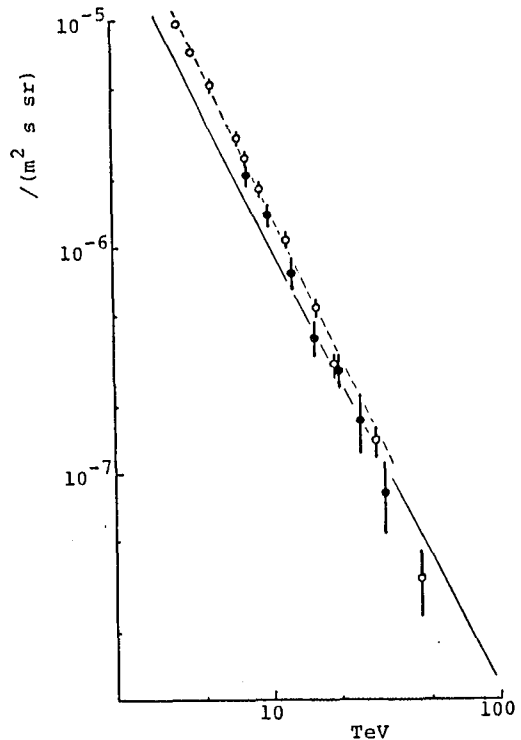


Fig. 3. Integral energy spectrum of showers induced by hadrons at Mt. Kanbala. The open and solid circles represent the results given from the Pb-EC and the Fe-EC, respectively. The dashed line is the best fit. The solid curve is expected by the assumptions mentioned in the text.

4. Discussions

There is no serious difference between both spectra derived from the Pb-EC and the Fe-EC. This indicates that on the experimental method and procedure, such as shower detection and energy determination, no systematic error is recognized for the Fe-EC. This gives a fundamental supporting factor for the reliability of the family data detected in the Fe-ECs(1).

According to the results of families, as described in another paper(1) and others(4),(5), the primary cosmic rays do not indicate

proton dominant in the energy around 10^{16} eV. It seems that the portion of heavy nuclei gradually increases. Also, on the nature of high energy interaction, the Feynman scaling is not appreciably broken in the fragmentation region of particle production and the collision cross section₂ of hadrons in air increases as $E^{0.06}$ corresponding to the \ln^2 's dependence. In Fig. 2 and Fig. 3 are displayed the results calculated with almost the same assumption as the above mentioned. Those spectra of atmospheric cosmic rays are genetically related to the primary cosmic-ray spectrum of a proton equivalent in which the primary cosmic-ray nuclei are broken up into nucleons. Those spectra, therefore, do not much sensitive to the composition of primary cosmic rays. It is, however, interesting to indicate in these figures that the atmospheric cosmic ray spectra may be also interpreted by the same assumption in a slightly lower energy region.

On the atmospheric cosmic rays, the spectral measurements have been performed with emulsion chambers of a similar type at Mt. Fuji (3750 m, 650 g/cm^2) (3), (6) and other mountain altitudes (7), (8), (9). The present results are compared with those intensities in Fig. 4. The comparison shows the attenuation length also to be consistent with the assumption mentioned above.

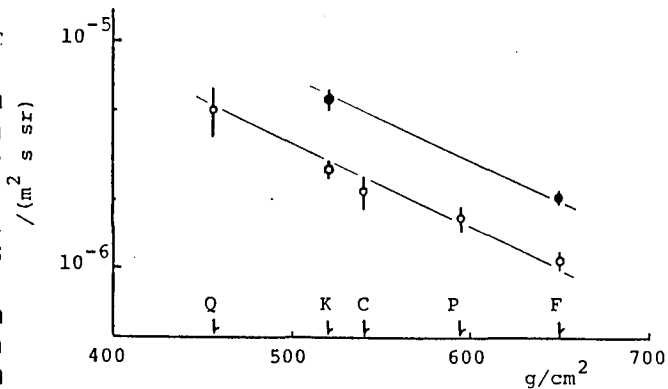


Fig. 4. Comparison of intensities of atmospheric cosmic rays at mountain altitudes. The open and solid circles represent the fluxes of gamma-ray and showers induced by hadrons, respectively, with the energy above 5 TeV; the present results (K) and the results at Mt. Fuji₂ (650 g/cm^2) (6) (F), at the Pamir plateau (594 g/cm^2) (7) (P), at Mt. Chacaltaya₂ (540 g/cm^2) (8) (C) and at the Qomolangma root (455 g/cm^2) (9) (Q). The curves represent the expected attenuation.

Acknowledgements

This work is supported by the grants from Academia Sinica in China and Japanese Ministry of Education including the Grant in Aid for Scientific Research. Data analysis was made with the computer FACOM M380R of Institute for Nuclear Study, University of Tokyo.

References

1. Ren, J.R. et al., the paper in this conference HE 3.7-5.
2. Ren, J.R. et al., 18th ICRC (Bangalore), **5**, 285 (1983).
3. Akashi, M. et al., Nuovo Cimento, **65A**, 355 (1981).
4. Akashi, M. et al., Phys. Rev. D, **24**, 2353 (1981).
5. Amenomori, M. et al., Phys. Rev. D, **25**, 2807 (1982).
6. Amenomori, M. et al., 18th ICRC (Bangalore), **11**, 57 (1983).
7. Pamir Collaboration, 17th ICRC (Paris), **5**, 297 (1981).
8. Brasil-Japan Emulsion Chamber Collaboration, Suppl. Prog. Theor. Phys., No. 47, 1 (1979).
9. Lu, S.L. et al., 17th ICRC (Paris), **5**, 254 (1981).

HIGH ENERGY GAMMA-RAYS AND HADRONS AT Mt.FUJI

Mt. Fuji Collaboration

Amenomori, M., Nanjo, H. and Konishi, E.
 Hirosaki University, Hirosaki, Aomori
 Hotta, N.

Utsunomiya University, Utsunomiya, Tochigi
 Mizutani, K.

Saitama University, Urawa, Saitama
 Kasahara, K., Kobayashi, T., Mikumo, E., Sato, K. and Yuda, T.
 ICR, University of Tokyo, Tanashi, Tokyo
 Mito, I.

Shibaura Institute of Technology, Shibaura, Tokyo
 Shibata, M.

Yokohama National University, Yokohama, Kanagawa
 Shirai, T., Taira, T., Tateyama, N. and Torii, S.
 Kanagawa University, Yokohama, Kanagawa
 Sugimoto, H. and Taira, K.

Sagami Institute of Technology, Fujisawa, Kanagawa

The energy spectra of high energy gamma-rays and hadrons were obtained by the emulsion chamber with 40 c.u. thickness at Mt. Fuji (3750 m). These results are compared with the Monte Carlo calculation based on the same model which is used in a family analysis. Our data are compatible with the model of heavy-enriched primary and scaling in the fragmentation region.

1. Introduction.

The energy spectra of both gamma-rays and hadrons at high energies have been measured with the large-scale emulsion chambers at Mt. Fuji (3750 m, 650g/cm^2)^{1),2)}. The present scale of Fuji experiment is possible to cover the energy range of 2- \ast 100 TeV both for gamma-rays and hadrons with a sufficient statistics.

These spectra are known to be very sensitive to the proton component in the primary and also well reflect the particle production spectra in the fragmentation region, increasing cross sections. This problem has been frequently discussed by many authors, mainly based on the analytical calculation with some approximations.

In this report, we present new spectra of uncorrelated gamma-rays and hadrons observed with the emulsion chamber (FH) of 40 c.u. thickness and compare this with the Monte Carlo simulation made with the same model used in the family analysis.

2. Experiment

In the Mt. Fuji experiments, two types of emulsion chambers have been exposed, i.e., one is of thin-type, with the total thickness less than 10 c.u. and the other of thick-type. The total exposure amounts to about $1000\text{ m}^2\cdot\text{y}$. Among this, the chamber FH, exposed for two years

from 1982 to 1984, has high quality for detecting both gamma-rays and hadrons. The detection efficiency of hadrons is estimated to be 60 %. The X-ray films were inserted at every 2 c.u. from 4 to 40 c.u.. In the depth shallower than 10 c.u., two kinds of films with a different sensitivity (Sakura-N and Fuji-#100) were used.

The energy of each shower is estimated by comparing the transition of shower spots in the x-ray films extending over several layers with the theoretical one (note that the energy of hadron is that released as the electro-magnetic component in the chamber). The separation of gamma-rays and hadrons is made statistically referring to the starting point of showers observed in the chamber. That is, if the showers start in the depth less than 6 c.u., except ones with successive interactions, then they are regarded as gamma-rays (including electrons and positrons) and others as hadrons.

As discussed already in the previous paper²⁾, the Landau-Pomeranchuk effect becomes dominant at high energies over several 10 TeV. Showers become more penetrative at higher energies so that some of gamma-rays are misidentified as hadrons in the usual statistical method mentioned above. In our data processing, this problem is adequately taken into account.

3. Monte Carlo simulation.

The Monte Carlo simulation has been done to get some conclusive results from our experimental data. The model adopted here is the same one as used in the family analysis³⁾. That is, the scaling in the fragmentation region, increasing cross section as $E_0^{0.04}$ and the heavy enriched primary are assumed in the calculation. In the other papers, it has been shown that the scaling is not appreciably broken in the fragmentation region and the heavy enriched primary can well explain the family phenomena which are the products of nuclear interactions in air by primary particles at energies over 10^{15} eV. It is, therefore, of interest to examine whether the same model can also reproduce the energy spectra of uncorrelated gamma-rays and hadrons or not, since these are concerned in the wide energy range of primaries from several TeV to about 10^{16} eV. In Fig. 1 is shown the primary

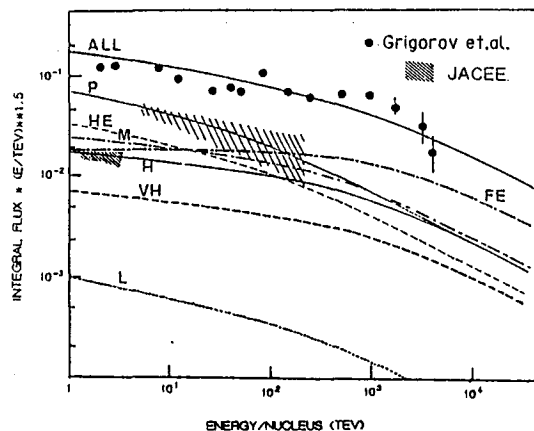


Fig. 1.

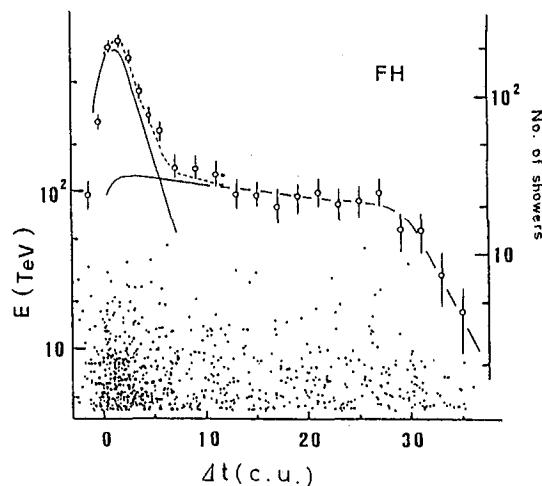


Fig. 2.

spectrum assumed in this calculation. A special feature of this spectrum is that the proton component becomes steeper (change of spectral index : 1.7 \rightarrow 2.0) at around 10^{14} eV, lower than the knee (3×10^{15} eV) appeared in the total spectrum. This proton spectrum is not inconsistent with the JACEE data⁴⁾, though statistics is still insufficient.

4. Results.

In Fig. 2, we show the starting point (Δt) distribution of showers with energy higher than 4 TeV, observed in the FH-chamber. The curves are the expectation of attenuation of high energy showers in the chamber calculated by the Monte Carlo method. In this calculation, the collision mean free path of hadrons is assumed to be 28 c.u. in lead. This data is used for obtaining the absolute vertical fluxes of gamma-rays and hadrons.

The energy spectrum of gamma-rays and hadrons, obtained with the chamber FH, is shown in Fig. 3 and 4, with the one presented at Bangalore Conference²⁾. As discussed in the previous paper²⁾, we revised the energy of showers by using a new energy-determination method. This change was made by a statistical way using a simple relation of $E_{\text{new}} = 1.3 \times E_{\text{old}}$, i.e., old energy is increased by 30%. On the other hand, the energy of each shower observed in the FH-chamber is determined individually by use of a new transition curve. A good agreement of both data means that the previous method is with considerable justification.

The absolute fluxes at 5 TeV and spectral indices are listed in Table 1 for gamma-rays and hadrons.

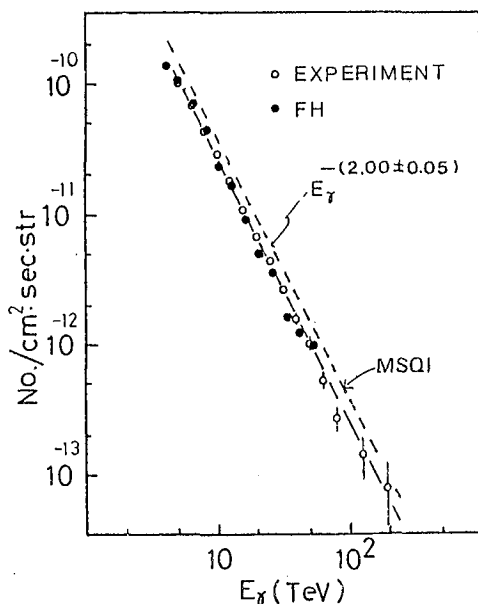


Fig. 3.

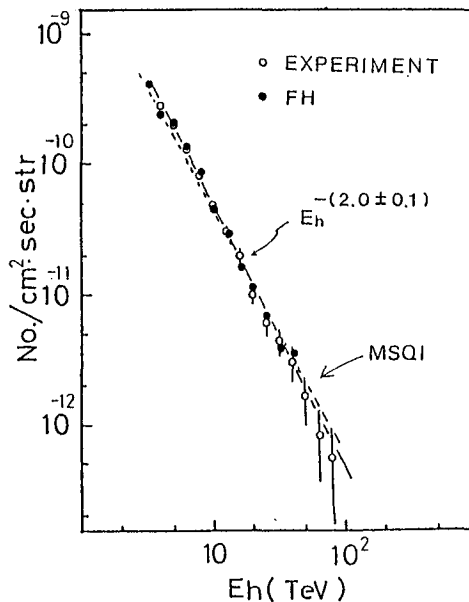


Fig. 4.

Table 1

	Spectral index	Flux value at 5 TeV ($\text{cm}^{-2}\text{sec}^{-1}\text{sr}^{-1}$)
gamma-rays	2.00 ± 0.05	$(1.1 \pm 0.1) \times 10^{-10}$
hadrons	2.0 ± 0.1	$(2.1 \pm 0.1) \times 10^{-10}$

5. Discussions.

We compare our data with the Monte Carlo result (dotted curve) in Fig. 3 and 4. As noticed from these figures, a slight difference may be found between the data and the calculation. But, this is not serious problem if we consider the uncertainty involving in the assumption of primary composition. Of course strong scaling break in the fragmentation region is compatible with proton dominant primary at least up to about 10^{15} eV. However, there is little hope for this possibility, because the primary energy responsible for generating these particles is not so high compared with the energy of CERN SPS collider where the strong scaling break has not been observed.

Our conclusion is that the model of scaling and heavy enriched primary can well explain both of uncorrelated particle spectra and family phenomena which are originated by the primary particles ranging from several TeV to about 10^{16} eV. The implication is that the fraction of primary proton decreases with increasing energy and reaches about 20 % at energies around 10^{15} eV. The proton spectrum should become steeper at least at around 10^{14} eV. This is very interesting result when we consider the problem of acceleration and confinement of high energy cosmic rays in our galaxy.

6. Acknowledgements

The authors would like to express their sincere thanks to Sengen Shrine, Kawaguchi-ko Office of the Ministry of environment Maintenance for extending every facilities necessary for carrying out the experiment at Mt. Fuji to us.

References

- 1) Akashi, M. et al, Nuovo Cimento, 65A, 355 (1981).
- 2) Amenomori, M. et al, 18th ICRC(Bangalore), 11, 57 (1983).
- 3) Ding, L.K. et al, Proc. Int. Symp. of Cosmic Rays and Particle Physics (ICR, Univ. of Tokyo), 142 (1984, Tokyo).
- 4) JACEE Collaboration, *ibid*, 468 (1984, Tokyo).

ON THE CHARACTERISTICS OF EMULSION CHAMBER
FAMILY EVENTS PRODUCED IN LOW HEIGHTS

Jing Gu -ru, Jing Cai-liu, Zhu Qing-qi, Ding Lin-kai
Institute of High Energy Physics, Academia Sinica
P.O.Box 918, Beijing, China

1. Introduction.

The uncertainty of the primary cosmic ray composition at 10^{14} - 10^{16} eV is well known to make the study of the nuclear interaction mechanism more difficult. Experimentally considering, if one can identify effectively the family events which are produced in low heights, then an event sample induced by primary protons might be able to be separated. It is undoubtedly very meaningful. In this paper we simulate the family events under the condition of mountain emulsion chamber experiments with a reasonable model. The aim is to search for the dependence of some experimentally observable quantities to the interaction height.

2. Method.

The model used is: proton incidence, total inelastic cross section rising with energies ($\sigma \propto E_0^{0.06}$), Feynman scaling in fragmentation region holding and mean transverse momentum increasing with energies ($\langle Pt \rangle \propto E_0^{0.05}$). The electromagnetic cascade and the multiple Coulomb scattering are also treated by Monte-Carlo method. Because the stress point is on the study of the qualitative characters of the production height dependence on the transverse distribution of family events, the model used may be a suitable one.

The observation height is assumed at Mt. Kanbala (520 g/cm²). The incident axis is taken uniformly on 40x50 cm² X-ray film, and the particle outside this area are ignored. Hadron showers are recorded by the same method as experiment with chamber thickness of 28 c.u. Pb. The criteria of a family are $\sum(E_Y + E_h^{(\gamma)}) (\equiv \sum E) \geq 30$ TeV, $n_Y \geq 4$ and $n_h \geq 0$ (all symbols are in the common meaning). 546 family events with $\sum E \geq 100$ TeV are analysed.

The $\langle R \rangle$ and $\langle ER \rangle$ of a group of testing events with $\langle Pt \rangle = 330$ MeV/c are shown in Table 1 to compare with M. Shibata's results (in parentheses) using model PRS⁽¹⁾. The difference between them may be reasonable owing to the different observation levels. For families with $\sum E \geq 100$ TeV ($E_{min} = 4$ TeV), we have $\langle \bar{R} \rangle = 2.75$ cm which is close to the experimental value 2.5 cm⁽²⁾.

Table 1 $\langle R \rangle$ and $\langle ER \rangle$ of family events

E (TeV)	30-50	50-100	100-200	200-500
$\langle R \rangle$ (cm)	3.20 (3.3)	3.45 (3.1)	2.82 (2.5)	2.43 (2.3)
$\langle ER \rangle$ (TeV.cm)	12.5 (13.6)	14.1 (13.7)	12.2 (11.7)	10.7 (10.6)

3. Average interaction times, mean interaction height and purity.

The average interaction times, N_{int} , for all observed particles of each family event is calculated. In Fig.1 is shown the N_{int} distribution with mean value 3.74. The

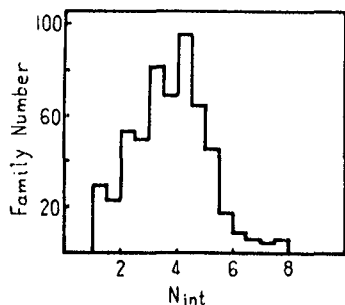


Fig.1

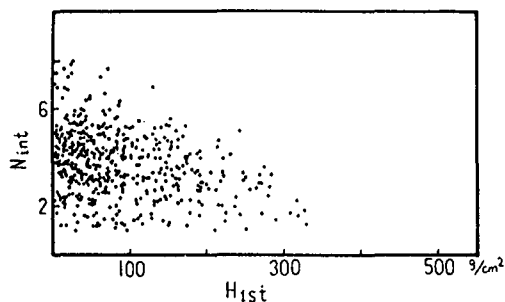


Fig.2

relation between N_{int} and the first interaction height, H_{1st} is seen in Fig.2. It is obvious that the events having both single interaction only and low interaction height are very rare.

For each event with multi-time interactions, imagine that there exists a main interaction. We divide the 520 g/cm^2 atmosphere into 21 layers with step 25 g/cm^2 . Define the layer in which the produced particles contributes the most fraction of family energy ΣE as the main interaction layer and the corresponding height as main interaction height (H_{main}). The fraction mentioned above is defined as purity of the family (abbreviate as p hereafter).

The distribution of main interaction height is rather flat, slight favorable to lower height (or larger H_{main}) (see Fig.3). It is noticed that the events with larger H_{main} are not always very pure (Fig.4). The low-height event which we are interested in, of course, should those with lower main interaction heights and high purities.

R and ER.

The analysis shows that $\langle R \rangle$ and $\langle ER \rangle$ of family events are significantly dependent on H_{1st} (Fig.5): events with larger $\langle R \rangle$ and $\langle ER \rangle$ have smaller H_{1st} , events with larger H_{1st} have smaller $\langle R \rangle$ and $\langle ER \rangle$, but incorrect inversely. As to the dependence of $\langle R \rangle$ and $\langle ER \rangle$ on H_{main} , it is insensi-

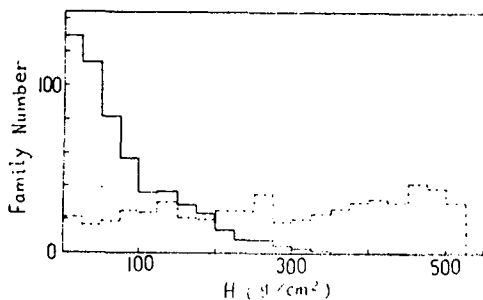


Fig. 3 H_{1st} (real line) and H_{main} (dotted line) distribution

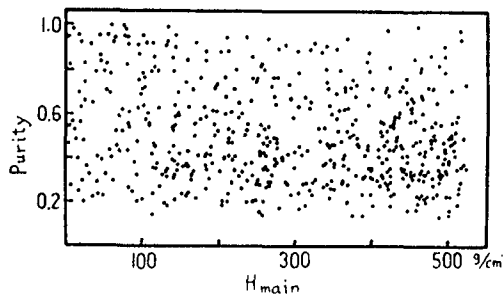


Fig. 4 Purity vs. H_{main}

tive (Fig. 6).

The rejuvenation treatment^[3], or taking R as the distance to event axis, or taking $\langle R \rangle$ as the energy weighted mean R , all induce the $\langle R \rangle$ and $\langle ER \rangle$ with the same qualitative characters as shown in Fig. 5 and 6.

"Decascading" treatment with full efficiency gives weak dependence of $\langle R \rangle$ on H_{main} (fig. 7). Besides, $\langle ER \rangle$, mean energy ($\langle E_y \rangle$) and maximum energy (E_y^{max}) of γ -rays of a family event show the same tendency as $\langle R \rangle$. But at the other hand γ -ray number of a family, n_y , shows opposite tendency. In

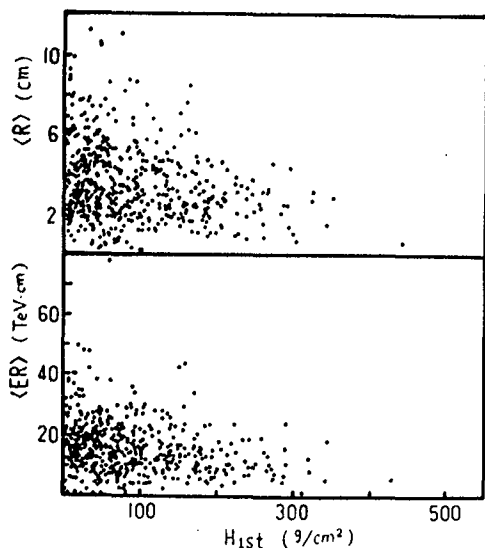


Fig. 5

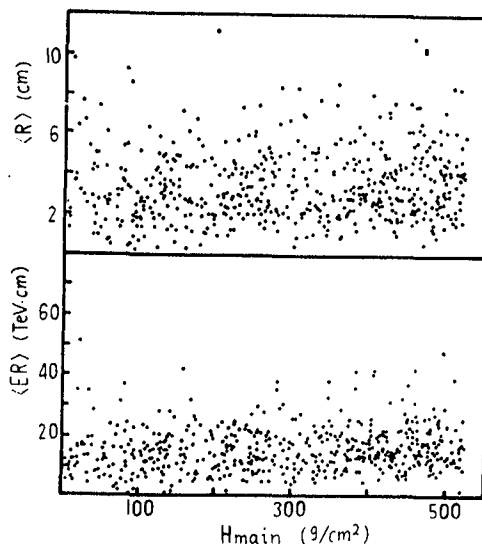


Fig. 6

Fig. 8 is shown the dependence of $\langle E_y \rangle$ on H_{main} . When we analyse the relation between the composite quantity $C \equiv \langle R \rangle \cdot \langle E_y \rangle E_y^{max} / n_y^2$ and H_{main} (Fig. 9), it is seen that some low height events are condensed near $C=0$. Taking a C value cut (say $C=5$), the event sample selected will be dominant for low-height events.

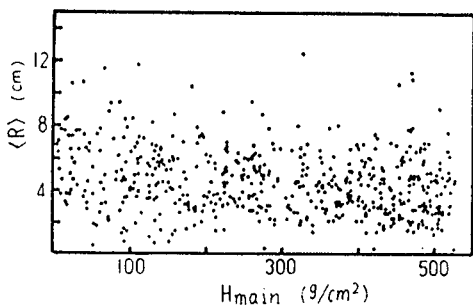


Fig.7

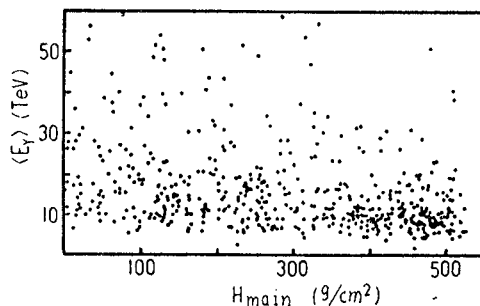


Fig.8

For the families not treated by decascading procedure, the composite quantity $A \equiv n_Y^2 / (\langle R \rangle \langle ER \rangle \langle E_Y \rangle \cdot E_Y^{\max})$ can also be used to separate the the concerned events. For example, there are 28 events satisfying the conditions $A < 0.05$ and $\langle R \rangle < 3$ cm, among which 12 have $H_{main} > 450$ g/cm, 7 events have both $H_{main} > 450$ g/cm and $p > 0.7$. Considering the whole events satisfying these two conditions are not very rich (Fig. 4), this method may be useful.

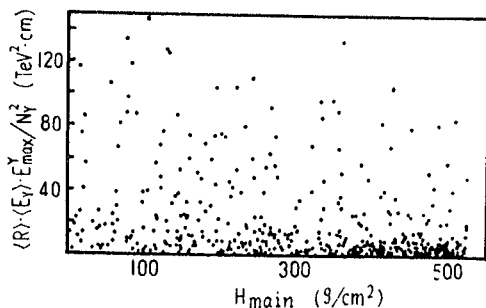


Fig.9

The condition $\langle ER \rangle < 10$ TeV.cm and $\langle E_Y \rangle > 12$ TeV can also separate about one half events having $H_{main} > 450$ g/cm and $p > 0.8$.

Summary.

Due mainly to the multi-interactions in thick atmosphere target above the mountain emulsion chamber, the dependence of the observable quantities of family events on the main interaction height H_{main} is strongly smearing. However, weak dependence on H_{main} still exists in $\langle R \rangle$, $\langle ER \rangle$, $\langle E_Y \rangle$, n_Y and E_Y^{\max} etc. A small sample with low-height and high purity is not impossible to be separated by suitable composing and cutting of these quantities.

References.

1. M. Shibata, Phys. Rev., D24(1981)1847.
2. T. Yuda, 18th ICRC, Rapporteur talk on HE 5.
3. Pamir Collaboration, 14th ICRC, 7(1975)2370.

HADRON INTENSITY AND ENERGY SPECTRUM
AT 4380 m ABOVE LEVEL

Cananov S.D., Chadranyan E.Kh., Khizanishvili L.A.,
Ladaria N.K., Roinishvili N.N.

Institute of Physics, Academy of Sciences of the
Georgian SSR, Tbilisi, USSR

The flux value of hadrons with $E_k^{(n)} \geq 5$ TeV, where $E_k^{(n)}$ is the energy transferred into electromagnetic component is presented. It is shown that the energy spectrum slope β of hadrons with $E_k \geq 20$ TeV is equal to 1.9.

The present work is based on the experimental data obtained by means of "Pamir" carbon X-ray chamber. [1] contains the detailed description of detectors's arrangement.

Two sets of experimental data are used.

The first of them represents the result of exposure of "Pamir 77-78" chamber $ST = 60 \text{ m}^2 \times 11$ months. The lead thickness t in hadron block is equal to 10 c.u. For each spot coordinates, zenith and azimuthal angles and darkness have been measured. Hadrons with zenith angle $\theta \leq 20^\circ$ have been used only.

The second set of the experimental data is composed by selection of spots with darkness $D_{140} \geq 0.6$, measured by aperture of the radius $r = 140 \mu\text{m}$, that approximately corresponds to $E_k^{(n)} \geq 25$ TeV. On the total area $S = 471 \text{ m}^2$ hadrons with zenith angles $\theta \leq 20^\circ$ have been selected in the chambers with lead thickness in hadron $t = 8$

In all used chambers carbon layer was 60 cm thick.

Connection between E^\pm and $E_k^{(n)}$ spectra is given in the [2] (here E^\pm is an energy estimated by means of the dependence $E(D)$ for e^+e^- -pair, the so-called " e^+e^- -pair curves", and $E_k^{(n)}$ is an energy in fact transferred into

electromagnetic component):

$$I(>E_k^{(r)}) = C 10^{B\beta} (E^\pm)^\Delta (E^\pm)^{-\beta} \quad (1)$$

According to [2], in the case of $r = 140\mu\text{m}$, if E^\pm will be estimated by "e⁺e⁻-pair curves" for $t_0 + \Delta t$, where t_0 is the lead thickness in chamber and Δt is equal to 2 c.u., the parameters will take the following values: $B = 0$, $\Delta = 0$.

Hence, to obtain the correct estimate of $E_k^{(r)}$ one can use curves for lead thickness $t = 12$ c.u. in the first set of experimental data and $t = 10$ c.u. in the second one.

Both sets of data are presented in Table 1.

Table 1

No of set	Area (m ²)	$N(E_k^{(r)} \geq 7 \text{ TeV})$	$N(E_k^{(r)} \geq 30 \text{ TeV})$	$N(E_k^{(r)} \geq 100 \text{ TeV})$
1	60	422	24	-
2	471	-	197	29

The value of vertical intensity of hadron flux is calculated by well-known formula:

$$I_0(>E_k^{(r)}) = \frac{N}{ST\omega} \frac{1}{\rho(\theta_0)} \frac{m+2}{2\pi} \quad (2)$$

where N is number of hadrons with $E_k^{(r)}$ greater than the threshold; S is chamber area; $T = 2.7 \cdot 10^7$ s exposure time; $\omega = 0.55$ is the probability of hadron interaction in C-chamber; $\rho(\theta_0) = 1 - \cos^{m'+2} \theta_0$ is the angular factor, which converts hadrons intensity for $\theta < \theta_0$ to the global one with $\theta_0 = 90^\circ$ (m' is the exponent of angular distribution of hadrons, registered in hadron block); $(m+2)/2\pi$ is converting factor from global intensity to the vertical one. Here m is the exponent of angular distribution for hadrons falling on the chamber. According to [1], $m = H/\lambda + 2 = 8 \pm 1$. Here $H = 600 \text{ g/cm}^2$ is atmospheric depth, $\lambda = 90 + 100 \text{ g/cm}^2$ is the attenuation length for protons.

The experimental value of m' , obtained by formula

$$(m'+2)/(m'+3) = \langle \cos \theta \rangle \quad (3)$$

where $\langle \cos \theta \rangle = 0.92 \pm 0.01$ is the average cosinus of zenith angle is equal to $m = 9.5 \pm 1.5$, that is in a satisfactory agreement with results of Monte-Carlo simulations for $m = 8$.

Thus, vertical intensity values obtained from experimental sets turned out to be in a good agreement with each other

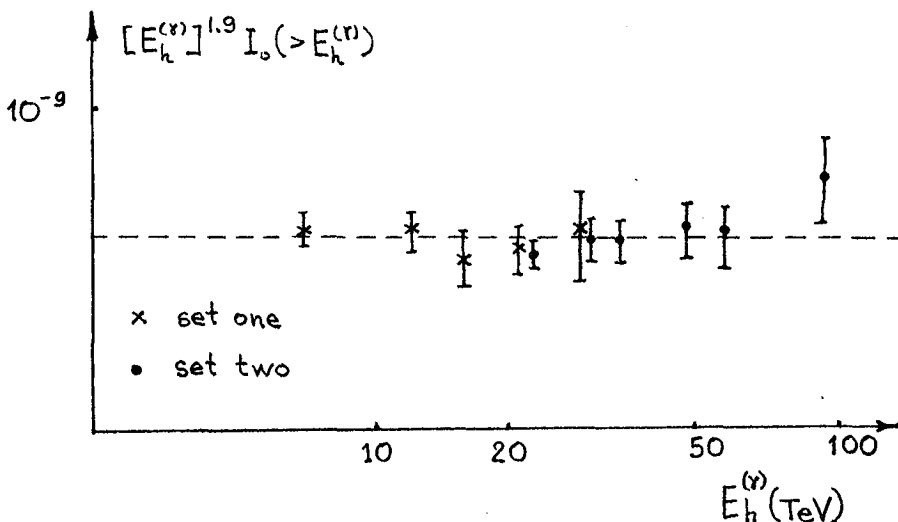
$$I_0(E_h^{(r)} \geq 5 \text{ TeV}) = (2.7 \pm 0.1) \cdot 10^{-10} \text{ cm}^{-2} \text{ s}^{-1} \text{ sr}^{-1} \quad (4)$$

$$I_0(E_h^{(r)} \geq 30 \text{ TeV}) = (0.7 \pm 0.1) \cdot 10^{-11} \text{ cm}^{-2} \text{ s}^{-1} \text{ sr}^{-1} \quad (5)$$

The slopes of energy spectra are in a good agreement also. In Fig.1 the concluding $E_h^{(r)}$ spectrum with the slope 1.9 ± 0.1 is presented (here after the statistical errors are only given).

For chambers under investigation the value of effective coefficient $K_{\text{eff}} = E^{\pm}/E_h$ (here E_h is the energy of incident hadron) is given in [3]. At $E^{\pm} = 5 \text{ TeV}$ K_{eff} it is equal to 0.25. As energy $E^{\pm} = 5 \text{ TeV}$ turns into $E = 20 \text{ TeV}$, and since the value $E^{\pm} = 5 \text{ TeV}$ corresponds to $E = 7 \text{ TeV}$:

$$I_0(E_h^{(r)} > 7 \text{ TeV}) = I_0(E_h > 20 \text{ TeV})$$



Thus, we can obtain energy spectrum of hadrons in the interval 20 + 300 TeV:

$$I_0(>E_h) = (1.4 \pm 0.1) \cdot 10^{-10} \left(\frac{E_h}{20 \text{ TeV}} \right)^{-(1.9 \pm 0.1)} \text{ cm}^{-2} \text{ s}^{-1} \text{ sr}^{-1} \quad (6)$$

In Table 2 the comparison with data from different installations is given. Each value of hadron flux intensity is calculated for Pamir altitude ($H_0 = 600 \text{ g/cm}^2$) and energy $E_h^{(0)} \geq 5 \text{ TeV}$.

Table 2.

Experiment	$I_0(E_h^{(0)} \geq 5 \text{ TeV}) (\text{cm}^{-2} \text{ s}^{-1} \text{ sr}^{-1})$	The slope
Fudji [4]	$(3.2 \pm 0.2) \cdot 10^{-10}$	2.0 ± 0.1
Canbala [5]	$(2.9 \pm 0.1) \cdot 10^{-10}$	1.85 ± 0.1
"Pamir" Pb chamber [1]	$(1.9 \pm 0.4) \cdot 10^{-10}$	1.96 ± 0.1
This work	$(2.7 \pm 0.1) \cdot 10^{-10}$	1.9 ± 0.1

REFERENCES

1. Trudy FIAN, v.154, p.39 (in Russian)
2. Wlodarczyk et al. (in press)
3. Pamir collaboration, 18th ICRC v.11, p.122, 1983
4. Mt.Fuji collaboration, 18th ICRC v.11, p.57, 1983.
5. China-Japan collaboration, 18th ICRC v.5, p.411, 1983

Some characteristic cosmic ray events and an attempt
at their explanation

S. Bhattacharyya
Physical and Earth Science Division
Indian Statistical Institute
Calcutta-700035,
India

«ABSTRACT»

Some cosmic ray events with very large multiplicities and very high transverse momenta have recently been reported in balloon-borne emulsion chamber experiments. The explanation for these events by the standard approaches has become a bit problematical. We have attempted here to understand and interpret them in the light of a dynamical model of multihadron production phenomena with power-law nature of average multiplicity and automatic scale-breaking derived in the model.

1. Introduction

In the recent past some cosmic ray events with very high multiplicities and large average transverse momenta have been observed in a balloon-borne emulsion chamber experiment⁽¹⁾ in the collisions between Si-AgBr nuclei. The charged multiplicity range is $750 \sim 1000$ and the range of the average transverse momentum lies between 550-700 Mev/c and the observed event number is two. The rising behaviour of the average transverse momentum with energy is also confirmed by the CERN PP collider experiments.⁽²⁾ But the CERN PP collider results, it is believed, set an upper limit ($\langle n \rangle \sim \ln^2 S$) to the nature of growth of multiplicity which cannot accommodate such high multiplicity events. Herein lies the problem.

There has in recent times been a lot of theoretical studies⁽³⁾ in understanding these events which are just *not* flukes. We would like to apply here a model for production of secondaries by BANDYOPADHYAY and BHATTACHARYYA⁽⁴⁾ in order to see whether such events can be explained with the help of the expressions we arrive at from the viewpoint of this model.

2. The model and the method.

We will put our model for nucleon-nucleon reactions into use here for nucleus-nucleus collisions on the assumption that all nucleus-nucleus collisions can be treated with the basic dynamics of nucleon-nucleon interactions and taking into account an A-dependence term into final calculation in a somewhat hand-inserted manner, at least for the present.

According to the present model, nucleons are thought to be composed of pions and spectators so far as strong interactions are concerned and all hadronic collisions thus boil down to pion-pion interactions. The interactions proceed in a sequential chain through some ρ - ω - π exchanges with emission of free secondary pions at each vertex on both sides of the horizontal ρ - ω chain giving rise to the spray-like nature of emission of the secondaries (and thus contributing to some form of 'jettiness'). The chain ends as soon as both the mediating and final ρ meson is absorbed by the pions in the target. Kaons are produced from the decay of the virtual ϕ^0 mesons which are generated through $\rho\pi\phi^0$ coupling and the secondary baryons-antibaryons (non-leading) are the products the decays of pions arising out of the sequential $\rho\omega\pi$ chains as prescribed in the pion production. This model gives a unified description for production of both low and large p_T secondaries, an explanation for the leading particle effect and accounts for the by-now established <<universality>> of all hadron-involved interactions as well as of e^+e^- annihilations.

3. Theoretical Results

By applying the Feynman diagram techniques and some standard high energy assumptions the following expressions, very crucial for our cosmic ray physics purpose, were derived

$$E \frac{d^3\sigma}{dp^3} \Big|_{PP \rightarrow \pi^-x} \approx G_{\pi} \exp \left[- \frac{26.88}{\langle n_{\pi^-} \rangle} \frac{k_T^2 + m_{\pi}^2}{1-x} \right] \exp \left[- 2.38 \langle n_{\pi^-} \rangle x \right] \quad (1)$$

with

$$\langle n_{\pi^-} \rangle_{PP} = \langle n_{\pi^+} \rangle_{PP} = \langle n_{\pi^0} \rangle \approx 0.335^{1/3} \quad (2)$$

and

$$E \frac{d^3\sigma}{dp^3} \Big|_{PP \rightarrow \pi^+x} \approx \left[1 + 2.75^{-1/3} \right] E \frac{d^3\sigma}{dp^3} \Big|_{PP \rightarrow \pi^-x} \quad (3)$$

and the inclusive crosssection for the π^0 production is just the mean of inclusive (secondary) π^+ and π^- crosssections.

The expression for the average transverse momentum of any type of particle C is defined by

$$\langle p_T \rangle_C = \frac{\int F(x, p_T)_C p_T dp_T^2}{\int F(x, p_T)_C dp_T^2} \quad (4)$$

Using the above definition and making use of the expressions (1-2) deduced by our dynamical model we finally arrive at

$$\langle p_T \rangle_{\pi^-} \simeq 1.1 \times 10^{-1} s^{\frac{1}{6}} \text{ GeV}/c \quad \text{--- (5)}$$

The expression (2) with incorporation of a maximum $A^{\frac{1}{3}}$ (actually $\leq A^{\frac{1}{3}}$) dependence can account for the observed range of multiplicity events and the expression (5) gives their average transverse momenta in the expected limit. Why the number of such events is limited to two only could probably be explained in terms of phase transitional probability^(3a) occurring in the structure of hadrons; the pion clusters in the strong interaction domain might exhibit further structures leading to a change in the nature of interactions at such high energies. This aspect is now under study. Side by side, the explicit nature of A dependence is also being looked into.

4. Discussion and Conclusions

Our brief study shows that the problem might not be linked up with the validity or violation of the KNO scaling⁽³⁾ or be connected with the unknown heavies as proposed by Sukuyama and Watanabe⁽³⁾. Some further comments are in order here: (i) it is seen and supported here that " $\langle p_T \rangle$ increases gradually with energy and this increase is associated events corresponding to average multiplicities - not with events higher than average multiplicity" as was argued by Halzen,⁽⁵⁾ (ii) our multiplicity pattern follows power law (although the rate is a bit larger here) as advocated by Maraki.⁽⁶⁾ This inevitably leads to the violation of both Feynman and KNO scaling as argued and/or observed by many authors.^(7,8) But the fair agreement that we claim here might be proven wrong by the uncertainties in the correctness of the measurement of the average transverse momentum as pointed out by Hagedorn.⁽⁹⁾

We would like to emphasise here a few ^{more} points. Unless the experimental results from the Fermilab PP collider at higher energies than the CERN PP collider are to hand no one can and should put a *quies* to the power law nature - whatever its magnitude *far* less than unity - of average multiplicity practically on the basis of quasi empirical type of QCD predictions. QCD has many intrinsic loop-holes⁽¹⁰⁾ even in its philosophy of confinement, the very kernel of the theory. Thus we hope our model might have had a modest prospect in future studies vis-a-vis this QCD state and the so far illusive⁽¹¹⁾ (experimental) behaviour of the quarks.

References

1. Burnett T.H. et al (1983) Phys. Rev. Letts. 50, 2062;
Iwai J. et al (1982) Nuovo Cimento 69A, 295.
Bhattacharyya, D.P. (1983) Canadian Journal of Phys.
61, 434.
2. UA(1) Collaboration (1982) Phys. Letts. 118B, 173
3. Stanev Todor (1985) Phys. Rev. D31, 1155
Fajares, C. and A.V. Romallo (1984) Phys. Rev. Letts.
52, 407; Sukuyama, H. and K. Watanbe, (1984) Lett.
Nuovo Cimento 40, 243; Sukiyoshi, H. (1983) Phys.
Letts. 131B, 343.
4. Bandyopadhyay, P. and S. Bhattacharyya (1978) Nuovo
Cimento 43A, 305, 323, (1979); Nuovo Cimento 50A, 133
with D.P.B. and R.K.R.C. (1980) Phys. Rev. D21, 1861.
5. Halzen Francis (1984), Invited talk at the Interna-
tional Symposium on Cosmic Rays and Particle Physics,
Tokyo, Japan (March 19-23) and Preprint; University
of Wisconsin Madison (USA)
6. Muraki, Y. (1983) Proceedings of the 18th ICRC Vol.5
499 (Bangalore-India).
- 7(a). Kiang, D. et al. (1985) Phys. Rev. D31, 31 and
the references therein UA(5) Collaboration (1984)
Phys. Letts. 138B, 304 and the references therein
(b) Sreekantan, B.V., S.C. Tonwar and P.R. Biswanath
(1983) Phys. Rev. D28 1050; Fakinuto, F. et al.
(1983) Jour. of Phys. G9, 339; Tasaka, S. et al.
(1982) Phys. Rev. D25, 1765;
Amenomori, M. et al (1982) Phys. Rev. D25 2807;
Akasi, M. et al (1981); Phys. Rev. D24, 2353;
Shibata M (1981) Phys. Rev. D24, 1847.
8. Wdowczyk, J. and A.W. Wolfendale (1984) Jour. of
Phys. G10, 257; (1979) Nuovo Cimento 54A, 433;
(1973) Jour. of Phys. A6 L48.
9. Hagedorn, R. (1983) La Riv. Nuovo Cimento 6, p.37.
10. Altarelli, G. (1984) La Rivista Nuovo Cimento 7
(No.3); p5.
Hagedorn, R. (1984) CERN Preprint TH3918/84
11. Trower, W.P. (1985) Nucl. Phys. B252, 285.

NOTE ADDED : In getting the order of magnitude of the multiplicity and the average transverse momentum we make use here of the relation $S = 2 i M_A E$ where i = number of nucleons involved in each collision and the other letters have their usual significances. It is seen that in order to have a good fit one has to take here $i \sim 30$.

The Nucleon Intensity in the Atmosphere and the p_t Distribution

A. Liland
N-9785 Veidnesklubben
Norway

ABSTRACT

The diffusion equation for cosmic ray nucleons in the atmosphere has been solved analytically, taking into account the transverse momentum distribution of nucleons produced in nucleon-air nucleus collisions. The effect of the transverse momentum distribution increases the nucleon intensity at large zenith angles and low energies.

1. Introduction

The intensity of cosmic ray nucleons in the atmosphere, due to cosmic ray primary protons, can be expressed by (1)

$$N(E, x) = C_p E^{-(\gamma + 1)} e^{-x/\lambda} \quad (1)$$

where $N(E, x=0) = C_p E^{-(\gamma + 1)}$ is the primary proton spectrum, x the atmospheric depth and λ the diffusion length for nucleons in the atmosphere. This solution is obtained by the assumption that the secondary nucleons are moving in the same direction as their parent nucleons. It can be used for deriving the intensities of cosmic ray mesons in the atmosphere and muons at sea-level (1) because the energies of interest here are high such that the average transverse momentum of secondary nucleons $\langle p_t \rangle$ is very small compared to the energy E of the nucleon, $\langle p_t \rangle \ll E$. If $\langle p_t \rangle$ is no longer much smaller than E , as is the case, for instance, for low energy cosmic rays in the upper part of the atmosphere, equation (1) will give too low nucleon intensity at large zenith angles θ , as we shall see below.

2. The Atmospheric Depth

From the U.S. Standard Atmosphere (1976) (2) we obtain the atmospheric depth at sea-level and zenith angle 0° , $x_0 = 1035.6 \text{ g/cm}^2$. We approximate the Standard Atmosphere by an exponential atmosphere and obtain for the atmospheric depth at height Z (km) above sea-level $x = x_0 \exp(-Z/H)$, $H = 6.95 \text{ km}$. The error is less than 12% for $x < 1 \text{ g/cm}^2$ compared to the Standard Atmosphere. For an inclined direction, $0^\circ < \theta < 90^\circ$, we obtain for the atmospheric depth $x_{\max}(\theta)$, at sea-level,

$$(2) \quad x_{\max}(\theta) = \frac{\rho_0 \sqrt{\frac{\pi}{2} HR}}{\frac{1+\alpha}{2} \sqrt{\frac{\pi}{2} \frac{R}{H}} \cos \theta + \beta} \begin{cases} \theta \geq 87^\circ \begin{cases} \alpha = 0.398 \\ \beta = 0.96 \end{cases} \\ \theta < 87^\circ \begin{cases} \alpha = 0.96 \\ \beta = 0.398 \end{cases} \end{cases}$$

ρ_0 is the density of air at sea-level

R is the radius of the earth, 6366 km.

The error, due to approximations, is less than 5%.

From the figure we obtain:

$$\cos(\hat{\theta}) = \cos(\theta) \cos(\alpha) + \sin(\theta) \sin(\alpha) \cos(\varphi)$$

α will be given by $\frac{P_t}{E}$ later on

and is small so that we can take

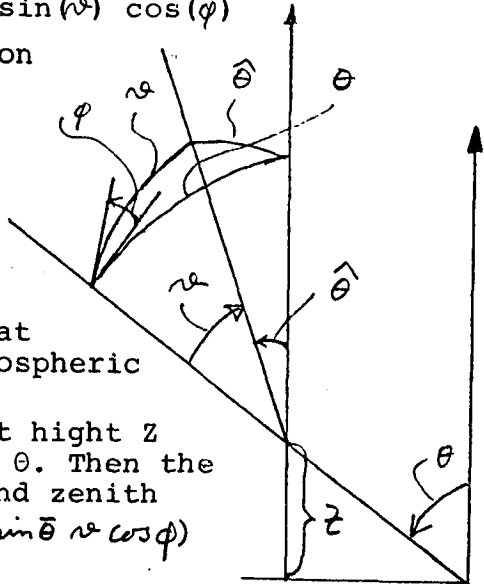
$$\cos \hat{\theta} = \cos \theta + \sin \theta \alpha \cos \varphi$$

We introduce the reduced zenith angle $\bar{\theta}$,

$$\cos \bar{\theta} = \sqrt{1 - \left(\frac{\sin \theta}{1 + \frac{2+3\cos \theta}{6.364}} \right)^2}$$

which is the local zenith angle at approximately half the total atmospheric depth $x_{\max}(\theta)$.

Let x be the atmospheric depth at height Z above sea-level and zenith angle θ . Then the atmospheric depth \hat{x} at height Z and zenith angle $\hat{\theta}$ is given by $(\cos \hat{\theta} = \cos \bar{\theta} + \sin \bar{\theta} \alpha \cos \varphi)$



$$\hat{x} = x \frac{x_{\max}(\hat{\theta})}{x_{\max}(\theta)} = \frac{x}{1 + \frac{\sin \bar{\theta} \alpha \cos \varphi}{\cos \bar{\theta} + \eta}}$$

$$\eta = \frac{2\beta}{1+\alpha} = \begin{cases} 0.0362 & \theta \geq 87^\circ \\ 0.0107 & \theta < 87^\circ \end{cases}$$

3. The Diffusion Equation

Let the differential production cross section for nucleon production by nucleons have the following transverse momentum distribution

$$\frac{d^2\sigma}{dp_{\perp 1} dp_{\perp 2}} \sim e^{-\alpha p_{\perp}^2} \quad \alpha = \text{const.}$$

where p_{\parallel} is the longitudinal momentum and p_{\perp} is the transverse momentum of the produced nucleons. With $\alpha = \frac{P_t}{E}$ we then obtain for cosmic ray nucleons

$$g(E, E', \alpha, \varphi) = g(E, E') \frac{1}{2\pi} \frac{\pi}{4} \frac{1}{\langle p_{\perp}^2 \rangle} e^{-\frac{\pi}{4} \left(\frac{E}{\langle p_{\perp} \rangle} \right)^2 \alpha^2}$$

$$\text{with } G_{NN} = \int_0^1 g(E, E'/\alpha) u^x du \quad (1)$$

We use the generation method and obtain the diffusion equation for the first generation nucleon

$$\frac{d\hat{N}_1}{dx} = -\frac{\hat{N}_1}{\lambda_N} + \int_E^{\infty} \frac{1}{\lambda_N} C_p E' \int_0^{\pi} \int_0^{2\pi} e^{-\frac{\hat{x}}{\lambda_N}} g(E', E', \alpha, \varphi) d\varphi.$$

$$\cdot 2E^2 \alpha^2 d\alpha \frac{dE'}{E'} \quad \lambda_N = 84 \text{ g/cm}^2 \text{ is the interaction length for nucleons,}$$

The analytic solution is

$$\hat{N}_1(E, X, \theta) = C_p E^{-(\alpha+1)} G_{NN} \frac{X}{\lambda_N} e^{-\frac{X}{\lambda_N}} \frac{1}{1 - \left\{ \epsilon_1 \sqrt{\frac{\pi}{4}} \frac{X}{\lambda_N} \frac{\langle p_L \rangle}{E} \pi(\bar{\theta}, E) \right\}^2}$$

$\epsilon_1 = 0.2845$

$$\pi(\bar{\theta}, E) = \frac{\sin \bar{\theta} / (\cos \bar{\theta} + \eta)}{1 + (\sin \bar{\theta} \langle \frac{p_L}{E} \rangle \frac{\pi}{4}) / (\cos \bar{\theta} + \eta)}$$

The solution for the m'th generation nucleon has the form

$$\hat{N}_m = C_p E^{-(\alpha+1)} \frac{1}{m!} \left(\frac{X}{\lambda_N} G_{NN} \right)^m e^{-\frac{X}{\lambda_N}} \prod_{n=1}^m g_{m,n}$$

$$g_{m,n} = \frac{t_m}{1 - \left\{ s_{m,n} \frac{X}{\lambda_N} \frac{\langle p_L \rangle}{E} \right\}^2}$$

If we define an average for $g_{m,n}$, for instance:

$$g(E, X, \theta) = \frac{\langle t_m \rangle}{1 - \left\{ \langle s_{m,n} \rangle \frac{X}{\lambda_N} \frac{\langle p_L \rangle}{E} \right\}^2}$$

we can sum over m and write an approximate solution for the nucleon intensity in the atmosphere

$$\hat{N}(E, X, \theta) = C_p E^{-(\alpha+1)} e^{-\frac{X}{\lambda_N} (1 - G_{NN} g(E, X, \theta))}$$

$g(E, X, \theta) > 1$ and $\hat{N}(E, X, \theta)$ is increasing with increasing $\frac{X}{\lambda_N} \frac{\langle p_L \rangle}{E}$ and zenith angle θ .

If the differential production cross section is $\sim e^{-\alpha p_L}$ we obtain for the first generation nucleon

$$\hat{N}'_1(E, X, \theta) = C_p E^{-(\alpha+1)} G_{NN} \frac{X}{\lambda_N} e^{-\frac{X}{\lambda_N}} \frac{1}{1 - \left\{ \epsilon'_1 \frac{1}{2} \frac{X}{\lambda_N} \frac{\langle p_L \rangle}{E} \pi(\bar{\theta}, E) \right\}^2}$$

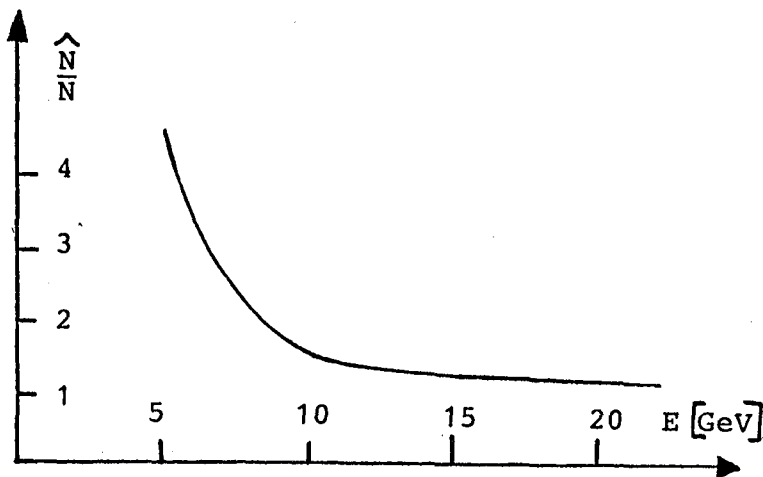
$$\epsilon'_1 \approx 1.$$

and we see that this flatter transverse momentum

distribution gives a greater effect.

4. Discussion and conclusion

$\hat{N}(E, x, \theta)$ is the solution of the 3 - dimensional diffusion equation for nucleons in the atmosphere and $N(E, x)$ the 1-dimensional solution as given above. The figure shows, as an example, the ratio $\hat{N}(E, x, \theta)/N(E, x)$ at 30 km above sea-level ($x(\theta = 0^\circ) = 12.4 \text{ g/cm}^2$) for $\theta = 90^\circ$, $x = 350 \text{ g/cm}^2$ as a function of energy E .



We see that below 10 GeV the ratio \hat{N}/N is increasing rapidly with decreasing energy. This is because \hat{N}/N is a function of E^{-2} as we see from the solution for \hat{N} above.

In the case of $\frac{d^2\sigma}{dp_u^2 dp_L^2} \sim e^{-\alpha p_L}$, we obtain approximately the same curve, but with the energy a factor 2 higher and the rapid increase is between 20 GeV and 10 GeV. We see that the effect of the transverse momentum distribution is not only a function of the average transverse momentum $\langle p_t \rangle$, but depends also on the shape of the transverse momentum distribution.

References

1. A. Liland, Fortschritte der Physik 23, 571 (1975)
2. U. S. Standard Atmosphere (1976), Handbook of Chemistry and Physics. The Chemical Rubber Co., 1984.

ENERGY SPECTRA OF PROTON AND NUCLEI OF PRIMARY
COSMIC RAYS IN ENERGY REGION > 10 TeV/PARTICLE

Mandritskaya K.V., Sazhina G.P., Sokolskaya N.V.,
Varkovitskaya A.Ya., Zamchalova E.A., Zatsepin V.I.
(Moscow University Balloon Emulsion Experiment - MUBEE)

Institute of Nuclear Physics, Moscow State University,
Moscow 119899, USSR.

To investigate the chemical composition of primary cosmic rays, several emulsion chambers were exposed at a 10.8 g/cm^2 depth in the stratosphere. Each chamber has the area of $0.92 \times 0.46 \text{ m}^2$ and the depth of 14 c.u. The exposure time of chambers processed by now is 260 hours. The detecting layers were X-ray films and nuclear emulsions, which allowed to measure an energy of cascade and a type of primary particle. Previous results and technique were described in /1,2/

Results. The obtained results are listed in Table 1. All cascades were divided into six groups, according to the type of a primary. He and Z denote here the cascades produced in a chamber by He nuclei and nuclei with $Z \geq 3$. SH denotes the cascades produced in the chamber cover, these cascades were observed as a shower in the emulsion layer just below the cover. A fraction of cascades was induced by secondaries generated in the residual atmosphere (A-cascades). The cascades observed as groups of two or more members with the same zenith and azimuth angles are called A_p cascades. The events belonging to none of the above enumerated types were attributed to p-cascades. This group consists of proton cascades with a small addition of single A-cascades. A small number of cascades were failure to identify due to technique causes (?-cascades). The third line in Table 1 lists the value of exposure factor $\langle S \Omega \varphi \eta \rangle \cdot T$, where S is the chamber area, Ω is the solid angle, φ is the efficiency of registration of given-type particles in

a chamber, η being the coefficient of intensity attenuation in the residual atmosphere, T - exposure time. The angular intervals for which the processing was made also presented here.

Table 1.

primary θ°	P		He		Z > 3		SH		A _p		?	
	25-60	10-72	25-60	10-72	25-60	10-72	25-60	10-72	25-60	10-72	25-60	10-72
G·T, m ² hr sr	434	62.5	50	70.5	M 45 63 H 37 51 VH 31 43							
ϵ , TeV	>1.6	292	39		58		68		60		39	
	>2	170	35		41		44		49		23	
	>2.5	115	23		30		30		40		13	
	>3	80 99	18 23		27 30		25 34		36 40		10 17	
	>4	43 53	13 14		25 27		15 22		25 27		3 6	
	>5	26 31	10 11		17 19		11 12		18 18		1 4	
	>10	6 9	6 6		3 4		6 6		3 3		1	
	>20	1 2	1 1				2 2					
	>40		1 1									

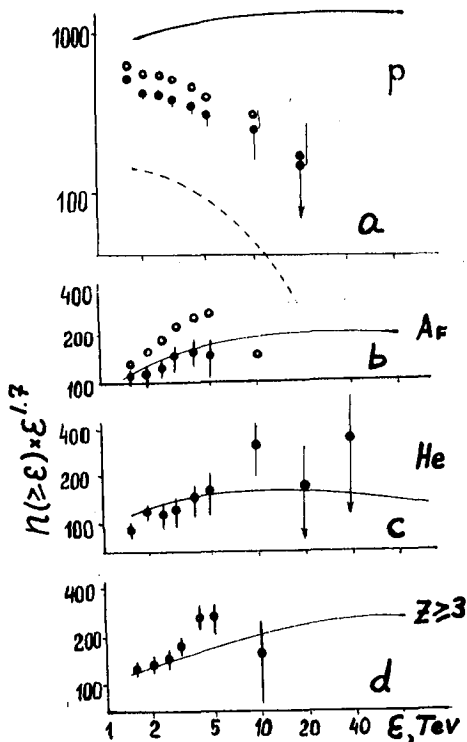
In Fig.1 the data for p, He and Z - cascades are shown along with the expected dependencies calculated for a primary composition model implying all spectra can be described by power-law dependences of the form $i_j = i_{0j} E^{-\beta_j}$, where E is the particle energy in TeV, and the values of parameters i_{0j} and β_j for various groups are given below:

Group	p	He	M	H	VH
$i_{0j}, m^{-2}hr^{-1}sr^{-1}$	240	90	75	107	67
β_j	1.7	1.8	1.7	1.7	1.7

These parameters were chosen when analysing experimental data obtained in /4-7/.

The expected number of cascades with energy $>E$ was calculated by the formula: $n_j(>E) = i_j(>E(E)) \cdot \langle S \Omega \psi \eta \rangle T \xi$, where $\xi = 1.25$ is the factor allowing for overestimation of the measured intensity due to fluctuations. A relationship between the measured energy ϵ and the total particle energy regarding fluctuations of the interacting nucleons number, fluctuations of K_X and diversity of a nucleon cascade from an electromagnetic one has been considered in /1,3/.

Fig.1 shows a good agreement between the observed and expected spectra of He and Z-cascades and the difference between the observed and expected p-cascade spectrum being small at low energies and rapidly increasing with energy.

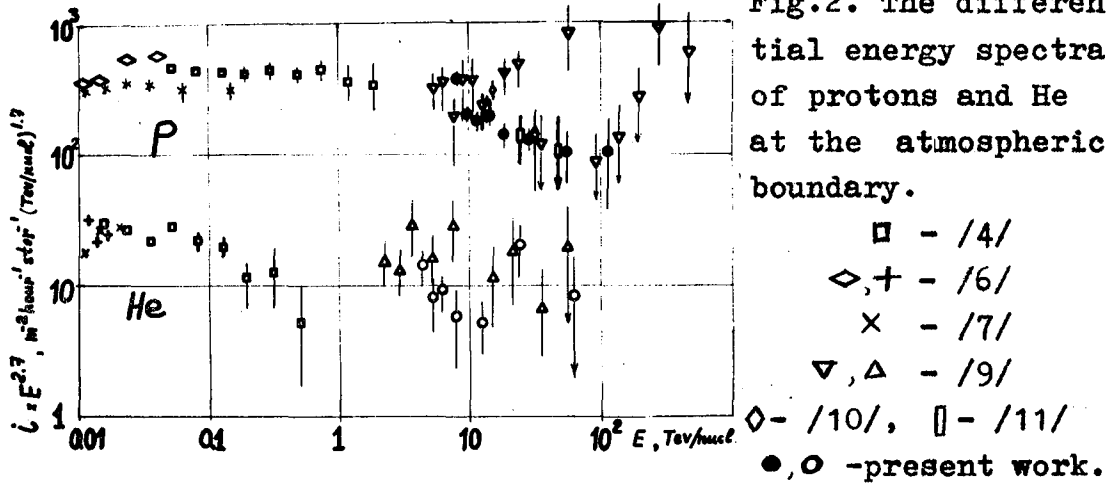


As note above, p-cascades include some fraction of single A-cascades. To estimate this fraction we performed simulations, which results are shown in Fig.1. The simulation was made by the program /8/, where interaction was assumed to quasi-scaling type, and a superposition model was used for nucleus-nucleus interaction. The expected number of single A-cascades is shown in Fig.1a by dashed line, the black circles denoting the corrected spectrum of proton cascades. Thus made correction is not quite reliable that follows

from Fig. 1b, where the expected and observed numbers of A_F -cascades are shown (solid line and open circles). The observed number of A_F -cascades can be seen to somewhat exceed the calculated number. It must be note that the number of A_F -cascades is the strongly fluctuating magnitude. For instance, if one of 31 observed families is exclude from the A_F -cascades, the calculated and observed (black circles) spectra would coincide. However, it is desirable to have a reliable experimental identification procedure, that is our aim in the nearest future.

Discussion. Fig.2 summarizes the data available on the p and He-components. One can see that there is a discrepancy between our and JACEE proton data. Unfortunately, JACEE spectrum in various energy ranges was obtained over different exposures, that makes it difficult to analyse the

origin of discrepancy.



Furthermore the steepening of the proton spectrum measured in our experiment shows that the proton spectrum problem in the range $10^{12} - 10^{14}$ eV is still unsolved and requires further explorations. The proton spectrum being steep in the range $10^{12} - 10^{14}$ eV and the normal amount of protons being present at $E > 10^{15}$ eV may indicate the existence of two proton components of different origin /2/.

References.

1. Abulova V.G. et al, Proc. 18th ICRC, 1983, v9, p 179.
2. Abulova V.G. et al, Izv. AN SSSR, ser. fiz., v 48, p2083
3. Dezurko M.D. et al, Proc. 17th ICRC, 1981, v 9, p 324.
4. Ryan M.G. et al, Phys Rev Lett, 1972, v 28, n 5, p 985.
5. Simon M., Ap.J., 1980, v 239, p 712.
6. Ormes J.P. et al, Proc ICRC, 1965, London, v 1, p 349.
7. Smith L.H. et al, Ap.J., 1973, v 180, p 987.
8. Mukhamedshin R.A. Thesis, 1981, Inst. for Nucl. Reas., Moscow, USSR.
9. Burnett T.H. et al, Phys Rev Lett, 1983, v 51, 11, p.1010.
10. Tasaka S. et al, Proc 17th ICRC, 1981, v 5, p 126.
11. Vakulenko E.S. et al, Vestnik MGU, ser.fis., 1985, v 26, n 4 (in Russian).

SCALING VIOLATION IN FRAGMENTATION REGION AT
ENERGIES ABOVE 10^{15} EV BASED ON THE DATA ON
COSMIC RAY HADRON COMPONENT

"Pamir" Collaboration 4

The ratio of intensity of energetic hadrons, having no visible accompaniment, to the total flux of hadrons of the same energy at 4380m above sea level is given. The ratio is much more than expected for scaling model with proton primaries. This result could not be explained by complex chemical composition of primary cosmic ray and indicates the scaling violation in fragmentation region.

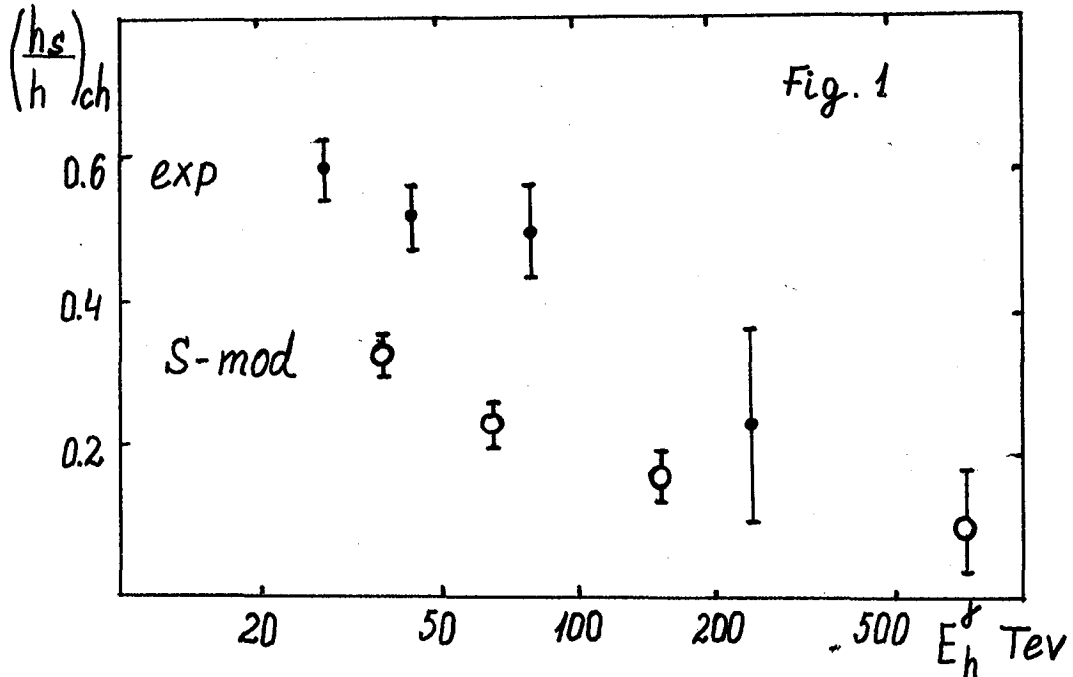
1. Experimental procedure. A special search of high energy hadrons in thick carbon type X-ray chambers [1] was made for investigation of hadron fraction having no accompaniment. 5 most energetic spots were selected in each X-ray sheet having 0.5 m^2 area. For them energy E^\pm was determined by means of darkness dependence on E for e^+e^- -pair. Then energy transferred by hadrons into electromagnetic component $E_h^{(e)}$ was estimated using method described in [2]. For this procedure effective coefficient $K_{\text{eff}} = E_h^{(e)}/E_h \approx 0.35$ [2]. Only hadrons having $E_h^{(e)} \geq 25 \text{ TeV}$ (we call them leaders) are including in the following analysis. The scanning efficiency for such hadrons is very good, since their average number of them is approximately 1 per 1 m^2 and beforehand selected one was 10 times higher.

A search of hadron accompaniment for each leader was made on the same X-ray sheet in a circle with $R = 30 \text{ cm}$. Energy threshold for accompanying particles was $E_h^{(e)} = 3 \text{ TeV}$.

Total area treated by the described method was 615 m^2 , 608 leaders were found and among them 332 were single one*.

*Note that here single hadron means that it has no visible accompaniment. Only part of them are primaries which did not interact in the atmosphere.

2. Results. Energy dependence of single hadron fraction $(h_s/h)_{ch}$ is shown in Fig.1. Up to $E_h^{(r)} \sim 100$ TeV it is



rather weak. The average value for $E_h^{(r)} \geq 25$ TeV $(h_s/h)_{ch} = 0.55 \pm 0.03$. Sign ch-marks the value h_s/h determined for the given type of chambers. To estimate the corresponding value for incident hadrons one needs to take into account interaction probability in the chamber and restore total energy of leaders and accompanying particles.

Correction for interaction probability ($\omega \approx 0.6$) was made in the following way. It was supposed that multiplicity distribution of accompanying hadrons is $(n+1)^{-\alpha}$. Constant α was found from experimental value $(h_s/h)_{ch} = \frac{\sum_0^{\infty} (n+1)^{-\alpha} C_n (1-\omega)^n}{\sum_0^{\infty} (n+1)^{-\alpha}} = 0.55 \pm 0.03$. It turns out to be $\alpha = 1.6 \pm 0.1$.

To check hypothesis about n distribution experimental distribution N_m of accompanying particle multiplicity m was compared with expected at $\alpha = 1.6$:

$$N_m = \frac{\sum_0^{\infty} (n+1)^{-\alpha} C_n^m (1-\omega)^{n-m} \omega^m}{\sum_0^{\infty} (n+1)^{-\alpha}}$$

The experimental and expected distribution were in good agreement. This was the argument for estimation of incident single hadron fraction as $h_s/h = 1/\sum_0^{\infty} (n+1)^{-\alpha} = 0.45 \pm 0.05$.

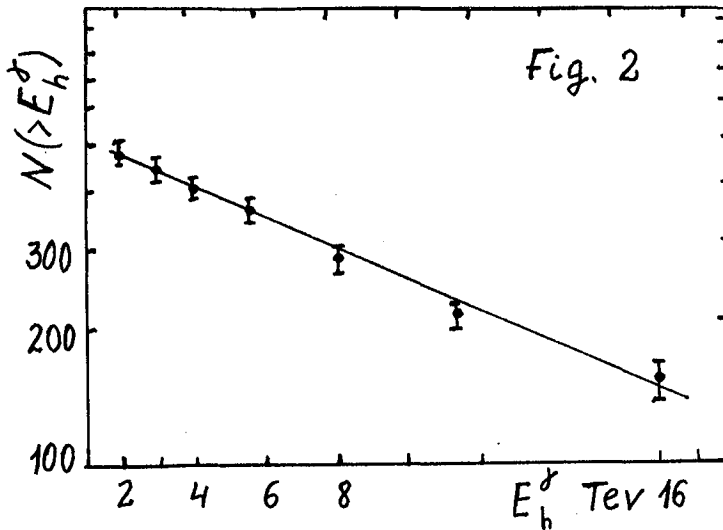
It was mentioned that effective coefficient connected total energy of a hadron $E_k^{(r)}$ with measured $E_k^{(s)}$ is equal to ~ 0.35 . Therefore investigated energy ($E_k^{(r)}$) interval of leaders corresponds to E_k interval (60 - 400) TeV, and threshold energy of accompanying hadrons is approximately (10 + 15) TeV.

3. Comparison with the calculation. Results of the scaling type S-model [3] for proton primaries simulation are shown in Fig.1 by open circles. Interaction probability in the chamber, size of X-ray sheet and K_Y distribution ($\bar{K}_Y = 0.17$, $\sigma = 0.12$ for nucleons, and $\bar{K}_Y = 0.23$, $\sigma = 0.13$ for pions has been taken into account in calculations.)

As it is seen, experimental value $(h_s/h)_{ch}$ up to $E_k^{(r)} = 100$ TeV is essentially larger than simulated one.

Two methodical effects have to be analysed before final conclusions. The first is possible systematical error in $E_k^{(r)}$. No exact correspondence of $E_k^{(s)}$ in the experiment and simulation could lead to false disagreement between them due to $(h_s/h)_{ch}$ dependence on $E_k^{(s)}$. But Fig.1 shows that overestimation of $E_k^{(r)}$ in the experiment has to be too large to explain observed discrepancy.

The second effect is the influence of bad correspondence between energy threshold of accompanying particles in the experiment and calculation. It turns out that change of $E_k^{(s)}$ from 3 TeV to 7 TeV in the simulation increases $(h_s/h)_{ch}$ from 0.30 ± 0.02 to 0.36 ± 0.02 only. The experimental situation looks rather interesting. Integral spectrum of accompanying particles is shown in Fig.2, It has exponential form without any threshold effect up to 2 TeV. About 33% of particles has $E_k^{(s)}$ less than 7 TeV. But they practically do not influence on $(h_s/h)_{ch}$ value. While one changes threshold energy from 3 to 7 TeV it increases only by 0.01. This is



because most of the low energy particles are in groups of accompanying hadrons with multiplicity more than 1 or even 2.

4. Conclusions.

a. The experimental data on single hadron fraction

are in disagreement with S-model prediction.

b. This disagreement could not be explained by experimental inaccuracy.

c. As it is shown in [4], an account for interaction cross-section increase leads to the decrease of $(h_s/h)_{ch}$, i.e. to the increase of contradiction between the experiment and the model.

d. An account for complex chemical composition of primary cosmic ray leads to the same effect. This was shown in a small set of simulation for Fe primaries.

Thus an agreement between experimental data and calculation can be found only in the frame of models with scaling violation in the fragmentation region, in which either number of secondaries with large X is essentially less or (and) inelasticity coefficient is significantly larger than in scaling type models.

REFERENCES

1. Pamir collaboration ZNUZ S 2 z 60, p.9-21, 1977.
2. S.D.Canonov et al. This proceedings HE-5.
3. A.Krys et al. ZNUZ S 2 z 32, p.5-45, 1980.
4. Y.Malinovski et al. 18th ICRC v.5, p.429, 1983.

CONNECTION BETWEEN VARIATIONS OF THE ATMOSPHERE TEMPERATURE PROFILE AND VARIATIONS OF THE MESON COMPONENT INTENSITY

Ya.L.Blokh, S.I.Rogovaya

Institute of Terrestrial Magnetism, Ionosphere and Radio Wave Propagation, USSR Academy of Sciences, I42092 Troitsk, Moscow Region, USSR

The influence of temperature effects on intensity variations of the cosmic ray meson component are now studied in detail. The intensity variations caused by temperature variations are known to have the form /1/

$$\frac{\Delta I^i(t)}{I} = \int W^i(h) \Delta T(h,t) dh \quad (1)$$

where $W^i(h)$ are densities of temperature coefficients. These coefficients were calculated by Dorman /1/ for a wide energy spectrum. Miyazaki and Wada /2/ were the first to consider the possibility to solve the problem inverse to (1) - to predict variations of the atmosphere temperature from intensity variations of the meson component measured on the Earth. With this purpose they proposed a model simple at first glance, in which the temperature variations for each isobaric level were determined linearly from the intensity variations of the meson component registered by several ground-base devices

$$\Delta T_j = \sum_i A_{ij} \Delta I_i \quad (2)$$

Here ΔT is temperature variation of j -th isobaric level. ΔI is intensity variation of the i -th device. The coefficients A_{ij} were found by the method of least squares. The number of devices is as a rule limited to $i \leq 3$.

The present paper is aimed at establishing connection between the temperature variation ΔT and the intensity variation ΔI by using the temperature coefficient density technique developed by Dorman. To this end we divide the atmosphere into some number of isobaric levels n ; let inside each level the temperature variations be constant in magnitude, although vary in time. Then the relation (1) can

be reduced to the form

$$\Delta I^i(t) = \sum_{j=1}^n A_{ij} \Delta T_j, \quad (3)$$

where

$$A_{ij} = \int_{h_j}^{h_{j+1}} W^i(h) dh \quad (4)$$

Since the temperature coefficient densities are known for a large number of devices, the coefficients A_{ij} can be obtained in any set. And if we choose the number of devices equal to the number of isobaric levels, the system of equations (3)-(4) can be solved exactly relative to the temperature variations

$$\Delta T_j = \sum_i B_{ij} \Delta I^i \quad (5)$$

The relation (5) resembles by its form the model (2) used by Japanese authors, but the coefficients B_{ij} are easily expressed through the temperature coefficient densities

$$B_{ij} = A_{ij}^{-1} \quad (6)$$

To realize how much devices are actually needed on the Earth for predicting the temperature variation of the atmosphere profile with a reasonable accuracy, we have carried out concrete calculations for 10 isobaric levels and 10 devices. As the components we have taken: I_1 - mesons registered by a cubical telescope with a 10-cm lead absorber. I_2 - mesons observed by ionization chamber at the sea level. I_3 - mesons underground at a depth of 25 mwe. I_4 - slow mesons of energy 200-350 MeV. I_5 - I_{10} are mesons observed, respectively, underground at a depth of 55 mwe, at the sea level with $\text{Cos}\theta = 0.2$, at the sea level with $\text{Cos}\theta = 0.6$, underground at a depth of 55 mwe with $\text{Cos}\theta = 0.4$, at a depth of 25 mwe with $\text{Cos}\theta = 0.8$, at a depth of 55 mwe with $\text{Cos}\theta = 0.6$. Table I presents the values of the coefficients B_{ij} calculated for 10 isobaric levels in atmosphere from 0 to 1000 mb.

Table I
Values of the coefficients B_{ij}

0.872	0.577	-0.163	0.789	0.058	-0.026	-0.345	0.596	-1.096
-4.742	-2.376	0.63	-2.174	-9.191	0.075	0.834	0.295	4.33
-64.21	-43.40	11.21	-45.03	6.453	1.365	18.60	1.207	72.59
60.18	74.74	25.20	153.3	2.211	-3.665	-68.83	-3.998	-169.3
-12.21	15.37	-6.088	46.21	-1.534	-0.599	-20.06	-0.435	3.55
17.81	41.97	4.689	38.83	7.456	-2.198	-42.69	-1.44	-37.69
-35.02	-85.67	13.07	-254.9	-6.845	5.377	123.1	3.809	118.7
56.95	36.82	-8.23	40.74	-1.642	-1.237	-18.02	-1.261	-57.75
-0.553	-0.551	0.197	-1.767	-0.023	1.555	-0.399	1.026	1.169
-24.36	-13.16	3.013	13.56	1.298	-1.105	-15.28	0.353	20.44

We have varied the set of initial elements of the cosmic ray meson component. The calculation has shown that the matrix of the coefficients B_{ij} is rather sensitive to their choice. Moreover, the analysis of the results shows that if for the calculations of the atmospheric temperature variations the model (2) is used, the number of meson components, essentially exceeding 3, should be taken into account.

REFERENCES

1. Dorman L.I. Cosmic Ray Variations. M. Gostekhizdat, 1957, 492 p.
2. Miyazaki Y., Wada M. Proc. II-th ICRC, Budapest, 1969, v.2, p. 592.

High Sensitive X-Ray Films to Detect Electron Showers in 100 GeV Region

Taira, T., Shirai, T., Tateyama, N. and Torii, S.

(Kanagawa University, Kanagawa)

Nishimura, J., Fujii, M. and Yoshida, A.

(Institute of Space and Astronautical Science, Tokyo)

Aizu, H. and Nomura, Y.

(Kanagawa Prefectural J. College, Kanagawa)

Kazuno, M.

(Toho University, Chiba)

Kobayashi, T.

(Aoyama Gakuin University, Tokyo)

Nishio, A.

(Kyoto University, Kyoto)

ABSTRACT

Non-screen type X-ray films have been used in emulsion chamber experiments to detect high energy showers in cosmic rays. Ranges of the detection threshold is from about 1 to 2 TeV as depending on the exposure conditions. In order to improve this threshold, we have tested different types of X-ray films and sheets i.e. high sensitive screen type X-ray films (Fuji G8-RXO) and luminescence sheets (Fuji 'Imaging Plate'). For these, the threshold of the shower detection is found to be about 200 GeV, which is much lower than that of non-screen type X-ray films. These films are useful to detect showers in the medium energy range, a few hundred GeV, of the cosmic ray electrons¹⁾.

1. Introduction.

In emulsion chamber experiments, the detection of high energy electron showers is usually carried out by naked eye scanning on X-ray films. This reduces a lot of labour for microscope scanning of high energy showers. The detection threshold, if we use non-screen type films such as the Sakura N-type, is about 1 to 2 TeV as depending on the exposure conditions. In order to improve this threshold, we tested other types of X-ray films and sheets i.e. the screen type X-ray films (Fuji G8-RXO), and the luminescence sheets (Fuji 'Imaging Plate').

These photographic materials have been irradiated to the INS electron synchrotron beams to obtain the characteristic curves for the particle densities²⁾. The net optical density, D_n , of the RXO at the electron density of $10^6/\text{cm}^2$ has been confirmed to be about 10 times higher than that of the N-type. This result suggests that the detection threshold for G8-RXO is by a factor of 10 less than that of N-type. For 'Imaging Plate', the computer-aided laser beam scanning was performed for the measurements of D_n ³⁾.

These films and sheets have been also tested to detect electron showers in the emulsion chamber exposed at balloon altitude. By track counting of the observed showers in nuclear emulsions, the detection threshold of G8-RXO has been found to be around 200 GeV, which is consistent with results of the accelerator experiment.

2. Characteristic Curve of X-Ray Films and 'Imaging Plate'.

Several types of X-ray films (Sakura N type, Fuji #200 type and G8-RXO) and 'Imaging Plate' have been irradiated vertically to the 760 MeV electron beams. The setup of these materials is shown in Figure 1. The electron beam densities in this irradiation are covering from 6.7×10^4 to 2.7×10^6 /cm² at the center of the beams.

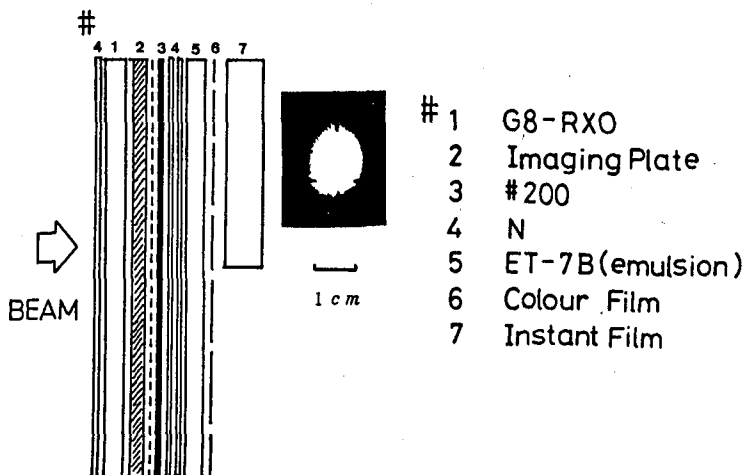


Fig.1 Setup of photographic materials.

The development times were 15 min., 20 min. and 25 min. for N-type and #200, and 10 min., 12 min., and 15 min. for RXO respectively, under the condition that Konidol developer was used at 20°C. After the development, the optical densities, D , on the films were measured with the microphotometer with the slit size of $200 \times 200 \mu\text{m}^2$. The electron densities were determined by the track counting in the emulsion plates. Figure 2 shows examples of the beam profiles on these films.

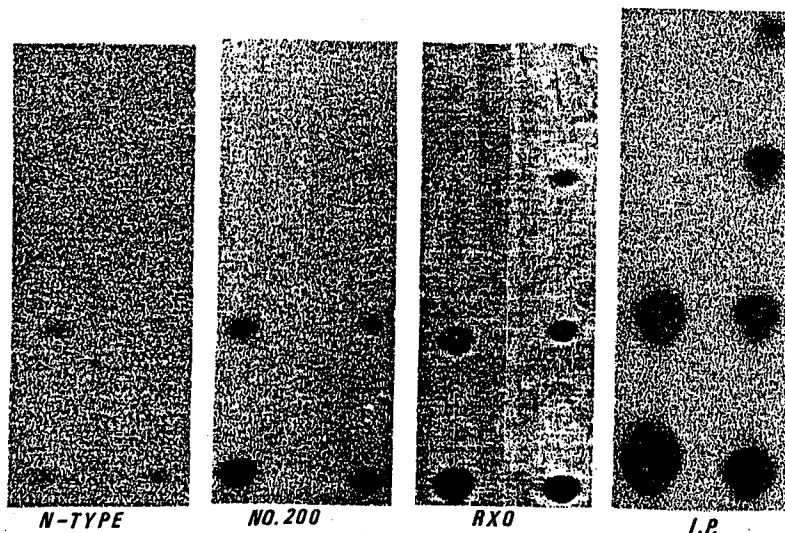


Fig.2 Beam profiles on different types of films are shown for comparison. Each black spot at the same relative position on a film corresponds to the same intensity of beam.

The characteristic curves for these films and sheets are shown in Figure 3. The data on N-type and #200 are those for the development time of 15 min. The D_n 's of N-type and #200 increase with development times, but the ratio of sensitivities of #200 to N-type remains constant, keeping the value of ~ 2.5 . The D_n of RXO, however, does not change with the development time. As shown in Figure 3, the characteristic curve for RXO shows a non-linear dependence on the electron density. This is due to the characteristics of the screen type X-ray films. As to 'Imaging Plate', the characteristic curve is derived after the computer processing. We can chose the most appropriate condition which is suitable for detecting the electron shower.

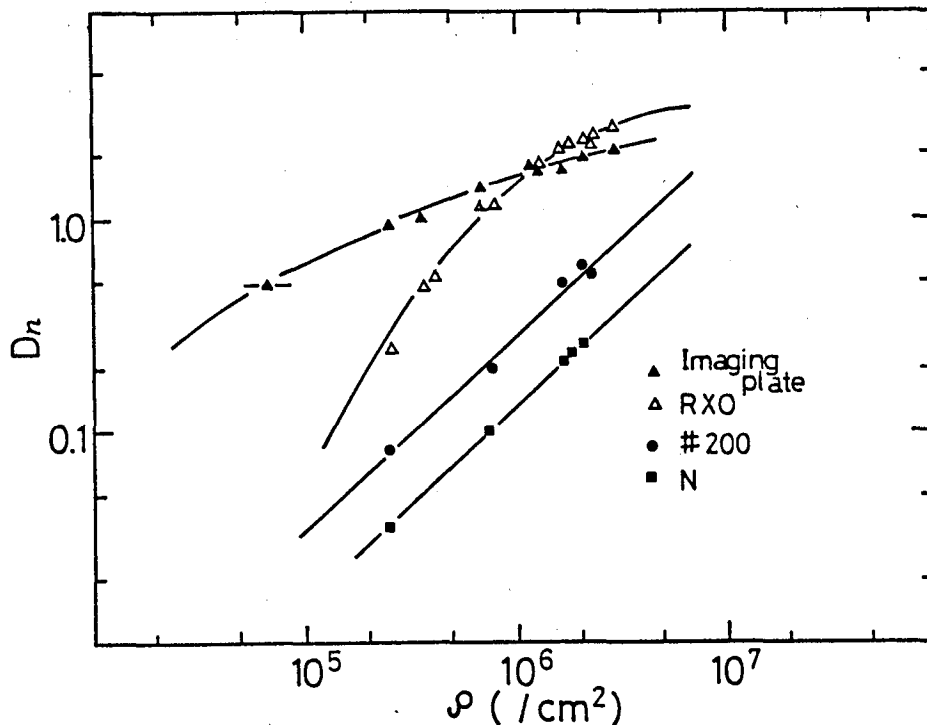


Fig.3 Characteristic curves of different types of films.

3. Discussion.

From the characteristic curves, we observe that the ratios of the sensitivities from N-type via, #200 and G8-RXO to 'Imaging Plate' are of 1:2.5:8:80 at the D_n of 0.1. This seems to indicate that the ratios of the detection threshold of electron showers are of 1:0.4:0.13:0.013 with respect to the foregoing ratios.

In actual case, however, the threshold is determined not only by sensitivity of the film, but also the signal to noise ratio of D , the noise in which is produced by the background tracks and chemical fogs. Fluctuations of the D due to background tracks depend on the number of grains developed by these tracks, and depend on the sensitivities and grain sizes of the films. Grain size in non-screen type X-ray films are larger than that in screen type X-ray films. The average area of grains in N-type and RXO are $16.5 \mu\text{m}^2$ and $4.8 \mu\text{m}^2$ respectively.

The sensitivity of each grain in N-type is high, and almost of all grains are developed when thin tracks penetrate through the grains. The sensitivity remains almost unchanged even for slow protons or electrons contained in the background tracks. This is the reason why non-screen type X-ray films have been used in the shower detection for long exposure experiment.

The screen type X-ray films have quite different characteristics. The sensitivity is almost proportional to the ionization loss of the penetrating particles. Thus screen type X-ray films and 'Imaging Plate' could be thought as the most effective in detecting showers for short exposure experiment such as the balloon's. Referring to these fact, we exposed the emulsion chamber with G8-RXO and 'Imaging Plate' at balloon altitude in September, 1984. The experiment was to observe the cosmic ray electrons at medium energy range of a few hundred GeV.

The detection threshold in this exposure has been made clear to be around 200 GeV. Detailed analysis has also been made for the fluctuations of the background D , and confirmed the detection threshold energy is around 200 GeV for this exposure by considering the signal to noise ratio of D . 'Imaging Plate' is much more sensitive than RXO, but as seen from the signal to noise ratio consideration, the threshold energy in this experiment is a little lower than the RXO's. We are now trying to find the most favorable condition for the computer-aided process of 'Imaging Plate' to get a lower threshold for the detection of electron showers.

Acknowledgements.

The authors would like to express their gratitude to Mr. Miyahara and his collaborators, Fuji Photo Film Co., Ltd., for extending every facility necessary for the test of 'Imaging Plate'. They are also indebted to the staffs of the electron synchrotron of the Institute for Nuclear Study, the University of Tokyo, for carrying out the irradiation of films to the electron beams.

References

1. Nishimura, J. et al.: Ap. J. 238 (1980) 394.
2. Ohta, I. et al., Nuclear Instrum. and Methods 161 (1979) 35.
3. Miyahara, J. et al., Journal of Luminescence 31 & 32 (1984) 266; RADIOLOGY 148 (1983) 833.

JETS IN AIR-JET FAMILY

NAVIA O., C.E. and SAWAYANAGI, K:
 Depto.RC, IFGW, Univ. Estad. Campinas
 Cx.Postal 6165, Campinas-13100-SP, BRAZIL

ABSTRACT

The A-jet families of the Brazil-Japan Collaboration on Chacaltaya Emulsion Chamber Experiments are analyzed by the study of jets which are reconstructed by a grouping procedure. It is demonstrated that large- E_{JR_J} events are characterized not only by small number of jets and two-jet like asymmetric shape, i.e. the binocular events, but also by the other type. This type has a larger number of jets and more symmetrical shape in the p_t plane.

INTRODUCTION

Event shape is examined by using the following two quantities;

- a) energy-weighted distance from the center of a family of reconstructed jet, $\overline{E_{JR_J}}$ (TeVcm),
 b) symmetry coefficient/1/ of jet, b_J , as defined

$$b_J = (\sum E_{Ji} Y_{Ji}^2)_{\min.} / (\sum E_{Ji} X_{Ji}^2)_{\max.}$$

The symmetry coefficient measures azimuthal symmetry, which will have a value of 0 for the case of in-line event and of 1 for the completely symmetrical azimuthal distribution. All the quantities with a letter of J are obtained after a grouping procedure to reconstruct jets. The energy weighted distance used is defined as $\chi_{ij} = R_{ij} E_i E_j / (E_i + E_j)$ and the cut-off value $\chi_c = 25$ TeVcm as usual. For this grouping procedure cascades with $E \geq 2$ TeV are used, γ -ray and hadronic components are treated equally and energies of hadronic cascades are used without correction of K_γ .

RESULT

To grasp gross features of the A-jet families, are used all the 218 A-jet families including hadron-rich and exotic events. After the jet-grouping, 215 events have more than one jet. Then $\overline{E_{JR_J}}$ and the symmetry coefficient are calculated for each event.

We can see from Fig.1 that $\overline{E_{JR_J}}$ distribution has a peak at around 20 TeVcm and a very long tail over 300 TeVcm. On the other hand the b_J distribution is almost flat with a sharp peak at around $b_J = 0$. This sharp peak should include the contributions of the binocular events/3/ and some excess

of the experimental ^{data} can be seen at b_J near to 1, comparing with the tendency of the Monte-Carlo simulation/1/. While we can see the correlation between b_J and $\overline{E_{JR_J}}$ exists, the dependence of b_J on $\overline{E_{JR_J}}$ is shown clearly in Fig.2, in which b_J distributions are given separately for three intervals of $\overline{E_{JR_J}}$. As increasing $\overline{E_{JR_J}}$ the fraction of $b_J=0$ is rising. It means that large $\overline{E_{JR_J}}$ is realized by two-jet like events, i.e. binocular-type events. We note that in spite of the very rapid decreasing of the fraction towards larger b_J 's there exist non-zero experimental data at b_J near to 1 even at the highest- $\overline{E_{JR_J}}$ group.

The correlation between number of jet N_J and $\overline{E_{JR_J}}$ as given in Fig.3 shows that larger $\overline{E_{JR_J}}$'s are shared by less number of jets. That is large $\overline{E_{JR_J}}$ region is occupied by binocular-type events. And also some events are found to have very large N_J even at the highest- $\overline{E_{JR_J}}$ group.

It may be concluded that there exist those A-jet families which have large and comparable $\overline{E_{JR_J}}$ with the binocular events, but which contain many jets so as to give rise to very symmetrical azimuthal distribution. The reconstructed jets with the use of the cut-off value $\chi_c=25$ TeVcm seem to have a jet-size less than the actual size of the two clumps, because the N_J distribution of the group $\overline{E_{JR_J}} \geq 80$ TeVcm has a rather broad peak between 2 and 10.

ACKNOWLEDGMENTS

The author acknowledges financial supports by the local committee of the 19th ICRC and by the Conselho Nacional de Desenvolvimento Científico e Tecnológico—CNPq in BRAZIL.

REFERENCES

- /1/ KRYS, A. et al., Proc. 17th ICRC(Paris, 1981), vol.11, p.187.
- /2/ SEMBA, H., Proc. Intern. Symp. on Cosmic Rays and Particle Physics, edit. OHSAWA, A. and YUDA, T., 1984, Inst. for Cosmic Ray Research, Univ. of Tokyo, p.211.
- /3/ LATTES, C.M.G. et al., Phys. Rep. 65(1980), p.151.

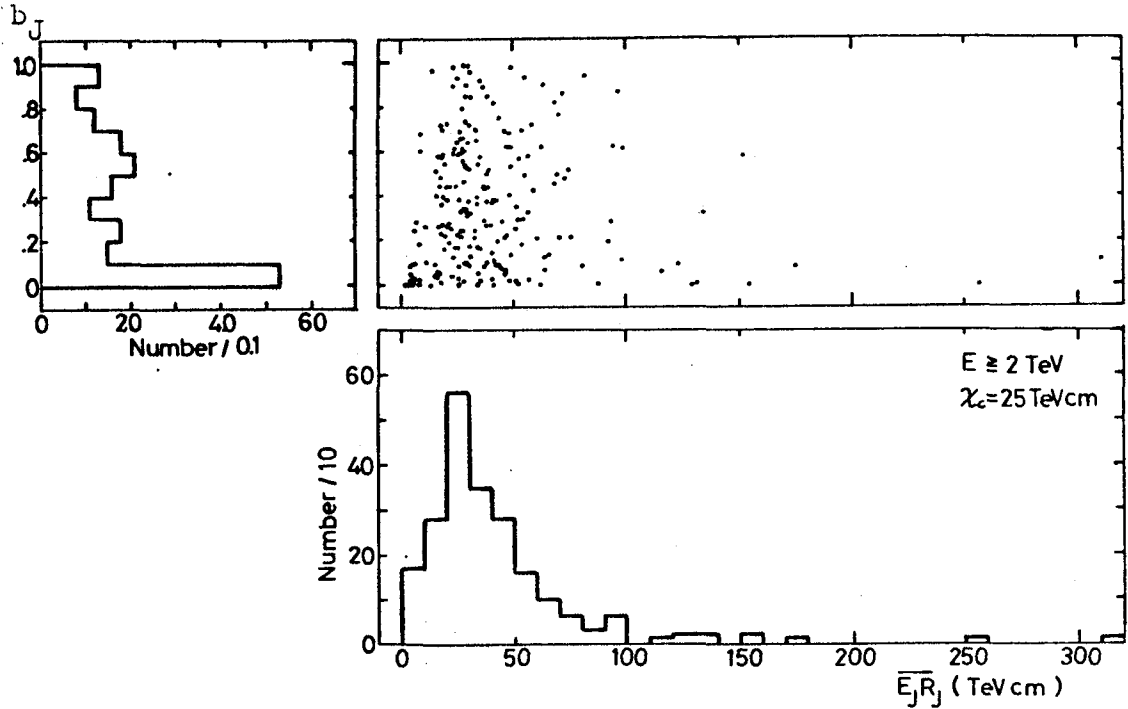


Fig. 1 The scatter plot of symmetry coefficient $b_j/1/$ of jet vs. $\overline{E_j R_j}$ of the A-jet families.

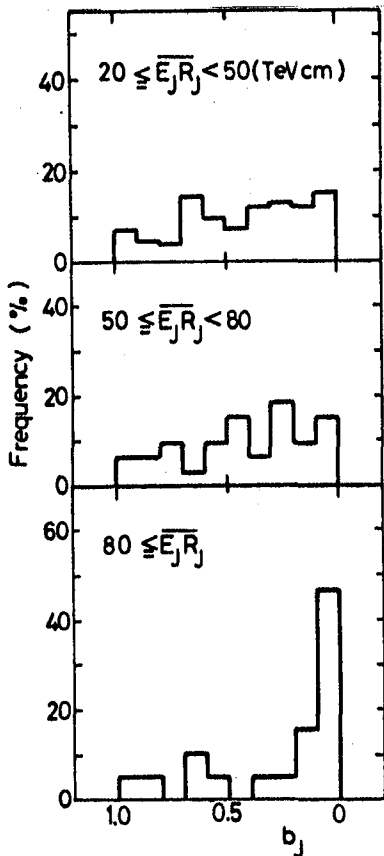


Fig. 2 The symmetry coefficient b_j distribution.

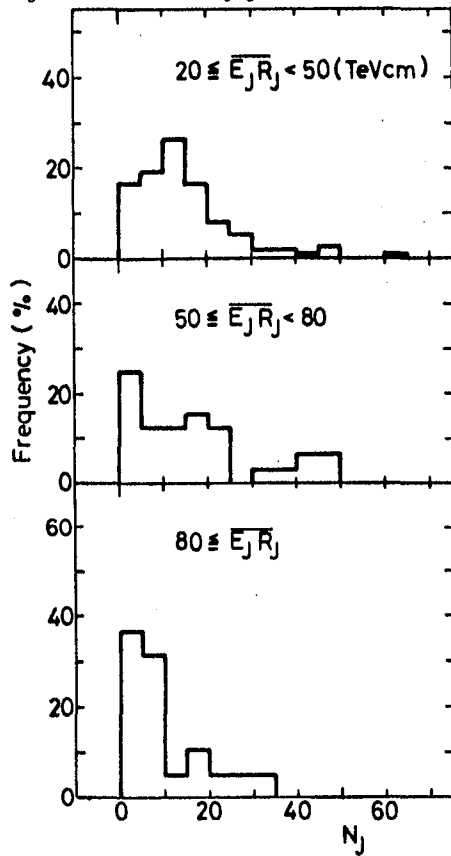


Fig. 3 The distribution of number of jet.

Search for Anomalous C-jets
in Chacaltaya Emulsion Chamber Experiment

H. Kumano

Science & Engineering Research Lab.,
Waseda University, Tokyo, Japan

Abstract

A search for anomalous C-jets is made in Chacaltaya emulsion chamber No.17 exposed by Brasil-Japan collaboration. Up to date, measurement of 150 C-jets (nuclear interactions occurred in the target layer in the chamber itself) with total visible energy greater than 5 TeV was completed. They are recorded in area of 11 m^2 , corresponding to $17.1 \text{ m}^2 \cdot \text{year}$ exposure.

Among them, 7 events has no pinpoint and two events are peculiar in that 3 showers out of 4 show abnormal cascade development. Especially, two of them show remarkable characters indicating that they are coming from exotic interactions in the target layer. We present here some illustrations of these events and short discussions on the threshold of this type of events.

1. Introduction.

After the discovery of exotic interactions such as Chiron, Centauro and so on, among cosmic-ray induced nuclear interactions by Brasil-Japan collaboration of Chacaltaya emulsion chamber experiment, there has been studied extensively about the detailed structure of these events through the observation of atmospheric interactions. /1/ But there are no reports so far that these types of events are found in CERN SPS experiment at energy region around 200 TeV in lab. system nearly equal to C-jet energy region. As to the multi-pion production phenomena, we can see good agreement between the two. /2/ It is therefore urgent question what is the threshold energy of these events. Recently, the systematic survey of C-jets is carried out on chamber No.19 (abbreviated as CH19 hereafter) partly to answer this question. And it is found that there exist some exotic events with $\Sigma E(\gamma)$ (sum of all visible energies) greater than 5 TeV. Present work is made to improve the statistics of exotic events in target interactions to give better understandings of the problem of exotic events.

2. Experimental Procedure.

C-jets recorded in the two-storeyed emulsion chamber No.17 exposed on the top of Mt.Chacaltaya are measured and partly re-analysed. Detailed description of the structure of the emulsion chamber and the method of observation is found elsewhere./2/,/3/

3 Result.

Up to date, 150 C-jets are accumulated from 55 blocks in CH17 corresponding $17.1 \text{ m}^2 \cdot \text{year}$ of exposure. In Fig.1 we present $\Sigma E\gamma$ spectrum with the straight line power of which is -1.7 . Fig.2 is the distribution of invariant masses of every possible pair of gamma rays from 78 newly measured events. The peak of pinaught is clearly seen which assures the accuracy of energy measurement. Fig.3 is the scattered diagram of observed showers of 120 events with multiplicity greater than 4. These figures show that the present measurement of C-jets is carried out without severe systematic errors.

Among 150 events, there are 7 pinaught-less events, i.e., there is no pair of showers whose invariant mass falls into pinaught region ($100 - 170 \text{ MeV}$). In addition, two events show peculiar behavior indicating that constituent showers of these events are not simple gamma-ray originated showers. In table 1 these 9 events are summarized.

Among them, two-prong events with invariant mass about 4 or 5 hundreds of MeV can be interpreted as the result of fluctuation of normal multiple meson production. The remaining events are highly probable candidates of non-pion interactions. Two events are illustrated here in detail. One is the event 17-151-3, which consists of 4 showers with energy 2.6, 1.3, 1.5 and 1.3 TeV, respectively. Careful search for another lower energy showers were in vain. Invariant masses are shown in Fig.4 with target map of the event. Numerical values in brackets are energies of showers. The constituent showers in this event have no partner to make up pinaught. Further, shower No.1 and 2 are not observed in 3 c.u. layer and shower No.2 shows abnormal development of track numbers in transition as well as shower No.4. Therefore, only No.3 can be considered as gamma-ray shower. In addition, transverse momenta of these showers are very large compared with the average ones $\sim 200 \text{ MeV}$. Sum of transverse momenta, $p_T(\gamma)$, of the four is $2.0 \text{ GeV}/c$ which gives $500 \text{ MeV}/c$ as the average.

The other event 17-135-A is also shown in Fig.5, as in the same way in the former event. Shower No.1 has multi-core structure from 4 c.u. layer down to the last layer 12 c.u. peculiar to Pb-jet in the lower chamber (local nuclear interaction in the lower chamber). No.2 has two maxima in transition of track numbers. No.4 has only 12 tracks within the circle with radius $25 \mu\text{m}$ at 5c.u. and then develops and attenuate abruptly. No.3 has also double maxima in transition, but rather smooth fitting to the calculated curve can be made. Consequently only No.3 can be interpreted as gamma ray originated shower as in the former event. As well as the event 17-151-3, transverse momentum of showers in this event as large as $0.38 \text{ GeV}/c$ on the average which value of transverse momentum is close to that of Mini-Centauro event observed by atmospheric interactions.

4. Discussions.

Preliminary comparison with Monte-Carlo simulation tells us that above two events can not be seen in the artificial events so far which reproduce well the over-all feature of multiple meson production phenomena observed in C-jets. It is highly probable that several events found by the present analysis are coming from the same origin as the exotic events found in the atmospheric interactions. Frequency of these anomalous events is the same as in the result of the analysis of CH19 as a first approximation, several percent of the whole events.

If we assume that gamma-ray inelasticity of these showers are usual one (average is about $1/4 \sim 1/3$) and all showers are from the local nuclear interactions in the lower chamber itself, average energy of parent particles producing these events is estimated as about 100 TeV which is within the limit of accelerator experiment. This seems to be a contradiction, which might be a fringe of the secrets of the nature.

Acknowledgement

The author expresses the sincere gratitude to all the members of Brasil-Japan collaboration of Chacaltaya emulsion chamber experiment for encouragement and offering him the data.

References

1. Brasil-Japan collaboration; Proc. of Workshop on Cosmic Ray Interactions High Energy Results, La Pas Rio de Janeiro (1982) 319.
2. Brasil-Japan collaboration; Supplement of Progress of Theoretical Physics, 1, and H. Kumano; *ibid*, 51.
3. Brasil-Japan collaboration; this issue, HE 3.2-6.

Table 1. List of Events

Event name	No. of showers	$\Sigma E(\gamma)$ (TeV)	Remarks
17-89-2	5	8.00	Non pinaught
17-93-2	3	7.32	Non pinaught
17-116-3	2	6.90	Non pinaught, 560 MeV
17-122-14	2	5.55	Non pinaught, 519 MeV
17-140-C	2	5.60	Non pinaught, 559 MeV
17-144-24	2	> 6.9	Non pinaught, > 484 MeV One shower is pb-jet lower ($\Delta t=8.3$)
17-151-3	4	6.70	Non pinaught, See text
17-135-A	4	5.65	See text, at most one gamma ray
17-135-B	4	7.26	At most one gamma ray

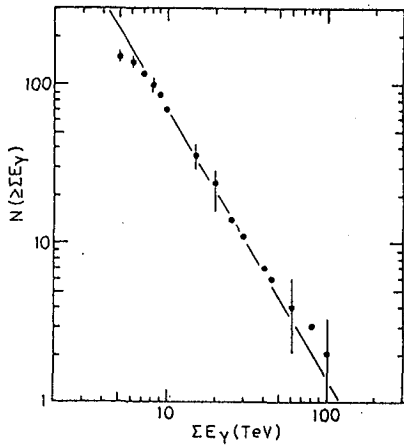


Fig. 1 $\Sigma E(\gamma)$ Spectrum

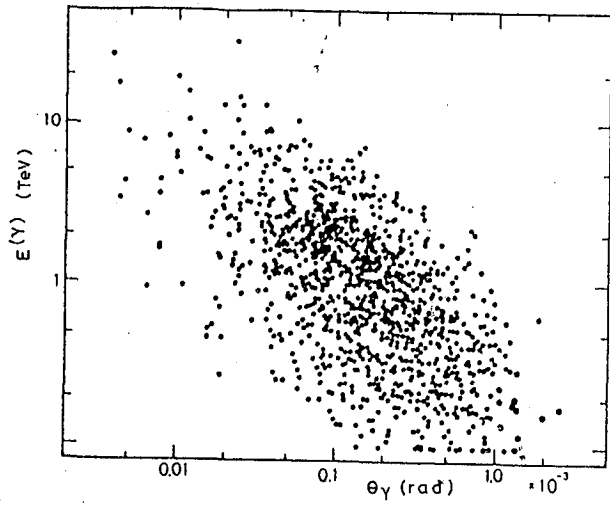


Fig. 3 $\Sigma E(\gamma) - \theta_\gamma$ correlation

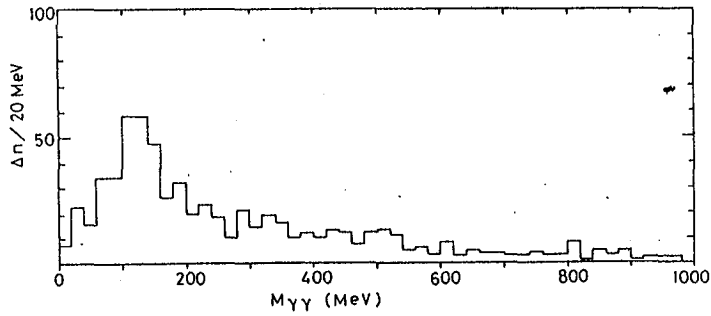


Fig. 2 Invariant mass spectrum

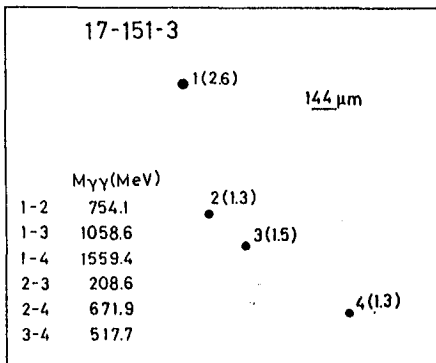


Fig. 4 Target map

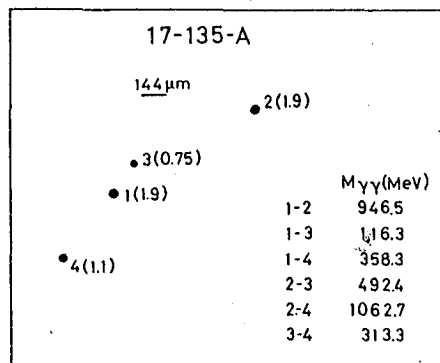


Fig. 5 Target map

Exotic Interactions among C-jets and Pb-jets
 Brasil-Japan Emulsion Chamber Collaboration

ABSTRACT

Systematic survey of C-jets and Pb-jets is carried out on the part of Chacaltaya Emulsion Chamber No.19 amounting to an exposure of 28.8 m²yr. 198 C-jets with two or more constituent shower cores and with $\Sigma E_{\gamma} \geq 5$ TeV are adopted and analysed. It is shown that the adopted events make up an unbiased sample of C-jets for $\Sigma E_{\gamma} \geq 7$ TeV. Among the adopted events, 16 are found to be pinaught-less. Fluctuation of ordinary multi-pion production can account for only a small fraction of them. Mini-Centauro interaction gives the most natural explanation for the eight pinaught-less C-jets with three or more constituent shower core. Out of the eight double-cored pinaught-less events, three are found to have visible invariant masses > 1.8 GeV/c, which strongly reminds us of the event "Castor-Pollux", the first clear example of a Geminion interaction.

In addition, three Pb-jets-lower are found to be composed of double cores whose respective visible transverse momenta are greater than 0.5 GeV/c, suggesting that they are of Geminion origin or chiron origin.

The energies of the parent particles are estimated to be 100 to 200 TeV for all the above-mentioned three kinds of events.

Discussions are made on the implications of this energy estimate and of the frequency of observed exotic events.

1. Introduction.

In mountain emulsion chamber experiments, several types of exotic nuclear interactions have been found among A-jets, i.e., nuclear interactions occurring in the atmosphere above the chamber/1/2/. The decisive characteristics common to all these exotic interactions are follows:

- (i) they produce secondary particles with unusually large transverse momenta.
- (ii) they are "pinaught-sterile", i.e., they produce practically no pinaught.

Some of the above-mentioned exotic interactions were expected to occur at the CERN \bar{p} -p collider, but the search met with no success.

The present work is the report on a least biased systematic survey of the local nuclear interactions occurring within the emulsion chamber, aiming at making a guess on the threshold energy for the exotic interactions.

2. Experimental Procedure.

C-jets and Pb-jets-lower recorded in the two-storeyed Chacaltaya Emulsion Chamber No.19 are detected and analysed. The chamber consists of the upper chamber (area 44m², thickness 6cmPb), nuclear interaction producer (area 44m², thickness 23 cm asphalt), air gap(1.5m) and the lower chamber (area 33m², thickness 7cmPb). C-jets and Pb-jets-lower are the local nuclear interactions occurring in the producer and in the lower chamber, respectively. The chamber contains nuclear plates and N-type X-ray films under 1.5cm, 2cm, 2.5cm, 3cm, 4cm and 6cm of Pb. It was exposed for 667 days to cosmic rays at Chacaltaya(540 gr/cm²). It is worth remarking that all the nuclear plates maintained excellent and uniform level of sensitivity even after this long exposure. 16m² of the lower chamber has been used in the

present work, which amounts to the exposure $28.8 \text{ m}^2\text{yr}$.

Scanning of C-jets and Pb-jets-lower are made in the same way as the previous works, and so is the energy measurement of their constituent showers/4/.

An electron shower satisfying one of the following criteria is identified as of a hadronic origin:

- (i) It becomes observable only in greater depths, typically under at least 6 c.u.
- (ii) The change with depth of electron number deviates significantly from that of a pure electron-photon cascade shower.
- (iii) Clear multi-core structure is observed and traced at two or more successive layers.

3. Quality of Experimental Data

215 C-jets with $n \geq 2$ are found, where n denotes the number of constituent showers. Out of them 198 have visible energy $\Sigma E \geq 5 \text{ TeV}$, of which 155 are isolated and 43 are accompanied by γ -hadron families (i.e., bundle of parallel γ -rays and hadrons). These 198 events are adopted and used for analysis.

The 145 C-jets with $n \geq 2$ and $\Sigma E_{\gamma} \geq 7 \text{ TeV}$ yield quite consistent and reasonable results for ΣE_{γ} -distribution, the zenith angle distribution and the vertical flux. This shows that the event detection has been made in the way free from any serious biases.

As for constituent showers, the detection efficiency turns out to be nearly uniform down to $E_{\gamma} \approx 0.2$ to 0.3 and up to $r = 1.5$ to 2.0 mm . Also the invariant mass distribution of all possible γ -ray pairs has quite a reasonable shape. This shows, firstly, that the present experimental method is free from any serious systematic errors and, secondly, that the overwhelming part of the C-jets in the present experiment are due to ordinary multi-hadron production.

4. Morphology of Pinaught-less C-jets

Eight events with $n=2$ and another eight with $n \geq 3$ are found to be "pinaught-less", i.e., every pair out of the constituent showers either has visible invariant mass $M(ij) > 200 \text{ MeV}/c$, or contains at least one identified Pb-jet-lower.

As ΣE_{γ} of all the above 16 events are rather small ($< 30 \text{ TeV}$), the question arises whether they are accounted for as the fluctuation tail of usual C-jets. In order to answer the question, simulation C-jets are constructed and compared with experiment. 200 Mirim-type C-jets (scaling multi-pion production via H-quanta) and 200 Acu-type C-jets (scale-breaking multi-hadron production via SH-quanta) are constructed. The rest masses of an H-quantum and an SH-quantum are assumed to be $2.3 \text{ GeV}/c^2$ and $18 \text{ GeV}/c^2$, respectively. For simplicity, SH-quanta are assumed to decay exclusively into pions in the present simulation.

Fig. 1 shows the E_1/E_2 vs. n plot of the observed and the simulated pinaught-less events, where E_1 and E_2 stand for the highest and the second highest, respectively, energies of the constituent showers.

Firstly one observes that the simulation produce only $n=2$ and $n=3$ events, while about one-third of the observed events have $n \geq 4$.

Secondly, only two Mirim-type C-jets (one double-cored and the other triple-cored), out of the 18 simulated pinaught-less events, are observed to reproduce the experiment. The remaining 16 yield E_1/E_2 far too large to be reconciled with experiment.

The conclusion is that a minor part of pinaught-less C-jets might represent the fluctuation tail of Mirim-type ordinary C-jets, but that the main part is of genuinely different origin.

5. Nature of $n \geq 3$ Pinaught-less C-jets

Fig. 2 shows the superposed integral $p_T(\gamma)$ -distribution of the constituent showers of the eight pinaught-less C-jets with $n \geq 3$, where $p_T(\gamma)$ denotes the observed part of the shower transverse momentum with respect to the respective energy-weighted center of each event. Also shown in the figure by a solid line is the same distribution of Event Centauro I. Both agree well with each other, giving

$$\langle p_T(\gamma) \rangle = 0.35 \pm 0.05 \text{ GeV}/c,$$

which, at the same time, coincides with that of Mini-Centauro interactions.

Fig. 3 shows the superposed fractional energy distribution of the constituent showers of the same eight events in an integral form. It fits well with an exponential form, and extrapolation down to zero energy gives

$$\langle m \rangle = 6 \pm 1 / \text{event},$$

as the average observed multiplicity of cores.

Now let us assume that the events are due to bundle of non-rapid-gamma-decaying hadrons having the same nuclear mean free path as nucleons. Then the correction for escaping hadrons gives

$$\langle m_0 \rangle = 18 \pm 3$$

as the average multiplicity of hadrons produced in the parent interaction. Again this is in good agreement with

$$\langle m_0 \rangle = 15 \text{ to } 20$$

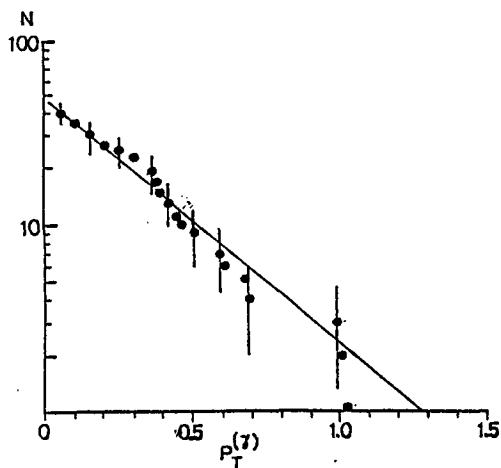


Fig. 2. Integral $p_T(\gamma)$ -distribution.

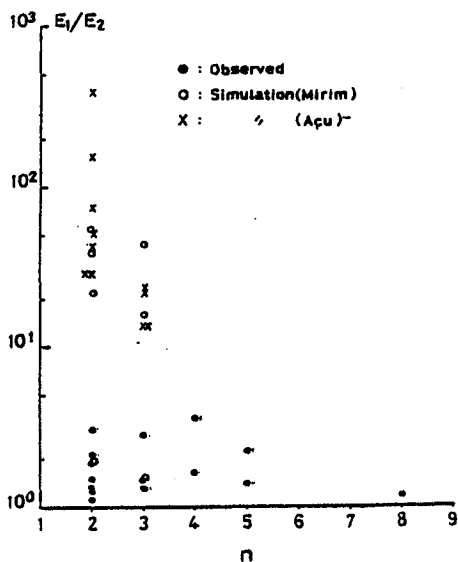


Fig. 1. E_1/E_2 vs. n plot

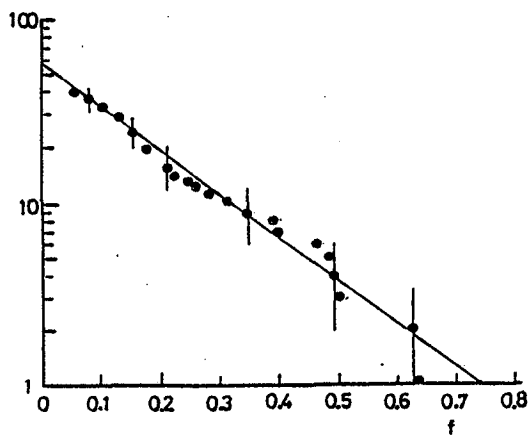


Fig. 3. Fractional energy distribution in the integral form.

of the Mini-Centauro interaction.

In view of the above results for $\langle p_T(\gamma) \rangle$ and $\langle m_0 \rangle$, the Mini-Centauro interaction seems to be the most natural explanation of the pinaught-less C-jets with $n \geq 3$.

Now the average energy of the parent particle responsible to these C-jets, $\langle E_0 \rangle$, is estimated by $\langle E_0 \rangle = \langle \Sigma E_h(\gamma) \rangle / (\langle K \rangle \langle f \rangle \langle k_\gamma \rangle)$, where $\langle E_h(\gamma) \rangle$ is the average observed energy sum of the hadron bundle, $\langle K \rangle$ the average inelasticity at a Mini-Centauro interaction, $\langle f \rangle$ the energy fraction of the released energy given to the detected hadrons, and $\langle k_\gamma \rangle$ the average fraction of the energy released to γ -rays at a successive interaction in Pb. Assumption $\langle K \rangle \sim 1/2$, $\langle f \rangle = 1/3$ to 1, $\langle k_\gamma \rangle = 1/5$ to $1/4$ yields

$\langle E_0 \rangle \approx 100$ to 400 TeV.

6. Double-cored Pinaught-less C-jets.

Out of the eight double-cored pinaught-less C-jets, three has striking features. The constituent shower-core pairs yield quite large visible invariant masses, $M(1-2)$: 3.3 GeV/c², 1.85 GeV/c² and 2.9 GeV/c². They strongly remind us of the Geminions, whose first clear example is the "Castor-Pollux" with $M(1-2)=5.8$ GeV/c². The event with $M(1-2)=3.3$ GeV/c² has still another striking feature. Its constituent showers originate from a point in the air gap, indicating a decay of some unknown matter.

Now, the assumption that the constituent showers are due to ordinary hadrons gives an estimate $\langle E_0 \rangle \approx 100$ to 200 TeV. The remaining five events have $M(1-2)$ falling between 0.2 GeV/c² and 1.0 GeV/c², and can be explained either as the fluctuation of Mini-Centauros or as that of Mirim-type C-jets.

7. Pb-jets-lower with High- p_T Double Cores.

Three Pb-jets-lower are found to be composed of two shower cores whose mutual opening angles are large enough to be measured. Their $M(1-2)$ are 3.3 GeV/c², 2.77 GeV/c² and 1.1 GeV/c². They again strongly remind us of Geminions. Here also the "ordinary hadron assumption" gives an estimate $\langle E_0 \rangle \sim 100$ TeV.

8. Summary and Discussions.

- 1) A least-biased systematic study of C-jets is made in Chacaltaya Emulsion Chamber No.19. It is found out that 5-10 % of the C-jets with $\Sigma E_\gamma \geq 5$ TeV are genuine exotic events. This corresponds to an estimated incident frequency of ~ 1 exotic-interactable particle per m²yr at Chacaltaya.
- 2) Average energy of the parent particles responsible to the above exotic events are estimated to be 100 to 200 TeV, irrespective of types.
- 3) If a nuclear collision of ordinary hadrons can produce an exotic interaction directly, either the versioned-up CERN SPS Collider or the coming FNAL TEVATRON must produce one.
- 4) On the other hand, if we assume that only the secondary particles from a chiron interaction can produce exotic interactions/3/, the upper bound of the threshold energy for chiron production will be estimated, from flux consideration, as $E_0 \sim 10^{16}$ eV.

References

1. C.M.G.Lattes, Y.Fujimoto and S.Hasegawa: Phys. Rep. 65 No.3('80),p151.
2. S.Hasegawa: Proc. Intern. Symp. on Cosmic Rays and Particle Physics, 1984, Tokyo, p.319.
3. S.Hasegawa: ibid., p.718.
4. Brasil-Japan Emulsion Chamber Collaboration: ICR-Report-91-81-7, Institute for Cosmic Ray Research, Univ. of Tokyo, 1981.

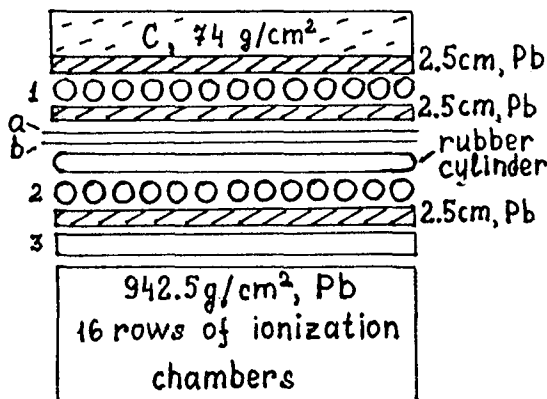
X-RAY FILM CHAMBER WITH CARBON TARGET
OF TIEN-SHAN COMPLEX ARRAY

K.V.Cherdyntseva, A.P.Chubenko, A.G.Dubovy,
N.P.Krutikova, N.M.Nesterova, S.I.Nikolsky,
N.M.Nikolskaja, E.I.Tukish, N.G.Vildanov,
T.I.Yakovleva

P.N.Lebedev Physical Institute
Moscow, USSR

The experiment was carried out at Tien-Shan highmountain station. X-ray films were exposed inside the ionization calorimeter under 74g/cm^2 of carbon and 5 cm of lead. The X-ray film chamber area is 36 m^2 . To perform more reliable time selection of events in this experiment moving X-ray films have been used. 50% of events, in which we succeeded to determine incidence time, were identified with corresponding EAS. For such events the size spectrum of associated EAS was derived. Two methods of energy measurement using X-ray films (E_x^g) and ionization calorimeter (E_{jet}^g) have been compared. We obtained that $E_x^g/E_{\text{jet}}^g = 0.95$. In this work the plot is presented to illustrate energy transfer from selected hadron to electromagnetic component. We find cascades with high energy release into electromagnetic component and in which the hadron component is practically absent.

The experiment was carried out at Tien-Shan highmountain station /1/. The complex array included the big ionization calorimeter (BIC), the scintillation set for the size shower (N_e) determination with $N_e \geq 5 \cdot 10^4$, the central hodoscope for the size shower determination with $N_e < 5 \cdot 10^4$, the chronotron for the arrival angles detecting of EAS etc. The big ionization calorimeter consists of the 19 rows of ionization chambers, its thickness is 1040 g/cm^2 . The area of calorimeter is 36 m^2 . The dead time of recording system of EAS data including calorimeter data was 17.5%. The BIC construction with the X-ray film chamber (X-chamber) is shown in Fig.1. Time selection of the events found in the X-chamber was performed. For this purpose the upper layer of the X-ray film was moved on several centimetres along the lower layer and a special time mark was put on the upper layer. When an electromagnetic cascade (EMC) crosses the both layers of the X-ray film, it marks them. Putting then together the two dark spots formed by the same EMC we can find the upper layer shift value along the lower layer. The inci-



- 1,2,3-the ionization chambers
 a-upper moving layer of X-ray films
 b-lower moveless layer of X-ray films

Fig.1. Construction of BIC with X-ray films (side view).

dence time was determined by the shift value. The accuracy of incidence time determination is several days in our experiment.

Every day the ionization calorimeter was stopped for several hours for the purpose of the maintenance and checks. To correlate the running time of X-chamber and ionization calorimeter EMC were not recorded on the X-ray films when calorimeter stopped running. That has been made as follows.

As one can see in Fig.1 the rubber cylinders were placed under the X-ray films. They had been pumped up to some surplus pressure, that caused the close contact between X-ray films and the lead plates. If the cylinders were not pumped up, air clearance was formed between the X-ray films and the lead. The EMC electrons

are dispersed in the clearance and the marks did not arise.

The ionization calorimeter and the X-chamber run together for 2600 hours. The handled area of the X-ray films is 18.8 m^2 . We have determined incidence time at 300 events which have been found in the X-chamber. 50% of these events have been combined with corresponding EAS. Some results of 150-event analysis are presented in this paper.

The X-ray films have been handled by the method used in the Pamir experiment /2/. The energy of EMC has been determined by means of theoretical curves calculated for primary photon /3/.

The EAS size (N_e) was obtained by scintillation counter data for $N_e \geq 5 \cdot 10^4$. The size of small EAS was determined by hodoscope data according to the following expression

$$N_e \approx 10^3 \frac{K(\theta)}{C_0} \ln\left(\frac{n}{n-m}\right),$$

where C_0 -the hodoscope channel area, $K(\theta)$ -a coefficient depending on the arrival angle of EAS, n - the total number of channels, m -the number of fired channels.

The ionization calorimeter data have been handled as follows. The jet corresponding to the event found in the X-chamber have been separated in the ionization calorimeter. For these jets the energy E_{jet} and the energy E_{jet}^0 transferred into first electromagnetic peak have been calculated.

Two methods of the EMC energy measurement using the X-ray films (E_x^0) and using ionization calorimeter (E_{jet}^0) have been compared. For this purpose the hadron jets satisfying the following criteria have been selected:

HE 3.2-7

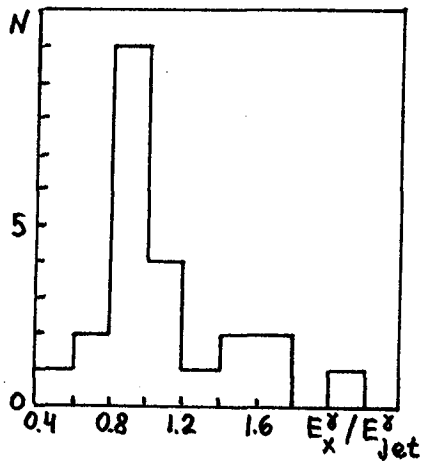


Fig.2.

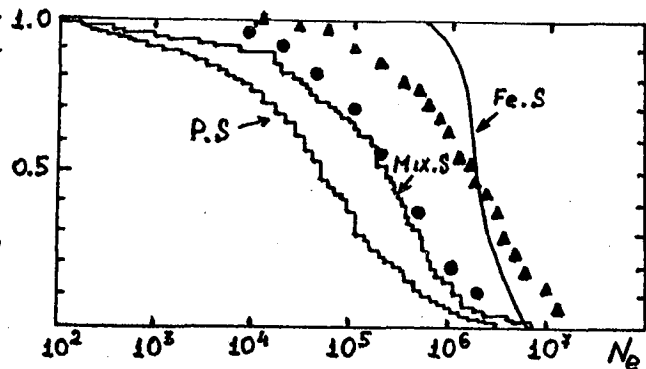
1. The ionization in the first row chambers is less than that in the second row chambers of the calorimeter. This condition selects the events with a small contribution to the ionization from the cascades caused by low energy particles of EAS.
2. The energy, transferred into the first electromagnetic peak is about half part of the jet total energy. This condition allows us to escape the influence of the secondary interaction in the lead on the determination of the EM peak energy.
3. The shape of experimental electromagnetic peak is close to that of calculating curve for primary photon /4/. There are no obvious

secondary interactions.

The 23 events satisfying these conditions have been selected. The ratio of the energy determined by X-chamber (E_x^γ) to the energy determined by the calorimeter (E_{jet}^γ) is presented in Fig.2. The mean value of this ratio is 0.95. According to these data one can say that there is quite good agreement of these two methods of the energy measurement.

The shower size spectrum of associated EAS was derived on the basis of the obtained data. Similar distribution has been obtained in the work performed at the Norikura mountain /5/. Comparison of the results is presented in Fig.3. The shower size of our experiment does agree with the simulation for Mixed primary mass composition and the scaling model /5/ and differs from the Norikura experimental result.

Fig.4 shows the $E_{jet}^\gamma - E_{jet}$ plot for our combined events. We find 16 cascades with high energy release into electromagnetic component and in which the hadron component is practically absent, that is $E_{jet}^\gamma \approx E_{jet}$. Out of them 8 events had equal EMC energies determined by means of both



- Δ - $\Sigma E_{\gamma,H} \geq 10\text{TeV}$, $n_{\gamma,H} \geq 1$, Norikura/5/
- simulation, S implies a scaling model /5/
- \bullet - $\Sigma E_x^\gamma \geq 10\text{TeV}$, $n_x^\gamma \geq 1$, our experiment

Fig.3. Normalized integral size spectrum of showers combined with γ, H -families ($\Sigma E_x^\gamma \geq 10\text{TeV}$).

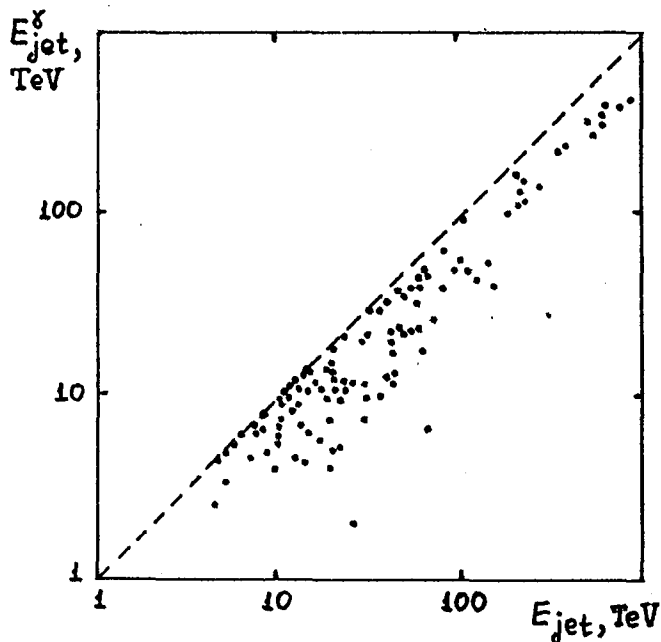


Fig. 4.

HE 3.2-7

the X-ray film and the ionization calorimeter (Table 1) that is in these events the hadron energy is transferred most likely into one or two electromagnetic particles mainly. To make the definite conclusion it is necessary to estimate the probability of such events in similar experiments.

Table 1.

No.	$\Sigma E_x^\gamma, \text{TeV}$	$E_{jet}^\gamma, \text{TeV}$	E_{jet}, TeV	n_x^γ	N_e
1	8.4	9.8	10.4	1	$1.6 \cdot 10^4$
2	83.3	87.2	91.7	2	$6.3 \cdot 10^4$
3	8.1	4.7	4.9	1	$2.9 \cdot 10^3$
4	6.4	7.1	8.1	2	unknown
5	9.8	10.9	11.3	2	$4.4 \cdot 10^4$
6	9.2	4.3	4.4	1	$1.8 \cdot 10^5$
7	5.5	6.3	6.5	1	$3.7 \cdot 10^4$
8	2.9	3.3	3.4	1	$1.8 \cdot 10^4$

References

1. Erlykin A.D., Nesterova N.M. et al., (1965), Proc. 9th ICRC, London, 2, 731.
2. "Pamir" coll., (1984), Trudy FIAN, 154, p. 14-27
3. Belyaev A.A., Ivanenko I.P. et al., (1980), Electron-photon cascades in cosmic rays at superhigh energies, Nauka, Moscow (in russian), p. 197.
4. Ivanenko I.P., Samosudov B.E., (1967), Yad. phys., 5, 622.
5. Nakatsuka T., Nishikawa K., Saito T. et al., (1983), Proc. 18th ICRC, Bangalore, 11, 346.

SCALING VIOLATION IN HADRON-NUCLEUS
INTERACTION

Yu.G.Verbitski, L.P.Garsevanishvili, D.M.Kotlyarevski, N.K.Ladaria, N.G.Tatalashvili, P.V.Tso-maya, N.I.Sherer, Yu.M.Shabel'ski, G.Z.Stemanetyan

Institute of Physics, Academy of Sciences of the
Georgian SSR, Tbilisi, USSR

Summary. The scaling violation within the pionization region in the energy range of 0.2 - 2.0 TeV is shown on the basis of the analysis of angular characteristics in the interactions of the cosmic radiation hadrons with the nuclei of various substances (CH₂, Al, Cu, Pb).

The investigation of multiple processes in hadron-nucleus interactions allows to obtain the information on the space-time structure of strong interactions.

It is rather paradoxical, but at present, the so called soft processes of particle generation making the overwhelming contribution to the inelastic interaction cross-section, remain the most obscure.

The most natural method to the understanding of the structure of such interactions is the investigation of hadron-nucleus interactions at high energies using nuclei of various atomic numbers A.

The experimental data presented in this work have been obtained at Chikovani Tskhra-Tskaro Station at the height of 2500 m above the sea level by means of the installation consisting of the magnetic spark spectrometer and the ionization calorimeter /1/.

The targets of Al, CH₂, Cu, Pb with the thickness of 0.1 λ int. were exposed. Some interesting results have been obtained in the energy region of 0.1 + 5.0 TeV using the data of several thousand of events.

Here the results of the investigation of interactions with the energy above 0.9 TeV are presented. The selected events have been generated, mainly, by primary protons which have had passed through the atmosphere without any interactions. That condition has been achieved by means of selection of showers without of other particles accompanying ($N_{acc} \leq 0.3/m^2 /6/$).

The aim of the present investigation is to reveal the dominating mechanism of the secondary particle generation. In the present paper the experimental data are analyzed with respect to the variable $\chi^2 = -\ln \text{tg } \Theta_{pr}/2$, where Θ_{pr} is the projection of the secondary particle escape angle on the photography plane.

The experimental data have been corrected for the efficiency of secondary particle recording in wide-gap spark

chambers (depending on the track direction with respect to the electric field) and for the conversion of γ -quanta due to π^0 -meson decay /7,8/. The resolution of the apparatus does not allow us to make some definite conclusions on the particles generated within the angle interval narrower than 0.1° (i.e. at $\eta' > 6.5$). The experimental distributions given in Fig.1 take into account the corrections over the whole rapidity region excluding ($0^\circ \pm 0.1^\circ$) where the uncertainty in the estimations may be significant.

The experimental distributions have been compared with the predictions of additive quark model /9/. According to the latter, the component interact independently with the cross-section equal to 1/3 of nucleon-nucleon one, while the generated objects do not interact within the nucleus. In addition, the comparison has been made with the active leader model, according to which the leading object interacts with nucleons, while the newly-generated particles do not interact in the nucleus: as it follows from Fig.1, a considerable discrepancy with the experimental data takes place. To achieve the agreement of theoretical predictions with the experimental data, one may: assume 1) a significant violation of scaling laws within the fragmentation region or a significant decrease of the cross-section of secondary interactions of the leading object (quarks, diquarks) with the nucleons in the nucleus; and 2) take into account the cascade of particles generated in the nucleus, which is, apparently, growing with increasing E. Table and Fig.2 present the data on the extent of the scaling violation increasing with the growth of A within the pionization region in hadron-hadron and hadron-nucleus interactions.

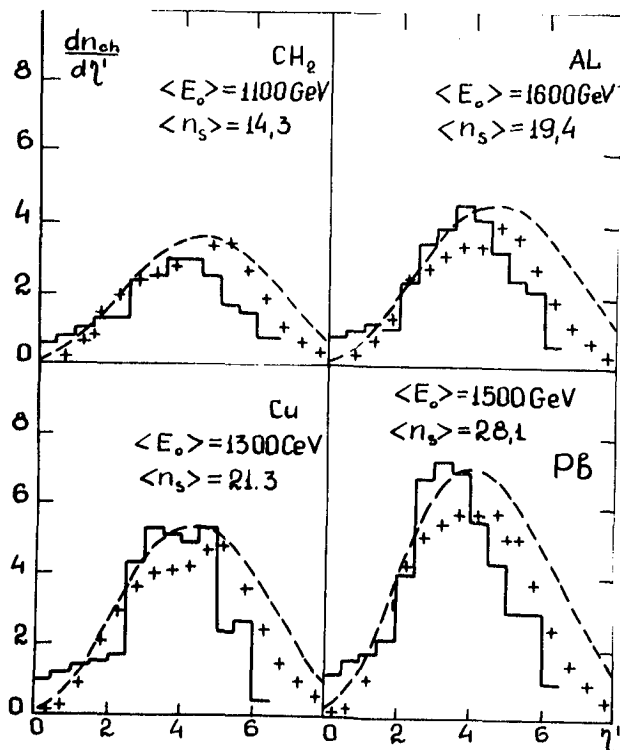


Fig.1 Inclusive distributions over η' of secondary particles in hadron-hadron interactions. The histogram corresponds to the corrected data (see the text). Dotted line - the active leader model. Crosses-additive quark model with the shifts in distribution due to the errors in the determination of the primary particle direction, introduced by means of Monte-Carlo method.

Reaction	Δn_s in the interval in the vicinity of		$R = \frac{\Delta n_s(2.0)}{\Delta n_s(0.2)}$
	0.2 TeV	2.0 TeV	
pH	2.8 ± 0.1	4.0 ± 0.1	1.42 ± 0.08
pCH ₂	3.9 ± 0.3	5.4 ± 0.6	1.38 ± 0.28
pH	4.2 ± 0.4	8.1 ± 1.0	1.93 ± 0.42
pC	4.0 ± 0.4	10.3 ± 1.1	2.58 ± 0.53
pPb	4.8 ± 0.5	12.1 ± 1.2	2.52 ± 0.51

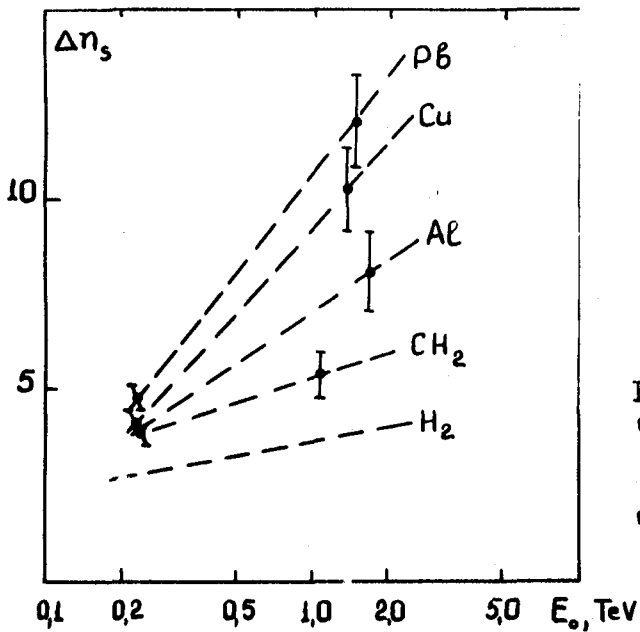


Fig.2 The multiplicity of the charged particles Δn_s within the central $\eta' = 4.0 - 1.0$ region of the distribution over η'

References

1. M.I.Atanelishvili et al., Izvestiya Akad.Nauk SSSR, 42, No.7, 1479 (1978)
2. M.I.Atanelishvili et al., Yadernaya Fizika, 24, 369 (1976)
3. O.L.Berdzenishvili et al., Bangalore, India XYIII ICRC HE 3-18 L.P., p.51 (1983)
4. M.I.Atanelishvili et al., Plovdiv XY ICRC, HE 7, p.66 (1977)
5. O.L.Berdzenishvili et al., Kioto XYI ICRC, HE 3-43, p.210 (1979)
6. O.L.Berdzenishvili et al., Kioto, XYI ICRC, HE 3-43, p.337 (1979)
7. D.M.Kotlyarevski. Pis'ma v JETP, 28, 4, 254 (1978)
8. K.G.Gulyamov et al. In: "Multiple Generation of Particles in pA-Interactions", ed. FTI of Izv.SSR, Tashkent, 78 (1976)
9. Yu.M.Shabel'ski, Proc XIII School of the LNPI, Leningrad, 90 (1978)

FEW-PARTICLES GENERATION CHANNELS IN
INELASTIC HADRON-NUCLEAR INTERACTIONS
AT ENERGY ≈ 400 GeV

Tsomaya P.V.

Institute of Physics, Academy of Sciences of
the Georgian SSR, Tbilisi, USSR

Abstract. On the basis of experimental data obtained at "Tskhra-Tskaro" installation we investigate the behaviour of the few-particles generation channels in interaction of hadrons with nuclei of CH_2 , Al, Cu and Pb at mean energy 400 GeV. The values of coherent production cross-sections σ_{coh} at the investigated nuclei are given. A dependence of coherent and noncoherent events is investigated. The obtained results are compared with the simulations on additive quark model (AQM).

The presented data were found experimentally on G.Chikovani mountain cosmic rays station "Tskhra-Tskaro" (atmosphere depth ≈ 760 g/cm²).

The installation consists of magnetic spark spectrometer and ionizational calorimeter /1/. We've got and analysed about three thousands of hadron nuclear interactions in CH_2 , Al, Cu and Pb targets.

The incoming hadrons flux consisted of 27% of pions and 73% of nucleons /1/. To estimate the multiplicity interval n_s where the contribution of coherent events was the most essential the angular distribution for various intervals were tested by means of dispersional analysis using F-criterion /2/. Such analysis is possible due to more narrow angular distribution of coherent generation particles events comparing with the rest ones. We found that multiplicity interval is equal to: $n_s = 3 + 5$. On the other intervals n_s the coherent generation event contribution was less than

5%. We must note here that because of different methodical effects the events with $n_s < 3$ were not taken into consideration /1/.

The most simple and generally accepted criterion of coherent production on nuclei processes selection was the criterion /3/:

$$\sum_i \sin \theta_i \leq A^{-1/3}$$

where θ_i is the angle of produced particle.

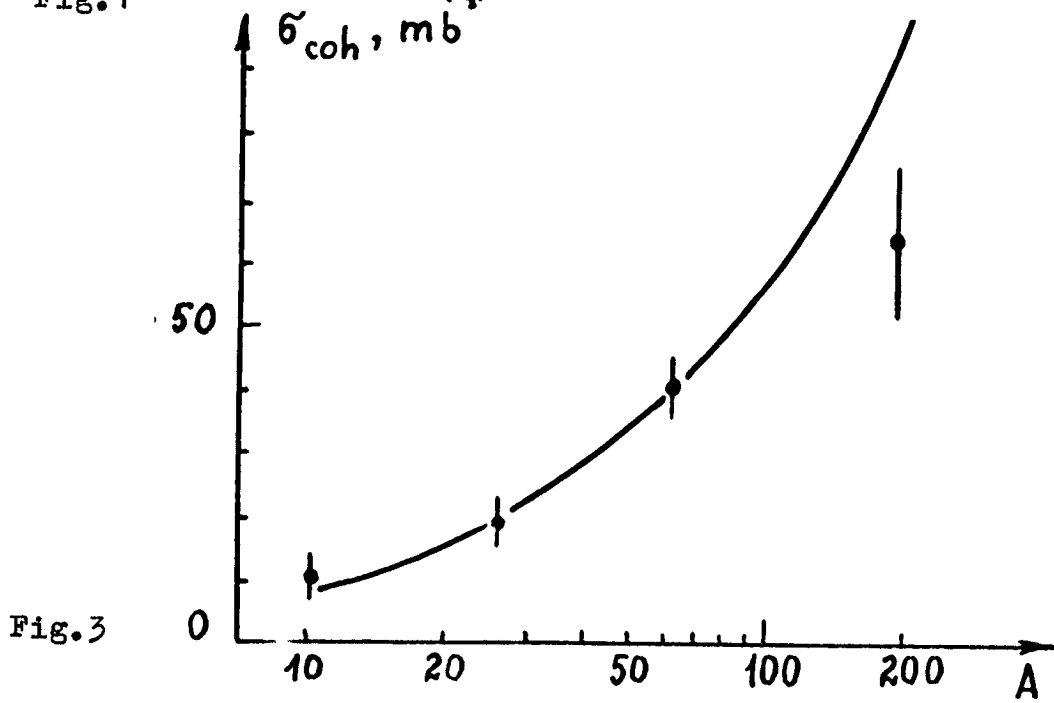
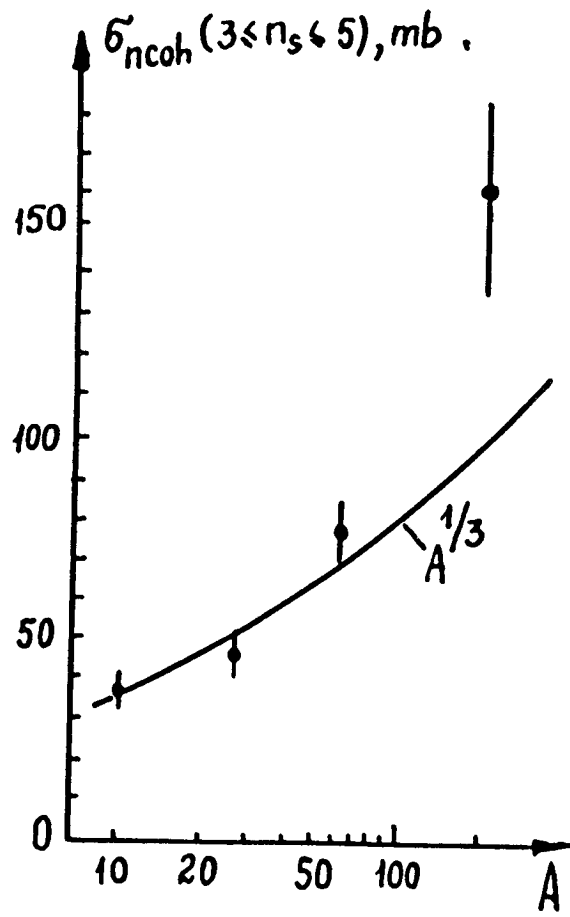
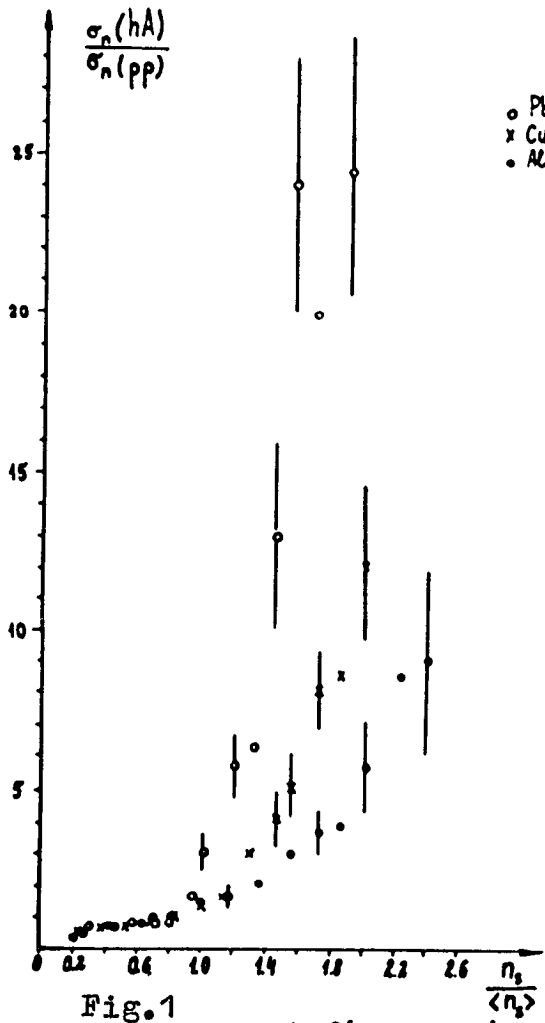
This criterion is necessary because of the small impulse value transferred to the nucleus target in these processes. The most of multiplicity production events fit this condition as the secondary events distribution becomes more narrow with the increase of primary energy. That's why this background should be taken into account. It can be evaluated starting from the fact that up to the mean multiplicity the hadron in nucleus interacts only with a nucleon. This can be seen from Fig.1 where we give a probability of fixed multiplicity production n_s on the nucleus as a function of the same probability in pp-interaction. We see that up to $\langle n_s \rangle$ this function doesn't depend on atomic number and is equal to ~ 1 . That's why the events, concerning the investigations with only one nucleon which satisfies this criterion were subtracted.

For this we used the data on pp-interaction at energy of 400 GeV /4/.

The selection results are given in the Table where we also give a full statistics of the observed events.

Table

Nucleus	A full number of interactions	A number of coherent events	A number of incoherent events	σ_{coh}^{mb} ($n_s=3+5$)
CH ₂	589	26	95	9 ± 2
Al	680	27	77	16 ± 3
Cu	1173	50	110	33 ± 5
Pb	457	11	41	40 ± 12



With the help of experimental data for $n_s < 3/5$ the received values of $\sigma_{\text{coh}}(n_s = 3 + 5)$ were restored to the full ones and compared with theoretical simulation on additive quark model results /6/. This comparison is given in Fig.2. We see that AQM describes light intermediate nuclei rather well, and σ_{coh} isn't in accordance with simulation

On Fig.3 we've plotted the noncoherent events (with $n_s = 3 + 5$) dependence on atomic number. The curve corresponds to $A^{1/3}$ parametrisation. Such a dependence suggests a particle production at the nucleus edge. It can be seen from Fig. that this suggestion is true for light and intermediate nuclei.

The behaviour on Pb nucleus for coherent and noncoherent processes, evidently, is the consequence of the fact that "passive" quark states on heavy nuclei introduced into AQM manage to transform into active ones. This reduces coherent probability and respectively increases noncoherent events probably.

References.

1. M.I.Atanelishvili et al. Izvestiya Akad.Nauk SSSR, 42, 1479, (1978)
2. S.A.Azimov et al. In: "Many Particles Processes at High Energies" ed. FTI of Izv.SSR (1976)
3. C.M.Fisher, W.H.Gibson et al. Nuov. Cim., 27, 761(1963)
4. Leningrad-Moscow-Gatchina-Tashkent Collaboration (Russian) Preprint IFHE 75-79, Akad.Nauk Kazakh.SSR, (1979)
5. W.Mollet, I.Biel, T.Ferbel. Phys.Rev.Lett., 39, 1646, (1977)
6. V.M.Brown, Yu.M.Shabelski. YaF, 37, 1011(1983)

THE MODEL OF INDEPENDENT PARTICLES
EMISSION IN THE MULTIPARTICLE
PRODUCTION THEORY

V.V.Uchaikin, V.A.Litvinov
Altai State University, Barnaul, USSR

ABSTRACT

It is shown, that it is possible to obtain the degree dependence of average multiplicity from energy, KNO-scaling and the effect of leading, taking into account the law of energy preservation.

The following model of multiple process is offered for discussion. Particles are born independently of each other from some distribution $f(E)$, but a chance set of E_1, \dots, E_n turns into realization of the multiple process only under the condition, that the sum

$$S_n = \sum_{i=1}^n E_i$$

will fall into the small interval ΔE_0 about E_0 (primary energy). The density of distribution $f(E)$ is assumed to be independent of E_0 .

The distribution of the thus obtained events on multiplicity n will be:

$$P_n = \text{Prob}\{S_n \in \Delta E_0\} / \sum_n \text{Prob}\{S_n \in \Delta E_0\} = f_n(E_0) / \sum_n f_n(E_0), \quad (\text{I})$$

where

$$f_n(E) = \underbrace{f(E) * f(E) * \dots * f(E)}_n$$

is fold single particle distributions. From the theory of probabilities it is known that if the second distribution $f(E)$ moment exists, then the sum S_n is distributed according to the normal law:

$$f_n(E) \sim \frac{1}{\sqrt{2\pi n \sigma^2}} \exp \left\{ -\frac{(E - n\bar{E})^2}{2n\sigma^2} \right\}, \quad n \rightarrow \infty, \quad (2)$$

where

$$\bar{E} = \int_0^{\infty} E f(E) dE, \quad \sigma^2 = \int_0^{\infty} E^2 f(E) dE - \bar{E}^2.$$

It is clear from here that the maximum of distribution falls on

$$\tilde{n} \sim E_0 / \bar{E} \quad (3)$$

and the relative distribution width is

$$\Delta n / \tilde{n} \sim (\sigma / \bar{E}) \tilde{n}^{-1/2}. \quad (4)$$

Thus, in this case we have the linear increase of the average multiplicity and the decrease of relative fluctuation according to the Poisson's law - both are inconsistent with the character of multiple processes.

Another case is discussed in the theory of probability too: when no second and even first moments of distribution $f(E)$ exist [1,2].

If that satisfies the condition

$$\int_E^{\infty} f(E') dE' \sim \alpha E^{-\alpha}, \quad E \rightarrow \infty, \quad \alpha \in (0, 2), \quad (5)$$

then instead of (2) there is a tendency to the stable law with the index α and parameter $\beta = 1$ (for positive random values)

$$\text{Prob} \left\{ \frac{S_n}{B_n} - A_n < x \right\} \Rightarrow G(x, \alpha, 1),$$

here

$$B_n = [\alpha n]^{1/\alpha}$$

and A_n is determined by the index α . For $\alpha > 1$ the first moment exists and can be used for centering consequence $A_n = n\bar{E}/B_n$ for $\alpha = 1$ $A_n \sim \ln n$ and for $\alpha < 1$ $A_n = 0$ [3].

Using this result for each of these cases, we obtain:

$$\alpha > 1: \quad \tilde{n} \sim E_0, \quad \Delta n / \tilde{n} \sim \tilde{n}^{\frac{1}{\alpha}-1}; \quad (6)$$

$$\alpha = 1: \quad \tilde{n} \ln \tilde{n} \sim E_0, \quad \Delta n / \tilde{n} \sim [\ln \tilde{n}]^{-1}; \quad (7)$$

$$\alpha < 1: \quad \tilde{n} \sim E_0^\alpha, \quad \Delta n / \tilde{n} \rightarrow \text{const} \neq 0. \quad (8)$$

From here it is clear, that at $\alpha \in (1, 2)$, when only the second moment doesn't exist \tilde{n} is proportional E_0 , although the relative fluctuations decrease at a slower rate; at $\alpha = 1$

when the first moment ceases to exist, the linear dependence $\bar{n}(E_0)$ is violated and the decrease of fluctuations is slow, until finally at $\alpha < 1$ the dependence of multiplicity from E acquires a degree character (with index α), and the distribution width of quantity (n/\bar{n}) stops to change with the increase of energy. Thus, at $\alpha < 1$ we find the characteristic features of the multiple processes.

At $\alpha = 1/2$, the analytical form of density of the stable law is

$$g(x, \alpha, 1) = G'(x, \alpha, 1) = \frac{1}{2\sqrt{\pi}} x^{-3/2} e^{-1/4x}$$

leading to one of the known approximation KNO-distribution

$$\psi(z) = \frac{\pi z}{2} e^{-\pi z^2/4}$$

and the average multiplicity $\bar{n} \sim E_0^{1/2}$, which doesn't disagree the experiment (if E_0 means the energy of the particles in the center-of-mass system).

For more detailed study of the given model, a Monte-Carlo simulation was carried out with the distribution function:

$$f(E) = \begin{cases} \alpha E^{-\alpha-1}, & E > 1, \\ 0, & E < 1, \end{cases}$$

$$\alpha = 1/4, 1/2, 1, 2, 4.$$

Results are shown in fig.1-3. Besides the confirmation of the above theoretical conclusions (3-8), it is clear from these calculation, that at $\alpha < 1$ there exists a particle separated by energy, which carries away about a half all the energy of the born particles (effect of leading), and the distribution along the variable $z = n/\bar{n}$ has the typical form of KNO distribution and doesn't depend from primary energy (KNO-scaling). This circumstance, in particular, may be used for the working out of the simple algorithm for simulation the act of multipartical production by Monte-Carlo method in calculations of extensive air showers and perhaps, is of interest to the theory of multiparticle production.

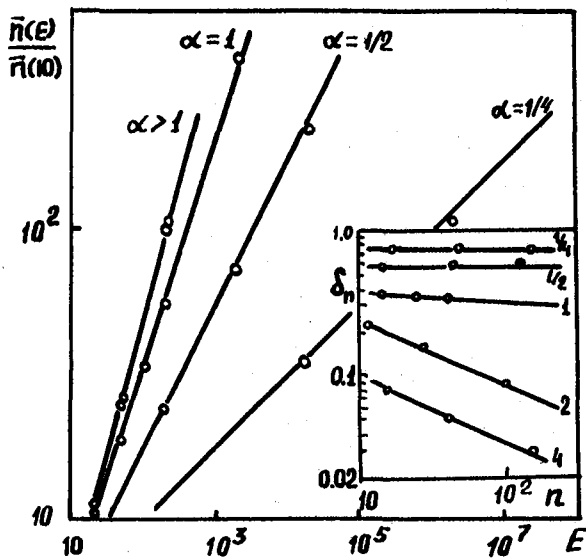


Fig. 1. Average multiplicity and relative fluctuations.

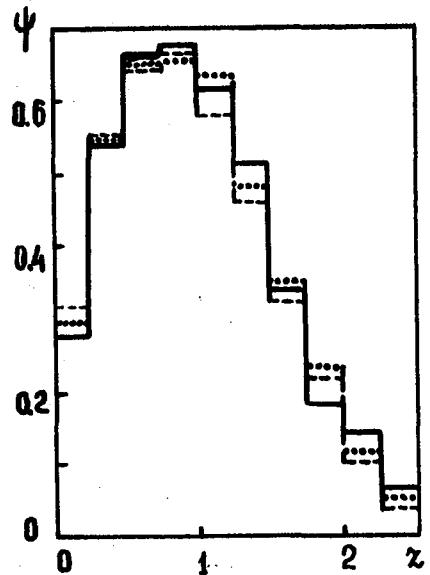


Fig. 2. Distributions of multiplicity for E_{01} , $E_{02} = 10E_{01}$, $E_{03} = 100E_{01}$ ($\alpha = 1/2$)

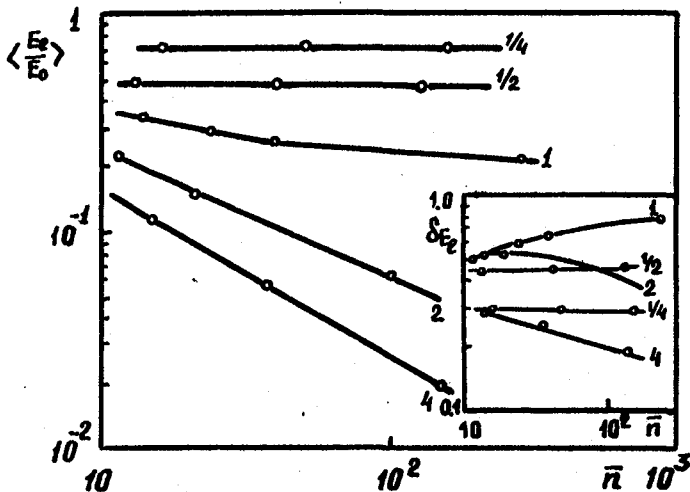


Fig. 3. Average value and relative fluctuations of the leading particle energy.

References:

1. Gnedenko B.V., Kolmogorov A.N. Limit distributions for sums independence random values. Moscow, Gostehizdat, 1949, 264 p.
2. Zolotarev V.M. One dimensional stable distributions. Moscow, Nauka, 1983, 304 p.
3. Borovkov A.A. The theory probability lectures. Moskow, Nauka, 1972, 287 p.

THE MULTIPLICITY AND THE SPECTRA OF SECONDARIES
CORRELATED WITH THE LEADING PARTICLE ENERGY

N.A.Kruglov, A.S.Proskuryakov,
L.I.Sarycheva and L.N.Smirnova

Institute of Nuclear Physics, Moscow State University,
Moscow II9899, USSR

Abstract. The spectra of leading particles of different nature in pp-collisions at $E_0 = 33$ GeV are obtained. The multiplicities and the spectra of secondaries π^+ , π^- , K^+ -mesons, γ -quanta, Λ and $\bar{\Lambda}$ -hyperons and protons for different leading particle energy ranges are determined.

The interactions in which the leading particle conserves a great fraction of the initial energy are essential for the development of nuclear cascades in the atmosphere. The leading particles form a deeply propagating part of the cosmic rays. The accompaniment of these particles is determined by the peculiarities of the low-inelasticity interactions. Besides, the events with a leading particle are reliably identified in the cosmic-ray detectors.

The main information on the multiple production of particles obtained from accelerators, is averaged over all types of events. This paper reports the multiplicities of π^+ , π^- , γ , K^+ , Λ and $\bar{\Lambda}$ -particles, the partial coefficients of inelasticity and the spectra of particles in $p\bar{p}$ -interactions at $E_0 = 33$ GeV in the lab.system that are correlated with the origin and energy of the leading particle.

The experimental conditions

The experimental material consists of 200 thousands of inelastic interactions of antiprotons with the momentum 32 GeV/c observed in the liquid hydrogen Mirabelle bubble chamber. The large dimensions of the chamber provided high detection efficiency of photons, K_s^0 -mesons and $\Lambda/\bar{\Lambda}$ -hyperons. We use the events where all charged tracks are measured.

For the particles with the momentum $p_{\text{lab}} < 1.2$ GeV/c the protons were discriminated from the π^+ -mesons by comparing track ionization. Neutrons and antineutrons are the only unobservable species in the chamber. Their mean characteristics are restored proceeding from the condition of energy balance /1/. In the present paper all inelastic interactions are analyzed in the system of an incident antiproton which will be mark in following as lab-system. This choice of system enabled us to establish the nature of a leading particle with the fraction of initial energy $\alpha_{\text{lead}} = E/E_0 \geq 0.4$.

Classification of events

The particle carrying away the maximum, as compared with other particles, fraction of energy in the lab.system in an event is assumed to be the leading particle. When

the total energy of unobservable neutral particles exceeds the energy of the leading particle, a neutral system χ^0 is regarded to be the leader. Table I presents the cross sections of the events with the leading particle of different nature in different ranges of \mathcal{U} lead.

Table I
The cross sections of the picked out classes of interactions
 \mathcal{G}, mb

leader	leading energy ranges		\mathcal{U} lead
	0.4 - 0.6	0.6 - 0.8	0.8 - 1.0
p	2.83 ± 0.03	3.43 ± 0.03	3.55 ± 0.15
π^+	1.23 ± 0.02	0.23 ± 0.01	0.015 ± 0.002
π^-	0.59 ± 0.01	0.084 ± 0.005	0.007 ± 0.002
χ^0	7.46 ± 0.04	6.78 ± 0.03	4.49 ± 0.03
Λ	0.35 ± 0.04	0.24 ± 0.03	0.07 ± 0.02
γ	0.15 ± 0.09	0.017 ± 0.015	0.004 ± 0.004
K_S^0	0.09 ± 0.02	0.007 ± 0.005	-

$$\mathcal{G}_{tot}^{pp} (32^{GeV/c}) = 45.6 \pm 0.3 \text{ mb}, \mathcal{G}_{in}^{pp} = 37.2 \pm 0.5 \text{ mb}, \mathcal{G}_{nonann}^{pp} = 30.7 \pm 0.5 \text{ mb} / 2/.$$

The events with the leader p, π^+, π^- and \mathcal{U} lead ≥ 0.4 make up 12 mb, i.e. $(32 \pm 0.4)\%$ of the inelastic $p\bar{p}$ -cross section. The events with the leaders $\Lambda, \gamma, K^0 (= K^0 + \bar{K}^0)$ at \mathcal{U} lead ≥ 0.4 with the cross section 1.04 ± 0.11 mb are observed.

The total energy of the particles attending the charged and neutral leader is presented in units of $\mathcal{U} = \sum E_i/E_0$ in fig. I. It is seen that the taking account of $\langle \mathcal{U} \text{ lead} \rangle$ in the events with the charged leader permitted the complete recovery of the interaction energy. The measured fraction of energy of the attending particles in the events with the leader χ^0 is higher as compared with the events with the p and π^\pm -leader. In this case according to the selection criteria a fraction of energy of the neutral leader χ^0 is carried by photons and the mean value of this energy is measured in the chamber for each group of events. The unobservable energy is carried away by an outgoing neutron. The mean fraction of this energy is indicated in fig. I. Consequently, the class of events with the leader χ^0 contains mainly the events with a leading neutron. The groups with \mathcal{U} lead (χ^0) ≥ 0.6 correspond to the events with \mathcal{U} lead (n) ≥ 0.4 , since the mean value of \mathcal{U}_γ in these events is ≤ 0.2 . The events with the leader χ^0 and \mathcal{U} lead ≥ 0.6 are considered in what follows as two groups of events with a leading neutron: $\langle \mathcal{U} \text{ lead} \rangle = 0.78 \pm 0.01$ and 0.50 ± 0.01 . The cross sections of the events with a leading proton and neutron with \mathcal{U} lead ≥ 0.4 are actually the same. This means that the leader in $(68.8 \pm 0.5)\%$ of the nonannihilation $p\bar{p}$ -interactions is a nucleon with \mathcal{U} lead ≥ 0.4 .

In fig. I there is no evidence for a fast neutron in the events with the π^\pm -leader and we therefore conclude that these events are mainly due to the $p\bar{p}$ -annihilation. The cross sections of the events are in accord with this conclusion.

Experimental Results

The spectrum of leading protons is uniform within $u_{\text{lead}} = 0.5 \div 0.9$ [2]. The spectra of leading π^\pm and K^\pm -mesons with $u_{\text{lead}} \geq 0.5$ decrease with increasing u_{lead} and are described by the function $A \exp(-B u_{\text{lead}}^2)$ with the parameters $B_{\pi^+} = 12.4 \pm 0.9$ and $B_{\pi^-} = 12.6 \pm 0.4$. To the spectrum of leading Λ with $u_{\text{lead}} \geq 0.5$ there corresponds the parameter $B_\Lambda = 8.1 \pm 0.3$.

The total multiplicity of the particles attending the leading p, n, π^+ , π^- , Λ is shown in fig.2a. The right scale shows the ratio of the observed multiplicity to the estimated total multiplicity $\langle n_{\text{tot}} - 1 \rangle$ for pp-interactions at 32 GeV/c [3]. It is seen that at u_{lead} close to 0.5 the multiplicity reaches the mean value.

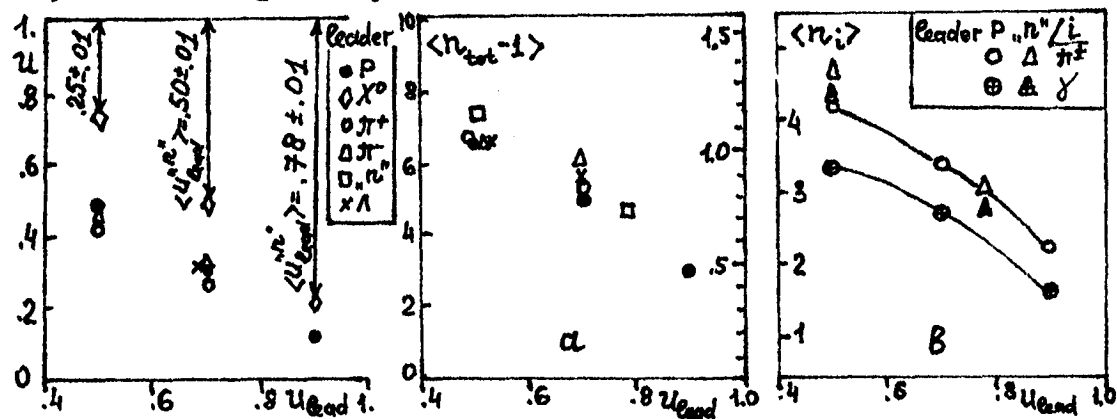


Fig.1. A fraction of Fig.2. Total multiplicity (a) and multiplicity of the attending particles of species i (b) for different leaders in the events with different leaders

The multiplicity of π^\pm and K^\pm -mesons and photons attending the leading nucleon is shown in fig.2b. The total multiplicity of π^\pm -mesons is similar in the events with a leading proton and "neutron". The value of $\langle n_\gamma \rangle$ proves to be higher for a leading "neutron" which can be connected with the identification procedure used.

The mean fraction of energy carried away by the attending π^+ , π^- , K^\pm , γ is shown in fig.3. The mean fraction of energy per π^+ and γ is the same whether the leader is a proton or a "neutron". The total fraction of energy carried away by these particles is plotted in fig.4 versus u_{lead} of a proton and "neutron".

The spectra of the attending particles are rather complex and concentrated in the region of low u for high u_{lead} . The parameters of the function describing these spectra are listed in table 2.

In the events with a leading proton a great fraction of the "invisible" energy carried away by the photons. In this case $\sum E_\gamma \approx E_0 - \sum E_\pm - \sum E_{K^\pm} - \sum E_\Lambda$ and the spectrum of photons can be obtained from the variable $u_\gamma = E_\gamma / \sum E_\gamma$ used in the cosmic rays. The spectra $d^2/d u_\gamma$ are presented in fig. 5

for the events with a leading proton at $u_{lead} > 0.8$ and $u_{lead} = 0.4 \div 0.8$.

Table 2
Parametrization of the spectra of the particles attending the leading protons and "Neutrons" by the function $f = u^N \exp(-B1u - B2u^2)$

leader	u_{lead}	type of a secondary particles	N	B1	B2
p	0.4-0.6	π^+	-1.00 ± 0.01	-5.5 ± 0.3	22.6 ± 0.6
		π^-	-1.61 ± 0.01	-7.51 ± 0.07	24.6 ± 0.3
		γ	0.027 ± 0.014	34.3 ± 2.6	-9.0 ± 13.6
	0.6-0.8	π^+	-1.31 ± 0.06	-11.0 ± 1.3	41 ± 2
		π^-	-1.85 ± 0.01	-7.91 ± 0.08	32.5 ± 0.4
		γ	0.027 ± 0.014	44.1 ± 2.3	-28 ± 10
	0.8-1.0	π^+	-0.21 ± 0.01	31.0 ± 0.9	-15.6 ± 5.4
		π^-	-2.62 ± 0.01	10.8 ± 0.2	-6.7 ± 1.4
		γ	-1.15 ± 0.05	32.5 ± 1.8	58.3 ± 6.3
χ^0 ("n")	0.6-0.8 $\langle u_n \rangle = 0.50$ ± 0.01	π^+	-1.25 ± 0.02	-14.9 ± 0.4	54.8 ± 0.7
		π^-	-1.20 ± 0.05	-2.3 ± 1.1	39.8 ± 2.3
		γ	-2.41 ± 0.02	-20.2 ± 1.3	83.4 ± 8.4
	0.8-1.0 $\langle u_n \rangle = 0.78$ ± 0.01	π^+	-2.66 ± 0.01	64.0 ± 0.1	287.4 ± 0.9
		π^-	-1.98 ± 0.01	-20.1 ± 1.0	179 ± 7.8
		γ	-2.3 ± 0.1	-17.2 ± 4.3	83.4 ± 8.4

References:

1. Vinitzkii A.A. et al., Sov.Journ.Nucl.Phys., 1984, 40,474.
2. Hanumehah B. et al. Nuovo Cim., 1982, 68A, 161; 17 ICR, 1981, HE 1-7, v.5, p.22.
3. Nikitaev D.N., Smirnova L.N. Sov.Journ.Nucl.Phys., 1985, 41, No.3.

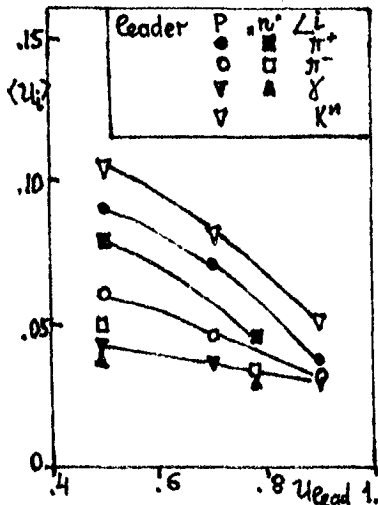


Fig. 3. Mean fraction of energy per particle of species i for different leaders

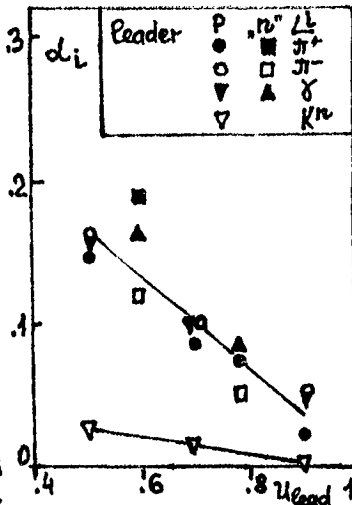


Fig. 4. Partial coefficients of inelasticity of particles α_i for different leaders: $\alpha_i = \langle u_i \rangle \langle n_i \rangle$

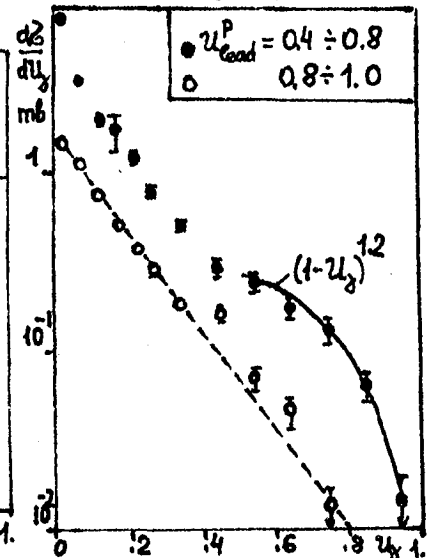


Fig. 5. Spectra of γ in $u_\gamma = E_\gamma / \sum E_\gamma$ for the events with a leading proton

CHARACTERISTICS OF ANOMALOUSLY HIGH MULTIPLICITY
COSMIC RAY INTERACTIONS.

I.Ya.Chasnikov, Yu.A.Eremenko, D.T.Madigozhin,
T.Kh.Sadykov, V.G.Voinov

HEPI of Kazakh Academy of Sciences, Alma-Ata, USSR

Six events with the number of secondaries ranging from 250 to several thousands have been registered by means of the installation consisting of a thin graphite target above and under which were placed photolayers followed by the usual lead X-ray film and emulsion chambers. Data concerning the number of secondaries and their angular distribution are given. A comparison of the variance of the angular distribution with that obtained at accelerator energies is made.

It was planned to create the experimental installation described in paper [1] at cosmic ray station (3340 m above sea level) of HEPI of Kazakh Academy of Sciences. The altered version of such full-automatic installation has been created in 1984 [2]. It consists of a replaceable target, the X-ray film and emulsion chambers (XREC) and of the ionization calorimeter (total absorber spectrometer) with the area being equal to 44 m^2 . While this installation was putting into the operation an experiment using XREC consisting of the graphite target of 5 cm thickness above and under which were placed photolayers followed by the layer of lead of 3 cm thickness and by other photopackets was in progress. Each photopacket contained two sheets of bilateral X-ray film RT-6 and one sheet of nuclear emulsion R-2T. The aim of the experiment was the searching of high multiplicity cosmic ray interactions the existence of which was indirectly confirmed by extensive air showers (EAS) data analysis (see, for instance, [3]). The idea of this experiment has been proposed in [4], where, in particular, the ground for the choice of a target thickness has been made.

The total exposure time and the area of the installation are equal to $83.8 \text{ m}^2 \text{ year}$. Under the target we have registered 6 dark spots which could not be explained by trivial

reasons: mechanical action on the X-ray films or electrization processes. The fact that the spots are formed by charged relativistic particles is confirmed by the examination of nuclear emulsion under a microscope. One does not able to find by the naked eye any dark spots on the X-ray film placed above the target. This means, that if there exists some microstructure of EAS, the particle density will be less than 200 particles per 1 mm^2 . At present only the photomaterial placed under the target has been treated utterly.

The scanning of X-ray films was performed by means of laser beam of 20 microns in diameter on the special installation created at HEPI of Kazakh Academy of Sciences [5]. The calibration of readings (calculation of darkness density and charged particles density) was made by control X-ray film which were obtained by fixed flux of charged particles from a radioactive source, by dark spots from electromagnetic cascades with known darkness density, and also by direct comparison of readings with the number of particles registered in nuclear emulsion. Some characteristics of the events found are given in the table.

Table.

1	2	3	4	5	6
1240	750	3800	1040	2500	950
0.4 ± 0.08	0.32 ± 0.08	0.48 ± 0.06	0.31 ± 0.07	0.35 ± 0.06	0.33 ± 0.07

The number of particles in the spots was evaluated by the dependence of their number $N(\leq R)$ in a circle of radius R on the value of R (Fig.1). The variance of the angular distribution has been found as follows. If H is the height from the generation point to the observation level, R_i - is the distance of i -th particle from the centre of gravity of all secondaries, then $R_i/H \approx \tan \theta_i$, where θ_i is the emission angle of i -th particle in the laboratory system, and $\log R = \log \tan \theta_i + \log H$ distribution is actually the angular distribution of secondary particles in $\log \tan \theta_i$ coordinates displaced for the given event by the constant value

$\log H$ (Fig.2).

If the registered dark spots are actually the result of inelastic interactions, then one can evaluate the lowest limit for primary energy. Considering the secondaries as pions and assuming that the coefficient of inelasticity is equal to unit as well as that transverse and longitudinal momenta in CMS are equal, we get $E_{0 \min} \approx 800 \text{ Tev}$, if $P_{\perp} = 0.4 \text{ GeV}/c$.

Fig.3 shows the dependence of the variance δ of the angular distribution on primary energies according to the data of [6].

The value of the variance of the summarized angular distribution for all six events is also shown. Fig.4 gives the dependence of δ on the multiplicity of secondaries n_{\perp} at 200 GeV and at more high energy. One can see, that δ -values do not depend within experimental errors on the multiplicity of secondaries, but they are systematically lower than those at our energies. We emphasize once again that if the observed dark spots in X-ray film are produced by inelastic interactions in the target, then these events not only confirm the existence of high multiplicity inelastic interactions, but also show that the variance of the angular distribution of secondaries can be essentially changed at superhigh primary energy.

The analysis of such events will of course be continued.

References

1. Buya S., Dobrotin N.A., Takibaev Zh.S. et al. Preprint of the institute of Nuclear Physics, N 100, Alma-Ata, 1969.
2. Alibekov M.I., Baigubekov A.S., Eremenko Ju.A. et al. Preprint HEPI, N 84-09, Alma-Ata, 1984.
3. Nickolsky S.I. "Proc. of Intern. Seminar on high energy Physics problems", Dubna, 1978, P 160.
4. Eremenko Yu.A., Lukin Yu.T., Sadykov T.Kh., Preprint HEPI N 81-12, Alma-Ata, 1981.
5. Voinov V.G., Kuntukov E.Yu., Chasnikov I.Ya. et al. Preprint HEPI, N 84-26, Alma-Ata, 1984.
6. Eremenko L.E., Chasnikov I.Ya., Shahova Z.I., Preprint HEPI, N 65-78, Alma-Ata, 1978.

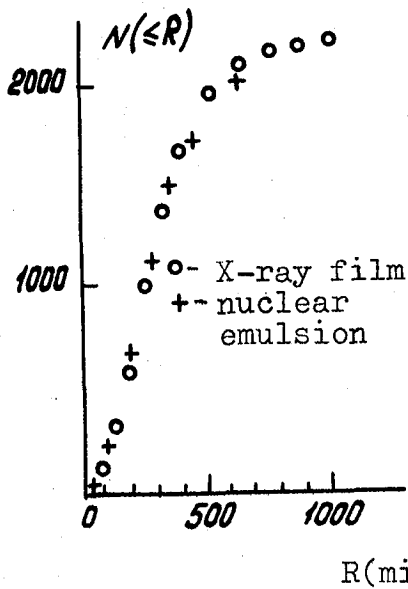


Fig. 1

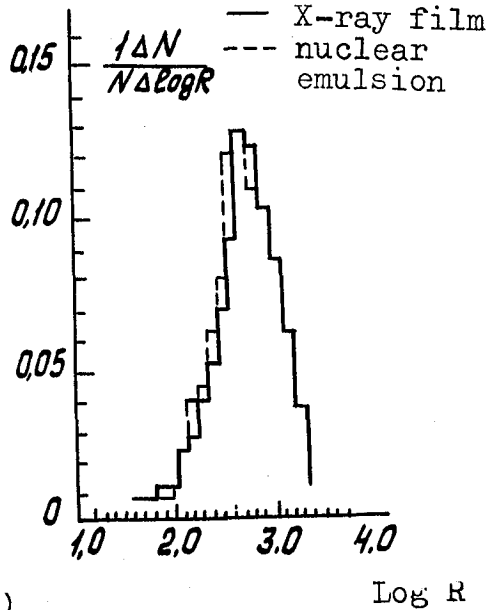


Fig. 2

Fig. 2. The angular distribution of charged particles for one of the events.

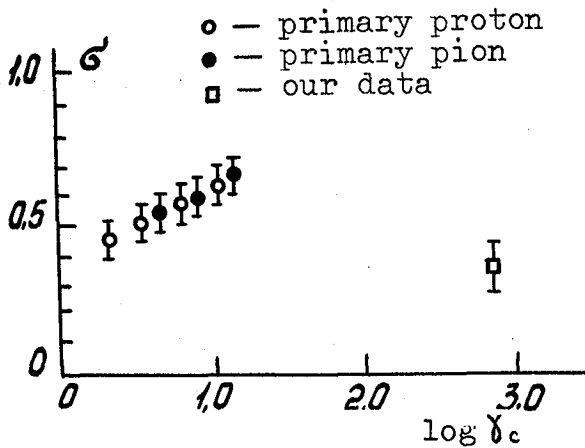


Fig. 3

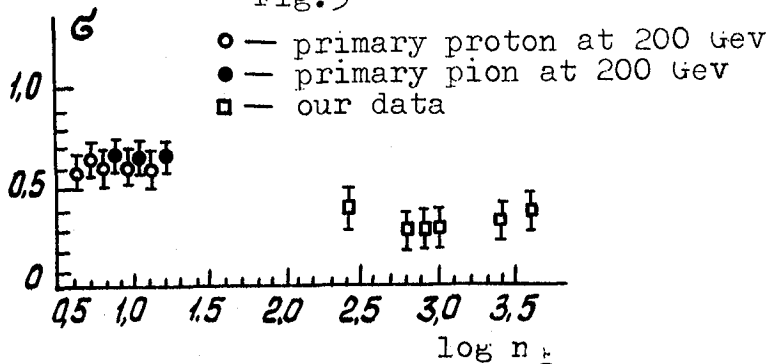


Fig. 4

TRANSVERSE MOMENTUM DISTRIBUTION OF π^0 IN THE FRAGMENTATION
REGION OF SUPER HIGH ENERGY INTERACTIONS

Ren, J.R., Kuang, H.H., Huo, A.X., Lu, S.L., Su, S., Wang, Y.X.,
Xue, Y.G. Institute of High Energy Physics, Academia Sinica,
China

Wang, C.R., He, M., zhang, N.J., Cao, P.Y., Li, J.Y.
Shandong university, China

Wang, S.Z.
Zhengzhou University, China

Bai, G.Z., Liu, Z.H., Li, G.J., Geng, Q.X.
Chongqing Architecture College, China

Zhou, W.D., He, R.D.
Yunnan University, China

The lateral distribution of γ -familige observed by emulsion chamber is sensitive to test transverse momentum of high energy interaction. But most part γ -families are successive interation's results. so it is necessary to analyse the propagation of γ -ray in atmosphere. A γ -ray with energy E_r and transverse momentum P_{tr} is producted at the altitude h above the observation level (Fig.1). After cascade, the total observation energy reduce to E_{ob} , the $P_{tr} = \frac{RE_r}{h} = R E_{ob} \left(\frac{1}{h} \frac{E_r}{E_{ob}} \right)$. The arerage valne $\langle h \frac{E_{ob}}{E_r} \rangle$ has been calculated by Monte-Carlo simulation, Fig 2 give the relation between $\langle h \frac{E_{ob}}{E_r} \rangle$ and h . From $h=1.5\text{km}$ to 30km and difference E_r , the $\langle h \frac{E_{ob}}{E_r} \rangle$ approximately is a constant, $\langle h \frac{E_{ob}}{E_r} \rangle \sim 1.7\text{km}$. From here, the transeverse momentum of π^0

$$P_{t\pi^0} \simeq 2P_{tr} \simeq 2R E_{ob}/1.7\text{km}. \quad \langle 1 \rangle$$

In the emulsion chamber experiment, E_{ob} can be estimated by decascade method. There are 30 γ -families observed by Ganbala emulsion Chamber with total observation energy $\sum E_r \geq 100\text{Tev}$ and lateral spread $\langle ER \rangle \geq 15\text{Tev}\cdot\text{cm}$ selected. The value $X_{ij} = \sqrt{E_i E_j} R_{ij} \leq 2.5\text{Tev}\cdot\text{cm}$ is used to decasecade. the value R is measmed from energy center, then the $P_{t\pi^0}$ distribution have been estimated by use relation $\langle 1 \rangle$, In order to test this method, a group of Monte-Carlo simulation γ -families are used to compare with

experimental data by same treatment. Fig 3 shows both distributions are consistent and consistent with a result of another analysis [2], but they have some difference with the Pt distribution of the model --- $\frac{dN}{dP_T^2} \propto e^{-7.5 P_T}$. It means the relation $\langle 1 \rangle$ is a approximate average, but Fig 3 shows only few π^+ are with large Pt value, the mean value $\langle P_T \rangle = 0.46 \pm 0.3$ in the $E \geq 10^{15}$ ev and $\eta > 2.5$ region.

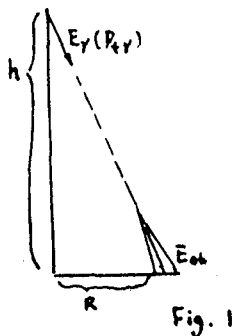


Fig. 1

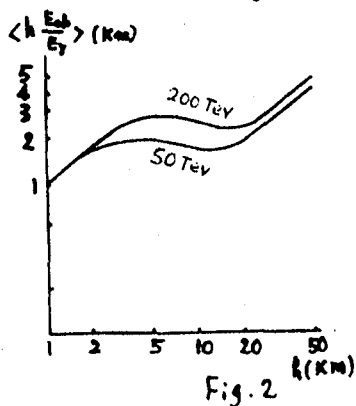


Fig. 2

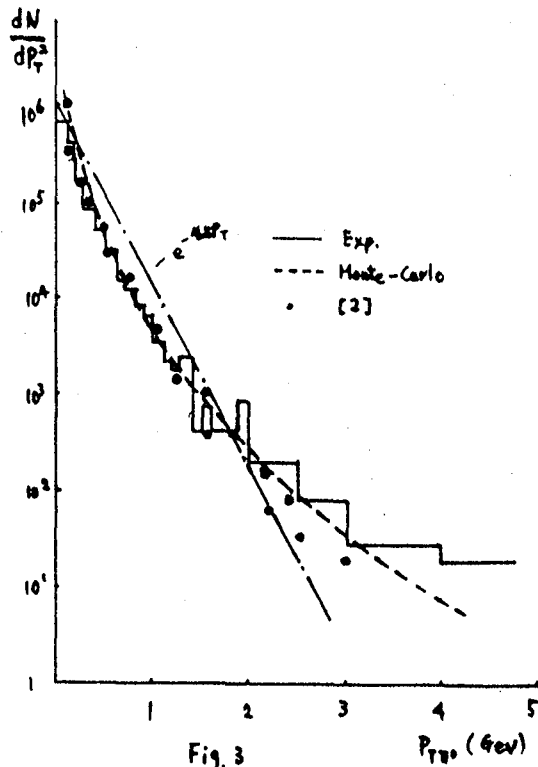


Fig. 3

Reference

- [1] Jing et al., This volume
- [2] Huo et al., Journal of Wuhan University, 1983, p.45

STUDY OF HADRON BUNDLES OBSERVED IN CHACALTAYA
TWO-STORY EMULSION CHAMBER

AOKI, H.

SCIENCE AND ENGINEERING RESEARCH LAB.
WASEDA UNIV.

17, KIKUICHO, SHINJUKU-KU, TOKYO, JAPAN

1. INTRODUCTION

The existence of hadron-rich families associated with few gamma-ray emission named Centauro and Mini-Centauro phenomena was reported by Brasil-Japan collaboration. (1) Since, it is important to make clear whether these are produced by the special type of interaction different from the ordinary pion multiple production or not, a number of studies have been made by various authors. (2)

We have already presented the result of the systematic study of hadron bundles, detected by Chacaltaya emulsion chamber No. 15, 17 and 18. (3)

In this paper the experimental results are compared with simulation calculation based on ordinary multiple pion production model.

2. EXPERIMENTAL PROCEDURE

We analyzed 172 blocks of the lower detector of each two-story emulsion chamber No. 15, 17 and 18.

Through the general scanning of X-ray films in the lower detector, we select parallel incident showers which pass through the upper chamber as hadron bundles, since such showers detected in lower chamber are originated by hadronic interactions in the chamber itself.

We studied core structure of showers in nuclear emulsion plates under microscope for all the detected X-ray film dark spots, and classify them into the following categories, (1) Pb-jet-upper with diffuse core structure, (2) C-jet with clean multi-core structure and (3) Pb-jet-lower with single collimated core structure.

We observed 90 hadron bundles in the present analysis. Among these hadron bundles, the following special events are included which were identified as Centauro I and IV, Mini-Centauro (7 events), and hadron-rich families (2 events).

Energies of showers are estimated by track-counting method for C-jets and by micro-photometry measurement for the others. The detection threshold energy was estimated around 2.0 TeV.

3. SIMULATION CALCULATION FOR HADRON BUNDLES.

In order to study hadron bundle phenomena originated from ordinary multiple pion production, a simulation calculation was carried out, based on the scaling model for nuclear interactions. (4)

Two kinds of primary particles are assumed for the contrast, (a) proton primary and (b) iron nucleus, respectively. In both cases, the energy spectrum of primary particles is assumed to be $F(\geq E_0) \propto E_0^{-\beta}$ and the power index β is given

as 1.8 in integral form. The minimum energy of primary particle in the calculation, E_{\min} , is chosen as 500 TeV for proton primary and 1000 TeV for iron nucleus. The structure and geometry of Chacaltaya chamber is taken into account exactly. The unit of detection for hadron bundles is taken to be the size of one block of chamber 40cm \times 50cm. In order to adjust to the experimental conditions, the family center is randomly moved inside the size of one unit block. 76 hadron bundles ($N_h \geq 2$, $E_h^{(s)} \geq 1$ TeV) are obtained from 600 proton primaries and 36 from 600 iron primary.

4. COMPARISON

Fig.1 shows the differential distribution of observed multiplicity, N_h , for all hadron bundles (90 events). Simulation results (76 events) are shown by the dotted line in the same figure.

Fig.2 shows the differential distribution of $\langle E_R \rangle$, and simulation results are shown by the dotted line in the same figure.

Fig.3 shows scattering plots of $\langle E_R^{(s)} \rangle$ v.s. N_h , where \bullet is simulation data based on proton primary, \times based on iron primary, \otimes is Centauro events, \circ is Mini-Centauro events, \odot is hadron-rich families and \bullet is the other observed events.

5. CONCLUSION.

As is seen in Fig.1, both hadron multiplicity distribution, obtained from the present observation and the simulation calculation, show almost the same distribution in the range $0 < N_h < 8$. It means that hadron bundles of such smaller multiplicities are considered to be originated from successive interactions of surviving nucleon with the nature of multiple production during passing through the atmosphere. One cannot find, however, larger multiplicity hadron bundles, $N_h > 9$, in the simulation data.

Especially, Centauro I ($N_h = 27$), Centauro IV ($N_h = 13$) seems to be far beyond the fluctuation which is expected from the ordinary pion multiple production originated from proton primary.

Fig.2 shows similar tendency between the $\langle E_R^{(s)} \rangle$ distribution obtained from the present observation and the simulation calculation in the range $0.80 < \langle E_R^{(s)} \rangle < 6.7 \times 10$ TeV.cm. One cannot find, however, smaller $\langle E_R^{(s)} \rangle$ hadron bundles, $\langle E_R^{(s)} \rangle < 0.80$ TeV.cm, in the simulation data.

The comparison of scattering plots of $\langle E_R^{(s)} \rangle$ v.s. N_h between the experimental results and the simulation data, based on proton and iron primary, shown in Fig.3 give the same conclusion. They are in the similar tendency for the events with $N_h < 13$.

6. ACKNOWLEDGMENT.

The author would like to express his gratitude to all the members of Chacaltaya emulsion chamber collaboration, Prof.Y.Fujimoto and S.Hasegawa. In particular, to Prof.M. Sibata for his kind support.

REFERENCES.

- (1) C.M.G.Lattes et al, Phys. Report Vol.65, No.3 (1980)151
 (2) A.S.Borisov et al, Proceeding of Workshops in La Paz
 Rio De Janeiro (1982)445
 T.K.Gaisser and T.Stanev, Proceeding of Workshops in La
 Paz Rio De Janeiro (1982)281
 B.S.Acharya et al, 16th Intern. Cosmic Ray Conf. Vol.6
 (1979)289
 (3) H.Aoki; Proc. of 18th ICRC 11(1983)96.
 (4) M.Shibata, Private Communications.

Fig. / Differential Distribution
of Multiplicity

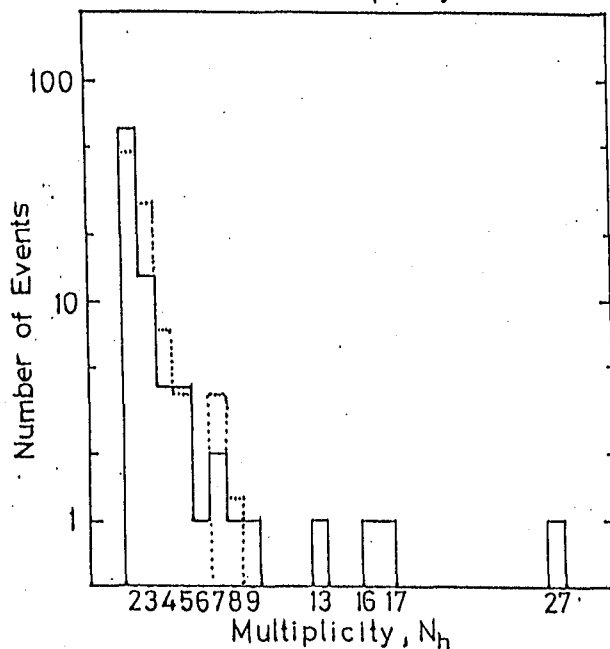


Figure shows the differential distribution of observed multiplicity, N_h .

———— is the experimental result for all hadron bundles (90 events).

..... is the simulation results (76 events from proton primary).

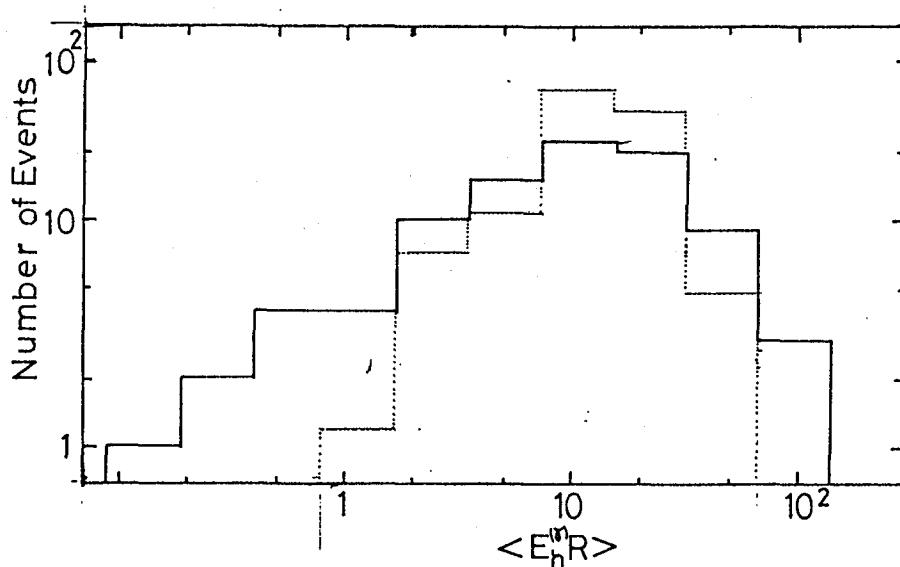


Figure 2; The differential distribution of $\langle E_h R \rangle$ is shown. is the experimental result for all hadron bundles (90 events).
 is the simulation results (76 events from proton primary).

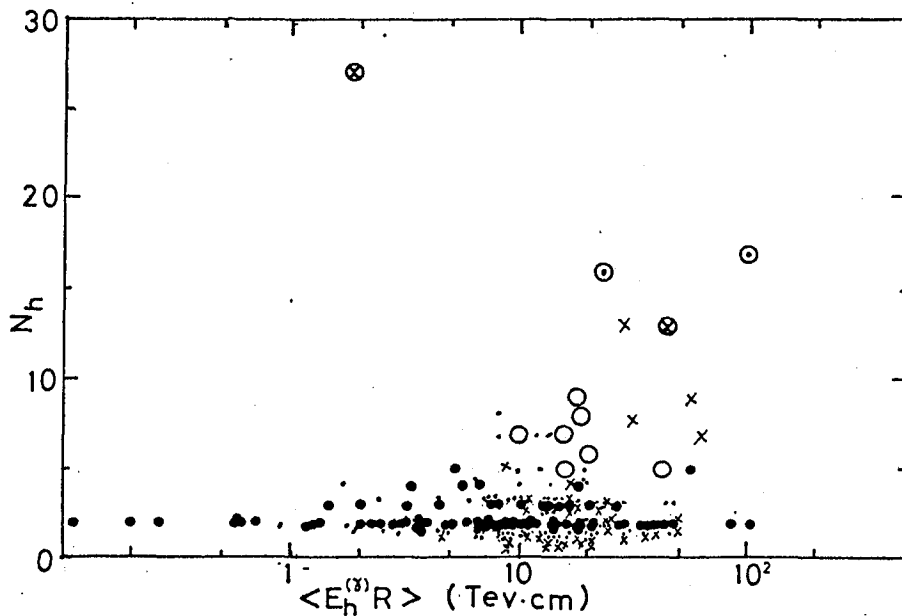


Figure 3; The scattering plots of $\langle E_h R \rangle$ v.s. N_h is shown.

- is simulation data based on proton primary.
- × based on iron primary.
- ⊗ is Centauro events.
- ⊙ is Mini-Centauro events.
- ⊙ is hadron-rich families.
- is the other observed events.

Penetrative nature of high energy showers
observed in Chacaltaya Emulsion chamber

Y. Funayama and M. Tamada

Science and Engineering Research Laboratory,
Waseda University, Tokyo 162, JAPAN

ABSTRACT

It is shown that about thirty percent of single core showers with $E^{(\gamma)} > 10$ TeV, which have been observed in the air families with $\sum E^{(\gamma)} > 100$ TeV, have stronger penetrating power than that expected from electromagnetic showers (e, γ). On the other hand, their starting points of cascades in the chamber are found to be as shallow as those of (e, γ) components. Then, we can consider that those showers are very collimated bundles of hadron and (e, γ) component. Otherwise, we must accept that the collision mean free path of those showers in the chamber is shorter than that of hadron with geometrical value.

1. Introduction

Chacaltaya experiment has reported the existence of mini-cluster, which has been observed as the daughter product of the exotic interaction, such as Chiron[1] and Geminion[2]. This is the shower bundle observed as narrowly collimated cluster structure and looks like an early stage of (e, γ) cascade showers in the upper chamber. But, we can identify at least one hadron in it, and then we must consider that this is the collimated bundle of hadrons and electromagnetic showers.

On the other hand, we have often observed a number of showers in these families penetrating strongly through the whole chamber, although they are found to start at the shallower depth in lead of the upper chamber.

Here, we discuss the characteristics of those penetrating showers with $E^{(\gamma)} > 10$ TeV, observed as single core structure in the upper chamber.

2. Experimental apparatus and method

2.-1 chamber

Chacaltaya E.C. no.19 has two storey structure and consists of four parts, the upper chamber of 6 cm thick in lead, the target layer of 23 cm pitch, the air gap of 158 cm and the lower chamber of 8.4 cm thick in lead. Both the upper and the lower chamber are multi-layered sandwiches of lead plates and photo-sensitive materials (nuclear emulsion plates and X-ray films).

2.-2 selection of families

We here select 19 air families with $\sum E^{(\gamma)} > 100$ TeV, which have been

obtained by the systematic study of Chacaltaya E.C. no.19 (Japan part, $\sim 30 \text{ m}^2 \cdot \text{yr}$). They have at least two showers which are detected both in the upper chamber and in the lower chamber.

2.-3 measurement of showers

In the present analysis, we pick up only single core showers with penetrative nature. Here, the penetrating shower means that it has at least two layers where its spot darkness on X-ray films is greater than 0.1 in the lower chamber. The spot darkness is measured by microphotometer with $200 \mu\text{m} \times 200 \mu\text{m}$ square slit. The energy of shower with maximum darkness 0.1 is about 1 TeV, and it is the threshold energy obtained by X-ray film. We call showers as 'single core showers' which accompany no showers within 1 mm around them. The energy measurement of each shower is also carried out by the track-counting method on nuclear emulsion plates.

3. Results

3.-1 (e, γ)-like behaviour of penetrating showers

Fig.1 is the integral energy distribution of observed single core showers (O) and those with penetration (\bullet). That of simulated gamma-rays is also shown in the same figure. (—; all showers, - - - -; with penetration). Statistics of calculations is about 10 times larger than that of observed showers. Here, we consider the only showers with $E_\gamma > 10 \text{ TeV}$, because the penetration probability of gamma-ray with $E_\gamma < 10 \text{ TeV}$ is found to be negligible small by the same calculations.

Fig.1 Integral energy distribution

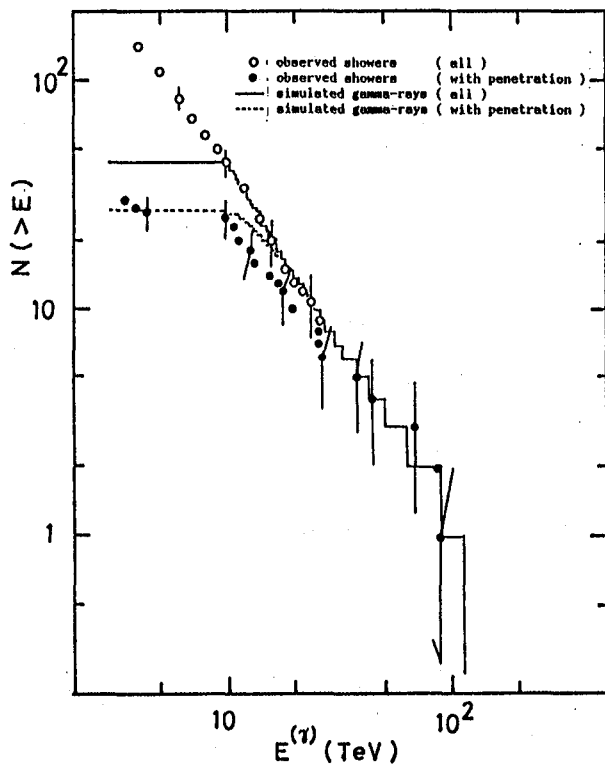
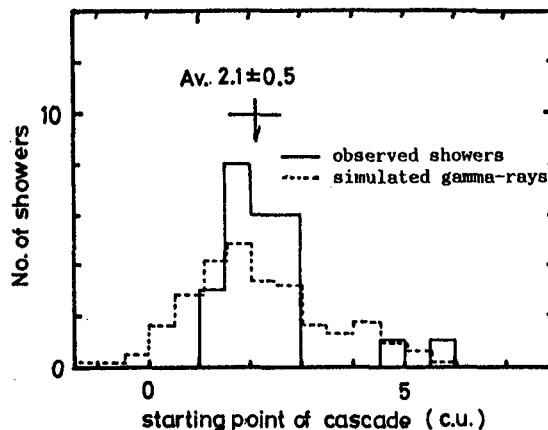


Fig.2 Starting point distribution of cascade in the chamber for penetrating showers $E^{(1)} > 10 \text{ TeV}$



Simulation calculation is constructed by T. Shibata et al. [3]. The exact structure of E.C. no.19, L.P.M. effect and spacing effect are taken into account. Fig. 2. is the starting point distribution of cascades in the chamber only for penetrating showers with $E^{(\gamma)} > 10$ TeV (—; experiment, ----; simulated gamma-ray). We can see from these figures that the observed showers with $E^{(\gamma)} > 10$ TeV show the (e, γ) -like behaviour on the penetration probability and the starting point of cascades.

3.-2 hadron-like behaviour of penetrating showers

In order to investigate the penetrating power of showers, we define the quantity n_i at the i -th layer in the lower chamber, and introduce $\sum n_i$ as follows. (Fig.3)

$$\sum n_i = \sum (\log D_i - \log \langle D \rangle_i) / \log \sigma_i$$

D_i denotes the observed spot darkness on X-ray films at the i -th layer in the lower chamber. For each shower, we fit the observed spot darkness in the upper chamber to the transition curve, using the least square method. Here, the transition curve is constructed by the simulated (e, γ) cascade showers of electron pair origins in the chamber without air gap of 158 cm. $\langle D \rangle_i$ and σ_i is the average darkness and its one standard deviation at the i -th layer in the lower chamber, respectively, estimated from the above fitted curve. \sum means summing up of the quantity n_i only for the layers in the lower chamber where the spot darkness D_i is greater than 0.1. We assume $n_i = 0$ if $D_i < \langle D \rangle_i$. Then, it is considered that the showers with larger $\sum n_i$ have long tails with strongly penetrative nature.

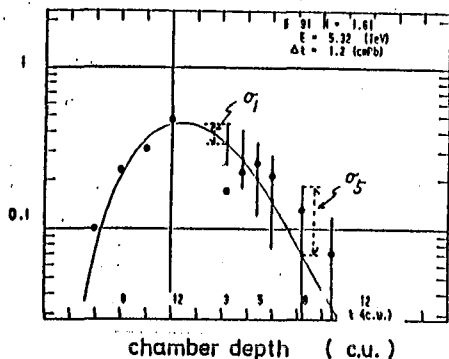


Fig.3 Procedure of calculating $\sum n_i$

We get $\langle D \rangle_i$ and σ_i at the i -th layer in the lower chamber from the fitted curve and calculate n_i .

where,

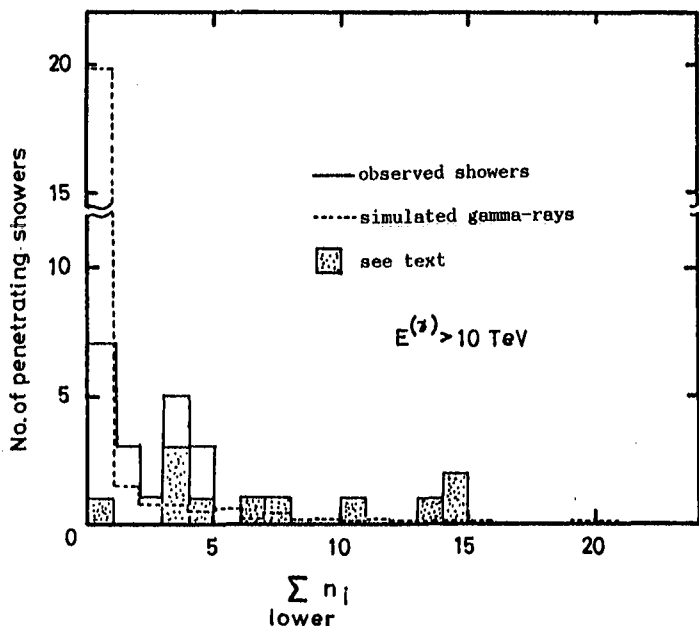
$$n_i = 0 \quad \left(\begin{array}{l} \text{at } D_i < 0.1 \\ \text{or } D_i < \langle D \rangle_i \end{array} \right)$$

$$n_i = \frac{(\log D_i - \log \langle D \rangle_i)}{\log \sigma_i} \quad \text{(otherwise)}$$

(see text.)

In this case,
 $n_1 = n_2 = n_6 = n_7 = n_8 = 0$
 $n_3 = 0.40, n_4 = 0.55, n_5 = 0.66$
 then, $\sum_1 n_i = 1.61$

Fig.4 $\sum n_i$ distribution of penetrating showers



Σn_i distribution is shown in Fig.4 (—;experiment, - - - - -;simulated gamma-rays). That for simulated gamma-rays is obtained by applying the same method. We can expect that the showers with larger Σn_i have the new shower cores in the lower chamber, which make this quantity bigger. Thus, the showers, which were identified to have these new cores in the lower chamber under the microscopic observation, are shown by the \otimes marks.

As is seen from this figure, about one half of observed penetrating showers with $E(\gamma) > 10$ TeV, that is, about thirty percent of observed single core showers with this energy region, have long tails of cascade developments in the lower chamber, which cannot be explained by the fluctuation of (e, γ) showers.

4. Conclusion and Discussion

About 30 % of single core showers with $E(\gamma) > 10$ TeV, which have been observed in the families with $\Sigma E(\gamma) > 100$ TeV detected by Chacaltaya E.C. no.19, start at the shallower depth in the upper chamber like (e, γ) components, but they penetrate strongly into the lower chamber like hadron components. This suggests that they consist of very collimated a gamma-ray and a hadron, the distance between the two is $< 100 \mu\text{m} \sim 200 \mu\text{m}$. That is, the gamma-ray starts cascade development in the upper chamber and the hadron interacts in the target layer, so that they look like just continuing single core shower, because there is an uncertainty of about $100 \mu\text{m} \sim 200 \mu\text{m}$ in the geometrical position when we identify the showers observed in the lower chamber with the continuation of the shower in the upper chamber. Then, when the hadron happen to interact in the upper chamber, we might recognize those showers as mini-clusters. Otherwise, from the argument on the detection probability of hadrons in the chamber, the collision mean free path of these showers is about one third of that of hadron with geometrical value [4].

Acknowledgement

The authors would like to express their gratitude to Prof.Y.Fujimoto and Prof.S.Hasegawa and to all the members of Chacaltaya emulsion chamber experiment for their valuable discussions and comments, especially to Dr.T.Shibata for simulation calculation.

References

- [1] Brazil-Japan collaboration ; Proc. of Workshops on Cosmic-Ray Interactions High Energy Results, La Pas Rio de Janeiro (1982) 319
S.Hasegawa ; Proc. of Int. Sympto. on Cosmic Rays and Particle Physics, Tokyo (1984) 319
- [2] Brazil-Japan collaboration ; AIP Conf. Proc. no.49 (1979) 145
- [3] M.Okamoto and T.Shibata ; Conf. Paper, 17th Cosmic Ray Conf., Paris 5 (1981) 214,218
- [4] Y.Funayama and M.Tamada ; to be published.

Anomalous correlation between hadron and electromagnetic particles in hadron and gamma-ray families

M. TAMADA

Science and Engineering Research Laboratory, Waseda University, Tokyo 162, JAPAN

Abstract

Correlations between hadrons and electromagnetic particles are studied in the hadron-gamma families observed in Chacaltaya emulsion chamber experiment. It is found that there exist a number of hadrons which associate electromagnetic showers in extraordinarily close vicinity. The probability to have such large number of hadrons associating electromagnetic showers, expected from background calculation, is found to be negligibly small, $\sim 10^{-5}$, and it means there exists anomalous correlation between hadrons and electromagnetic particles in the characteristic spread of atmospheric electromagnetic cascade.

1. Introduction.

Through the analysis on the structure of hadron and gamma-ray families, especially of the families with hadron-rich nature, we have noticed that there were a number of showers which penetrate through the hole chamber, the upper and the lower chamber. The core structure seen in the lower chamber tells us that considerable number of those penetrating showers are not simply pure electromagnetic cascades but are coming from nuclear interaction of hadrons in the chamber, that is, they are hadronic origin.[1][3] During studying on the core structure of those penetrating showers, we found some of showers which are considered as hadronic origin have separate multi-core structure in the upper chamber, not single core structure. That is, there exist hadron and electromagnetic showers which are located extraordinarily close each other, in the extreme case the relative distance between the two is $\sim 30 \mu\text{m}$. Here we show how closely a hadron accompanies electromagnetic showers in its neighbourhood in the high energy hadron and gamma-ray families observed in Chacaltaya chamber no.19.

2. Experimental procedure.

Chacaltaya chamber no.19 The Chacaltaya chamber no.19 has two-storey structure with air-gap, that is, the upper chamber of 6 cmPb thick, target layer of 23 cm pitch, air-gap of 1.5 m and the lower chamber of 8.4 cmPb thick. The special character of the chamber no.19 different from the other chamber is that in all the area of the upper chamber nuclear emulsion plates together with X-ray films are inserted under 3, 4 and 6 cm lead plates. Then we can study very precisely on the core structure of showers, with accuracy of $10 \mu\text{m}$, observed in the upper chamber as well as in the lower chamber.

The energy of each shower is estimated by track-counting method. Photometric measurement is also applied for high-energy showers.

Selection of the events Among the events observed in the chamber no.19 we pick up only the events which have at least one identified hadron and pass through the whole chamber, in order to get enough information on hadron component. In the Japanese part ($\sim 30 \text{ m}^2$ year, a half of the total area) of the chamber no.19, we found 19 events

with total observed energy greater than 100 TeV, incident energy $E_0 \sim 10^{15}$ eV, which satisfy the above criteria. The detection threshold energy is put to 2 TeV.

Identification of hadrons The showers in the lower chamber are those from local nuclear interactions in the target layer (C-jet with clean multi-core structure), those from local nuclear interactions in the lower chamber (Pb-jet-lower with clean single-core structure) and tails of showers from the upper chamber (with diffuse core structure). Thus almost all showers observed in the lower chamber are hadronic origin. The showers observed in the upper chamber are mixture of electromagnetic showers from the atmosphere and those from local nuclear interactions in the upper chamber itself (Pb-jet-upper). Among showers observed in the upper chamber, we consider the showers as hadrons when the showers can be seen only after 8 cascade unit of emulsion plate, that is, no electron shower track can be seen at the expected place of emulsion plate at 6 cascade unit, and/or when the showers continue to the lower chamber and new core can be seen in the lower chamber. The above procedure for identification of hadrons in the upper chamber can not pick up all hadrons interacted in the upper chamber, 20 ~ 30% of them are left unidentified.

3. Results.

Here we study how closely hadrons accompany electromagnetic showers in their neighbourhood by comparing with background calculation where only azimuthal angle ϕ of observed hadrons are randomly chosen in the observed families. Fig.1a shows a distribution of relative distance, R_{min} , between a hadron and its nearest neighbouring shower, and Fig.1b shows a distribution of energy-weighted relative distance, X_{min} , between a hadron and a shower nearest neighbouring in X_{ij} -space for the events of Chacaltaya chamber no.19. X_{ij} is defined by $X_{ij} = \sqrt{E_i E_j} \times R_{ij}$ where E_i and E_j are visible energy of hadrons and of electromagnetic showers and R_{ij} is relative distance between the two. The distributions are compared with background calculation. As is seen in the figures, there exists a bump above the background distribution both in small R_{min} region, $R_{min} < 400 \mu m$ and in small X_{min} region, $X_{min} < 2 \text{ GeV.m}$. Figs.2a and 2b are the same distributions shown above in $\log R$ and in $\log X$ scale but here hadrons are divided into four parts depending on their distance R_h measured from energy-weighted center of a family. The background distribution in small R_{min} and in small X_{min} becomes negligibly small when distance R_h of hadrons becomes larger, in contrast to that in the experimental data there still exist hadrons which accompany a shower in very small R_{min} and X_{min} even when R_h is large. There exist two hadrons which accompany a shower in R_{min} less than $160 \mu m$ and in X_{min} less than 0.6 GeV.m for the case of $R_h = 5 \text{ cm}$ where no hadrons are expected to accompany a shower in such small R_{min} and X_{min} region from the background calculation. The probability, p , that a hadron accompanies a shower at (energy-weighted) relative distance less than R_{min} or X_{min} is given by the background calculations. Then the probability Q_n that at least n hadrons accompany a shower at (energy-weighted) relative distance less than R_{min} or X_{min} is given by a binomial formula,

$$Q_n = \sum_{r=n}^{n_h} \binom{n_h}{r} p^r (1-p)^{n_h-r} \quad (1)$$

here n_h is the total number of observed hadrons. The observed number

of hadrons which accompany a shower in small R_{min} or X_{min} is very large compared with background distributions and the probability that such large number of hadrons accompany a shower in such small R_{min} or X_{min} is negligibly small, for example, we have 21 hadrons which accompany a shower in R_{min} less than $400 \mu m$ and 19 hadrons which accompany a shower in X_{min} less than 2 GeV.m. The probability that these two cases are realized, expected from background calculation, is $\sim 8.3 \times 10^{-7}$ and $\sim 2.1 \times 10^{-5}$ respectively. Thus we can conclude that there exist hadrons which accompany electromagnetic showers extraordinarily close to them, and such closeness in relative distance R_{min} and in energy-weighted relative distance X_{min} can not be reproduced simply by chance.

4. Discussions.

Those hadron and accompanied electromagnetic showers form isolated cluster of collimated showers, mini-cluster[2][3]. Then one may say that those cluster of showers are due to nuclear interaction at low altitude. However, if we interpret those clusters of showers as products of atmospheric nuclear interaction of normal type, $\langle p_t \rangle \sim 350$ MeV/c, the interaction height of them always gives very small value, around several to several ten meters above the chamber. We can estimate the number of hadrons arriving at the chamber by the observed number of C-jet and Pb-jet-lower under the assumption of a collision mean free path of hadrons. Then we can estimate the number of atmospheric interactions at low altitude, $H = 50$ m above the chamber for example. Table 2 shows a summary of the above argument for hadrons with visible energy, $E_h(\gamma)$, greater than 10 TeV. Almost all of shower clusters have their energy greater than 10 TeV. The estimated number of atmospheric interactions should be compared with the number of hadrons which accompany electromagnetic showers in the close vicinity of them. As one can see in the Table, the number of atmospheric interactions at such low altitude is very small compared with those hadrons unless we assume very short collision mean free path, $\sim 1/5 \lambda_{geo}$, of hadrons. The effect of the zinc roof of $\sim 1mm$ thick ($\sim 0.01 \lambda_{geo}$) which is located 3m above the chamber is also negligible. Thus if we assume that those mini-clusters are due to nuclear interaction in the atmosphere, the interaction point should be much higher and the average transverse momentum of produced particles should be much smaller (~ 10 times smaller) than normal one. In many of mini-clusters, a hadron carries a large portion of energy of a cluster. This fact indicates that a hadron is a core of a cluster and electromagnetic showers are accompanied by unknown mechanism.

Acknowledgement

The author would like to express his gratitude to Professors Y.Fujimoto and S.Hasegawa and to all the members of Chacaltaya emulsion chamber experiment for their valuable discussions and comments.

References

- [1] Y.Funayama and M.Tamada ; 19th ICRC HE 3.3-5
- [2] Brasil-Japan collaboration ; AIP Conf. Proceedings No.85(1981) p.500
S.Hasegawa ; Proceedings of Int. Sympo. on Cosmic Rays and Particle Physics, Tokyo(1984) 319
- [3] H.Bielawska et al. ; Proceedings of Int. Sympo. on Cosmic Rays and Particle Physics, Tokyo(1984) 374

no. of hadrons with $R_{\min} \leq 400$ μm	number of 'single hadrons'			arriving number of hadrons expected from C-jet and Pb-jet-lower			
	Pb-jet-upper identified	C-jet	Pb-jet-lower	λ geo.	$1/2\lambda$ geo.	$1/3\lambda$ geo.	$1/5\lambda$ geo.
21	12	8	1	23 ± 7 (1.0 ± 0.3)	21 ± 7 (1.8 ± 0.6)	24 ± 8 (3.2 ± 1.1)	41 ± 14 (9.5 ± 3.2)

Figures in parenthesis are estimated number of atmospheric interactions at the heights less than 50 m above the chamber.

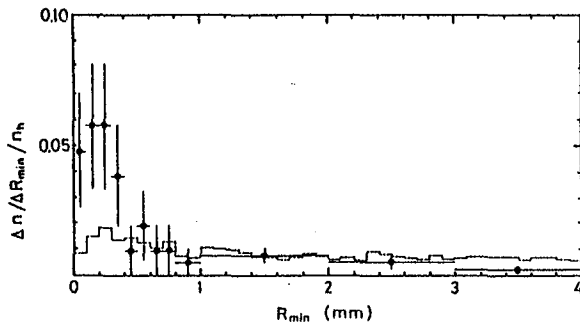


Fig.1a: Distribution of relative distance, R_{\min} , between a hadron and its nearest neighbouring shower. Histogram is a background distribution.

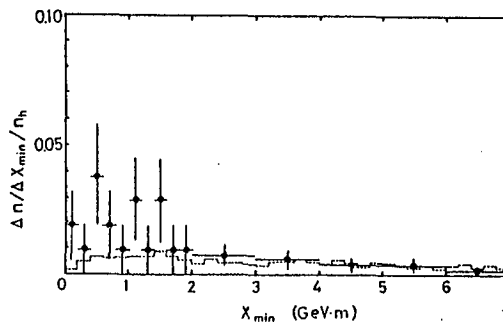


Fig.1b: Distribution of energy-weighted relative distance, X_{\min} , between a hadron and its nearest neighbouring shower in X_{ij} -space.

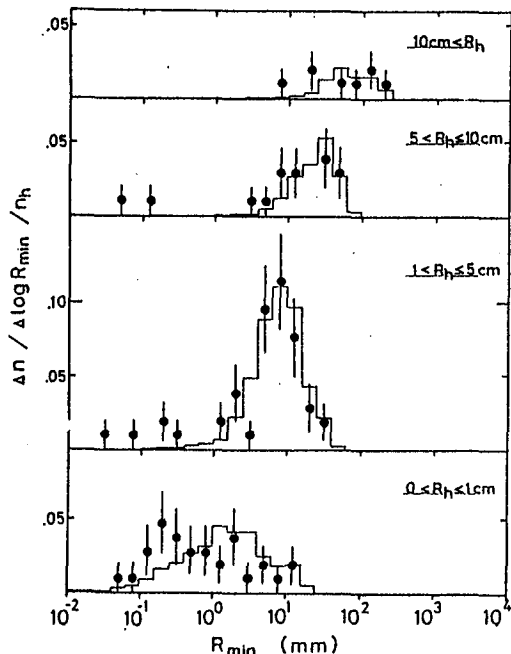


Fig.2a: Distribution of relative distance, R_{\min} , between a hadron and its nearest neighbouring shower for four different intervals of distance R_h of hadrons measured from the energy-weighted center of the event. Histograms are background distributions.

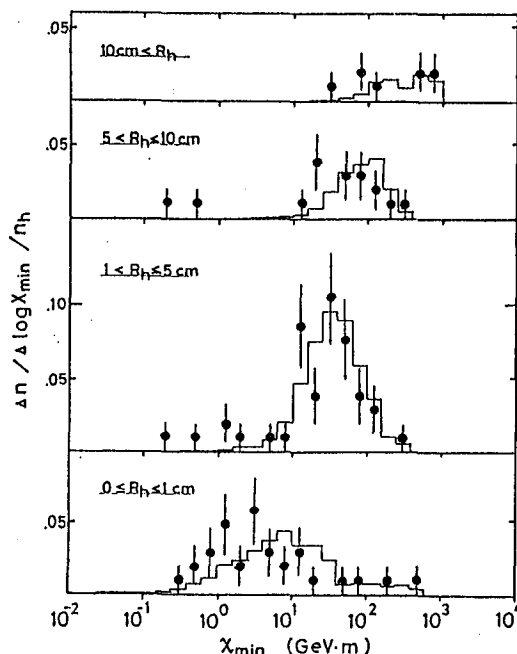


Fig.2b: Distribution of energy-weighted relative distance, X_{\min} , between a hadron and its nearest neighbouring shower in X_{ij} -space for four different intervals of distance R_h of hadrons.

Atmospheric Interactions detected in both the
Upper and the Lower Chambers at Chacaltaya

N.M.Amato*, N.Arata* and R.H.C.Maldonado**

* Centro Brasileiro de Pesquisas Físicas
Rua Dr. Xavier Sigaud 150
22290 Rio de Janeiro, RJ, Brasil

** Instituto de Física
Universidade Federal Fluminense
Niteroi, RJ, Brasil

1. Introduction

Brasil-Japan Collaboration has been studying the cosmic ray interactions in the energy region $10^{13} - 10^{17}$ eV by means of emulsion chambers exposed at Chacaltaya, 5220 m above sea-level, Bolivia[1]. The recent chambers have a two-storied structure, and the events which are observed both chambers have given us important informations on the phenomena. For example, the first Centauro event was detected as a small shower at the bottom of the upper chamber and as a big fraction of energy deposit in the lower chamber, which indicated a high contribution of hadronic showers[1].

We are almost finishing the complete analysis of the events of atmospheric interactions with such continuation for the Rio part of the 19th chamber. In this paper, we describe some results of the events with continuation in the rather low energy region which are often eliminated in the discussion only because of their low energy.

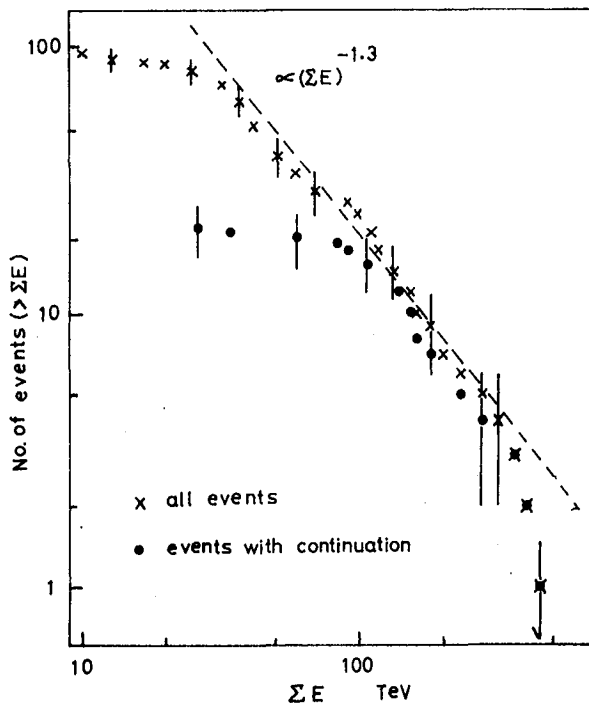


Fig.1 The integral distributions of total visible energy. (x) for all the events and (•) for the events with continuation.

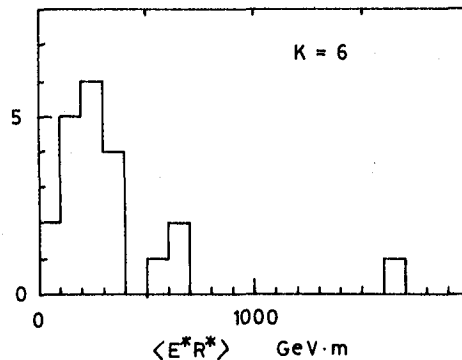


Fig.2 The histogram of $\langle E^*R^* \rangle$, where $K=6$ GeV·m is used for decascading.

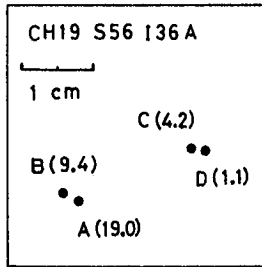
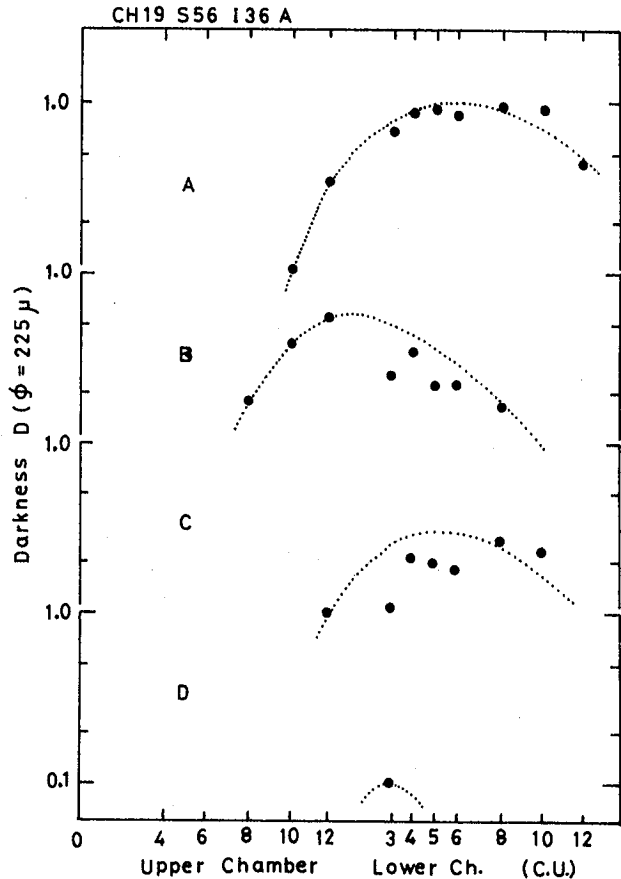


Fig.3 The target diagram of CH19 S56 I36 A. The name and energy of each core is shown.

Fig.4 The transition of darkness D with slit diameter 225μ for 4 cores in S56 I36 A. The fitting curves are also shown.



2. Experiment

The 19th chamber is two-storied, and for the whole upper and lower chambers, nuclear emulsion plates were inserted in sandwiches of lead plates together with X-ray films. The exposure time was 677 days. The upper chamber has total area of 44.2 m^2 and the lower chamber 32.4 m^2 . They are formed by unit blocks of dimension $40 \times 50 \text{ cm}^2$; in Rio de Janeiro have been analyzed 59 blocks of the upper chamber and 48 blocks of the lower chamber.

We must observe at least two penetrative shower cores in both the upper and the lower chambers, in order to determine the relative geometrical position of all the showers in both chambers. We have observed 21 events with such continuation. Fig.1 shows the integral distributions of the total energy visible in the form of electro-magnetic cascade showers for all the events and for the events with continuation. We notice that the distribution for all the events obeys $\propto (\Sigma E)^{-1.3}$, which is consistent with the previous measurements [1].

Fig.2 shows the distribution of average energy-weighted lateral spread, $\langle E^*R^* \rangle$, for the 21 events, where the so-called decascading constant $K = 6 \text{ GeV}\cdot\text{m}$ was chosen [2]. We usually have a larger interest in the region of large ER, but in the following we describe three events in the small ER region.

3. Results

We have two events with continuation in the interval of

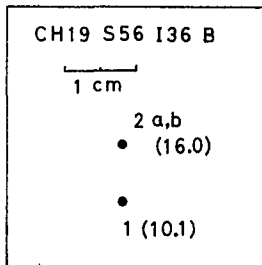
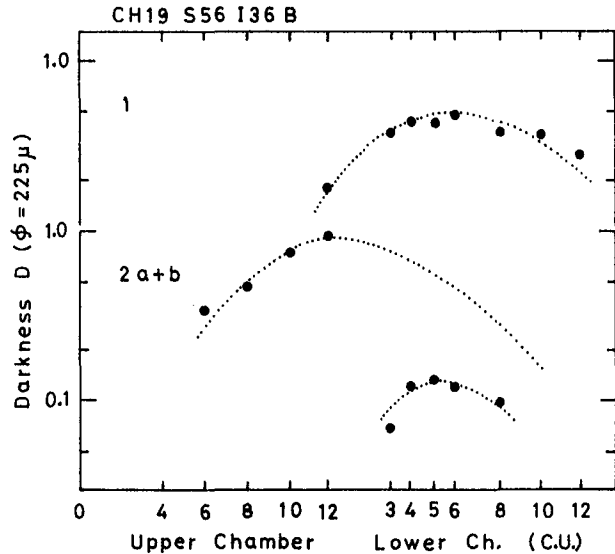


Fig.5 The target diagram of CH19 S56 I36 B.

Fig.6 The transition of D for 2 spots in S56 I36 B.



$\langle E^*R^* \rangle$ less than 100 GeV.m.

The names of the events are CH19 S56 I36 A and CH

19 S56 I36 B; it is a coincidence that these two events were

observed in the same blocks.

CH19 S56 I36 A Fig.3 shows the target diagram of this event. The event consists of only four shower spots with the total visible energy 33.7 TeV. Fig.4 shows the transition of darkness D on the N-type X-ray films for the four spots of the event. The slit size is 225 μ in diameter. The depth of lead is indicated by the cascade unit of each chamber.

#A starts to be observed at the very deep layer, 8 cu on the emulsion plate and 10 cu on the X-ray film, as a sharply collimated shower core. #B starts to be observed at 8 cu and we can not find any track on the corresponding position at 6 cu. #C starts to be observed at 12 cu. #D is observed only in the lower chamber as a diffused small shower.

Down to 6 cu in the upper chamber, this event does not appear for detection, and the cores B, A, C and D start to appear, one by one, to form the event.

We can identify all the four cores as hadronic because of their deep penetration. This event is lacking in electromagnetic components at the entrance of the chamber within the limit of detection threshold (~ 1 TeV).

CH19 S56 I36 B Fig.5 shows the target diagram of this event. The event consists of two spots (#1 and #2) with the total visible energy 26.1 TeV. #2 consists of two constituent cores (a and b) with the very short mutual distance 33 μ . Both the two spots continue into the lower chamber.

Fig.6 shows the transition of spot darkness on the N-type X-ray films. #1 starts to appear at 12 cu in the upper chamber as a collimated core and in the lower chamber as multi-cores. #2 starts to be observed at 6 cu and the spacing effect of air-gap between the upper and the lower chambers is clearly seen in Fig.6.

We can identify #1 as a hadronic core, but we can not judge whether #2 contains hadronic nature.

CH19 S83 #200 This event is observed only in the upper chamber. Fig.7 shows the target diagram of this event. The event consists of two spots (#1 and #2) with the total visible energy ~ 30 TeV. #1 consists of two constituent cores (a and b) with the mutual distance 175μ .

Fig.8 shows the transition of electron number counted on the nuclear emulsion plates in the area $78 \times 78 \mu^2$. #1a appears as a normal shower, but #1b starts to appear at 8 cu and grows up remarkably down to 12 cu. #2 is observed only at 12 cu in the upper chamber.

We can identify #1a and #2 as hadronic cores. We can not judge #1b as a hadronic core.

4. Discussions

We have encountered interesting (exotic) events in the high energy region, $\Sigma E > 80 - 100$ TeV [1,3]. But as shown in the previous section, we can pick up some events with an impressive character even in the lower energy region.

In the energy interval, 25 - 35 TeV, we have analyzed 18 events, among which 3 events showed a hadron-rich nature. If we use the power fit of $(\Sigma E)^{-1.3}$ in Fig.1, these 3 events are in the unbiased sample of ~ 40 events in that energy interval.

More details on the events with continuation will be presented at the Conference.

5. Acknowledgement

The authors wish to acknowledge all the members of the Brasil-Japan Collaboration for their kind support. They are grateful to Profs. F.M. Oliveira Castro and H.M. Portella for their continuous encouragement. They also thank T.T.Villar, N.Miranda and I.A.Lopez in CBPF for their help in scanning work. Thanks are also due to the CNPq, Brasil, for a financial support.

References

- [1] C.M.G.Lattes, Y.Fujimoto and S.Hasegawa, Phys.Rep. 65 (1980) 151 and references therein.
- [2] H.Semba, Supplement of Prog.Theor.Phys. 76 (1983) 111.
- [3] Brasil-Japan Collaboration, AIP Conference Proceedings, 85 (1981) 500.

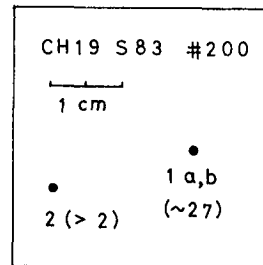


Fig.7 The target diagram of S83#200.

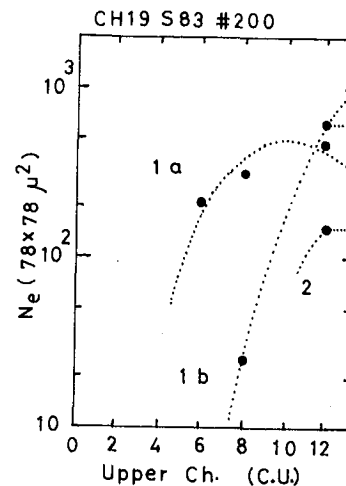


Fig.8 The transition of electron number inside the counting area $78 \times 78 \mu^2$.

LATERAL DISTRIBUTION OF HIGH ENERGY HADRONS AND GAMMA RAY
IN AIR SHOWER CORES OBSERVED WITH EMULSION CHAMBERS

Matano, T. and Machida, M.

Department of Physics, Saitama University,
338 Urawa, Japan

Kawasumi, N., Tsushima, I., Honda, K. and Hashimoto, K.

Department of Physics, Yamanashi University,
400 Kofu, Japan

Navia, C., Martinic, N. and Aguirre, C.

Instituto de Investigaciones Fisicas
Universidad Mayor de San Andres, La Paz, Bolivia

1. Introduction

We have observed a high energy event of a bundle of electrons, γ rays and hadronic γ rays in an air shower core. This bundle were detected with an emulsion chamber with thickness of 15 cm lead installed in the central part of SYS air shower array at Mt. Chacaltaya. The size of air shower accompanying the bundle is 1.5×10^7 and the age parameter is determined 0.17 from the steepness of the lateral structure. This air shower is estimated to be initiated with a proton with energy around 10^{17} to 10^{18} eV at a altitude of around 100 gcm^{-2} above Mt. Chacaltaya. We have determined lateral distributions of the electromagnetic component (for simplicity, we call this component as gamma ray) with energy above 2 TeV and also the hadronic component of energy above 6 TeV of this air shower core respectively. These lateral distributions may also ones at the very early stage of air shower development.

We have also studied so-called $E_\gamma R_\gamma$, $E_H R_H$ distribution. Here E_γ , E_H are the energy of each gamma ray and hadronic γ ray respectively. R_γ , R_H are the radial distance from the center of the bundle of these particles. As well known, we can determine the transverse momentum from the product of energy and distance of a particle (ER) divided with a production height (H).

Since particles in the bundle are produced with process of the development of the nuclear cascade, we can not know the primary energy of each interaction in the cascade which produces these particles. In order to know the primary energy dependence of transverse momentum, we study the average products of energy and distance ($\langle ER \rangle$) for various average energies of secondary particle ($\langle E \rangle$).

2. Lateral distribution of gamma rays and hadrons

Centers of the bundle are determined from the energy weighted mean of positions of gamma rays and hadrons respectively. The deviation between two centers is only less than 1 mm and both are in agreement.

Lateral distributions of gamma rays and hadrons are shown in Fig.1 and Fig.2 for two different threshold energies. The slopes of these distributions are in agreement.

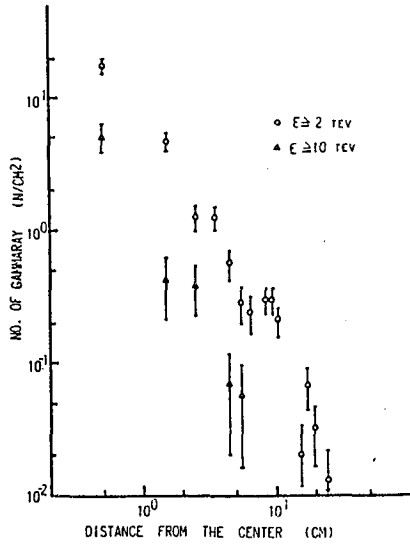


Fig. 1. Lateral distribution of gammarays.

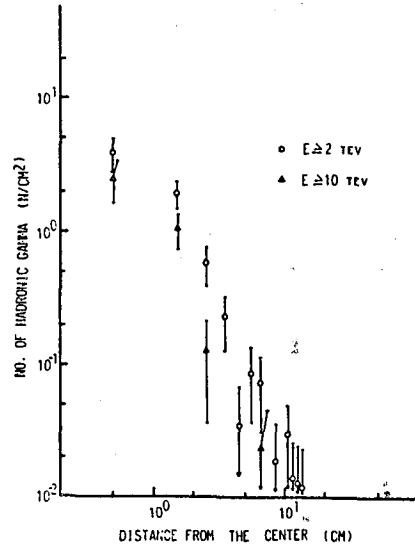


Fig. 2. Lateral distribution of hadrons.

Distributions are represented by the power law of the form r^{-n} . The exponent (n) is about 1.8 for gamma rays and about 1.9 for hadrons.

3. ER distributions

ER is the parameter which reflect the transverse momentum of that particle. Fig. 3 and Fig. 4 show ER distribution for gamma rays and hadrons respectively. The distributions for hadrons with energy more than 10 TeV is flatter than others untill higher ER values.

The relation between the averages, $\langle ER \rangle$ and $\langle E \rangle$, are

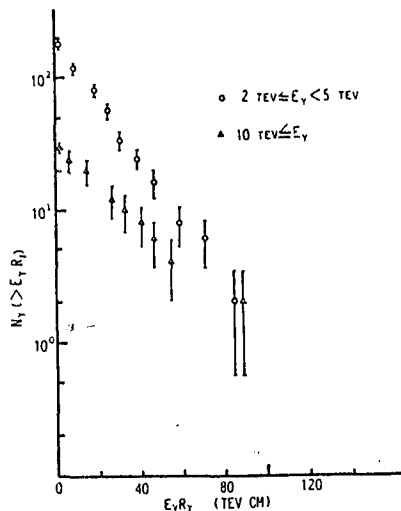


Fig. 3. ER distribution of gammarays.

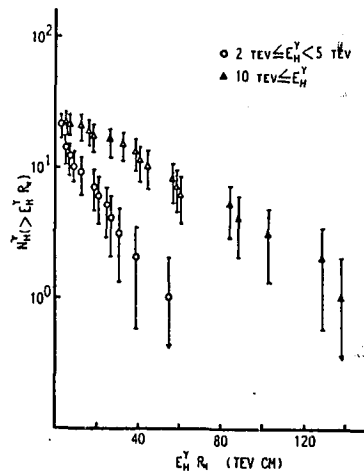


Fig. 4. ER distribution of hadrons.

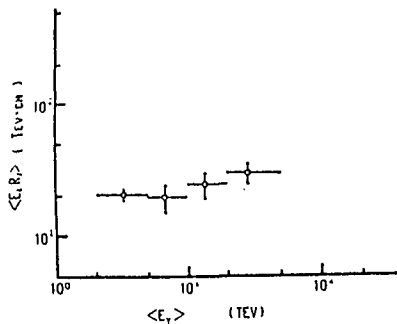


Fig. 5. Relation between the average of ER and E of gamma rays.

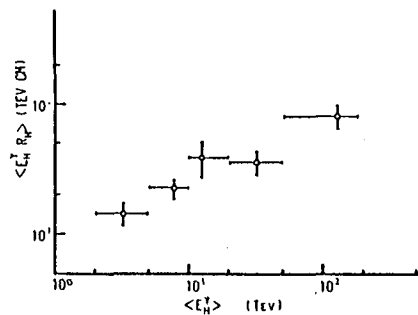


Fig. 6. Relation between the average of ER and E of hadrons.

shown in Fig. 5 and Fig. 6 for gamma rays and hadrons. The average $\langle ER \rangle$ increase with increasing the mean energy $\langle E \rangle$. This tendency is remarkable for high energy hadrons. This tendency is found in ER distributions of gamma rays and hadronic gamma rays of events Andromeda and M.A.M. These events are the most high energy events among five families of the highest energy range, $\sum E_T > 1000$ TeV observed by Chacaltaya Emulsion Chamber Experiment of Brasil-Japan Collaboration.¹⁾

4. Energy dependence of transverse momentum

Transverse momentum is determined from ER divided by production height. In the air shower, hadrons are not produced in a single interaction, but individual interactions at different stages in a nuclear cascade of air shower development. Radial distance R, however, corresponds to radial deviation caused by final interaction in which that particle is produced. Therefore, we can estimate P_T with these R and an estimated most probable production height above the observation level. In the present case, we use 80 gcm^{-2} which is consistent to a height estimated from calculations of air shower development. We estimated P_T with $P_T = (E_H^T \times 3 \times R)/H$ for hadron and $P_T = (E_T \times 2 \times R)/H$ for gamma ray. Factor 3 comes from the charge symmetry in hadron interaction and factor 2 from two gamma decay of a neutral pion. Result are shown in Fig. 7. In the figure, we show also data obtained from CERN experiments.²⁾ In order to compare the accelerator results with present results, interaction energy in the laboratory system transferred from colliding particle energy is divided with the average multiplicity of secondary particles.³⁾ Two points obtained from ISR and $P\bar{P}$ collider are connected with a dashed line. The present results are on the extrapolation of this line. In spite of uncertainty of air shower experiments, these data seem to be in good agreement. In the higher energy region, P_T increase much largely apart from the extrapolation of the energy dependence of lower energy region.

This figure shows that P_T increase with the power law of the average energy of shower particle of the form E^n of the

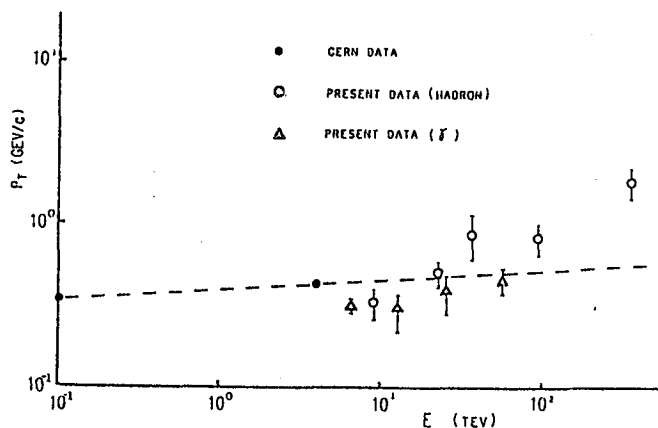


Fig.7. Relation between $\langle P_T \rangle$ and shower particle $\langle E \rangle$.

exponent $n=0.06$. However, in the extremely high energy region, the exponent increase to $n=0.44$.

In model calculations on the nuclear cascade of energy around 10^{17} eV, high energy hadrons can not be produced by secondary pion after passing through 80 gcm^{-2} . Consequently, hadrons with energy more than 100 TeV may be produced in fragmentation region of nucleon interaction.

We can conclude that this remarkable increase of P_T for hadrons above 100 TeV with increasing average hadron energy may be a noteworthy characteristics of the energy dependence of transverse momentum especially in the fragmentation region.

Acknowledgements

This work was supported by the Grant-in-Aid for Oversea Survey of the Ministry of Education, Science and Culture in Japan. The authors wish to thank prof. C. Grupen, Siegen University, for fruitful discussion during his stay in Japan.

References

- 1) Yamashita, S., et al, ICR-Report-112-83-6, 123(1983)
- 2) Arnison, G., et al, UA1 Collaboration, Proc. Third Topical Workshop, CERN 83-04, 75(1983)
- 3) Ward, D., et al, UA5 Collaboration, Proc. Third Topical Workshop, CERN 83-04, 75(1983)

SIZE DISTRIBUTIONS OF AIR SHOWERS ACCOMPANIED WITH HIGH ENERGY GAMMA RAY BUNDLES OBSERVED AT MT. CHACALTAYA

Matano, T. and Machida, M.

Department of Physics, Saitama University,
338 Urawa, Japan

Tsushima, I., Kawasumi, N., Honda, K. and Hashimoto, K.

Department of Physics, Yamanashi University,
400 Kofu, Japan

Martinic, N., Zapata, J., Navia, C., Aguirre, C., Siles, L.
and Magnani, R.

Instituto de Investigaciones Fisicas
Universidad Mayor de San Andres, La Paz, Bolivia

ABSTRACT

We report size distributions of air showers accompanied with bundle of high energy gamma rays and/or large size bursts under emulsion chambers, in order to study the composition of primary cosmic rays and also characteristics of high energy nuclear interaction.

Air showers initiated by particles with a large cross section of interaction may develop from narrow region of the atmosphere near the top. Consequently, fluctuations of sizes of air showers are not so large.

On the contrary, starting levels of air showers by particles with smaller cross section fluctuate in wider region of the atmosphere. Air showers of extremely small size accompanied with bundle of gamma rays may be ones initiated by protons at lower level after penetrating deep atmosphere without interaction. In such cases, the air shower size distribution may be flatter than previous case.

We have determined the relative size distribution according to the total energy of bundle of gamma rays and the total burst size observed under 15 cm lead absorber. These results are discussed on the point of view mentioned above.

EAS ACCOMPANIED BY GAMMA-FAMILIES AT MT. NORIKURA AND COMPARISON
WITH MONTE CARLO SIMULATION

Shima, M., Saito, To., Sakata, M. and Yamamoto, Y.

Konan University, Kobe, Japan

Kasahara, K. and Yuda, T.

Institute for Cosmic-Ray Research, University of
Tokyo, Tanashi, Japan

Torii, S.

Kanagawa University, Yokohama, Japan

Hotta, N.

Utsunomiya University, Utsunomiya, Japan.

ABSTRACT

The experimental data of EAS accompanied by gamma-families, with total energy greater than 10 TeV, obtained at Mt. Norikura, were compared with a Monte Carlo simulation with a rising cross section proportional to $E^{0.04}$ for the p-air inelastic cross section. It is found that the absolute intensity of size spectrum of such EAS is strongly affected by the primary protons intensity at 10^{15} - 10^{16} eV region and the experimental size spectrum agrees with the simulated spectra for the p-poor (<15%) primary composition better than the p-rich ($\geq 30\%$) one.

1. Introduction

The longitudinal development of EAS cores, especially at its early stages, depends on the collision mean free path and/or mass number of primary cosmic-ray particle in the atmosphere. The penetrated protons through the upper atmosphere without collisions or with a few semi-elastic collisions, even though their primary energies are a little low, are more advantageous to yield gamma-families at high mountains than the survival nucleons with normal fraction of energy in the normal EAS development. The inverse power form of the primary energy spectrum hastens this tendency. On the other hand, primary heavy nuclei are quite disadvantageous to generate gamma-families at mountain altitudes, because their primary energies are rapidly splitted into a lot of particles in the upper atmosphere due to their short mean free path and the plenty of initial constituent nucleons. Then, the observation of EAS accompanied by gamma-families with total energy greater than a certain value in an appropriate size range at mountain altitudes is nearly equivalent to observe EAS initiated by primary protons preferentially.

The combined EAS with gamma-families, which were obtained by the cooperative experiment between the EX chamber and the EAS array at Mt. Norikura (738 gcm^{-2}), were compared with the simulation with respect to the shape of size spectrum once at Bangalore (Nakatsuka et al., 1983). After that, the experimental data were reanalysed and a few combined events were added. The summary of the new results is presented in this Conference (HE-3.3-11). On the other hand, the simulation calculation was thoroughly renewed by employing the rising cross section, zenith angle distribution of incident particles and by extending the Monte Carlo

calculation to lower energy than the former calculation by three orders. The results of new simulation are fairly different from the old one due to those changes, especially due to the last procedure described above. Then, we must abandon the former conclusions reported at Bangalore and the new results are presented here.

2. Assumptions and procedures in the simulation

First, the models about the hadronic interactions are summarized. The inelastic cross section of p-air collision has an energy dependence of a form E^δ instead of the constant cross section $\sigma(p\text{-air})=300$ mb in the old model of simulation (Kasahara et al., 1979). When the energy dependence of $\bar{p}p$ cross section is expressed by E^δ , that of p-A cross section (A: mass number) is roughly given by $\propto (2E^\delta - 1 + A^{1/3})^2 / (1 + 2A^{1/3} + A^{2/3})$ by a simple consideration that the increase of nuclear radius is due to swelling of only surface nucleons. This function is approximated by $\sigma(p\text{-air}) \propto E^{\delta'}$ again. For instance, the values $\delta=0.073 \sim 0.11$ representing the $\bar{p}p$ cross section from ISR data up to SPS data (Matthiae et al., 1983) are converted to the values $\delta'=0.044 \sim 0.068$ for p-air collisions. In this paper we use a moderate rising cross section $\delta'=0.04$ as shown in Fig. 1. The multiplicity of secondary particles satisfies the KNO scaling in all energy region but the mean multiplicity depends on collision energy in the form $a + b \ln s + c \ln^2 s$ with $a=0.88$, $b=0.44$ and $c=0.118$ as shown in Fig. 2, which is nearly equivalent to the old one. The inelasticity distribution is not changed from the old one. The rapidity distribution of secondary particles keeps nearly the form $(1-x)^4/x$ as in the scaling model although the cross section of QCD large p_T jets is added to the normal cross section in the new simulation. The calculation was done by the full Monte Carlo method until the energy of each shower particle becomes lower than 1 GeV. Hadronic jets in the iron EX chamber were simulated for the high energy hadrons arrived at the chamber and those which released electromagnetic energy greater than 3 TeV in the chamber were joined into gamma-families. We picked up only the simulated showers accompanied by a gamma-family with total cascade energy $\Sigma E_{\gamma, H} \geq 10$ TeV, $n_{\gamma, H} \geq 2$ for $E_{\min}=3$ TeV, involving hadron initiated cascades, at the level of Mt. Norikura in accordance with the experimental conditions. And, the total number of shower particles (Ne) of them is calculated by connecting the one dimensional

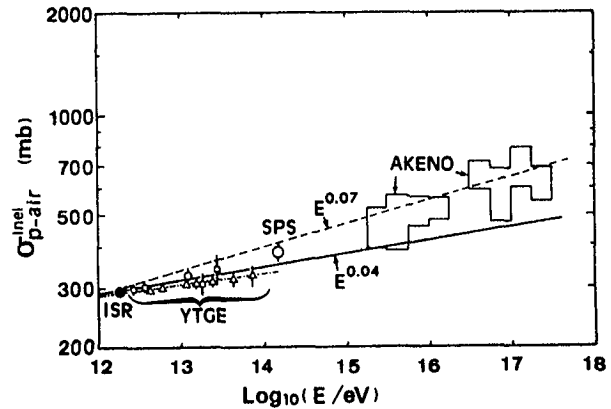


Fig. 1 Energy dependence of p-air inelastic cross section. $\bar{p}p$ accelerator data by ISR and SPS are transformed to p-air cross section. The solid curve with $\delta'=0.04$ is assumed in the simulation. YTGE means the calculation by Yodh et al. (Yodh et al., 1983).

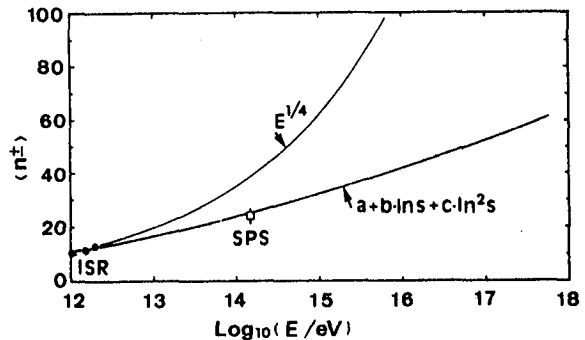


Fig. 2 Energy dependence of mean charged multiplicity. The solid curve is employed in the simulation.

cascade function to each shower particles generated by the full Monte Carlo method. The contribution of hadrons with energies less than 1 GeV is neglected. The conversion factor, i.e., primary energy per maximum EAS size is about 1.5 ~ 1.7 GeV/particle for the normal EAS with sizes from 5×10^5 - 10^7 in this simulation.

Second, the models about the energy spectrum of primary cosmic rays are described. The experimental data are briefly summarized in Fig. 3 (a). The total energy spectrum is represented by the solid curve which is smoothly connecting the Grigorov's data (Grigorov et al., 1972) and the air shower data at Akeno (Nagano et al., 1983). In this simulation are assumed two extreme models about the primary composition, especially about the fraction of iron nuclei. One is the p-rich spectrum as shown in Fig. 3 (b), where the fraction of iron nuclei is very small. Another one is the p-poor spectrum as shown in Fig. 3 (c), where iron nuclei are extremely abundant. The fractions of proton, helium and iron are tabulated at several energies in Table 1. The flat distribution of zenith angle with which the primary particles rush into the atmosphere is adopted instead of the vertical incidence.

3. Results of calculation

The primary spectrum is cut at 10^{15} eV as its lower end in the calculation. This primary energy is corresponding to a mean shower size $\sim 6 \times 10^5$ at the shower maximum. Because EAS accompanied by such gamma-families we concern are generally at stages before the shower maximum and their sizes have a narrower correlation with primary energies than the general EAS, the size spectrum of them is surely free from the

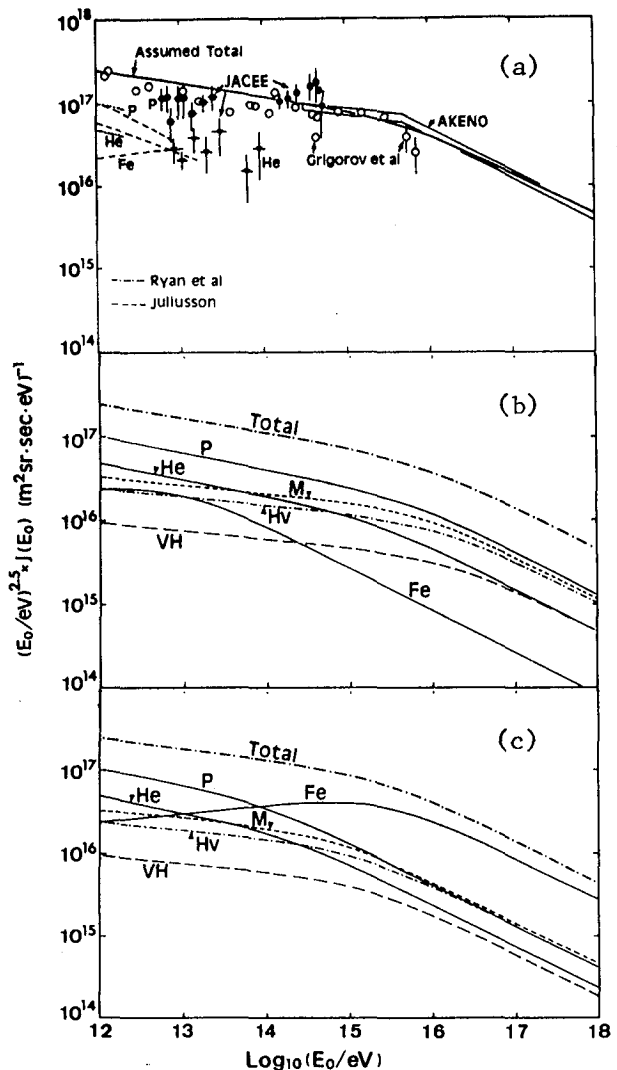


Fig. 3 Differential energy spectrum of primary cosmic rays.

- (a); summary of experimental data. Some points are converted from integral form by Juliusson's way (Juliusson, 1975).
 (b); p-rich primary spectrum assumed in the simulation.
 (c); p-poor primary spectrum assumed in the simulation.

Table 1

Energy	(eV)	10^{14}	10^{15}	10^{16}	10^{17}
p-rich	P	31.8%	34.3%	32.8%	28.6%
	He	17.3	15.7	12.2	10.7
	Fe	8.9	3.7	2.3	1.9
p-poor	P	25.4	14.8	10.0	8.1
	He	13.1	8.0	5.6	4.6
	Fe	30.0	45.5	58.5	61.4

bias due to the cutoff at the lower end of the primary spectrum for the size region $N_e \geq 10^6$ at the observation level. Then, the comparison with the experimental size spectrum is done in this size region.

The number of primary particles sampled is 480 for the p-rich spectrum and 561 for the p-poor spectrum. Out of them the number of EAS accompanied by gamma-families with $\Sigma E_{\gamma, H} \geq 10$ TeV, $n_{\gamma, H} \geq 2$ for $E_{\min} = 3$ TeV is 45 events for the p-rich spectrum and 25 events for the p-poor one. The zenith angle distribution of these EAS are shown in Fig. 4 for the two cases of assumed primary spectrum. Both of them are represented by the theoretical curve with $x_0/\Lambda_{\text{att}} = 7.0$, which is consistent with the experimental data (Mitsumune et al, 1985). The integral size spectra of those EAS accompanied by gamma-families are shown by step lines in Fig. 5. From this figure we can see that the experimental data agree with the p-poor primary spectrum but not with the p-rich one.

4. Conclusions

Using the moderate rising cross section proportional to $E^{0.04}$ for p-air collision in the simulation calculation, the experimental size spectrum of EAS accompanied by gamma-families with $\Sigma E_{\gamma, H} \geq 10$ TeV, $n_{\gamma, H} \geq 2$ for $E_{\min} = 3$ TeV agrees with the simulated result in the p-poor (<15%) case better than in the p-rich ($\geq 30\%$) case.

5. Acknowledgements

The calculation was carried by the computer FACOM 380R of the Institute for Nuclear Study, University of Tokyo.

6. References

- Nakatsuka et al., 1983; Conf. Papers of 18th ICRC (Bangalore), 11, 346.
 Kasahara et al., 1979; Conf. Papers of 16th ICRC (Kyoto), 13, 75.
 Matthiae, 1983; Proceedings of Int. Europhys. Conf. on H. E. P., 714.
 AKENO; Hara et al., Phys. Rev. Letters, 50 (1983), 2062.
 Yodh et al., 1983; Phys. Rev. D, 27 (1983), 1183.
 Grigorov et al., 1971; Conf. Papers of 12th ICRC (Hobart), 5, 1746.
 Nagano et al, 1983; J. Phys. G, 10 (1984), 1295.
 Juliusson, 1975; Conf. Papers of 14th ICRC (Munich), 8, 2689.
 Ryan et al, 1972; Phys. Rev. Letters, 28 (1972), 987.
 JACEE; Burnett et al, Proceedings of Int. Symposium on Cosmic Rays and Particle Physics at Tokyo (1984), 468.
 Mitsumune et al, 1985; this Conference, HE-3.3-11.

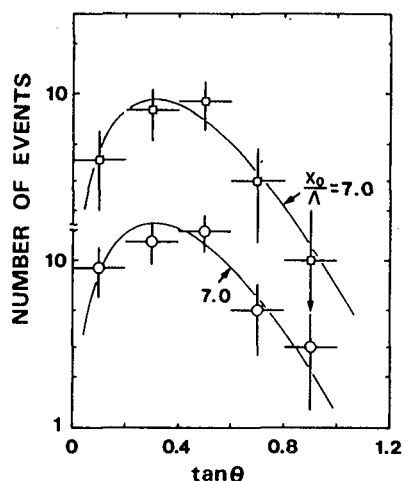


Fig. 4 Zenith angle distribution of simulated events with gamma-families. Open circles are for the p-rich spectrum and open squares for the p-poor one.

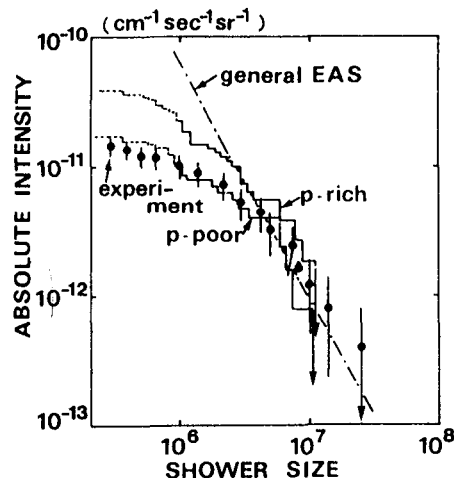


Fig. 5 Size spectra of EAS accompanied by gamma-families with $\Sigma E_{\gamma, H} \geq 10$ TeV, $n_{\gamma, H} \geq 2$ for $E_{\min} = 3$ TeV at the level of Mt. Norikura (738 g cm^{-2}).

COMPARISON OF ABSOLUTE INTENSITY BETWEEN EAS WITH GAMMA-FAMILIES
AND GENERAL EAS AT MT. NORIKURA

Mitsumune, T., Nakatsuka, T., Nishikawa, K., Saito, To.,
Sakata, M., Shima, M. and Yamamoto, Y.

Konan University, Kobe, Japan.

Dake, S. and Kawamoto, M.

Kobe University, Kobe.

Kusunose, M., Ohmori, N. and Sasaki, H.

Kochi University, Kochi, Japan.

Hotta, N.

Utsunomiya University, Utsunomiya, Japan.

ABSTRACT

Gamma-families with total energy greater than 10 TeV, found in the EX chamber which was cooperated with the EAS array at Mt. Norikura, were combined with EAS triggered by big bursts. The absolute intensity of the size spectrum of these combined EAS was compared with that of general EAS obtained by AS trigger. EAS with sizes greater than 2×10^6 were always accompanied by gamma-families with $\Sigma E_{\gamma, H} \geq 10$ TeV, $n_{\gamma, H} \geq 2$ and $E_{min} = 3$ TeV, although the rate of EAS accompanying such gamma-families decreases rapidly as their sizes decrease.

1. Introduction

The results of the cooperative experiment of the 20 m² iron EX (emulsion and/or X-ray film) chamber and the EAS array at Mt. Norikura (738 gcm⁻²) were reported once at Bangalore (Nakatsuka et al., 1983). Thereafter, the reanalysis of combination between gamma-families and EAS was done and a few new combined events were obtained. And, some of the old data were revised, especially the EAS size N_e and age parameter s were renewed by taking account of the transition effect of the materials over the scintillation counters and of the plastic scintillator itself for EAS density measurement. The data of general EAS obtained by the AS trigger in the same period of this experiment were analysed. In this report the EAS combined with gamma-families of total energy greater than 10 TeV is compared with the general EAS thus obtained with respect to the absolute intensities of EAS size spectrum.

2. Experiment

The experimental apparatus was described before (Yamamoto et al., 1981). The EAS data were taken by two kind of triggers. One was a burst trigger under the 14 r.l. thick EX chamber when any one of 72 burst scintillation counters responded to bursts greater than about 2000 particles per detector of 0.25 m² unit area. These EAS events with big bursts were provided for the analysis of combination with gamma-families. Another one was an AS trigger by four sets of four-fold coincidence of the nearest four out of the central nine non-covered scintillation counters.

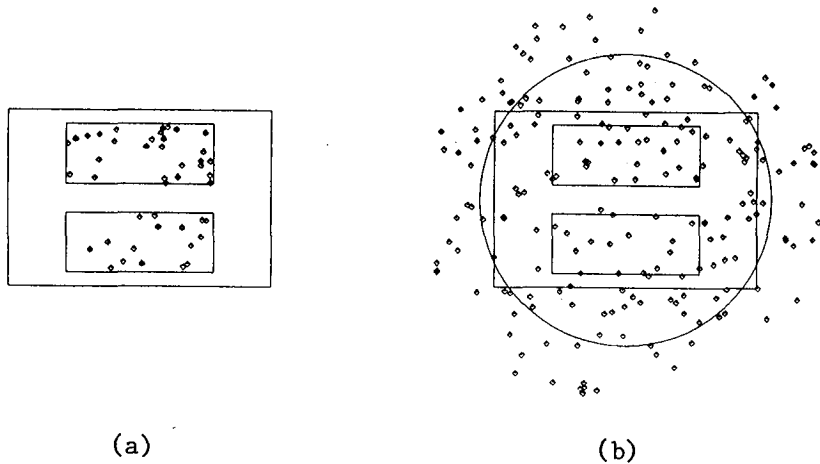


Fig. 1 Map of EAS axis locations.

(a): the EAS combined with gamma-families of $\Sigma E_{\gamma, H} \geq 10$ TeV. Two small rectangles indicate the EX chambers (10 m^2 each) and a big one is the spark area ($9 \times 6 \text{ m}^2$).

(b): the general EAS with $N_e \geq 2 \times 10^6$. Only the events hit the area within $r=5 \text{ m}$ were used for the analysis.

The period of the experiment was 302.5 days and the live time of recording system of EAS data was 292.2 days (95.7 %). The total number of EAS recorded by the burst trigger in this period was about 12000 events and the number of EAS obtained by the AS trigger was about 6000 events during about 240 days. The arrival angles of EAS, which are necessary for combining them with gamma-families and for deducing absolute intensity of EAS size spectrum, were detected by four sets of spark chambers. The live time of spark chamber system was a little higher than 80 %.

3. Selection of events

53 gamma-families with total energy $\Sigma E_{\gamma, H} \geq 10$ TeV and $n_{\gamma, H} \geq 2$ for $E_{\text{min}} = 3$ TeV were found in our EX chamber and 44 events out of them were combined with EAS triggered by big bursts. The rate of combination was 83 %. Nine gamma-families were not combined with EAS. This is mainly due to the lack of arrival angle data of EAS because of dead time of the spark chamber system. The data of these 44 combined events were used for deducing the absolute intensity of EAS with big gamma-families assuming that the residual nine unknown EAS have the same size distribution as the combined events. The EAS size N_e and age parameter s were determined by fitting the experimental shower particle density to the NKG lateral function with the Moliere unit 110 m, where the shower axis was put on the location of the gamma-family whose map was given in Fig. 1 (a). On the other hand, about 4200 EAS recorded during the last 170 days by the AS trigger were served for the size spectrum of general EAS. The axis locations of the general EAS whose axes hit the area within radius $r=7 \text{ m}$ from the array center are shown in Fig. 1 (b) for $N_e \geq 2 \times 10^6$. But, only the EAS whose axes hit the area of $r \leq 5 \text{ m}$ were employed for the analysis here.

4. Results

Using the experimental result about the transition effect of EAS shower particle density by thin materials (Saito et al., 1983) the corrections were made on the raw values of Ne and s for the response excesses of 3 cm thick plastic scintillator and also for the transition effect due to the roof and ceiling materials for indoor counters and due to the counter box material for all counters. As a result, the age parameter s was increased by the amount of 0.18 ~ 0.16 and the shower size Ne was multiplied by a factor 0.65 ~ 1.16 depending on the raw values of s from 0.4 to 1.2. The Ne-s scatter plot of the combined events after the correction is shown in Fig. 2. In this figure are also shown the Ne-dependences of average age parameters for combined events (crosses) and for the general EAS (open diamonds).

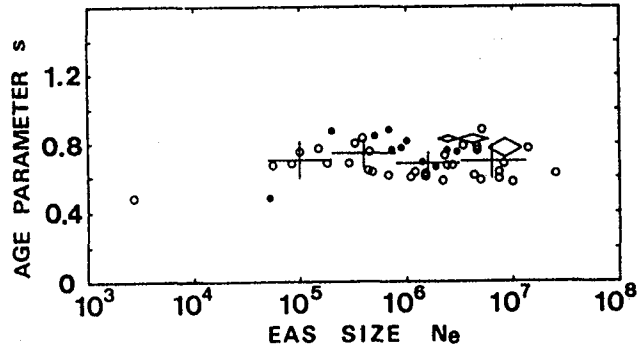


Fig. 2 Ne-s correlation for the combined EAS with gamma-families with $\Sigma E_{\gamma, H} \geq 10$ TeV (scatter plot and crosses) and for the general EAS with sizes $Ne \geq 2 \times 10^6$ (open diamonds).

In order to get the vertical intensity of size spectrum of EAS it is necessary to know the zenith angle distribution of them. In Fig. 3 (a) are shown the distributions for the combined EAS with gamma-families of $\Sigma E_{\gamma, H} \geq 10$ TeV (closed circles) and for the general EAS with $Ne \geq 2 \times 10^6$ (open circles). It is natural that the zenith angle distribution of the combined EAS is steeper than the general EAS but almost same as the gamma-families shown in Fig. 3 (b). Using the values of a factor x_0/Λ_{att} in the

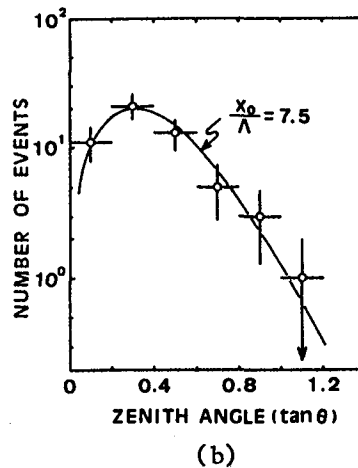
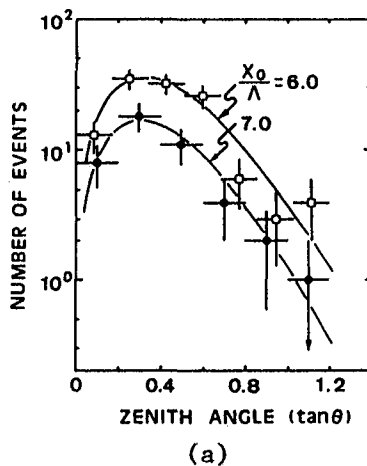


Fig. 3 Zenith angle distributions.

- (a): the general EAS with $Ne \geq 2 \times 10^6$ (open squares) and the combined EAS with gamma-families with $\Sigma E_{\gamma, H} \geq 10$ TeV (closed circles).
 (b): all gamma-families with $\Sigma E_{\gamma, H} \geq 10$ TeV, $n_{\gamma, H} \geq 2$ and $E_{min} = 3$ TeV.

theoretical zenith angle distribution fitted to the experimental data, we can easily get vertical intensity of EAS size spectrum as shown in Fig. 4. The spectrum of the general EAS, marked by open squares in this figure, is considered to be free from detection bias in the size region $N_{e \geq 2 \times 10^6}$. Closed circles and open triangles indicate the combined EAS with $\Sigma E_{\gamma, H} \geq 10$ TeV and ≥ 20 TeV, respectively. It is concluded from this figure that the EAS with $N_{e \geq 5 \times 10^6}$ are always associated with gamma-families with $\Sigma E_{\gamma, H} \geq 10$ TeV at the altitude of Mt. Norikura ($x_0 = 738$ gcm $^{-2}$). This is consistent with the fact seen in Fig. 2 that both the average values of s agree each other for $N_{e \geq 5 \times 10^6}$ between the general EAS and the combined EAS with gamma-families with $\Sigma E_{\gamma, H} \geq 10$ TeV. Also, the figure 4 suggests that the EAS with $N_{e \geq 10^7}$ are always accompanied by gamma-families with $\Sigma E_{\gamma, H} \geq 20$ TeV at the same altitude. These results are important to study the absolute intensity of energy spectrum of the primary protons in the energy region $E_0 = 10^{15} \sim 10^{17}$ eV.

5. Conclusions

EAS with sizes greater than about 5×10^6 are always accompanied by gamma-families with $\Sigma E_{\gamma, H} \geq 10$ TeV, $n_{\gamma, H} \geq 2$ for $E_{min} = 3$ TeV at the altitude of Mt. Norikura. This size at Mt. Norikura is nearly equivalent to the primary proton's energy 10^{16} eV. The size of EAS which are always accompanied by gamma-families with $\Sigma E_{\gamma, H} \geq 20$ TeV seems to be greater than about 10^7 . Then, if the gamma-families with higher cutoff energy are observed together with EAS, the data will provide an available key to get the absolute intensity of the primary proton's spectrum up to 10^{17} eV.

6. Acknowledgements

The authors would like to express their thanks to the members of the Norikura Air Shower Group for kind offer of the EAS array and assistance and also to staffs of Norikura Observatory of the Institute for Cosmic Ray Research for kind offices and continuous support. This work is supported financially by a Grant-in-aid for Scientific Research from the Ministry of Education, Science and Culture.

7. References

- Nakatsuka et al., 1983; Conference Papers of the 18th ICRC (Bangalore), Vol. 11, 346.
 Saito et al., 1983; *ibid* Vol. 11, 217.
 Yamamoto et al., 1981; Conference Papers of the 17th ICRC (Paris), Vol. 11, 130.

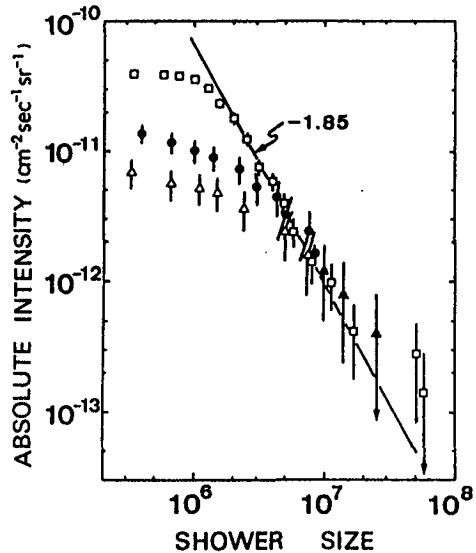


Fig. 4 Integral size spectra for the general EAS (open squares) and the combined EAS with gamma-families of $\Sigma E_{\gamma, H} \geq 10$ TeV (closed circles) and of $\Sigma E_{\gamma, H} \geq 20$ TeV (open triangles).

A COSMIC RAY SUPER HIGH ENERGY MULTICORE FAMILY EVENT (I)
EXPERIMENT AND GENERAL FEATURES

CHINA-JAPAN EMULSION CHAMBER COLLABORATION

Ren, J.R., Kuang, H.H., Huo, A.X., Lu, S.L., Su, S., Wang, Y.X., Xue, Y.G.

Institute of High Energy Physics, Academia Sinica, China

Wang, C.R., He, M., Zhang, N.J., Cao, P.Y., Li, J.Y., Zou, B.T.

Shandong University, China

Wang, S.Z.

Zhengzhou University, China

Bai, G.Z., Liu, Z.H., LI, G.J., Geng, Q.X.

Chongqing Architecture College, China

Zhou, W.D., He, R.D.

Yunan University, China

Amenomori, M., Konishi, E., Nanjo, H.

Hirosaki University, Japan

Hotta, N., Ohta, I.

Utsunomiya University, Japan

Mizutani, K., Sato, T.

Saitama University, Japan

Kasahara, K., Yuda, T.

Institute for Cosmic Ray Research, University of Tokyo, Japan

Torii, S.

Kanagawa University, Japan

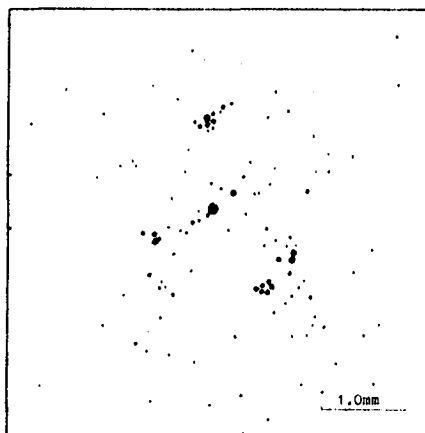
I. Introduction. Information on the fragmentation region in super high energy hadronic interactions can be obtained through the observations of γ -ray families produced by cosmic rays. γ -ray families with $\Sigma E_{\gamma} > 1000$ TeV are receiving increasing interests in emulsion chamber experiments. There exist some complications caused by the superposition of nuclear and electromagnetic cascades and the uncertainty in the nature of the primary particles. These complications usually make the conclusions drawn from various interesting phenomena observed in family events not so definite. Here we describe an interesting family event KO E19, which is likely to have suffered only very slight disturbances. It was found in Mt. Kambala emulsion chamber experiment. The production height of the event is determined to be $H = (70 \pm 30)$ m and some conclusions are given.

II. Experiment. The event KO E19 was found in 14.8 m² of emulsion chamber (thickness 14 c.u.) exposed on Mt. Kambala during 1980.9-1981.9. The photosensitive materials of the emulsion chamber consist of x-ray films of Sakura N type and Fuji 100 type and nuclear emulsion plates of ET7C type. On the N type x-ray films, the central part of the event is completely blackened, forming a halo. The visible energies of the event are determined independently on the three kinds of photosensitive plates and crosschecked, yielding a consistent result.

The optical density distributions in the halo part are determined on all layers of N type films. From the variation of the density distributions on consecutive layers, we can determine the electron number densities n_i and obtain the total number of electrons N and their total track length Z on the basis of the approximation B, thus giving the visible energy of the halo (1) $\Sigma E_{\gamma} = 1200$ TeV. Every shower in the central part of the event are clearly separated from each other on the 100 type x-ray films and the ET7C type nuclear emulsion plates (Fig.1). On the 100 type films, we can make accurate measurements of the positions and

optical densities, shower by shower, using the Mitaka-Hamamatsu automatic microphotometer. From the darkness-energy relation with Landau effect correction, we can determine the total visible energy(2), yielding $\Sigma E_{\gamma} = 1300$ TeV ($E_{min} = 2$ TeV). On the ET7C emulsion plates, the electron track counting method is used for the energy determination of the majority of showers except those of very high energies, for which the photometric method is applied. The resultant visible energy is $\Sigma E_{\gamma} = 1537$ TeV ($E_{min} = 1.5$ TeV), which is somewhat higher due to the lower threshold in the energy determination.

Fig.1



With the photometer system used, x and y distances can be measured accurate to about $1 \mu\text{m}$ and shower centers (points of maximum optical density) can be determined with a small aperture.

III. General Features of KO E19. The general statistical characteristics of the event are listed in Table I, where N_{γ} is the number of γ -rays ($E_{\gamma} \geq 3$ TeV) and R the distance from the energy center of the event to the center of a shower. For families produced not too high above the detector, the electromagnetic cascades are usually not fully developed and thus $\langle ER \rangle$ will be small and $\langle E_{\gamma} \rangle$ large, while the energy spectrum will be exponential in form. This is the case for KO E19, as can be seen from Table I and Fig.2. Fig.3 shows the ER-R correlations of the showers in the event, points within the dashed circle representing those in the central part. It is this portion which is the least disturbed during the super high energy hadronic interactions.

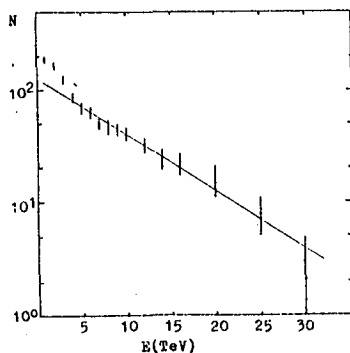


Fig.2

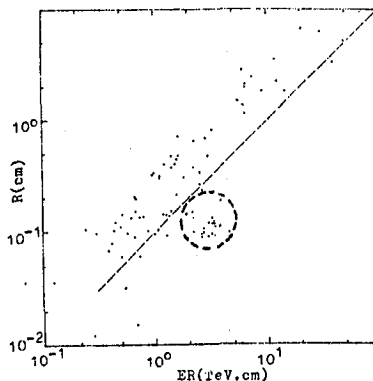


Fig.3

Table I. Statistical characteristics of KO E19

$N_{\gamma}(E \geq 3\text{TeV})$	$\Sigma E_{\gamma}(\text{TeV})$	$\langle E_{\gamma} \rangle(\text{TeV})$	$\langle R \rangle(\text{cm})$	$\langle ER \rangle(\text{TeV.cm})$
131	1083	8.3	0.39	3.23

IV. Production Height and Pseudorapidity Distribution. The exponential energy spectrum, the very low value of $\langle ER \rangle$ and the relatively high value of $\langle E_{\gamma} \rangle$ show some evidences of the small production height H of the main part of KO E19. For an accurate determination of H , a triangulation method is used. Among showers with $E_{\gamma} \geq 10$ TeV and penetrating through the whole thickness, 14 c.u., of the chamber, choose those with favorable measuring conditions. Take a pair of such showers i, j and determine the separations between them, R_{ij}^k and R_{ij}^{k+m} , on the k -th and the $(k+m)$ -th layers respectively. Repeat the same for every pair. Then the production height H can be calculated from

$$H = (m\Delta H \sum_{ij} R_{ij}^k) / \sum_{ij} (R_{ij}^{k+m} - R_{ij}^k)$$

where ΔH is the distance between two consecutive x-ray film layers. In our actual measurements, $k=1$, $m=5$ and $\Delta H=1.3\text{cm}$. The result is $H=(70 \pm 30)\text{m}$. As a rough check of this result, we make a mass distribution obtained from the coupling of the above showers pair by pair, where we take $m_{ij} = R_{ij} \sqrt{E_i E_j} / H$, with $H=70\text{m}$. This is compared with a simulation calculation shown in Fig.4. There are two peaks at $m_{ij} = 150$ MeV and 500 MeV in the experimental distribution, corresponding to the masses of π^0 and η^0 respectively, and thus confirming the result from triangulation.

With $H=70$ m, calculate the pseudorapidity $\eta = -\ln \tan(\theta/2)$ where θ is the emission angle of a secondary particle. The distribution of η is shown in Fig.5. There is a hump near $\eta=12$, which may be attributed to the showers in the cores of the central part. The magnitude of the plateau is roughly $\Delta N / \Delta \eta = 40$, a value about four times as large as that of the scaling extrapolation of accelerator results. The energy dependence of $\Delta N / \Delta \eta$ is shown in Fig.6, indicating a more rapid increase in $\Delta N / \Delta \eta$ above 10^{16} eV.

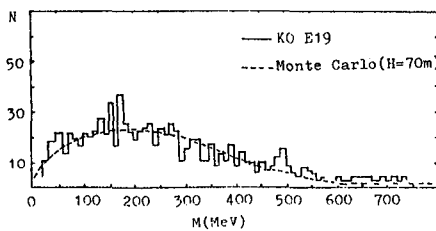


Fig.4

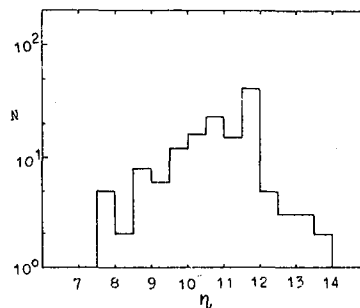


Fig.5

Taking $H=70$ m, the p_t distribution in the family is shown in Fig.7, where "o" represent data of KO E19 ($E_{min}=4$ TeV) and "+" come from C-jets ($E_{min}=0.5$ TeV). In the $p_t < 800$ MeV/c region, the p_t distribution of KO E19 is consistent with that of C-jets and both of them take the exponential form e^{-5p_t} . The central portion of the family will be treated in (5).

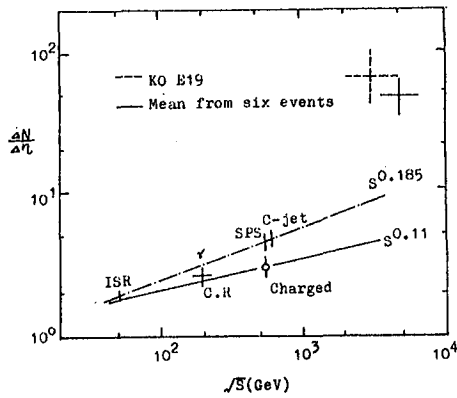


Fig.6

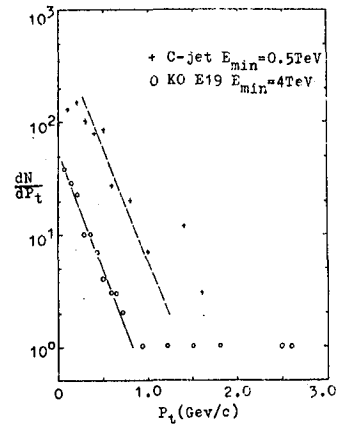


Fig.7

References.

- (1) T.Yuda, Utsusen Kenkyu (in Japanese) 24(1981) 92.
- (2) K. Kasahara, 18th ICRC, 5(1983) 303.
- (3) T. Yuda, 18th ICRC, 12 (1983) 341.
- (4) C.M.G. Lattes, Physics Reports, 65 (1980) 151.
- (5) J.R. Ren et al., HE 3.4-2, this conference.

A COSMIC RAY SUPER HIGH ENERGY MULTICORE FAMILY EVENT (II)
STRUCTURE AND FRAGMENTATION CHARACTERISTICS OF THE JETS

China-Japan Emulsion Chamber Collaboration*

I. Introduction. Quarks and gluons are not directly observable, but may be displayed through fragmentation in the form of hadronic jets, the evidence of which was first revealed in cosmic ray interactions before the advent of the modern theory of strong interactions. Experimental results from ISR(1) and SP \bar{P} S collider rendered the jet phenomena more confident and definite. All the properties of jets observed up to now at ISR and SP \bar{P} S collider are in agreement with the predictions of QCD(2-4). In order to make further test of QCD in still higher energy regions, detailed study of super high energy jet events in cosmic rays is very desirable. The event KO E19 observed in Mt. Kambala emulsion chamber is an interesting event for such study. The general features of KO E19 is described in (5). Its total visible energy is $\Sigma E_{\gamma}=1537$ TeV ($E_{min}=1.5$ TeV) and production height $H=(70\pm 30)$ m, with a hadron as its primary particle. Besides about forty small clusters, there are five super high energy cores or jets, one lying near the center of the event while the other four surrounding it, having incident directions making small angles (about $5^{\circ}-6^{\circ}$ in CMS) with that of the primary particle. Detailed analysis is done on the emulsion plates inserted in the chamber, making full use of their fine granularity, superior in detecting and analyzing jet events, especially their substructures.

II. Jets and jetty event. By jet we generally mean a bundle of fairly collimated hadrons in the final states of high energy interactions. It can also be considered as a cluster of particles in the pseudorapidity-azimuth ($\eta-\varphi$) space. We adopt a procedure for the jet clusterization similar to that in accelerator experiments as follows. Assign an energy vector to every shower (track), directed from the vertex of the event to the point of recording. Find out the largest of these vectors and compute the quantities d of other ones relative to the largest in $\eta-\varphi$ space, where $d=\sqrt{(\Delta\eta)^2+(\Delta\varphi)^2}$. Add all energy vectors with $d\leq 1.0$ to the largest one vectorially, we then obtain a jet. Next find out the largest vector among the remaining ones and repeat the above procedure to get another jet, etc. A transverse energy threshold is taken, which may be 10-60 GeV. For the four outer jets in KO E19, the minimum $E_t=10$ GeV and the maximum $d=0.82-1.0$, corresponding to $\varphi=38^{\circ}-44^{\circ}$ and $\theta=4.8^{\circ}-6.1^{\circ}$. Adopt $\sum_n (E_{jet})_n / \Sigma E_{\gamma} \geq 70\%$ as a criterion for the so-called jetty events, conforming to the convention in accelerator experiments. In our case, the total energy of the four outer jets is 756 TeV and corresponds a fraction of 76% of the total visible energy 994 TeV ($E_{min}=4$ TeV). If the energy of the central jet is also included, the fraction will increase to 79%. Therefore we may consider KO E19 as a jetty event. The characteristics of jetty events are closely related to the production and fragmentation behaviors of jets.

III. Structures and fragmentation characteristics of jets. The transverse momentum p_t of a jet can be obtained by vector addition of the p_t 's of all its constituent particles. If the jet particles are assumed to be π 's, then the p_t of the four outer jets are 12.77, 11.42, 6.81 and 8.63 GeV/c. Fig.1 gives the vector diagram of these jets. The sphericity of a jet is defined as $S_n = 3(\sum p_{ti}^2)_n / 2(\sum j_i^2)$, where j_i is the momentum

* For full list of authors, see HE 3.4-1, this conference.

of the i -th particle and j_{ti} is its transvers component relative to the axis of the n -th jet. For an event with n jets, the total sphericity is the sum over all jets. The total sphericity of KO E19 is $S=0.0074$ and the total neutral transverse energy $E_{\perp}^0 = 148$ GeV, which are compared with accelerator results qualitatively in Fig.2, showing no inconsistency

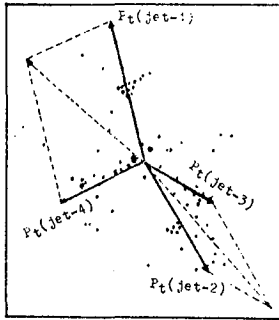


Fig. 1

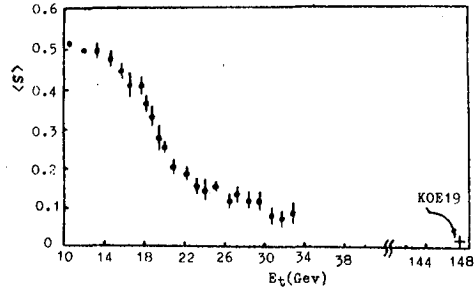


Fig. 2

in its trend. The distribution of θ_j^* , the angle between the particle momentum and the jet axis in CMS, is shown in Fig.3 for the four outer jets. The peak value of θ_j^* for KO E19 lies near 0.5° , consistent with the most probable values 7° and 2° in ISR and SPFS collider energy regions, respectively. Take $H=70m$, $\langle J_{tr} \rangle = 0.04$ GeV/c, corresponding to $\langle j_{tr} \rangle = 0.08$ GeV/c, smaller than the average from $p\bar{p}$ collider.

The fragmentation variable is a useful quantity in jet analysis. It is defined as $z = 2E_{||}\gamma / 3(\Sigma E_{\perp})_{\perp}$, representing the fraction of the component of shower energy along the jet axis in total visible jet energy. The factor $2/3$ takes account of the fact that the secondary particles are mainly γ -rays, coming from the decay of π^0 's. The distribution of z is called the fragmentation function of jet: $D(z) = (1/N_j) dN_{ch} / dz$. Fig.4 gives the fragmentation function of the five jets in KO E19, which

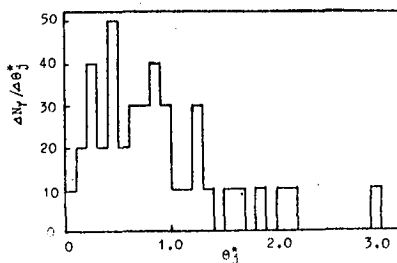


Fig. 3

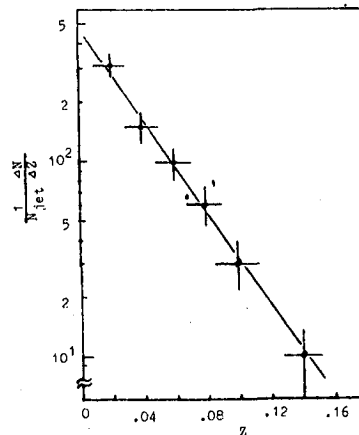


Fig. 4

is in the exponential form $\text{Exp}(-Bz)$, with $B=27.4$. Data from ISR and FNAL are also included for comparison. In the ISR range, ABCS Collaboration gave an exponential $D(z)$ for small z , with $B \approx 7$, while CCOR Collaboration obtained $B \approx 5.3$ at lower energies. FNAL(9) obtained $B \approx 4.6$,

using jets with p_t lower than ABCS Collaboration. As noted in (7), when the energy of the scattered parton increases, the number of fragmentations increases also, resulting in a decrease in z and an increase in the slope. KO E19 is a super high energy event and the value of B should be correspondingly larger. By integration of the jet fragmentation function, we can obtain the charged particle multiplicity in the jet. For the five jets of KO E19, $\langle N_{ch} \rangle \approx 18$, $\langle E_{jet} \rangle \approx 95$ GeV in CMS. A comparison between KO E19 and accelerator results(10) is shown in Fig.5. There is an evident increase in N_{ch} in KO E19.

IV. Comparison with QCD calculations at TeV energies. It is shown in the phenomenological QCD study of the properties of the jets produced in hadronic collisions in $\sqrt{s} = 10$ TeV range(11), that hadronic jets are mixtures of quark jets and gluon jets and that 50% of the energy of quark jets is carried by particles with $z=0.06$ while the corresponding value for gluon jets is $z=0.025$. From KO E19 data, 50% of the jet energy is carried by particles with $z=0.045$, in reasonable agreement with the above estimation. The particle multiplicity of jets as a function of jet energy is shown in Fig.6(11). The value of $\langle N_{ch} \rangle$ is

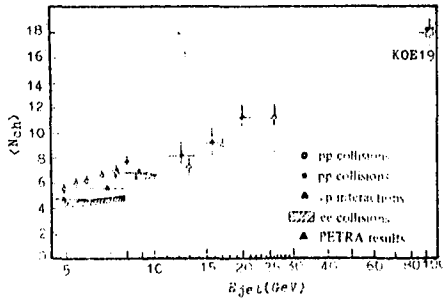


Fig. 5

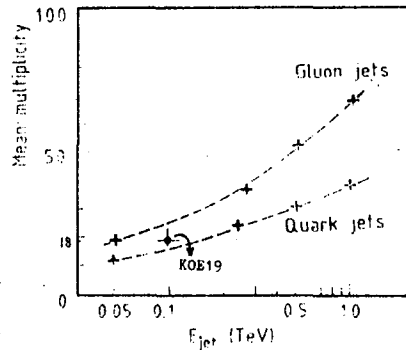


Fig. 6

about 18 and lies between the theoretical values for quark and gluon jets. The fractions of the numbers and energies of jet particles outside the jet cone in KO E19 are also close to the theoretical results. The high p_t Monte Carlo events generated by the ISAJET program are shown to have core structures. This is also the case for the four outer jets in KO E19. Fig.7 gives the jet number distribution reconstructed from

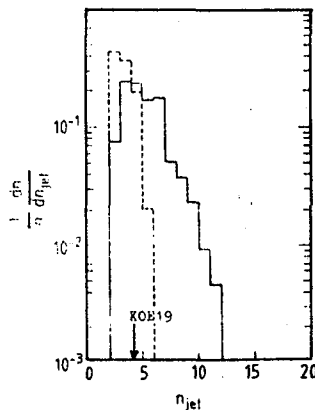


Fig.7

the TeV range Monte Carlo events by means of the clusterization techni-

que, where the solid line represents events with $E_{\text{t}} > 10$ GeV and the dotted line those with $E_{\text{t}} > 100$ GeV. For the four outer jets in KO E19, $E_{\text{t}} > 10$ GeV, $N_{\text{jet}} = 4$, lying within the theoretical prediction. From the above analysis, it can be seen that the characteristics of KO E19 are in agreement or not inconsistent with the predictions of the phenomenological QCD. Further analysis and confirmation require more events.

References

- (1) M.Jacob et al., Phys. Rep. 48(1978) no.4.
- (2) T.Akesson et al., 14th Inter. Symposium on Multiparticle Dyn. Lake Tahoe, CA(1983).
- (3) M.Banner et al., Phys. Lett. 118B(1982)203; P.Bagnaia et al., Phys. Lett. 138B(1984)430; G.Arnison et al., Phys. Lett. 123B(1983)115.
- (4) R.Horgan and M.Jacob, Nucl. Phys. B179(1981)441; R.Field, La Jolla Summer Institute, 1978; AIP Conf.Proc., no.53(1979); R.Horgan and M.Jacob, CERN Rep. 81-04(1981).
- (5) Ren Jingru et al., Physica Energiae Fortis et Physica Nuclearis (in Chinese); Ren Jingru et al., see HE 3.4-1, this conference.
- (6) G.Arnison et al., Phys. Lett. 132B(1983)214.
- (7) C.Kourkouvelis et al., Phys. Lett. 86B(1979)391.
- (8) A.L.S.Angelis et al., Physica Scripta, 19(1979)116.
- (9) C.Bromberg et al., Nucl. Phys. B134(1978)189.
- (10) E.Leader and E.Predazzi, An Introduction to Gauge Theories and the 'New Physics', Cambridge Univ. Press 1982, P.421.
- (11) T.Akesson et al., LHC in the LEP Tunnel, (CERN 84-10) Vol.I, P.165 (1984).

OBSERVATION OF SUPER HIGH ENERGY BIG FAMILY
WITH LARGE SCALE Fe EMULSION CHAMBERS

China-Japan Emulsion Chamber Collaboration*

I. Introduction. In order to get higher efficiencies for detecting hadrons and to make technical improvements in the chamber structure, the Mt. Kambala Emulsion Chamber Collaboration constructed 57 m² of Fe chamber, with thickness 29 c.u. (1c.u.=17.6 mm Fe), using 300 tons of Fe plates and made the first exposure from Sept., 1982 to May, 1984. The photosensitive layers consist of x-ray films of Sakura N type, Fuji No. 100 type and Tianjin III type, some of them contain also emulsion plates of Fuji ET7B type. They are inserted between the Fe plates at every 2 c.u., beginning at 5 c.u. from the chamber top. In a number of blocks, 3 mm spacings are provided at every 2 c.u. of Fe plates to facilitate the replacement of photosensitive layers, without disassembling the chamber. On the bottom of the chamber Fe plates of thickness 9 mm are placed in order to shield the chamber from the radioactivities of the ground. An event, numbered K2 58 of visible energy $\Sigma E_{\gamma} = 7345$ TeV was found in this exposure. It is the event with the highest energy obtained in Mt. Kambala emulsion chambers up to now. No obvious halo is seen in the event and all the showers are clearly separated and easy to measure. A brief report of the preliminary results is given here.

II. General characteristics of the event. There are 566 showers with visible energies greater than 3 TeV, distributed as shown in Fig.1. It is evident that the event is a single core family. On the map of the event, 161 high energy showers of total visible energy $\Sigma E_{\gamma} = 4228$ TeV are concentrated within a circle of radius 8 mm, therefore it is not necessary to carry out clusterization of the showers. Fig.2 is the optical density distribution contours of K2 58, obtained by the automatic photometer NGD-17 \times 17, with optical aperture 300 \times 300 m².

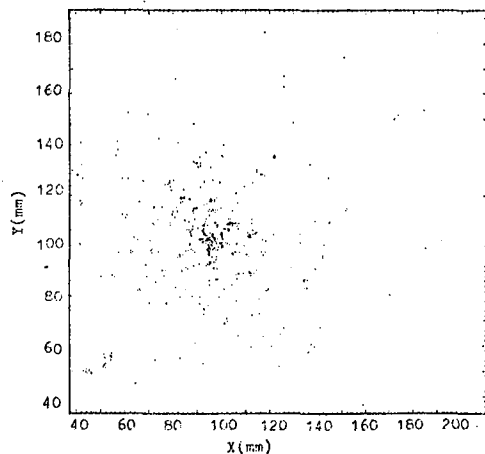


Fig. 1

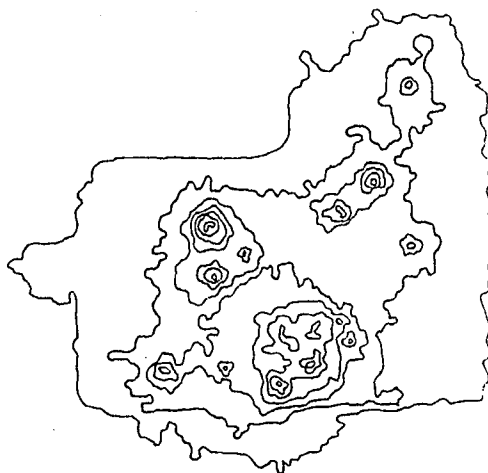


Fig. 2

Various statistical averages are given in the table I, where Δt is the depth of the starting point of a shower. The various averages remain unchanged when Δt is taken either as ≤ 4 c.u. or as ≤ 6 c.u..

The data in the last row of the table I are the corresponding quantities

* For full list authors, see HE 3.4-1, this conference.

for events with visible energies $\Sigma E_{\gamma} \geq 1000$ TeV obtained in earlier exposures at Mt. Kambala (2). Both results agree well.

Table I. Statistical Averages for Big Families ($E_{\min} = 4$ TeV)

Event	t (c.u.)	N	R (cm)	ER (TeV.cm)	E (TeV)	E (TeV)
K2 58	4	417	2.02	19.9	15.1	6300
	6	455	2.04	19.9	14.9	6800
Mean for 5 Events	6	134	1.94	16.3	11.7	1530

III. Energy spectrum and ER distribution. Shower energy spectra and ER distributions taken with different values of Δt are shown in Fig.3. The shape of the energy spectrum remains almost unchanged as the value of Δt is varied. It is nearly of the form $N(>E) \propto E^{-\beta}$, where $\beta=1.2$. All the energy spectra of showers in circles with different radii R and centered

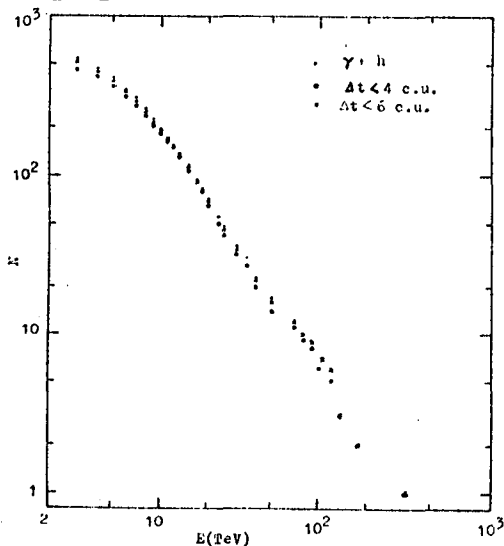


Fig. 3a

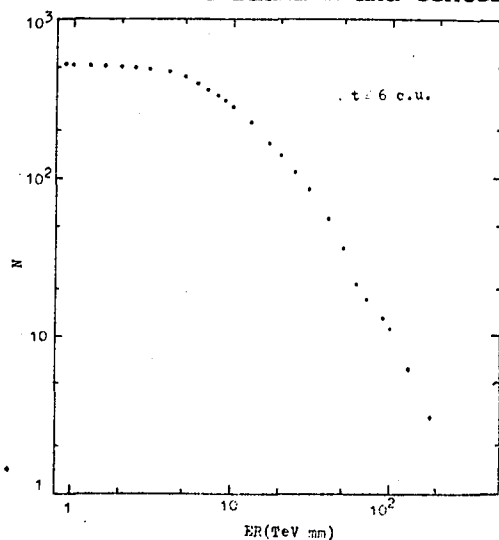


Fig. 3b

at the center of energy of the event are in power form (Fig.4). Further-

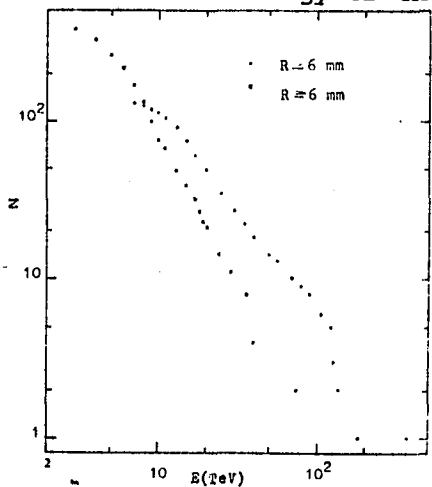


Fig. 4

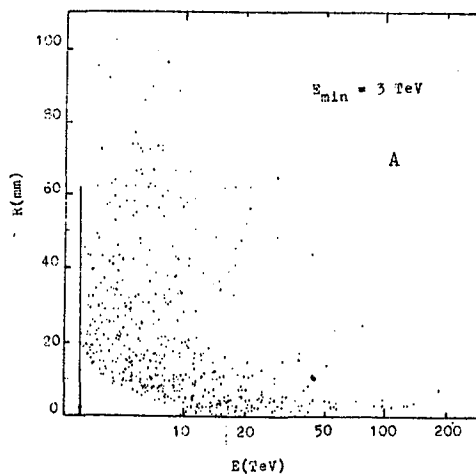


Fig. 5

more, the energy spectrum of showers with $E_\gamma \geq 10$ TeV remains almost the same when R has increased to 8 mm. These indicate that the production height of the event is so high that both the central and the peripheral parts of the event have already undergone sufficient electromagnetic processes. In the $R < 12$ mm region, are concentrated a large number of showers of energies in the interval 3-10 TeV, making the optical densities in their neighborhood greatly exceeding those of the background and rendering the showers with lower energies obscure (see the triangular blank region A in Fig.5). From the energy spectrum $N(>E) \propto E^{-\beta}$ at $E_\gamma \geq 10$ TeV, it is estimated that there should be about 180 showers with $E_\gamma \geq 3$ TeV in the blank region A, with a corresponding total energy $\sum E_{\gamma A} = 808$ TeV.

Fig.6 gives the energy spectrum for showers with $\Delta t = 6$ c.u., corresponding to the energy spectrum of a part of the Pb-jets in Pb chambers. The result is the same as that in Fig.3.

Thick Fe chambers are more effective than Pb chambers in the detection of hadrons, but the method for discriminating Fe-jets and γ -rays (electrons) remains to be further explored. Criteria based on the difference in Δt are unfavorable but considerations about the consecutive interactions of hadrons in Fe may be more adequate. Fig.7 gives an example of the transition curve in Fe of a high energy shower, with $\Delta t \sim 0$. It is seen that the trend of the shower development distinctly deviates from the transition curve of the showers produced by γ -rays (electrons), corrected for the L-M effect (3). However, this is applicable only to high energy showers but is difficult for low energy ones.

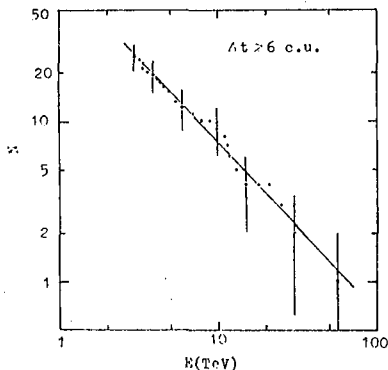


Fig. 6

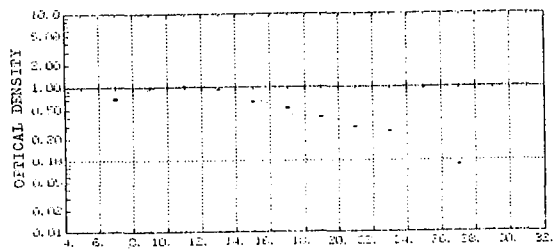


Fig.7

References

- (1) I.Onta, Uchusen Kenkyu (in Japanese), 24(1980)147.
- (2) J.R.Ren et al., Physica Energiae Fortis et Physica Nuclearis (in Chinese), to be published.
- (3) K.Kasahara 1984, unpublished.

A Halo Event Created at 200 m above
the Chacaltaya Emulsion Chamber

N.M. Amato, N. Arata (CBPF, Rio de Janeiro, RJ, Brasil) and
R.H.C. Maldonado (UFF, Niteroi, RJ, Brasil)

1. Introduction

We present the results of analysis on a cosmic-ray induced nuclear event with the total visible energy ~ 1300 TeV which is characterized by the central (halo) part of a strong energy concentration and the outer part of a large lateral spread. The event (named as P06) was detected in the 18th two-storied emulsion chamber exposed at Chacaltaya by Brasil-Japan Collaboration. As the nuclear emulsion plates were inserted at every layer of the concerned blocks in the upper and the lower chambers together with RR- and N-type X-ray films, we can study the details of the event.

Some results on P06 have already been reported [1] based on the general measurement of opacity on N-type X-ray films: (1) the total energy of halo is ~ 1000 TeV; (2) the shower transition reaches its maximum at ~ 16 cu; and (3) the radius of halo is 6.5 mm (at the level of 10^6 electrons/cm²). The results in more details will be described here.

2. Results

Fig.1 shows the target diagram of P06, where we notice a large lateral spread of the event and richness in hadrons in the outer region.*

Fig.2 shows the contour map of opacity ($D=.2, .3, .4, .6, .8$ and $1.$) for the central part of halo on RR-type X-ray film at 14 cu in the upper chamber with slit diameter 113μ , together with the high energy shower cores ($E > 10$ TeV). A clear asymmetry is seen in both distributions of D and shower cores. Notice that it also holds for both γ -rays and hadrons.

Fig.3 shows the distributions of opacity in the upper and the lower chambers, where the measurement was made along the straight line on the film passing through the two hadronic cores (#40 and #58) which can be well recognized in both chambers because of their strong and sharp penetration. We notice that the halo part contains at least two peaks.

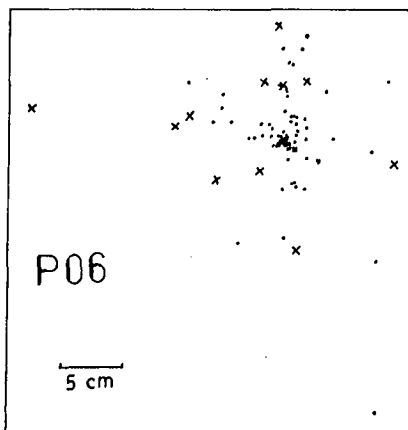


Fig.1 Target diagram of P06. γ -rays (\bullet) and identified hadrons (\times).

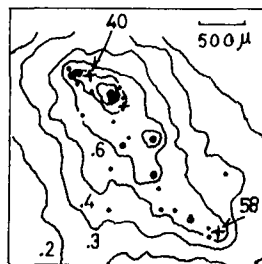


Fig.2 Contour map of opacity of RR-type X-ray film at 14 cu and shower cores: γ -rays (\bullet : > 20 TeV, \circ : $10-20$ TeV) and hadrons (\times). The cores (#40 and #58) are indicated.

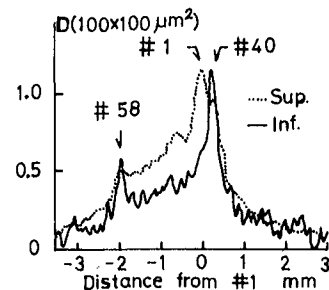


Fig.3 Distributions of opacity on RR-type X-ray film at 14 cu in the upper chamber (Sup) and on N-type X-ray film at 4 cu in the lower chamber (Inf).

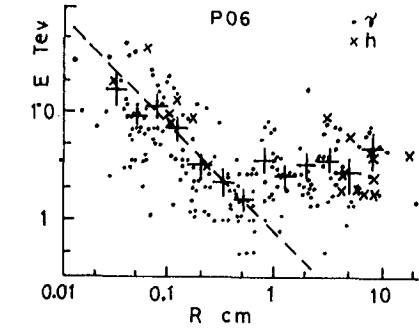
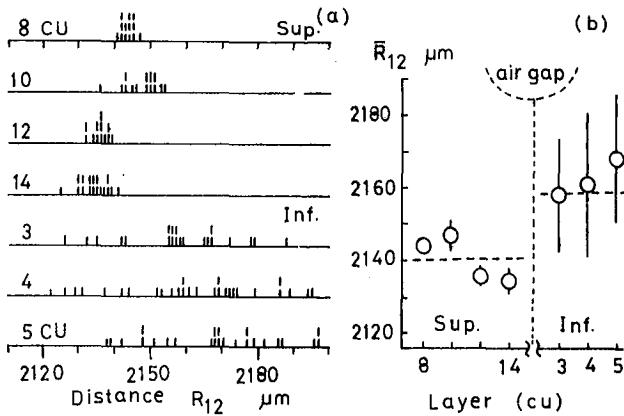


Fig.4(a) Measurement of the relative distances, R_{12} , between #40 and #58 in the upper (Sup) and the lower (Inf) chambers. 4(b) Variation of \bar{R}_{12} at 8, 10, 12 and 14 cu in the upper chamber and at 3, 4 and 5 cu in the lower chamber. The best fitted straight line is also shown.

Fig.5 Correlation Diagram between energy and distance of P06. γ -rays(\bullet) and hadrons(\times). $+$ are for the average values.

Fig.4-a shows the results of measurement on the relative distance, R_{12} , between #40 and #58 on the nuclear emulsion plates which was done repeatedly after some blank days enough long to forget the previous measurement. Fig.4-b shows the average values of R_{12} at 7 layers together with the best fitted straight line given by the least-square method which corresponds to the interaction height $H = 208 \pm 245$ m. The value of χ^2 is rather large, 16.4 for the 7 points, of which 4 points in the upper chamber share 98% of the total; we could not resolve the fluctuation seen in the upper chamber. If we use the average value of 4 points, $H = 177 \pm 165$ m; if we take only the point at 10 cu, $H = 263 \pm 784$ m. In the following, we take 208 m as the vertical height above the chamber which corresponds to $H_0 \sim 250$ m after the correction on zenith angle (35°).

Fig.5 shows the diagram of energy, E , and distance, R , for all the shower cores observed in P06, where R is measured from the energy-weighted center of shower cores which are located inside the halo radius, 6.5 mm. The dashed line stands for the fit to the averages in the central region,

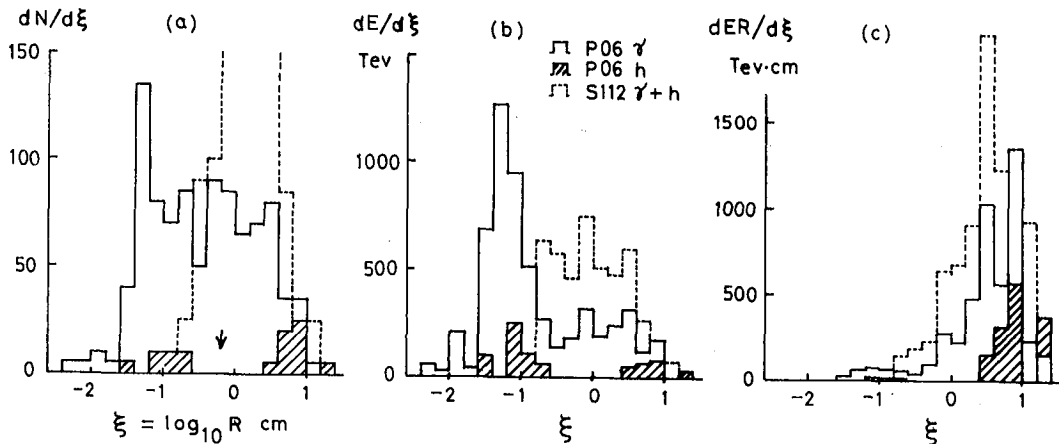


Fig.6 (a) Histogram of $\log_{10}R$, (b) energy-flow and (c) energy-weighted lateral distance ER-flow in $\log_{10} R$, for γ -rays and hadrons in P06, and for all the shower cores in the event S112.

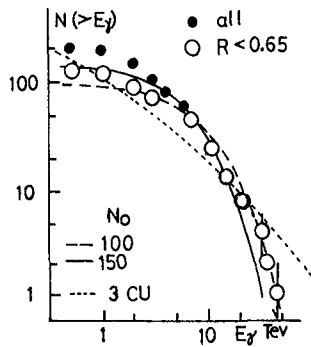


Fig. 7 Energy distribution. All the γ -rays (•) and γ -rays in the halo radius (o) in P06.

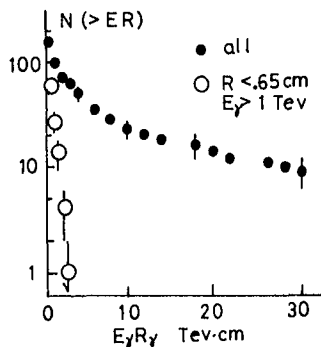


Fig. 8 ER distribution. All the γ -rays (•) and γ -ray inside the halo radius (o) in P06.

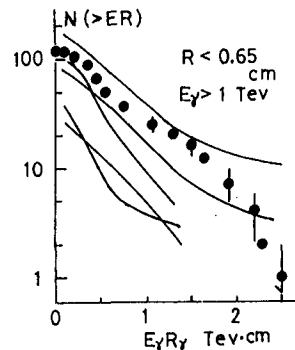


Fig. 9 ER distribution for γ -rays in the halo of P06, and those for other 5 events [3].

$\langle ER \rangle = 8 \text{ GeV m}$ which corresponds to $p_T = 32 \text{ MeV/c}$ under $H_0 = 250 \text{ m}$. In the central region, the correlation between E and R shows some constancy of ER (or p_T) but the behavior in the outer region is quite different.

Fig. 6 (a-c) show the flows of number, energy and energy-weighted lateral spread in the space of $\log_{10} R$, respectively. The γ -rays and the hadrons are shown separately. Also shown for the comparison are the results of the event S112 which is classified as Guaçu-type meson production characterized by the large p_T and the high multiplicity [2]. As the total energy (878 TeV) and the interaction height ($\sim 250 \text{ m}$) of S112 are nearly equal to those of halo part of P06, we can compare the two events with each other without any normalization. We notice that P06 contains a strong concentration of particles and energy in the small angular region as a clear peak of halo (75% of the total energy being inside the radius) but S112 not, and that the outer region of P06 is similar to S112.

Fig. 7 shows the energy distribution of γ -rays in P06 in an integral form. The dashed and the solid lines stand for the exponential distributions of the form $N_0 \exp(-E_\gamma / \Sigma E_\gamma)$ with $N_0 = 100$ and 150, respectively. The dotted line is the result of analytic calculation with $t = 3 \text{ cu}$ and $N_0 = 6$ where required are 1 TeV for the energy threshold and 1000 TeV for the total visible energy. We notice that a long passage in air does multiply the number of γ -rays and electrons, but that the original exponential form is greatly distorted.

Fig. 8 shows the distributions of energy-weighted lateral spread, ER , of γ -rays in P06. A large difference of lateral spread between the halo and the outer region is impressive (of a factor ~ 30). The average value of ER for the outer region is obtained from the slope to be $\sim 0.2 \text{ GeV km}$.

Fig. 9 shows the distribution of ER in the halo of P06. The average value of ER is 7.2 GeV m , which corresponds to $\langle p_T \rangle = 29 \text{ MeV/c}$ under $H_0 = 250 \text{ m}$. Also shown are those of other five events similar to the halo of P06 [3].

3. Discussions and Conclusion

The event P06 is realized in the upper part of the upper chamber as a rather small size of dark spot on N-type X-ray films, but it develops remarkably in the lead material of the chamber and appears as a generally darkened wide area [1]. This area is called as "halo".

The total visible energy is 1275 TeV, 217 shower cores being observed

on the nuclear emulsion plates. Within the halo radius (0.65 cm), 965 TeV is emitted in 127 shower cores. To explain this large particle density in a small region, one might imagine a long passage in the atmosphere to include the cascade multiplication process. But the experimental results of P06 do not seem to support such a naive consideration:

- (1) The halo energy estimated by the general measurement of opacity is nearly equivalent to the energy sum, ΣE_{γ} , of shower cores. The former should include the contribution of low energy showers which are not visible in the latter. In case of the event Andromeda, $E(\text{halo}) \sim 3.5 \Sigma E_{\gamma}$ [4];
- (2) The depth of shower maximum is very deep in P06 (~ 16 cu). In case of Andromeda, it is ~ 10 cu [4];
- (3) The sharp alignment on azimuth is seen for both γ -rays and hadrons;
- (4) The energy distribution is almost exponential.

The above results indicate that the halo of P06 does not suffer from a large cascade degradation during its passage in the atmosphere, and that the high energy shower cores observed on the nuclear emulsion plates play a decisive role in the halo.

The triangulation method gives us a direct check on that point. The interaction height is obtained to be ~ 250 m although some fluctuation is seen in four layers in the upper chamber. Taking 250 m, the halo part of P06 comes to be of abnormally small p_T (~ 30 MeV/c on the average) and of high γ -ray density in rapidity (~ 59 at the maximum). There is a possibility that a new phenomena happens to appear in the super high energy region which is characterized by a very small p_T (a few tens of MeV/c).

The large lateral spread with richness in hadrons is seen in the outer region of P06, which seems to be a common feature in the halo events [5]. It may be plausible to speculate that the mechanism of large p_T phenomena could produce some new character to create the halo.

The new characteristics seen in the halo of P06 could be compared with those of the so-called "mini-cluster" which is also characterized by the small p_T , 10-20 MeV/c [6].

4. Acknowledgement

The authors wish to express their thanks to all the members of the Brasil-Japan Collaboration for their kind and continuous support. They are grateful to Profs. C.M.G.Lattes, S.Hasegawa and S.A.Slavatinsky for their valuable comments. Thanks are also due to the CNPq, Brasil, for their financial support.

References

- [1] N.M.Amato et al., Proc. of Internat. Symposium on Cosmic Rays and Particle Physics, Tokyo, 1984, p.123.
- [2] H.Semba, Nuovo Cimento 49A (1979) 247.
- [3] S.Hasegawa, Proc.of Internat.Symposium (see [1]), Tokyo,1984, p.62.
- [4] A.Ohsawa, ICR-Report-112-83-6 (1983) 65.
- [5] S.Yamashita, Journal of Phys.Soc.Japan 54 (1985) 529.
- [6] Brasil-Japan Collaboration, AIP Conf.Proc., 85 (1981) p.500.

* We used the following criteria to identify hadrons: the starting point of cascade is estimated to be deeper than 4 cu and/or the transition curve indicates a successive interaction.

A Binocular-type Atmospheric Interaction
Generating Sequential Exotic Features

N.M.Amato^{*}, N.Arata^{*} and R.H.C.Maldonado^{**}

^{*} Centro Brasileiro de Pesquisas Físicas
Rua Dr. Xavier Sigaud 150
22290 Rio de Janeiro, RJ, BRASIL

^{**} Instituto de Física
Universidade Federal Fluminense
Niteroi, RJ, BRASIL

Abstract A cosmic-ray induced nuclear event is presented, which is of clear binocular-type and contains several exotic features through its passage in the atmosphere and the emulsion chamber.

1. Introduction

Brasil-Japan Collaboration has observed some exotic events (Centaurus family) in the high-energy cosmic-ray interactions, and they are classified into four categories as (original-) Centaurus, Mini-Centaurus, Geminion and Chiron according to their multiplicity and average p_T ./1,2/ Their common feature is a lack of γ -ray emission in their interactions, and they are regarded as phenomena quite distinct from the normal pion production.

In this paper, we present a very special event which shows several exotic features in three generations of interactions.

2. Experiment

The event was observed in the 19th emulsion chamber at Chacaltaya. The chamber is two-storied, which consists of an upper chamber, a lower chamber and a target layer in-between. The chamber is multi-layered sandwiches of lead plates and photo-sensitive materials. In the unit block where the present event was detected, nuclear emulsion plates were inserted with N-type X-ray films at 6,8 and 12 cu in the upper chamber and 3,4,5,6,10 and 12 cu in the lower chamber. At 4 and 10 cu in the upper chamber and at 8 cu in the lower chamber, only X-ray films were inserted. Thanks to the high spatial resolution of nuclear emulsion, we can study a fine structure of shower cores in detail which is quite powerful to pick up and examine the exotic features.

3. Results

As the event was observed in the unit block 109 in the upper chamber and in the block 69 in the lower chamber, we name this event as CH19 S109 I69. In the following, the results corrected on the incident zenith angle (15 degrees) will be presented.

Fig.1 shows the target diagram of the event, which already visualizes the first impressive feature, i.e., a clear double-core structure. In the group A, 83.7 TeV is observed in the form of electro-magnetic cascade showers, and

51.3 TeV in the group B. The relative distance between A and B is 22 cm, and the value $\chi(A,B) = R(A,B) \sqrt{E(A)E(B)}$ is 1440 TeV·cm. We notice how large the spread of this event is, comparing the average value ~650 TeV·cm of the binocular-type events observed by the Brasil-Japan Collaboration./1,2/

3-1. Group A The group A contains 3 high energy hadrons and 4 low energy showers as shown in Fig.1 and Table 1.

(#A1) #A1 has two cores in the upper chamber (10.5 TeV and 5.8 TeV with the relative distance 152 μ), and continues into the lower chamber where five weak and diffused showers and one very new core are observed inside the radius ~400 μ . Thus we can know that one of the two cores observed in the upper chamber or another hadron interacted to produce the showers observed in the lower chamber.

(#A2) #A2 starts to appear at 12 cu in the upper chamber as a very collimated core which can be realized only in the emulsion plate, and appears in the lower chamber as a multi-core event inside the radius 114 μ . The energy was determined for each of the 7 cores, and π^0 -coupling confirms that they were born in a normal pion production at the lower part of the upper chamber. Outside the multi-cores, one new core of 8 TeV starts to appear at 10 cu in the lower chamber, its distance from the multi-cores being 187 μ . But we can not test whether it came from the emission point of the multi-cores or from the atmosphere. In case of the former, the electro-magnetic component of p_T of this hadron with respect to the emitted direction of the multi-cores is 0.80 MeV/c.

(#A3) #A3 starts to appear at 3 cu in the lower chamber as a single core, but at 4,5 and 6 cu as double cores, their energies being 17 TeV and 3 TeV. The relative distance between the two cores increases gradually at the deeper layers as shown in Fig.2. The convergence shows that #A3 is an interaction in lead plate in the lower chamber, and that the

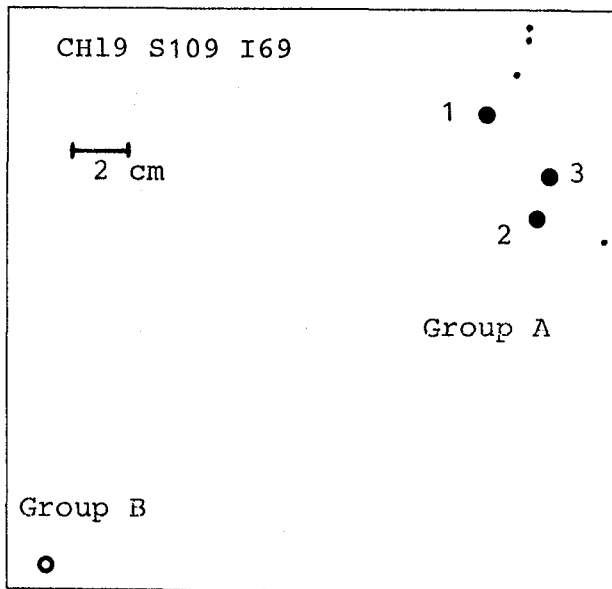


Fig.1 The target diagram of the event CH19 S109I69.

	Energy (TeV)	Comments
A1	16.3	A-jet
A2	31.5	Pb-jet-upper
A3	20.0	Pb-jet-lower
A4-7	15.9	A-jet
B	51.3	A-jet

Table 1 Groups A and B.

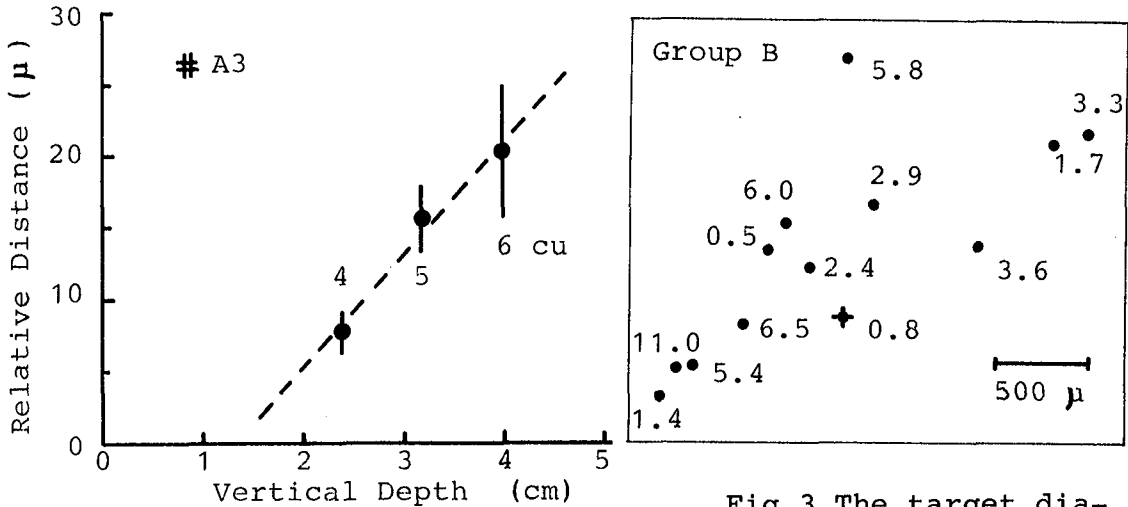


Fig.2 Variation of relative distances in #A3 at 4,5 and 6 cu.

Fig.3 The target diagram of B. + stands for a hadron.

opening angle is $(7.6 \pm 1.8) \cdot 10^{-4}$ rad.. Their invariant mass is calculated only for the electro-magnetic component to be $5.4 \text{ GeV}/c^2$.

(#A4-7) #A4-7 are observed in the upper chamber as normal low energy showers.

The triangulation method was applied to determine the interaction height of the group A by measuring the relative distances between the higher energy core of #A3 and one of the multi-cores of #A2 at 3,4,5,6 and 10 cu in the lower chamber and between the higher energy core of #A3 and the new core of #A1 at 4 and 5 cu in the lower chamber. Within the error, the measurements on both pairs are consistent with parallelism, so we can say that the interaction height of the group A is higher than the limit of accuracy on the height determination, $\sim 500 \text{ m}$ above the chamber.

3-2. Group B The group B contains 13 shower cores with a quite small lateral spread; the average spread is 745μ which is $\sim 1\%$ of the average of atmospheric interactions. The target diagram of B is shown in Fig.3. One core indicated by the cross in Fig.3 appears at 6 cu as a very collimated shower core whose starting-point of cascade is estimated to be 2.2 cm Pb , which is identified as a hadron.

4. Discussions and Conclusion

The event S109 I69 is of clear binocular-type consisting of two groups of particles well separated to each other. In the view-point of Centauro family, this event can be a Geminion-type. Using the average mass of Geminion ($k_{\gamma} M \sim 5 \text{ GeV}/c^2$), the production height is calculated to be $\sim 3 \text{ km}$.

In the group A, the fraction of the energy sum of hadrons over the total visible energy is 81% . This large fraction satisfies the criteria/3/ that the event can be of Mini-Centauro type. Using the average p_T of Mini-Centauro ($k_{\gamma} p_T \sim$

0.35 GeV/c), the interaction height is calculated as ~ 1 km.

#A1 is an atmospheric interaction. If we assume that the two cores observed are decay-products of $\pi^0 \rightarrow 2\gamma$, the height is 8.8 m. If we assume that they are from mini-cluster/2,4/ with $p_T = 20$ MeV/c, the height is ~ 30 m above the chamber.

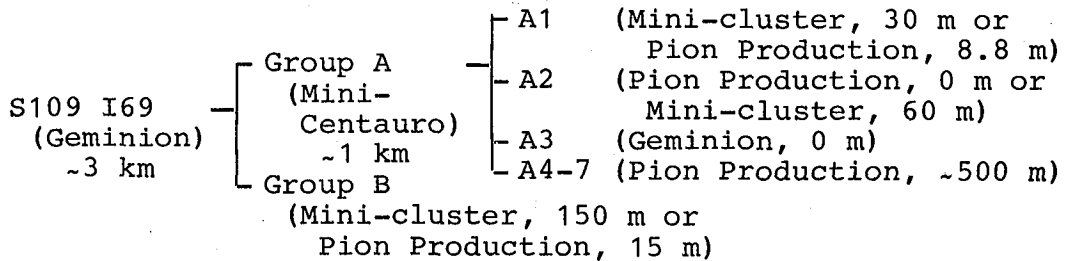
#A2 is an interaction in the upper chamber. If the hadronic core came from the same emission point of the multi-cores, #A2 can be a normal pion production in the chamber. If the hadronic core came from the atmosphere with another hadron producing the multi-cores, #A2 can be of mini-cluster. Using $p_T = 20$ MeV/c, the height is ~ 60 m.

#A3 is an interaction in the lower chamber, in which two cores are well separated with a very large transverse momentum ($k_T p_T \sim 1.9$ GeV/c). #A3 can be a Geminion.

#A4-7 may be products of normal pion production in the atmosphere.

The group B is an atmospheric interaction very near the chamber. If we assume that the interaction is of normal pion production with $\langle p_T \rangle = 200$ MeV/c, the height is 15 m. If we assume a mini-cluster, the height is 150 m.

Summarizing the results and discussions on the event CH19 S109 I69 whose total visible energy is 135 TeV, our conclusion is as follows:



Sequential appearance of exotic features in this event can be well understood by the hypothesis on genetic relation/4/ that an exotic interaction is generated by an exotic particle produced out of the exotic interactions.

5. Acknowledgement The authors wish to acknowledge all the members of the Brasil-Japan Collaboration for their kind and continuous support. Thanks are due to the CNPq, Brasil, for their financial support.

References (PIS=Proc.of Internat.Symposium on Cosmic Rays and Particle Physics, Tokyo, 1984; CFL=Contribution to a Festschrift for Prof.C.M.G.Lattes)

- /1/ C.M.G.Lattes et al., Phys.Rep.65 (1980) 152.
- /2/ Brasil-Japan Col., AIP Conf.Proceedings, 85 (1981) 500.
- /3/ A.S.Borisov et al., PIS, 1984, p.248.
- /4/ S.Hasegawa, PIS, 1984, p.718 and CFL, 1984, vol.1, p.71. Brasil-Japan Col., CFL, 1984, vol.1, p.62.

GAMMA-HADRON FAMILIES AND SCALING VIOLATION

T.K.Gaisser(*), T.Stanev(**) and J.A.Wrotniak(***)

Bartol Research Foundation of the Franklin Institute,
 University of Delaware,
 Newark, DE 19816, U.S.A.

For three different interaction models we have simulated gamma-hadron families, including the detector (Pamir emulsion chamber) response. We compare with experiment rates of gamma families, of hadrons, and hadron-gamma ratios.

The Monte Carlo data on families in large emulsion chambers indicate, that simulations made for primary vertical protons are sufficient for the interpretation of observed gamma families (except of their intensity rates). However, for gamma-hadron families the increase in air thickness and the presence of heavier primaries may be important, as the hadron component has different penetrating power than the electromagnetic one.

Therefore we used our three different nuclear interaction models embedded in the same simulation framework, including heavy primaries and zenithal angles from 0 to 45 degrees.

Summary of models used in simulation

- @ FF-Y00 - scaling extrapolation of ISR data, constant AA and pA cross-sections.
- @ RR-F00 - energy dissipation increasing with energy; at 1.5 TeV as FF-Y00, at 150 TeV y-distributions reflect the SPS p \bar{p} data (what by itself does not say much about the x-distributions, decisive for the family features), with fraction of neutral pions increasing with energy, rapidly rising AA and pA cross-sections.
- @ ST - based on a parametrization of hadron-nuclear collisions at accelerator energies, tuned to fit the balloon data in the TeV region. Scaling holds in the fragmentation region, while the central rapidity density increases as log E. Leading hadron energy is skewed towards smaller values and energy-dependent cross-sections correspond to log²E rise of the pp one.

(*) Work supported in part by the U.S.Department of Energy under contract No. DE-AC02-76 ER 05007.

(**) Work supported in part by the U.S.National Science Foundation under grant No. PHY 84-10989.

(***) On leave from the $\dot{\text{B}}\text{o}\dot{\text{d}}\text{z}$ University, Poland.

First two models are described in detail by Wrotniak [4] (see also [7] in this volume), the third one - by Gaisser et al.[8]. Simulations were done in frames of the SHOWERSIM/84 standard [4], with Nikolskii [11] primary mass/energy spectrum; sampling threshold effects were avoided.

Simulation of the chamber response

The chamber [1,2] consisted of a 5 cm lead layer (gamma block), 60 cm (66 g/cm²) of carbon and another 5 cm of lead (hadron block), with increase at non-zero zenithal angles.

Mean free path for nuclear interaction in carbon was 70, 91 and 102 g/cm² (nucleons, pions and kaons, respectively), and in lead - 168, 218 and 245 g/cm².

The effective gamma inelasticity of interacting hadrons was distributed as in [5] with mean value of .24 (nucleons) or .29 (mesons). Particles in the gamma block (including few interacting hadrons) were processed as in [9] (energy distortion, resolving power and a 15 cm cut-off).

Results

We compare our results with the Pamir Experiment data from Bangalore [1,2]. Both these papers refer to basically the same experimental results from a 250 m²y exposure [1], expanded to 308 m²y in [2].

Table 1 The ratio of gamma families with $\Sigma E_\gamma > 100$ TeV to primary flux above 1000 TeV/nucleus.

Primary	FF-Y00	RR-F00	ST	Exp [1]
p	.077(4)	.0153(11)	.039(5)	.
Alpha	.028(3)	.0051(9)	.016(5)	.
M	.007(2)	.0021(5)	.003(2)	.
LH	.011(3)	.0013(6)	.002(2)	.
VH	.0075(23)	.0011(2)	-	.
Total	.037(2)	.0073(5)	.018(2)	.0056(5)

Obviously, one can adjust the overall rate just by assuming different primary composition (cf Amenomori et al.[10]). However, at $\Sigma E_\gamma > 100$ TeV there were 133 gamma families in experiment, versus 874 (FF-Y00), 173 (RR-F00) or 430 (ST) predicted by us for this exposure. Assuming the spectrum used by Gaisser (cf [3]) will reduce these numbers by about 6%; the spectra used by Kasahara et al. or M.Shibata (compared in [3]) - by 30-40%.

The experimental rates for hadron families (>100 TeV in total detected energy, at least 1 hadron) have not been published, but this should be not too difficult [6]:

Table 2 The ratio of hadron families with $\Sigma E[\text{detected}] > 100 \text{ TeV}$ to primary flux above 1000 TeV/nucleus .

Primary	FF-Y00	RR-F00	ST
p	.020(2)	.0017(4)	.0034(15)
Alpha	.013(2)	.0017(2)	.0012(7)
M	.004(1)	.0008(3)	.0022(16)
LH	.007(2)	.0005(4)	-
VH	.005(2)	.0006(1)	-
Total	.012(1)	.0013(2)	.0024(8)

The $308 \text{ m}^2 \text{ y}$ exposure [2] gave 144 hadrons above 50 TeV (electromagnetic component energy in the chamber) and 41 hadrons above 100 TeV. We can compare these figures with ours:

Table 3 The ratio of hadrons with $E > 50 \text{ TeV}$ and $E > 100 \text{ TeV}$ to primary flux above 1000 TeV/nucleus .

Model:	FF-Y00	RR-F00	ST	Exp [2]
$E > 50 \text{ TeV}$.0164(11)	.0024(3)	.0051(11)	.0049(4)
$E > 100 \text{ TeV}$.0049(6)	.0006(1)	.0017(6)	.0014(2)

The hadron to gamma-family ratio is often quoted for the experimental data, being independent on the absolute primary flux: $H = N[\text{hadrons} > 100 \text{ TeV}] / N[\text{gamma families} > 100 \text{ TeV}]$.

Table 4 The hadron/gamma family ratio, H (as defined above)

Model:	FF-Y00	RR-F00	ST	Exp [1]
H	.13(2)	.08(2)	.09(4)	.27(5)!

The pattern emerging from Tables 1-3 is lost here! Also, simulations presented in [1] indicate, that H decreases with rising cross-section and increases with energy dissipation in nuclear interaction. This makes the experiment harder to explain with a quasi-scaling model with rising cross-section (needed to account for absolute rates); the rise assumed for non-scaling models should be much slower than ours.

Of course, higher effective gamma inelasticity and/or shorter interaction paths in the chamber would also bring

simulations closer to experiment. However, more than 2/3 of hadrons interact in the sensitive volume of our chamber, so the mean free paths will not give us even a 50% increase in H, and an approximate argument shows, that we need a much higher effective inelasticity to bring our results into agreement with experiment (the average of .4 for FF-Y00 or .5 for two other models).

Finally, let us compare the data on the accompaniment of high-energy hadrons:

S - the ratio of hadrons with neither gamma nor hadron accompaniment (above visible 2 TeV) to all hadrons above 50 or 100 TeV,

S' - the ratio as above, but no hadron accompaniment only,

S'' - as above, but no gamma accompaniment only.

Table 5 The percentage of 50 and 100 TeV hadrons with no accompaniment at all, with no other hadrons and without gamma accompaniment.

	E > 50 TeV				E > 100 TeV			
	FF-Y00	RR-F00	ST	Exp[2]	FF-Y00	RR-F00	ST	Exp[2]
S	11(2)	25(5)	25(10)	45(4)	07(3)	10(7)	29(17)	41(8)
S'	23(3)	47(6)	40(11)	49(4)	14(5)	30(9)	43(19)	49(8)
S''	15(3)	26(5)	25(10)	71(4)	09(4)	10(7)	29(17)	61(8)

Once again, the discrepancy lies in the hadron/gamma ratio, as the S' values fit two of our models. One possible explanation is, that there are more hadrons produced than we assume (though there are no Centauros in Pamir), another - serious underestimation of gamma-ray energy or (perhaps more probable) overestimation of energy in the hadron block.

References

1. J.Malinowski et al.; 18th ICRC, Bangalore, 11, 179 [1983]
2. Pamir Collaboration; 18th ICRC, Bangalore, 5, 433 [1983]
3. T.K.Gaisser et al.; Bartol Report BA-81-21 [1981]
4. J.A.Wrotniak, SHOWERSIM/84; Univ.Md.Rep. PP 85-191 [1985]
5. J.Malinowski et al.; Pamir Coll.Workshop, Lodz, 49 [1980]
6. Pamir Collaboration; 17th ICRC, Paris, 11, 148 [1981]
7. J.A.Wrotniak and G.B.Yodh, HE 4.1-7 in this volume
8. T.K.Gaisser et al.; 18th ICRC, Bangalore, 5, 174 [1983]
9. H.Bielawska et al.; 18th ICRC, Bangalore, 11, 149 [1983]
10. M.Amenomori et.al.; Phys.Rev.D25, 2807, [1982]
11. S.I.Nikolskii; Izv.Akad.Nauk, Ser.Fiz., 39, 1160 [1975]

SUPER-FAMILY P2 C-96-125 OBSERVED BY JAPAN-URSS
JOINT EMULSION CHAMBER EXPERIMENT

JAPAN-URSS JOINT EMULSION CHAMBER EXPERIMENT and
EDISON HIROYUKI SHIBUYA S
INSTITUTO DE FÍSICA 'GLEB WATAGHIN'
UNIVERSIDADE ESTADUAL DE CAMPINAS
CAMPINAS, SÃO PAULO BRASIL

1. INTRODUCTION: Since 1969, when it was observed the event 'Andromeda' by Brasil-Japan Emulsion Chamber Collaboration-BJECC, others events, looking like the pionner one, was detected and are turning to be one of the main themes of Cosmic Ray experiments. Nowadays, in 4 mountain stations (Kambala-China, Chacaltaya-Bolivia, Pamir-Soviet Union and Fuji-Japan), huge Cosmic Ray exposed Emulsion Chambers are constructed under name of International Collaborations, and constitute a world-wide effort to catch such type of events. This paper aims to be a detailed description of the event detected in the second chamber of Japan-Urss Collaboration. A preliminary description was already published(1) and from that time a careful microscopic scanning was carried out.

2. METHODS: Fig.1 is the sketch of the chamber. As the Japanese sensitive X-ray films are inserted only in 4 layers, being 2 in the I-Block and the other 2 in the H-Block, the usual way of BJECC for energy determination is not applicable, a different method of energy determination was developed by T. Shibata(2), method that was used in the present paper. Japanese and Sovietic groups, using their respective materials and their own methods, made energy determination of this event. A check was recently made, obtaining consistent energy values.

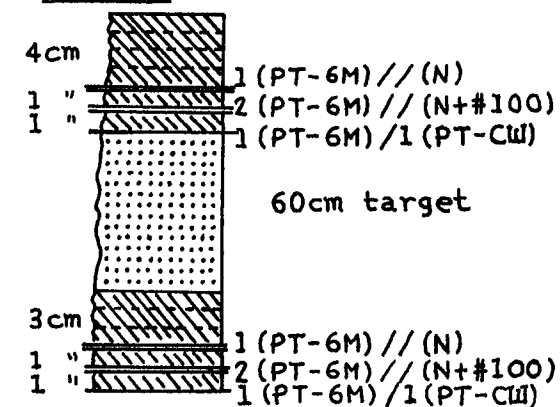




Fig.1 Sketch of the chamber

 lead plates

 rubber plates

3. RESULTS: Main characteristics of the event are summarized in Table I. From there we see that around half (56%) of the scanned individual showers are inside the central area of $(1.5 \times 1.5) \text{ cm}^2$. They carries about 76% of the energy ($\Sigma E_{\gamma} + \Sigma E_h^{\gamma}$) of the individual showers and the energy inside the central square of $(1.5 \times 1.5) \text{ cm}^2$ is equal to 2.5×10^3 TeV, approximately equal to the energy determined by halo measurement ($= 2.9 \times 10^3$ TeV). So, the remaining 400 TeV are distributed into many showers with energy less than 1 TeV and that causes the blacked region of the event.

TABLE I

Zenith angle: (18±2) degrees

Detection: e, γ and hadrons (efficiency for hadrons = 80%)

Halo	}	Radius $R_{\text{halo}} = 1.2 \text{ cm}$
		Energy = $2.9 \times 10^3 \text{ TeV}$
$(E_{\gamma} > 1 \text{ TeV})$	}	Number 177
		112 inside central square of $(1.5 \times 1.5) \text{ cm}^2$
	}	Energy 2,000
		$\Sigma E_{\gamma} / \text{TeV}$ 1,651 inside central sq. of $(1.5 \times 1.5) \text{ cm}^2$
Hadrons	}	Number 35(44)
		7(9) inside central sq. of $(1.5 \times 1.5) \text{ cm}^2$
$(E_h^{(\gamma)} > 1 \text{ TeV})$	}	Energy 1,254(1,567)
		$\Sigma E_h^{(\gamma)} / \text{TeV}$ 822(1,028) inside sq. of $(1.5 \times 1.5) \text{ cm}^2$

- Notes: a) the efficiency was calculated as ref.4, i.e.
 $\text{efficiency} = \exp(-4/\lambda_h \cos \theta) - \exp\{- (T - T_0)/\lambda_h \cos \theta\}$,
 where the nuclear collision mean free path λ_h was assumed as 30 c.u.Pb, T_0 = vertical traverse in lead over which an electron shower develop above the detection threshold (assumed $T_0 = 4$ c.u.Pb) and T is the thickness of Pb layers + target.
- b) radius of halo, R_{halo} is defined as the distance from the center to the point where the electron density is $10^6 / \text{cm}^2$.
- c) hadrons was identified as shower spots observed only in H-Block(22) + shower spots showing transition curve with 2 peaks(6) + shower spots showing transition curve adjustable to analytical γ transition curve(7).
- d) figures in the parentheses gives the value after correction of detection efficiency.

Fig.2 shows the integral fractionary energy spectrum of electrons/gamma-rays. Others events are included and the marks are: Δ for the concerned event, \circ for Andromeda, \times for Ursa Major, \bullet for Mini-Andromeda III and the smooth curve is the average of five families with $\Sigma E_{\gamma} = (1,000 \sim 3,000) \text{ TeV}$ of Mt. Fuji experiment(3). Fig.3 shows the same kind of spectrum for hadrons. Marks are the same as Fig.2. From the comments of Table I, it is clear that the number of identified hadrons is the minimum, because it was used a very restrictive criterion. Also, looking for the figures (13 continuing showers from Γ -Block to H-Block and labeled as hadrons) and the 22 hadrons observed only in H-Block, we confirm the above affirmation. Fig.4 is the lateral distribution of energy flow, where R is the distance of shower from the energy weighted center, center of γ 's only. Hatched areas are for identified hadrons.

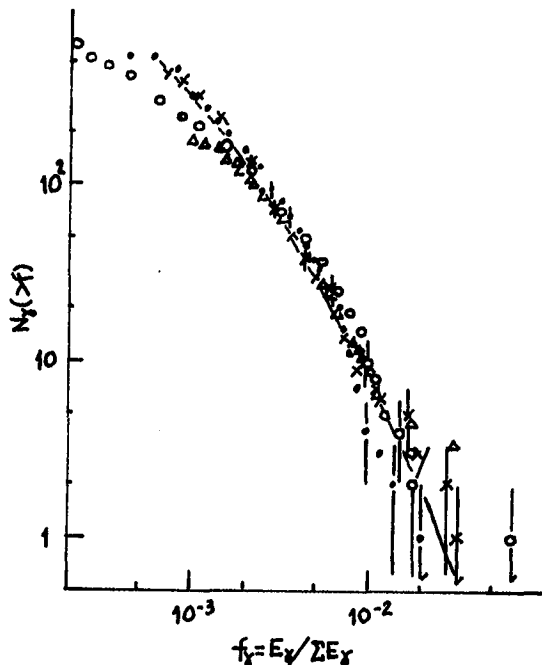


Fig.2

The individual showers was observed in the central (1.5x1.5) cm² area, by microscopic scanning in the #100 type Fuji X-ray films (fine grains) added to showers scanned by naked eyes in the N-type Sakura X-ray films (high sensitivity). From this scanning it is clear the existence of two clusters, formed by 76 spots, each one containing γ 's and also hadrons. The showers of these two clusters are distributed in the distances smaller than R_c , that characterizes the pronounced peak of Fig.4.

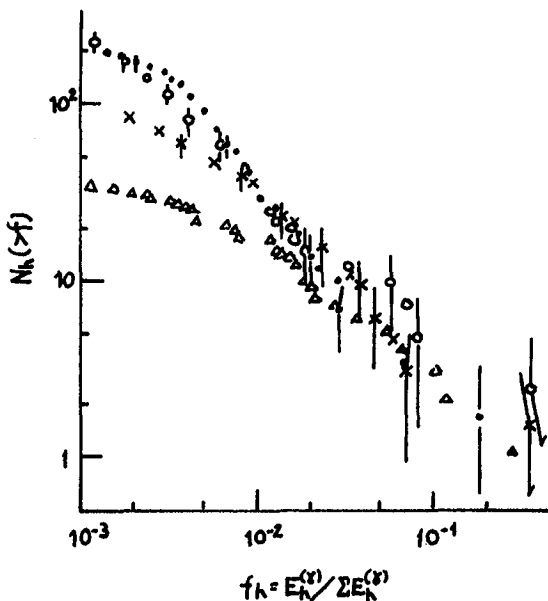


Fig.3

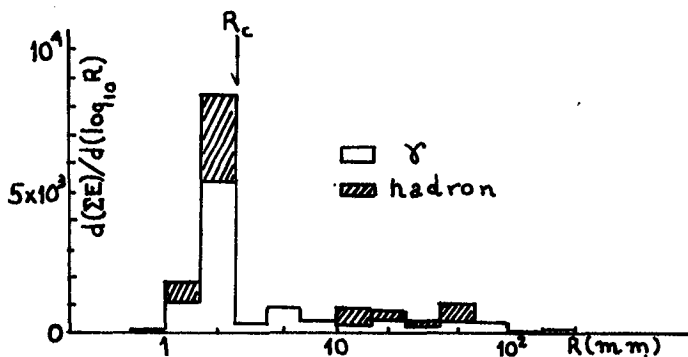


Fig.4

Table II *

event name	lateral spread	energy	energy-normalized
	R_c (mm) *	ΣE_{γ} (TeV) $R < R_c$	lateral spread $R_c X \Sigma E_{\gamma}$ (GeV.Km) $R < R_c$
P2 C-96-125	2.5	1,338 (66.9%) **	3.3
Andromeda	1.0	323 (7.2%)	0.32
Ursa Maior	4.0	700 (52.1%)	2.8
M.A.I	6.3	734 (55.0%)	4.6
M.A.II	1.6	390 (43.9%)	0.62
M.A.III	2.5	796 (31.5%)	2.0

Notes:* For definition of R_c and data of other events see(4)

**Figures in the parentheses are the fraction of energy to the total energy of electromagnetic component

4. SUMMARY AND DISCUSSIONS: Comparison of this event shows similar features with other events. Remarkable difference is the existence of two central clusters carrying 67% of electromagnetic energy and 64% of hadronic energy. Under the

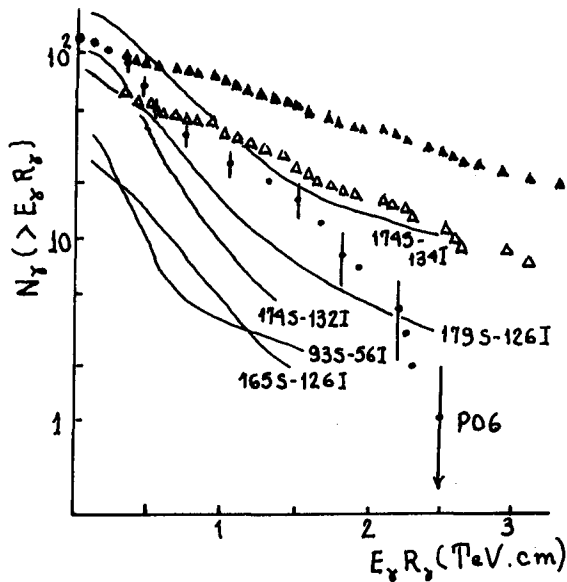


Fig. 5

same restrictive criterion for hadron identification, from where it was obtained the above figures, it was made a $E_\gamma R_\gamma$ integral distribution (fig. 5). Marks are Δ for this event considering γ 's with $R_\gamma < R_c (=2.5\text{mm})$ and \blacktriangle for $R_\gamma < R_{\text{halo}} (=12.0\text{mm})$. The distribution for event P06 is from article: A Cosmic-Ray Nuclear...-Amato, Arata and Maldonado in this issue. Full lines are from ref. 5. So, the distribution obtained for this event is similar to that one obtained for events containing the so-called Giant-Mini-Cluster phenomena (see article of BJ ECC in this issue).

References:

1. Shibuya, E.H. - Proc. Int. Sympo. on Cosmic-Rays and Particle Physics, Tokyo, (1984), 127
2. Shibata, T. - Internal Colloquium of Japanese Group of Japan-USSR Collaboration
3. Mt. Fuji Collaboration - Nuovo Cimento Ser. 11, 67A, (1982), 221
4. Yamashita, S. - Jour. Phys. Soc. of Japan, vol. 54, n. 2, (1985), 529
5. Hasegawa, S. - Proc. Int. Sympo. on Cosmic-Rays and Particle Physics, Tokyo, (1984), 62

§ Permanent address of E.H.S. is UNICAMP, Campinas-São Paulo, Brasil. He was visiting researcher during 1984 at the Institute for Cosmic Ray Research-University of Tokyo and Science and Engineering Research Laboratory-Waseda University, where the present work was developed.

Acknowledgments: The Japanese part of the JAPAN-USSR Collaboration is financially supported by Grant-in-Aid of Ministry of Education and Waseda University. One of the authors (EHS) was recipient of a Conselho Nacional de Desenvolvimento Científico e Tecnológico, Brasil during the year of 1984 - CNPq fellowship (Processo nº 200.881/83-FA), which is also gratefully acknowledged.

On the halo events observed by Mt.Fuji and Mt.Kanbala
Emulsion Chamber Experiments

--- Mt.Fuji Collaboration , Japan-China Collaboration ---

Ren J.R., Kuang H.H., Huo A.X., Lu S.L., Su S., Wang Y.X.,
and Xue Y.G.

(Institute of High Energy Physics, Academia Sinica, China)

Wang C.R., He, M., Zhang, N.J., Cao P.Y. and Li J.Y.

(Shandong University, China)

Wang S.Z. (Zhengzhou University, China)

Bai, G.Z., Liu, Z.H., Li, G.J. and Geng, Q.X.

(Chongqing Architecture College, China)

Zhou, W.D. and He, R.D. (Yunnan University, China)

Amenomori M. and Nanjo H. (Hirosaki University, Japan)

Hotta N. and Ohta I. (Utsunomiya University, Japan)

Mizutani K. (Saitama University, Japan)

Kasahara K. and Yuda T.

(Institute for Cosmic Ray Research, University, of Tokyo, Japan)

Mito I. (Shibaura Inst. of Technology, Tokyo),

Shibata M. (Yokohama National University, Japan)

Shirai T., Tateyama N., Taira T. and Torii S.

(Kanagawa University, Japan)

Sugimoto H. and Taira K. (Sagami Institute of Technology, Japan)

ABSTRACT

The intensity of big gamma-ray families associated by "halo" is obtained from Mt.Fuji experiment (650 g/cm^2 atmospheric depth) and Mt.Kanbala experiment (515 g/cm^2). The results are compared with Monte Carlo calculation based on several assumptions on interaction mechanisms and the primary cosmic ray composition. The results suggest more than 3 times lower proton abundance among primaries than that of $10^{12} - 10^{13}$ eV region within the framework of quasi-scaling model of multiple production.

1. Introduction Emulsion chamber experiments at high mountain altitudes are extending the concerned energy region over 10^{15} eV by the scale up of installations and accumulation of the exposure time. The integrated exposures have reached about $1000 \text{ m}^2\text{y}$ and $300 \text{ m}^2\text{y}$ at Mt.Fuji¹⁾ and Mt.Kanbala²⁾, respectively, where the latter is already more than half of the former taking into account of the detection yield of the events. Some of the most energetic events ($\Sigma E_{\gamma} > 1000 \text{ TeV}$) observed by these experiments show a remarkable character of extremely high optical density on the X ray films at the gamma-ray family center, which we call halo. Some methodical problems connected to the energy estimation and the method of the analysis on the halo events are already reported in other papers^{3), 4)}. The responsible interaction energies for these events are estimated as $10^{16} - 10^{17}$ eV. Since the extremely high energy density at the central part of the gamma-ray family is attributed to a number of energetic secondaries produced at the nuclear interactions in the atmosphere, the physical interest in the halo phenomena is connected to the feature of the multiple production mechanism in the fragmentation region at such a high energy

and also to the primary cosmic ray composition, especially to the portion of protons. As already reported in preliminary works^{4), 5)}, the experimental data show less intensity of the halo type event than expected one based on simple extrapolation of lower energy data on multiple production and primary composition. Some possibilities resulting to the decrease of the halo intensity are considered in this paper. Namely, the fast increase of interaction cross section, breakdown of scaling law as expected from the extrapolation of ISR-SPS^{6), 7)} results and possible change of the primary cosmic ray composition connected with the magnetic rigidity in the galaxy magnetic field are taken into account in the simulation.

2. Intensity of the halo events The number of big families with observed gamma ray energy more than 1000 TeV is 10 and 8 in Mt.Fuji and Mt.Kanbala experiment, respectively. The details of those events are described in ref. 2) and 5). The intensity of the halo events is examined in terms of the geometrical halo size defined as:

$$S_{\max} = \int_{D > D_{\min}} dS \quad (\text{cm}^2) , \quad D_{\min} = 0.7 \quad (1) ,$$

where D_{\min} is a given threshold for high optical density corresponding to the electron density of $3.24 \times 10^6 / \text{cm}^2$ in case of double side coating N type X ray films. The integration is carried out over the area where the net optical density exceeds given threshold D_{\min} . We can obtain the transition curve of the halo size measuring on X ray films of every layers of the chamber, then the maximum value is adopted as S_{\max} . Thus defined halo size well describes the feature of the energy flow at the gamma-ray family center. The integral spectrum of the halo size S_{\max} is shown in Fig.1 (Mt.Fuji) and in Fig.2 (Mt.Kanbala) together with the results of Monte Carlo calculation made by one of the authors (M.Shibata). The main characters of models used in the simulation are as followings.

PS, α S, CNOS : Complete scaling model in entire energy range with constant interaction cross section, assuming primary cosmic ray particles as proton, helium and CNO group, respectively (pure composition).

PC : Proton primary with CKP model⁸⁾.

PSq : Proton primary with quasi-scaling model, where increasing cross section ($\sigma \propto E_0^{0.06}$) and breakdown of scaling in pionization part is taken into account to be consistent with ISR-SPS results as shown in Fig.3. In this model, x-distribution in the fragmentation part shrinks very weakly with increasing energy as shown in Fig.4.

MSq : The same interaction model as PSq but assuming mixed primary composition of heavy nuclei dominance as shown in Table 1.

Table 1. The primary composition in mixed composition model (in %)

E_0 eV	P	α	CNO	LH	MH	Fe
$\langle A \rangle$	1	4	15	25	35	56
10^{15}	10.8	4.4	6.9	22.9	3.0	51.9
10^{16}	7.3	3.1	5.0	20.3	2.6	61.6
10^{17}	6.0	2.6	4.5	19.2	2.5	65.1

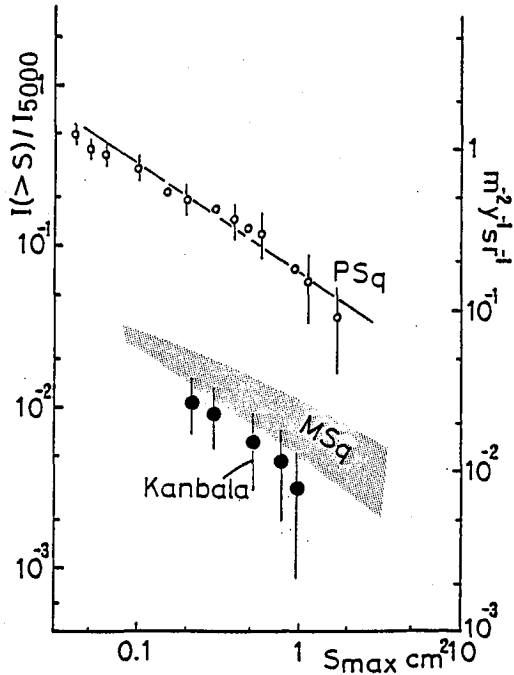
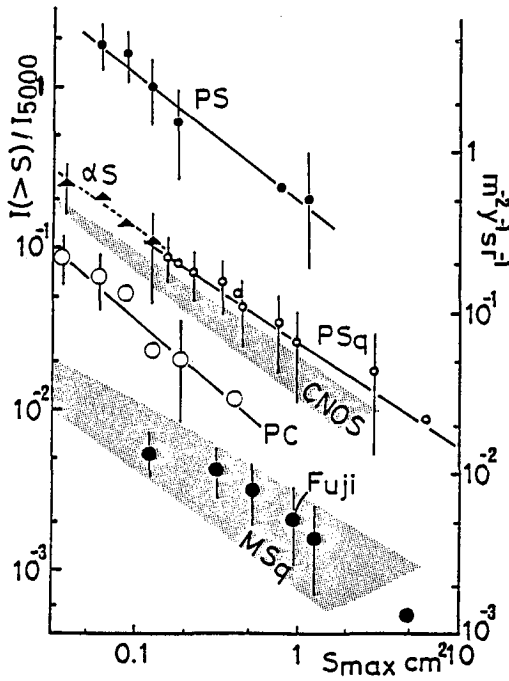


Fig.1 Intensity of the halo at Mt.Fuji. See eq.(1) for the definition of S_{max} .

Fig.2 Intensity of the halo at Mt.Kanbala.

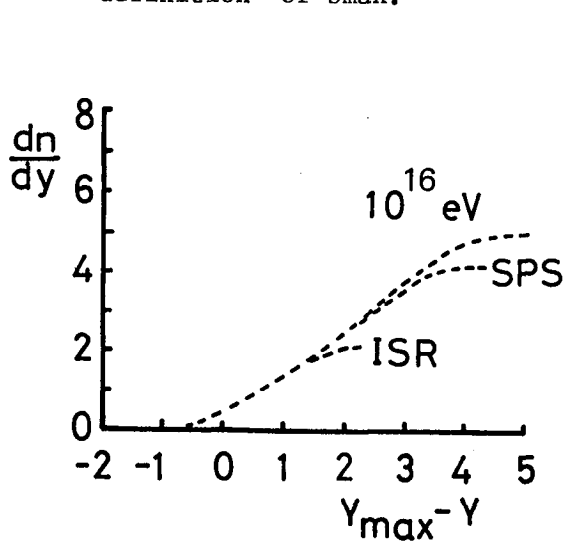


Fig.3 Rapidity distribution for quasi-scaling model.

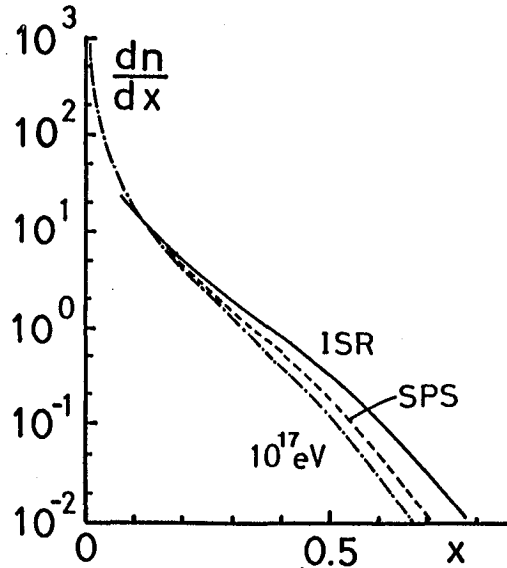


Fig.4 x -distribution for quasi-scaling model.

The intensities in Fig.1 and 2 are normalized to the number of primary cosmic rays at $E_0 > 5000$ TeV (left hand side scale) and to absolute intensity (right hand side scale) using $I_{\text{tot}}(E_0 > 5000 \text{ TeV}) = 2.5/\text{m}^2 \text{ y sr}^{-1}$. As is clearly seen from Fig.1, PS model is far from agreement with experimental data even if the portion of protons among total flux is considered. The quasi-scaling model with proton primary (PSq) still gives more than 10 times higher intensity. Therefore we can get agreement with experimental data within the framework of quasi-scaling model only when the portion of protons among total primary flux is less than 10 %, which is more than 3 times lower than the proton abundance known in 10^{12} - 10^{13} eV region. The contribution of heavy nuclei for the creation of the halo events is expected to be very small from the results of α S and CNOS models (about 10 times lower efficiency compared with PS). In fact, the results of calculation with mixed composition described above (MSq:heavy nuclei dominance, quasi-scaling model) show most of the big events come from proton primary even its ratio is less than 10 % of total flux. (In present simulated statistics, only two events, one from helium nucleus and another from LH nucleus, contribute to the halo event among 25 observable events.)

Another possibility to interpret the low intensity of the halo events is to assume stronger breakdown of the scaling in fragmentation part than quasi-scaling model. But CKP type model is not suitable for this discussion because PC model in Fig.1 gives about 30 times less intensity than PS model. Therefore it cannot reproduce the halo intensity if the increase of cross section and primary composition is adequately incorporated.

Both results from Mt.Fuji and Mt.Kanbala experiments are in agreement with the discussion above within statistical error.

References

- 1) M.Akashi et al., Phys. Rev. D, Vol.24, No.9 (1981) 2353
- 2) J.R.Ren et al., Proceedings of International Symposium on Cosmic Rays and Particle Physics, Tokyo, (1984) 87
- 3) M.Shibata, 18th International conference on Cosmic Rays, Bangalore, India, 1983, HE 5-16, Vol.11 (1983) 106
- 4) M.Amenomori et al., 18th International conference on Cosmic Rays, Bangalore, India, 1983, HE 5-15, Vol.11 (1983) 102
- 5) M.Amenomori et al., Proceedings of International Symposium on Cosmic Rays and Particle Physics, Tokyo, (1984) 76
- 6) W.Thome et al., Nucl. Phys. B129(1977)365
- 7) K.Alpgard et al., Phys. Lett. Vol.107B, No.4 (1981) 310
- 8) G.Cocconi et al., Lawrence Radiation Laboratory, High Energy Physics Study Seminars, Report No. 28.2 (UCID-1444,1,1961) (unpublished)
- 9) N.L.Grigorov, Proc. of 12th ICRC, Hovart (1971) 1746

EXPERIMENT "PAMIR"-II. "FIANIT" - A GIANT SUPER-FAMILY WITH HALO ($E_0 \sim 10^{17}$ eV)

Collaboration of experiment "Pamir" *)

1. Introduction. A supefamily with halo of extremely high energy named "Fianit" was recorded in X-ray emulsion chamber (XEC) at the Pamirs (atmospheric depth 600 g/cm²). Here we present detailed description of the superfamily and results of its analysis.

2. Experimental set-up and description of the event. The "Fianit" was recorded in the XEC consisted of two registration blocks separated by the 1 m air gap which permit to evaluate (by a triangulation method) the height of the initial interaction in the atmosphere up to several kilometers. The method and the structure of the XEC were described elsewhere [1,2]. The superfamily was traced in all six layers of the XEC with selection of the cascades in the circle of $R = 40$ cm. Zenith angle of particle arrival was 18° the height of the initial interaction determined from the relative distances between the single γ -cascades at various depths in nuclear emulsions is equal to $3,5 \pm 1,5$ km.

The γ -quanta of high enough energy used for the estimation of the height were located at distances from 4 to 12 cm from the family center.

In the center of the family there is a large dark dif-fused spot ("halo"), and on the background of it the separate cascades are visible in the upper layer of the XEC.

The energy determination for individual cascades was performed at the depth of 7.5 c.u., i.e. above the air gap. About 900 cascades are located out of the central circle with $R = 2$ cm, and they need no corrections taking into account the halo. On the background from halo, in the ring $0.5 < R < 2.0$ cm the energies of nearly 700 cascades were measured after the corrections connected with halo by the technique described in / 3/. The results of the measurements of cascade energies are given in Table 1. In the region $R > 2$ cm integral spectrum of γ -quanta has the power index $\beta = 1.8 \pm 0.1$. As far as the total depth of XEC is equal (taking into account the inclination) to 13.3 c.u. the hadron registration efficiency is $\sim 15\%$ only. Selection of hadrons was made at the depth of 13.3 c.u. (the 6th layer) and as a criterion of a hadron-induced cascade served the absence of it at a depth 7.5 c.u. (it corresponds to depth of origin $\Delta t > 6$ c.u.). In the region with $2 < R \leq 40$ cm 46 of such the cascades were observed, 26 of them be-

*) Full list of authors see in HE 1.2-12. The author of this paper is also G.T.Zatsepin (Institute for Nuclear Researches, Moscow).

ing with energy $E_h^{(n)} \geq 4$ TeV. The power index of this hadron spectrum occurred to be $\beta_h = 1.5 \pm 0.2$. Some results of measurements for γ -quanta and hadrons are given in Table 1.

Table 1

	Particles with $2\text{cm} < R < 40\text{cm}$		All γ -quanta	
	N_γ or N_h	$\sum E_\gamma$ or $\sum E_h^{(n)}$, TeV	N_γ	$\sum E_\gamma$, TeV
γ -quanta, $E_\gamma \geq 4$ TeV	250	$2.7 \cdot 10^3$	720	$1.0 \cdot 10^4$
hadrons, $E_h^{(n)} \geq 4$ TeV	26	192	-	-

2. Lateral distributions. The interesting feature of the superfamily "Fianit" consists in some structure of lateral distribution of γ -quanta. In the target diagram of the family (Fig.1) points the mean centers of the close groups of γ -quanta (clusters), obtained by the method of "nuclear decascading": to be included in the same cluster each pair of the cascades has to satisfy the condition

$$R_{ik} \cdot (E_i + E_k)^{-1} \leq Z_0, \quad Z_0 = 30 \text{ TeV} \cdot \text{cm} \quad (R_{ik} - \text{the mutual distance, } E_i, E_k - \text{the energies of the cascades}).$$

The number of clusters so obtained with energy $E_{cl} \geq 4$ TeV is equal to $N_{cl} = 55$, while 38 of them are located outside the circle of radius 2 cm. Differential distributions of R and ER for clusters are shown in Fig.1, the average values being $\langle R_{cl} \rangle = 10.5 \pm 1.4$ cm, $\langle E_{cl} \cdot R_{cl} \rangle = 5.8 \pm 0.6$ GeV.km. After the comparison with results of /4/ it can be stated that the high values of $\langle E_{cl} \cdot R_{cl} \rangle$ are connected with large ($\gg 1$ GeV/c) transverse momenta at least for the part of the initial hadrons or jets.

3. Properties of halo. To evaluate the energy of the halo the scanning of the area $4 \times 4 \text{ mm}^2$ with a slit size $500 \times 500 \mu\text{m}^2$ was performed in the central part of "Fianit" for 5 depths: 3.8, 5.7, 7.5, 11.4 and 13.3 c.u. *) Analysis of the densitograms has shown, that the total number of particles reaches the maximum at 11.4 c.u. although the darkness density is still growing up to the last level, 13.3 c.u. The total numbers of particles at various depths is given in Table 2.

The energy of the halo can be calculated from the total number of particles at maximum of the transition curve and the typical average energy $\sim 10^8$ eV:

$$E_{\text{halo}} \cong 1.7 \cdot 10^8 \cdot 10^8 = 1.7 \cdot 10^{16} \text{ eV}$$

*) Scanning was done in P.N. Lebedev Physical Institute (Moscow) and in the Institute of Cosmic Ray Research (Tokyo).

Table 2

$t, \text{c.u.}$	3.8	5.7	7.5	11.4	13.3
$N_{\text{tot}} \cdot 10^{-7}$	1.2	6.3	13.4	16.6	15.1

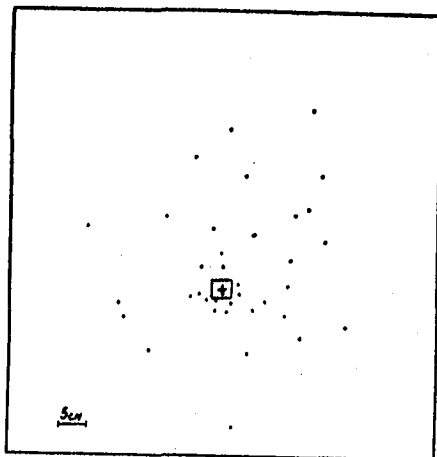


Fig.1. Target diagram of cluster lateral distribution (+ - central region of halo)

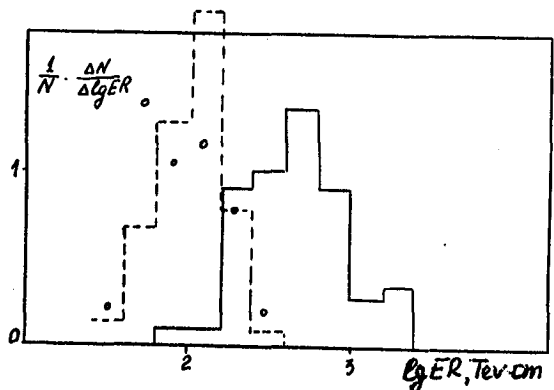


Fig.2. ER distributions of clusters:
 - "Fianit", O - big families of Fuji group,
 - - - calculations by model of high multiplicity

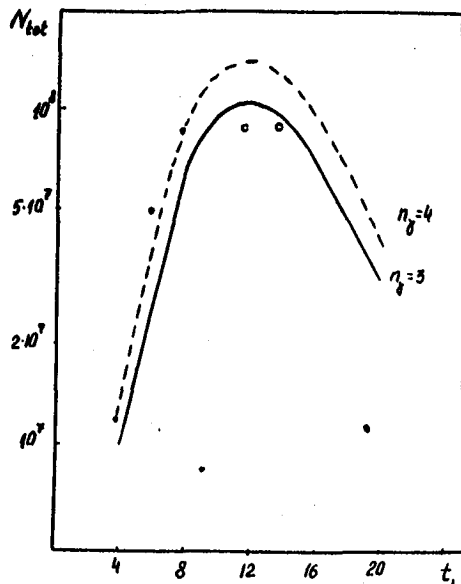


Fig.3. Transition curve of halo particles: • - experiment, — - and - - - - calculations for various number of initial δ -quanta with energy 10^{16} eV

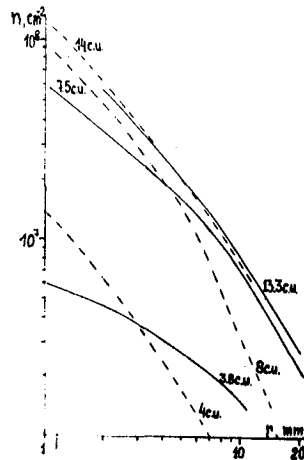


Fig.4. Lateral distributions of halo particles at various depths: — - experiment, - - - - calculation /5/

Because of the possible influence of the large air gap this energy estimate is considered as a lower limit.

The comparison of the longitudinal and lateral development of the halo with calculations is given in the Figs.3 and 4. The last 2 experimental points in Fig.3 are measured under the air gap, so they are underestimated. It can be seen that the longitudinal development can be explained /5/ by the production of 4 initial γ -quanta with energies of each of them $\sim 10^{16}$ eV at the height ~ 12 c.u. above the chamber. However for the lateral structure of halo the calculation differs from reality: it gives too high density in the center and ~ 2 times lower at the distance ~ 1 cm. This discrepancy cannot be explained by methodical reasons and it is necessary to admit the production of the considerable number of γ -quanta with initial lateral divergence.

4. Conclusions. The total energy of γ -component of superfamily "Fianit" occurred to be $\sim 3.5 \cdot 10^{16}$ eV, the total multiplicity of γ -quanta ~ 1500 so it is now the most energetic event ever recorded by XEC. Its peculiar feature is the large number of clusters (55) anomalously wide distributed over $E_{cl} R_{cl}$ values.

References

1. Puchkov V.S. Proc. 15th ICRC, V.9, p.190, 1977
2. S.G.Bayburina et al., Trudy FIAN, t.154, p.11, 1484 (In Russian)
3. Baradzei L.T. et al., preprint N 51, FIAN, 1976
4. Mt.Fuji collab., ICR-Report, 95-81-11
5. Ivanenko I.P., Managadze A.K., Proc. Inst. Symp. on Cosmic Rays and Particle Physics, Tokyo, March 1984, p.101

EXPERIMENT "PAMIR"-IV. ANALYSIS OF SUPERFAMILY WITH HALO OF ELECTROMAGNETIC NATURE DETECTED IN DEEP XEC

Collaboration of Experiment "Pamir"*

1. Introduction. The family Pb2-11 was detected in the multi-layer lead XEC with total thickness of 100 c.u. exposed at the Pamirs. Each lead layer was 1 cm thick, the first registering layer being located under 2 cm of Pb (≈ 4 c.u.). The family comprised a narrow group of gamma-rays which near the maximum of cascade development (≈ 14 c.u.) produced a dark spot of optical density $D \approx .4$ over area $S \approx 25\text{mm}^2$. The narrow group of gamma-rays was traced up to 14th layer corresponding to 30 c.u. Deeper in the chamber, for the space of 70 c.u. no hadron cascade was observed. Thus, the pure electromagnetic halo could be assumed.

Preliminary results of the analysis of the family Pb2-11 has been presented in /1/. We consider here in more detail the methods of estimation of energy of primary particle and height of nuclear interaction responsible for the observed halo.

2. Longitudinal and lateral characteristics of halo. To determine $\sum E_\gamma$ released in the halo, the area of halo was scanned by two instruments at various depths in lead. From the measured optical densities we inferred the density of number of secondary electrons $n(r)$ and subsequently the total number of particles $N(4\text{mm})$ within a circle of radius 4 mm. When determining $\sum E_\gamma$, restriction of the scanned area should be regarded. The ratio of the total number of secondary electrons in lead to the particle number within a circle of 4 mm, $K(4\text{mm})$, was calculated for maximum of an electron-photon cascade (EPC) induced by primary gamma-ray and electron with various energies E_γ . The value of $K(4\text{mm})$ weakly depends on E_γ and is equal to $2A$. Thus, $\sum E_\gamma = K(4\text{mm}) \cdot \beta \int_0^{\infty} N(4\text{mm}) \cdot t dt$, where $\beta = 7.5$ MeV. After taking into account the scattering of shower particles within a gap, the total energy was found to be $\sum E_\gamma = 560$ and 610 TeV, respectively, for two scanning instruments.

In /2,3/, the EPC from one or few high-energy gamma-rays have been shown to dominate halo production. To evaluate the height (C_{air}) and the energy (E_0) of the primary interaction producing the halo, experimental characteristics of halo were compared with the characteristics calculated in /2,3/ for air-lead EPC induced by high-energy gamma-ray. The Table below lists the interaction parameters used in three calculational versions.

The choice of the best version of calculations was made by comparison of experimental and calculated lateral

* Full list of authors see in HE 1.2-12. The author of this paper is also Zatsepin G.T., Institute of Nuclear Research, Academy of Sciences of the USSR, Moscow

distributions for 9 depths in the chamber, because the comparison on a single depth turned out to be insufficient. As an example the distribution $n(r)$ for three depths are plotted in Fig.1. The best agreement of experimental and calculated distributions is obtained for version II.

If lateral distribution in the halo at various depths are available, the transition curve for the halo longitudinal development within circles of vari-

Versions of calculations	I	II	III
E_0, TeV	100	700	1400
$t_{012}, \text{c.u.}$	3	3	9
n_r	7	1	1

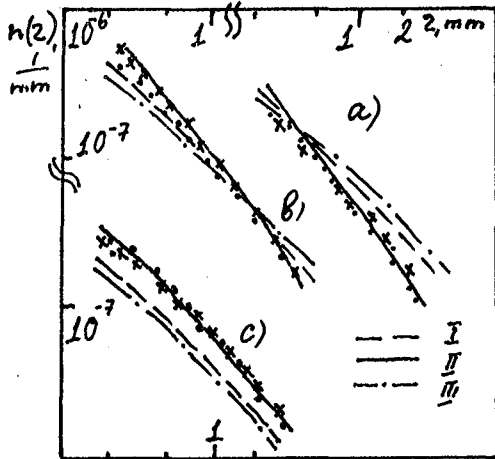


Fig.1. Lateral distributions $n(r)$ for the depths in XEC equal to 8 c.u.(a), 14 c.u.(b) and 20 c.u.(c). Experimental data is observed with scanning systems of University of Tokyo (.) and P.N.Lebedev Physical Institute (x). Curves present results of three versions of calculations listed in Table

Fig.3 presents the experimental energy spectrum of gamma-rays in the halo and calculated spectra for three versions of calculations and for version II with $E_0=1000 \text{ TeV}$. The best description of experimental data gives version II with $E_0=1000 \text{ TeV}$.

Experimental lateral characteristics and multiplicities obtained for gamma-rays within halo area for two different threshold (4 TeV and 10 TeV) were compared with calculated ones/6/ and thus the values $E_0=1000 \text{ TeV}$ and $t_{012} \approx 3-5 \text{ c.u.}$

ous radii in the chamber can be obtained. Fig.2 presents the experimental and calculated transition curves for a circle of radius 4 mm. The best agreement is also achieved for version II.

3. Lateral and energy distributions of individual gamma-rays in the halo

To obtain the characteristics of individual particles in the halo, spots from them were photometered at a depth of 6 c.u. taking into account overlapping /4,5/.

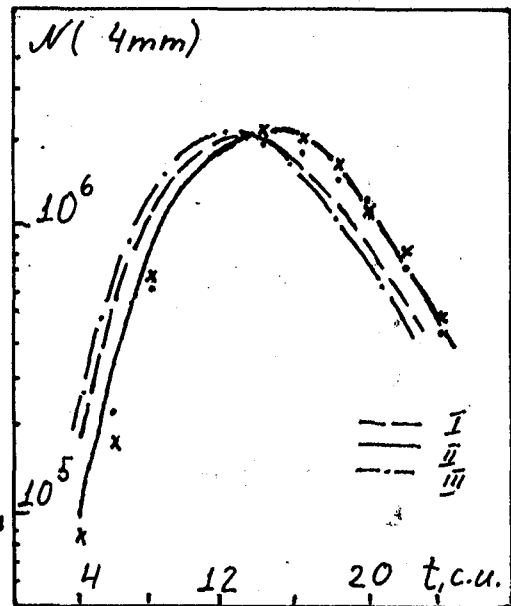
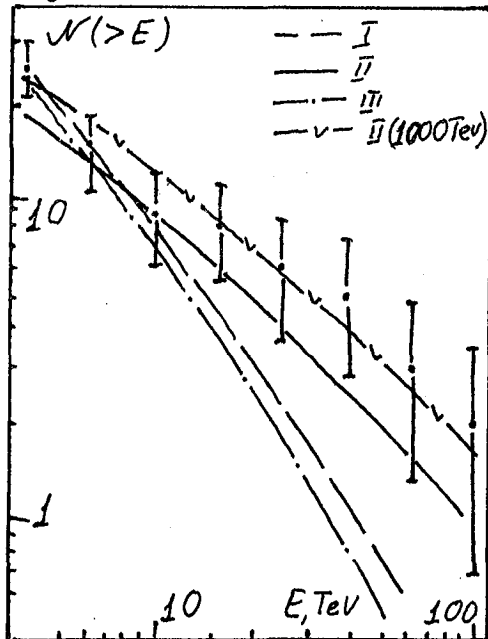


Fig.2. Transition curve $N(4\text{mm})$. Symbols are the same as in Fig.1.

were obtained.

Distribution of the relative transverse momentum z_{ik} for gamma-rays in the halo and for all gamma-rays in the family are shown in Fig.4. The distribution for all gamma-rays has two maxima. The first maximum corresponding to the



component with momentum $p_{em} \sim 2 \cdot 10^7$ eV/c, i.e. typical value for Coulomb scattering of electrons in the EPC, is caused mainly by gamma-rays in halo. The second maximum is caused by the component with characteristic nuclear transverse momentum $p_{nucl} \sim 2 \cdot 10^8$ eV/c. The height of nuclear interaction (τ_{air}) derived from the dependence $z_{ik}(\tau_{air})/7$ is equal to $\tau_{air} \sim 5$ c.u. both for gamma-rays in the halo and for all particles in the family.

The same analysis was also applied to the integral distribution of relative transverse momenta of particles with respect to the direction of the particle with the highest energy (z_{10}), and obtained estimation of the height is $\tau_{air} \sim 4$ c.u. also both for gamma-rays in halo and for all particles.

Fig.3. Experimental and calculated energy spectrum of gamma-rays in the halo. Calculations are made for three versions listed in Table and for version II with $E_0 = 1000$ TeV. $E_0 \sim 1000$ TeV and production height $\tau_{air} \sim 3-5$ c.u. is due to the nuclear interaction which has occurred at a

4. Conclusion. Summarizing the results of the analysis, we can infer that the observed halo is caused by the EPC induced by a single gamma-ray with energy $E_0 \sim 1000$ TeV and production height $\tau_{air} \sim 3-5$ c.u. The family is due to the nuclear interaction which has occurred at a height of 3-5 c.u. above the XEC.

It is important that the values of E_0 and τ_{air} obtained by analysing the halo development in the chamber and by analysing the lateral and energy distributions of family particles are in a good agreement.

Thus, the information on the longitudinal and lateral characteristics of electromagnetic halo allows estimation of the parameters of primary interaction producing the halo.

Energy of the primary interaction E_{int} can be obtained as a sum of energy of gamma-rays and hadrons outside halo/1/ and above estimated energy of halo equal to 700-1000 TeV, and the result is $E_{int} \sim 1200-1500$ TeV.

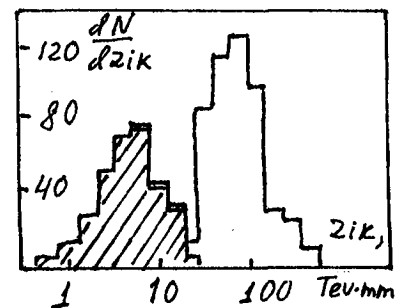


Fig.4. Distribution of z_{ik} for gamma-rays in halo (dashed) and for all gamma-rays in the family

The transfer of the large energy fraction into the electromagnetic component is an important feature of the family. The observed event can be treated as detection of the charge exchange process $\pi^{\pm} \rightarrow \pi^0$ with Feynman variable $\alpha \approx .6 \pm .1$.

References

1. Borisov A.S. et al. - Proc. of Int. Symp. on Cosmic Ray and Particle Physics, Tokyo, 1984, p.3-29.
2. Fedorova G.F., Managadze A.K. - Proc. 18th ICRC, 1983, v.5, p.466-469.
3. Ivanenko I.P., Managadze A.K., Roganova T.M., Osipova L.A. - Proc. 15th ICRC, 1977, v.7, p.267-280.
4. Aminava T.P., Lazareva T.V., Managadze A.K. - Acta Univ. Lodz. ZNUL, 1980, ser.II, v.32, p.199-216.
5. Ivanenko I.P., Managadze A.K., Roganova T.M. - Proc. 15th ICRC, 1977, v.7, p.280-284.
6. Adachy A. et al. - Prog. Theor. Phys., Suppl., 1964, v.32, p.154-191.
7. Baradzey L.T., Smorodin Yu.A., Solopov E.A. Preprint NN 103, 104, M.: FIAN, 1974.

PARTICLE INTERACTIONS AT ENERGIES OVER 1000 TeV INFERRED
FROM GAMMA-FAMILIES OBSERVED AT Mt. FUJI

Mt. Fuji Collaboration

Amenomori, M., Nanjo, H. and Konishi, E.
Hirosaki University, Hirosaki, Aomori
Hotta, N.

Utsunomiya University, Utsunomiya, Tochigi
Mizutani, K.

Saitama University, Urawa, Saitama
Kasahara, K., Kobayashi, T., Mikumo, E., Sato, K. and Yuda, T.
ICR, University of Tokyo, Tanashi, Tokyo
Mito, I.

Shibaura Institute of Technology, Shibaura, Tokyo
Shibata, M.

Yokohama National University, Yokohama, Kanagawa
Shirai, T., Taira, T., Tateyama, N. and Torii, S.
Kanagawa University, Yokohama, Kanagawa
Sugimoto, H. and Taira, K.

Sagami Institute of Technology, Fujisawa, Kanagawa

Scaling, mean P_t , high P_t jets and others at energies over 1000 TeV are discussed on the basis of gamma-family data with $\Sigma E_\gamma > 100$ TeV, observed at Mt. Fuji (3750 m). These quantities are examined in connection with the primary composition.

1. Introduction.

At present, an observation of cosmic ray phenomena is a unique source to get a direct information about particle interactions at energies over 10^{15} eV. Among these, emulsion chamber experiments produce fruitful results for this purpose. Since 1970, the large-scale emulsion chamber experiments have been continued at Mt. Fuji (3750 m, 650 g/cm^2). Now, the total exposure of chambers reaches about $1000 \text{ m}^2 \cdot \text{y}$ and about 200 family events with $\Sigma E > 100$ TeV have been observed. Also we have reliable data about particle interactions at energies up to 150 TeV and this energy will go higher at Felmilab in very near future. So, within one or two years, we may give a definite answer to the alternative of 1) scaling break in the fragmentation region and proton dominant primary or 2) scaling and heavy enriched primary, which have been repeatedly discussed for a long time.

In this report, we discuss general features of particle interactions expected from the Mt. Fuji experiment, comparing with the Monte Carlo results, and also describe some characters of

super-families.

2. Problem of the Feynman scaling in the fragmentation region.

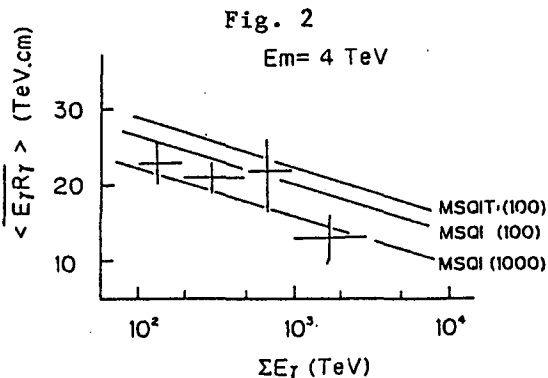
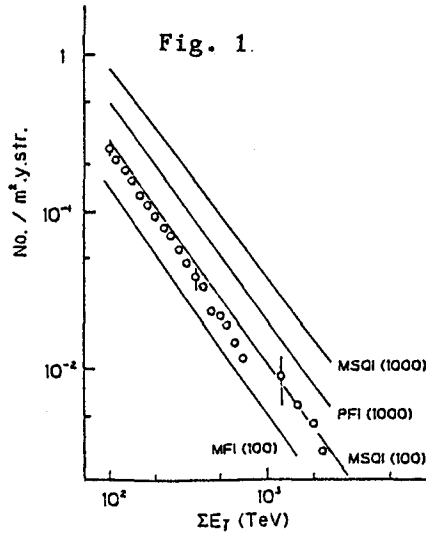
It is well confirmed that the absolute flux of gamma-ray families at mountain altitude is the most sensitive to the energy spectra of particles in the fragmentation region, inelastic cross sections and also primary composition, 1).

In Fig.1 we compare our data with the Monte Carlo results which are simulated on the basis of the conventional model of the interaction and primary. The symbols used for classifying the model are : P means the proton primary, M the mixed composition (heavy dominant), S the scaling, F the fire-ball model (normalized to SPS data at 150 TeV), Q the QCD-jet, I the increasing cross section as $E^{0.04}$ and T the transverse momentum increasing with energy as $E^{0.04}$. The bending energy (E_b in TeV) of primary proton is denoted in the bracket (spectral index changes from 1.7 to 2.0) and other nuclei also become steeper at $Z \cdot E_b$. The absolute intensity of assumed total spectrum is normalized to the Grigorov's one at energies around 10^{15} eV. Details of the simulation will be found in the other paper, 2).

It can be understood that the scaling with heavy enriched primary is compatible with the experimental data. In this case, the proton component should become steeper at energies around 10^{14} eV. Of course, a strong scaling break and proton dominant primary ($E_b \sim 10^3$ TeV) can also explain our data, but the fraction of protons to the total would not exceed 50 % at around 10^{15} eV (bending energy of proton spectrum).

3. Mean P_t at high energies.

The lateral spreads of constituent gamma-rays in the families give a measure of the mean P_t of secondaries at collisions. In Fig. 2 is shown the lateral spread, $\langle ER \rangle$, averaged in the respective energy range, with the Monte Carlo results. In the accelerator energy region, the mean P_t near



the central region seems to increase with energy as $E^{0.04}$. If this increasing rate is hold up to higher energies, it takes about 450 MeV/c at 1000 TeV. However, as learned from this comparison, our data do not favour to increasing P_t (Here we discuss the P_t in the small P_t region. Note that the QCD jets are speciously taken into account in the simulation.). This result may suggest that the mean P_t depends very weakly on the primary energy, if any, or remains almost constant, since the family phenomena are very sensitive to the fragmentation region.

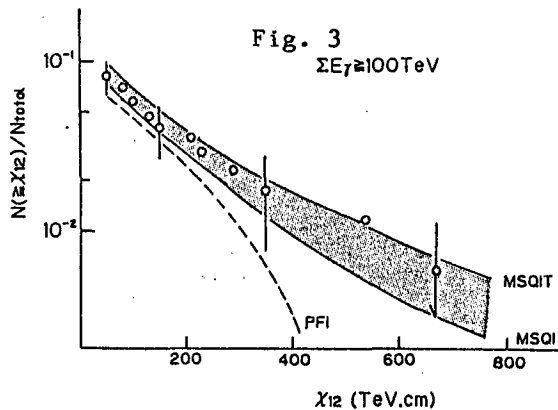
4. High P_t phenomena.

In order to enhance the effect of high P_t , a clustering method t is applied to the family phenomena. This method is already described in the paper, 3). Here we present the frequency of double-core events. In order to pick up such events, first we clusterize the gamma-families with $\Sigma E_\gamma > 100$ TeV, then impose the following conditions : $E_1 + E_2 > 0.8 \Sigma E_\gamma$ and $E_1, E_2 > 10$ TeV ; $R_{12} > 5 \max(r_1, r_2)$, where $E_1(E_2)$ and $r_1(r_2)$ is the energy and lateral spread of cluster 1(2) and R_{12} the distance between two clusters. In Fig.3 we show our data together with the Monte Carlo results. The frequency of double-core events with $\chi_{12}(=R_{12}/\sqrt{E_1 E_2}) > 100$ TeV.cm is about 7 %. This figure teaches us that such events are within the scope of expectation of the model based on the scaling with QCD-jets, and also a rapid energy dissipation model such as fire-ball is incompatible with the data.

Concerning to high P_t jets, we should note here that the peculiar event "TITAN", t observed in 1977 and composed of 6 very high energy showers with $E > 100$ TeV, 4), is by no means produced by the conventinal interaction models according to our Monte Carlo simulation.

5. Super-families.

Here, we describe some features of super-families with $E > 1000$ TeV. The primary energy responsible for generating such families would mostly exceed 10^{16} eV. A general feature of these super-families is expected to bring us a new clue for the study of particle interactions at energies $10^{16} - 10^{17}$ eV. A remarkable structure is that the majority of super-families is accompanied by a halo. In Fig. 4, we show the flux of gamma-families with $\Sigma E_\gamma > 1000$ TeV ($E = 4$ TeV) and halo events at Mt.Fuji. Here, the energy of halos is estimated by using a relation of $E = C * Z_0$, where Z_0 is the total track length and C the conversion factor of 10 MeV/c.u.. As discussed in other paper, the flux of halo events can also be explained by the model mentioned above, 5).



At present, we have 6 halo events with energy exceeding 1000 TeV. The biggest event is the FC-31 with energy of about 9000 TeV. Two patterns are found about halo structure, i.e., single and axial-symmetric core or multi-cores. Examples of the event, FH-89 (2500 TeV) and FC-104(4000 TeV) are shown in Fig. 5 and 6. Three among 6 events have a single-core structure. In

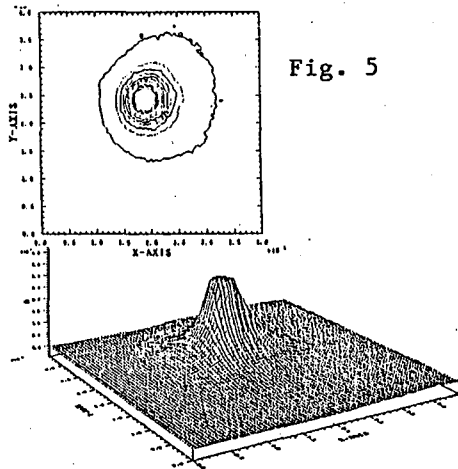


Fig. 5

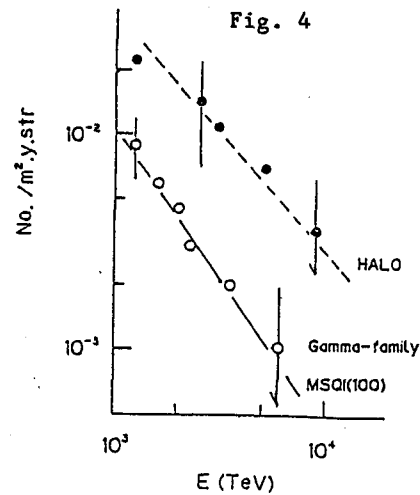


Fig. 4

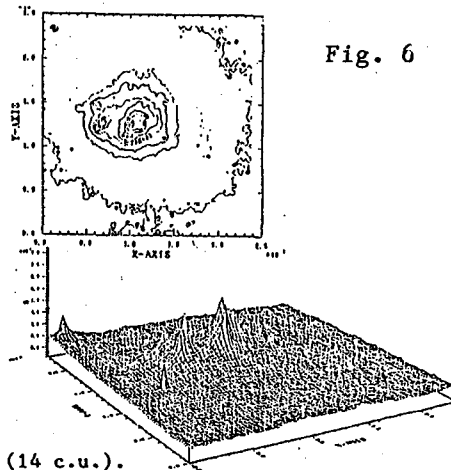


Fig. 6

Fig. 5 : FH-89 (36 c.u.), Fig. 6 : FC-104 (14 c.u.).
Density map of X-ray film measured by photometer.
Area : 24x24 mm², Slit size : 300 microns, Z-axis :
Density from 0-3.0.

particular, no high energy showers are found in the outskirts of the halo of the event FH-89, strikingly different from other two, as noticed from Fig. 5. According to the Monte Carlo simulation, such type of events are possibly produced by protons deep in the atmosphere and the structure of the event FH-89 may suggest a look of very high multiplicity. We need more events to reach some conclusive results.

- 1) Akashi, M. et al, Phys. Rev., D24, p2353 (1981).
- 2) Ding, L. K. et al, Proc. Int. Symp. on Cosmic Rays and Particle Physics, p142 (1984, ICR, Univ. of Tokyo).
- 3) Amenomori, M. et al, Phys. Rev., D25, p2807 (1982).
- 4) Akashi, M. et al, 15th ICRC, Vol.7, p184 (1977, Plovdiv) ; Amenomori, M. et al, Proc. Int. Symp. on Cosmic Rays and Particle Physics, p382 (1984).
- 5) Ren, J. R. et al, HE3.4- 9, in this volume.

A SEARCH FOR MINI-CLUSTERS IN JAPAN-USSR JOINT EXPERIMENT AT PAMIR

JAPAN-USSR JOINT EXPERIMENT (II)

Abstract

A search for mini-clusters, very collimated shower clusters of hadrons and electromagnetic particles, is made for the hadron and gamma families observed by Japan-USSR joint carbon chamber at Pamir. The existence of anomalous correlation between hadrons and electromagnetic particles is found. The decascading method is applied to the families and it is found that 11 clusters which include hadrons as members have smaller spread, $\langle E_r \rangle < 3.5 \text{ GeV.m}$ and larger lateral spread, $E^* R^* > 100 \text{ GeV.m}$, from the family center. In the simulated events, we have found very rare such clusters. The results are compared with those of Chacaltaya experiment.

1. Introduction.

In the cosmic-ray nuclear interactions of incident particle energy $E_0 > 10^{15} \text{ eV}$, there exist several kinds of exotic phenomena[1], Centauro is a typical one, which are not yet observed in the accelerator experiments. The characteristics of those exotic phenomena is seen in the composition and in the magnitude of transverse momentum of produced particles, that is, particles unaccompanied with pions are produced with large transverse momentum. Recently, the existence of a new shower phenomenon is reported from Chacaltaya experiment, that is, there exist hadrons accompanied by electromagnetic showers in very close vicinity and those hadrons and electromagnetic showers form very collimated shower cluster, the mini-cluster[2]. And now, it is one of the most important problems to make clear the physical nature of the mini-cluster. The carbon chamber is thick enough to detect hadrons and is suitable to detect mini-clusters. Here we show the results of systematic analysis on hadron and gamma families observed in USSR-Japan joint carbon chamber[3] exposed at Pamir plateau, paying special attention to the mini-clusters.

2. Experimental procedure.

The chamber, so-called carbon chamber, consists of three parts, i.e., Γ -block of 6 cmPb, H-block of 6 cmPb and carbon layer of 60 cm thick between the two. The detail structure of the chamber and the method of energy determination is described in the separate paper[3].

Identification of hadrons The showers observed in H-block are those from local nuclear interaction in the carbon layer(C-jet), those from local nuclear interactions in the H-block itself(Pb-jet-H) and tails of showers from Γ -block. Thus almost all showers in H-block are hadronic origin. The showers observed in Γ -block are mixture of electromagnetic showers from the atmosphere and those from local nuclear interactions in Γ -block itself(Pb-jet- Γ). Among showers observed in Γ -block, we consider the shower as hadronic-origin when the shower continues to H-block and the darkness of the shower in H-block is far above the expected darkness in case of electromagnetic shower. The detail argument on the identification is described in the Ref.[4]. The above procedure for identification of hadrons in Γ -block can not pick up all hadrons interacted in Γ -block, and also the threshold energy for them becomes 5 ~ 10 TeV although the detection threshold energy of showers is around 2 TeV. The detection probability of hadrons with

energy $E_E^{(\gamma)}$ greater than 2 TeV is estimated as $\sim 70\%$.

Selection of the events The systematic measurement of gamma- and/or hadron- families is done in one section (24 m²) of the joint chamber 'Pamir-2' [4], and we have about 110 unbiased events with total visible energy greater than 20 TeV. Among 52 families of total visible energy greater than 50 TeV, 21 events have hadrons in their member showers. Our main concern is to see correlations between hadrons and electromagnetic showers. Then we pick up only the events which have showers penetrating from Γ -block to H-block. Among 21 hadron and gamma families, 14 events have penetrating showers. In the following analysis, three high energy events (in the another section where systematic measurement is going on) together with 14 events above mentioned are used.

3. Results.

Correlation between hadrons and electromagnetic showers Fig.1a shows a distribution of relative distance, R_{min} , between a hadron and its nearest neighbouring shower and Fig.1b shows a distribution of energy-weighted relative distance, X_{min} , between a hadron and its nearest neighbouring shower in $X_{ij}(=\sqrt{E_i E_j} R_{ij})$ -space, where E_i , E_j are energies of showers and R_{ij} is a relative distance between the two. Histogram in the figure shows a background distribution which is obtained by randomly changing azimuthal angle, ϕ , of hadrons in the observed events. As is seen in the figures, in contrast with that the background distribution is almost uniform, in the experiment there exists a peak, which is not seen in the background distribution, in small R_{min} region, $R_{min} < 400 \mu\text{m}$ and in small X_{min} region, $X_{min} < 2.2 \text{ GeV.m}$. We have 11 hadrons which accompany a shower in R_{min} less than 400 μm and 9 hadrons which accompany a shower in X_{min} less than 2.2 GeV.m. The number of those hadrons expected from the background distribution is ~ 0.8 and ~ 0.6 respectively. And the probability that the observed number of hadrons accompany showers in such small R_{min} and X_{min} is estimated $\sim 5 \times 10^{-10}$ and $\sim 8 \times 10^{-9}$. The result well agrees to that obtained in the Chacaltaya experiment [5], and the observed closeness in (energy-weighted) relative distance between hadrons and electromagnetic showers can not be simply accidental.

Mini-clusters Mini-cluster is a narrowly collimated shower cluster and it looks like pure young electromagnetic cascade in the atmosphere. The characteristic of mini-clusters different from pure electromagnetic cascade is its hadronic nature, that is, hadrons are included as members. Here we apply the decascading method [6] to the families in order to study cluster structure of hadrons and electromagnetic particles. Decascading method is a way to trace back to the original gamma-rays from the observed cluster of electromagnetic showers. The showers are amalgamated to one if $Z_{ij} = E_i E_j R_{ij} / (E_i + E_j)$ is less than a constant value k where E_i , E_j are energies of showers and R_{ij} is relative distance between the two. Here the decascading method is applied to all the members, including hadrons and electromagnetic particles, of the family, and we put parameter $k = 11 \text{ GeV.m} (= k_s X_0)$, characteristic spread of electromagnetic cascade at Pamir altitude. In this case, the decascading method loses its original meaning but simply means 'clustering'. Fig.2a shows a correlation diagram on the energy-weighted lateral spread $E^* R^*$ of clusters with energy E^* greater than 10 TeV and the average lateral spread, $\langle E_r \rangle$, of showers in the clusters, obtained by the above procedure. E^* , R^* are the energy and the

distance of the cluster from the family center. E and r are energy of shower in a cluster and distance of it from cluster center. In the figure, clusters which include hadrons as constituents are marked by triangles. For the comparison, the clusters with hadrons, obtained by the same procedure, in the Chacaltaya events are shown in the figures. Fig.2b shows the same diagram for the simulated events. Simulations are carried out under the assumption that the primary particles are protons with power energy spectrum. Two types of interaction model are assumed. One is fire-ball(H-quantum) model[7], Model-I, and the other is C-jet data model[8], Model-II, where C-jet events observed by Chacaltaya experiment are boosted to cosmic-ray energies. The above two interaction models can well reproduce results of accelerator experiment of ISR and SPS. As is seen in the figure, in the simulated events, too, there exist clusters which accidentally include hadrons as members. Those clusters which include hadrons, however, are distributed in the region of larger $\langle Er \rangle$ in the above diagram. The striking characteristics in the experiment is that there exist clusters including hadrons which have smaller $\langle Er \rangle$ and larger E^*R^* . For example, 11 among 16 clusters with hadrons in the events of joint chamber and 11 among 26 clusters in the Chacaltaya events are with $\langle Er \rangle < 3.5 \text{ GeV.m}$ and $E^*R^* > 100 \text{ GeV.m}$, the region is indicated by broken lines in the figure, while in the simulated events almost all clusters with hadrons are distributed outside of the above region. Such smallness of $\langle Er \rangle$ of experimentally observed clusters with hadrons are coming from the anomalous closeness of hadrons and electromagnetic showers, discussed in the previous section. In Fig.2a we put special mark to the clusters which include hadrons with $R_{\min} < 400 \mu\text{m}$ and/or $X_{\min} < 2.2 \text{ GeV.m}$.

4. Conclusion.

We have observed 11 clusters, mini-clusters, of anomalously collimated hadrons and electromagnetic particles through the systematic analysis on 17 hadron and gamma families, with total observed energy greater than 50 TeV, observed by joint carbon chambers at Pamir. Though the structure of the chamber and the accuracy of measurement are different from the Chacaltaya chambers, we have obtained good agreement on the characteristics of mini-clusters between the two experiments.

Acknowledgement. The collaboration experiment is financially supported in part by Grant-in-Aid from the Ministry of Education and Waseda University, in Japan.

References.

- [1] C.M.G.Lattes et al.; Physics Report 65 no.3(1980) 151
L.T.Baradzei et al.; Proceedings of 18th ICRC, Bangalore(1983) p.441
A.S.Borisov et al. ; Proceedings of 18th ICRC, Bangalore(1983) p.491
- [2] Brasil-Japan collaboration ; AIP Conference Proceedings (1981) p.500
H.Bialawska et al. ; Proceedings of Int. Sympo. on Cosmic Rays and Particle Physics, Tokyo (1984) 374
- [3] Japan-USSR Joint Experiment ; 19th ICRC (1985) HE 3.1-1
- [4] M.Koike, T.Hibi, H.Tanaka, M.Tsuchiya and K.Teramura ; to be published
- [5] M.Tamada ; 19th ICRC (1985) HE 3.3-6
- [6] H.Semba ; Supple. Prog. Theor. Phys. no.76(1983) 111
- [7] T.Maeda ; to be published
- [8] I.Takatsuka ; 'Uchusen Kenkyu' (in Japanese) vol.28 no.1(1984) 1

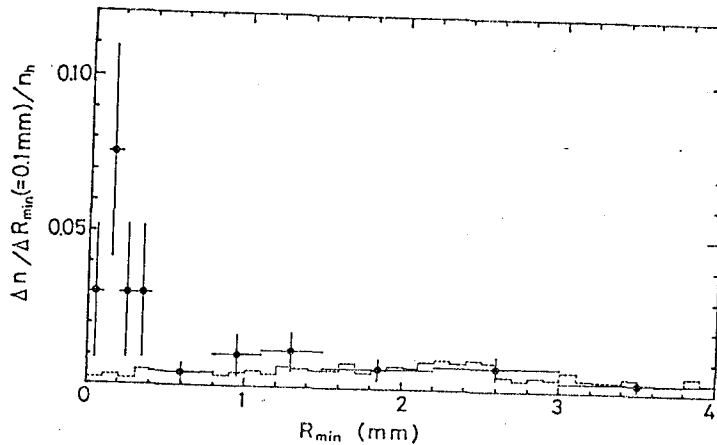


Fig. 1a: Distribution of relative distance, R_{min} , between a hadron and its nearest neighbouring shower. Histogram is a background distribution (see text).

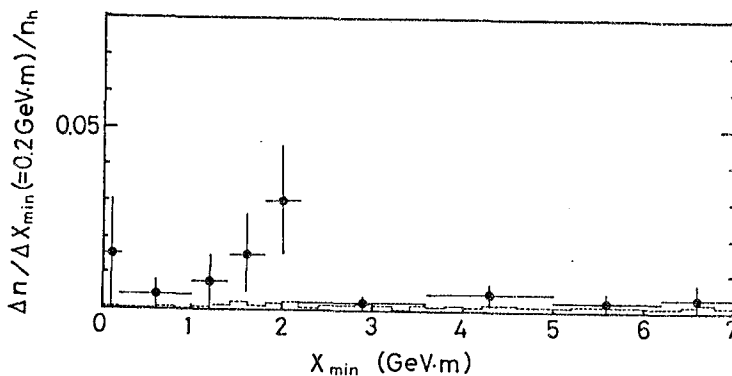


Fig. 1b: Distribution of energy-weighted relative distance, X_{min} , between a hadron and its nearest neighbouring shower in X_{ij} -space.

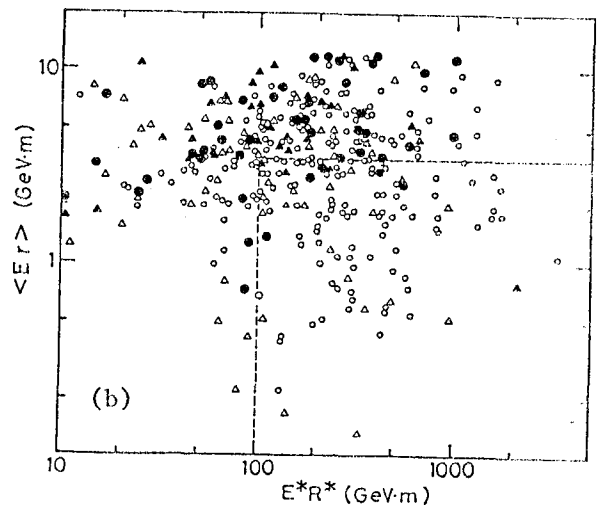
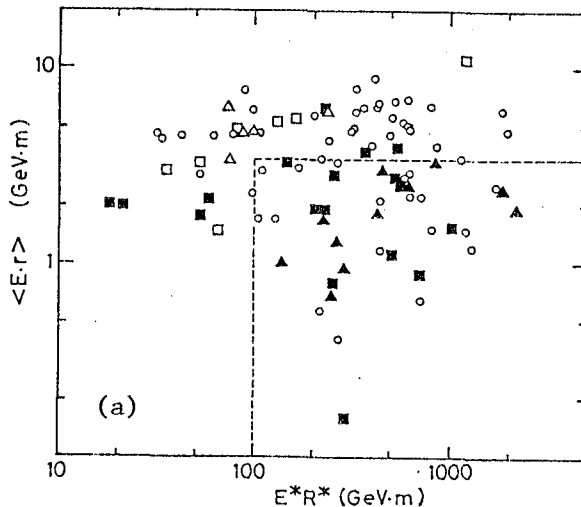


Fig. 2a: Correlation diagram on energy-weighted lateral spread, ER of clusters and the average $\langle E_r \rangle$ of showers in a cluster for the clusters with energy greater than 10 TeV.

○: clusters without hadrons, △: clusters which include hadrons,
 ▲: clusters which include hadrons with $R_{min} < 400 \mu m$ and/or $X_{min} < 2.2 \text{ GeV.m}$ for the events of joint chamber.
 □: clusters which include hadrons, ■: clusters which include hadrons with $R_{min} < 400 \mu m$ and/or $X_{min} < 2.2 \text{ GeV.m}$ for the events of Chacaltaya chamber no.19.

Fig. 2b: Same to Fig. 2a for the simulated events. △, ▲: for Model-I and ○, ●: for Model-II. ▲, ●: clusters which include hadrons.

Mini-clusters

Brasil-Japan Collaboration of Chacaltaya Emulsion Chamber Experiment

J.A.Chinellato, C.Dobrigkeit, J.Bellandi Filho, C.M.G.Lattes, M.J.Menon, C.E.Navia O., A.Pamilaju, K.Sawayanagi, E.H.Shibuya and A.Turtelli Jr. ; Institute de Fisica Gleb Wataghin, Universidade Estadual de Campinas, Campinas, S.P.

N.M.Amato, N.Arata and F.M.Oliveira Castro. ; Centro Brasileiro de Pesquisas Fisicas, Rio de Janeiro, R.J.

R.H.C.Maldonado ; Instituto de Fisica, Universidade Federal Fluminense, Niteroi, R.J.

H.Aoki, Y.Fujimoto, Y.Funayama, S.Hasegawa, H.Kumano, H.Semba, M.Tamada and S.Yamashita ; Science and Engineering Research Laboratory, Waseda University, Tokyo

T.Shibata and K.Yokoi ; Department of Physics, Aoyama Gakuin University, Tokyo

A.Ohsawa ; Institute for Cosmic Ray Research, University of Tokyo, Tanashi, Tokyo

Abstract

Experimental result of 'mini-clusters' observed in Chacaltaya emulsion chamber no.19 is summarized. The study was made on 54 single core shower upper and 91 shower clusters of $E(\gamma) > 10$ TeV from 30 families which are visible energy greater than 80 TeV and penetrate through both upper and lower detectors of the two-storey chamber. The association of hadrons in mini-cluster is made clear from their penetrative nature and microscopic observation of shower continuation in lower chamber. Small $p_t(\gamma)$ of hadrons in mini-clusters is remained in puzzle.

1. Introduction.

The new shower phenomena named "mini-cluster" was first found through the study of shower clusters associated with families of large spread called Chiron type in Chacaltaya emulsion chamber no.19[1]. Chacaltaya chamber no.19 is one of the series exposure of two-storey structure and what is special for no.19 is that the whole area of the upper chamber, 44 m^2 , is covered with three layers of nuclear emulsion plates as well as the lower chamber, 33 m^2 , with seven layers of nuclear emulsion plates[1]. It allowed us to study the behaviour of shower cores in fine resolution under the microscopic observation.

A mini-cluster is a narrowly collimated shower core bundle ; so narrow that, in many cases, it gives a single dark-spot in X-ray films, and it reveals itself a very closely distanced shower core cluster under the microscopic observation in nuclear emulsion plates. The characteristic dimension of lateral spread is of the order of a few GeV.m, the same as the spread of young atmospheric cascade showers. The difference is seen in the strong penetrative nature of mini-cluster, showing the shower cluster is not of simple electromagnetic nature but hadrons must be inside. The present paper describes the summary of study on mini-clusters in Chacaltaya chamber no.19 of 677 days exposure.

2. Statistics of families.

30 families with $\Sigma E(\gamma) > 80$ TeV are selected under the following

criteria.

- i) A family penetrates through both upper and lower chambers.
- ii) A family has wide spread ; $\langle ER \rangle > 180 \text{ GeV.m}$ after the decascading procedure with constant $Kc=6 \text{ GeV.m}$.

3. Shower core observation under microscope.

Every dark spots in X-ray films in the upper chamber are studied in nuclear emulsion plates under microscope, especially asking whether a dark spot in X-ray films is single core structure or closely distanced multiple cores. The track counting method is applied to all individual shower cores for their energy determination with radius $r=25$ and/or $50 \mu\text{m}$.

4. High energy showers ($E(\gamma) > 10 \text{ TeV}$) in the upper chamber.

The high energy showers show the following characteristics.

(1) About one third of high energy showers are of single core structure. More than 60% of them penetrate into the lower chamber, indicating the majority are of hadron origin showers in the chamber materials.

(2) The rest are of multi-core clusters spreading over area $0.1 \sim$ a few mm of radius. About one half of them are penetrative into lower chamber, indicating they all are not pure electromagnetic cascade in the atmosphere.

Table 1 gives the summary of observation of high energy shower-upper.

Table 1.	Summary of high energy shower-upper		
	no. of shower	no. of penetrative showers	%
single core	54	35	65 ± 12
mini-clusters	91	41	45 ± 8

Fig.1 shows the average transition curve of spot darkness in X-ray films (measured by slit size $200 \times 200 \mu\text{m}^2$) for 37 single core and 57 mini-clusters. The results of simulation calculations are drawn together for pure electromagnetic cascades of gamma-ray incidence with energies 10 and 20 TeV, respectively, since the average energies of single core shower-upper and the highest one in mini-clusters are 20 and 15 TeV, respectively. One sees qualitatively different behaviour between the two, especially in the deepest region in the lower chamber ; that is, experimental results have much larger and longer tail for both single and mini-cluster cases than the case of pure electromagnetic cascades in the chamber materials.

5. Mini-clusters.

5-1. Multiplicity Fig.2 gives the distribution of number of shower cores, m , for 91 mini-clusters ($E > 10 \text{ TeV}$). We see most of mini-clusters are ranging $m =$ a few ~ 10 . There are observed mini-clusters with extreme large multiplicity, say $m \sim 30$, for which we put the name "Giant-mini-cluster" and we shall discuss specially the properties of those huge shower clusters in details in the separate paper[2].

5-2. Small pt of mini-clusters It is expected $p_t(\gamma)$ of shower cores at the mini-cluster formation must be small from their very small lateral spread. Fig.3 gives the scatter plots between the spread of 91 mini-clusters, $\langle ER \rangle$, versus that of parent Chiron family, $\langle ER \rangle$, measured by high energy showers ($> 10 \text{ TeV}$) by mark (O). The broken lines show the cases where the ratio of both spreads are $1/1000$, $1/300$ and $1/100$,

respectively. Most of them are distributed in the region smaller than $1/100$ and the average is given by $\sim 1/300$. If we accept $\langle p_t(\gamma) \rangle$ of parent Chiron interaction is $2 \sim 3$ GeV/c, the $\langle p_t(\gamma) \rangle$ of mini-cluster formation is obtained $10 \sim 20$ MeV/c. In the same figure, we present the relation of spreads on binocular families by mark (●). We see the same small ratio in more than half of clusters from binocular families as in the case of Chiron families. The large pt nature at the geminon interaction, $\langle p_t(\gamma) \rangle = 2 \sim 3$ GeV/c, the same order of magnitude with the Chiron interaction, is suggesting that there might work the similar dynamics for secondary particle production.

5-3. Hadrons in mini-clusters Mini-clusters show strong penetrative nature than expected from pure electromagnetic cascades from X-ray film observation as shown in Table 1 and Fig.1. Table 2 gives the results of microscopic observation of shower continuation in the lower chamber for mini-clusters as well as single core shower-upper of $E(\gamma) > 10$ TeV.

Table 2 Microscopic observation of shower continuations in lower chamber.

	Pb-jet-upper	C-jets	Pb-jet-lower	any	not studied	sum
single-core	14	7	3	7	4	35
mini-clusters	22	8	5	6		41

Hadrons in mini-clusters are studied in much detail by observing the core configuration and by comparing transitions of electron number in individual shower cores with the expected behaviour of pure electromagnetic cascades of single gamma-ray incidence on the basis of a large number of simulation calculations by T. Shibata. The results show there are not small cases where mini-clusters include plural hadrons[3]. A study on hadron association in mini-clusters are made from the side of correlation analysis by M. Tamada[3]. Using 19 families of Japanese part of the chamber no.19, the distribution of the relative distance (and energy-weighted relative distance) between detected hadrons and the nearest shower in each family is constructed and compared with the one of random background (Fig.4). The anomalous correlation was found in the range $R \lesssim 1$ mm which show the probability is nearly equal or less than 10^{-6} if the hadrons and electromagnetic particles are produced without any correlation.

6. Discussions.

A systematic search of mini-clusters was carried in the first carbon chamber at Pamir by USSR-Japan joint exposure[4]. There are found 11 penetrative mini-clusters among 17 families with energy greater than 50 TeV in ~ 24 m²year exposure. There was a report on study of penetrative cascade showers in Pamir carbon chamber, giving the consistent results[5]. Exotic behaviour of secondary particles of Chiron-type families is remarkable when one consider the small collision mean free path ($1/2 \sim 1/3 \lambda_{geo.}$) and small pt of hadrons and electron/gamma-rays seen in the mini-clusters.

Acknowledgement.

The collaboration experiment is financially supported in part by Conselho Nacional para o Desenvolvimento Cientifico e Tecnologico, Fundacao de Amparo a Pesquisa do Estado de San Paulo, in Brasil, and Institute for Cosmic-Ray Research, University of Tokyo and Grant-in-Aid from the Ministry of Education, in Japan.

References.

- [1] Brasil-Japan Collaboration ; AIP Conf. Proc. Vol.85(1981) 500
- [2] S.Hasegawa; Proceedings Int. Sympo. on Cosmic Rays and particle Physics, Tokyo (1983) 62 and 319
- [3] M.Tamada ; 19th ICRC, HE 3.3-6
- [4] USSR-Japan joint experiment ; 19th ICRC, HE 3.5-2
- [5] H.Bielawska et al. ; Proceedings of Int. Sympo. on Cosmic rays and Particle Physics, Tokyo(1983) 374

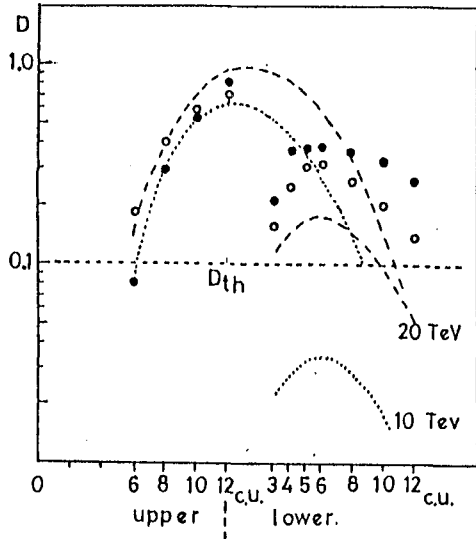


Fig.1 Penetrative nature of high energy($E > 10$ TeV) single shower-upper and mini-clusters.
 ● : single shower-upper
 ○ : mini-clusters
 Dth means threshold darkness of shower spot in X-ray films.

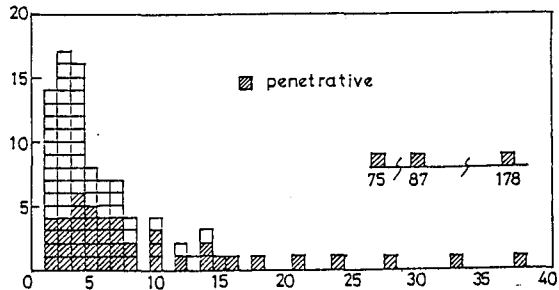


Fig.2 Histogram of shower core number in a mini-cluster.

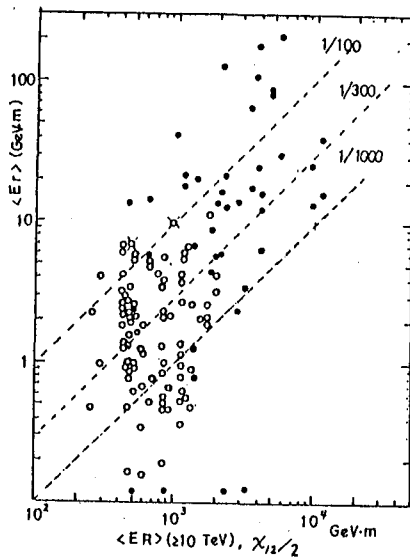


Fig.3 Scatter plot between two spread, $\langle Er \rangle$ of individual shower clusters and family clusters, of Chirons and binocular families.

- ; Chirons
- ; binocular families.

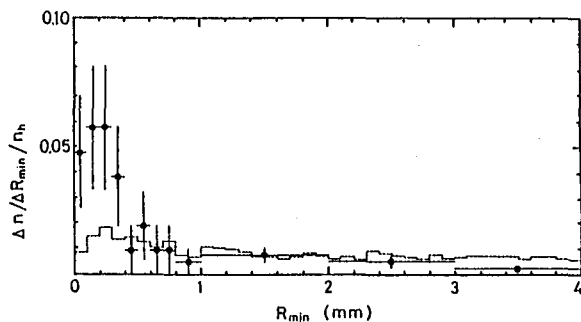


Fig.4 Distribution of relative distance, R_{min} , between a hadron and its nearest neighbouring shower. Histogram is background distribution obtained by changing randomly azimuthal angle, ϕ , of hadrons in the observed events.

Giant Mini-clusters as Possible Origin of "Halo" Phenomena Observed in Super-families

Brasil-Japan Collaboration of Chacaltaya Emulsion Chamber Experiment

ABSTRACT

Among 91 mini-clusters from 30 high energy Chiron-type families in Chacaltaya emulsion chambers, there are observed several extremely large multiplicity clusters in the highest energy range, far beyond the average of ordinary type clusters. We put the name giant mini-cluster for them. The present paper describes some details of microscopic observation of those giants mini-clusters in nuclear emulsion plates and some phenomenological regularity found in common among them. It is discussed such giant mini-clusters will be a possible candidate of origin of narrow symmetric single halo phenomena in X-ray films which is frequently observed in super-families of visible energy greater than 1,000 TeV.

1. Introduction

Since the observation of a super-family with a spectacular halo named "Andromeda" in Chacaltaya chamber no.14 in 1969, there have been a number of reports on observation of such halo phenomena from large scale mountain emulsion chamber experiments, and the existence of such halo is now considered to be a remarkable general characteristics of cosmic-ray families of visible energy greater than 1,000 TeV. A halo is a general darkened area in X-ray films, ranging from several to several ten mm in diameter, in the central area of super-family. The microscopic observation in nuclear emulsion plates reveals that it is a bundle of great number of shower particles, hadrons and electron/gamma-rays. Since the frequency argument excludes the possibility that those halo phenomena are the results from ordinary type pion multiple production under the scaling rule starting from proton primary incidence, the origin of halo phenomena seems to suggest us new mechanism of particle production.

The recent observation of new shower phenomena named "mini-cluster" in Chacaltaya chamber shows unusual nature of shower particle production. It is a shower cluster which consists of hadrons and electron/gamma-rays with small spread, as small as $\langle E(\gamma)r \rangle$ a few several GeV.m, the same order of magnitude as young atmospheric cascade shower of electromagnetic origin. Among 91 mini-clusters in Chacaltaya chamber no.19, we found several huge mini-clusters with very large multiplicities in higher energy and larger $\langle E_r \rangle$ ranges in mini-cluster statistics, far beyond the average of ordinary mini-clusters. The present paper describes some details of such huge mini-clusters, the giant mini-clusters, as the possible origin of halo phenomena in X-ray film observation.

2. Characteristics of huge shower core bundles

We present in Fig.1 the relation between $\sum E(\gamma) - N$, total visible energy and multiplicity of shower cores with $E(\gamma) > 1$ Tev, and in Fig.2

$\langle Er \rangle - N$, average spread and multiplicity, respectively, for all the observed 91 mini-clusters from 30 Chiron families in Chacaltaya chamber no.19[1] and one from no.18[2]. One sees most of the ordinary mini-clusters gathered around in small N and $\langle Er \rangle$ region and, at the same time, we find a group of shower clusters of large multiplicities, say $m > 30$, with large ΣE and $\langle Er \rangle$ values as indicated by the mark(⊙). Since we see the multiplicity and spread of those clusters are significantly greater than the average of the ordinary mini-clusters, we separate them from the ordinary mini-clusters and put the name "giant mini-cluster" for them. Table 1 gives details of those selected giant mini-clusters.

Table 1. Some details of giant mini-clusters

Event no.	$\Sigma E(\gamma)$ (TeV)	N (>1 TeV)	$\langle r \rangle$ (mm)	$\langle Er \rangle$ (GeV.m)	family energy (TeV)
#174S-134I	1,056	158	2.88	10.00	1,164 (91 %)
#P06 (no.18)	961	123	1.77	7.40	1,272 (76 %)
#179S-126I	394	85	2.82	7.10	757 (52 %)
#174S-132I	270	98	2.84	4.80	342 (79 %)
# 93S- 56I	169	38	1.33	4.30	182 (93 %)
#165S-126I	126	30	1.79	5.73	156 (81 %)

Figures in bracket mean the energy fraction of giant mini-cluster to total visible family energy.

The following characteristics are remarkable to all the giant mini-clusters above selected. The first, they all show strong penetrative nature into lower chamber and we are able to see not small number of shower cores which could not be attributed to pure electromagnetic cascade originated from atmospheric electrons/gamma-rays. The second, shower bundles show small spread and extremely high rapidity density of number of shower cores in very narrow collimated region, as seen in Fig.3. Since the families are of very simple structure for all, the position of the origin of those giant mini-clusters is estimated to be near above the chamber, say less than 1 km or so. Microscopic observation in nuclear emulsion plates for central region of giant mini-cluster shows that there are none or very rare of scattered background electron tracks in space among shower cores. Especially, it is reported[2] that the central halo part of the event P06(no.18) is produced ~ 200 m above the chamber by the triangulation measurement. These facts show the unusual large rapidity density which reflects approximately just the initial state of the production as it is, not severely distorted by the multiplication due to atmospheric degradation. The third, these giant mini-cluster occupy the substantial part of family energy as shown in Table 1, different from the ordinary mini-clusters of Chiron families.

Fig.4 gives the distribution of Er of individual shower cores in giant mini-clusters. The shape of the distribution is the same among them and seems to be well expressed by common exponential law. The average values are given in Table 1.

3. Mini-clusters and giant mini-clusters

At present, we are not able to explain fully the exotic nature seen in either mini-cluster and giant mini-cluster from the present knowledge of the particle production. However, simultaneous observation of those two in the same Chiron family is very suggestive to explore the nature of giant mini-cluster.

At one glance, we immediately noticed that the giant mini-cluster is not of simple symmetrical structure but there are recognized a number of localized sub-clustering. And it is clear enough to hypothesize that giant mini-cluster will be an ensemble of mini-clusters. Then, here is presented the results of sub-clustering into mini-clusters by computer algorithm[3] where the constant is assumed to be $Kc = 6 \text{ GeV.m}$, which corresponds to assume the giant mini-cluster be an ensemble of mini-clusters with the average spread $\langle E^*r^* \rangle = 1 \sim 2 \text{ GeV.m}$. Fig.5 gives the distribution of E^*r^* of mini-clusters in giant mini-clusters of the present examples, together with the big halo events Ursa-Maior and M.A.III[4] as the reference, for both of them the detailed microscopic observation in nuclear emulsion plates was carried out. We see good regularity of the spread E^*r^* for all the present samples except the case M.A.III, which is wide spread halo in X-ray film observation. The average value is given as $\langle E^*r^* \rangle \approx 30 \sim 50 \text{ GeV.m}$. The hypothesis seems to be promising when we are required so rapid energy partition into a large number of minute low energy showers as is seen in experimental results.

4. Discussion

When we see two dimensional contour map of darkness of halo in X-ray films, we find varieties of core configuration. Some cases, it is of narrow single symmetrical core and the other cases, it is of multi-core structure. The event P06(no.18) is of clean single core halo in X-ray film observation, total darkness maximum of which is seen at $\sim 14 \text{ c.u.}$ The shower clusters of event #174S-134I passes through the upper chamber before making a single definite halo in X-ray films. From these observation, single and narrow core halo in X-ray films seems to be nothing but huge shower clusters, the giant mini-cluster. When one looks multi-core events, like M.A.III, it seems it is an ensemble of the narrow single cores showing large spread as found in Fig.5.

Acknowledgement

The collaboration experiment is financially supported in part by Conselho Nacional para o Desenvolvimento Cientifico e Tecnologico, Fundacao de Amparo a Pesquisa do Estado de San Paulo, Financiadora de Estudos e Projetos, in Brasil, and Institute for Cosmic-Ray Research, University of Tokyo and Grant-in-Aid from the Ministry of Education, in Japan.

Reference

- [1] Brasil-Japan Collaboration ; this issues HE 3.5-3.
- [2] N.M.Amato, N.Arata and R.H.Maldonado ; Proc. Intern. Symp. on Cosmic-Rays and Particle Physics (1984) 123
- [3] H.Semba ; Suppl. Prog. Theor. Phys. no.76 (1983) 111
- [4] S.Yamashita ; Jour. of the Phys. Soci. of Japan Vol.54 No.2(1985) 529

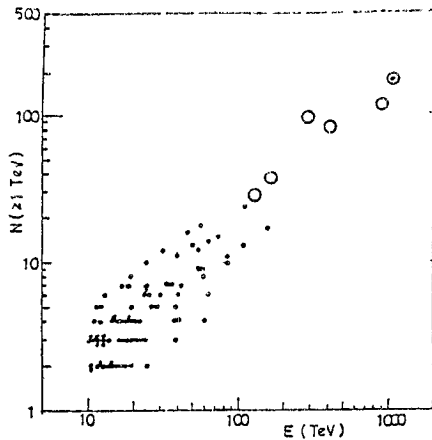


Fig.1 Relation between energy sum, E, and multiplicity, $N(>1\text{TeV})$, of shower cores in mini-clusters. \odot : giant-mini-clusters (Table 1)

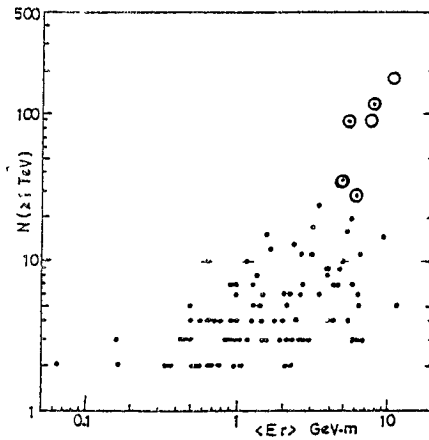


Fig.2 Relation between average spread, $\langle E_r \rangle$, and $N(>1\text{TeV})$ of shower cores in mini-clusters. \odot : giant-mini-clusters.

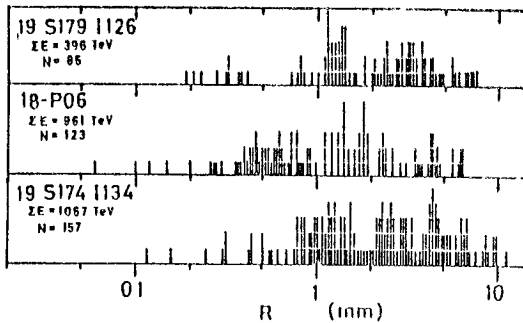


Fig.3 Log r -plot for shower cores of giant-mini-clusters.

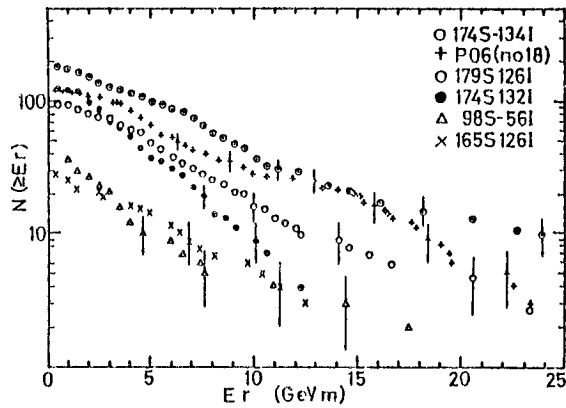


Fig.4 Integral distribution of E_r of shower cores in giant-mini-clusters.

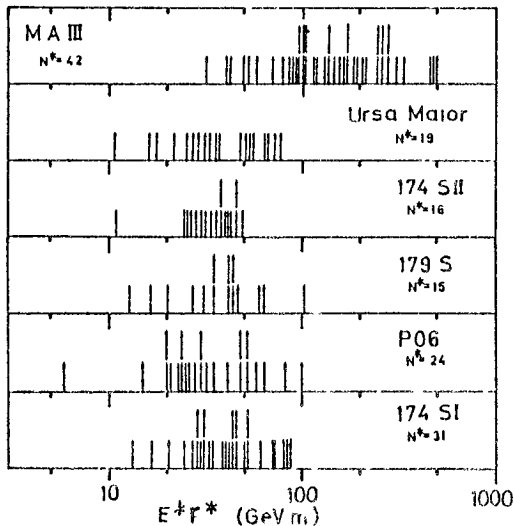


Fig.5 Distribution of E^*r^* of mini-clusters in giant-mini-clusters and huge core bundles of halo in super-families Ursa-Maior and M.A.III.

Structure of Super-Families

S. Yamashita, A. Ohsawa⁺ and J. A. Chinellato[°]

Science and Engineering Res. Lab., Waseda Univ., Shinjuku, Tokyo.

⁺Inst. Cosmic Ray Res., Univ. of Tokyo, Tanashi, Tokyo.

[°]Instituto de Fisica, UNICAMP, Campinas, Sao Paulo.

I. Introduction.

At present study of nuclear interactions induced by cosmic rays is the unique source of information on the nuclear interactions in the energy region above 10^{15} eV. The phenomena in this energy region are observed by air shower array or emulsion chamber installed at high mountain. Emulsion chamber is the pile of lead plates and photo-sensitive layers (nuclear emulsion plate and/or X-ray films) to detect electron showers. High spatial resolution of photographic material used in the emulsion chamber enables us to observe the phenomena in detail, and recently experiments of emulsion chamber with large area are being carried out at high mountains by several groups in the world [1].

They are to observe the mixture of high energy hadronic and e.m. (= electromagnetic) particles produced through the nuclear and e.m. cascade process in the atmosphere, induced by high energy primary cosmic rays. The phenomenon observed by the emulsion chamber is called family, and that with high energy (say, $\Sigma E_Y > 10^{15}$ eV) is called super-family.

All the super-families, observed so far, consist of, on N-type X-ray films of high sensitivity, the black core and halo of radius $l \sim 3$ cm in the center (called halo) and several hundreds of shower spots scattering over ~ 30 cm around the center. It is found by the microscopic observation in the nuclear emulsion plates that the halo is made of numerous number of electrons distributed densely and continuously, and that there exist many high energy shower spots even inside the halo.

Super-families carry the information of high energy nuclear interaction. However, since the events are very complicated, it is most important, we think, at first to make clear the whole structure of the events from the observed data. In other words the first step is to make clear how is the behaviour of the showers incident upon the chamber, and the second is what can produce such behaviour of the showers on the chamber. For the purpose of the first step we assume an appropriate function of energy-lateral distribution for the particles produced through the cascade process, and examine the inter-relation between the halo and detected high energy showers.

The five events analysed here are those with the energy above 10^{15} eV, observed by the series of emulsion chamber experiment at Mt. Chacaltaya (5,200 m, Bolivia), carried out by Brazil-Japan collaboration. Those are among 14 events, observed so far, and the rest are under measurement and analysis. Full description of the events is made elsewhere [2]. Table 1 gives a summary of the events.

II. Energy-Lateral Distribution of Showers

We here approximate the energy-lateral distribution of high energy showers incident upon the chamber, $F(E,r) dE 2\pi r dr$, to be,

$$F(E,r) = AC r^{s-1} \exp\left[-\frac{1}{\sigma^2} \left(\ln \frac{Er}{a}\right)^2\right] \quad (1)$$

The distribution, Eq.(1), has the following nature which is fundamental for the particles produced through the cascade process.

- (1) The relation, $Er \sim a$, holds with the dispersion σ around $Er = a$ in log-scale.
- (2) Integration with respect to r gives the energy spectrum of, $2\pi A(E/a)^{-s}/E$.

The parameters in Eq.(1) are four; A relating to the absolute number of showers, s to the power index of the energy spectrum, a to the lateral spread and σ to the dispersion around the average of the lateral spread. And we determine the four parameters by comparing the energy spectrum and Er -distribution, obtained from the Eq.(1), with the experimental data.

The parameter values determined are tabulated in Table 2 for e.m. and hadronic particles. As to Urça Maior, only several showers have large Er -values and it is difficult to fit the distribution by one set of values.

(a) Lateral distribution of high energy showers.

Fig.1 shows how the lateral distribution, Eq.(1), of high energy e.m. showers, with the parameter values in Table 2, can reproduce the experimental data in case of Andromeda. The expected distribution can reproduce the experimental data in case of shower energy > 5 TeV and > 10 TeV, while the experimental data is short in number for $E > 3$ TeV. And the agreement becomes good if we adopt the observed number of showers at 3 TeV (the chain line in the figure) instead of the one extrapolated from the energy spec-

Table 1.

	Andromeda	Urça Maior	M.A. I	M.A. II	M.A. III
Halo	$\times 10^{16}$	$\times 10^{14}$	$\times 10^{15}$	$\times 10^{15}$	$\times 10^{15}$
Total energy (eV)	(2.1±0.5)	(9.8±0.2)	(3.2±0.2)	(1.3±0.2)	(5.1±0.5)
e.m. (eV)	1.6×10^{16}				4.4×10^{15}
hadronic (eV)	5.3×10^{15}				6.6×10^{14}
High Energy Showers					
(1) Central region					
Observed number					
e.m.	288	113	96	24	264
hadronic	45	14(22)	11(73)	-	60(101)
Total obs. energy					
e.m. (TeV)	3,585	582	958	437	1,566
hadronic (eV)	1,401(3,417)	281(439)	143(953)	-	516(875)
(2) Outer region					
Observed number					
e.m.	322	108	50	89	227
hadronic	75(183)	25(39)	2(13)	-	92(166)
Total obs. energy					
e.m.	833	355	212	520	782
hadronic	317(773)	267(417)	8(53)	-	622(1,054)
[Numbers in the parentheses are the corrected ones due to the detection efficiency for hadrons.]					

trum. The agreement is good for M.A. I, II and III.

Fig.2 is that for the hadrons in the case of Andromeda. Deviation of expected distribution from the experimental data, suggests the hadron distribution is rather of exponential type.

(b) Comparison with halo data.

In this paragraph we examine whether the energy-lateral distribution, Eq. (1), with the parameter values in Table 2, can reproduce the behaviour of the halo. It is to see the behaviour of low energy showers, incident upon the chamber and not to be observed individually.

Energy cut, E_{th} , at the low energy side is necessary to be introduced to reproduce the transition curve of the total electron number in the halo. The values of E_{th} for the events are listed in Table 2. One can see the values for four events except Andromeda are similar to the value of detection threshold of high energy showers of $E_d \sim 3$ TeV. It indicates the observed high energy showers are sufficient to produce the halo in the chamber. In the case of Andromeda the behaviour of the transition curve necessitates a number of low energy showers with the average energy of ~ 0.4 TeV. However, if we assume those showers follow the distribution of Eq. (1), those showers should fall around $r = z_{max} / E = 25$ cm, far from the central region.

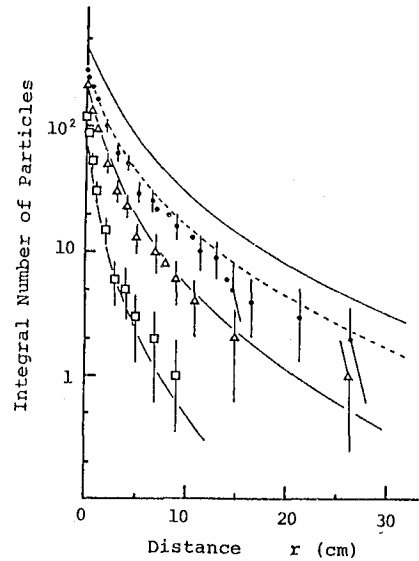


Fig.1. Lateral distribution of e.m. particles in integral form (Andromeda). The marks are for different energy thresholds; \bullet for $E > 3$ TeV, Δ for $E > 5$ TeV, and \square for $E > 10$ TeV. The curves are the expected ones from the assumed energy-lateral distribution with parameter values given in Table 2. The chain line is the case when we adopt the observed number of showers instead of the one expected from the parameter values listed in Table 2.

Table 4

Event	$A(\text{cm}^{-2}\text{s})$	s	$a(\text{TeV}\cdot\text{cm})$	σ	$E_{th}(\text{TeV})$	$z_{max}(\text{TeV}\cdot\text{cm})$
(e.m. particles)						
Andromeda	7.8×10^2	1.36	6.7×10^{-1}	1.5	0.1	10.4
Urca Maior	-	1.87	-	-	2.0	-
M.A. I	9.8×10^6	1.94	7.5×10^{-3}	2.0	1.3	3.0
M.A. II	8.3×10^2	1.17	1.0×10^{-1}	2.0	1.0	8.2
M.A. III	5.6×10^5	1.85	2.1×10^{-2}	2.0	2.0	5.7
(hadrons)						
Andromeda	1.9×10	0.97	2.0	1.5	-	5.0
Urca Maior	-	0.94	-	-	-	-
M.A. III	8.6×10^2	1.25	2.6×10^{-1}	2.0	-	38.0

[z_{max} is the value of Er where Er -distribution becomes the maximum.]

The fact that those showers exist inside the halo to contribute to the transition curve, indicates that they have smaller lateral spread. If these particles have the lateral spread characterized by the e.m. cascade process, their spread is, $r = z_{\text{max}}(\text{e.m.})/E = 1.5 \text{ cm}$, which is consistent with the size of the halo.

It means Andromeda consists of two different kind of showers; one is characterized by $z_{\text{max}} = 10 \text{ TeV}\cdot\text{cm}$ and the other by $z_{\text{max}} = 0.6 \text{ TeV}\cdot\text{cm}$. The former value may be due to nuclear cascade process and the latter due to pure e.m. cascade process.

The lateral distribution of the halo in Andromeda, in terms of track length density, is also consistent with the conclusion of two component of showers, stated above.

III. Conclusion.

We analysed five highest energy events, $\Sigma E > 10^{15} \text{ eV}$, observed by Chacaltaya γ emulsion chamber experiment. The results are;

(1) We tried to approximate the behaviour of high energy showers, e.m. and hadronic, by the function Eq.(1). The behaviour of e.m. particles can be described well by Eq.(1), both longitudinally and laterally, while hadrons have the lateral distribution of rather exponential type.

(2) We examined whether the halo can be explained by extrapolating the shower energy to lower energy side in Eq.(1). The four events except Andromeda can be explained by the behaviour of the observed high energy showers, while, as to Andromeda, low energy showers with average energy $\sim 0.4 \text{ TeV}$ contribute significantly. And these showers has the spread consistent with that of pure e.m. cascade showers.

The authors thank to the member of Chacaltaya emulsion chamber experiment of Brazil-Japan Collaboration for their valuable discussions.

References

- PISCRPP = Proc. Intern. Sympo. on Cosmic Rays and Particle Physics (Tokyo) (1984), Inst. Cosmic Ray Research, Univ. Tokyo, Tokyo.
- [1] For example, contributions to PISCRPP and, S. G. Bayburina et al., Nucl. Phys. B191 (1981) 1.
- [2] S. Yamashita et al., ICR-report 112-83-6 (1983), Inst. Cosmic Ray Res. Univ. Tokyo, and PISCRPP (1984) 30.

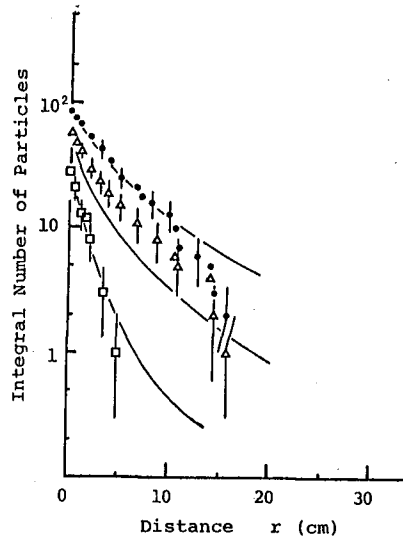


Fig.2 Lateral distribution of hadrons in integral form (Andromeda). See the caption of Fig.1 for the explanation of marks and curves.

Extremely High Energy Hadron and Gamma-ray Families(III)

--- Core Structure of The Halo of Superfamily ---

* ** **

Yamashita, S., Ohsawa, A. , Chinellato, J.A. , Shibuya, E.H.

Science and Engr. Research Lab., Waseda University, Japan

* Institute for Cosmic Ray Research, University of Tokyo, Japan

** Instituto de Fisica, Universidade Estadual de Campinas, Brazil

Abstract

The study of the core structure seen in halo of Mini-Andromeda III(M.A.III), which was observed in Chacaltaya emulsion chamber, is presented. On the assumption that lateral distribution of darkness of the core is exponential type, i.e. $D=D_0\exp(-r/r_0)$, subtraction of D from halo darkness is performed until the cores are gone. The some quantity on cores obtained by this way are summarized. The analysis is preliminary and is going to be developed.

1 Introduction

Since one of the most powerful event, Andromeda($E_{\text{halo}} = 21,000$ TeV), was observed in 1969, eight events with halo were detected by Brazil-Japan emulsion chamber collaboration experiment, at Mt. Chacaltaya, 5200 m at sea level, in Bolivia(1)(2)(3)(4)(5). The detailed study of halos tells the existence of various pattern of the core structure in halo, i.e., single core structure and/or multi-core structure.

Pamir group of emulsion chamber experiment, already, paid attention to this multi-core structure of halo and has derived the important results such as relative P_c of each core and alignment of the cores, etc.(6)(7).

On the other hand, Chacaltaya group has pointed out that the cores in halo correspond to the Jet-clusters obtained by the clustering analysis for individual high energy shower-particles and to the vestige of the nuclear interaction(5). Then in this article, we pick up the M.A.III for example of typical multi-core event and investigate the characteristic of the core structure in halo. The detailed description on M.A.III is presented elsewhere(5).

2 Method

2-1) Core structure of the halo

Fig.1 shows the two-dimensional distribution of darkness of halo in RR type X-ray film at 10 c.u. on M.A.III. The figure is processed by the micro-computer after getting the data by automatical photometry measurement at Institute for Cosmic Ray Research, University of Tokyo. The measurement is carried out by the square slit with the size of 300 μm and number of steps of measurement are 80 to both horizontal and vertical direction, i.e., the figure is made of the darkness of 80 x 80 cells. The numerals in the figure show the darkness $D(D=-\log_{10} I/I_0)$, where I_0 and I , respectively, express flux of the incident and transmitted light. In the figure, four cores are recognized and are

named as H, I, J and L, respectively. The center of halo, \vec{R}_G , is defined by the following way to be presented by a mark of + . $\vec{R}_G = \frac{\sum \vec{r}_i D_i}{\sum D_i}$, where D_i and \vec{r}_i , respectively, represent the darkness and position vector of each cell.

2-2) Determination of incident direction

As an air family generally comes into the chamber with inclined direction and halo looks like an elliptical shape which extends to the incident direction, the correction for inclined incidence must be made. For the correction, we make the following way. One subtracts the $D = D_0(x_0, y_0) \exp(-r/r_0)$, (x_0, y_0) is the position of halo center and r_0 is arbitrary, from the all D_i of the cell. As the function, $D = D_0 \exp(-r/r_0)$, is a circular symmetrical one on r , subtraction of this function from elliptical halo makes the plus area in both edge of long axis of ellipse and the minus area in both edge of short axis of ellipse when we chose suitable size of r_0 . If we can get a line which is joined at two plus area, we determine the direction of the line as incident one and correction for inclined direction is made along the direction. In fact, the coefficient of correlation, R_{xy} , of the first degree is calculated and in the case when absolute value of it is greater than 0.5, we consider there is a linear correlation on x and y and determine the line of incident direction by the least square method.

2-3) Subtraction of the core from halo

We assume that the lateral distribution of the darkness of the core is $D(r, x, y, r_0) dr = D_0(x, y) \exp(-r/r_0) 2\pi r dr$, and we input the position of the core, (x, y) , and its mean spread, r_0 . D_0 is the darkness of the core center and we can get the electron density, ρ_0 ($1/\text{cm}^2$) at $r=0$ by transforming D_0 to ρ_0 .

The distribution, $D(r, x, y, r_0)$, thus defined is subtracted from the darkness of halo made of 80×80 cells (contour map) at each r in order of the magnitude of the core size and new contour map is constructed. In this time, correction for inclined incidence is made with the way described in preceding paragraph. Fig.2 shows the new map thus obtained by subtraction of the highest energy core L on the assumption of $r_0 = 1.5$ mm. In the figure, we can see the core L disappears and H, I and J cores survive. The same procedures are applied to the second highest core J with $r_0 = 1.5$ mm and to the cores H, I with $r_0 = 0.5$ mm, respectively and the new map are shown in Fig.3. In the figure we can see all the four cores disappear.

3 Discussion

Table 1 shows the summary of some quantity on cores H, I, J and L thus obtained. In the Table 1, ρ_0 and R_0 present electron density of the cores at $r=0$ and mean lateral spread of the cores, respectively. R is the distance from the center of halo to the core and N_e is a total electron number in the core obtained by $N_e = \int_0^\infty \rho_0 e^{-r/r_0} 2\pi r dr$. According to the simulation calculation by Makio Shibata, we can get the energy of core by transforming the number of electrons in core at 10 c.u. to the energy(8). E in Table 1 shows the energy of each core thus estimated. R_{ij} is a relative distance among each core and Z_{ij} is a quantity induced by Pamir group as $Z_{ij} = R_{ij} (1/N_i + 1/N_j)^{-1}$, which is connected with the relative transverse momentum of each core(6)(7). ER_{ij} is the relative lateral spread of each core obtained by $R_{ij} (1/E_i + 1/E_j)^{-1}$ using the energy of the cores instead of N_i . Fig.4 shows the scatter plot of

the cores in E-R diagram together with that of computer-constructed A-jets. The triangles with capital letters H, I, J and L show the plots of the cores of M.A.III and the closed circles with small letter i, j and l show the A-jets of M.A.III which should correspond to the cores I, J and L as seen in ref.(5). The cores J and L well correspond to the A-jets j and l but correspondence of the core I to A-jet i is not so good. We suppose it is caused by using the unfit r_0 . The core H is originated from hadronic component as seen in ref.(5) and the shower development does not still reach the maximum at 10 c.u..

This report is preliminary one and shows the new method of investigation of the core structure. There remain problems to be solved, such as the way of determination of r_0 , the order of subtraction of the cores and derivation of the P_t from Z_{1j} , etc.. These problems are under considerations and we will make the answer on their problems in separate publication.

Acknowledgment

The authors would like to express their thanks to all the members of Chacaltaya emulsion chamber experiment. Special thanks are also to Profs. Y. Fujimoto and S. Hasegawa for their kind advices.

Figure captions

- Fig.1: Contour map of halo in RR-type X-ray film at 10 c.u. on M.A.III. Cores H, I, J and L are recognized in it. Darkness are shown by numerals in figure.
- Fig.2: Contour map of halo on M.A.III after subtracting the core L from Fig.1 with $R_0=1.5$ mm.
- Fig.3: Contour map of halo on M.A.III after subtracting the core J from Fig.2 with $R_0=1.5$ mm and the cores H and I with $R_0=0.5$ mm.
- Fig.4: Scatter plot of the cores in E-R diagram together with that of computer-constructed A-jet. Marks are \triangle for the cores of M.A.III, \circ for A jet of Andromeda, \times for A-jet of Ursa Maior and \bullet for A-jet of M.A.III.

Reference

- (1) A. Ohsawa: ICR-Report-112-83-6(1983)65
- (2) J.A.Chinellato: Dr Thesis; Universidade Estadual de Campinas (1981).
- (3) K. Sawayanagi : Proc. Int. Sym. on Cosmic Ray and Particle Physics , Tokyo (1984)116.
- (4) N.M. Amato et al.: Proc. Int. Sym. on Cosmic Rays and Particle Physics (1984)123.
- (5) S. Yamashita: Jour. of the Phys. Soci. of Japan Vol.54 No.2(1985) 529.
- (6) Pamir collaboration: Proc. 18th Int. Cosmic-Ray Conf. Vol.5 (1983)126.
- (7) L.T. Baradzei et al.: Proc Int. Sym. on Cosmic Rays and Particle Physics, Tokyo(1984)136.
- (8) M. Shibata et al.:Uchusen Kenkyu(in Japanese) Vol.26 No.4(1983)13

Table 1

#	$\rho_0(1/cm^2)$	$R_0(mm)$	$R(mm)$	N_e	$E(TeV)$
L	2.63×10^7	1.5	1.65	3.72×10^6	580
J	1.91×10^7	1.5	0.55	2.69×10^6	420
H	2.27×10^7	0.5	2.84	3.56×10^5	56
I	6.25×10^6	0.5	1.86	9.81×10^4	15

#--#	$R_{ij}(mm)$	$Z_{ij}(els.mm)$	$ER_{ij}(TeV.mm)$
L--J	2.20	3.44×10^6	536
L--H	3.67	1.19×10^6	187
L--I	3.13	2.99×10^5	46
J--H	2.66	8.37×10^5	131
J--I	1.54	1.46×10^5	22
H--I	1.24	9.58×10^4	14

Fig.1

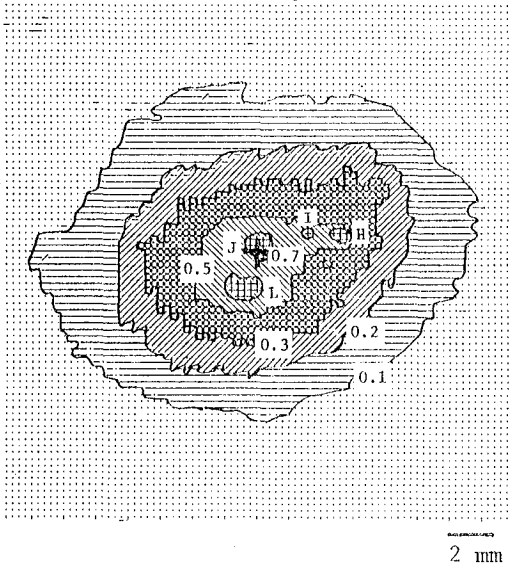


Fig.2

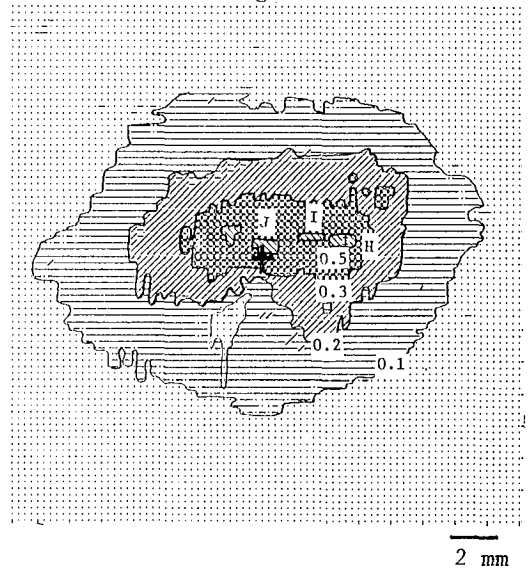


Fig.3

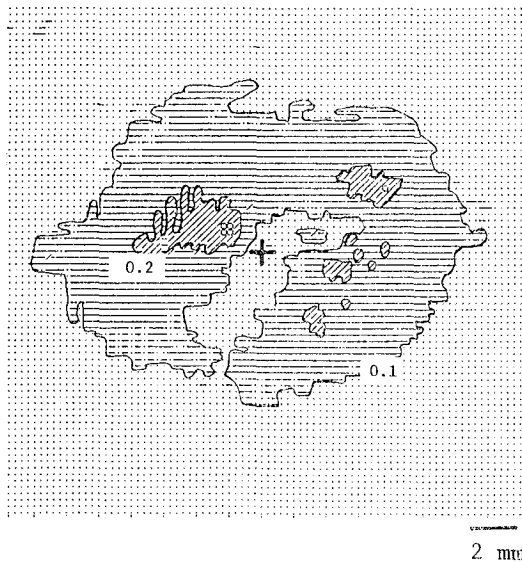
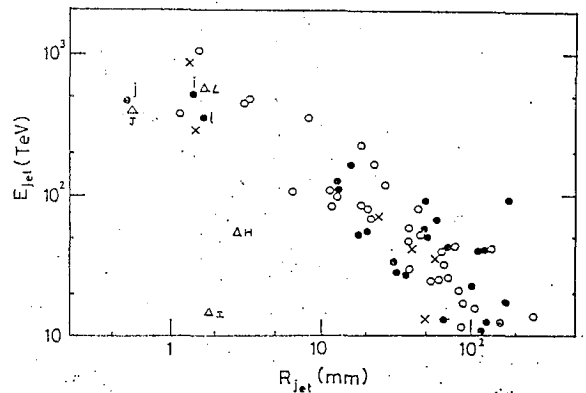


Fig.4



NUMERICAL ANALYSIS OF ELECTROMAGNETIC
CASCADES DEVELOPMENT IN EMULSION CHAMBERS

Plyasheshnikov, A.V., Vorobyev, K.V.
Altai State University, Barnaul,
USSR

1. Introduction. A new calculational scheme of the Monte-Carlo method assigned for the investigation of the development of high and extremely high energy electromagnetic cascades (EMC) in the matter was elaborated in the work [1]. In the works [2] the scheme [1] was applied to the analysis of angular and radial distributions of EMC electrons in the atmosphere. In the work [3] by means of this scheme the EMC development in dense medium is investigated and some preliminary data are presented on the behavior of EMC in emulsion chambers. In the present article the results of more detailed theoretical analysis of the EMC development in emulsion chambers are discussed.

2. Method. The calculational scheme used here consists in the combination of the usual Monte-Carlo method (the transport of the low energy part of the cascade ($E \leq 56\text{eV}$) is calculated by this method) and a method of numerical solution of adjoint cascade equations (to calculate the development of the high energy cascade part).

Our calculations were carried out for the cascade energy region ($10^2 - 10^5$) Gev, the Landau-Pomeranchuk-Migdal effect was taken into account in a number of calculations. Some improvement was made in the computational code [1,3] concerning the electron multiple scattering sampling quality.

This improvement allowed us to get better agreement with experimental data [4].

3. Results. Our calculational data are compared in fig.1 with the experimental data of FNAL [4] and some results of other Monte-Carlo method calculations. As can be seen from

fig.1 our data are in good agreement with experimental results [4] and calculations of Okamoto and Shibata [5] (for $R = 50, 100 \mu\text{m}$ and the upper side of emulsion our results and data [5] practically coincide). At the same time there exists considerable difference of all results presented in fig.1 from the Monte-Carlo method data [6]. To our opinion this difference may be explained by the not quite correct account of the multiple scattering of cascade electrons in [6].

A comparison of our data for homogeneous medium with analytical data [7] evaluated in the core approximation is given in fig.2. As can be seen, our data for $R = 200 \mu\text{m}$ are in a rather good agreement with analytical results corresponding to the simple saddle point method condition, but there exists considerable disagreement with the data using complicated condition of this method.

It is well known that core approximation data on average number of EMC electrons in a small radius circle are invariant with respect to production $E_0 R$ of primary energy E_0 and radius R . Fig.3 shows that such invariance takes place only approximately and only for relatively small values of $E_0 R$.

Fig.4 illustrates the difference in the development of EMC in homogeneous medium of lead and a real emulsion chamber. Analytical data [8] taking into account only single emulsion layer are given there too. A qualitative agreement between numerical and analytical data is observed.

References:

1. Plyasheshnikov, A.V., Vorobyev, K.V., (1981), 17th ICRC, 5, 206.
2. Lagutin, A.A., et.al., (1981), 17th ICRC, 5, 198; 5, 202.
3. Plyasheshnikov, A.V., Vorobyev, K.V., (1983), 18th ICRC, 11, 73.
4. Hotta, N., et.al., (1980), Phys.Rev.D, 22, 1,
5. Okamoto, M., Shibata, T., (1981), 17th ICRC, 5, 214.
6. Van Ginneken, A., (1978), Preprint Fermilab.FN - 309.
7. Fedorova, G.F., Roganova, T.M., (1980), Pamir Collaboration Workshop, Gedzina (Poland), p.26.
8. Guzhvin V.V., Ivanenko, I.P., et.al., (1975), 14th ICRC, 7, 2637.

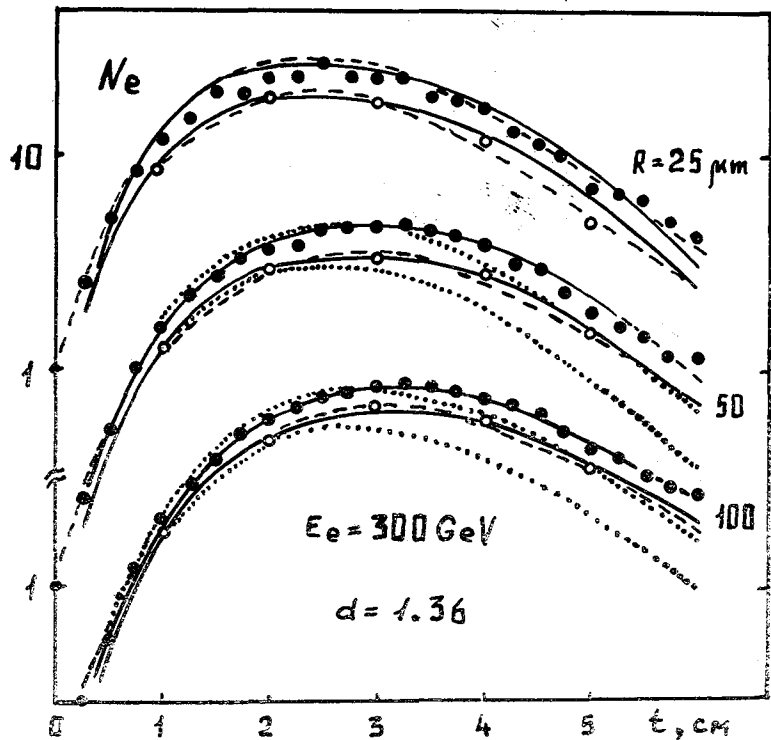


Fig. 1. The average number of electrons N_e within 25, 50 and 100 μm for the chamber of the structure described in [4]. \bullet, \circ - experimental data [4] corresponding to the upper (\bullet) and lower (\circ) emulsion sides, — - our data, ---- data [5], ... - data [6]

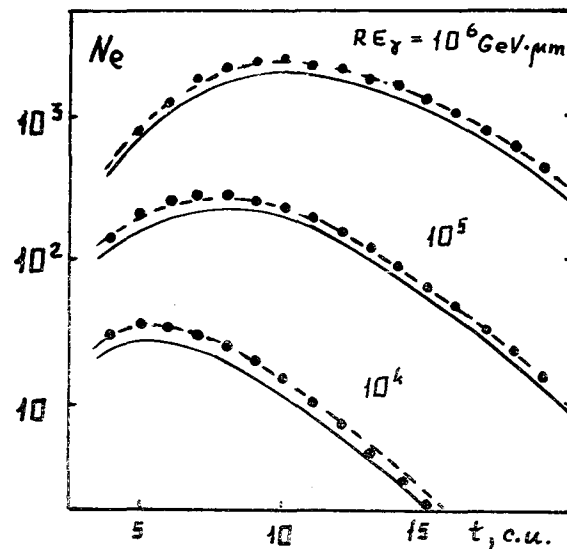


Fig. 2. The average number of cascade electrons N_e within radius $R = 200 \mu\text{m}$ for the homogeneous lead absorber. \bullet - our calculation, curves are the core approximation data [7] corresponding to usual (----) and complicated (—) saddle point method conditions.

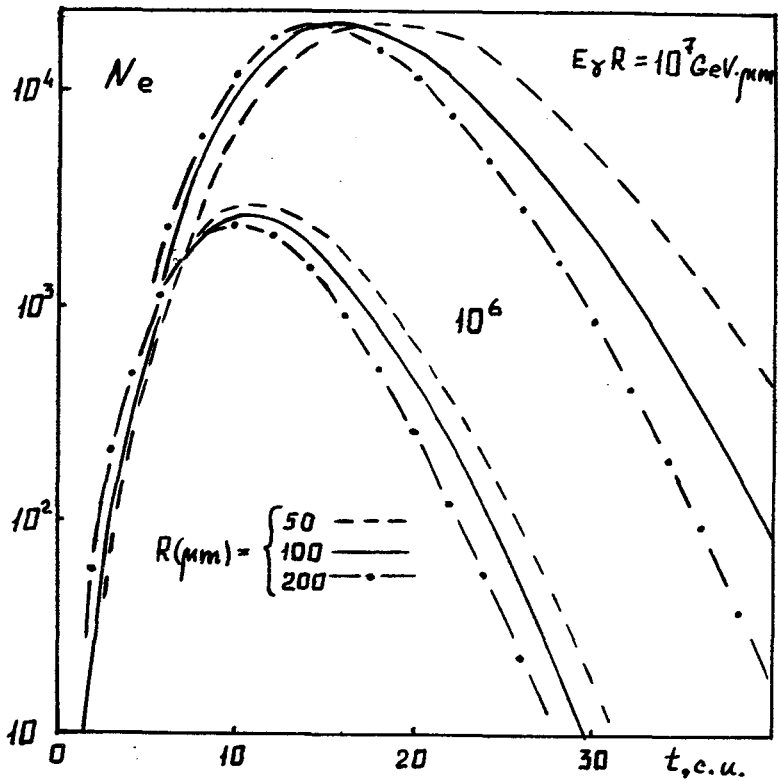


Fig.3. The average number of cascade electrons N_e in the homogeneous lead absorber. The LPM effect is taken into account.

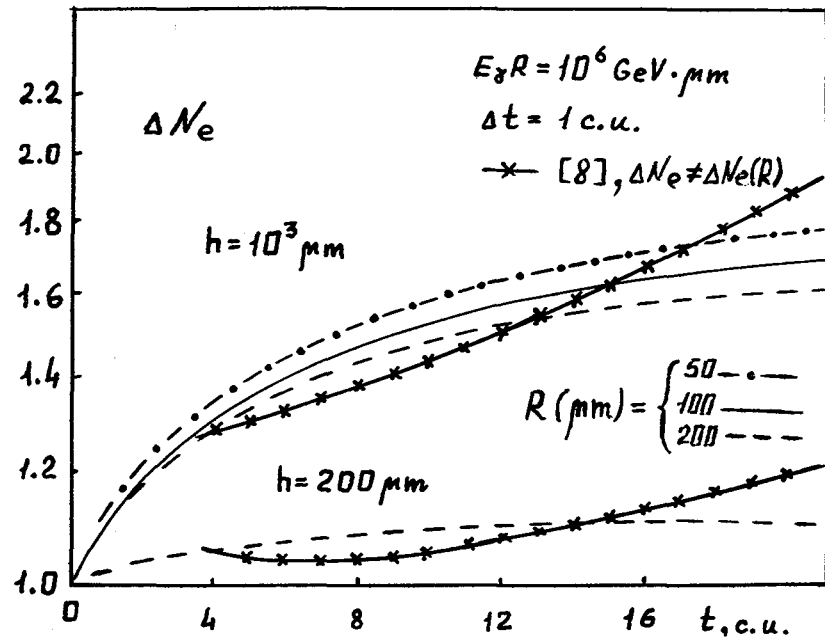


Fig.4. The ratio ΔN_e of average number of electron tracks for homogeneous medium of lead and the lower emulsion side of the chamber having the lead layers thickness $\Delta t = 1 \text{ c.u.}$ and emulsion (or film) layers thickness h .

AN EXPERIMENTAL STUDY OF CORRELATIONS IN THE
DEVELOPMENT OF THE ELECTRON-PHOTON CASCADES

Kratenko, Yu.P. and Charishnikov, S.A.

Tashkent State University, Tashkent 700095, USSR

ABSTRACT

In terms of the experimental data on the development of the electron-photon cascades (EPC) in Pb from electrons and photons of cosmic rays in the tens GeV energy region a calculation of correlations between the characteristics of longitudinal and lateral development of the EPC as well as those between fluctuations of the cascade particle numbers at different stages of the cascade development, is being carried out. The results obtained are compared to the numerical EPC calculations.

1. INTRODUCTION

Among methods characterizing the properties of the cascade processes special attention is drawn to the calculation of correlation between different features of the cascade. Note, a sequence of the correlation coefficients (time-correlation $r(\tau)$) determining a random relation between fluctuations of the cascade particle number $u(E_0, t) = n(E_0, t) - \overline{n(E_0, t)}$ at the depth t in a given cascade with the energy E_0 and $u(E_0, t+\tau)$ at the depth $t+\tau$ in the same cascade, gives a fairly deep insight into the inner structure of the process. The available data on correlations in the longitudinal development of the EPC obtained by numerical methods [1+4] needs to be experimentally tested.

2. EXPERIMENTAL SET-UP "PHOTON"

With the aid of the experimental set-up PHOTON [5] the EPC's from single electrons and photons of cosmic rays in the energy range of tens GeV have been measured. The EPC-detecting section is a single Pb-Ar calorimeter made as a steel tank filled with argon at a pressure of 16 atm, inside of which 16 Pb plates are placed (the width of the first 11 plates is $0.9t_0$, of the rest 5 - $1.77t_0$, where the ra-

diative unit t_0 is $7,4 \text{ g/cm}^2$). Between the plates on the isolators 16 steel strings $0,5 \text{ mm}$ of thickness spaced between 3 cm are stretched. Thus obtained 16 ionization chambers (IL) lack in each IL hollow walls and diaphragms, therefore, there is practically no transition effect. To study a spatial development of the EPC strings in the neighbouring IL's were perpendicular placed. PHOTON was exposed at the height of 3160 m over the sea level. Principles of the initial information selection allowed us to take 383 EPC's for analysis. Statistical simulation of experimental conditions and IL calibration showed that the error in measuring E_0 , and the number of cascade particles $n(E_0, t)$ is approximately the same being averaged as $\sim 7\%$.

3. RESULTS AND DISCUSSIONS

Comparison of a typical experimental time-correlation $r(\tau)$ with results from [4] by the incomplete Monte-Carlo method shows good agreement (Fig.1). Fit of $r(\tau)$ to the time-correla-

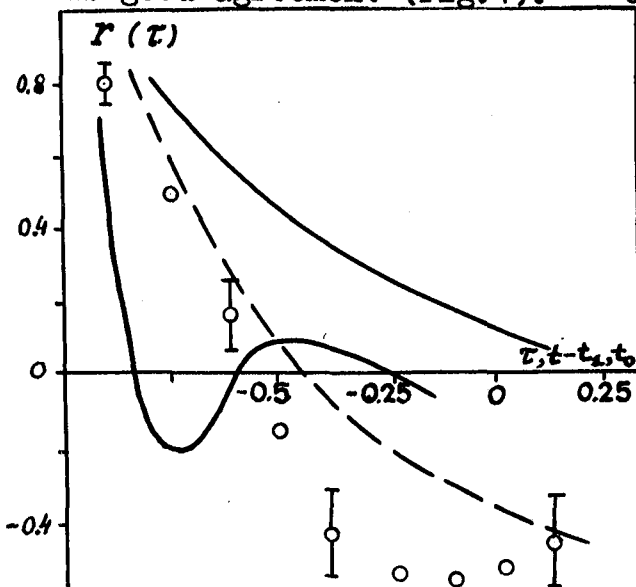
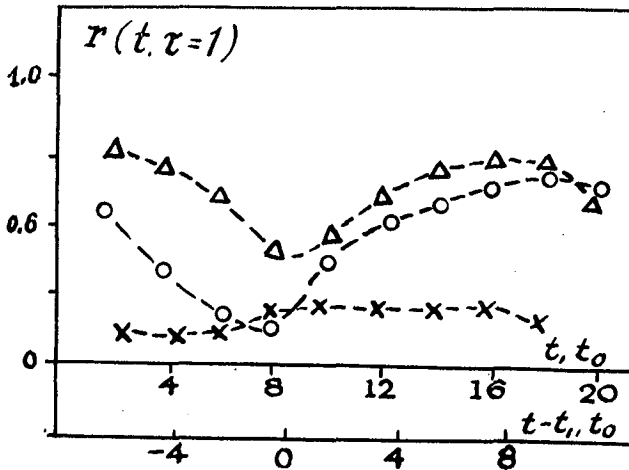


Fig.1 Time-correlation $r(\tau)$ in the EPC. \circ - the present experiment, (---) calculation 4, 1-Marcoff model, 2 - Yule model.

tions of simple autoregression Marcoff and Yule models in Fig.1 is unsatisfactory, especially for large τ . However, the rms deviation of $r(\tau)$ values is known to increase with τ and after a small quantity of runs ($\sim 20-30$) is comparable with $r(\tau)$ for large τ , the significance level being $\sim 0,4$ [6,7]. In this case

following [7] there are no $u(t)$ fluctuations, a series of $u(t)$ where t is determined by t_0 , can be described by the Marcoff model, i.e. there is a correlation only between $u(t)$ and $u(t+1)$. The corre-

lation interval being $\tau_0 = \int |r(\tau)| d\tau$ [8], or "separation" between depths in t_0 at which cascade fluctuations can be considered as independent, fairly strongly changes with E_0 from $2,5t_0$ for $E_0 \approx 30$ GeV up to $3,5t_0$ for $E_0 \approx 80$ GeV. Therefore, with the increase of E_0 the values of $r(E_0, t, \tau=1)$ grow through t_0 , and the minimum of $r(E_0, t, \tau+1)$ shifts towards the deep depth (Fig.2).



The profile of $r(E_0, t, \tau+1)$ coincides with the calculation results [2,3]. Note, that occurrence of anticorrelations for large τ is readily explained by the EPC energy conservation law: fluctuations for one region of depths should be compensated by those in the other part of the

Fig.2 Experimental correlations of cascade development. It is known that the central approach [8] allows us to study separately fluctuations directly of the cascade shape u_c and those of the shift u_λ . As our calculations showed the experimental time-correlations for fluctuations u_c are typical for a set of independent random quantities (Fig.2), the distribution of u_c being obeyed to the Gauss law within the EPC development. Consider a relation between fluctuations u_λ and those of the "center-of-gravity" of the cascade curve $t_1 = \int t n(E_0, t) dt / \int n(E_0, t) dt$, the latter being rather considerable: $\sigma_{t_1} = 1,5$ for $E_0=30$ GeV. The value of the area under the transition curve $\rho(t)$ can serve as an estimate for the absorbed energy in the cascade, and thus, characterize the cascade particle behaviour [9]. Correlations between $\rho(t)$ at the early stages of the EPC development ($t \leq 2t_0$) and t_1 turned out to

be rather high: $\sim 0,55$ and $\sim 0,70$ for the EPC^e from the primary electrons and the EPC^γ from photons, respectively. That is, fluctuations of t_1 are generally determined by those of the shift u_1 . At the same time a correlation between $\rho(t \leq 2t_0)$ and the second central momentum $\mu_2^{1/2}$, characterizing the longitudinal EPC dimension, is small: for EPC^e $\sim 0,16$, for EPC^γ $\sim 0,27$. Finally, a correlation between the rms deviation of r_3 of the spatial cascade ionization distribution within different depths is not considerable: $\sim 0,3$, being independent of the primary particle type and the depth t . A correlation between r_3 and $\mu_2^{1/2}$ is practically independent of the primary particle type and E_0 tends towards zero in the region of depths up to $(\ln(E_0/\beta) + 2)t_0$, then it gradually grows to 0,4 in the deep depth region. Thus, in the wide range of depths lateral and longitudinal dimensions of the EPC are independent.

References

1. Borkovsky M.I., Reprint of Leningrad Nuclear Physics Institute, No 566, 1980.
2. Betman R.G., Gedalin E.N., in "Nuclear interactions in high energy region", Tbilisi, USSR, 1976, v.2, p.13.
3. Lagutin A.A., Plyasheshnikov A.V., Uchaikin V.V., Vetoshkin V.V. The 17th ICRC, Paris, 1981, v.5, p.198.
4. Kirillov A.A., Lyotov Yu.G. Reprint FIAN USSR, No278, 1982
5. Asimov S.A., Glukhov G.A., Daudov Z.H. et al., Reprint of Tashkent Nuclear Physics Institute, NoP-7-22, 1981.
6. Kendall M.G., Stuart A., Design and analysis and time-series, in Russian, Moscow, Nauka, 1976.
7. Chetyrkin E.M., Kalikhman I.L. Probability and Statistics, Moscow, 1982.
8. Kokoulin R.P., Petrushin A.A. Nucl. Phys. USSR, 1980, v.32, 4(10), p.1030.
9. Ivanenko I.P. Electromagnetic cascade processes.- Moscow, 1972.

THE ELECTROMAGNETIC COMPONENT OF ALBEDO FROM
SUPERHIGH ENERGY CASCADES IN DENSE MEDIA

Golynskaya R.M., Hein L.A., Plyasheshnikov A.V., Vorobyev K.V.

Institute of Nuclear Physics, Moscow State University,
Moscow 119899, USSR

Albedo from cascades induced in iron by high-energy gamma-quanta were Monte-Carlo simulated. Thereafter the albedo electromagnetic component from proton-induced cascades were calculated analytically. The calculations showed that the albedo electromagnetic component increases more rapidly than the nuclear-active component and will dominate at sufficiently high energies.

1. Introduction. When a calorimetric installation is used to detect high energy particles essential methodical difficulties are caused by albedo from absorber. Experiment shows that at energies of several TeV the nuclear-active component contributes the most into the albedo effect, and the dependence of albedo on primary energy is rather weak, i.e. logarithmic. Calculations of the albedo from electron-photon cascades so far performed to energies of 100 GeV show that the albedo electromagnetic component increases more rapidly, according to a power law. It indicates that further rapid increase being present, the electromagnetic component will dominate and provide a rapid increase with energy of the overall albedo flux.

A semi-analytical Monte-Carlo method described in /1/ allowed calculations of albedo from the electron-photon showers to highest energies of interest now. In /2/, the results for lead have been reported. We present here the results on the albedo from iron. The results obtained were used to calculate the electromagnetic component of albedo from a primary proton-induced cascade. Since, according to the calculations, the albedo electron flux is 2-3 orders less than the gamma-quantum flux, results on the gamma-quantum albedo only are presented.

2. Results for primary gamma-quantum. Fig.1 shows the energy dependence of the albedo gamma-quantum flux for three angles of incidence of a primary gamma-quantum. One can see that this dependence is, with a high accuracy, a pure power law $N_{\gamma} \sim E^{\mu}$.

Fig.2 presents the albedo gamma-quantum flux versus cascade production depth. The results are for two primary energies and two incidences (production depth is measured along the normal to the entrance plane). It can be noted that i) the exponent $N_{\gamma}(t) \sim e^{-\mu t}$ provides a good description; ii) the rate of albedo attenuation somewhat increases with energy, e.g. $\mu(3 \text{ GeV}) = .92$, $\mu(10^3 \text{ GeV}) = .71$. iii) the results for various incidence angles demonstrate a very high similarity. In Fig.3 the dependence of the mean

energy of albedo gamma-quanta on the primary gamma-quantum energy is shown for three incidence angles. The mean energy can be seen to somewhat increase with primary energy.

In Fig.4, the energy spectrum of albedo gamma-quanta is presented for a primary energy of 10^3 GeV and a normal incidence. It can be noted that about 90% of the photons are confined within the energy interval to 1 MeV.

Fig.5 shows the rms radius versus primary energy. We present the results for a normal incidence and two production depths $t=0$ and $t=2$. With an increase of primary energy the area of albedo emission first apparently broadens, but at higher energies one could suppose some narrowing. In Fig.6, the albedo gamma-quanta radial distribution is shown for energy 3 GeV and a normal incidence.

The angular distribution of albedo gamma-quanta is practically isotropic in the angular range from 30° to 70° , the mean cosine being equal to $\cos\theta = .7$ and independent of both energy and shower incidence angle.

3. Discussion of results for primary gamma-quantum. We make here an attempt to obtain the general features of the albedo behaviour by constructing a rather simple model of its production and applying the results of cascade theory. It proved to be feasible to deduce a simple formula which represents a good reflection of the dependence of albedo on energy and incidence angle

$$N_\gamma(E, t, \cos\theta) \sim \left(\frac{E}{\beta}\right)^S e^{-\mu t} / \lambda_1(s)$$

where β is the critical energy, $\lambda_1(s)$ being the known cascade theory function, and s is found from the equation

$$\lambda_1(s) = \mu \cos\theta.$$

This formula can be thought to be approximating over E , t , and $\cos\theta$, i.e. the values of N and μ being once taken from calculations for one energy, the albedo values can be found for all energies and incidences. The agreement with calculations is demonstrated by the following comparison: if the value of μ at $E=3$ GeV is taken, $N \sim E^{.48}$ / calculations yield $E^{.48}$ / is obtained for a normal incidence and $N \sim E^{.62}$ / calculated value is $E^{.63}$ / for the incidence angle $\cos\theta = .6$.

4. Primary proton. The above discussed features of the behaviour of albedo from a primary gamma-quantum allowed analytical going over to the albedo from a primary proton. The expression for the mean albedo value reads

$$N_\gamma^p = \left\{ \frac{2}{s+1} \frac{f_{\pi\pi}(s)}{\mu \lambda_{\pi+1} - f_{\pi\pi}(s)} \left[1 + \frac{2 f_{\pi\pi}(s)}{\mu \lambda_{\pi+1} - 2 f_{\pi\pi}(s)} \right] \right\} N_\gamma^\delta(E_p)$$

Here $f_{ij}(s) = \int dx \frac{h_i}{\lambda_i} \frac{d\sigma_{ij}}{dx}$

in the $h_i + A = h_j + x$ -reaction, where a h_i hadron is either nucleon or pion, λ_i being the nucleon or pion interaction length. The above expression shows that the contribution of the secondary interactions is about 25%, i.e. the albedo is mainly determined by the first interaction characteristics and primary proton path. Only the variation of these characteristics and μ with energy provides a weak energy dependence of the expression in the figure brackets, i.e. the albedo energy dependence maintains to be a power law with about the same exponent S . For the inclusive distributions and

interaction lengths corresponding to the modern accelerator data the calculated values for the coefficient of transition from a primary gamma-quantum to a proton/expression in the figure brackets/ are the following

$$\{ \dots \}_{\cos\theta=1} = 0.16, \quad \{ \dots \}_{\cos\theta=0.6} = 0.022$$

5. Conclusion. The gamma-quantum albedo indicates a rapid power law increase of $N \sim E^s$, where $s \approx 0.5$, to the highest energies for which the calculation was performed. The mean energy of albedo gamma-quanta slightly increases with primary energy, the lateral distribution becomes broader, and the angular distribution maintains its shape, being close to the isotropic one. We should notice finally, our simulations do not incorporate the Landau-Pomeranchuk effect. The effect should reveal itself in Fe at energies $> 10^{14}$ eV, i.e. providing far deeper cascade development the albedo should sharply decrease with energy (see /2/).

References

1. Plyasheshnikov A.V., Vorobyev K.V., 1981, Proc. 17th ICRC, 5, 206.
2. Plyasheshnikov A.V., Vorobyev K.V., 1983, Proc. 18th ICRC, 11, 73.

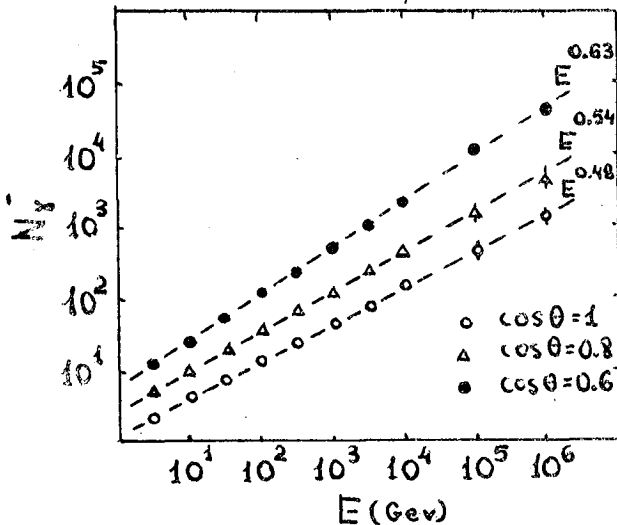


Fig.1. The dependence of the albedo flux on the energy of the primary gamma-quantum. Lines are for the power approximation.

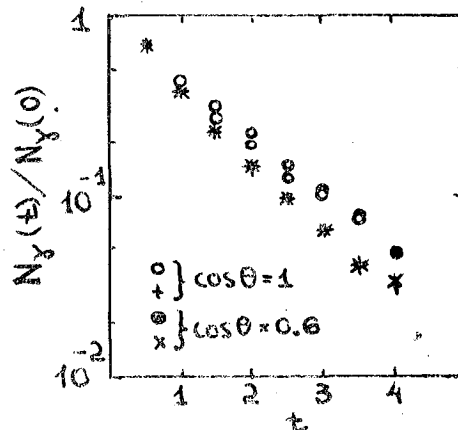


Fig.2. The albedo attenuation with the shift of the cascade generation point.

Crosses are for primary energy $E = 3$ GeV;
circles - 10^3 GeV.

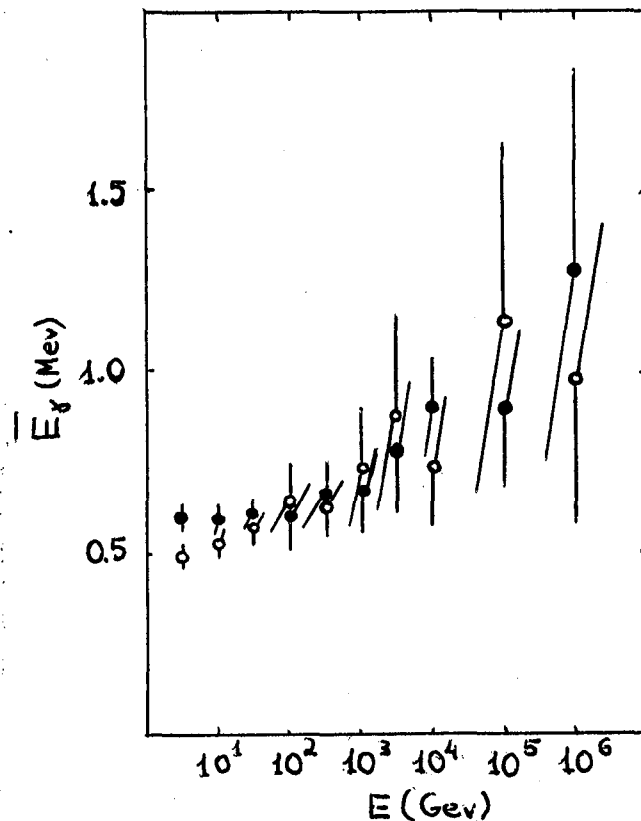


Fig.3. Mean energy of the albedo quanta versus the primary quantum energy

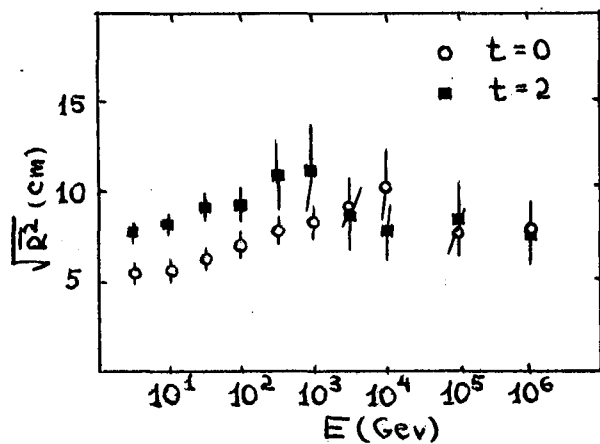


Fig.5. The albedo RMS radius vs primary energy, for two depths of the cascade generation, normal incidence

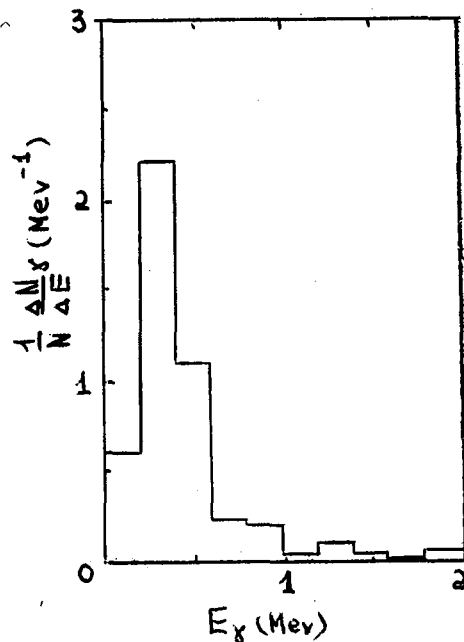


Fig.4. The energy spectra of the albedo quanta. The primary quantum energy is 10^3 GeV, normal incidence

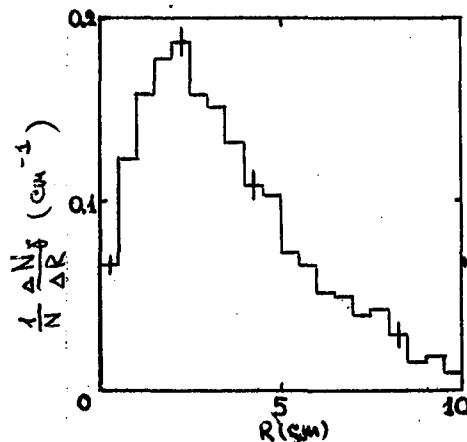


Fig.6. The albedo quanta radial distribution. Primary energy is 3 GeV, normal incidence

INTEGRAL FUNCTIONS OF ELECTRON LATERAL DISTRIBUTION AND
THEIR FLUCTUATIONS IN ELECTRON-PHOTON CASCADES

Ivanenko I.P., Kanevsky B.L., Kirillov A.A., Linde I.A.,
Lyutov Yu.G.

Institute of Nuclear Physics, Moscow State University,
Moscow 119899, USSR

The paper presents Monte-Carlo simulated lateral distribution functions for electrons of EPC developing in lead, at superhigh energies (.1-1 PeV) for depths $t \lesssim 60$ c.u. $\Delta t = 1t_0$ c.u. The higher moment characteristics, i.e. variation, asymmetry, excess, are presented along with analytical solutions for the same characteristics at fixed observation level calculated to theory approximations A and B by using numerical inversion of the Laplace transformation. The conclusion is made of a complex, usually non-Gaussian shape of the function of the particle number distribution within a circle of given radius at fixed depth.

To analyse experimental data obtained by an X-ray emulsion chamber technique, the detailed information on mean EPC characteristics and their fluctuations in dense media is necessary. Therefore, in the high energy region The Landau-Pomeranchuk effect should be regarded, in the low energy region ionization losses and the Compton effect should be allowed for, and it is necessary to describe rather correctly the scattering processes. The problem being extremely complex requires the Monte-Carlo method to be used. For a simplified problem (one-dimensional theory approximations A and B, i.e. consideration of the number of particles with energy higher than the given energy), it is possible now to analyse analytically the problem of the distribution function for the particle number at fixed depth using higher moments, unlike to /1/, where only the second moment has been used. This approach allows qualitative comparison with the Monte-Carlo results and is of interest in itself as an approbation of the technique (e.g. when using the latter to analyse quark-gluon cascades).

1. A cascade from a primary of energy E_0 was Monte-Carlo simulated up to energies about $E = 10^{-2} - 10^{-3} E_0$, then each branch of 130-150 branches of the cascade was ended by statistically with a mean cascade from a previously calculated data bank. In calculations the above mentioned processes were regarded, and scattering at each segment of the free path was considered in the Fermi approximation/2/. An estimate by the method of standards assuming the initial distribution to be non-Gaussian/3/, showed that, in the range $(1/2 \pm 2)t_{\max}$, where t_{\max} is the depth of a mean shower maximum ($t_{\max} \gg 20t_0$), a statistics of 100 events yielded an error (standard) of the mean to be 2-3%,

of variation $\sim 10\%$, of asymmetry 20-30%, and of excess 40-80%. Calculations were made on a net of 14 radii (1-400 μm) given uniformly in logarithm of spatial variable, ($\lg r$), that made it feasible to plot the differential $P(E_0, r, t)$ lateral distribution function: the particle number at distance r from the axis at depth t . The obtained differential functions were integrated and approximated.

Figs. 1 and 2 compares our calculations (see the solid lines) with the experiment/4/ for the differential and integral distribution functions. The experimental results are presented for front-side film of a type C-chambers with delution factor $d=1.18$ leading to a decrease of the particle number in cascade with increasing depth.

Fig. 3 shows the results for 8 values of primary γ . The bundles of curves are parametrized by the product $E_0 R$. The point in Fig. 3 are for the results/5/. This figure illustrates violation of the core approximation of the Landau-Pomeranchuk effect. The investigation of fluctuations of the particle number within a circle of given R substantiates the general picture of evolution of the density distribution function/6/ - at $t \leq 1/2 t_{\text{max}}$ and $t \geq 3/2 t_{\text{max}}$, the distributions are narrow-peaked and skewed towards the small particle number (to the left), at $1/2 t_{\text{max}} \leq t \leq 3/2 t_{\text{max}}$ these distributions shift to the right transforming through symmetric distributions into asymmetric ones with a flat maximum (or several maxima), Gaussian distributions in the region of t_{max} are rather an exclusion than a rule. The results under consideration give a considerable qualitative clarification of the earlier data and allow investigation of the dependence on R or, what is the same, on the efficient value of threshold energy. Figs. 4-6 shows $\text{Var}(E_0, t) = \sigma^2/m$, $A_3(E_0, t) = m_3/\sigma^3$, $E_x(E_0, t) = m_4/\sigma^4$ where $m_i = \frac{1}{n} \sum (N(E_0, r, t) - m)^i$ the numbers are for energy in TeV, $R=140 \mu\text{m}$ (a) and radii in μm (b). The influence of the Landau-Pomeranchuk effect can be clearly seen in Fig. 4 - the curve minima at $E_0 = 10 \text{ TeV}$ (see Fig. 4a); degrading (see Fig. 4b) with increasing R corresponds to a decrease of efficient threshold energy, i.e. a weaker influence of the Landau-Pomeranchuk effect on a cascade.

2. To analyse analytically the set of equations for higher moments of the function of distribution over the particle number in approximation A, it is written in the similar form as in /1/. The solution of this set of equations can be obtained to approximation A for homogeneous cross sections and any moment using the Mellin transformation in energy $E_0/1/$. For the first, second, third etc. moments of the functions of distribution over the particle number in a shower induced by a primary electron the solutions can be represented as follows /7/:

$$\overline{N_e^2}(E_0, E, t) = \frac{1}{2\pi i} \int_{-i\infty+A}^{+i\infty+A} dS (E_0/E)^S \psi_2(S, t) \frac{1}{S}$$

$$\overline{N_e^4}(E_0, E, t) = \frac{1}{(2\pi i)^2} \int_{-i\infty+A}^{+i\infty+A} \int_{-i\infty+A}^{+i\infty+A} dS_1 dS_2 \left(\frac{E_0}{E}\right)^{S_1+S_2} \psi_2(S_1, S_2, t) \frac{1}{S_1 S_2}$$

$$\overline{N_c^3}(E_0, E, t) = \frac{1}{(4\pi i)^3} \int_{-i0+\Delta}^{+i0+\Delta} ds_1 \int ds_2 \int ds_3 \left(\frac{E_0}{E}\right)^{s_1+s_2+s_3} \varphi_3(s_1, s_2, s_3) \frac{1}{s_1 s_2 s_3}$$

etc.

In the cascade theory approximation B similar formulae for higher moments can be obtained. These integrals for a moderate values ($n = 1, 2, 3, 4$) can be calculated using the numerical Laplace inversion. These calculational results are listed in Table 1 and show qualitative agreement with the simulation results. Around the shower maximum we can perform the detailed analysis of higher moments and structure of the distribution function at $E_0/E(E_0/\beta)$. Using the saddle point method (S_{sp}-1) it can be shown that in the region of shower maximum

$$\text{Var} \sim A_2 / \sqrt{\ln E_0/E}$$

i.e. Var decreased slowly, as $\sqrt{\ln E_0/E}$, with increasing ratio E_0/E . Asymmetry and excess increases

$$A_x \sim A_3 \sqrt{\ln E_0/E}, \quad E_x \sim A_4 \ln E_0/E$$

This behaviour of higher moments contradicts the assumption of the Gaussian shape of the distribution functions for the particle number.

The investigation showed that fluctuations of the distribution functions for the particle number within a circle of fixed radius and those of the function of the number of particles with energy higher than the given energy are of similar character, oscillations of higher moments show evidence of a complex structure of the distribution functions and indicate that Gaussian distribution is rather an exclusion than a rule.

References

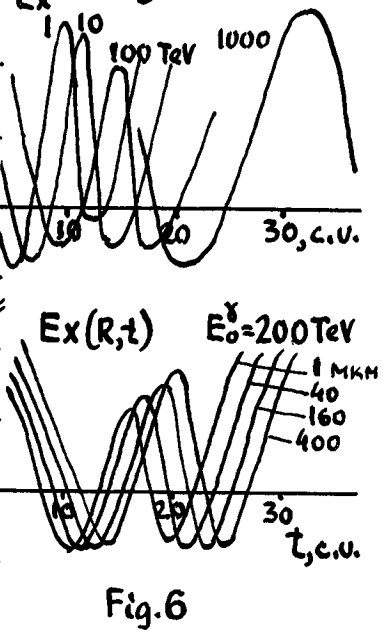
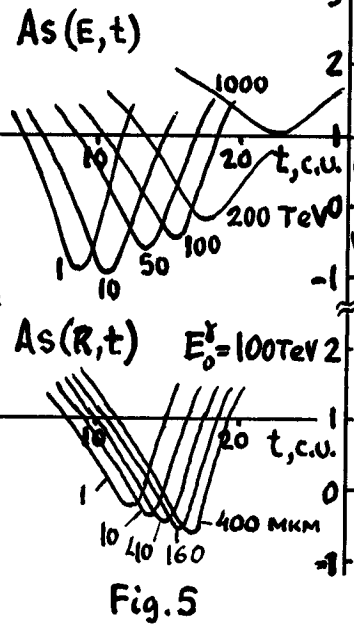
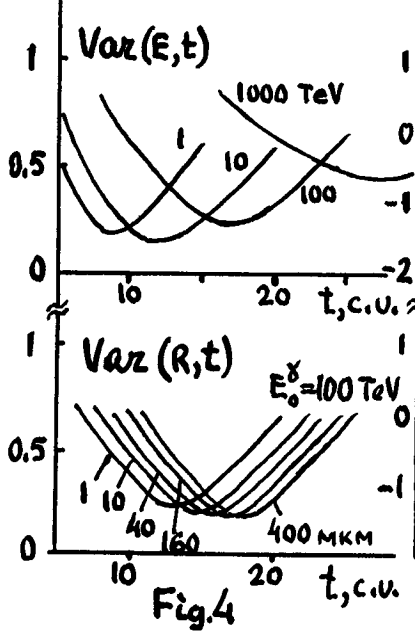
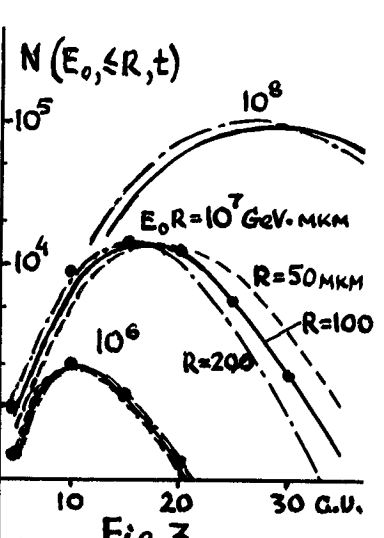
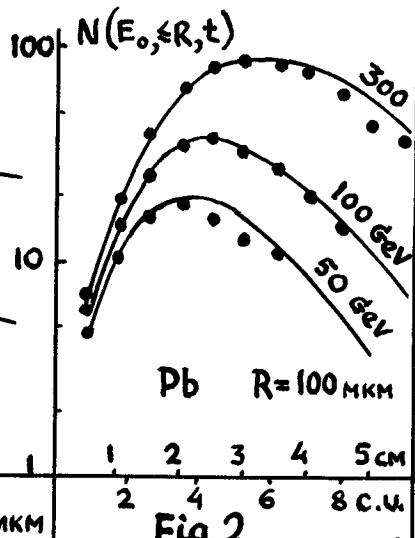
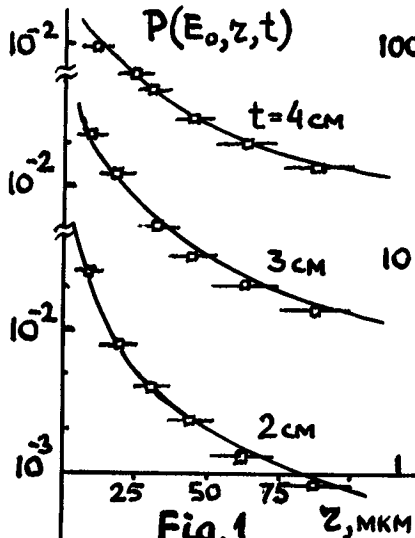
1. Yanoshi L., JETP, 26, 386, 518, 1954.
Gerasimova N.M., Trudy FIAN, 26, 192, 1964.
2. Belenky S.Z. Shower processes in cosmic rays, Gostechizdat, 243, 1948.
3. Kramer G. Mathematical methods of statistics, "Mir", Moscow, 648, 1976.
4. Hotta N. et al. Phys. Rev. D1, 22, 1, 1980.
5. Vorobyev K.V., Plyasheshnikov A.B., Uchaikin V.G., Half-analytical Monte-Carlo method. Dep. VINITI, 120, 1984.
6. Ivanenko I.P. et al. Proc. 16th ICRC, 9, 247, 1979.
7. Kanevsky B.L., Linde I.A. Proc. 17th ICRC, 6, 268, 1981.
8. Gerasimova N.M. Proc. 16th ICRC, 9, 216, 1979.

Table 1

t	\bar{N}	Var^2	A_s	\bar{N}	Var^2	A_s	\bar{N}	Var^2	A_s
2	64.8	.25	1.0	30.1	.17	1.92	.12+2	.25	.99
4	415	.14	.3	110.2	-.11	-.12	.13+4	.15	.52
6	982	.7-1	-.45	157.9	.48-1	-1.1	.45+4	.94-1	-.4-2
8	1333.31	-1-.78	145	.33-1	-1.3	---	---	---	-.2+1
10	1272.17	-1-1.26	91.9	.76-1	.76-1	.12+5	.24-1	-3.34	

Table 1(continued)

t	\bar{N}	Var^2	A_S	\bar{N}	Var^2	A_S	\bar{N}	Var^2	A_S
14	600	.9-1	.6	24.5	.49	1.75	.95+4	.15-1	.87
18	167	.43-1	.91	4.44	2.29	4.99	.40+4	.10	1.77



ANALYTICO-NUMERICAL METHODS OF CALCULATIONS OF ENERGY AND THREE-DIMENSIONAL PARTICLE DISTRIBUTIONS IN ELECTROMAGNETIC CASCADES

Ivanenko I.P., Kanevsky B.L., Roganova T.M., Sizov V.V.,
Triphonova S.V.

Institute of Nuclear Physics, Moscow State University,
Moscow 119899, USSR

The paper reports on analytical and numerical methods of calculation of the energy and three-dimensional EPS characteristics. The angular and lateral functions of electrons in EPS have been obtained to the Landau and small angle approximations A and B and compared with the earlier data /1,2/. A numerical method of solution of cascade equations for the EPS distribution function moments has been constructed. Considering the equilibrium rms angle as an example, we analyse errors appearing when approximating the elementary process cross sections by their asymptotic expressions.

1. Analytical method of solution of a lateral problem

For EPS, in /3/, an analytical method to solve a joint equations for the electron LDF in EPS has been proposed. The method allowed obtaining the accurate moments of LDF and the function itself. The energy-integral LDF being represented as the Mellin inverse transformation

$$N(E_0, > E_1, t, \rho) = \frac{1}{2\pi i} \int ds (E_0/E)^s \frac{1}{s} H_1(s) e^{\lambda_1(s)t} P_{n_2}(s, \tilde{\rho}), \quad (1)$$

where $\tilde{\rho} = \rho E/E_0$, the structure function can be presented as the infinite power series

$$P_{n_2}(s, \tilde{\rho}) = P^{(0)} + (P^{(1)} - P^{(0)}) + (P^{(2)} - P^{(1)}) + \dots \quad (2)$$

Δ is written in the form of a linear combination of the Meier G-functions

$$\Delta = P^{(n)} - P^{(n-1)} = \sum_{k=0}^{2n} C_k(s) G_{26}^{60} \left(f(s) \tilde{\rho}^2 \middle| \begin{matrix} a_p(s) \\ b_q(s) \end{matrix} \right), \quad (3)$$

where s is the shower age parameter, the first $2n-2$ lateral moments of the function transform, $N^{(n)}$, identically coincide with exact function moments.

Proceeding from the properties of Meier G-functions /4/, one can determine the asymptotic behaviour of P_{n_2} at small and large core distances

$$\begin{aligned} \tilde{\rho} \rightarrow 0 & \quad P_{n_2} \sim \tilde{\rho}^{2-s} \\ \tilde{\rho} \rightarrow \infty & \quad P_{n_2} \sim \exp[-4f^{1/4}\sqrt{\tilde{\rho}}] \tilde{\rho}^{2-s + \frac{1-s}{4}} \sum_{k=0}^{\infty} M_k(s) \tilde{\rho}^{-k/2} \end{aligned} \quad (4)$$

2. Asymptotic method of calculation of the EPS lateral-angular functions. The method proposed consists in reducing the solution for angular and lateral functions to a (3)-type contour integral based on the known asymptotics of the solution and calculation of the latter by a saddle-point method. The angular and lateral parts of a cascade equation solution in approximation A can be presented in

the form /2/

$$P(s, \theta) = \frac{1}{4\pi^2 i} \int dp \Gamma(p+1) m_\theta(p, s) \left(\frac{\theta E}{E_k}\right)^{-2p} \frac{1}{\theta^2} \quad (5)$$

$$P(s, z) = \frac{1}{4\pi^2 i} \int dp \Gamma(p+1) m_z(p, s) \left(\frac{z E}{E_k}\right)^{-2p} \frac{1}{z^2}$$

The asymptotics of angular and lateral functions (5) at $p \rightarrow \infty$ ($z \rightarrow \infty$) and $t \gg 1$ reads, respectively

$$m_\theta(p, s) \sim \Gamma(p+1) \alpha_\theta(s)^{-2p}; \quad m_z(p, s) \sim \Gamma(3p+1) \alpha_z(s)^{-2p} \quad (6)$$

In the region $\text{Re } p < 0$ ($z > 0$) the energy-integral angular and lateral distribution functions have the closed singularities $1/p+1, 1/p+s/2$ (7)

Patching of the two asymptotics for the angular and lateral functions yields, respectively:

$$m_\theta(p, s) \sim \frac{\Gamma(p+1)\Gamma(p+s/2)}{\Gamma(s/2)} \alpha_\theta(s)^{-2p}; \quad m_z(p, s) \sim \frac{\Gamma(2p+2)\Gamma(2p+s)}{\Gamma(s)} \alpha_z(s)^{-2p} \quad (8)$$

The integral in (5) is then represented as a product of singularities by some function $G(p, s)$ without singularities in the region $-s/2 < \text{Re } p < \infty$.

The function $G(p, s)$ is developed into Taylor series in the vicinity of a point p_0

$$G(p, s) = G(p_0, s) + (p-p_0) G'(p_0) + (p-p_0)^2/2 G''(p_0) + \dots \quad (9)$$

and a term with the first derivative $G'(p_0)$ is required to be zero. From this condition we find a point " p_0 " and calculate integrals (5):

$$P(s, \theta) = K_{(2-s)/2} (2\alpha_\theta z_\theta) (\alpha_\theta z_\theta)^{2+s} G_\theta(p_0, s); \quad P(s, z) = K_{3-s} (2\sqrt{a_z z_z}) (\alpha_z z_z)^{2+s} G_z(p_0, s) \quad (10)$$

where

$$p_0^\theta = -1 + K_{(2-s)/2} (2\alpha_\theta z_\theta) \alpha_\theta z_\theta / K_{(2-s)/2} (2\alpha_\theta z_\theta); \quad p_0^z = -1 + K_{3-s} (2\sqrt{a_z z_z}) \sqrt{a_z z_z} / K_{2.5} (2\sqrt{a_z z_z}) \quad (11)$$

The expression for the angular part of the distribution function at $G=1$ coincides with the Belenky's function /1/. However, in the expression for $\alpha_\theta(s)$ in $1/d = \sqrt{s(\lambda)}/\lambda$ at $\lambda = \lambda_1(s)$. In the present case, $\alpha_\theta(s)$ is determined from the condition of coincidence of first moments of angular distribution function (9) with a point. If the functions are normalized to the first moment, an accuracy of the functions obtained from (9) is considerably better, and in the core approximation region ($z > 0$) these functions practically coincide. At $-s/2 < p < 3$ $G(p) \sim 1$, and the term with second derivative is negligible. A parameter $a_z(s)$ for the lateral distribution function is determined from a condition of coincidence of the second moments with a point and approximation function. In the integer points ($p=n$) the function $G(n, s, t)$ is thought to be known, since the lateral function moments in approximation A are known. In a wide range of the variable $-s/2 \cdot p_0 < 3$, $G_z(p_0)$ varies slightly and a term with $G_z''(p_0)$ can be neglected. Table 2 compares lateral distribution function (9) with Kamata-Nishimura's calculations /2/. Within 5-10%, even zero approximation yields good results. The lateral-angular distributions can be similarly constructed in cascade theory approximation /5/.

3. Numerical method of solution of cascade theory problems for EPC. To solve analytically the cascade theory problems, simplified expressions for elementary process cross secti-

ons are used. The influence of these simplifications on the results of calculations is considered for an "equilibrium"

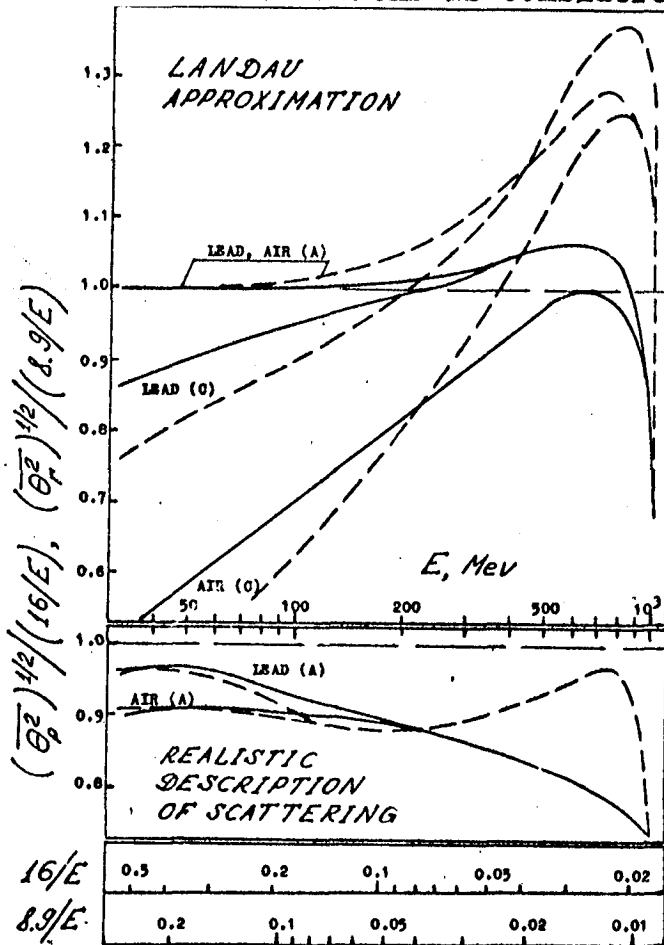


Fig.1

those in Approximation A and from each other. At the bottom of Fig.1, the curves calculated to Approximation A for scattering described realistically are shown - the Thomas-Fermi equation was taken to present atomic potential, a nucleus being considered to be a uniformly charged sphere. By comparing these curves with curves (A) at the figure top a physical accuracy of the Landau approximation can be estimated. On the whole, it can be stated that the differential angular characteristics are sensitive to the details of a description of elementary interactions in the energy range, where their cross section differs from the asymptotic values.

References.

1. Belenky S.Z. Shower processes in cosmic rays, M.: Gostechizdat, 1949, 243p.
2. Nishimura J.N. Handbuch der Physik, Berlin, Springer Verl., 1967, 46/2, 1-113.
3. Roganova T.M., Triphonova S.V., Proc. 18th ICRC, 1983,

rms angle. A numerical method of cascade equation solution has been reported in /6/. For showers induced in lead and air by a primary electron, Fig.1 shows the rms angles of electrons, (see the dashed curves) divided by the Landau analytical expressions /7/ for these magnitudes (see their table below the figure). The top of Fig.1 presents the values of $\bar{\theta}_r^2$ obtained for scattering described in the Landau approximation, in the standard theory approximation A and in approximation C allowing for ionization losses, realistic expressions for bremsstrahlung and pair production cross sections and the Compton effect. The values of $\bar{\theta}_r^2$ obtained to Approximation C for air and lead considerably differ from

- 5, 32.
4. Luke J.L. The special functions and their approximations, New York, 1969.
 5. Ivanenko I.P., Kanevsky B.L. Asymptotic methods of solution of lateral-angular problems in cascade theory (in print).
 6. Ivanenko I.P., Ivanova E.V., Maximenko V.M., Sizov V.V. Preprint FIAN, 1985.
 7. Landau L.D. JETP, 1940, 10, 1107.

Table 1

The ratio of moments of exact and approximate function for normalization to the first moment and at

		$S = 0.6$	$S = 1$	$S = 2$		
1	1	0.82	1	0.87	1	0.95
2	0.90	0.60	0.92	0.67	0.96	0.83
3	0.82	0.41	0.87	0.48	0.90	0.60

Table 2

The EPS lateral function in cascade theory Approximation A. Comparison with the Nishimura-Kamata's calculation /2/ for the zero approximation, parameter $\alpha_{\nu}(s)$ being normalized to the second moment

$s \setminus \tilde{\alpha}$	0	0.01	0.03	0.1	0.3	1.0	3.0
0.6	0.38	0.33	0.26	0.15	---	0.04	0.00006
	0.38	0.34	0.27	0.17	0.05	0.04	0.00009
1	1.12	0.91	0.71	0.4	---	0.017	0.00050
	1.01	0.91	0.70	0.38	0.15	0.019	0.00065
1.4	2.5	1.8	1.31	0.72	---	0.038	0.0016
	2.5	1.9	1.35	0.69	0.27	0.041	0.0019
	0.53	3.0	1.9	0.94	---	0.060	0.0040
	0.54	2.7	1.8	0.99	0.37	0.060	0.0037

MULTIDIMENSIONAL ANALYSIS OF DATA OBTAINED IN EXPERIMENTS
WITH X-RAY EMULSION CHAMBERS AND EXTENSIVE AIR SHOWERS

A.A.CHILINGARYAN, S.KH.GALFAYAN, M.Z.ZAZYAN

Yerevan Physics Institute, Markarian st.2
375036, Yerevan, Armenia, USSR

A.M.DUNAEVSKII

Lebedev Physical Institute
Leninsky prospect 53, Moscow, USSR

1. Introduction

The traditional approach to the analysis of data available from experiments with X-ray emulsion chambers consists in considering one-dimensional distributions or the dependences of one experimentally observed value on the other.

Recently the analysis of two- and three-dimensional distributions /1/ as well as the presentation of averages of two variables together with their errors led to the possibility of drawing a conclusion on the scaling violation in the secondary particle fragmentation region at the energies $\sim 10^{16}$ eV and estimating the degree of its violation /2/.

Thus, the increase of simultaneously analyzed features seems to be attractive, but it is apparent that the analysis of three and more features is connected with the necessity to have the quantitative measure of distinction of multidimensional distributions presented by limited samples.

The other main problem of cosmic ray physics may be formulated as the problem of determining the portion of experimental events belonging to one of described types. That is the problem of determining the portion of photon-hadron ($\gamma - h$) families generated by various primary nuclei or the determination of the primary component chemical composition by the EAS data.

In the present paper we shall show that the solution of the above problems may be realized in the multidimensional space by the nonparametric statistic methods developed in /3,5/. Note that the use of these methods for processing the experimental data from the cosmic ray physics installations has demonstrated their advantage over the traditionally applied techniques /4,6,7/.

This is a methodical work, i.e. the experimental events are replaced by the model ones. Thus we have an opportunity to determine the limits of applicability of the methods suggested and to estimate the expected accuracies of determining the desired physical values.

Among the models used, there is a pure-scaling one - M6, the models with increasing cross section and scaling violation in the pionization region - M4, Femin, Femax (the detailed

description of the models may be found in /8/). Some models are obviously nonrealistic (e.g. M6), but for the methodical purposes the use of the family banks corresponding to these models is admissible.

2. The Distinction of Strong Interaction Models

The selection of the feature set optimal for the discrimination purposes is performed with account of the averages differences and the correlation information. The feature pairs with the statistically significant difference in correlations are included in the set. Finally each set is characterized by the so-called Bayesian risk R - the probability to misclassify the models (or the model and experimental data) in classification procedure performed with the optimal Bayesian decision rule (for details of the method and used features see /9/).

The R^B use in one-dimensional analysis leads to the same conclusions as the standard statistical methods of two samples averages difference significance calculation (T-test and Wilcoxon test). The more is the difference between R and 0.5 (corresponding to the classes total overlapping) the stronger is the difference between the distributions.

The Bayesian risk calculation method /10/ allows to obtain unbiased effective estimates and to judge of the model describing the experiment in the best way by the successive comparison of the experimental and alternative model training samples.

The estimation accuracy depends on the sizes of the used training samples. Besides there is an interrelation between the sample size and maximum dimensionality of the space where one may realize the effective local reconstruction of the probability multidimensional density. As we see from Table 1, the samples limitation (100+400) leads to that the addition of low-informative features may even deteriorate the discrimination due to the scarcity of points in N-dimensional feature space.

Table 1. The comparison of the M4 and M6 models by means of χ -family various characteristics.

Combination	Space dimensionality	R^B
\bar{R}_χ	1	0.38 \pm 0.3
$\bar{R}_\chi, \bar{E}R_\chi$	2	0.37 \pm 0.3
$\bar{R}_\chi, \Sigma'E_\chi, d'_\chi$	3	0.35 \pm 0.3
$\bar{R}_\chi, \Sigma'E_\chi, d'_\chi, b'_\chi$	4	0.34 \pm 0.3
$\Sigma'E_\chi, n_\chi, \bar{R}_\chi, \bar{E}R_\chi, d_\chi, \Sigma'E_\chi, \dots$	10	0.38 \pm 0.3
$\Sigma'E_\chi, n'_\chi, \bar{R}'_\chi, \bar{E}R'_\chi, d'_\chi, b'_\chi, \dots$	15	0.40 \pm 0.3

The comparison of the M4 and M6 models by means of various feature combinations has shown that the addition of in-

formation from the hadronic block or the shower installation to the γ -family information does not reduce the classification errors. That is, in the problems related to the study of strong interaction cross sections and scaling violation in the pionization region it is enough to analyze only the photon family characteristics.

3. Separation of Families from the Light and Heavy Nuclei. Determination of the Portion of Families from Fe Nuclei.

Let us take as prototypes (training samples) the samples containing the events from the light nuclei and, respectively, the events from the banks Femin and Femax. Various combinations of both types from the events not included in the training samples will be taken as the "experimental" one. Such a choice imitates the case of precise knowledge of the strong interaction model. The portion of "iron" events in these samples is set to be $P_H = 0.05, 0.07, 0.1$.

The estimate of the portion of families initiated by the Fe nuclei will be obtained after the experimental data classification and calculation of the probabilities to misclassify the events of both types.

$$\hat{R}_H = \frac{R_H^* - R_{L \rightarrow H}}{1 - R_{H \rightarrow L} - R_{L \rightarrow H}}$$

where P_H^* is the portion of families referred to the "iron" type, $P_{L \rightarrow H}$ and $R_{H \rightarrow L}$ are the probabilities of the classification possible errors.

Table 2 shows that the reconstructed P_H value is rather close to the true one. Besides, it may be shown that the classification allows one to enrich 5+7 times the selected events with the families from the heavy nuclei, this possibly enabling one to study Fe - N¹⁴ interaction at the energies more than 10^{16} eV.

Table 2. Reconstruction of the portion of families from the Fe nuclei. The training and control samples are taken from the banks M6 and Femin.

Installation	Features	P_H	P_H^*	\hat{P}_H
γ -block	$\Sigma E_\gamma, \bar{R}_\gamma, \alpha_\gamma$	0.05	0.194	0.042±0.060
		0.07	0.202	0.055±0.058
		0.1	0.217	0.080±0.058
γ -block + shower part	$\Sigma E_\gamma, \bar{R}_\gamma, \alpha_\gamma, E_0$	0.05	0.09	0.048±0.025
		0.07	0.115	0.074±0.024
		0.1	0.138	0.098±0.023
γ -h -block	$\bar{R}_\gamma, n_h, \bar{R}_h$	0.05	0.125	0.044±0.028
		0.07	0.149	0.076±0.026
		0.1	0.171	0.099±0.025

However, if the strong interaction model is unknown (this case was simulated by the use of "experimental" data from the banks not coinciding with the prototypes), the reconstruction is carried out with great errors. Therefore, to treat the real experimental data one should use either more realistic models or combinations of features weakly dependent on the strong interaction model, but simultaneously highly sensitive to the primary nucleus type.

4. Conclusion

The use of nonparametric statistic methods allows one to carry out the quantitative comparison of the model and experimental data. The same methods enable one to select the events initiated by the heavy nuclei and to determine the portion of the corresponding events. For this purpose it is necessary to have the banks of artificial events describing the experiment sufficiently well. At present, the model with the small scaling violation in the fragmentation region /11/ is the closest to the experiments. Therefore, the treatment of γ -families obtained in "Pamir" experiment is being carried out at present with the application of these models.

REFERENCES

- /1/ Danilova T.V., Erlykin A.D., VANT, ser.tekhn.fiz.eksp., issue 1(13), p.13-19, 1983.
- /2/ Pamir Collaboration, 18th ICRC, v.5, p.425-428, 1983.
- /3/ Chilingaryan A.A., VANT, ser.tekhn.fiz.eksp., issue 2(8), p.59-68, 1981.
- /4/ Chilingaryan A.A., VANT, ser.tekhn.fiz.eksp., issue 3(12), p.90-91, 1982.
- /5/ Chilingaryan A.A., 18th ICRC, v.5, p.524-526, 1983.
- /6/ Chilingaryan A.A., VANT, ser.tekhn.fiz.eksp., issue 1(13), p.81-84, 1983.
- /7/ Chilingaryan A.A., VANT, ser.tekhn.fiz.eksp., issue 1(13), p.61-68, 1983.
- /8/ Dunaevskii A.M., Uryson A.V., Preprint FIAN, No.150.
- /9/ Chilingaryan A.A., Galfayan S.Kh., Zazyan M.Z., Dunaevskii A.M., 18th ICRC, v.5, p.487-490, 1983.
- /10/ Galfayan S.Kh., Chilingaryan A.A., in: Statistical Problems of Control, issue 66, Vilnius, 1985.
- /11/ Vernov S.N., Khristiansen G.B. et al., 15th ICRC, v.8, p.32-35, 1976.

A NEW METHOD OF DIFFERENTIAL STRUCTURAL ANALYSIS
OF γ -FAMILY BASIC PARAMETERS

L.G.MELKUMIAN, S.V.TER-ANTONIAN

Yerevan Physics Institute, Markarian st. 2
375036, Yerevan, Armenia, USSR

YU.A.SMORODIN

Lebedev Physics Institute, Leninsky Prospekt 53
117312 Moscow, USSR

ABSTRACT

The maximum likelihood method is used for the first time to restore parameters of electron-photon cascades registered on X-ray films. The method allows to carry out a structural analysis of the γ -quanta family darkening spots independent of the γ -quanta overlapping degree and to obtain maximum admissible accuracies in estimating the energies of the γ -quanta composing a family. The parameter estimation accuracy weakly depends on the value of the parameters themselves and exceeds by an order the values obtained by integral methods.

In our previous papers /1,2/ we have proposed for the first time to use the maximum likelihood method for the solution of the traditional inverse problem of X-ray emulsion experiments. The essence of the method consisted in the reconstruction of source parameters (the energy E , zenith and azimuth angles Θ and φ , the spot center coordinates X, Y) of the darkening spot on the X-ray emulsion film according to the matrix of darkening densities $\{P_{ij}\}$ measured by a densitometer in the cells (i, j) $i = 1, \dots, N_i$, $j = 1, \dots, N_j$. The scanning cell dimensions ΔX , ΔY and the number of cells $n_i \cdot n_j = N$ are fixed. It has been shown in /1,2/ that the maximum likelihood method gives consistent, efficient and nonshifted estimates for the parameters E, Θ, φ, X, Y in the wide range of scanning cell dimensions $\Delta X = \Delta Y = 10, 20, \dots, 50 \mu\text{m}$. The accuracy of parameter estimation slightly depends on the value of the parameters themselves and exceeds by an order the values obtained by the momenta method and by integral methods.

The results of /1,2/ are obtained for the darkening spots caused by a single γ -quantum (electron) with the energy E in the range $2 + 100 \text{ TeV}$ and zenith angle in the interval $1 + 0.5$.

In /3/ the results of solution of the inverse problem for the general case - the number of the darkening spot

sources (γ -quanta) is greater than 1 with the strongly marked structure of the spot overlapping, are given.

Remaining within the framework of notations accepted in /1,2/, one may present the likelihood function for the realized density matrix $\{\rho_{ij}\}$ at the unknown but fixed vector of parameters $\vec{\eta} = \eta(E_1, \dots, E_n, X_1, \dots, X_n, Y_1, \dots, Y_n, \Theta, \Psi)$ in the form

$$\Phi(\{\rho_{ij}\} | \vec{\eta}) = \prod_{i=1}^{N_i} \prod_{j=1}^{N_j} f_e(n_{ij} / \vec{\eta}); \quad (1)$$

where $n_{ij} = \rho_{ij} \cdot S$ is the number of electrons in the cell (i, j) ; $S = \Delta x \cdot \Delta y$ is the cell area; N_i, N_j is the corresponding number of scanning cells along the X and Y axes; $f_e(n_{ij} / \vec{\eta})$ is the probability of n_{ij} electrons having been registered in the cell (i, j) at the given $\vec{\eta}$ vector of parameters; $\ell = 1$, if $n_{ij} < n_{\min}$; $\ell = 0$, if $n_{\min} \leq n_{ij} \leq n_{\max}$; $\ell = 1$, if $n_{ij} > n_{\max}$. The boundary values of the electron number are defined by the operation properties of the film and are chosen by us as in /1-3/ $\rho_{\max} = n_{\max} / S = 0.5 \mu \text{km}^{-2}$, $\rho_{\min} = n_{\min} / S = 0.002 \mu \text{km}^{-2}$. The distribution function $f_e(n_{ij} / \vec{\eta})$ is assumed to be Poisson with the mean value $\bar{n} = \sum_{m=1}^n \bar{n}_m + \bar{n}_\phi$, where n_γ is the number of γ -quanta (electrons), $\bar{n}_m(E_m, X_m, Y_m, \Theta, \Psi)$ is the average number of electrons in the cell (i, j) generated by the source with the energy E_m , whose trajectory crosses the film at the point X_m, Y_m at the zenith and azimuth angles Θ and Ψ respectively; \bar{n}_ϕ is the average number of "background" electrons ($\rho_\phi = \bar{n}_\phi / S = 0.04 \mu \text{km}^{-2}$).

The determination of the $\vec{\eta}$ vector components is performed numerically by minimizing the likelihood function negative logarithm:

$$\Omega_0 \equiv \min \Delta(\vec{\eta})_{n_\gamma} \equiv \min \left\{ -\ln \Phi(\{\rho_{ij}\} / \vec{\eta}_{n_\gamma}) \right\} \quad (2)$$

The inverse problem may also be solved in the case when the number of darkening spot sources n_γ is unknown. In this case one should minimize the functional

$$\Omega_1 \equiv \min \left\{ \min \Delta(\vec{\eta}) \right\}_{n_\gamma}, \quad n_\gamma = n_0, n_0 + \Delta n, \dots, n', \quad (3)$$

where n_0 and n' determine the boundaries of search for the darkening source number.

The inverse problem was solved by the maximum likelihood method basing on the density matrix $\{\rho_{ij}\}$ generated by the Monte-Carlo method at the given vector of parameters $\{\rho_{ij}\}$. The average number of equivalent electrons in the cell (i, j) was calculated according to the cascade theory axial approximation. Fluctuations were assumed to be Poisson-distributed. The BESM-6 computer main memory allowed one to analyze the rasters with the cell number $N_i \cdot N_j \leq 7000$ and the summary number of unknown parameters $3(n_\gamma + 1) \leq 99$.

Consider the possibilities of the elaborated method at

1) $n_\gamma = 1$, 2) $n_\gamma = 2$, that is of interest for calibrating the emulsion technique on $\pi^0 \rightarrow 2\gamma$ decays; 3) $n_\gamma > 2$ for processing γ -families; 4) $n_\gamma = ?$, i.e. when the number of the darkening spot sources is the component of parameter vector and is unknown.

1. $n_\gamma = 1$

The simulated rasters parameter reconstruction was carried out for discrete series of γ -quanta energy ($E_0 = 2, 5, 10, 20, 50, 100$ TeV) $\Delta x = \Delta y = 10, 20 \mu\text{km}$ cell dimensions and various thicknesses of absorbers (d).

The relative accuracy of estimates of E, Θ, φ made a few per cent. The accuracy of the definition of the spot center coordinates is $2-5 \mu\text{km}$.

2. $n_\gamma = 2$

For the darkening spot pair the calculations were performed at various energies $E_1 = 2 \cdot E_2 (2, 4, 5, 10, 20 \text{ TeV})$ and distances between the spot centers $\mathcal{D} = (0.1+100 \mu\text{km})$ at the scanning step of $10, 20, 50 \mu\text{km}$.

The results may be formulated as follows:

- the accuracy of determining the zenith Θ and azimuth φ angles differs insignificantly from the single spot results and makes $\sigma_{\cos\Theta} \leq 5 + 7 \%$;
- the accuracy of determining the spot center coordinates is $\sigma_x \approx \sigma_y \leq \Delta x / 2$, the distances between centers are $\sigma_{\mathcal{D}} \approx \Delta x$;
- the accuracy of determining the energy for the overlapping spots is not worse than 10% at the summary energy reconstruction accuracy of 5-7%.

3. $n_\gamma > 2$

For the overlapping families of γ -quanta the inverse problem was solved for the energies distributed uniformly in the 2-20 TeV interval. The number of γ -quanta was varied in the region 2-20 over the area 0.25 mm^2 .

The accuracies of determining the parameter vector components at $3 \leq n_\gamma \leq 10$ were independent of the n_γ number and on the average equalled the corresponding values at $n_\gamma = 2$.

The accuracy of determining the zenith angle cosine made $4 + 5 \%$ and also was independent of n_γ .

4. $n_\gamma = ?$

The n_γ value varied in the interval $1 + 5$ due to the complexity of solving the problem at the unknown number of the darkening spot sources.

No noticeable variation of the estimation accuracy was observed. Note also that at the known values of $n_\gamma \leq 10$ the efficiency of solving the inverse problem equalled $90 + 100 \%$. At the unknown n_γ the efficiency decreased to 80%, and the computer counting time grew 5 - 7 times.

REFERENCES

- /1/ Melkumian L.G., Ter-Antonian S.V., Preprint EPI-649(39)-83, Yerevan, 1983.
- /2/ Melkumian L.G., Ter-Antonian S.V., Preprint EPI-725(40)-84, Yerevan, 1984.
- /3/ Melkumian L.G., Ter-Antonian S.V., (1984), sb. Voprosi atomnoi nauki i tekhniki, ser.tekhn.fiz.eksp., 3(20), p.60-64.

LPM EFFECT AND PRIMARY ENERGY ESTIMATIONS

M.F. Bourdeau and J.N. Capdevielle
 Laboratoire de Physique Théorique, Université de Bordeaux I
 Rue du Solarium, 33170 GRADIGNAN, FRANCE

1. Introduction

The distortion of the electron cascade development under LPM effects is now currently admitted (1, 2, 3) ; it consists in an increase of depths of showers origin, of shower maximum T_{\max} , a decrease of the number of particles at maximum N_{\max} and results in a flattening and a widening of the cascade transition curve. Connected with the influence of multiple Coulomb scattering on basic electromagnetic processes (bremstrahlung, pair production), this effects appears at high energy with a threshold dependent on the density of the medium (more than 10 TeV for lead, more than 10^6 TeV in air).

We examine here, consequently, the electromagnetic components of hadron induced showers in lead and EAS in air, calculated for the same hadronic cascades in the different alterlative, including or not LPM effect.

2. Analytical representation of cascade curve

We have used in lead our Monte-Carlo data (1) to estimate from numerical values of γ -induced showers the different moments at fixed primary photon energy E_0 .

$$p_n(E_0) = \int_0^{\infty} t^n N_e(E_0, t) dt$$

The longitudinal spread τ and the integral track length S_0 have therefore been obtained from the relations between appropriate moments

$$[\tau(E_0)]^2 = \frac{p_2(E_0) - [p_1(E_0)]^2/p_0(E)}{p_0(E)}$$

and

$$S_0(E_0) = \sqrt{2\pi} \tau(E_0) N_{\max}(E_0) = \int_0^{\infty} p(E_0, t) dt$$

We found convenient to describe the data including LPM effect by the following formula (replacing Greisen's formula when $E_0 > 1$ TeV in lead) :

$$N_e(E_0, t) = 15.3 [1 + \alpha_2 B_0^{\beta_2}]^{-1} E_0^{0.9773} \exp[-(t-T_0)^2/2\tau^2]$$

with $T_0 = T_{\max}^{\text{LPM}}$, $\tau = \tau^{\text{LPM}}$ and $B_0 = \ln(E_0/10^3)$, where

$$T_{\max}^{\text{LPM}} = 4.98 + \ln E_0 + \alpha_1 [\ln E_0]^{\beta_1} \quad (\alpha_1 = 0.0001477, \beta_1 = 4.64)$$

and $\tau^{\text{LPM}} = 3.78(1 + \alpha_2 B_0^{\beta_2}) E_0^{\delta} \quad (\alpha_2 = 0.008446, \beta_2 = 2.7936)$

This formula is inserted in our Monte-Carlo programm of hadronic

cascade for all γ rays of different energy emitted at different depth.

Similar procedure has been adopted for air, from Monte-Carlo data (2) leading to the formula for $E_0 \geq 10^5$ TeV

$$N_e(E_0, t) = 0.00825 E_0 (100 - 0.88B_0 - 1.62B_0^2) \exp [-(t-T_0)^2/2\tau^2]$$

where $B_0 = \text{Ln}(E_0/10^8)$, $T_0 = 1.363B_0 + 21.09$

$$\tau = 5.2 \quad \text{if } E_0 \leq 10^{10} \text{ GeV}$$

$$\tau = 5.2 - 0.426 \text{Ln}(E_0/10^{10}) \quad \text{if } E_0 \geq 10^{10} \text{ GeV}$$

(E_0 in GeV, t in c.u.). This formula is also inserted in our hybrid Monte-Carlo-analytic simulation in air in place of Greisen's formula.

3. Simulation in lead calorimeters

The model used for production of secondary hadrons is SBM extended in lead following HE 4.1-9 with $\langle \nu \rangle = 3.2$. The energy lost in disintegration of the struck nucleus is $E_D(\text{MeV}) = 124 N_H^{+30}$, the number of tracks N_H being obtained from $N_H = 3.46 E_0^{0.33} A^{0.19} H(4)$. The Monte Carlo procedure gives the quantities E_{ion} , E_D , E_{out} at different depth of a calorimeter 1000 g/cm^{-2} deep built with lead plates of 50 g.cm^{-2} .

$$E_{\text{ion}} = (N_1 + N_2 + 0.75 N_3) 32 \times 7.4 \text{ (MeV)}$$

$$(N_1 = \frac{1}{2}(N(100)+N(200)), N_2 = ([N(300)+N(400)]/2) \dots)$$

is the energy lost by secondary particles and γ initiated cascades, E_D is the total energy spent by disintegration, E_{out} is the energy leaking out the considered slide (or the bottom of the calorimeter) estimated as the sum of the individual energies of outgoing hadrons. The behaviour of those quantities with depth are given in fig. 1 for incoming protons of 10^5 GeV. E_{ion} is given with and without LPM. It can be ascertained that for short calorimeters ($\sim 3\lambda$) E_{ion} is 1.6 times lower at 10^6 GeV when LPM is taken into account and a systematic underestimation, rising with energy, occurs when the primary E_0 is estimated from E_{ion} without consideration of LPM. A first approach of the amended Grigorov spectrum is shown in fig. 2. Similar consequences will also be detailed for emulsion chamber data.

4. EAS with LPM

EAS induced by proton have been simulated between 10^9 - 10^{11} GeV, for scaling model (5) and CKP model. For 1st model according to the small number of more energetic secondaries an important distortion occurs in cascade curve (fig. 3 - 4) at 10^{10} and 10^{11} GeV. The discrepancy is not visible at 10^9 GeV. For CKP model, LPM can be neglected even at 10^{10} GeV. If we postulate, following (6) the validity of scaling at such energies, the primary energy near 10^{11} GeV estimated from the Fly's eye could be underestimated by 30% without LPM correction.

5. Conclusion

LPM effect implies higher intensities near 10^6 GeV, estimated from direct measurements. The tendency of fig. 2 where Grigorov

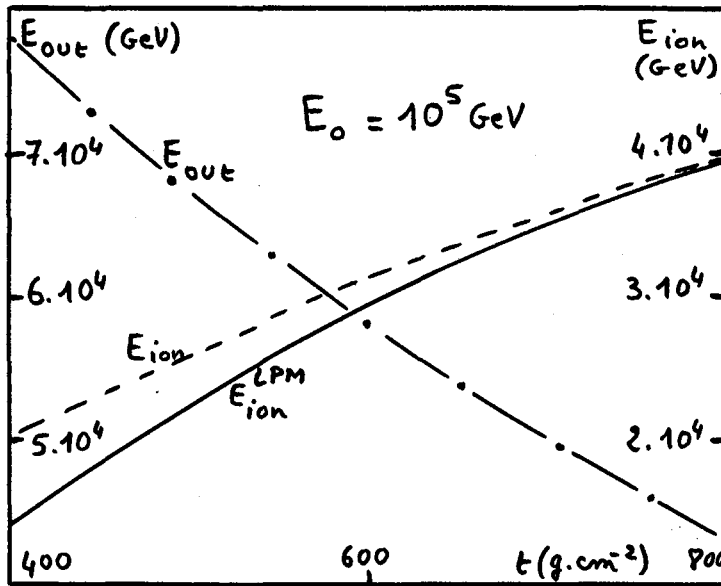


Fig. 1

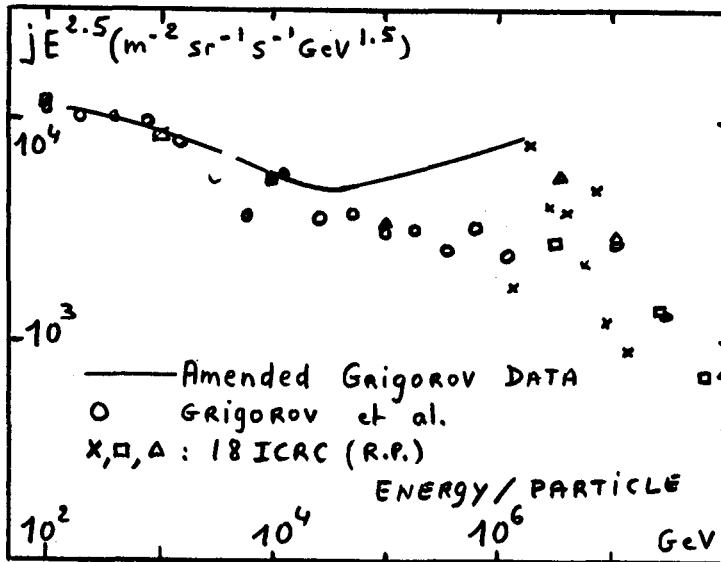


Fig. 2

amended spectrum is nearer of EAS data (7) could be stronger, if we consider in nuclear model the decrease of inelasticity with primary energy (HE 4.1-9,10). In atmosphere, it's difficult to know at present if scaling model is valid at so high energy, but we have considered here at least, the extremal distorsion due to LPM.

References

1. Bourdeau M.F. et al., 1981, J.Phys. G7, 1571.
2. Misaki A. et al., 1981, 17th ICRC, Paris, 5, 162.
3. Amineva T.P. et al., 1984, Proc.Symp.Cosmic Rays and Particle Physics, Tokyo, 420.
4. Bourdeau et al., 1977, Proc. 15th ICRC, Plovdiv, 15, 133.
5. Capdevielle J.N. et al., 1981, Proc. 17th ICRC, Paris, 6, 66.
6. Linsley J. et al., 1981, Phys.Rev.Lett. 46, 459.
7. Wdowczyk J., 1984, 9th ECRS, Kosice

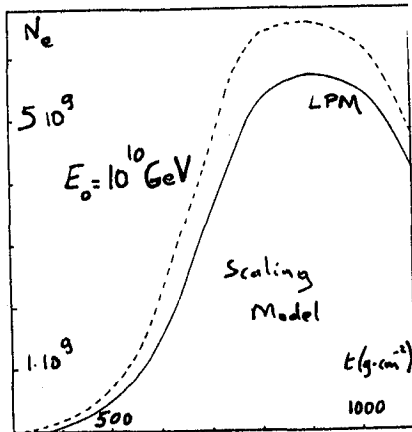


Fig. 3

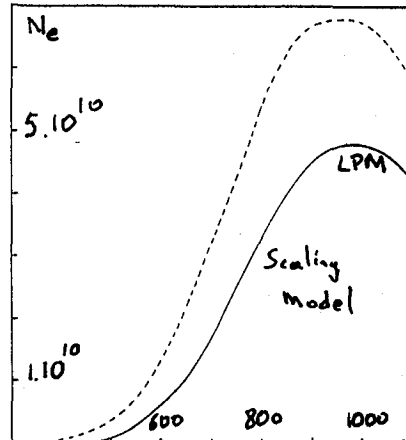


Fig. 4

EXPERIMENTAL BASIS FOR THE MODELS OF CASCADE PROPAGATION IN
ATMOSPHERE

Strugalski Z.

Institute of Physics of the Warsaw Technical University
ul. Koszykowa 75
00-662 Warsaw, Poland
and

Joint Institute for Nuclear Research, High Energy Labor.
Dubna, USSR

ABSTRACT

The picture of the hadron-nucleus collision process is presented as emerged on the basis of newly obtained experimental data. The picture is applicable for models of cascade propagation in Earth atmosphere.

1. Introduction

Results from studies of cascades and of their propagation in the Earth atmosphere form a basis for our knowledge about ultra-high energy cosmic ray particles; these results are fundamental for the cosmic ray astrophysics as well. But, the knowledge about the cascade propagation in a medium rests on the information about the hadron-nucleon, hadron-nucleus, and nucleus-nucleus collision processes first of all.

Now, various models of the hadron-nucleon and hadron-nucleus collision processes, and of the particle-producing reactions in them, are in use, based on different almost arbitrarily introduced physical processes assumed. The assumptions do not correspond in many cases to the reality - they are inadequate. The question: "Is an assumption adequate or not?" should find its answer primarily in experiments.

We have studied experimentally the hadron-nucleus collisions at the conditions when the reaction outcome was almost totally identified, Strugalski Z. et al. (1981 a, b; 1982 a - c; 1983 a - e); experimental data have been obtained as well on the hadron-nucleon collision processes in their initial stages - before decays of produced resonances, using massive target nuclei as detectors, Strugalski Z. (1981 a,b; 1982; 1984 a-d; 1985). The results are crucial for any model of the hadron-nucleon, hadron-nucleus, and nucleus-nucleus collisions and, therefore, for a more adequate model of the cascade propagation in media - in the Earth atmosphere in particular.

2. Experimental procedure

In experiments, the 26 and 180 litre xenon bubble chambers, Kanarek T. et al. (1959), Kuznetsov E. V. et al. (1970), were used. The smaller chamber was exposed to beams of pions with 2.34, 5, and 9 GeV/c momentum from the synchrophasotron of the Joint Institute for Nuclear Research in Dubna; the bigger chamber was exposed to pion beam at 3.5 GeV/c momentum from the accelerator of the Institute of Experimental and Theoretical Physics in Moscow.

General experimental information about the pion-xenon nucleus collisions is contained in series of Communications of the JINR: Strugalski Z. et al. (1981, 1982, 1983, 1984, 1985). Additional appropriate information has been found in various emulsion works: Andersson B. et al. (1978), Babecki J. and Nowak G. (1978), Bannik B.P. et al. (1980), Gurtu A. et al. (1979), Meyer H. et al. (1963), Otterlund I. et al. (1978), Tsai-Chü et al. (1977), Winzeler H. (1965); the accelerator data there are at energies up to about 400 GeV in the lab, the cosmic ray data are up to a few thousands GeV.

3. Results

Four main phenomena are usually observed, when hadrons collide with atomic nuclei: a) The emission of nucleons with energies from about 20 up to about 400 MeV; b) The production of particles; c) The evaporation of target fragments; d) The fission of residual target nucleus.

3.1. Nucleon Emission. Any hadron with kinetic energy higher than the pion production threshold may pass through some layer of nuclear matter before to come into particle-producing reaction in it; there are events in which incident hadrons with energies of a few GeV traverse nuclei or are stopped in them without causing particle production. In any case, are the particles produced or not, any hadron causes emission of nucleons in passing through atomic nucleus. The number n_N of the emitted nucleons equals the number of nucleons contained within the volume $v = \pi D_0^2 \lambda$ centered on the hadron path λ in nuclear matter, where D_0 is the diameter of the nucleon. The particle production process does not effect an influence on the nucleon emission.

Any hadron loses its kinetic energy monotonically along its path in nuclear matter, by nucleon emission. Energy spectra and angular distributions of emitted nucleons are practically the same in pion-xenon nucleus collisions with and without particle production; they do not depend neither on the multiplicity of emitted protons nor on the multiplicity of produced pions. The spectra and distributions are the same for pion-xenon collisions at 3.5 GeV/c momentum and for the proton-nucleus collisions in emulsions at 400 GeV/c.

3.2. Particle Production. Particles are produced via intermediate objects, we have called them "generons", created firstly in $2 \rightarrow 2$ type endoergic reactions and decay-

ing after the lifetimes $\tau \approx 10^{-22}$ s into particles and resonances. Generons behave themselves in passage through nuclear matter as usual hadrons do it - in particular, they can produce new generons in colliding with the downstream nucleons. A quasilinear cascade of generons may develop in nuclear matter, therefore. This way, the outcomes in hadron-nucleus collisions at an energy E are the compositions of m outcomes in hadron-nucleon collisions at energies in average E/m , where m is the number of particle-producing collisions of the incident hadron.

The nucleon emission process does not depend on the particle production process. The region of the particle production process in the target nucleus is not larger than the region of the nucleon emission, therefore; it is rather almost linear and situated collinearly with the incident hadron course in predominant number of collisions.

3.3. Evaporation of Target Fragments. Relation between the multiplicity of the emitted protons and the mean multiplicity of the charged fragments in collisions with a given proton multiplicity allows to determine the size and localization of the fragment evaporation region, Strugalski Z. (1984). Nuclear fragments are evaporated from the surface of the damaged part of the target nucleus; the damage is due to the nucleon emission process accompanying the passage of any hadron through nuclear matter.

3.4. Fission of the Residual Target Nucleus. In any hadron-nucleus collision the target nucleus is damaged, and relatively large part of it is removed, as it may be concluded from experimental results on the nucleon emission and target fragment evaporation. Obviously, such damaged nucleus is instable and it must decay into stable smaller nuclei in the final state.

More information about the experimental picture of the hadron-nucleus and hadron-nucleon collision processes can be found in series of works: Strugalski Z. (1982, 1984, 1985).

References

- Andersson B. et al., 1978, Phys. Lett., 73B, 343.
 Babecki J. et al., 1978, Acta Phys. Polon., B142, 445.
 Bannik B.P., 1980, Comm. JINR, Dubna, R1-13055.
 Gurtu A. et al., Pramana, 3, 311.
 Meyer H. et al., 1963, Nuovo Cim., 28, 1399.
 Otterlund I. et al., 1978, Nucl. Phys., B142, 445.
 Strugalski Z. et al., Comm. JINR, Dubna: 1982, a) E1-82-718, b) E1-82-719, c) E1-82-841; 1983, a) R1-83-68, b) R1-83-237, c) R1-83-564, d) R1-83-568, e) R1-83-234.
 Strugalski Z. Communications JINR, Dubna: 1981 a) E1-81-576, b) E1-81-577; 1982, a) E1-82-718, b) E1-82-719, c) E1-82-841; 1983, a) E1-83-155, b) E1-83-850; 1984, a) E1-84-195, b) E1-84-268, c) E1-84-853, d) E1-84-854; 1985, E1-85-231.
 Tsai-Chü et al., 1977, Nuovo Cim. Lett., 20, 257.
 Winzeler H., 1965, Nuclear Phys., 69, 661.

RELATION BETWEEN GAMMA-RAY FAMILY AND EAS CORE
- MONTE-CARLO SIMULATION OF EAS CORE -

Tomotake YANAGITA
Takakura-cho 5-4-301, Nishinomiya, 662 JAPAN

ABSTRACT

Preliminary results of Monte-Carlo simulation on EAS($N_e=10^5$) core is reported. As the first collision at the top of atmosphere, high multiplicity (high rapidity density) and large Pt (1.5GeV average) model is assumed. The most of the simulated cores show complicated structure.

1. Introduction. Several simulation studies on the EAS core structure were performed previously(Ref.1). Although various models or assumptions (fire ball, CKP, heavy primary or energy dependent Pt etc.) were tested in these works, the prominent frequency of the multi- or complicated core structure has not been simulated.

Recently, in the direct and pseudo-direct observation of nuclear interaction by EC (JACEE and CONCORDE, Ref.2, 3), very high multiplicity (high rapidity density) and comparatively large transverse momenta events were detected. The feature of these events gives us a motive for another EAS core simulation. We performed the core simulation taking these interaction feature in the simple model.

2. Simulation. The final output of the simulation calculation is the electron density map. We postulate 16×10 of packed array consist of 50×50 cm² density detectors, then area is 40 m² which is similar to the Norikura Spark Chamber Array(Ref.4).

The first collision depth (hereafter it is abbreviated as Z_0) is not sampled randomly, but is fixed to 10, 50 and 100 g/cm². The nuclear cascade is traced to observation depth(750g/cm²) and the gamma-rays produced through neutral pion decay are filed (x,y,z-coordinate, directional cosine and the energy). From the gamma-ray file the core density map is generated superposing each electromagnetic cascade. As the electron lateral distribution function of the electromagnetic cascade, the NKG-formula is used.

Tracing the nuclear cascade, only the forward region in the rapidity space is concerned but the central and backward regions are neglected in each interaction.

Model and Postulate for the first interaction :

- survival particles are not in concern
- total energy of produced particles is fixed to 600TeV.
- multiplicity of charged hadrons is fixed to 20.
- multiplicity of neutral pion is fixed to 10.
- production energy spectrum is exponential type.
- transverse momentum distribution is $\exp(-Pt/P_0)$,
 $P_0 = 1.5$ GeV/c

Other Interaction :

- collision mean free path is 90 g/cm².

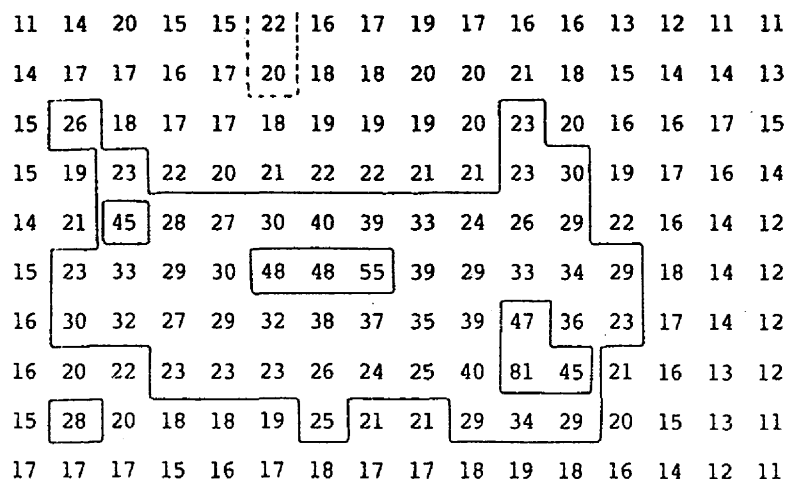
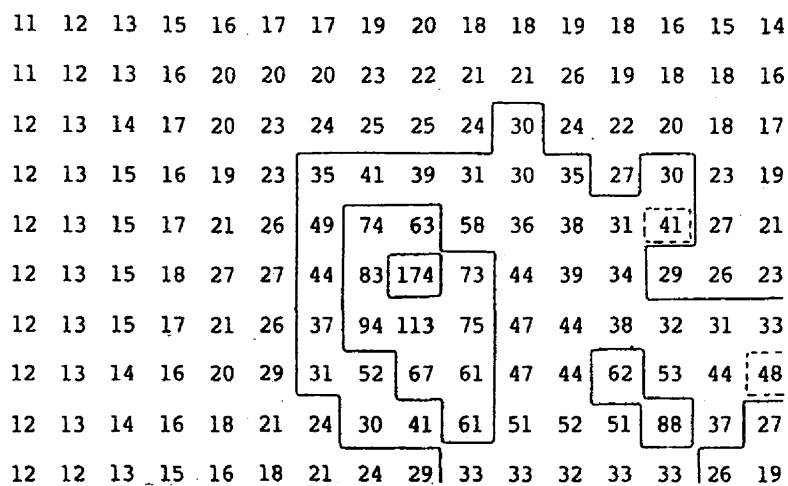
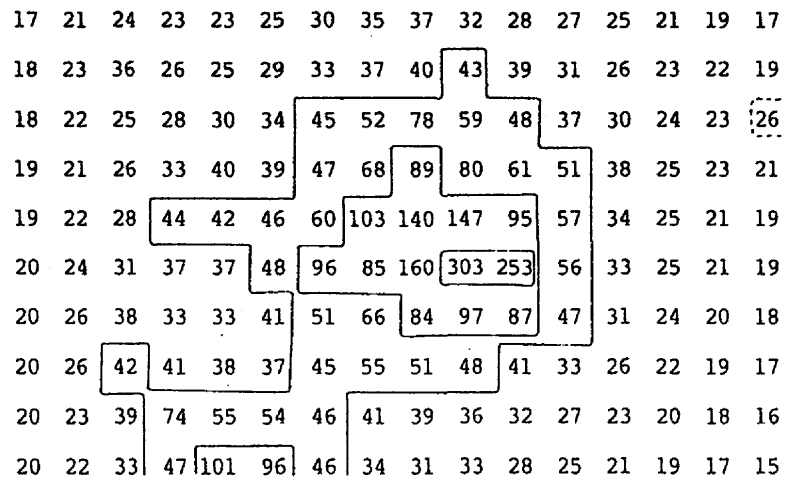
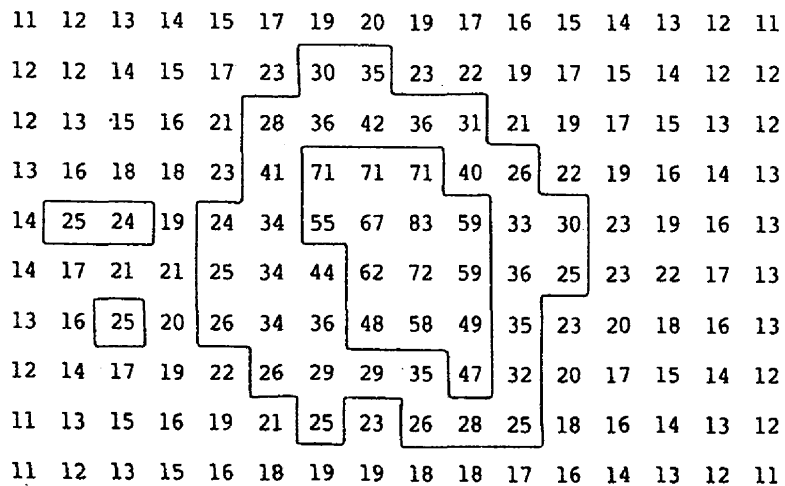


Fig.1-a,b,c,d. Core density maps for $Z_0=10\text{g/cm}^2$. One of the most simple example is in (a). Typical complicated examples are in (b), (c) and (d).

(a) (b)
 (c) (d)

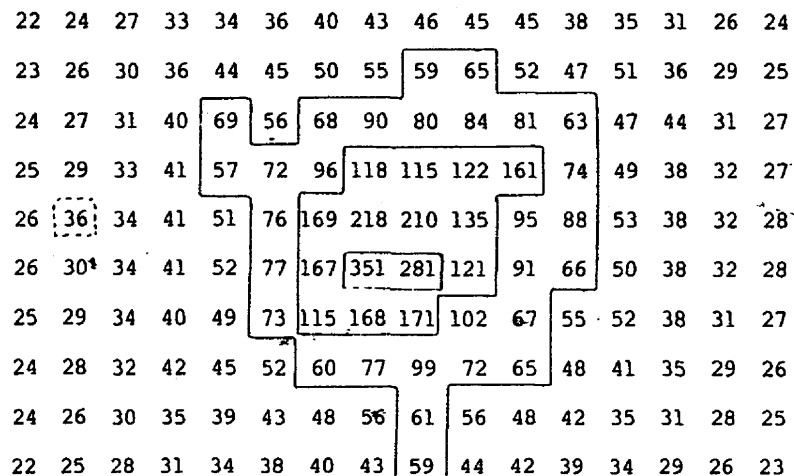
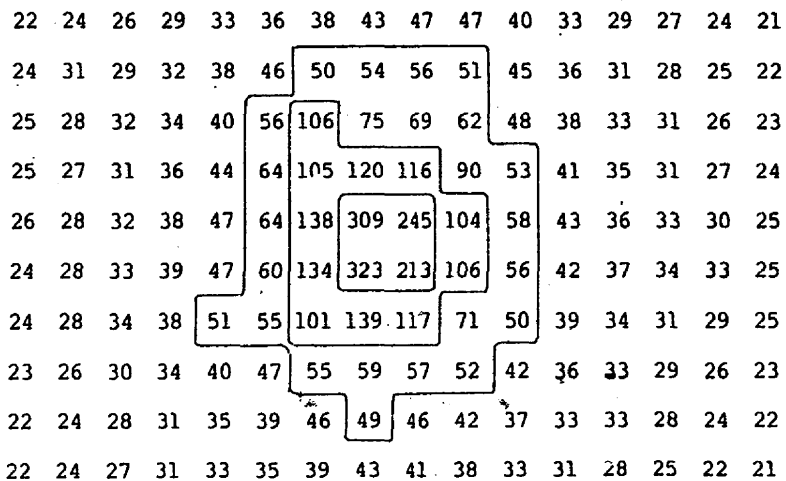
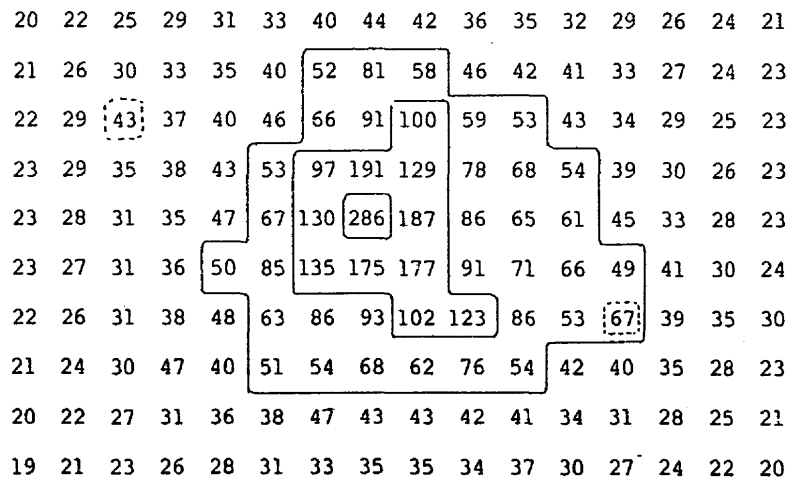
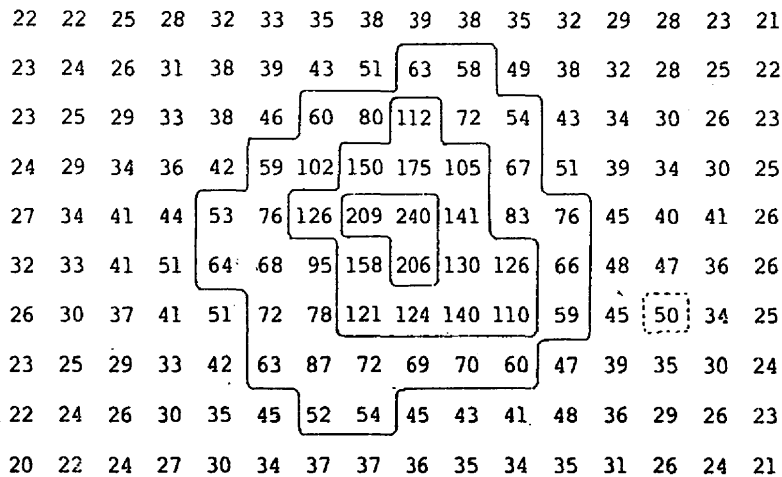


Fig.1-e,f. Core density maps for $Z_o=50g/cm^2$.
 Fig.1-g,h. Core density maps for $Z_o=100g/cm^2$.

(e)	(f)
(g)	(h)

inelasticity is uniform distribution of 0-1.
multiplicity is fixed to 9 and 1/3 of these are pi-zero.
production energy spectrum is exponential type.
transverse momentum distribution is $\exp(-P_t/P_m)$,
 $P_m = 0.4 \text{ GeV}/c$.

Decay of hadrons were not concerned except neutral pion.
Atmosphere is isothermal and the scale height is 7.0 km.

3. Results. In the case of $Z_0=10\text{g}/\text{cm}^2$, almost 50 percent of the cores have multi- and/or complicated structure. On the other hand, scarce cores (10 or less percents) have complicated structure, when $Z_0=50$ and $100\text{g}/\text{cm}^2$.

In Fig.1, typical examples of the core map are presented. The contour lines in the maps are drawn at the densities of (average density of the 16×10 detectors) $\times 2^n$, where $n=0, 1$, and so on. Small sub-peaks are marked by the broken line.

Even in the most simple structured cores, we can find some small scale sub-peaks in the case of $Z_0=10\text{g}/\text{cm}^2$. There is no examples having well separated multi-core, when $Z_0=50$ and $100\text{g}/\text{cm}^2$.

4. Discussion and Concluding Remarks. Multi-cored EAS was observed at the prominent rate at a mountain altitude (Ref.4). And, the balloon and airplane born EC detected gamma-ray families with large multiplicity, high rapidity density and large transverse momentum. And in the JACEE events the projectiles are identified to He and heavier nuclei.

Our simulation results indicate that these phenomena are closely connected. It can be said that the interaction feature like the gamma-ray families mentioned above and the sufficiently high first interaction point can produce multi-cored EAS at the prominent rate, but steep and simple structured cores scarcely.

References:

1. Ogita, N. et al. Canad. J. Phys., Vol.46, (1968)S164.
Thielheim, K.O. et al. Acta Physica 29, Supl.3(1970)519.
Dake, S. et al. Contribution to Workshop on Cosmic Ray and High Energy Gamma Ray Experiments for the Space Station Era, Baton Rouge (1984), and ICR-Report=121-85-2, University of Tokyo, (1985).
2. Burnett, T.H. et al.
3. Iwai, J. et al. Nuovo Cimento A, Vol.69, (1982)295.
4. Kino, S. et al. Rproc. ICCR, Vol.8, EA(1977)79.
Sasaki, H. et al. Proc. ICCR, Vol.8 EA(1979)190.
5. Nakatsuka, T. et al. proc.ICCR, Vol.11, (1981)326.

COMPARISON OF BIG EVENT WITH CALCULATIONS
OF THE AIR SHOWER DEVELOPMENT

Niwa, M., Misaki, A. and Matano, T.

Department of Physics, Saitama University,
338 Urawa, Japan

Honda, K., Tsushima, I., Kawasumi, N. and Hashimoto, K.

Department of Physics, Yamanashi University,
400 Kofu, Japan

ABSTRACT

We calculate high energy hadrons and electron-photons in air showers at various stages of developments.

We use the numerical calculation for solving the diffusion equation for nuclear cascade following Dedenko and the analytical calculation for cascade shower induced gamma rays. From these calculation, we can get the longitudinal development of high energy hadron and electron-photon component, and energy spectra of these components at various depth of air shower development. The total number of hadron (N_H) and electron-photon component (N_γ) are related according to stages of air shower development and primary energy as shown in Fig.1. From such a figure, we can understand the relation between both components. We can show the relation of the total energy of hadron and electron-photon component above the threshold energy as Fig.2. The energy balance between both components is also useful parameter to study high energy events accompanying air showers. The relation of N_H and fractional hadronic energy ($\Sigma E_H^r / (\Sigma E_H^r + \Sigma E_\gamma^r)$) is calculated like Fig.3. This relation is helpful to understand the stage of air shower development (t) and primary energy (E_P).

These calculations has been done and compared with experimental results, especially Big event.

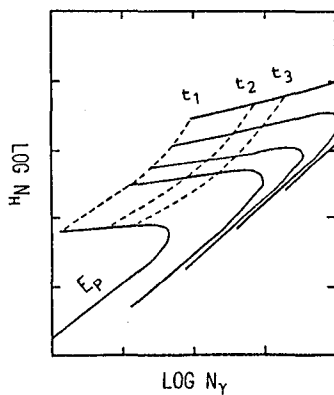


Fig.1

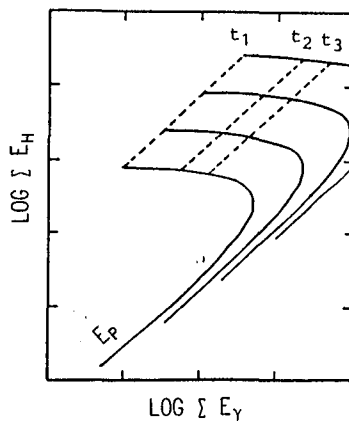


Fig.2

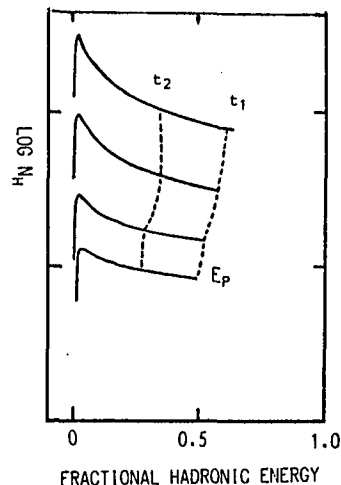


Fig.3

THE LATERAL DISTRIBUTIONS OF CHARGED PARTICLES OF ENERGY
GREATER THAN $0.3 E_{crit}$ IN ELECTRON-PHOTON CASCADES
IN LEAD AND AIR

A. Wasilewski^x, E. Kryś^{xx}

^xInstitute of Nuclear Studies, Łódź, Poland

^{xx}University of Łódź, Phys. Department, Łódź, Poland

In the recent investigations, both theoretical and experimental, the disagreement between cascade theory and experimental data is pointed out. In the present paper the radial distributions obtained from the Monte-Carlo simulations are compared with the well known results of the analytical theory for all particles in cascades. In the paper the data on mean radius of the electron lateral distribution in air are compared with those in lead.

Lateral development of the electromagnetic cascades

In order to study the three dimensional behaviour of electromagnetic cascades, our simulation was made for the cascades initiated at the top of atmosphere and at a depth of 712 g/cm² for different energies. It shows, that the lateral distributions of particles are narrower than the NKG distributions with an age parameter describing the longitudinal development of the cascades /6,7/. We also found that the initiating point of the cascade development has an effect on the width of the electron lateral distribution. It appeared that the width of the distribution is determined by the density of the atmosphere at so-called effective height above the considered level and this gives the possibility of removing the differences in the shape of distributions for different starting points of the cascades. The effective height was estimated as equal to 2 cascade units. The investigation of the effect of primary particle energy on the width of the electron lateral distribution shows that the mean distance of particles from the cascade axis corrected for the density effect increases with primary particle energy. Basing on our simulations we have approximated the electron lateral distribution by a simple formula:

$$\rho(x) = C(s, z) \cdot X_1^{s+0.5 \cdot z-2} \cdot (1+X_1)^{z-5.3}$$

where: $x=r/r_0$; $X_1 = x \cdot \eta(t-2) / (m \cdot \eta(t))$; $m=0.8-0.2 \cdot s$

r - the distance from the cascade axis ;

r_0 - the Molier unit ; C - the normalization param.,

$\eta(t), \eta(t-2)$ - the density of air for the observation level, the density 2 c.u. above the observation level

$$s = \frac{3t}{t+2\ln(E_0/\epsilon_k)} \quad z = \frac{3(t-2)}{(t-2)+2\ln(E_0/\epsilon_k)}$$

From that formula we derived the value of so-called the local age parameter for different distances from the cascade axis. The local age parameter is defined as the age parameter obtained from the NKG formulae on the basis of particle density at two distances from the axis. The result is shown

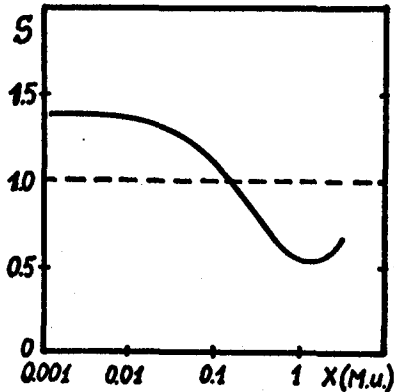


Fig.1 The value of the local age parameter as a function of distance X from the cascade axis: solid line - our approximation, broken line - the age parameter describing the longitudinal development. The ratio of electron densities at distances from the axis X_{i-1} and X_i where $X_i = X$, $\lg X_{i-1}/X_i$ was taken.

in Fig.1. This analysis shows that the local age parameter changes from a value clearly greater than the NKG age parameter at small distances to significantly lower one at distances greater than the 0.1 Molier unit. It means that the method of describing the lateral distributions of electrons by the NKG function with one parameter can lead to different results depending on the distances at which this parameter is estimated.

The comparison of simulation of the electromagnetic cascades with the other results

In this part we compare our approximation with those proposed by Nishimura-Kamata/1/, Greisen/2/, Hillas/4/ and Uchaikin/5/.

The comparison of the mean distances of particles from the cascade axis obtained from our results with the Hillas ones is shown in Fig.2a. Comparison of the analytical results

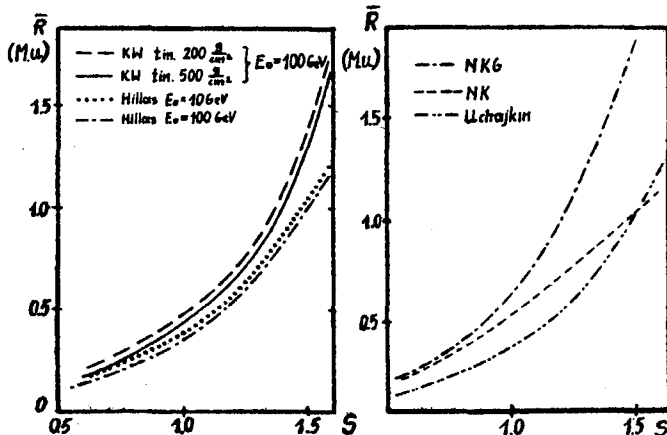


Fig.2 The mean distances of electrons from the cascade axis as a function of age parameter s .

for the same stage of the cascade development /NKG, NK and Uchaikin formulae / is shown in Fig.2b. Thus it is seen that reconstruction of such parameters as age parameter and number of particles on the basis of the proposed lateral distributions cannot give the same results.

The comparison of the relative numbers of particles at small distances from the cascades axis for two different stages of the cascade development with the Hillas, NKG, NK and Uchaikin formulae is shown in Fig.3

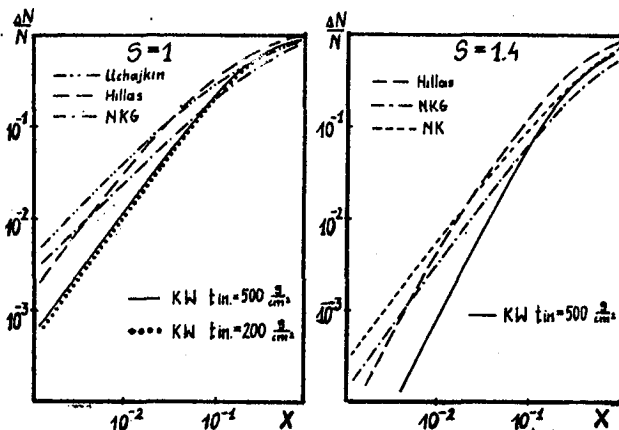


Fig.3 The relative numbers of electrons as a function of X

The present situation is such that near the axis the evident differences between the curves exist. These deviations have significant consequences for the experimental investigations. For instance, that flat distributions of electrons at small distances from the axis would lead to underestimation of the energy in subcores in EAS.

The comparison of simulation of the electromagnetic cascades with various energy threshold in different absorbers.

In simulations of the electromagnetic cascades the lateral distributions were obtained for various energy thresholds. The comparison of the mean distances of particles with threshold $30 m_{ec}^2$ and $60 m_{ec}^2$ in cascade initiated by primary photon of energy 50 GeV in air as a function of age parameter is shown in Fig.4. In lead, the mean distances of particles with the similar value of ratio E_{thr}/E_{crit} is also shown / $E_{thr}=4 m_{ec}^2$ / in Fig.4. for cascades initiated by primary photons of energy 10 GeV /for this energy the LPM effect does not play any role/ the mean distances of particles are compared in Molier units. It can be seen that there is a good agreement between the values of mean distances of particles obtained from the simulation in very differing absorbers - lead and air. It is demonstrated that the mean radii of the lateral distributions in lead can be obtained from those in air, if the same ratio of the threshold energy to the critical energy is taken.

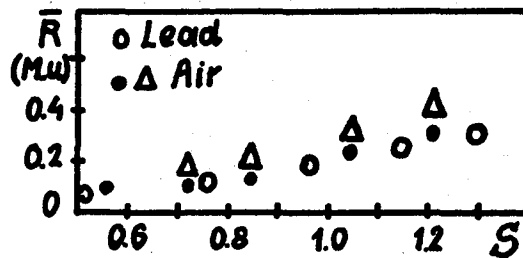


Fig.4 The mean distances of electrons with threshold $30 m_e c^2$ and $60 m_e c^2$ in air and $4 m_e c^2$ in lead for cascades initiated by primary photons of energy 50 GeV at the depth $712 g/cm^2$ in air and 10 GeV in lead.

Conclusions

The method applied in EAS research for estimation of parameters / i.e. age parameter and a number of particles / is based on assumption that the lateral distributions of particles in air showers are of the same type as in the electromagnetic cascades. The lateral distributions are always reconstructed by fitting the NKG function to the experimentally measured densities of particles at several distances from the shower axis. The signalized incoherences in EAS research / 8 / i.e. change of the age parameter with distances can be explained as a results of applying the incorrect formula / NKG ones /. This effect may be still better visible for higher energy threshold of secondary particles.

The formula proposed by us though not so easy for direct use in EAS research explain the discrepancies between experimental data and NKG formula, for instance the change of age parameter with distance.

The present results show that the applied Monte - Carlo method for significantly different absorbers seems to be good.

Acknowledgments

We would like to express the sincere thanks to Prof. J.Wdowczyk from the Institute of Nuclear Studies for helpful discussions.

References

- /1/ Kamata.K, Nishimura J., Suppl.Prog.Theor.Phys. 6, 93, 1958
- /2/ Greisen K, Progress of Cosmic Ray Physics, 1956
- /3/ Allan H., XIV ICRC, Munich, 6, 3071, 1975
- /4/ Hillas A.M., Lapikens J., XV ICRC, Plovdiv, 8, 460, 1977
- /5/ Uchaikin V.V., XVI ICRC, Kyoto, 7, 1979
- /6/ Kryś E., Wasilewski A., IX ECRC, Kosice, 1984
- /7/ Kryś E., Acta Physics Polonica, v B16, 1985
- /8/ Miyake, XVII ICRC, Paris, 10, 1981

RESULT OF MONTE-CARLO SIMULATION OF ELECTRON-PHOTON
CASCADES IN LEAD AND LAYERS OF LEAD-SCINTILLATOR

A. Wasilewski^X, E. Kryś^{XX}

^XInstitute of Nuclear Studies, Łódź, Poland

^{XX}University of Łódź, Phys. Department, Łódź, Poland

Results of Monte-Carlo simulation of electromagnetic cascade development in lead and lead-scintillator sandwiches are analysed. It is demonstrated, that the structure function for "core approximation" is not applicable in the case in which the primary energy is higher than 100 GeV. The simulation data has shown that introduced inhomogeneous structure of chamber gives subsequent reduction of secondary particles.

Introduction.

In this paper we present results of detailed simulations, including the LPM effect, of electromagnetic cascades in lead and lead-scintillator sandwiches which are often used in emulsion chamber experiments. The following processes were taken into account in calculations: pair production, bremsstrahlung including LPM effect with energy dependent cross - sections /Fig.1/, ionisations loss, Compton effect, single and multiple Coulomb scattering, the electron and positron inelastic scattering, photoelectric effect, annihilation of the positron.

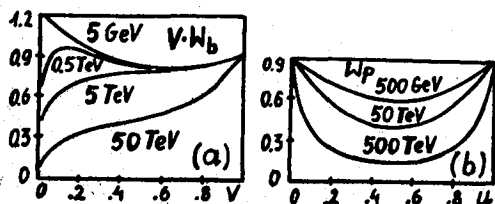


Fig.1.a The product of differential cross-section of bremsstrahlung and v , where $v = E/E_0$.
b The differential cross-section of pair production, where $u = E/E_0$.

The simulations were performed:

- in lead, for primary photons of energy 100 GeV, 10 TeV and 100 TeV and for primary electrons of energy 100 GeV,
- in sandwiches of lead and scintillator: for primary electrons of energy 100 GeV /Tab.1, No.1/, primary photons of energy 10 TeV and 100 TeV /Tab.1, No.2/.

absorber		Pb	Sc	Pb	Sc	Pb	Sc	Pb	Sc	Pb	Pb
thickness of	1	1	.5	.5	.5	.5	.5	.5	.5	.5	.5
aborb. /cm/	2	4	2	1	2	1	90	3	2	1	1

Tab.1 The structure of chambers investigated in our simulation. No.1: this sandwich is similar to that used in FNAL experiment [1]. No.2: this one is similar to the big gamma-hadron detector used in cosmic rays research /for instance Pamir Collaboration [2] /.

General procedure was following. All particles with energies exceeding certain value of $k = E_0/E_k$ were followed individually. Particles below E_k down to the threshold energy were followed using the so-called "thinning" method. The value of k

was usually taken to be 1000 or 100 and the threshold energy was $2 m_{ec}^2$.

Longitudinal and lateral development of the electromagnetic cascades

In the emulsion chamber technique, the energy of an incoming electron or photon is measured by the behaviour of cascade showers near the shower axis. In "core approximation" it is assumed that the lateral structure functions depend on $E_0 r / K_s$ and s only and not of separate variables E_0 and r . In this paper we analyse validity of this statement for wide range of energies and for different structure of chambers. In Fig.2 one can see the transition curves for primary electrons and photons of energy 100 GeV for shower radii 100 μm together with the cascades obtained in chamber C1 of FNAL experiment.

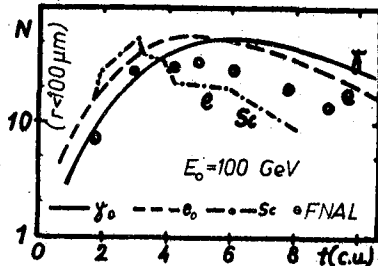


Fig.2 Cascades curves of electrons in photon and electron initiated showers for radius 100 μm .

Our results are presented separately for cascade passing only through lead and for cascades initiated in lead-scintillator /sandwich No.1/. As can be seen the introduced scintillator plays important role, giving subsequent reduction of secondary particle numbers. The transition curve obtained for sandwich's structure shows similar tendency as is seen in experiment, i.e. the smaller electron size than in pure lead chamber. We conclude that the agreement with experiment can be achieved by employing as an absorber in our simulations the precise structure of FNAL sandwiches.

Let's compare the shape of transition curves when the energy of primary particles increases.

In Fig.3a we present the transition curves with $E_{thr}=2m_{ec}^2$ for $E_0=10$ TeV and $E_0=100$ TeV for pure lead chamber and for sandwich No.2. Fig.3b gives the transition curves for "core approximation" i.e. for shower radius 100 μm and for the same primary energies of particles. For these cascades the LPM effect plays an important role in transition curves as the energy increases giving a deeper position of shower maximum and smaller size at maximum. In Fig.3 one can see that even primary photons of energy 10 TeV can penetrate through all chamber /sandwich No.2/. This effect is stronger when the primary energy of photon increases. The most of EAS experiments have one or more layers of carbon: this enhances the detector capability to discriminate hadrons from photons and electrons. The interesting results of the present simulations is that the number of particles after penetration of

the thick /90 cm/ scintillator and 3 cm lead increases if the lead follow this scintillator. Furthermore the numbers

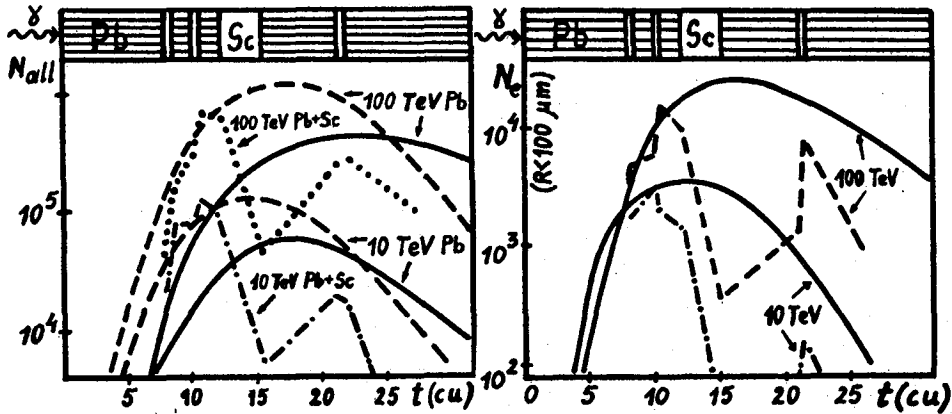


Fig. 3 Cascade curves of electrons in photon initiated shower.

- a. for all particles with threshold $2 m_{ec}^2$,
- b. the same threshold but in radius 100 μm .

of electrons after first 4-5 cm in lead is comparable with ones after 90 cm of scintillator and 3 cm of lead for primary photons of energy 100 TeV. A detailed simulation would be necessary to quantify this effect with respect to different experiment.

The comparison of the simulation transition curves for different energies shows that validity of statement "core approximation" for all range of energies and depths is not good - Fig.4 .

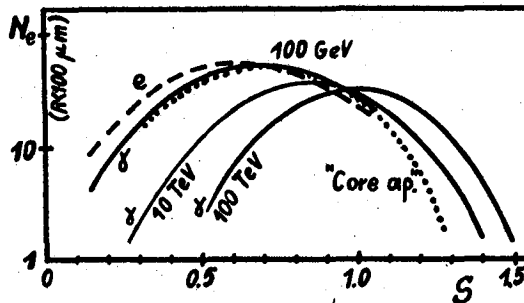


Fig.4 The transition curves of electrons obtained in our simulation /solid ones/ are compared with "core approximation" /the numbers of electrons for 10 TeV and 100 TeV are scaled to 100 GeV - i.e. divided by 100 and 1000 respectively/.

Our results show that applied "core approximation" for lower energies than 100 GeV is rather good, but for higher energies LPM effect makes this relation wrong.

On the basis of presented transition curves we estimated the energy of primary particle for different depths of development cascades according to "core approximation". It is

shown in Tab.2 . The value of energy determined from our data changes from a value lower than the energy of primary particle at low s to the value greater than ones at higher s . In the other words, our results show that the method of describing lateral distributions of electrons by "core approximation" leads to underestimation of the energy of the primary particle at low value of s and to overestimation at higher s .

	s	0.5	0.6	0.7	0.8	0.9	1.0	1.1	1.2	1.3	1.4
a	$t/cm/$	2.9	3.6	4.5	5.3	6.3	7.3	8.5	9.7	11.2	12.8
	$E_e/TeV/$	5.0	7.1	9.2	10.1	12.8	15.0	17.0	22.3	26.6	31.0
b	$t/cm/$	6.6	8.3	10.1	12.0	14.2	16.6	19.2	22.1	25.3	29.0
	$E_e/TeV/$	7.0	21.0	40.0	77.0	107.0	170.0	280.0	370.0	670.0	1000.

Tab.2 The comparison of the energy of primary photon estimated according to "core approximation".
The energy of primary photon is : a. 10 TeV and b. 100 TeV.

As one can see, these discrepancies depend on the depth of the observation level and on the primary energy of particles.

Conclusions

1. It was stated that inhomogeneous structure of chamber has an effect on the transition curves. It appeared that numbers of secondary particles / for constant radii and constant primary photon energy / is determined by thickness, the kind of absorbers and their place in sandwiches.
2. It is not possible to describe the lateral distributions of particles with "core approximation" independent of the primary particle energy because the LPM effect plays an important role in transition curves. The method of describing lateral distributions of electrons by the "core approximation" used in chamber experiments lead to underestimation of the primary photon energy at low values of s and overestimation at higher s .

Acknowledgements

We would like to express the sincere thanks to Prof. J. Wdowczyk from the Institute of Nuclear Studies for critical advise about various aspects of interpreting the data discussed here. Thanks are also due to dr J. A. Wrotniak for his informations about "thinning" method.

References

- [1] Hotta N et al., 1980 Phys.Rev.D 22 1
- [2] Trudy FIAN, v.154, Moskva 1984

ON 'MINI-CLUSTER' OBSERVED BY CHACALTAYA EMULSION CHAMBER EXPERIMENT

T. Tati

Otsuka 6-36-8, Bunkyo-ku, Tokyo 112, Japan

It is mentioned that the phenomena of 'Mini-Cluster' observed by Chacaltaya emulsion chamber experiment support the model of hadronic matter based on the theory of finite degree of freedom.

1. Introduction

The world of elementary particles has been more and more enlarged and diversified and, at the same time, unifying relations in it have gradually been established basing on the quantum field theory. In this case, the quantum field theory itself has been unchanged in its foundation, though basic fields and their interactions have been effectively selected. The quantum field theory gives divergent results showing that the theory is not completely defined. The difficulty is avoided for practical problems by choosing the renormalizable type of theories. Even in the renormalizable case, the theory contains an undefined part left to future theories. The renormalization theory evades the divergence difficulty by replacing arbitrarily the undefined divergent part by an appropriate finite constant and considers only things independent of details of the undefined part. We want to consider, however, the difficulty or inconsistency in the fundamental theory as a moment for deeper recognition of the existence of elementary particles.

The divergence difficulty is due to the infinite degree of freedom of the quantum field given by the set of all possible values of momentum or equivalently of position of the particle associated to the field. The quantum field with a finite degree of freedom is contradictory to the space-time description so that the theory of finite degree of freedom requires the reformation of the concept of space-time based on the non-space-time description³. The theory of finite degree of freedom suppresses the high momentum part of the degree of freedom referring to a universal timelike vector¹ and gives consequences for the part left undefined in the renormalization theory³.

The ultrahigh energy nuclear interactions have long been investigated by the emulsion chamber experiments of Brasil-Japan collaboration and Soviet group. They found various kinds of fireballs as intermediate states of multi-hadron productions^{4,5}. It is considered that the approach using phenomenological models is effective for the interpretation of fireball phenomena. In this case, when the models reflect a basic idea, its validity can be tested by experimental facts. The model of hadronic matter² of which hadrons are made based on the theory of finite degree of freedom seems to give a picture which explains qualitatively the characteristic properties of hadrons and hitherto found fireballs^{9,3}.

The hadronic matter is made mainly of a great number of virtual urbaryon pairs (quark pairs) generated by vacuum polarization. Due to the finite degree of freedom of urbaryon, it is an extended matter with a fairly uniform density and a volume generally proportional to its mass apart from individualities. Recently the Brasil-Japan collaboration observed bundles of electromagnetic showers with very small

transverse momenta (some 10 MeV) accompanied by decay products of Chiron-type fireballs (Chiron and Geminion)⁶. The bundle of electromagnetic showers is called 'Mini-Cluster'. It is mentioned in this paper that the phenomena of 'Mini-Cluster' support the picture of fireballs made of the hadronic matter based on the theory of finite degree of freedom.

2. A Picture of Hadrons and Fireballs made of the Hadronic Matter

The basic particle (urbaryon) of the hadronic matter is a bare quark q having color and flavor and obeying the theory of finite degree of freedom. 'bare' is to distinguish q from the physical quark Q ⁸ mentioned below but we call q simply quark in the following. The hadronic matter consists of a certain number of quarks carrying quantum numbers of the system and a large number of virtual quark pairs generated by vacuum polarization. The position degree of freedom of the field of basic particle distributes with a density $(1/v)$ in the hyperplane perpendicular to a universal timelike vector N_μ , that is, the space in the Lorentz system (we call N -system) in which $N_\mu = (1, 0, 0, 0)$. The relative velocity between the N -system and our laboratory system on the earth is considered some $10^{-3}c$ (c is the light velocity) on cosmological grounds so that our laboratory system is considered approximately the N -system for high energy phenomena³. The volume v is given by

$$(4\pi/3)K_1^3 v \approx (2\pi\hbar)^3,$$

when the effective cutoff of the momentum degree of freedom is K_1 . (The cutoff function should have a sufficiently long tail.)

Due to the Fermi statistics, only a finite number of quarks can occupy the volume v . This acts to extend the volume of the system and to make its density uniform. Hadronic matter is assumed to be a superposition of states confined with the maximum compactness so that the mass is, apart from individualities, e.g. vibrational excitations, in general given by

$$M \approx \wp V \approx \wp(n/f)v,$$

where \wp is the density being a constant, f is the number of quarks in v and, V and n are expectation values of the volume and the number of quarks of the system, respectively. The quantum field theory implies that the hadronic matter has its proper V and n for each quantum state. In a broad view, it is assumed that all colorless ground states (hadrons) have nearly the same V and n given by

$$V \approx V_N \approx (4\pi/3)(1/M_N)^3, \quad n \approx n_N \approx f(V_N/v),$$

where M_N is the nucleon mass. Hadron resonances are considered excited states of hadrons by surface vibrations.

We consider that there exists a free physical quark Q clothed in a cloud of virtual quark pairs like a physical electron in QED clothed in a cloud of virtual electron pairs. In our picture, when Q and anti Q combine to form a meson ($Q'\bar{Q}'$) (Q' represents a deformed physical quark in the hadron), hadronic matter of the volume $2V_Q - V_N$ should disappear. This corresponds to the binding energy

$$B \approx \wp(2V_Q - V_N) \approx 2M_Q - M_N,$$

where M_Q is the physical quark mass. Conversely, in order to decompose ($Q'\bar{Q}'$) into Q and \bar{Q} , we should produce hadronic matter of the volume $2V_Q - V_N$. The produced giant hadronic matter is, however, a colorless fireball which decays into hadrons. This is a limited color confinement in our picture. For definiteness and simplicity, we assume that all colored ground states have nearly the same V and n given by

$V \approx V_Q \approx 10 V_N$, $n \approx n_Q \approx 10 n_N$,
so that $M_Q \approx 10 M_N$.

The effective cutoff momentum K of hadronic matter of size n is given by

$$K \approx nK_1,$$

where K_1 is the effective cutoff momentum of the basic particle (quark). The production probability of hadronic matter is suppressed when the momentum surpasses its effective cutoff K , although it can be accelerated when it is stable, e.g. by an electromagnetic field, far beyond K due to a long tail of the cutoff function. The effective cutoff for the Lorentz factor is given by, in the N -system,

$$\Gamma \approx K/M \approx (nK_1)/(\rho n v) \approx (K_1/\rho v),$$

which is insensitive to the size of hadronic matter. Cosmic ray experiments seem to suggest that there exists an effective cutoff around $10^4 - 10^5$ for Lorentz factors of fireballs insensitive to their sizes. When we take $K_1 \approx 10 M_N$ (in this case, $n_N \approx 10^4$), we have $\Gamma \approx 10^5$.

Hitherto found fireballs are three kinds of ordinary fireballs H, SH and UH quanta having masses about 3 GeV, 30 GeV and 300 GeV, respectively, which decay mainly into pions and four kinds of exotic fireballs Mini-Centauro, Centauro, Geminion and Chiron, the decay products of which contain almost no pions. The masses of Mini-Centauro and Geminion are about 30 GeV and the masses of Centauro and Chiron are considered as being around 300 GeV.

We assume that the fireballs decay in accordance with the schema mentioned below and, in each step of decays, the sum of masses of decay products is about equal on an average to half of the mass of the decaying fireball. This scheme gives the right order of magnitude of multiplicity and transverse momenta of decay products characterizing each fireball.

H quantum decays into several pions. SH quantum decays into several H quanta. UH quantum decays into several SH quanta. Mini-Centauro decays into several nucleon pairs (NN)'s. Centauro decays into several Mini-Centauros. Geminion decays into a physical quark pair $Q\bar{Q}$ ⁸. Chiron decays into several Geminions.

In view of the model of hadronic matter, H, SH and UH quanta are the hadronic matter of the volume around V_N , $10 V_N$ and $100 V_N$, respectively. (H quantum is considered an excited state hadronic matter of $V \approx V_N$ by volume vibration. In this case, H quantum is not a superposition of hadron resonances.) Centauro and Mini-Centauro are interpreted as UH quantum and SH quantum, respectively, in which the production of the participating H quanta in their decays is suppressed due to that the momenta of the H quanta surpass their effective cutoff and, instead of each H quantum, a nucleon pair NN is produced for which the effective cutoff momentum is larger than that of H quantum⁷. Chiron is interpreted as UH quantum in which the production of the participating SH quanta in the decay is suppressed due to that the momenta of the SH quanta surpass their effective cutoff and, instead of each SH quantum, a physical quark pair $Q\bar{Q}$ is produced for which the effective cutoff momentum is larger than that of SH quantum. The physical quark pair thus produced instead of a SH quantum is, regardless of whether the SH quantum belongs to decay products of a larger fireball or not, considered to be a Geminion.

3. 'Mini-Cluster'

The decay products of exotic fireballs have definite nuclear collision mean free paths so that they are considered to be

indestructible. In our picture, the decay products of Centauro type and Chiron type fireballs are nucleons and physical quarks, respectively. In this case, in order to produce physical quarks in the $p\bar{p}$ collider interaction, the colliding particles should have at least $\Gamma M_{\text{CH}} \approx 10^6$ GeV which is far beyond the present collider energies¹⁰. The observed collision mean free path of the decay product of Chiron type fireballs is considerably short compared with that of the nucleon. This fact is in accord with our model, since the physical quark is an indestructible hadronic matter of the volume much larger than that of the nucleon.

Owing to that the nuclear matter is a fairly homogeneous many body system, the liquid drop model is applied to heavy nuclei and the excitations being considered due to surface vibrations are observed. The hadronic matter in our picture is also a fairly homogeneous many body system so that the excitations due to surface vibrations should be observed. We consider that the hadron resonances are due to surface vibrations. The surface vibration of the physical quark should also have observable effects.

The frequencies of stationary surface waves of liquid drop is¹¹

$$\omega_\ell = [(4\pi\epsilon/3M_d)\ell(\ell-1)(\ell+2)]^{1/2}, \quad \ell = 2, 3, \dots,$$

where ϵ is the surface energy per unit area and M_d the mass of the drop. When ϵ is assumed to be the same for all hadronic matter and M_Q is taken to be 10 GeV, the ratio $\hbar\omega_\ell(Q)/\hbar\omega_\ell(N)$ of the quantum $\hbar\omega_\ell$ for the physical quark to that for the nucleon is about 1/3. In our picture, $\hbar\omega_\ell(N)$ is the spacing of hadron resonances for $\Delta J = 2$ and is about 500 MeV. Then $\hbar\omega_\ell(Q)$ turns out to be about the pion mass. In view of the oversimplification of our model, it is possible that $\hbar\omega_\ell(Q)$ is considerably smaller than the pion mass, e.g. some 10 MeV. In this case, the n quantum excited state of surface vibration of the physical quark, $E_n = n\hbar\omega_\ell(Q)$, decays emitting n photons of energy $\hbar\omega_\ell(Q)$. The transition probability per unit time for the γ emission of the liquid drop is given by¹¹

$$(\Gamma_\gamma/\hbar) = (1/4)[\omega_\ell(Q)/c]^5[QM]^2/\hbar,$$

where $[QM]$ is the quadrupole moment of the emitting system. The quark is considered to move fairly freely in its massive neutral clothes of virtual pairs. (For the hadronic matter, just as heavy nuclei, the liquid drop model and the degenerate Fermi gas model are considered valid for collective motions and individual particle motions, respectively.) Then the life time of the γ emission of the physical quark is estimated to be around 10^{-12} sec. (Γ_γ is the γ ray width.)

Thus we consider that the recently observed 'Mini-Cluster' accompanied by a decay product of the Chiron type fireballs is due to the surface vibration of the physical quark and accordingly supports the model of hadronic matter based on the theory of finite degree of freedom.

- 1 T. Tati, Prog. Theor. Phys. 24 (1960), 1.
- 2 T. Tati, Prog. Theor. Phys. 43 (1970), 1596.
- 3 T. Tati, Prog. Theor. Phys. Suppl. No. 76 (1983), 186.
- 4 C.M.G. Lattes et al., Phys. Rep. 65 (1980), 152.
- 5 Brasil-Japan EC Collab., Proc. 17th ICRC 11 (1981), 100.
- 6 Brasil-Japan EC Collab., Proc. 18th ICRC 11 (1983), 77.
- 7 T. Tati, Proc. 13th ICRC 3 (1973), 2311.
- 8 T. Tati, Proc. 16th ICRC 7 (1979), 367.
- 9 T. Tati, Proc. 17th ICRC 5 (1981), 356.
- 10 T. Tati, Proc. 18th ICRC 5 (1983), 495.
- 11 H.A. Bethe, Rev. Mod. Phys. 9 (1937), 69.

A COMPARATIVE ANALYSIS OF GAMMA AND HADRON
FAMILIES AT THE SUPERHIGH ENERGIES RECORDED
IN EXPERIMENT "PAMIR"

Azimov S.A., Mulladjanov E.J., Nosov A.N., Nuritdinov H.
Talipov D.A., Halilov D.A., Yuldashbaev T.S.

Physical-Technical Institute of Academy of
Sciences of the Uzbek SSR, USSR

In the paper a comparative analysis of hadron and gamma families were undergone the decascading procedure is made. Receive results are compared with different models of interactions. In hadron families with energies $\sum E_{\gamma}^n > 20$ TeV as well as in gamma families with energies $\sum E_{\gamma} > 70$ TeV increasing azimuthal anizotropy in events with large ER is observed.

INTRODUCTION

It's of interest compare different characteristics of the gamma and hadron families at superhight energies. However, electromagnetic multiplication of the initial γ -quanta in the atmosphere has a great influence on observed characteristics of the γ -families decreasing sensitiveness these characteristics (especially longitudinal) to different models of strong interaction. Hadron families characteristics are free the influence of those effects.

The decascading procedure suggested in /1/ allow to reduce essentially the influence of electromagnetic cascading multiplication of the initial γ -rays in the atmoaphere. All particles paires satisfied the condition $Z_{ik} < Z_0$ were combined in single group (initial quantum), where $Z_{ik} = R_{ik}(1/E_i + 1/E_k)^{-1}$, R_{ik} -the mutual distance of particle pair in mm, E_i , E_k -their energies in TeV. The decascading parameter was set equal to $Z_0 = 10$ TeV·mm. Thus the observed γ_0 -families are transformed in 0 the initial γ_i -family. The comparison characteristics of the hadron-families (h-families) with such γ_i -families is a more corred procedure than comporison with 0 observed families.

The experimental data about spatial characteristics of the γ_i and h-families compare with simulated families calculatedⁱ on different assumptions about mechanism of the strong interaction. Different assumptions about chemical composition of the primary cosmic radiation exert essential influence on the results of such analysis. Consequently, in the paper an new selecting criteria of γ -families are formed by primary nuclei or protons is proposed.

We considered such spatial characteristics as \bar{R} ($\bar{R} = \sum_{i=1}^{n_{\gamma}} R_i / n_{\gamma}$, R_i -distance of the γ -quanta from axis of family, n_{γ} -number particles of family) and α proposed in the

work /2/ for analyse the structure of the families.

$\alpha = \frac{\sum_{i \neq j}^n \text{Cos} 2\varepsilon_{ij}}{(n(n-1))}$, where ε_{ij} -the angle between the momentum projections of i-th and j-th particles in azimuthal XY-plane, perpendicular to the primary particles direction, n -number of particles in family.

The value α reaches magnitude $\alpha = 1$ for the completely complanar events and become minimal $\alpha_{\min} = -1/(n-1)$ in the case of an isotropic, uniform distribution of azimuthal angles.

I. The characteristics of the hadron and gamma families

To analyse the spatial structure of γ -families it is important to have more complete information about particles with large transverse momenta. Consequently it's were investigated the experiment "Pamir" data obtained under conditions when film scanning and particle selection were realised within the radius $R = 30$ sm relatively the energy weighted center of γ -family. In the result were selected $N=326$ γ -families with energies $\sum E_{\gamma} = 60+500$ TeV and number of particles $n_{\gamma} \gg 4$. The minimum energy of the γ -quants in the families was set $E_{\gamma} = 4$ TeV. Particle scanning and selection h-families were realised within the radius $R=30$ sm too. The minimum energy of the cascades in the h-families was set $E_{\gamma}^h = 4$ TeV. It were selected $N=181$ h-families with energies $E_{\gamma}^h = 20+500$ TeV.

At the analysis of the hadron families on record by "Pamir" carbon chamber, it is necessary to take account the formation structured events that is the groups of spots with mutual distances less than ~ 1 mm in X-ray film. These narrow groups of spots corresponds to one hadron above the chamber and originate from spatial fluctuations in nuclear-electromagnetic cascades (NEC) in the chamber /3/.

In the paper the groups of the electron-photon cascades (EPC) with mutual distance less than 1.7 mm are considered as one cascade is produced by only hadron.

In table presents data about $\langle \bar{R} \rangle$ and $\bar{\alpha}$ obtained from experiment and from CS -scaling and CS \check{C} j -models /4/.

TABLE

EXPERIMENT		CALCULATION		
γ_i -fam.	h-fam.	CS γ_i -fam.	CS \check{C} j γ_i -fam.	CS \check{C} j h-fam.
$\langle \bar{R} \rangle : 44.6 \pm 2.1$	45.3 ± 3.4	29.1 ± 1.3	42.1 ± 3.8	47.3 ± 4.8
$\bar{\alpha} : 0.19 \pm 0.01$	0.26 ± 0.02	0.11 ± 0.01	0.21 ± 0.02	0.28 ± 0.03

In CS \check{C} j-model the inelastic charge-exchange of leading charge pion into neutral one $\pi^{\pm} \rightarrow \pi^0 + \dots$ and the jet production processes was taken into account. The generation cross

section of jets with large transverse momenta P_{tj} is calculated according to /5/. As one can see from table I only jet generation model is in good agriment with experiment.

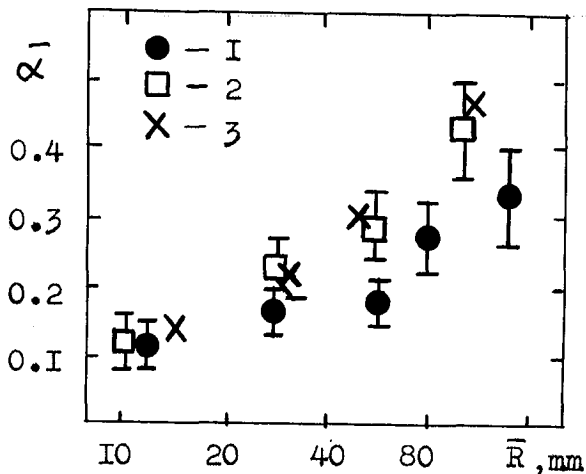


Fig. I

Fig. I presents data about the dependence of the value α_1 on the spatial parameter \bar{R} of γ_i and hadron families (1 - γ_i -families, 2 -h-families, 3 -h-families from CSCj-model). As one can see from figure I, the essential incrising of the azimuthal correlation in the range of the large values $\bar{R} > 50$ mm of the hadron and γ_i -families is observed. These results are in a good agriment with the jet production model while CS-model is led to smaller values α_1 , \bar{R} , than in experiment.

2. Gamma-families originated from nucleus-nucleus (AA) and proton-nucleus (PA) interactions

In the paper the selecting criteria of that families obtained from the analysis of the γ -families simulated on the basis MSF-model /6/.

The criterion: $\bar{R} > 40$ mm and $\alpha < 0.2$ for selection of γ -families, originated from nucleus-nucleus interactions (AA-families) is proposed, as for as AA-families are more wide (the majority of the families have the value $\bar{R} > 40$ mm) and isotropic in the azimuthal plane than PA-families. That criterion select 65% AA- and 35% PA- of simulated families with energy $\sum E_\gamma = 70-500$ TeV, contained EPC with energies $E_\gamma \geq 2$ TeV, lying within the radius $R=30$ sm from family center.

The using such criterion to experimental data showed, the fraction AA-families at the observation level is $15 \pm 4\%$. This value is agree with assumption about normal chemical composition of the primary cosmic radiation at energies $E_0 \geq 10^{15}$ eV.

Other proposed criterion: $d = n_0 / n_i$ where n_0 and n_i - number of the observed and initial γ -quants in the families. According to MSF-model, families with $d \geq 1.6$ originated from protons (the admixture of AA-families compose $\sim 9\%$), and events with $d \leq 1.2$ originated mainly from nucleus-

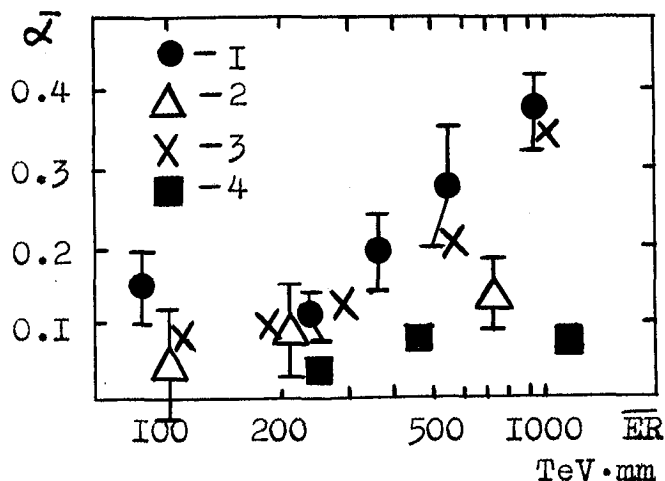


Fig. 2

tions increasing in the range of the large values \bar{R} and \overline{ER} connected with proton-nucleus interactions and described by CSČj-model. On the other hand for the nucleus-nucleus interactions the increasing azimuthal correlations is not observed.

nucleus collisions (among them 70% AA- and 30% PA-families).

At the Fig.2 data about the dependence azimuthal correlations from value \overline{ER} (E -energy R -distance of the γ -quanta from axis of family, 1 -experimental families with $d \geq 1.6$, 2 -experimental families with $d \leq 1.2$, 3 -CSČj-model, 4 -MSF-model for events with $d \leq 1.2$) is presented.

How one can see from Fig.2, effect of the azimuthal correla-

REFERENCES

1. L.T.Baradzey, Yu.A.Smorodin, E.A.Solopov Preprint FIAN N 103, 1974
2. S.A.Azimov, T.S.Yuldashbaev et.el. Zeszyty Naukowe Uniwersytety Lodzkiego, Lodz 1977; z.60, s.II, p.281
3. G.G.Leptuh et.el. Proc. of International Symposium on Cosmic Rays and Particle Physics, Tokyo, March 19-23, 1984, p.261
4. S.A.Azimov, E.J.Mulladjanov, H.Nuritdinov, D.A.Talipov, D.A.Halilov, T.S.Yuldashbaev Proc. 18-th ICRC, Bangalore, India 1983, v.5, p.458
5. L.V.Gribov, E.M.Levin, M.G.Ryskin Phys.Lett. 121B, 65, 1983
6. R.A.Mukhamedshin Proc. 17-th ICRC, Paris 1981, v.5, p.343

A STUDY OF γ -FAMILIES GENERATED IN NUCLEON-
NUCLEUS (NA) AND PION-NUCLEUS (π A)
INTERACTIONS

Azimov S.A., Mullaajanov E.J., Nuritdinov H.,
Yuldashbaev T.S.

Physical-Technical Institute of Academy of
Sciences of the Uzbek SSR, USSR

In the paper the separation of the γ -families generated in NA and π A interactions is realized from the analysis of simulated γ -families. Some characteristics of NA and π A families and the influence of the process of inelastic charge-exchange of charged pions into neutral ones type of $\pi^{\pm}A \rightarrow \pi^0 + \dots$ are studied.

In the paper the characteristics of γ -families generated in pion-nuclear π A-interactions (π -families) and nucleon-nuclear NA-interactions (N-families) in atmosphere is investigated.

The selecting criteria of π and N-families is proposed from the analysis of γ -families simulated on the basis of scaling CS and CSC -models.

The CS -model is based on extrapolation to the super-high energies of the interaction characteristics known in the accelerator energies in the assumption of Feynman scaling validity. For that there is made no difference between NA and π A interactions mechanism.

In the CSC -model the inelastic charge-exchange of leading charge pion into neutral one $\pi^{\pm} \rightarrow \pi^0 + \dots$ was taken into account. The inelastic charge-exchange probability W is set equal to 0.2 at $x_1 = E_1 / E_0 \geq 0.5$ (x_1 -Feynman's variable for leading particle, E_0 -energy of colliding particle).

The families are considered as a formed mainly in the pion-nuclear interactions (π -families), if the fraction of the energy from pion interactions

$$K^{\pi} = \frac{\sum E_{\gamma}^{\pi}}{\sum E_{\gamma}},$$

where $\sum E_{\gamma}^{\pi}$ -the summary energy of the cascades from π A - interactions, was satisfied the relation: $K^{\pi} > 0.5$. If the value

$$K^N = \frac{\sum E_{\gamma}^N}{\sum E_{\gamma}},$$

where $\sum E_{\gamma}^N$ -the summary energy of the γ -quanta from nucleon-nuclear cascades, was satisfied the relation: $K^N > 0.5$, than such families are considered as a formed in the nucleon-

nuclear interactions (N-families) ($\sum E_\gamma$ - the total energy of γ -family).

The spatial characteristic of the simulated γ -families $\bar{R} = \frac{\sum_{i=1}^{n_\gamma} R_i}{n_\gamma}$ (where R_i - distance of γ -quanta from axis of family, n_γ - number of γ -quanta in the family) is considered too. The simulated families were selected according to criteria analogous to those in Pamir experiment: the family summary energy $\sum E_\gamma = 30 + 500$ TeV, the number of particles $n_\gamma \geq 3$, the minimal energy of quanta was equal to $E_\gamma = 2$ TeV, only those quanta is included in families which were found in the round with radius $R = 30$ sm from the center. As we showed in the work /1/, the simulated families with $R > 40$ mm mainly consist of the π -families (them fraction compose 70 + 85% for both models), and families for which angles of arrival on plant $\Theta \leq 20^\circ$ and $R < 20$ mm mainly consist of the N-families. Therefore, those conditions used as a selecting criteria of π and N-families in the work.

The characteristics of simulated γ -families were compared with the experiment "Pamir" data. The film scanning and particle selection were realised within the radius $R = 30$ sm relatively the energy weighted center of γ -family. In the result it were selected $N = 539$ γ -families with energies $\sum E_\gamma = 30 + 500$ TeV and number of particles $n_\gamma \geq 3$. The minimum energy of the γ -quanta in the families was set $E_\gamma = 2$ TeV. At this, the conditions near to experimental in the simulated families were introduced. The registration efficiency of γ -quanta $E_\gamma = 2 + 4$ TeV in the energy region change from 0.3 to 1.0. The registration efficiency of γ -families reach 1.0 at energy $\sum E_\gamma \geq 70$ TeV. The error δE in the energy measuring and real spatial resolution of the close situated quanta (quanta, situated on distance $r_{1,2} = 40 + 100$ μ m with energies $E_1 + E_2 = 25 + 50$ TeV, were considered as an unified) were taken account.

In the paper an distributions of families arrived the installation under different angles Θ to vertical investigated. In the experiment the errors of the angles determination for the families arrived under small angles to vertical are large.

The registration probability of γ -quanta decrease in the large angles range $\Theta > 36^\circ$. Therefore, events with angles of arrival situating in interval $9^\circ \leq \Theta \leq 36^\circ$ were selected for analyse. At this, the error in the angle measuring of the arrival $\Delta\Theta \sim 1^\circ$ introduced in the simulated families.

All events divided on the groups of families arrived the installation under angles $\Delta\Theta_1 = 9^\circ + 18^\circ$ (number this families N_1), and arrived under angles $\Delta\Theta_2 = 18^\circ + 36^\circ$ (N_2).

The value

$$F = \frac{P_2}{P_1}$$

where $P_1 = N_1/(N_1 + N_2)$ -the fraction of families arrived on plant under angles $\Delta\Theta_1 = 9^\circ + 18^\circ$ and $P_2 = N_2/(N_1 + N_2)$ -the fraction of families arrived under angles $\Delta\Theta_2 = 18^\circ + 36^\circ$ is calculated for families of experiment "Pamir" and simulated families. In consequence an following values F : 0.82 ± 0.08 (CS -model), 1.45 ± 0.15 (CSC -model) and 1.64 ± 0.16 (experiment) were obtained.

Like that, the experimental data relatively value F agree with CSC -model.

In the paper the families selected according to selecting criteria of π and N -families ($R > 40$ mm and $R < 20$ mm) is investigated. At this, for value $\Delta = N_\pi / N_N$, where N_π -number of π -families, N_N -number of N -families the following values were obtained: 0.5 ± 0.07 (CS-model), 0.78 ± 0.12 (CSC-model) and 0.73 ± 0.09 (experiment).

How one can see from analyse of the angular distributions of γ -families and the correlation between π and N -families, the experimental data are described by CSC-model in that the inelastic charge-exchange of leading charge pion into neutral one $\pi^\pm \rightarrow \pi^0 + \dots$, was taken account.

R E F E R E N C E

- I. S.A.Azimov, E.J.Mulladjanov, H.Nuritdinov, T.S.Yuldash -baev Proc. 18-th ICRC, Bangalor, India 1983, v.5, p.462

HADRONS REGISTRATION IN EMULSION CHAMBER WITH CARBON BLOCK

A. Tomaszewski and Z. Włodarczyk

Institute of Physics, University of Lodz, Lodz, Poland and
 Institute of Physics, Pedagogical University
 Kielce 25-509, Lesna 16, Poland

NEC in X-ray emulsion chambers with carbon block, which are usually used in the "Pamir" experiment, was Monte-Carlo simulated. Going over from optical density to ΣE_{γ} is discussed. Role NEC in the interpretation of energy spectra is analysed.

1. Introduction. As a result of the nuclear-electromagnetic cascade (NEC) in C-layer and Pb-layer of hadronic block, we get a spot on X-ray film of emulsion chamber and then we get several optical densities of the spot corresponding to several radii of a photometer diaphragm. General methodical problem of the hadronic block measurements is how to obtain a value of energy of the hadron - E_0 (or energy of electromagnetic component of a cascade initiated by the hadron - ΣE_{γ}) from the data of the optical densities D .

2. Simulation Assumptions. Spots of the individual NEC were simulated. We took into account a chamber consisting of 6 cm Pb gamma block (0.35λ , 10.5 c.u.) and hadronic block having 65 cm C-generator (0.95λ , 2.7 c.u.) and 4 cm Pb-layer (0.23λ , 7.0 c.u.). The calculation were divided into following parts:

- For purely proton spectrum with integral slope $\delta=2$, NEC in the chamber was Monte - Carlo simulated, using scaling model
- For each particles of electromagnetic component at energy $E_{\gamma} > 0.05$ TeV the mean cascade function for electron density $\zeta(E_{\gamma}, r, t)$ at depths t was used. Target diagramme was constructed on the area $300 \times 300 \mu\text{m}^2$ with cells $12 \times 12 \mu\text{m}^2$ each.
- The electron density diagramme was transformed to the flux of light diagramme, assumed the characteristic curve $D(r) = 4.0 \{1 - \exp[-3.25 \zeta(r)]\}$ of X-ray film. At a position of diaphragm for X-ray film at depth 4 cm of Pb-layer was obtained.

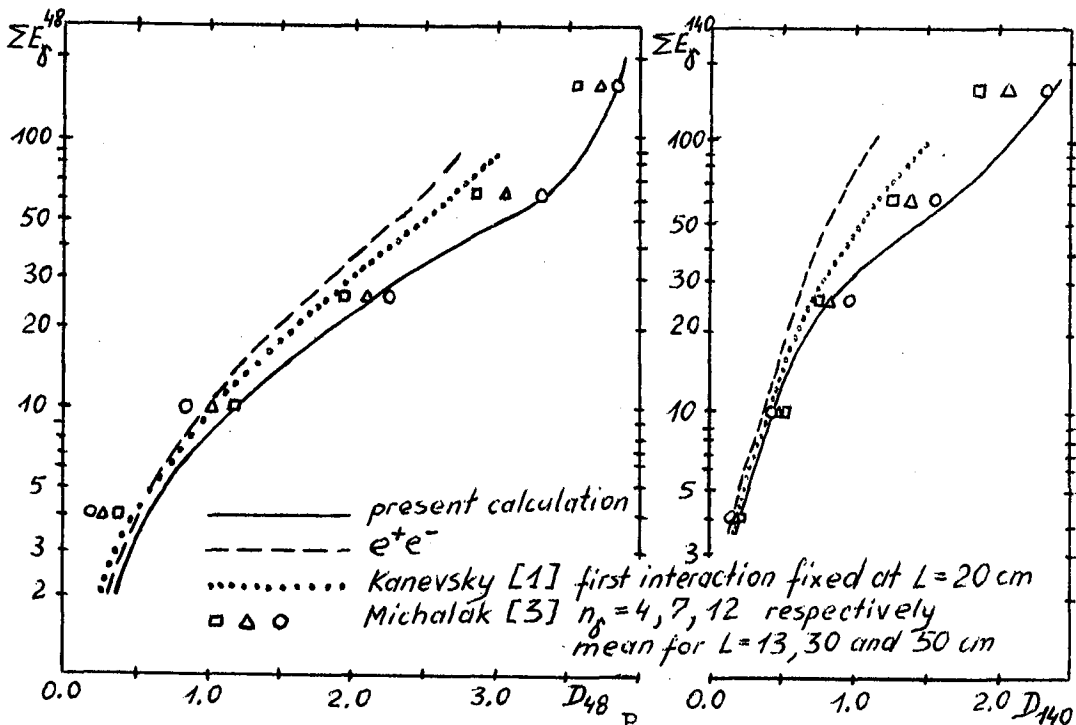


Fig.1. Mean cascade curves $D_R - \Sigma E_{\delta}^R$ for NEC at 4 cm Pb.

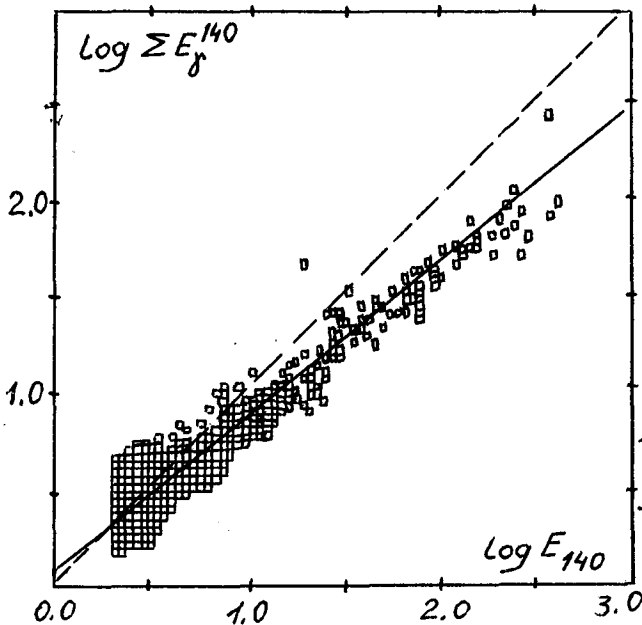


Fig.2. Scatter plot of ΣE_{δ} versus E for $R=140$ μ m and $\Delta t=0$. Dasched line is the dependence for the case $\Delta t = -2.0$ c.u.

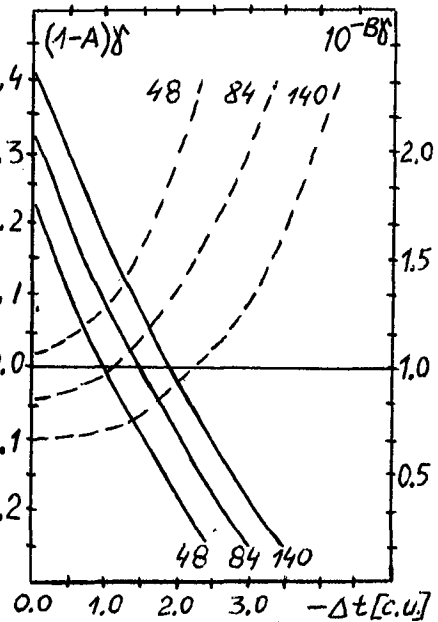


Fig.3. Dependence of $(1-A)\delta$ and $10^{-B\delta}$ on the Δt (solid and dashed curves, respectively).

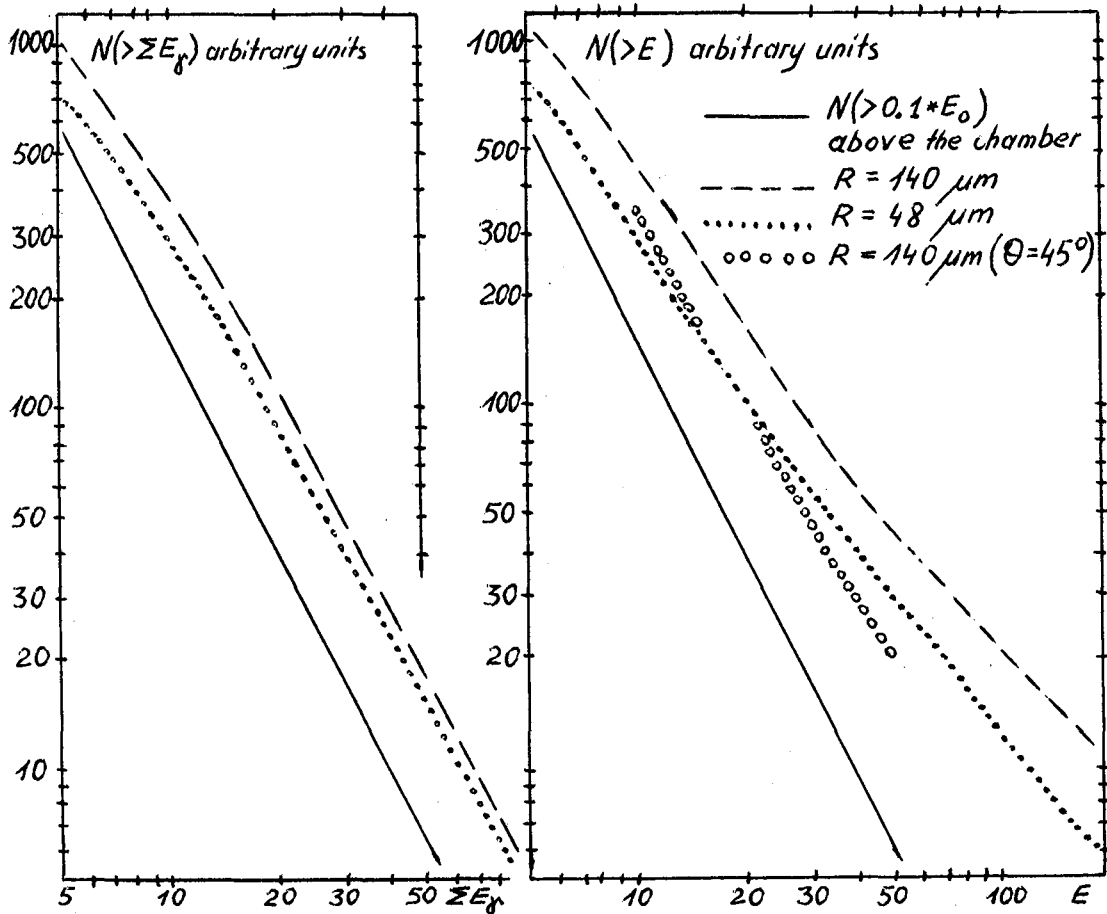


Fig.4. Integral spectra of ΣE_γ and E .

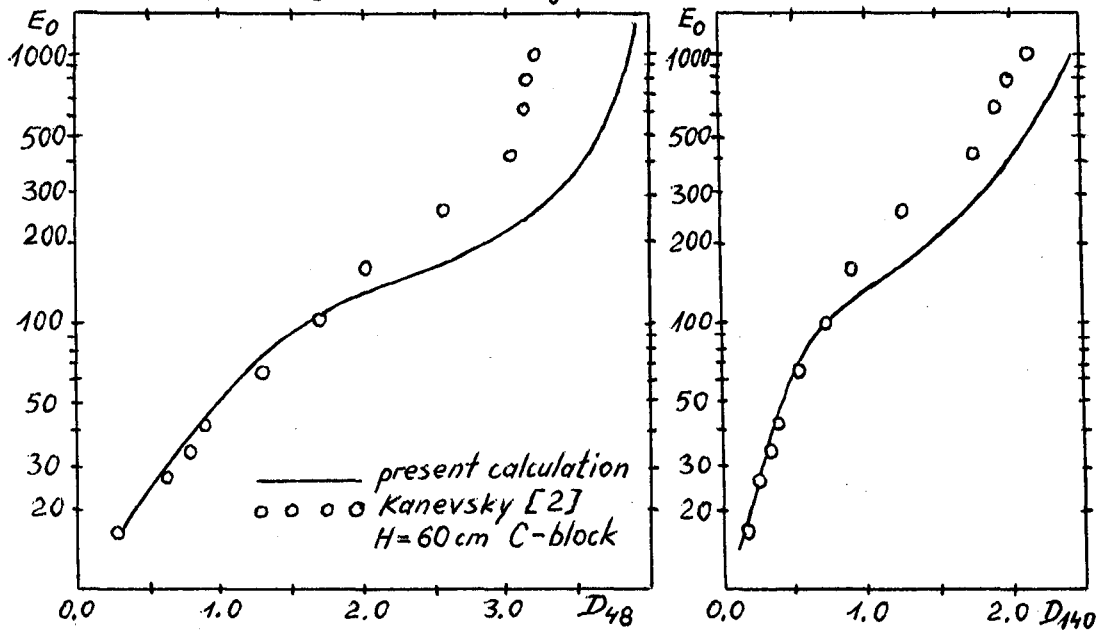


Fig.5. Mean cascade curves D_R-E_0 for NEC recorded at 4 cm Pb.

3. Results and Discussion. Mean cascade curves for D_R as a function of the energy $\sum E_\gamma^R$ (for radii of photometer diaphragm $R=48$ and $140 \mu\text{m}$) are plotted in Figure 1. The difference between the densities given by NEC in chamber and the ones corresponding to electron cascade is significant at energies above 30 TeV. The present calculation shows the much stronger difference than the one pointed out by [1] (the difference in the C-block thick is negligible at high energy, see Fig. 5)

In Figure 2 we presented scatter plot of $\sum E_\gamma$ and of energy E obtained using the "average transition curves" for e^+e^- (recorded by diaphragm with $R=140 \mu\text{m}$). The energy $\sum E_\gamma$ depend on E as $\sum E_\gamma = 10^B E^A$. Then the observed spectrum $N(>E) = C 10^{-B\delta} E^{(1-A)\delta} E^{-\delta}$ should be flattened by power index of $(1-A)\delta$ than the injection spectrum on $\sum E_\gamma$: $N(>\sum E_\gamma) = C(\sum E_\gamma)^{-\delta}$. The quantities $(1-A)\delta$ and $10^{-B\delta}$ are presented in Figure 3 (at $\Delta t=0$). Figure 4 shows the integral spectra of $\sum E_\gamma$ and E

Roughly, it is possible to estimate the energy spectra took into account the thick of carbon layer Δt penetrated by NEC. Nevertheless this manner is dangerous, because deepen in NEC development the difference is not so significant (see Figure 4, curve for $\Theta = 45 \text{ deg}$: $t = 4.0/\cos(45) \text{ Pb}$).

Mean cascade curves for optical density as a function of hadron energy E_0 are plotted in Figure 5. The difference between present calculation and Kanevski [2] data are caused by the difference in transition $\sum E_\gamma \rightarrow D$ mentioned above.

4. Conclusion. Using $D(\sum E_\gamma)$ corresponding to e^+e^- cascade or these calculated by [1,2] provide to flattenens of the observed hadron spectrum and decreases of attenuation m.f.p. (calculated from zenith angle distribution) at $\sum E_\gamma > 30 \text{ TeV}$.

References

- [1] Kanevsky B.L., in: Electron-Photon Cascade at High Energy Cosmic Rays, Moscow (1980), in Russian
- [2] Kanevsky B.L., et al., 17 th ICRC, 5, 335, Paris (1981) and Moscow State University Report-in Russian
- [3] Michalak W., Acta University of Lodz, 60, 137, Lodz (1977)

NEW ANALYSIS OF NUCLEAR INTERACTION OBSERVED
BY MT. KANBARA EMULSION CHAMBER EXPERIMENT

Nanjo. H

Hirosaki University, Hirosaki, Japan

1. Introduction. Up to date, the analysis of air cascade family has been performed mainly by using a full Monte Carlo simulation, because of the large fluctuation of the air cascade. Recently it has become clear, however, that it is difficult to draw a definite conclusion about the interaction mechanism by using only this kind of simulation, due to too many assumptions in relation to the amount of information.

On the other hand, some attempts to reproduce the original γ -ray at the interaction point, for example 'decascading¹', have also been made. This kind of method makes it possible to observe the interaction directly and to analyze the data from various angles. All of these methods, however, assume the constant ER in cascade shower, where E is energy and R is the distance from the center of cascade shower. This character is all-inclusive and changes according to the energy and the interaction height of original γ -ray. It is impossible, therefore, to reproduce the exact interaction height and energy by these methods. This work adopts a quite different way from the ER constant method; that is, a relative method in separating one cascade shower from others. This new method makes it possible to estimate the interaction height and energy by using information about the lateral spread of the cascade shower.

2. New method. Fig.1 (a) shows the correlation between E and R of γ -rays in a simulated family event. Open circle and closed circle represent the γ -ray produced by one original γ -ray and other original γ -rays, respectively. In this figure, we can find an energy gap at the boundary between groups of cascade shower γ -rays. The new method is nothing but a way to classify one cascade shower group from others by using of this energy gap.

We make a classification of each cascade shower according to the following procedure.

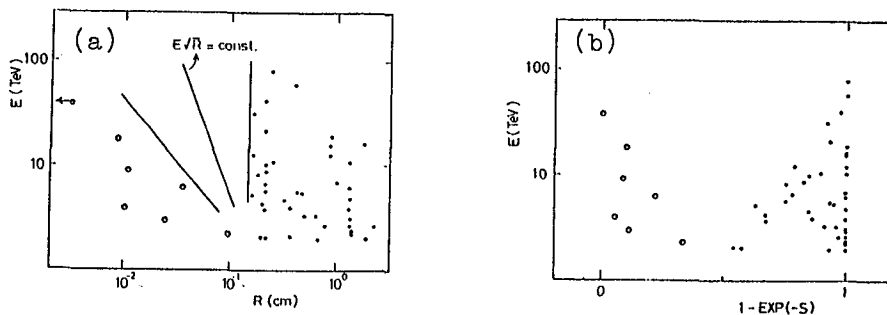


Fig.1 (a) Correlation between E and R in a simulated family event. Open and closed circle represent the γ -ray produced by one original γ -ray and other γ -rays, respectively. (b) Transformed figure of (a) in order to represent the energy gap symmetrically.

- 1) Take the i -th γ -ray as a temporary center of a cascade shower group. The selection of the i -th γ -ray is performed according to size of energy, because a high energy γ -ray should be located near the true center.
- 2) Calculate the following quantity S_{ij} representing a spread between the i -th γ -ray of a temporary center and all other γ -rays ($j=1\sim n$),

$$S_{ij} = (E_i + 5) R_{ij} \sqrt{E_j} / 15 \quad (1)$$

where R_{ij} is a length between the i -th and j -th γ -rays. As is seen in Fig.1 (a), a straight line of $R\sqrt{E} = \text{constant}$ has a mean inclination between the line of $ER = \text{constant}$ and $R = \text{constant}$.

- 3) Calculate the energy density for the following quantity W_j ,

$$W_j = 1 - \exp(-S_j) \quad (2)$$

for fixed i . W_j ranges from 0 to 1 and is effective to search for an energy gap impartially among various cases. The correlation between E and W is shown in Fig. 1 (b) for the same sample as in (a). We can see a symmetrical valley of energy in this Figure.

The energy density is defined as

$$P_j = \sqrt[3]{E_j \cdot E_{j+1} \cdot E_{j+2}} / (W_{j+2} - W_j) \quad (3)$$

The boundary is set up the position W_{\min} where P_j has the minimum value.

- 4) Select candidates, which satisfy the following criteria, as members of the same cascade shower with the i -th γ -ray.

$$W_j < W_{\min} \quad \text{and} \quad E_j < E_i$$

- 5) Proceed to the next γ -ray to be set as a temporary center. The γ -rays which have been already selected in (4) are excluded as new centers.
- 6) When a γ -ray is selected as a candidate of more than two groups, it is decided to belong the group which gives the smallest distance from its center.

3. Estimation of energy and production height. The energy and production height of γ -ray are estimated by using the mean spread of clustered γ -ray as members of a cascade shower. The mean lateral spread $\langle R \rangle$ is defined as,

$$\langle R \rangle = \Sigma R / N \quad (\text{cm}) \quad (4)$$

where R is a distance from the energy weighted center and N is the number of γ -rays in a cluster. Close investigation of the simulation data drew the estimation formula of energy E_{es} and interaction height H_{es} at Mt. Kanbara height (5500m) as follows,

$$E_{es} = \Sigma E \cdot 10^{2.5 \langle R \rangle} \quad (\text{TeV}) \quad (5)$$

$$H_{es} = 17000 \cdot \langle R \rangle^{1.5} \quad (\text{m}) \quad (6)$$

4. Check of new analysis method. Reproducibility by the new method was checked by using artificial data in a full Monte Carlo simulation. For the purpose of checking, only the standard model simulation was necessary. An outline of the simulation² is as follows.

- (1) Proton primary with energy spectrum as

$$I(E) dE \propto E^{-\beta-1} dE \quad (\beta=1.7)$$

- (2) Particle production spectrum is scaling law

$$f(X)dX \propto (1-X)^{3.5}/XdX$$

where $X=E/E_0$, E and E_0 are secondary and primary energy, respectively.

(3) Interaction mean free path

$$\lambda = \begin{cases} 80 \text{ g/cm}^2 & \text{for proton} \\ 96 \text{ g/cm}^2 & \text{for secondary pion} \end{cases}$$

(4) Mean transverse momentum

$$\langle Pt \rangle = \begin{cases} 330 \text{ MeV/c} & \text{for secondary particle} \\ 500 \text{ MeV/c} & \text{for leading particle} \end{cases}$$

For the investigation of large Pt , the double value $\langle Pt \rangle = 660 \text{ MeV/c}$ was also used.

All of the clusterized groups have not always one to one correspondence to the expected one. In the case of no one to one correspondence, the original γ -ray which gives the highest energy ratio within the cluster is selected as corresponding γ -ray and used for checking.

Fig.2 (a) shows the distribution of N_{es}/N_0 , where N_{es} is the number of γ -rays in an actual clusterized group and N_0 is the expected number in the corresponding cascade shower. The peak at $N_{es}/N_0=2$ is due to the case of $N_0=1$. Figure shows fairly strong agreement and the validity of the new method was confirmed.

Fig.2 (b) and (c) show the comparison of estimated energy E_{es} and estimated interaction height H_{es} of original γ -ray with expected true ones E_0 and H_0 , respectively. Fig. (c) for interaction height shows broad distribution. This is due to mainly the fluctuation in the traveling distance of the original γ -ray from the interaction point to the first pair creation point. We need the statistical analysis for the interaction height.

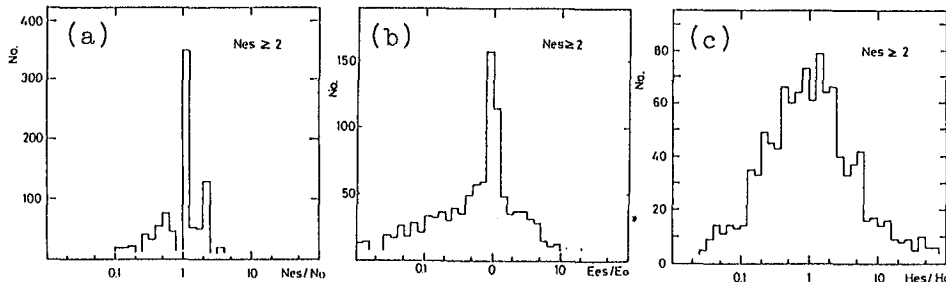


Fig.2. Comparison of the estimated value by new method with the expected one (a) Number of γ -rays in a clusterized shower (b) energy and (c) interaction height of original γ -ray

Fig.3 shows the reproducibility of the transverse momentum Pt distribution, (a) for normal Pt and (b) for double Pt . The full and broken lines represent the distributions of the estimated Pt and of the expected Pt of all γ -rays at the interaction point. The estimated and expected distribution does not necessarily coincide because of the detection bias and the error of estimated value. The positions of peak, however, coincide with each other, and the estimated distribution for normal Pt and for large Pt reproduce just a double difference. It is worth notice that the estimated Pt distribution has a large error but is independent of the interaction model.

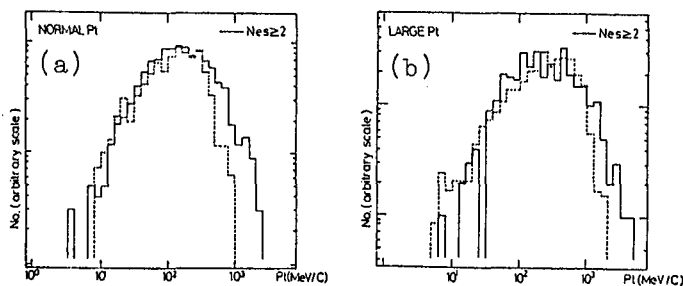


Fig.3 The transverse momentum P_t distribution of reproduced γ -ray for (a) normal P_t (b) double P_t , compared with the distribution of all γ -rays produced by the interaction (broken line).

5. Results. In Fig.4, is shown the result of the interaction height of the reproduced original γ -ray by the experimental data of the Mt. Kanbara emulsion chamber experiment, compared with the result of simulated data (broken line). The experimental data does not contradict the prediction of the simulation.

Fig.5 shows the lateral spread R distribution, where R is the distance between an energy weighted center of a family and of γ -rays in a cluster. Smoothed curves represent the distribution of the simulated data in the case of normal P_t and double P_t .

Fig.6 shows the transverse momentum P_t distribution by Mt. Kanbara experiment, compared with the simulated data. Smoothed curves in the figure are also the simulated distribution for normal P_t and double P_t .

Though the statistics of experimental data are not enough to reach a definite conclusion, the both results in Fig.5 and Fig.6 prefer large P_t ($\langle P_t \rangle \sim 600$ MeV/c) rather than normal P_t .

6. Acknowledgments. The author would like to express his thanks to the members of the Mt. Kanbara group for allowing the use of experimental data. He is much indebted to Dr. Shibata of Yokohama National University for using the Monte Carlo simulation method. The author thanks Mr. Y. Noto of Hirosaki University for help in calculation of the simulation.

References

1. H. Semba Prog. Theor. Phys. Suppl. No. 76, 111 (1983)
M. Amenomori et al. Phys. Rev.D 25, 2807 (1982)
2. M. Shibata Phys. Rev.D 24, 1847 (1981)

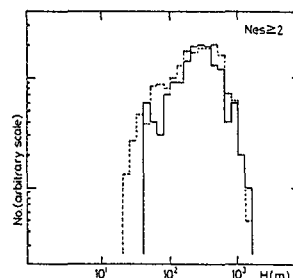


Fig.4 The interaction height distribution, compared with the simulated data (broken line)

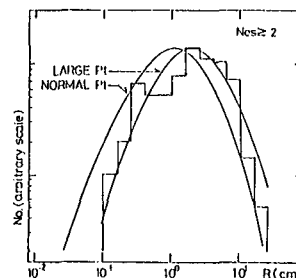


Fig.5 The lateral spread distribution of original γ -ray. Smoothed curves represent the simulated data for normal P_t and large P_t .

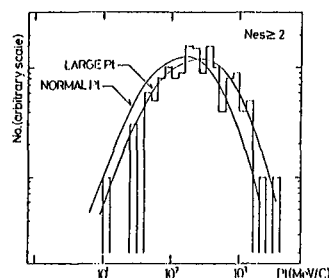


Fig.6 The transverse momentum P_t distribution of reproduced original γ -ray, compared with the simulated distribution for normal P_t ($\langle P_t \rangle = 330$ MeV/c) and large P_t (660 MeV/c)

ON THE MEAN CHARACTERS OF FAMILY EVENTS
OBSERVED AT MT.KANBALA

China-Japan Emulsion Chamber Collaboration *

ABSTRACT

General features of family events with $\Sigma E_{\gamma} > 200$ TeV, observed by the emulsion chambers at Mt.Kanbala, are presented in comparison with the Monte Carlo simulation. The lateral and cluster structure, and the energy spectra of constituent gamma-rays and hadrons are shown to be consistent with the Monte Carlo results calculated under the assumption of heavy-enriched primary, scaling, QCD jets and increasing cross-section.

1.Introduction.

Upto now, the total amount of exposure of emulsion chambers(ECs) at Mt. Kanbala has reached about $420 \text{ m}^2\text{year}$. We already observed 10 big family events with energies $\Sigma E_{\gamma} > 1000$ TeV. The main purpose of our experiment is to clarify what kinds of phenomena are new in the energy region beyond 10^{16} eV, though the problem of primary composition at these energies is inevitably intertwined with this subject.

In this paper we present the average behaviour of the family events in comparison with the Monte Carlo simulation made by an assumption on primary and interaction. First, we discuss the flux of gamma-families at Mt.Kanbala, since this is known to be very sensitive to the model of both interaction and primary composition. Then the average features of family events are shown.

2.Experiment.

Two types of chambers are assembled on the Mt.Kanbala station. One is the Pb-EC, usually used at the mountain experiments, and the other the Fe-EC. The exposure list is shown in ref. 1).

In our data processing, hadrons are defined as showers with its starting point deeper than 6 c.u. and/or with accompanying successive interactions in the EC, and others are identified as gamma-rays. The minimum energy of showers accepted in our analysis is set to be 4 TeV. The detection efficiency of hadrons is estimated to be about 40 % for Pb-EC and about 80 % for Fe-EC in an average.

Here, we use only the data taken from the Pb-chambers

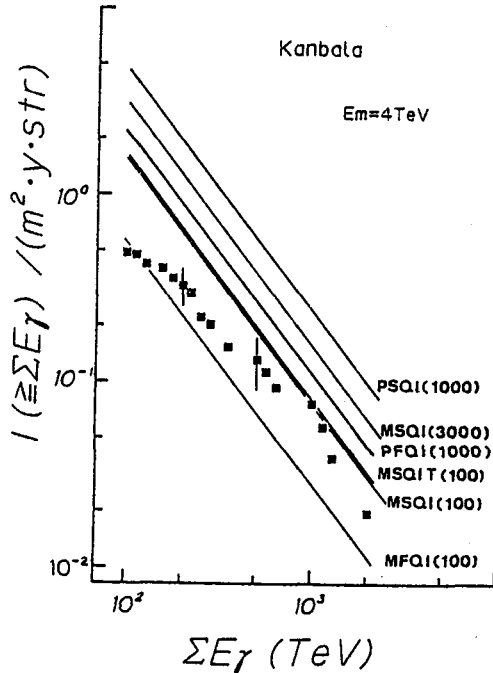


Fig. 1.

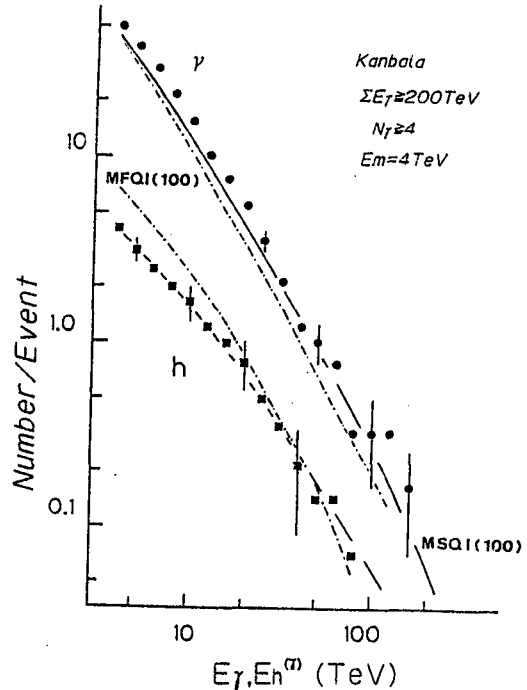


Fig. 2.

because the amount of exposure of the Fe-chambers is still insufficient to get quantitative results.

3. Monte Carlo simulation.

In order to make a standard picture on family phenomena and also to learn the size of its fluctuations, we have done the Monte Carlo simulations based on the conventional model of interaction and primary composition. Details of the simulation calculation are found in ref. 2). The meaning of the symbols appeared in this text is as follows ; M : Mixed chemical composition with a significant amount of heavy nuclei. The spectrum of Proton/He/L/M/H/VH/Fe becomes steeper at a bending energy (E_b) from 1.7/1.7/1.7/1.6/1.6/1.6/1.5 to 2.0 (all). The bending energy of proton spectrum is denoted in the bracket, and other nuclei steepen at energy of $Z \cdot E_b$. P : Proton dominant primary (In both cases, the total flux is normalized to the Grigorov's total spectrum at 10^{15} eV). S : Scaling in the fragmentation region. F : Fire-ball model normalized at 150 TeV. Q : QCD-jet. I : Increasing cross-section as $E^{0.06}$. T : Increasing average P_t as $E^{0.04}$.

4. Results

4.1. Intensity of gamma-families at Mt.Kanbala.

The absolute flux of gamma-families is compared with the Monte Carlo calculations as shown in Fig. 1. As learned from

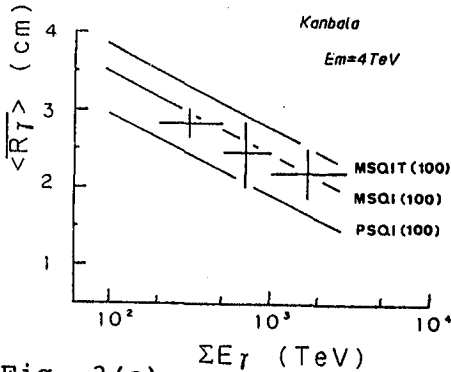


Fig. 3(a).

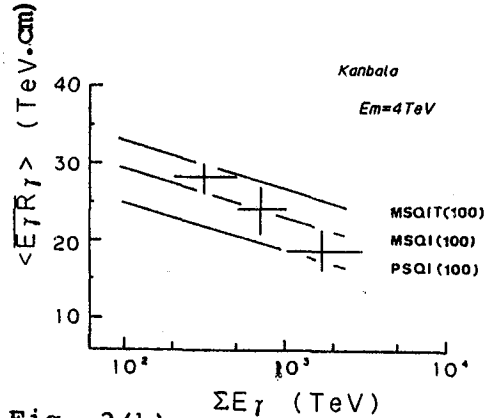


Fig. 3(b).

this figure, both cases of the model PSQI(1000) and MSQI(3000) give too high intensity compared with our data. In order to accord with the data, the proton spectrum must be bent at around 10^{14} eV. In this case, the fraction of protons and irons to the total is estimated to be about 20 % and 40 % at around 10^{15} eV, respectively. Even if we adopt the fire-ball model, the fraction of protons doesn't exceed 50 %.

4.2 Energy spectra of gamma-rays, hadrons.

Figure 2 shows the energy spectrum of gamma-rays and hadrons superposed in the energy interval of $\Sigma E_T > 200$ TeV. The solid and dotted line corresponds to the model MSQI(100) and MFQI(100), respectively. No clear difference is found between the data and the model MSQI(100) both on the number of showers and the slope of spectrum. However, the fire-ball model (MFQI, heavy enriched primary and scaling break) gives steeper spectrum compared with the experiment. That is, strong scaling break is incompatible with the heavy enriched primary and requires the proton dominant primary.

4.3 Lateral structure of gamma-families.

The mean values of $\langle R \rangle$ and $\langle ER \rangle$ of gamma-rays averaged in the respective energy range are shown with the Monte Carlo results in Fig. 3(a), (b). Our data come between the model MSQIT(100) and PSQI(1000), and remain close to the MSQI(100). At accelerator energy regions, the mean P_t near central region seems to increase with energy as $E^{0.04}$. But, it is also well confirmed that the behaviour of

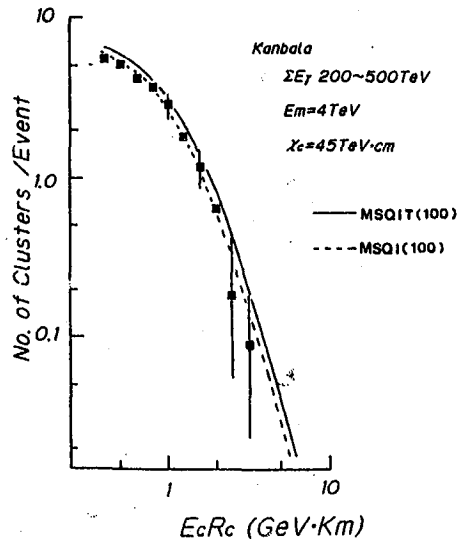


Fig. 4.

gamma-families is sensitive to the fragmentation region. If we take this into consideration, then we may say that the average P_t in the fragmentation region remains almost constant at least up to about 10^{15} eV (Here it should be noted that the QCD-jet effect is taken into account.).

The ER distribution of clusters in the gamma-families with $\Sigma E_\gamma = 200-500$ TeV is shown in Fig. 4, comparing with the results of the model MSQIT(100) and MSQI(100). This comparison tells us that the increasing mean P_t (smooth extrapolation from the accelerator energy region) gives merely a minor effect on the cluster structures.

5. Conclusions.

Our discussions are summarized as follows,

- 1) Scaling in the fragmentation region, increasing cross-section as E^δ , $\delta=0.04-0.06$, and the heavy enriched primary spectrum can well explain our experimental data.
- 2) A fraction of protons and irons to the total flux takes a value of about 20 % and 40-60 % at around 10^{15} eV, respectively. The proton spectrum should steepen at around 10^{14} eV.
- 3) The energy dependence of average P_t is very weak in the fragmentation region.

These conclusions are compatible with other data, i.e., uncorrelated gamma-ray/hadron spectrum and the behaviour of super-families³⁾. We also observed several family events with a peculiar structure, and some of these events are described in other paper⁴⁾.

This work is financially supported in part by IHEP, Academia Sinica in China and ICR, University of Tokyo, and Grant-in Aid from the Ministry of Education in Japan. Data analysis was made by using the Computer FACOM M380R of INS, University of Tokyo.

* For full list of authors, see HE 3.1-2.

- 1) Ren, J.R. et al, HE3.1-2, in this volume.
- 2) Ding, L.K. et al, Proc. Int. Symp. on Cosmic Rays and Particle Phys. (ICR, Univ. of Tokyo, 1984), p142.
- 3) Ren, J.R. et al, HE3.4-9, in this volume.
- 4) Ren, J.R. et al, HE3, in this volume.

STRUCTURED EVENTS IN "PAMIR" CARBON X-RAY CHAMBERS

G.G.Leptukh

Institute of Physics of Academy of Sciences of the
Georgian SSR, Tbilisi, 380077, USSR

ABSTRACT

Results of experimental and theoretical investigations of Structured Events or Narrow Groups of Hadrons in "Pamir" carbon chambers are presented.

It is shown that these events are formed by the usual fluctuations in in-chamber development of NEC initiated by a single hadron from the atmosphere.

1. Introduction. In the present article the revised data on Structured Events or Narrow Groups of Hadrons [1,2] are presented along with the final results of their Monte-Carlo simulation.

A Structured Event (SE) is a group of density spots on X-ray film in Hadron (H)-block of carbon emulsion chamber with mutual distances between spots in the interval (0.1 - 1.0) mm and energy registered in each spot $E_h^{(r)} \geq 2$ Tev.

Anomalously small distances in SE link these events with the so-called "Chiron"-type events and "mini-clusters" registered by Brazil-Japan Collaboration [3,4] and with the certain ones observed by Pamir Collaboration [5,6]. Usually, these phenomena are interpreted as an indication on an existence of narrow groups of particles in the atmosphere. However, to insist in this hypothesis the thorough investigation of all possibilities to obtain the observed events by the known physical processes is needed. This work has been performed for SE case and has led to the conclusion of SE origin triviality.

2. Properties of experimental Structured Events. From the data of 2×46 m² area of two-storey "Pamir-77778" C-chamber (60 cm of C and 5 cm of Pb in each H-block) as much as 85 SE have been selected. Since SE as a rule are consisted of two density spots the properties of two-spot SE are presented here:

a) The fraction of SE of the total number of registered hadrons with $E_h^{(r)} \geq 4$ Tev is:

$$\langle F \rangle = (8 \pm 2) \%, \quad (1)$$

while the ratio of SE fraction in lower H-block to the one in upper H-block is:

$$\langle Q \rangle = 1.3 \pm 0.3. \quad (2)$$

b) The spatial distribution within SE, i.e. the distribution of distances between spots in SE, is very narrow, con-

centrates at the lower edge of allowed interval and vanishes at 0.5 mm. The first two momenta of the distribution are:

$$\langle R \rangle = (0.21 \pm 0.03) \text{ mm}, \quad \sigma = 0.10 \text{ mm}. \quad (3)$$

Spatial distributions in both H-blocks are almost identical.

c) Energy-weighted spatial distribution in SE has the following mean value:

$$\langle E_h^{(\delta)} R \rangle = (0.38 \pm 0.03) \text{ Tev.mm}. \quad (4)$$

d) The average energy of SE as a whole is:

$$\langle \sum_1^2 E_h^{(\delta)} \rangle = (9.1 \pm 0.5) \text{ Tev}. \quad (5)$$

3. Out-of-chamber sources of Structured Events. Usually, to estimate the average height of parent interaction the $\langle ER \rangle$ characteristics of events under investigation is used along with the average transverse momentum of gammas produced in nuclear interaction ($\langle P_T^\gamma \rangle = 0.2 \text{ Gev/c}$). In case of SE one obtains the following:

$$\langle H \rangle = 0.4 \text{ Tev.mm} / 0.2 \text{ Gev} = 2 \text{ m}, \quad (6)$$

i.e. a source of SE seems to be above the chamber.

Investigations of possible out-of-chamber sources of SE have excluded them because in addition to the smallness of SE fluxes from these sources the experimental approximate equivalence of SE fractions in both H-blocks and narrowness of SE spatial distribution are not reproduced. For example, Monte-Carlo simulation of NEC in the atmosphere in the framework of quasiscaling model of strong interaction has resulted to almost uniform distribution of distances between hadrons in narrow groups of particles at the installation level:

$$\langle R \rangle = (0.61 \pm 0.06) \text{ mm}, \quad \sigma = 0.30 \text{ mm}, \quad (7)$$

which is in the striking discrepancy with the experiment.

4. Sources of SE inside the chamber. As the average height of the usual nuclear interaction in the chamber is estimated to be equal to $\approx 40 \text{ cm}$ above the observation level, i.e. above the level of X-ray films under investigation, it is possible to estimate the average transverse momentum of gamma-rays in interactions giving rise to SE:

$$\langle P_T^\gamma \rangle = 0.4 \text{ Tev.mm} / 400 \text{ mm} = 1 \text{ Gev}, \quad (8)$$

which is five times higher than usually accepted value.

However, simulation of high- P_T processes in the chamber have yield the negligible flux of SE [1]. This is due to the smallness of high- P_T processes cross-section, the smallness of transverse jet average energy and high energy threshold of X-ray film.

To check whether SE can be produced by hadron interactions inside the chamber the direct problem of NEC simulation in C-chamber has been solved along with the inverse problem of event processing, measurement and energy restoration[2].

Each simulated event is presented at the observation level in the form of secondary electron number density distribution (two-dimensional histogram, 80 x 80 channels). Note, that this allows a study of density spot microstructure on X-ray films in Hadron-block.

As regions of low density are not visible on film due to the latter low sensitivity it is obvious that only peaks of the distribution can be seen as density spots. Investigation of these distributions in simulated events in Gamma- and Hadron-block has shown the difference in their shapes: gamma-initiated events are of one-peaked narrow distribution whereas hadron-initiated ones result in rather wide complicated structure of electron number density distribution. It is evident that if two or more sufficiently well separated peaks (local maxima) of the latter distribution are above the certain threshold the event is seen as SE on X-ray film.

To select the required SE among the simulated ones a special method has been developed for the computer-search of local maxima which are candidates for separate density spots. The experimental procedure of optical density measurement by means of microphotometer with round diaphragm has been also simulated. Only peaks of electron number density distributions with corresponding energies above the accepted threshold value have been considered.

5. Results. The following properties of simulated SE have been obtained to be compared with similar ones in Sect. 2:

$$\begin{aligned}
 \langle F \rangle &= (20 \pm 4) \%, \\
 \langle R \rangle &= (0.23 \pm 0.03) \text{ mm}, \\
 \langle E_h^{(R)} \rangle &= (0.39 \pm 0.03) \text{ Tev. mm}, \\
 \langle \Sigma E_h^{(R)} \rangle &= (10.6 \pm 0.6) \text{ Tev}.
 \end{aligned}
 \tag{9}$$

As it can be seen the experimental and theoretical values are in good agreement. The excess in SE fraction in simulated events is related to its high sensitivity to handling parameters whereas it has been found the spatial and energy properties to be rather stable.

The interesting result is that the average energy of hadron interacted in the chamber and resulted in non-structured (usual) spot with $E_h^{(R)} \geq 4$ Tev is just the same as the average energy of hadron that generates SE. It means that SE are quiet normal events with $E_h^{(R)} \geq 4$ Tev and the selection of SE at the experiment does not biased energies of hadrons fallen on the installation from the atmosphere.

6. Discussion. Now the question is why simple estimates based on $\langle ER \rangle$ and $\langle P_n^s \rangle(H)$ relation have failed so drastically?

To study sources of this contradiction the genealogies of the certain number of simulated events have been analysed, i.e. it has been examined where from particles which form distant spots are originated. The investigation has shown that spots at distances greater than 0.1 mm from event's center are formed by rather low-energy particles from NEC nuclear interactions in the upper part of the chamber. All other particles in NEC give rise to more energetic central spot. When measuring optical density of distant spot the corresponding particle energy is overestimated due to overlapping effect. This effect was investigated in Gamma-block 7 where it was shown that "tails" of neighbouring electron-photon cascades (EPC) overlapped thus "amplifying" corresponding optical densities. In H-block the effect is stronger due to high multiplicity and narrowness of NEC secondary particles at film level. Overlapped EPCs of these particles form high "pedestal" for distant low-energy particle and lead to visible distant spot.

The second, rather trivial, source of simple formula (8) failure is that it can not be used in case of cascade. That is why in case of in-chamber NEC the average P_T was once more overestimated.

7. Conclusion. The investigation performed have shown that SE as a whole corresponds to a single hadron from the atmosphere. Distant spots in SE are formed by the usual fluctuations in in-chamber NEC development. Corresponding energies are overestimated due to overlapping effect.

It is recommended to treat SE as single "hadron" and to determine its energy by measuring optical density of SE as a whole by means of diaphragm of highest radius.

8. Acknowledgments. The author is indebted to N.N. Roinishvili, I.P. Ivanenko, V.I. Galkin, B.L. Kanevsky and A.K. Managadze for the aid in research and useful discussions.

References.

1. Khizanishvili, L.A. et al, (1983), Proc. 18th ICRC, Bangalor, vol. 11, p. 133.
2. Leptukh, G.G. et al, (1984), Proc. Intern. Symp. on Cosm. Rays and Particle Physics, Tokyo, p. 414.
3. Hasegava, S, (1984), ibid, p. 319.
4. Tamada, M, (1984), ibid, p. 352.
5. Bielawska, H. et al, (1984), ibid, p. 360.
6. Bayburina, S.G. et al, (1984), ibid, p. 426.
7. Denisova, V.G., Managadze, A.K., (1984), Lebedev P.N. Phys. Inst. preprint No. 20.

ULTRA HIGH ENERGY EVENTS IN ECHOS SERIES AND

PRIMARY ENERGY SPECTRUM

Capdevielle J.N., lab. Phys. Théorique, Bordeaux, rue
du Solarium, 33170 Gradignan, France

Iwai J. and Ogata T., ICR, University of Tokyo, Japan

1. ECHOS series. EMULSION chambers with X-ray film are boarded on the supersonic Concorde Air France liner from October 1978. Since, 6 chambers have been exposed at the highest altitude (about 16Km). The different flights of the French-Japanese collaboration (often quoted as Concorde Collaboration) have been scheduled on Atlantic between Paris and New York as listed in table 1. (ECHOS-Emulsion Chamber On Supersonic).

ECHOS	Altitude ₂ g-cm	Exposure (hours)	Area ₂ m	Depth c.u.	Type	Period
1	106	200	0.1	8.5	{producer no prod.	9-11 78
2	"	"	0.2	7.5	prod.	1-2 80
3	"	"	0.25	6.5	+spacer	1-2 82
4	"	"	0.2	8.5	+TLS sheet	8-10 82
5	"	500	0.2	8.5		11/84-8/85

Table 1

A description of the different chambers and sensitive materials can be found in previous reports (1,2,3) as well as the collection of remarkable events in ECHOS 1,2,3 between 10^6 - 10^7 GeV; we examine hereafter those events, jets, stratospheric ray family in view to point out some signature of phase transition quark gluon plasma and try from a general review of the data of flying experiments (Concorde, JAL cargo jets, JACEE) to situate the tendency of primary cosmic ray spectrum.

2. Correlation rapidity density- $\langle p_T \rangle$. A survey of ISR and \bar{P} -P data

has been taken from Hagedorn's compilation and joined to our data and analysis of cosmic ray jets (2) on Fig. 1. The accelerator data suggested a clear increase of $\langle p_T \rangle$ with rapidity density dn/dy and also that $\langle p_T \rangle$ levels off at highest densities (16). The total p_T distribution has been derived from well collimated and localized jets in emulsion chambers like JF1af1 in Concorde (2), Texas Lone Star in stack, C-C and Ca-C collisions in JACEE (5,6) or in Chacaltaya experiment (7). Admitting that $\langle p_T \rangle$ is the same for nucleon-nucleus collision, we can extend the behaviour of $\langle p_T \rangle$ versus dn/dy by one order of magnitude (fig. 1). Inside the experimental errors, the prediction of Barshay

$$\langle p_T \rangle = 0.32 \exp \left[\frac{1}{7} \ln \left(1 + \frac{3}{\exp(-0.519 \frac{dn^2}{dy}) Ei(-0.0516)} \right) \ln \left(3 - \exp \left(0.0516 \frac{dn^2}{dy} \right) Ei \left(-0.0516 \frac{dn^2}{dy} \right) \right) \right]$$

looks in better agreement than the hybrid model containing thermodynamic coupled with collective motions, which links phase transition and $\langle p_T \rangle$ flattening. (4)

3. Pseudo-rapidity distributions and phase transition.

It was advanced that the bumps occurring in pseudo-rapidity distribution could also be a signature of transition to quark-gluon plasma(8). We have carried out a Monte-Carlo simulation of 1500 p-Aluminium collisions for specific comparison with our typical event JFaf1 produced in Concorde cabin wall. The multicluster phenomenological model (MPM) has been used to extrapolate the collider data (see HE4.1-9, 10), assuming simultaneous rise in Lns of height and width of plateau, random production of small clusters decaying with Gaussian distribution and finally inclination of plateau for nucleon-nucleus collision. The average number $\langle \nu \rangle$ of successive collisions in Al target has been taken as 2 at low energy.

The pseudo-rapidity distribution plotted on fig.2 for $E = 26.10^6$ GeV includes all the possible fluctuations in multiplicity and inelasticity for p-Al collisions (where $\bar{n} = 73$). If the discrepancy of the left part can be easily explained by the γ -ray threshold of 100 GeV, the simulation cannot explain the large number of γ rays emitted (about 50%) at very high rapidity. Subtracting the forward part of simulated from experimental distribution, we obtain superposition of two components, one being consistent with the extrapolation of accelerator data (containing near 80 γ 's), also for n_c estimated to 45 in JFaf1, and one additive component characterized by a narrow peak with gaussian distribution centered at 2.7 unit of rapidity in CMS with FWHM near 1 unit.

This could be the rapidity signature of an explosive decay of phase transition fireball after compression of the projectile fragmentation fireball in the target. (the target fragmentation fireball cannot be seen with γ rays in emulsion chamber). Such procedure repeated with $E_0 = 10^6$ GeV lead to similar results even more pronounced.

5. Primary energy spectrum.

Using the relations previously developed between $E_0, \Sigma E_\gamma, r_\gamma, \langle E_\gamma, R_\gamma \rangle$ for stratospheric γ ray family with SBM model by Monte-Carlo simulation, we make a first attempt (now repeated with MPM) to estimate the integral primary spectrum from the primary energy E of ultra high energy jets in our Concorde and JAL cargo data (table 2,3) in "average conditions".

Name	ΣE_γ (TeV)	Comment	E (GeV)
JF2f1	1589	1Km above chamber	$0.9 \cdot 10^7$
JF1af1	260	From cabin wall	$1.9 \cdot 10^6$
JF3-1	55	jet	$4 \cdot 10^5$
JF3-2	51	jet	$3.9 \cdot 10^5$
JF1af2	34	600m above	$2.3 \cdot 10^5$
JFa1	18	jet	$1.55 \cdot 10^5$

Table 2. Concorde data.

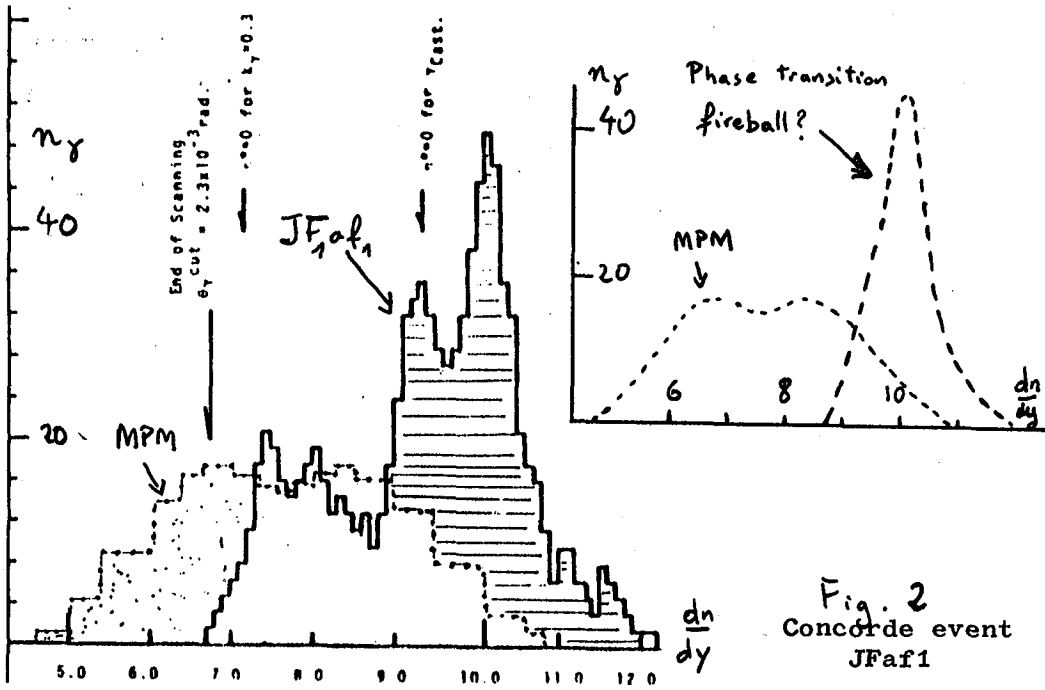


Fig. 2
Concorde event
JFaf1

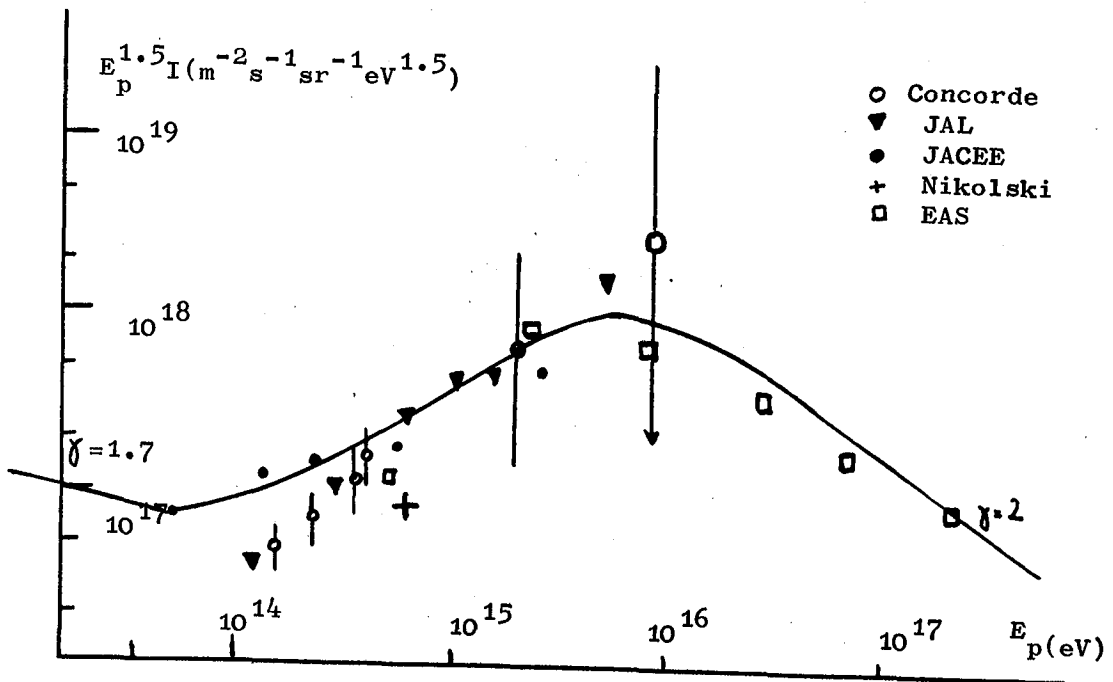


Fig.3

Name	$\sum E_i$	Comment	E
O#1	760	770m above	$5 \cdot 10^6$
AJ-c	239		$1.5 \cdot 10^6$
AJ-b	167		10^6
AJ-a	101		$6 \cdot 10^5$
CF1	74	3.2Km	$2.8 \cdot 10^5$
EF1	20.5	1.7Km	$1.2 \cdot 10^5$

Table 3.

JAL-cargo
data

Taking into account the exposure period and the area of the different chambers, we estimate the integral hadron energy spectrum at 260 G-cm^{-2} and 105 g-cm^{-2} and converted those spectra in total primary spectrum assuming $\Lambda = 105 \text{ g-cm}^{-2}$ for hadron absorption length in air. The situation obtained, together with JACEE data is shown on fig.3. The total 18 events (6 Concorde+6 JACEE+6 JAL) suggests a tendency for a bump in primary spectrum near $10^6 - 10^7 \text{ GeV}$. Furthermore, those intensities are close from those obtained by EAS near maximum (9).

6. Conclusion. The compilation of ultra high energy jets suggests at present the existence of a bump in primary energy spectrum (with the standard concept of high energy collisions). The pseudo rapidity distribution exhibits some typical anomalies, more than the $\langle p_T \rangle$ behaviour, which are, may be, the fingerprints of quark gluon plasma transition. The next results of ECHOS V will be in both cases determinant to confirm those tendencies, as well as an important effort of the cosmic ray community to develop in that sense flying emulsion chamber experiment.

References

1. Capdevielle J.N. et al., 1979, 16th ICRC, Kyoto, 6, 324
2. Iwai J. et al. 1982, NUOV. CIM., 469, 295
3. Capdevielle J.N., 1984, High Energy ASTROPH., Moriond, 129
4. Hagedorn R., 1983, Riv. Nuov. Cim., 6, 10
5. Jones W.v., 1983, 18th ICRC, Bangalore, 12, 279
6. Burnett T.h., 1982, proc. cosmic ray, Philadelphia, 236
7. Arata n., 1978, Nuov. Cim. A, 43, 455
8. Faessler A., 1983, Nucl. Phys., A400, 578c
9. Wdowczyk J., 1984, 9th ECRS, Kosice

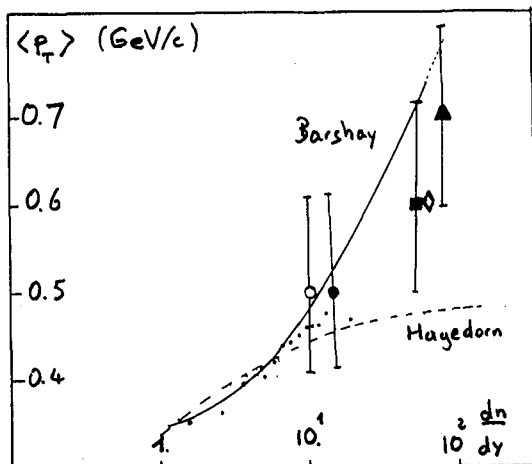


Fig. 1.

- ▲ Ca. C
- ◇ T.L.S.
- JF1af1
- C.C
- [7]
- .. collider

Peculiarities of gamma-quanta distribution at 20 Tev energy

P.M.Ermakov, A.A.Loktionov, Yu.T.Lukin, T.Kh.Sadykov.

HEPI of Kazakh Academy of Sciences, Alma-Ata, USSR.

The angular distribution of protons from the fragmentational region was analyzed. The gamma-quanta families were generated in a dense target by cosmic ray particles at 20 Tev energy. There were found the families which had dense groups (spikes) of gamma-quanta where the rapidity density was 3 times more than the average value determined for all registered families. The experimental data were compared with the results of artificial families simulation.

The fluctuations of particles density in the rapidity scale which were discovered in accelerator experiment [1] were discussed before when gamma-quanta families were studied in cosmic ray experiments [2]. It becomes interesting to study these fluctuations again because the mechanism of their appearance is connected with the effect of quark retention which leads to length restriction of gluons emission [3]. Thus, in the paper [4] there was discovered a structure of the angular correlations of charged secondaries in the inelastic proton-proton interactions at 400 Gev which gives new information about quark retention character.

The data concerning cosmic particles interaction were received by means of the installation consisting of the 9 m² ionization calorimeter and X-ray and emulsion chamber (XREC) of the same area, which was disposed just on the ionization calorimeter. At 11 m above the ionization calorimeter there was the paraffine target of 60 m² area and of 15 g/cm² thickness.

The photosensitive layers of XREC consisted of X-ray film RT-6 and nuclear emulsion R-2T. The registration energy threshold for gamma-quanta for about 100% detection efficiency was equal to $1.5 \cdot 10^{12}$ ev for X-ray films and $0.5 \cdot 10^{12}$ for nuclear emulsion.

The comparison of electron-nuclear cascades in the ionization calorimeter with dark spots in the X-ray film and emulsion chamber was made using coordinates of an entrance point of a high energy particle, zenith and azimuth angles and neutral pions energies measured by the ionization calorimeter and the XREC.

On ionization calorimeter and XREC give incomplete information about each individual interaction: not all secondaries are registered by XREC, besides, it is impossible to separate particles from first and second interactions. The limited spatial resolution of a calorimeter leads to confluence of electron-nuclear cascades initiated by near particles. Thus, the peculiarities of the experiment don't exclude the possibility of systematic distortion of some hadron-nucleons interaction characteristics. To reveal these systematic distortions there were made simulations of electron-nuclear and electromagnetic cascades applicable to the experimental conditions [5].

It was considered three-dimensional picture of electron-nuclear and electromagnetic cascade development for the case when cosmic particles went through layers of substance having different atomic weights, densities, cascade units and interaction mean free paths. The height was taken as 5200 m above sea level for simulation of artificial interactions. For this height there is known the experimental data concerning the composition and energy spectra of hadrons and electrons. In the simulations of hadron-nuclear interactions there was used the model which was based on an extrapolation of accelerator data into more than 10^{13} ev energy region. The model assumed scaling conservation in the fragmentational region.

The experimental statistics was 203 families of gamma-quanta initiated by particles at the mean energy which was equaled to 20 Tev. The mean number of gamma-quanta with energies above registration threshold was equaled to: $\langle N_p \rangle = 6.5$. The dense gamma-quanta jets (spikes) were looked for among the families with the number of gamma-quanta $N_p \geq 4$

Photon groups were taken for spikes when $N_{\mu} > 4$ and the densities on the rapidity scale were $N/\Delta\eta \geq 9$. Such spikes were found in 123 families.

Fig.1 gives the rapidity-distribution of the family photons against the spike rapidity. It can be seen that photons in spikes are in rather narrow rapidity interval. The width of the peak at half-height is equalled to: $\Delta\eta = 0.5$.

Fig.2 shows the number of spikes distribution against gamma-quanta density per rapidity unit.

Fig.3 shows the spike-distribution against the number of photons in the spikes (K).

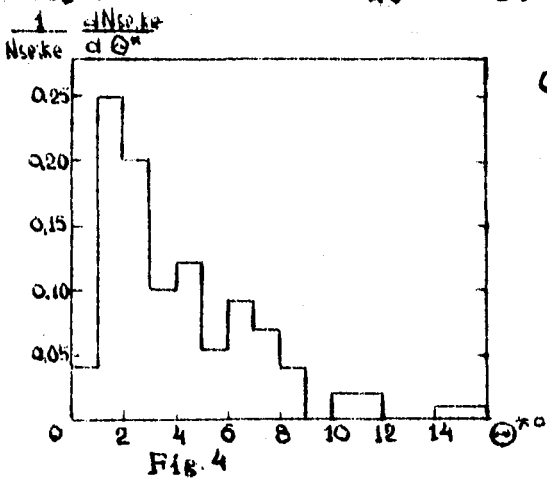
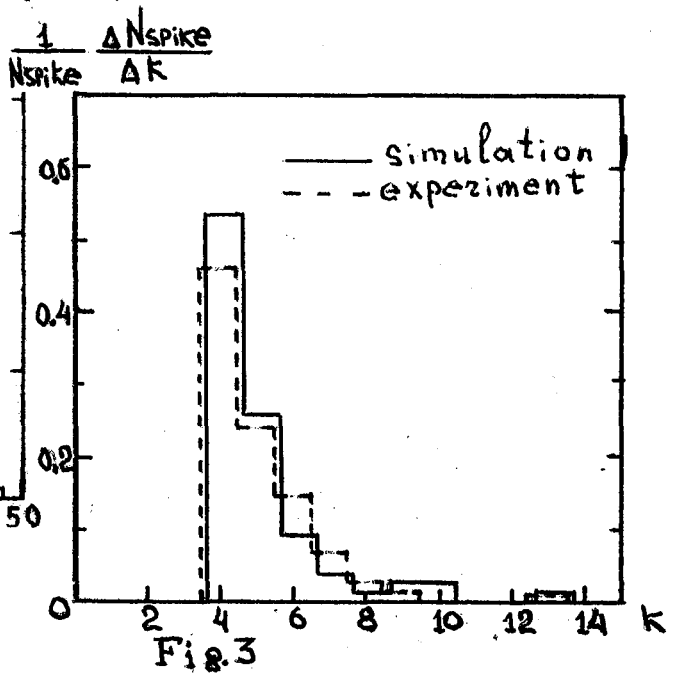
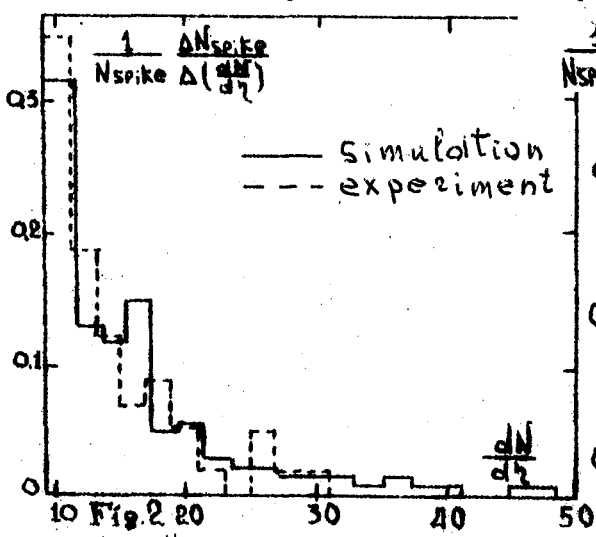
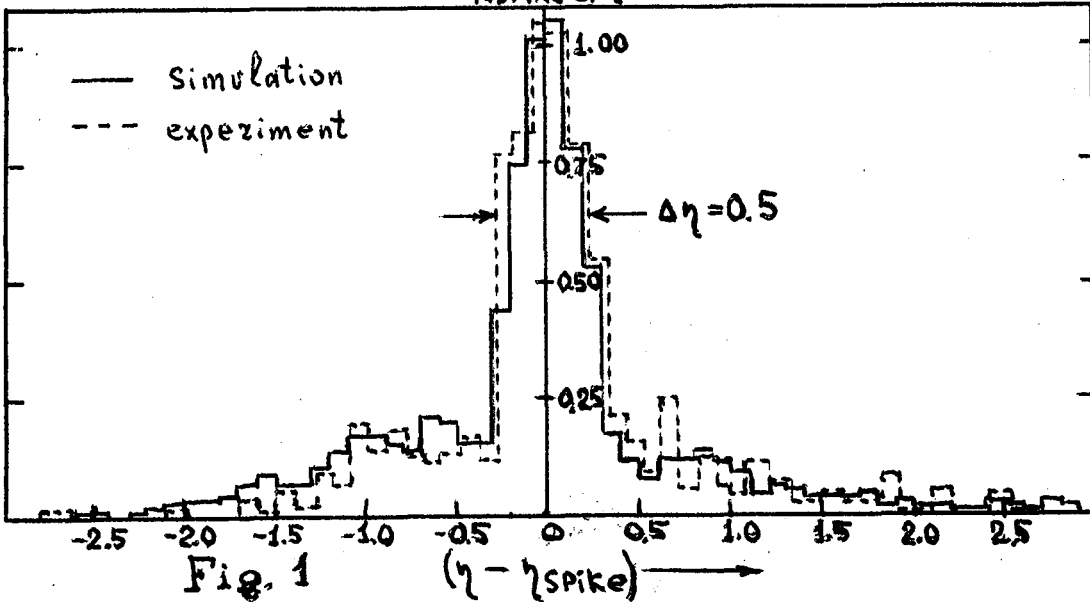
Fig.4 gives the distribution of the families against emission angles of jets in center-of-mass system. The emission angles in CMS range from 1° to 15° , the most probable value being $5-6^{\circ}$.

The estimations of the process of gamma-quanta generation with high density on rapidity scale are, probably, underrated because there were not taken into account the possible double-modal distributions of gamma-quanta in the families with high multiplicity.

Bibliography.

1. Rushbrooke J.G. Preprint CERN-EP/84-39, (1984).
2. Amanov K.A. et al., ICRC papers, Paris, v.5, p.307, (1981).
3. Dremin I.M., Nuclear Physics, v.37, p.649, (1983).
4. Dremin I.M. et al., Letters to JETP, v.40, p.320, (1985).
5. Ermakov P.M., Shorin B.F., Preprint HEPI, n.84-16, p.I-22, Alma-Ata, (1984).

$$\frac{1}{N_{\text{spike}}} \frac{dN_{\text{spike}}}{d\eta}$$



455
AUTHOR INDEX

AGUIRRE, C		BOBODJANOV, IB	
	296,300		200
AIZU, H		BORISOV, AS	
	239		200
ALEEM, FE		BOURDEAU, MF	
	21		400
AMATO, NM		BRASIL-JAPAN,	
	292,320		360
	324,356	BRAZIL-JAPAN,	
AMEEV, SSH			250
	180	BURNETT, TH	
AMENOMORI, M			172,156
	208,348		164,160
	336		152,76,168
AMINEVA, TP		CANANOV, SD	
	200		216
AMMIRAJU, P		CANANOV, SG	
	28		200
AOKI, H		CAO, PY	
	200,280		278,336
	356	CAPDEVIELLE, JN	
ARATA, N			447,400
	292,320	CASSIDAY, GL	
	324,356		5
ATWATER, TW		CHADRANYAN, EKH	
	100,184		216
AVAKIAN, VV		CHADRANYAN, LK	
	64,17		200
AZARIAN, MD		CHAE, IK	
	64		188
AZIMOV, SA		CHARISHNIKOV, SA	
	428,424		376
	200	CHASNIKOV, IYA	
AZIMOV, ZA			274
	200	CHEN, MY	
BAI, GZ			25
	278,336	CHERDYNTSEVA, KV	
BAKHTIGIREEV, SE			254,200
	200	CHILINGARYAN, AA	
BALASUBRAHMANYAN, VK			392
	137	CHINA-JAPAN COLLABORATION,	
BALTRUSAITIS, RM			317,313
	5		309,204
BARADZEI, LT			439
	200	CHINELLATO, JA	
BELLANDI, J			364,356
	356		368
BHATTACHARYYA, S		CHOU, TT	
	220		43
BIELAWSKA, H		CHUBENKO, AP	
	200		96,254
BLOKH, YAL		COOPER, R	
	236		5
BOBODJANOV, IB		DAKE, S	

456
AUTHOR INDEX

DAKE, S	172,156 164,160 152,76,305 168	FREIER, PS	100,104 184
DANILOVA, TV	35	FUJII, M	239
DEMIANOV, AI	270	FUJIMOTO, Y	200,356
DENISOVA, VG	200	FUKI, M	172,156 164,160 152,76,168
DERRICKSON, JH	160,152	FUNAYAMA, Y	200,284 356
DING, L	212	GAISSER, RK	55
DOBRIGKEIT, C	356	GAISSER, TK	47,9,328
DOBROTIN, NA	200	GALFAYAN, SK	392
DOKE, T	68	GARSEVANISHVILI, LP	258
DREMIN, IM	145	GENG, QX	278,336
DUBOVY, AB	254	GERHARDY, PR	5
DUNAEVSKII, AM	392	GOLYNSKAYA, RM	380
DUNAEVSKY, AM	200	GOULD, RJ	149
EBY, PB	133	GREGORY, JC	172,156 164,160 152,76,168
EBIYAN, KSH	64	GUBAR, NE	200
ELBERT, JW	5	GULOV, YA	200
ELLSWORTH, RW	55	GUSEVA, ZM	200
EMELYANOV, YA	200	HAGUENAUER, M	68
EREMENKO, YUA	274	HALILOV, DA	424
ERLYKIN, AD	92,35	HALZEN, F	47
ERMAKOV, PM	451	HASEGAWA, S	200,356
EROFEEVA, IN	196	HASHIMOTO, K	296,300 411
FAUTH, AC	243	HAYASHI, R	152
FIXSEN, DJ	104	HAYASHI, T	
FOUNTAINS, W	160		
FREIER, PS			

457
AUTHOR INDEX

HAYASHI, T	172,156 164,160 152,76,168	JURAK, A	152,76,168
HAYASHI, TO	160	JUSKIEWICZ, B	200
HEIN, LA	380	KAMBEROV, G	88
HE, M	278,336	KANEVSKAYA, EA	200
HE, RD	278,336	KANEVSKY, BL	31,384,388
HOLYNSKI, R	172,60,156 164,160 152,76,168	KARAGJOZIAN, GV	17
HONDA, K	296,300 411	KASAHARA, K	68,208,301 348,336
HOTTA, N	208,301 305,348 336	KASHIWAGI, T	68
HUANG, RQ	25	KAWAMOTO, M	305
HUO, AX	278,336	KAWASUMI, N	296,300 411
ILIJINA, NP	200	KAZANAS, D	137
INNOCENTE, V	68	KAZUNO, M	239
IVANENKO, IP	384,388 200	KEMPA, J	51
IWAI, J	172,156 164,160 152,76,447 168	KEROPIAN, MI	17
JAPAN-USSR,	352	KERTZMAN, MP	184
JING, C	212	KHALILOV, DA	200
JING, G	212	KHISANISHVILI, LA	200
JONES, WV	172,156 164,160,76 168	KHIZANISHVILI, LA	216
JONEW, WV	152	KIKUCHI, J	68
JURAK, A	172,156 164,160	KIM, CO	72,188
		KIM, DH	188
		KIM, SN	72,188
		KIRILLOV, AA	384
		KLOSINSKI, J	141
		KOBAYASHI, T	208,348
		KOBAYSHI, T	239

458
AUTHOR INDEX

KONISHI, E		LORD, JJ	
	208,348		172,156
KOSLOV, VD			164,160
	5		152,76,168
KOTLYAREVSKI, DM		LUKIN, YUT	
	258		451
KRATENKO, YUP		LU, SL	
	376		278,336
KRUGLOV, NA		LYUTOV, YG	
	270		384
KRUTIKOVA, NP		MACHAVARIANI, SK	
	92,254		96
KRYS, E		MACHIDA, M	
	412,416		296,300
KUANG, HH		MACIASZSZYK, A	
	278,336		200
KUBIAK, G		MADIGOZHIN, DT	
	51		274
KUCHIN, IA		MAGNANI, R	
	80,84		300
KUMANO, H		MALDONADO, RHC	
	200,246		292,320
	356		324,356
KUSUNOSE, M		MALINOWSKI, J	
	305		200
LADARIA, NK		MAMIDJANIAN, EA	
	216,258		64,17
LANZANO, S		MANAGADZE, AK	
	68		200
LATTES, CMG		MANDRITSKAYA, KV	
	356		228
LAZAREVA, TV		MARTINIC, NJ	
	200		296,300
LEPTUKH, GG		MARTIROSOV, RM	
	443,200		17
LI, GJ		MASUDA, K	
	278,336		68
LI, JY		MATANO, T	
	278,336		296,300
LILAND, A			411
	224	MAXIMENKO, VM	
LINDE, IA			200
	384	MEEFAN, CA	
LINSLEY, J			152
	1	MEEGAN, CA	
LITVINOV, VA			160
	266	MELKUMIAN, LG	
LIU, ZH			396
	278,336	MENON, MJ	
LOH, EC			356
	5	MIKHAILOVA, IA	
LOKTIONOV, AA			31,200
	451	MIKUMO, E	
LORD, JJ			208,348

459
AUTHOR INDEX

MILCZAREK, K	200	NIKOLSKAJA, NM	254
MISAKI, A	411	NIKOLSKY, SI	96,254
MITO, I	208,348	NISHIKAWA, K	305
	336	NISHIMURA, J	239
MITSUMUNE, T	305	NISHIO, A	239
MIYAMURA, O	172,156	NIWA, M	411
	164,160	NOMURA, Y	239
	152,76,168	NORMURADOV, F	200
MIZUMOTO, Y	5	NOSOV, AN	424
MIZUTANI, K	204,208	NURITDINOV, H	428,424
	348,336	NURITDINOV, K	200
MUKHAMEDSHIN, RA	200	ODA, H	164,160
MULLADJANOV, EJ	424		152,168
MULLAJANOV, EB	200	OGATA, T	172,156
MULLAJANOV, EJ	428		164,160
MURAKAMI, H	68		152,76,447
MURAKI, Y	68		168
MURZINA, EA	200	OHANIAN, GZH	64
MURZIN, VS	196	OHMORI, N	305
NAKADA, T	68	OHSAWA, A	364,200
NAKAMOTO, A	68		356,368
NAKATSUKA, T	305	OHTA, I	336
NAM, RA	200	OLIVERIRA CASTRO, FM	356
NANJO, H	208,348	OLSZEWSKI, A	76
	336,435	ORLOV, AM	145
NAVIA, CE	296,300	OVSEPIAN, GG	17
	356	PAMILAJU, OA	356
NEDEL'KO, OE	200	PAMIR COLLABORATION,	232,344
NESTEROVA, NM	254		192,340,39
NIKOLAEV, LP	200	PARK, IG	72

460
AUTHOR INDEX

PARNELL, TA
172,156
164,160
152,76,168
PASHKOV, SV
200
PIOTROWSKA, A
51
PLYASHESHNIKOV, AV
372,380
POMELOVA, EI
200
POPOVA, EG
200
POPOVA, L
88
PROSKURYAKOV, AS
270
PUCHKOV, VS
200
RAKOBOLSKAYA, IV
31,200
REN, GX
25
REN, JR
278,336
ROBERTS, E
160,152
ROGANOVA, TM
388,200
ROGOVAYA, SI
236
ROINISHIVILI, NN
200
ROINISHVILI, NN
216
RYABOVA, NG
200
SADYKOV, TKH
274,451
SAITO, T
172,156
164,160
152,76,301
305,168
SAKATA, M
301,305
SALEEM, M
21
SARYCHEVA, LI
270
SASAKI, H
305
SATO, K
SATO, K
208,348
SAWAYANAGI, K
243,356
SAZHINA, GP
228
SEMBA, H
200,356
SHABEL'SKI, YUM
258
SHABELSKI, YM
92
SHERER, NI
258
SHIBATA, M
208,348
336
SHIBATA, T
356
SHIBUYA, EH
332,200
356,368
SHIMA, M
301,305
SHIRAI, T
239,208
348,336
SHMONIN, VL
180
SHOBORONOV, K
200
SILES, L
300
SIVOKLOKOV, SYU
196
SIZOV, VV
388
SLAVATINSKY, SA
200
SMIRNOVA, LN
196,270
SMIRNOVA, MD
200
SMORODIN, YA
200
SMORODIN, YUA
396
SOKHOYAN, SO
17
SOKOLSKAYA, NV
228
SOKOLSKY, P
5
STANEV, T

461
AUTHOR INDEX

STANEV, T 55,328
 STECK, D 5
 STEMANETYAN, GZ 258
 STRAUSZ, S 172,164
 160,76
 STREITMATTER, RE 137
 STRUGALSKI, Z 404,108
 112,115
 118,122
 125,129
 SUGIMOTO, H 208,348
 SUKHATME, UP 9
 SU, S 278,336
 SVANIDZE, MS 200
 SVESHNIKOVA, LG 31,200
 SZABELSKI, 51
 SZARSKA, M 164,152,76
 TABUKI, T 172,156
 164,160
 152,76,168
 TAIRA, K 208,348
 TAIRA, T 239,208
 348,336
 TAKAHASHI, Y 172,156
 164,160,76
 133,168
 152
 TALIPOV, DA 424,200
 TAMADA, M 200,284
 288,356
 TATALASHVILI, NG 258
 TATEYAMA, N 239,208
 348,336
 TATI, T 420
 TER-ANTONIAN, SV 64,396
 TOMASZEWSKI, A 431,200
 TOMINAGA, T 172,156
 164,160
 168
 TOMINAGA, Y 76
 TORII, S 239,208
 301,348
 336
 TRETAKOVA, MI 145
 TRIPHONOVA, SV 388
 TSOMAYA, PV 258,262
 TSUSHIMA, I 296,300
 411
 TUKISH, EI 254
 TURTELLI, A 356
 UCHAIKIN, VV 266
 VARDANYAN, IN 270
 VARKOVITSKAYA, AYA 228
 VERBETSKI, YG 258
 VILDANOV, NG 254
 VOINOV, VG 274
 VOROBYEV, KV 372,380
 WADDINGTON, CJ 104
 WANG, CR 278,336
 WANG, SZ 278,336
 WANG, YX 278,336
 WASILEWSKI, A 412,416
 WATTS, J

462
AUTHOR INDEX

WATTS, J		YOON, CS	
	172		72
WATTS, JS		YOSHIDA, A	
	152		239
WATTS, JW		YUDA, T	
	164		68,208,301
WADOWCZYK, J			348,336
	51	YULDASHBAEV, TS	
WEFEL, JP			428,424
	164,76	YULDASHBAYEV, TS	
WILCZYNSKA, B			200
	172,156	ZAITSEVA, EG	
	164,160		200
	152,76,168	ZAMCHALOVA, EA	
WILKES, RJ			228
	172,156	ZAPATA, J	
	164,160		300
	152,76,168	ZATSEPIN, GT	
WLODARCZYK, Z			200
	431	ZATSEPIN, VI	
WOLTER, W			228
	172,156	ZAZYAN, MZ	
	164,160		392
	152,76,168	ZELEVINSKAYA, NG	
WOSIEK, B			200
	172,176	ZHAMKOCHIAN, VM	
	156,164		13
	160,152,76	ZHANG, NJ	
	168		278,336
WOZNIAK, K		ZHDANOV, GB	
	60		200
WROTNIAK, JA		ZHOU, WD	
	56,328		278,336
XUE, YG		ZHOU, YZ	
	336		25
YAKOVLEVA, TI		ZHU, Q	
	254		212
YAMAMOTO, Y		ZIMIN, MV	
	301,305		200
YAMASHITA, S			
	364,200		
	356,368		
YANAGITA, T			
	407		
YANG, CN			
	43		
YEREMIAN, SHS			
	13		
YERSHOV, AA			
	270		
YODH, GB			
	9,56		
YOKOI, K			
	200,356		

BIBLIOGRAPHIC DATA SHEET

1. Report No. NASA CP-2376 Volume 6	2. Government Accession No.	3. Recipient's Catalog No.	
4. Title and Subtitle 19th International Cosmic Ray Conference Conference Papers		5. Report Date August 1985	
		6. Performing Organization Code 665	
7. Author(s) Frank C. Jones, compiler		8. Performing Organization Report No.	
9. Performing Organization Name and Address Laboratory for High Energy Astrophysics Goddard Space Flight Center Greenbelt, MD 20771		10. Work Unit No.	
		11. Contract or Grant No.	
		13. Type of Report and Period Covered Conference Publication	
12. Sponsoring Agency Name and Address National Aeronautics and Space Administration Washington, D. C. 20546		14. Sponsoring Agency Code	
15. Supplementary Notes			
16. Abstract These volumes contain papers submitted for presentation at the 19th International Cosmic Ray Conference, held on the campus of the University of California, San Diego in La Jolla, CA., August 11-23, 1985. The conference is held every other year. The present volume contains papers with Paper Codes HE 1.1 through HE 3.6 and deals with cross sections, particle production, nuclei and nuclear matter, cosmic-ray jets, and emulsion chamber simulations.			
17. Key Words (Selected by Author(s)) cross sections, particle production, nuclei, nuclear matter, jets, emulsion chamber, simulations		18. Distribution Statement Unclassified - Unlimited Subject Category - 93	
19. Security Classif. (of this report) Unclassified	20. Security Classif. (of this page) Unclassified	21. No. of Pages	22. Price*



National Aeronautics and
Space Administration

Goddard Space Flight Center
Greenbelt, Maryland 20771